NATURALNESS-PRESERVING TRANSFORM PROCESSING OF DIGITAL SIGNALS

by

ADEWOLE OLUFOLAMI OSINUBI

A thesis submitted for the degree of
Doctor of Philosophy
in the Faculty of Engineering of the University of London
and for the Diploma of Imperial College.

Department of Electrical Engineering,
Imperial College of Science, Technology and Medicine
University of London,
London.
February 1990

ABSTRACT

This thesis develops Naturalness-Preserving Transforms and investigates their digital signal processing applications.

The Naturalness-Preserving Transforms (NPT) are linear combinations of orthogonal matrices. The problem of determining admissible NPT transforms for digital signal processing applications is addressed. A parametric family of NPT transforms are defined.

NPT coding of monochrome images is investigated. Conventional transform coding techniques are considered. The NPT is characterized by an infinite number of bases and the problem of determining the basis giving minimum mean-square error (MSE) for coding an image or image ensemble is addressed. An algorithm for determining the optimum basis (in MSE sense) is introduced. The optimum basis varies with image content and the parameters of the coder. Consequently, a block classification basis adaptive NPT coder featuring transform basis adaptation according to local image content in addition to conventional adaptation techniques (adaptive bit allocation/quantization) is proposed.

Subsequently, predictive NPT coding of images is investigated. The coding systems employ one-dimensional NPTs and a bank of DPCM (differential pulse code modulation) operators. The algorithm for selecting the optimum basis is developed.

A rate-distortion theoretic framework for NPT coders is developed. The emphasis is on ascertaining the minimum rate necessary to transmit or store a given image, in order to achieve a desired distortion level, when a specified NPT basis is used for coding the image. The bound is computed and compared with practical performance levels.

The problem of signal transmission through channels that are subject to non-stationary noise degradations, is considered. The basic problem can be stated as follows: We transmit a signal, and as a result of non-stationary channel noise, segments of the transmission are rendered unuseable due to unacceptable error levels. We develop pre-/post-transmission signal processing techniques that would permit the reconstruction of a useful version of the original transmitted signal.

The Hadamard NPT domain is proposed for signal transmission under this scenario. Signal degradation is modelled as a complete loss of segments of the transmitted signal and we subsequently address the problem of reconstructing a signal from segments of its Hadamard NPT. Closed-form reconstruction formulae are derived for typical formats of NPT segments. Both one-dimensional and two-dimensional NPT reconstruction formats are investigated. Empirical results of the reconstruction of first order stationary Gauss-Markov and speech signals, using the one-dimensional Hadamard NPT reconstruction algorithm, are presented.

Fast reconstruction algorithms applicable to some signal loss formats (one-dimensional and two-dimensional formats) which provide solutions in one iteration, are introduced.

The fast one-dimensional Hadamard NPT reconstruction algorithm is proposed for packetized imagery transmission applications. The reconstruction algorithm is investigated for intraframe two-layer packet transmission of image signals over an 'Orwell' ring based communication network. Good reconstructed pictures are obtained at up to fifty percent packet loss rate. For low bandwidth channel applications, the effect of data compression on the quality of reconstructed images is investigated. Both transform DPCM and vector quantization (VQ) techniques are studied for coding the Hadamard NPT samples necessary for reconstruction. VQ technique is shown to be effective for coding the Hadamard NPT samples used for reconstruction at low bit rates. The effect of channel errors is also considered.

The two-dimensional Hadamard NPT reconstruction algorithm is investigated for tactical imagery transmission. The problem of channel bandwidth limitations is also considered and VQ technique is shown to be effective for coding the two-dimensional Hadamard NPT transformed imagery at low bit rates i.e. bit rates in the range 0.5625-1.0 bit per sample. The effect of channel errors on the reconstructed image quality is also studied.

Hybrid coding systems which are based on fast Hadamard NPT signal reconstruction techniques are proposed. These are based on the fast one-dimensional Hadamard NPT reconstruction of each line of an image at the receiver. Empirical results of coded images, using the algorithms are presented.

NPT generalized Wiener filtering is developed; the formulation is in one dimension. The performance of an optimum NPT generalized Wiener filter is

shown to be equivalent to that of any optimum orthogonal transform generalized Wiener filter. Sub-optimum NPT generalized Wiener filtering is also investigated. The problem of determining the basis giving minimum MSE of filtering a given noisy signal, using sub-optimum NPT generalized Wiener filters, is considered. An approach to NPT generalized Wiener filter design which is different from classical design methods, is introduced. Empirical results of filtering first order stationary Gauss-Markov signals corrupted with additive white noise, are presented.

To my father, OLUSANYA OSINUBI

and

to my mother, OLUFUNSO OSINUBI

for their *sacrifices* to give me the very best.

ACKNOWLEDGEMENTS

I am indebted to Dr. R. A. King for his supervision, deep interest, guidance and commitment in the course of this work. I am also grateful for his interest in my welfare.

I wish to acknowledge Dr. T. Ibikunle for his encouragement and keen interest in the course of this work. His participation was at a supervisory level and the many discourses we have had contributed immensely to the findings reported in this thesis. I am also grateful to him for finding the time to go through most of the chapters of the thesis. Many thanks are also due to his wife, Dr Tokunbo Ibikunle for her encouragement, support and love. Their friendship has been invaluable.

I also wish to thank members of Dr King's research group who have showed interest, in one way or another, in the work.

I would like to thank the Imperial College Centre for Remote Sensing for allowing me to use their facilities. I acknowledge Dr Chris England for his assistance.

Many thanks are due to Mr. John Durodola for his encouragement, marvellous friendship and interest in the work; he has also found the time to help with some of the typescript. I am also grateful to Dr. Uwa Igiehon for helping with the preparation of the photographic prints and his friendship.

I express my gratitude to the members of my family for their encouragement, deep love and wholehearted support in the course of this work. I also acknowledge relations and many friends who have expressed sincere interest and concern about myself and my work. I am indeed grateful to you all.

I also wish to thank Mrs R. O. Sosanya for her support and encouragement, most especially during the writing up of the thesis.

My heartfelt thanks are due to my fiancée Omowunmi Sosanya for her devotion, invaluable love, encouragement and support throughout the course of this work.

Finally, I wish to thank God, the father of my Lord and Saviour Jesus Christ, for His faithfulness in meeting my needs at every point, in the course of this work and for His blessings over the years. God has indeed been real to me.

TABLE OF CONTENTS

		Page
ABSTRACT		2
DEDICATION		5
ACKNOWLEDGEMENTS		6
IMPORTANT NOTATION		13
CHAPTER 1	INTRODUCTION	17
1.1	Signal Transforms	17
1.2	Previous Work on The Naturalness-Preserving Transforms	17
1.3	Scope of Thesis	18
1.4	Outline of Thesis	20
PART I	THE NATURALNESS-PRESERVING TRANSFORM AND IMAGE DATA COMPRESSION	23
CHAPTER 2	THE NATURALNESS-PRESERVING TRANSFORM AND SOME DEVELOPMENTS FOR THE TRANSFORM	24
2.1	Introduction	24
2.2	Hybrid Transforms	25
2.3	Hybrid Transform Sub-Classes	25
2.3.1	Statement of the Problem of Determining Admissible Hybrid Transform Sub-Classes	26
2.3.2	Inversion of Hybrid Transforms	27
2.3.2.1	Hybrid Transform Inversion Theorems	28
2.3.2.1.1	Theorem 1 : The Inverse of A Linear Combination of Two Commuting Involutory Matrices	28
2.3.2.1.2	Theorem 2 : The Inverse of A Linear Combination of Two Anti-Commuting Involutory Matrices	28
2.3.2.2	Results and Discussion of Theorems	28
2.3.3	The Naturalness-Preserving Transforms	29
2.3.3.1	A Naturalness-Preserving Transform Sub-Class	30
2.3.3.1.1	Series Representation of The NPT	33
2.3.3.1.2	Properties of The NPT	36
2.3.3.1.3	Operation Count Required For Computing The NPT of A Data Sequence	46
2.3.3.2	An Alternative Definition of The NPT	47

2.3.4	The Original Pictures Used For Simulation	51
2.3.5	Simulation and Results	51
2.4	Summary and Conclusions	56
CHAPTER 3	NATURALNESS-PRESERVING TRANSFORM IMAGE DATA COMPRESSION	58
3.1	Introduction	58
3.2	The Data Compression Problem	59
3.3	Review of Image Data Compression Techniques	60
3.3.1	Predictive Coding	60
3.3.2	Transform Coding	61
3.3.3	Hybrid Coding	62
3.4	A Unifying Description of Data Compression Systems	62
PART A:	Conventional Pure Transform Coding of Images Using The Naturalness-Preserving Transforms	64
3.5	Naturalness-Preserving Transform Image Coding	64
3.5.1	The Optimum Basis Determination Problem	65
3.5.2	Determination of The Optimum NPT Basis	66
3.5.3	Simulation, Results and Discussion of Non-Adaptive NPT Image Coding	73
3.5.3.1	Bit Allocation	73
3.5.3.2	Variation of The Mean-square Error of NPT Image Coding With Transform Basis	74
3.5.3.3	Investigations on NPT Image Coding Correction Factor	80
3.5.3.4	Further Results on Non-Adaptive NPT Image Coding	87
3.5.4	Basis Adaptive NPT Image Coding	93
3.5.4.1	Introduction and Description of The Basis Adaptive NPT Image Coder (BANPTC)	93
3.5.4.2	Simulation and Results of Basis Adaptive NPT Image Coding	95
3.5.4.3	The Effect of Channel Errors	109
PART B:	Predictive Naturalness-Preserving Transform Coding of Images	111
3.6	The Intraframe NPT Hybrid Image Coding Scheme	111
3.6.1	Determination of The Optimum NPT Basis For Hybrid Coding of Images	114
3.6.2	Simulation, Results and Discussion	120

3.7	Summary and Conclusion	127
CHAPTER 4	RATE-DISTORTION THEORETIC ANALYSIS FOR NPT IMAGE CODERS	130
4.1	Introduction	130
4.2	Fundamentals of Rate-Distortion Theory	131
4.2.1	Rate-Distortion Theory and Transform Image Coding	134
4.3	Determination of The Rate-Distortion Function For NPT Image Coders	136
4.3.1	Problem Statement	138
4.4	An Upper Bound of The Rate-Distortion Function For NPT Image Coders	139
4.5	Evaluation of The Rate-Distortion Bounds For NPT Image Coders	142
4.6	Comparison of The Theoretical Bounds With The Performance of Sub-optimal NPT Compressors	145
4.7	Summary and Conclusion	147
PART II	ITERATIVE HADAMARD NATURALNESS-PRESERVING TRANSFORM PROCESSING OF SIGNALS	149
CHAPTER 5	ITERATIVE ONE-DIMENSIONAL HADAMARD NATURALNESS-PRESERVING TRANSFORM RECONSTRUCTION OF SIGNALS DEGRADED BY NON-STATIONARY NOISE PROCESSES OR JAMMING	150
5.1	Introduction	150
5.1.1	Problem Statement	150
5.1.2	Background to The Reconstruction Problem and Practical Applications of Hadamard NPT Signal Reconstruction	150
5.1.3	Scope of Research	151
5.1.4	Chapter Organization	151
5.2	Signal Reconstruction From Hadamard NPT Segments	152
5.2.1	Hadamard NPT Pre-processing	152
5.2.2	Classical Solution	153
5.2.3	Iterative One-Dimensional Hadamard NPT Reconstruction	155

5.2.3.1	Examples of Iterative One-Dimensional Hadamard NPT Reconstruction Formats	158
5.2.3.2	Fast Reconstruction Algorithms	182
5.2.3.3	Degenerate Formats	184
5.2.3.4	Signal Estimation From One-Dimensional Hadamard NPT Segments	186
5.3	Simulation, Results and Discussion	190
5.3.1	Reconstruction of Stationary First Order Gauss-Markov Signals	191
5.3.2	Reconstruction of Speech Signal	205
5.4	Application of One-Dimensional Hadamard NPT Reconstruction Formats in Intraframe Packet Transmission of Images	209
5.5	Summary and Conclusion	217
CHAPTER 6	ITERATIVE TWO-DIMENSIONAL HADAMARD NATURALNESS-PRESERVING TRANSFORM SIGNAL RECONSTRUCTION WITH APPLICATIONS TO TACTICAL IMAGERY TRANSMISSION	219
6.1	Introduction and Review of Previous Work	219
6.2	Signal Reconstruction From Two-Dimensional Hadamard NPT Segments	220
6.2.1	Two-Dimensional Hadamard NPT Pre-Processing	220
6.2.2	Iterative Two-Dimensional Hadamard NPT Signal Reconstruction	221
6.2.2.1	Examples of Iterative Two-Dimensional Hadamard NPT Reconstruction Formats	224
6.2.2.2	Fast Reconstruction Algorithm	232
6.2.2.3	Signal Estimation From Two-Dimensional Hadamard NPT Segments	233
6.3	Simulation, Results and Discussion	235
6.4	Summary and Conclusion	242
CHAPTER 7	CONSIDERATIONS FOR ONE-DIMENSIONAL AND TWO-DIMENSIONAL HADAMARD NATURALNESS-PRESERVING TRANSFORM RECONSTRUCTION APPLICATIONS	244
7.1	Introduction	244

7.2	Considerations For One-Dimensional Hadamard NPT Reconstruction Two-Layer Intraframe Packet Transmission of Images	245
7.2.1	Intraframe Packet Transmission of Images Over Low Bandwidth Channels	245
7.2.1.1	Reconstruction of An Image From Guaranteed Packets, Coded Using Hybrid Coding Techniques	245
7.2.1.2	Reconstruction of An Image From Guaranteed Packets, Coded Using Vector Quantization Techniques	250
7.2.1.2.1	Definition of Vector Quantization and Vector Quantizer Design	250
7.2.1.2.2	Application of VQ To Coding Hadamard NPT Samples For Transmission As Guaranteed Packets	252
7.2.2	The Transmission of Enhancement Packets	253
7.2.3	The Effect of Channel Errors	257
7.3	Considerations For Two-Dimensional Hadamard NPT Reconstruction, Tactical Imagery Transmission	259
7.3.1	Imagery Reconstruction From Compressed Two-Dimensional Hadamard NPT Segments	259
7.3.2	The Effect of Channel Errors On Reconstructed Imagery Quality	260
7.4	Hybrid Image Coding Techniques Based on Hadamard Naturalness-Preserving Transform Reconstruction	262
7.4.1	Introduction	262
7.4.2	The Hadamard Naturalness-Preserving Transform Reconstruction-Based Hybrid Image Coding Algorithm	263
7.4.2.1	Variations of The Hybrid Coding Algorithm	266
7.4.3	Simulation, Results and Discussion	268
7.5	Summary and Conclusion	270
PART III	NATURALNESS-PRESERVING TRANSFORM FILTERING	273
CHAPTER 8	NATURALNESS-PRESERVING TRANSFORM DOMAIN GENERALIZED WIENER FILTERING	274
8.1	Introduction	274
8.2	Mathematical Model of The NPT Generalized Wiener Filter	274

8.3	NPT Generalized Wiener Filter Design	276
8.3.1	Derivation of The Optimum NPT Generalized Wiener Filter Matrix	277
8.3.2	Minimum Mean-Square Error of The Optimum NPT Generalized Wiener Filter	280
8.4	Sub-optimal Wiener Filtering	281
8.4.1	Sub-optimal Filtering Using Relatively Large Magnitude Filter Coefficients	282
8.4.2	Sub-optimal Diagonal Filters	287
8.4.3	Determination of The Optimum Basis For Sub-optimum Filtering	289
8.5	A New Approach To Naturalness-Preserving Transform Domain Wiener Filtering	290
8.5.1	A Filtering Example	290
8.5.2	Other Filter Matrices	295
8.6	Summary and Conclusion	298
PART IV	SUMMARY, CONCLUSION AND RECOMMENDATIONS FOR FURTHER WORK	299
	CONCLUSIONS	300
	APPENDICES	312
APPENDIX I	DERIVATION OF THE HYBRID TRANSFORM INVERSION THEOREMS	313
APPENDIX II	PROOF OF CONVERGENCE OF THE ITERATIVE ONE-DIMENSIONAL HADAMARD NPT RECONSTRUCTION ALGORITHM	317
APPENDIX III	PROOF OF CONVERGENCE OF THE ITERATIVE TWO-DIMENSIONAL HADAMARD NPT RECONSTRUCTION ALGORITHM	321
APPENDIX IV	DERIVATION OF THE RESULT OF EQUATION (6.40), CHAPTER SIX	324
APPENDIX V	DERIVATION OF SOME RESULTS USED IN THE NPT GENERALIZED WIENER FILTER DESIGN	336
	REFERENCES	340

IMPORTANT NOTATION

NOTE:-

Only what is considered to be important notation for the thesis is listed here. Some symbols have been employed just for convenience at their time of use and these are not included here.

$\mathbf{A}$	-	Orthogonal transform matrix.
ALE	-	Adaptive line enhancer.
bits/pel	-	bits per picture element or bits per pixel.
$b(\alpha, \theta)$	-	Correction factor.
BANPTC	-	Basis adaptive NPT coder.
BER	-	Bit error rate.
$(CMEF)_{DC}$	-	Coefficient Magnitude Expansion Factor For "DC " values.
CRT	-	Cathode ray tube
$\mathbf{C_f}$	-	Data domain covariance matrix of the random process, $\mathbf{f}$.
$\mathbf{C_{t_f}}$	-	Covariance matrix of an NPT transformed random process, $\mathbf{f}$.
$\mathbf{D}$	-	Diagonal matrix.
$d(\alpha, \theta)$	-	Ratio of spatial to transform domain MSE.
D_{sp}	-	Spatial domain allowable total distortion.
D_{tr}	-	Encoding distortion in the transform domain.
D_I	-	Distortion due to inverse NPT transformation.
$d(\mathbf{v}, Q(\mathbf{v}))$	-	Distortion per vector of VQ.
$diag[\mathbf{B}]$	-	The diagonal of matrix $\mathbf{B}$.
$E\{\cdot\}$	-	Mathematical expectation operator.
$\mathbf{E}_S(\alpha, \theta)$	-	Spatial domain error array resulting from coding an image $\mathbf{F}$ with an NPT transform basis specified by α.
$\mathbf{E}_T(\alpha, \theta)$	-	Transform domain error array resulting from coding an image $\mathbf{F}$ with an NPT transform basis specified by α.
E	-	Vector of estimation errors.
$\underline{e}_i$	-	i^{th} sub-vector of equi-partitioned vector E.
$\mathbf{E}$	-	Matrix of estimation errors.
$\mathbf{f}$	-	N-length data vector.
$\mathbf{f}^T$	-	Transpose of $\mathbf{f}$.
$\mathbf{F}$	-	$N \times N$ data matrix.

$\bar{\mathbf{f}}$	-	Mean vector of a one-dimensional random process, $\mathbf{f}$.
$\mathbf{f_F}$	-	Vector of stacked two-dimensional data array $\mathbf{F}$.
$\hat{\mathbf{f}}$	-	A vector or sequence of encoded samples.
$\hat{\mathbf{F}}$	-	A matrix of encoded image samples.
$F(\cdot)$	-	one-dimensional signal estimation operator.
$\tilde{\mathbf{F}}$	-	Inverse two-dimensional Hadamard NPT of $\tilde{\mathbf{T}}_\mathbf{F}$.
$\hat{\mathbf{F}}^W$	-	Estimate of the original signal, derived from $\tilde{\mathbf{T}}_\mathbf{F}$.
$\hat{\mathbf{F}}_m$	-	Reconstruction of $\mathbf{F}$ at the m^{th} iteration.
$g(x,u)$	-	Forward one-dimensional NPT kernel.
$g(x,y;u,v)$	-	Forward two-dimensional NPT kernel.
$g_R(y,v)$	-	Row forward NPT kernel.
$g_C(x,u)$	-	Column forward NPT kernel.
g_m	-	Convergence parameter; m is the number of iterations.
$h(x,y;u,v)$	-	Inverse two-dimensional NPT kernel.
$\mathbf{H}_n$	-	Normalized natural Hadamard matrix of order $N = 2^n$.
$\mathbf{I}$	-	Identity matrix.
$\mathbf{I}_N$	-	Identity matrix of order $N = 2^n$.
KL	-	Karhunen-Loeve.
LBG	-	Linde, Buzo and Gray.
MSE	-	Mean-square error.
$M_N(\mathbf{f},\hat{\mathbf{f}})$	-	Mutual information between vector sequences $\{\mathbf{f}\}$ and $\left\{\hat{\mathbf{f}}\right\}$ when the vectors belong to an $N-$dimensional vector space.
$\mathbf{M}$	-	NPT generalized Wiener filter matrix.
NPT	-	Naturalness-Preserving Transform.
NPT(a)	-	NPT transform corresponding to the basis parameter $\alpha = a$.
$\underline{0}$	-	Null vector.
$\mathbf{0}$	-	Null matrix or null vector.
PSNR	-	Peak signal-to-noise ratio.
$Q(\mathbf{v})$	-	Vector quantizer or mapping of the vector $\mathbf{v}$.
$R_N(D)$	-	N-block rate-distortion function.
R	-	Hadamard NPT of S.
$\tilde{R}$	-	Truncated R, i.e. vector R with some segments excised.
$\hat{R}_m$	-	Reconstruction of R at the m^{th} iteration.
$\underline{r}_i$	-	i^{th} sub-vector of equi-partitioned vector R.
$\tilde{r}_j$	-	Entries of the truncated Hadamard NPT vector $\tilde{R}$.
RPM	-	Replacement processor module.

SCT	-	Symmetric cosine transform.
SC NPT	-	Symmetric cosine NPT.
$S(t)$	-	One-dimensional time-dependent signal.
S	-	N-length segment of $S(t)$.
$\tilde{S}$	-	Inverse NPT of $\tilde{R}$.
$\hat{S}^W$	-	Estimate of the original signal, derived from $\tilde{R}$; the components of $\hat{S}^W$ are zero at locations corresponding to the truncated samples of R.
$\hat{S}_m$	-	Reconstruction of S at the m^{th} iteration.
$\underline{s}_i$	-	i^{th} sub-vector of equi-partitioned vector S.
$\mathbf{S}(\cdot)$	-	Two-dimensional signal estimation operator.
SNR	-	Signal-to-noise ratio.
$\mathbf{t_f}$	-	One-dimensional NPT of $\mathbf{f}$.
$\mathbf{T_F}$	-	Two-dimensional NPT of $\mathbf{F}$.
$\bar{\mathbf{t}}_\mathbf{f}$	-	Mean vector of the NPT transformed random process, $\mathbf{f}$.
$\mathbf{t_F}$	-	Vector of scanned two-dimensional NPT coefficients of the transformed data array $\mathbf{F}$.
$\tilde{\mathbf{T}}_\mathbf{F}$	-	Truncated two-dimensional Hadamard NPT of the data array $\mathbf{F}$.
$\hat{\mathbf{T}}_{\mathbf{F};m}$	-	Reconstruction of $\mathbf{T_F}$ at the m^{th} iteration.
TDALE	-	Two-dimensional adaptive line enhancer.
$tr[\mathbf{B}]$	-	The trace of a matrix $\mathbf{B}$.
v_m	-	Error vector multiplying factor at the m^{th} iteration.
V_m	-	Error matrix multiplying factor at the m^{th} iteration.
VQ	-	Vector quantization.
α	-	NPT basis parameter.
$\underline{\alpha}$	-	Vector of NPT basis parameters.
$\psi\{\underline{\alpha}\}$	-	Forward NPT kernel.
$\psi^{-1}\{\underline{\alpha}\}$	-	Inverse NPT kernel.
$\delta_{x,u}$	-	Kronecker delta function.
$\mathcal{O}(\cdot)$	-	Operation count for computing the one-dimensional or the two-dimensional NPT of data.
$\psi_{ALT}\{\alpha\}$	-	Alternative NPT forward transform kernel.
$\psi_{ALT}^{-1}\{\alpha\}$	-	Alternative NPT inverse transform kernel.
θ	-	NPT image coder parameters specifying the dependence on bit rate and quantization scheme.
α_{opt}	-	Optimum NPT basis for coding a given image or

		image sub-array.
ρ	-	Inter-element correlation coefficient of first order stationary Gauss-Markov signal.
ρ_H, ρ_V	-	Horizontal and Vertical inter-element correlation coefficient for first order Gauss-Markov image.
$\mathcal{V}^N$	-	N-dimensional vector space.
ζ	-	Transform domain distortion parameter.
γ	-	Spatial domain distortion parameter.
ϕ_{ID}	-	One-dimensional replacement operator where the segments to be replaced are defined by an index vector ID.
$\Phi_{\mathbf{KD}}$	-	Two-dimensional replacement operator, where **KD** is an array of indices.
$\Re^z$	-	z-dimensional real Euclidean vector space.
ε_{min}	-	Minimum MSE of the optimum NPT generalized Wiener filter.
ε_d	-	MSE of sub-optimum diagonal NPT generalized Wiener filter.

CHAPTER ONE

INTRODUCTION

1.1 Signal Transforms

A very useful mathematical operation in digital signal processing is that involving a multi-dimensional rotation of co-ordinates of the data into another co-ordinate space which is more suitable for subsequent processing. The application of an inverse rotation yields an approximate* version of the original data. This rotation of the co-ordinates of the data is generally accomplished by applying a transformation.

Transforms have been widely used for signal processing applications [1,2]. For example, transforms have been used to extract features from images. In the Fourier transform domain, the average value or "dc " term is proportional to the average image brightness, and the high frequency terms provide information about the amplitude and orientation of edges within an image. In coding applications, the transform domain of data has been exploited for bandwidth reduction by discarding or grossly quantizing low-magnitude transform coefficients. Dimensionality reduction in the computational requirements for filtering, whereby low-magnitude transform coefficients are excluded from the processing operations without seriously affecting system performance, is another application area. A great deal of past research efforts have concentrated on the development, analysis and applications of unitary transforms in digital signal processing.

This thesis is concerned with the development, analysis and signal processing applications of a new class of transforms called *The Naturalness-Preserving Transforms (NPT).* These transforms are hybrid transforms in the sense that they lie in between various classical orthogonal transforms.

1.2 Previous Work on The Naturalness-Preserving Transforms

Recently, Hershey et al [3] suggested the possibility of defining linear combinations of weighted classical orthogonal matrices as transforms. Imposing the constraint that one of the matrices in the linear combination be the identity matrix,

*The approximation is brought about by processing operations that are performed on the transformed data.

they referred to the resulting transforms as The Naturalness-Preserving Transforms.

They considered the special case of a linear combination of the weighted identity matrix and the weighted Hadamard transform, and this was proposed for tactical imagery transmission. The problem of jamming or the excision of segments of two-dimensional Hadamard NPT transformed imagery by the opposition in the course of transmission, was considered. A so-called man-in-the-loop error correction procedure for reconstructing an approximate version of the original imagery data, was presented. However, their solution has the drawback of assuming the knowledge of flat pixel regions within the original image. Such an assumption is invalid for highly active images, images with a complicated texture and time-varying one-dimensional signals. Their algorithm also require a degree of operator intervention and no clear guideline was given for choosing the transform basis (or bases) that can be employed.

In chapter two of this thesis, we introduce a parametric family of Naturalness-Preserving Transforms. Admissible NPT transforms for signal processing applications are defined.

In chapter six, we examine the tactical imagery reconstruction problem in detail. A self-terminating iterative algorithm which does not require an apriori knowledge of the pixel values within the original image, is reported. A clear guideline on the choice of Hadamard NPT basis that can be employed for tactical imagery transmission is given. The problem of bandwidth limitations and channel error effects on the quality of reconstructed imagery data, are considered in chapter seven.

1.3 Scope of Thesis

The objectives of this thesis are to develop admissible NPT transforms for digital signal processing, investigate NPT properties and digital signal processing applications of NPT transforms. Accordingly, admissible NPT transforms are determined. Some useful NPT properties in addition to those reported in [3] have been developed. A number of digital signal processing application areas have been considered. These include data compression, signal reconstruction, packetized imagery transmission, tactical imagery transmission and generalized Wiener filtering.

Conventional transform coding of images, using the NPT transforms, is investigated. Block-classification basis adaptive transform coding systems are developed. Hybrid* image coding systems employing the NPT transforms, have also been developed. The work has been mainly concerned with intraframe coding of images. Algorithms for selecting the optimum basis (in the mean-square error sense) for coding a given image or image ensemble are introduced. A noiseless channel has been assumed although some results which demonstrate the effect of channel errors, based on a binary symmetric channel model, are presented. A rate-distortion theoretic analysis for NPT image coders have been presented. The emphasis is on ascertaining the minimum rate necessary to achieve a desired level of total distortion in the reconstructed image, when a specified NPT basis is used for coding a given image.

The transmission of signals through channels whose quality and characteristics are unpredictable due to non-stationary noise processes or jamming is considered in the thesis. The application of one-dimensional and two-dimensional Hadamard NPT in this scenario have been developed. The associated problem of determining the reliable transform segments that can be used for reconstruction is not within the scope of the investigation. The one-dimensional Hadamard NPT reconstruction algorithm has been applied to first order Gauss-Markov signals and speech signals. An intraframe two-layer packet transmission system, which is based on the one-dimensional Hadamard NPT reconstruction technique, has been proposed. One-dimensional Hadamard NPT reconstruction intraframe two-layer packet transmission of images over low bandwidth channels has also been investigated in the thesis. The effect of channel errors has also been considered.

Two-dimensional Hadamard NPT tactical imagery transmission has been investigated. The effect of data compression on the quality of the reconstructed imagery data is considered. The effect of channel errors is also examined in the thesis.

Generalized Wiener filtering using the NPT transforms is developed. Suboptimum NPT generalized Wiener filtering is also investigated in the thesis. The work has concentrated on one-dimensional signals. An approach to one-dimensional NPT generalized Wiener filter design which is slightly different from classical design techniques is also presented in the thesis.

* The word hybrid has been used in two contexts in the thesis: we have used it to describe a class of transforms in chapter two while we have used it to refer to an image coding technique in chapters three and seven.

1.4 Outline of Thesis

The thesis is organized into four parts. Part I is concerned with the development of the NPT transforms and their applications in image data compression. Chapter two defines hybrid transforms and considers the more general problem of determining admissible hybrid transforms for signal processing applications. Criteria governing admissible hybrid transforms are specified. Two theorems which define admissible hybrid transforms comprising a linear combination of two classical orthogonal matrices are derived. The NPT transforms are shown to be a sub-class of admissible hybrid transforms. Properties of the NPT transforms are developed. The NPT domain of typical imagery data is investigated empirically.

The development of image data compression schemes which are based on the NPT transforms is the subject of chapter three. A review of image data compression techniques is first given. NPT transform coding of images is then investigated within the context of conventional transform coding techniques, in part A of the chapter. The NPT is characterized by an infinite number of possible bases that can be used for coding a given image or image ensemble. The objective of an NPT image coder is to employ the basis or collection of bases giving minimum mean-square error (MSE) for coding a given image or image ensemble. Consequently, an algorithm for determining the optimum basis for pure two-dimensional NPT coding of a given image or image ensemble is developed. Empirical results of non-adaptive NPT coding of monochrome images are presented. Subsequently, a block-classification basis adaptive NPT image coder which features transform basis adaptation according to local image content in addition to conventional adaptation techniques (adaptive bit allocation/quantization) is proposed. The effect of channel errors on the subjective quality of the reconstructed pictures is also examined. Empirical results of basis adaptive NPT coding of monochrome images are presented. NPT hybrid image coding techniques are developed in part B of the chapter. The algorithm for determining the optimum basis for the hybrid coding of a given image or image sub-array is introduced. Empirical results of NPT hybrid coding of monochrome images are presented.

In chapter four, a rate-distortion theoretic framework for NPT image coders is presented. A Gaussian rate-distortion function which is effectively an upper bound for the minimum information rate required for coding image data with known second order statistics, using NPT based image coders, is derived. The bounds are

evaluated empirically and the theoretical results are compared with some of the practical compression levels of some of the algorithms of chapter three, using first order stationary Gauss-Markov images.

Iterative Hadamard NPT reconstruction of signals degraded by non-stationary noise processes or jamming is the subject of part II of the thesis. The reconstruction problem arises in applications where segments of a one-dimensional or two-dimensional signal could be rendered unuseable in the course of transmission. Chapter five deals with iterative one-dimensional Hadamard NPT reconstruction of signals. An iterative one-dimensional Hadamard NPT reconstruction algorithm is introduced. Closed-form solutions for the reconstructed signals from some examples of iterative one-dimensional Hadamard NPT reconstruction formats are presented. A clear guideline on the NPT basis that can be used for reconstruction is given. Empirical results of the reconstruction of first order Gauss-Markov signals and speech signals are presented. The application of one-dimensional Hadamard NPT reconstruction techniques to intraframe two-layer packet transmission of images is proposed. Pictorial results corresponding to fifty percent packet loss are presented.

Chapter six deals with two-dimensional Hadamard NPT reconstruction of signals. The work is basically an extension of the work of chapter five, to two dimensions. Closed-form expressions for reconstructed signals from some two-dimensional Hadamard NPT reconstruction formats are derived. A clear guideline on the Hadamard NPT basis parameter that can be used for reconstruction is given. A tactical imagery transmission application is considered. Empirical results of the reconstruction of imagery data are presented.

A variety of additional investigations on one-dimensional and two-dimensional Hadamard NPT reconstruction applications are reported in chapter seven. The performance of the one-dimensional Hadamard NPT reconstruction intraframe two-layer packet image transmission system, when used for the transmission of images over low bandwidth channels is investigated. Hybrid coding techniques as well as VQ (Vector Quantization) techniques are investigated for coding the transform samples to be transmitted as guaranteed packets. The transmission of additional information as enhancement packets, to improve the quality of reconstructed images, is considered. The effect of channel errors on the reconstructed image quality is separately studied for guaranteed and enhancement packets. For two-dimensional Hadamard

NPT tactical imagery transmission, VQ technique is investigated for coding the transform samples, at low bit rates. The effect of channel errors on the quality of reconstructed images is investigated. Hybrid image coding algorithms which are based on one-dimensional Hadamard NPT reconstruction, are developed.

Part III is concerned with transform domain generalized Wiener filtering. In chapter eight, one-dimensional NPT generalized Wiener filtering is developed. Sub-optimum NPT generalized Wiener filtering is investigated. The problem of determining the basis giving minimum MSE of filtering a noisy signal is considered. A new approach to NPT generalized Wiener filter design which is different from the classical design methods is introduced. Empirical results of filtering first order stationary Gauss-Markov signals corrupted by additive white noise are presented. The conclusions and suggestions for further work are presented in chapter nine, part IV.

Appendix I contains the derivation of the Hybrid Transform Inversion Theorems.

Appendix II contains the proof of convergence of the iterative one-dimensional Hadamard NPT reconstruction algorithm.

Appendix III contains the proof of convergence of the iterative two-dimensional Hadamard NPT reconstruction algorithm.

Appendix IV contains the derivation of equation (6.42); the material was extracted from chapter six to permit its easier reading.

Appendix V contains the derivation of some results used in NPT generalized Wiener filter design.

The simulations for this research were conducted mainly on the VAX 11/780 computer belonging to the Imperial College Centre for Remote Sensing Image Processing Laboratory. It should be noted that throughout the thesis, the comments made about processed images were those observed on the CRT display.
The pixel values in the pictures presented throughout the thesis were clipped to between 0 and 255.

PART I
THE NATURALNESS - PRESERVING TRANSFORM AND IMAGE DATA COMPRESION

CHAPTER TWO

THE NATURALNESS-PRESERVING TRANSFORM AND SOME DEVELOPMENTS FOR THE TRANSFORM

2.1 Introduction

The Naturalness-Preserving Transforms, which we investigate for their digital signal processing applications, are introduced and developed in this chapter. The transforms are a particular case of a general class of hybrid transforms [3].

Hybrid transforms are defined in section 2.2. The general transform operator is introduced. Section 2.3 discusses hybrid transform sub-classes and specifies criteria governing admissible hybrid transforms for signal processing applications. The problem of determining admissible hybrid transforms, based on the specified criteria, is addressed. This is shown to be equivalent to determining functional relationships for the inverse of a linear combination of fast orthogonal transforms subject to the constraint that the respective inverse transforms have fast algorithmic implementation.

Two theorems which define admissible hybrid transforms comprising a linear combination of two orthogonal matrices are derived in section 2.3.2 ; subsequently, a sub-class of the Naturalness-Preserving Transforms (NPT) are introduced in section 2.3.3. A series representation of this NPT sub-class is developed. Properties of the NPT are explored, some of which are confirmed empirically. An alternative form of the NPT is defined. An interesting property of this alternative NPT is highlighted.

Finally, clipped magnitude displays of one-dimensional and two-dimensional NPT of typical imagery data are presented in section 2.3.5. These confirm the contention made in section 2.3.3 that upon transforming imagery data with certain NPT bases, the image would still be visually comprehensible in the transform domain.

2.2 Hybrid Transforms

The hybrid transforms are linear combinations of orthogonal matrices. The general hybrid transform operator is denoted by $\psi\{\underline{\alpha}\}$, where $\underline{\alpha}$ is a vector of l components [3]. The operator $\psi\{\underline{\alpha}\}$ is defined as

$$\psi\{\underline{\alpha}\} = \sum_{i=1}^{l} \alpha_i \mathbf{A}_i \; ; \qquad l = 2, 3, \ldots, m \tag{2.1a}$$

where each $\mathbf{A}_i$ in (2.1a) is an orthogonal matrix, i.e. the $\mathbf{A}_i$ satisfy

$$\mathbf{A}_i \mathbf{A}_i{}^T = \mathbf{I} \tag{2.1b}$$

where $\mathbf{I}$ is the identity matrix, and α_i is constrained by

$$\sum_{i=1}^{l} \alpha_i = 1. \tag{2.1c}$$

We denote the inverse hybrid transform operator by $\psi^{-1}\{\underline{\alpha}\}$.

The one-dimensional hybrid transform of an N-length data vector

$$\mathbf{f} = [f_1 \quad f_2 \quad \ldots \quad f_N]^T \tag{2.2}$$

is given by

$$\mathbf{t_f} = \psi\{\underline{\alpha}\}\mathbf{f} \tag{2.3}$$

The two-dimensional hybrid transform of an $N \times N$ data matrix

$$\mathbf{F} = \begin{bmatrix} f_{11} & f_{12} & f_{13} & \cdots & f_{1N} \\ f_{21} & f_{22} & f_{23} & \cdots & f_{2N} \\ \vdots & \vdots & \vdots & \ddots & \vdots \\ f_{N1} & f_{N2} & f_{N3} & \cdots & f_{NN} \end{bmatrix} \tag{2.4}$$

is given by

$$\mathbf{T_F} = \psi\{\underline{\alpha}\}\,\mathbf{F}\psi\{\underline{\alpha}\} \tag{2.5}$$

2.3 Hybrid Transform Sub-classes

The hybrid transform operator $\psi\{\underline{\alpha}\}$ given by (2.1a) is very general and there are a variety of hybrid transform kernels resulting from possible linear combinations of orthogonal matrices. It is therefore necessary to determine hybrid transform kernels that would be useful for signal processing applications.

The choice of transforms for signal processing applications have been partly governed by the requirement that the transform be invertible. In addition , both the forward and inverse transforms should have fast computation algorithms, i.e. the transform of an N-length data sequence should be computable in the order of $Nlog_2N$ operations.

Orthogonal transforms having fast computation algorithms have been well documented in the literature [1,2,4,5] and have been widely used in signal processing applications. As an initial criterion, we limit hybrid transform kernels to those resulting from linear combinations of fast orthogonal transforms. The hybrid transform of a data sequence thus becomes a linear combination of fast orthogonal transforms of the data sequence. Additionally, we specify the criterion that the inverse hybrid transform should be definable functionally. The latter criterion is important from two standpoints. Firstly, if $\psi^{-1}\{\underline{\alpha}\}$ is not known functionally, its determination would have to be carried out numerically leading to additional computational cost. Secondly, if $\psi^{-1}\{\underline{\alpha}\}$ were unknown functionally, a fast algorithm may either not exist or it may only exist for certain transform orders. This would lead to increased computational cost in the former case and limit the usefulness of the transform in the latter case.

Based on the two criteria stated above, the problem of determining admissible hybrid transform sub-classes for signal processing applications is stated formally in the following sub-section.

2.3.1 Statement of The Problem of Determining Admissible Hybrid Transform Sub-classes

The problem of determining admissible hybrid transform kernels can be stated thus : Given the set $\mathbf{A} = \{\mathbf{A}_1, \mathbf{A}_2, \ldots, \mathbf{A}_m\}$ of fast orthogonal transforms and the vector of weighting parameters $\underline{\alpha} = [\alpha_1 \quad \alpha_2 \quad \ldots \quad \alpha_m]^T$, admissible linear combinations out of the ensemble $\Psi = \{\psi_1\{\underline{\alpha}_1\}, \psi_2\{\underline{\alpha}_2\}, \ldots \psi_\theta\{\underline{\alpha}_q\} \quad ; q \leq m\}$ of every possible linear combination of the members of $\mathbf{A}$, which are generated from (2.1a), are to be determined. From the criteria introduced in the previous sub-section, this problem is equivalent to that of determining the subset $\Psi' \subset \Psi$ of kernels for which there exists a functionally defined inverse transform with a fast algorithmic implementation, for each member of Ψ'.

2.3.2 Inversion of Hybrid Transforms

The problem of determining admissible hybrid transform kernels is solved by finding closed form analytic expressions for the inverse transforms of linear combinations of orthogonal transforms. Specifically, we seek to determine functional expressions for the inverse of the matrices

$$\psi\{\underline{\alpha}\} = \alpha_1\mathbf{A}_1 + \alpha_2\mathbf{A}_2 + \cdots + \alpha_l\mathbf{A}_l \; ; \quad l = 2, \ldots m \tag{2.6}$$

subject to the constraint that the respective inverse transform kernels, $\psi^{-1}\{\underline{\alpha}\}$, should have a fast algorithmic implementation. The solution of this problem is complicated by the fact that the inverse of the sum of two or more non-singular matrices is generally not known trivially as a function of the inverses of the matrices making up the sum [6]. Consequently, there is no established mathematical procedure available for solving this problem.

The approach that we adopt entails specifying apriori suitable functional expressions for the inverse transform, $\psi^{-1}\{\underline{\alpha}\}$, of the linear combinations of interest and solving for the unknowns in the expression such that

$$\psi^{-1}\{\underline{\alpha}\}\,\psi\{\underline{\alpha}\} = \mathbf{I} \tag{2.7}$$

is satisfied. As an example, for the transform

$$\psi\{\underline{\alpha}\} = \alpha_1\mathbf{A}_1 + \alpha_2\mathbf{A}_2 \tag{2.8a}$$

we consider

$$\psi^{-1}\{\underline{\alpha}\} = \psi\{\underline{\beta}\} = \beta_1\mathbf{B}_1 + \beta_2\mathbf{B}_2 \tag{2.8b}$$

as the inverse transform ; we then solve for the unknown parameters β_1 and β_2, and the matrices $\mathbf{B}_1$ and $\mathbf{B}_2$ satisfying (2.7).

Based on this approach, we derive two theorems which define a family of hybrid transforms comprising a linear combination of two orthogonal matrices. The first theorem [35] defines functionally, the inverse of a linear combination of two commuting involutory [6,pp 11] matrices, while the second theorem gives the functional definition for the inverse of a linear combination of two anti-commuting [6, pp 11] involutory matrices. These are stated in the following sub-section.

2.3.2.1 Hybrid Transform Inversion Theorems

2.3.2.1.1 THEOREM 1 : *The Inverse of a Linear Combination of Two Commuting Involutory Matrices*

We define

$$\psi\{\alpha\} = k_1(\alpha)\mathbf{A}_1 + k_2(\alpha)\mathbf{A}_2 \tag{2.9a}$$

then the inverse of (2.9a) *is*

$$\psi^{-1}\{\alpha\} = \frac{1}{k_1^2(\alpha) - k_2^2(\alpha)}[k_1(\alpha)\mathbf{A}_1 - k_2(\alpha)\mathbf{A}_2]\,; \quad k_1^2(\alpha) - k_2^2(\alpha) \neq 0 \tag{2.9b}$$

iff $\mathbf{A}_1$ *and* $\mathbf{A}_2$ *are commuting involutory matrices, where the* $k_i(\alpha)$ *are weighting functions dependent on the parameter* α.

The proof follows by establishing that

$$\psi^{-1}\{\alpha\}\,\psi\{\alpha\} = \mathbf{I} \tag{2.10}$$

under the stated conditions and is given in appendix I.

2.3.2.1.2 THEOREM 2 : *The Inverse of A Linear Combination of Two Anti-Commuting Involutory Matrices*

For the hybrid transform $\psi\{\alpha\}$ *, defined by* (2.9a)*, the inverse transform is*

$$\psi^{-1}\{\alpha\} = \frac{1}{k_1^2(\alpha) + k_2^2(\alpha)}[k_1(\alpha)\mathbf{A}_1 + k_2(\alpha)\mathbf{A}_2]\,; \quad k_1^2(\alpha) + k_2^2(\alpha) \neq 0 \tag{2.11}$$

iff $\mathbf{A}_1$*and* $\mathbf{A}_2$ *are anti-commuting involutory matrices, where the* $k_i(\alpha)$ *are as previously defined.*

This theorem can also be proved by establishing that (2.10) holds under the stated conditions and the proof is given in appendix I.

2.3.2.2 Results and Discussion of Theorems

The Hybrid Transform Inversion Theorems define functionally, the inverse of the weighted sum of two commuting (anti-commuting) involutory matrices. For the interesting case of the matrices $\mathbf{A}_1$ and $\mathbf{A}_2$ being fast orthogonal transforms, the theorems define admissible hybrid transforms comprising a linear combination of two commuting (anti-commuting) symmetric fast orthogonal transforms. Furthermore, they leave the choice of the weighting functions $k_i(\alpha)$ open to the

transform designer. For example they could be chosen to be either linear, logarithmic, exponential or other suitable functions of α. In addition, the theorems emphasize the fact that the $k_i(\alpha)$ need not necessarily satisfy the constraint of (2.1*c*).

For linear combinations of $l \geq 3$ orthogonal matrices, it has not been possible to find a simple functional expression for the inverse transform. Even if this were possible, the practical significance of the resulting transforms is not immediately obvious. Furthermore, since the hybrid transforms are computed via the fast algorithm of their component transforms, the computational load increases as the number, l, of orthogonal matrices in the linear combination increases. Consequently, we shall be concerned with hybrid transforms comprising a linear combination of $l = 2$ orthogonal matrices and by virtue of the result of the Hybrid Transform Inversion Theorems, we focus on symmetric orthogonal transforms.

Symmetric orthogonal transforms include the Hadamard transform [1,8,9], the sine transform [4,10], the symmetric cosine transform (SCT) [11] and certain members of the sinusoidal family of unitary transforms documented in [4].

An empirical investigation of commuting or anti-commuting classical orthogonal transforms was conducted but none were found. The investigation procedure entailed checking for whether the matrix products **AB** and **BA** are equal or not , where **A** and **B** are classical fast orthogonal transforms.

2.3.3 The Naturalness-Preserving Transforms

An interesting sub-class of hybrid transforms is obtained by requiring that one of the orthogonal matrices $\mathbf{A}_i$ in (2.1*a*) be the identity matrix. In this case, proper specification of the weighting parameters guarantees the preservation of a fraction of the signal in the transform domain. For an optical signal, such as an image, if the weighting parameter α_i corresponding to the identity matrix is large compared to the remaining weighting parameters, the image would be visually comprehensible in the transform domain. Hence this class of hybrid transforms are referred to as the *Naturalness-Preserving Transforms* (NPT).

By forming linear combinations of orthogonal matrices and an identity matrix, a variety of NPT transforms would be obtained. However, based on the criteria specified earlier for admissible hybrid transforms, useful NPT transforms are restricted to those derived from a linear combination of fast orthogonal transforms

and the identity matrix, and for which the inverse NPT transform is functionally defined in terms of fast transforms.

2.3.3.1 A Naturalness-Preserving Transform Sub-class

Since the identity matrix commutes with every matrix, the hybrid transform inversion theorem for commuting involutory matrices stated in section 2.3.2.1 defines a family of NPT transforms comprising a linear combination of the identity matrix and symmetric orthogonal transforms.

Thus we set $\mathbf{A}_1 = \mathbf{I}$ and $\mathbf{A}_2 = \mathbf{A}$ in (2.9a-2.9b) and define the weighting functions

$$k_1(\alpha) = \alpha \tag{2.12}$$

$$k_2(\alpha) = k(1-\alpha) \tag{2.13}$$

where α is a real valued parameter and k is an additional transform parameter whose significance will be made clear . The forward NPT transform for this choice of weighting functions is given by

$$\psi\{\alpha\} = \alpha I + k(1-\alpha)\mathbf{A} \tag{2.14a}$$

and by virtue of theorem 1, the inverse transform is

$$\psi^{-1}\{\alpha\} = \frac{1}{\alpha^2 - k^2(1-\alpha)^2}\left[\alpha I - k(1-\alpha)\mathbf{A}\right]; \quad \alpha^2 - k^2(1-\alpha)^2 \neq 0 \tag{2.14b}$$

where $\mathbf{A}$ is a symmetric fast orthogonal transform. The inverse NPT transform given by (2.14b) does not exist for

$$\alpha = \frac{k}{1 \pm k} \tag{2.15}$$

Thus, the parameter k determines the singularities of $\psi^{-1}\{\alpha\}$ and can be chosen to set the singularities of $\psi^{-1}\{\alpha\}$ at desired points on the real line; the singularities of $\psi^{-1}\{\alpha\}$, $\alpha_1 = \frac{k}{(1+k)}$ and $\alpha_2 = \frac{k}{(1-k)}$ are shown plotted in Fig. 2.1a over the range $-10 \leq k \leq 10$ and in Fig. 2.1b over the range $-0.5 \leq k \leq 0.5$. We observe that except for $k = 0$, there are two singularities corresponding to each choice of the parameter k. The choice $k = 0$ corresponds to having a weighted identity matrix and (2.15) gives $\alpha = 0$ as the singularity, meaning that a null transformation matrix would have to be specified, for the inverse transform not to exist. In the limit as $k \to \pm\infty$, $\alpha_1 \to 1$ and $\alpha_2 \to -1$.

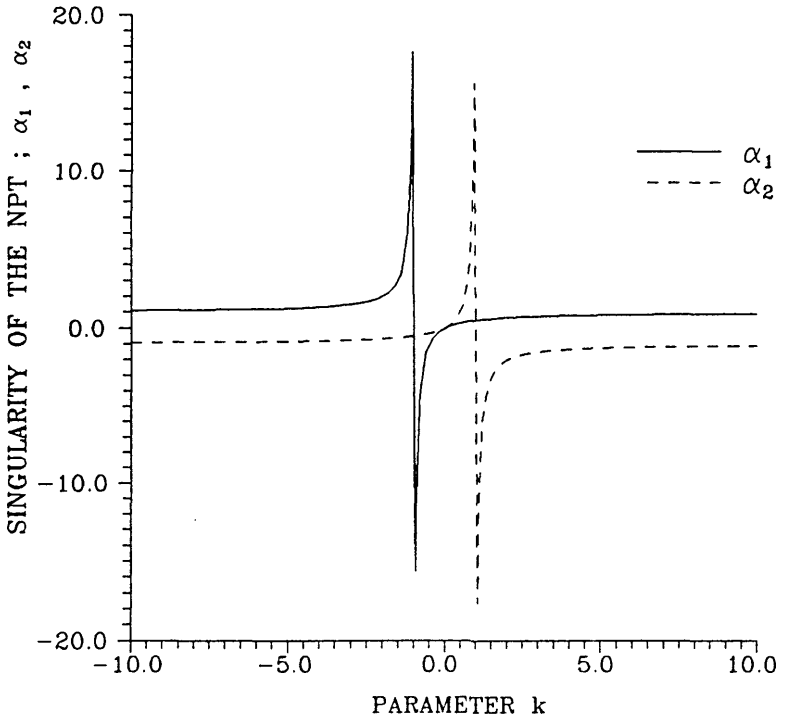


Fig. 2.1a : Singularities of the NPT as a function of the parameter k, $-10 \leq k \leq 10$.

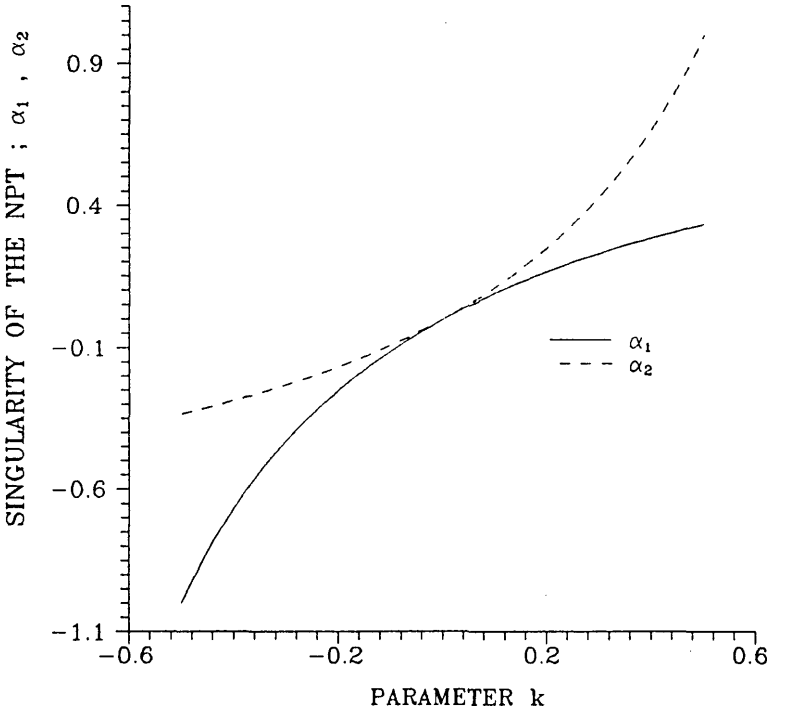


Fig. 2.1b : Singularities of the NPT as a function of the parameter k, $-0.5 \leq k \leq 0.5$.

The one-dimensional NPT of a data vector $\mathbf{f}$, is given by

$$\mathbf{t_f} = \psi\{\alpha\}\mathbf{f} \tag{2.16a}$$

$$= \alpha\mathbf{f} + k(1-\alpha)\mathbf{Af} \tag{2.16b}$$

while the two-dimensional NPT of an $N \times N$ data array ,$\mathbf{F}$, is given by

$$\mathbf{T_F} = \psi\{\alpha\}\,\mathbf{F}\psi\{\alpha\} \tag{2.17a}$$

$$= \alpha^2\mathbf{F} + k\alpha(1-\alpha)[\mathbf{FA} + \mathbf{AF}] + k^2(1-\alpha)^2\mathbf{AFA} \tag{2.17b}$$

Theoretically, the NPT transforms, (2.14a-2.14b), are defined for $-\infty < \alpha < \infty$ except at the singular points given by (2.15), which are determined by the parameter k. In addition, the parameter k can assume values over $[-\infty, \infty]$, excluding the extreme points of the interval. However, in order to permit a ready qualitative appraisal of the NPT domain of a transformed signal, we set $k = 1$ and restrict α to the range $[-1, 1)$. Thus, when $\alpha = 0.6$ for example, we are retaining 60 percent (36 percent) of the signal amplitude in the transform domain, for a one-dimensional (two-dimensional) NPT. The singularities of this NPT sub-class for $k = 1$ are at $\alpha_1 = 0.5$ and $\alpha_2 = \infty$

Discussion

An implication of the hybrid transform inversion theorem of section 2.3.2.1.1 is that the NPT transforms comprising a linear combination of the identity matrix and some classical orthogonal transforms such as the discrete cosine transform [15], Fourier transform [1,5], slant transform [16], Haar transform [1], high and low correlation transforms [17], are not admissible NPT transforms. However, for symmetric orthogonal transforms such as the Hadamard transform [1,8,9], the sine transform [4,10] and the symmetric cosine transform (SCT) [11], NPT transforms are defined and these shall be referred to as the Hadamard NPT, sine NPT and symmetric cosine NPT (SC NPT) respectively ; other symmetric orthogonal transforms can be found in [4].

Notation Adopted for Distinguishing Between The Various NPT Bases

For easy reference to the respective NPT transform bases, we shall adopt the following notation throughout this thesis. We shall, as an example, refer to the Hadamard NPT transform basis corresponding to $\alpha = \alpha_1$ as Hadamard NPT(α_1). Thus, the terms Hadamard NPT(0.2), sine NPT(0.8) and SC NPT(0.4) respectively

denote the Hadamard NPT transform corresponding to $\alpha = 0.2$, the sine NPT transform corresponding to $\alpha = 0.8$ and the symmetric cosine (SC) NPT transform corresponding to $\alpha = 0.4$.

2.3.3.1.1 Series Representation of The NPT

In this section, we develop series representations for the one-dimensional NPT of an $N \times 1$ data vector expressed in vector form by (2.16*b*) and the two-dimensional NPT of an $N \times N$ data array which is expressed in matrix form by (2.17*b*).

Series Representation of The One-Dimensional NPT of A Data Vector

We represent the data vector by $\mathbf{f}(x)$, $x = 0, 1, \ldots, N-1$ and denote the NPT kernel by $g(x,u)$, $x,u = 0, 1, \ldots, N-1$. Using (2.14*a*), we can express the NPT kernel as

$$g(x,u) = \alpha\delta_{x,u} + k(1-\alpha)a(x,u) \qquad ;x,u = 0,1,\ldots,N-1 \tag{2.18}$$

where $\delta_{x,u}$ is the kronecker delta function given by

$$\delta_{x,u} = \begin{cases} 1 & x = u \\ 0 & x \neq u \end{cases} \tag{2.19}$$

and $a(x,u)$ are the normalized basis elements of the symmetric orthogonal transform **A**.

The one-dimensional forward NPT of the data vector, using (2.16*a*) and (2.18) is thus given in series form by

$$\mathbf{t_f}(u) = \sum_{x=0}^{N-1} \alpha\delta_{x,u}\mathbf{f}(x) + \sum_{x=0}^{N-1} k(1-\alpha)a(x,u)\mathbf{f}(x) \tag{2.20}$$

for $u = 0, 1, \ldots, N-1$.

Theorem 1 permits the inverse one-dimensional NPT to be expressed in the series form

$$\mathbf{f}(x) = \frac{1}{\alpha^2 - k^2(1-\alpha)^2}\left[\sum_{u=0}^{N-1} \alpha\delta_{x,u}\mathbf{t_f}(u) - \sum_{u=0}^{N-1} k(1-\alpha)a(x,u)\mathbf{t_f}(u)\right] \tag{2.21}$$

for $x = 0, 1 \ldots, N-1$.

Series Representation of The Two-Dimensional NPT of A Data Array

The data array is represented by $\mathbf{F}(x,y)$, $x,y = 0, 1, \ldots, N-1$ and we denote the forward two-dimensional NPT kernel by $g(x,y;u,v)$, $0 \leq x,y,u,v \leq N-1$.

The two-dimensional forward NPT of the data array $\mathbf{F}(x,y)$ is given by

$$\mathbf{T_F}(u,v) = \sum_{x=0}^{N-1}\sum_{y=0}^{N-1} \mathbf{F}(x,y)g(x,y;u,v) \tag{2.22}$$

for $u,v = 0,1,\ldots,N-1$.

The two-dimensional inverse NPT of (2.22) is similarly given by

$$\mathbf{F}(x,y) = \sum_{u=0}^{N-1}\sum_{v=0}^{N-1} \mathbf{T_F}(u,v)h(x,y;u,v) \tag{2.23}$$

for $x,y = 0,1,\ldots,N-1$ where $h(x,y;u,v)$, $0 \le x,y,u,v \le N-1$ denotes the inverse two-dimensional NPT kernel. The notation for the indices $x,y;u,v$ for the domains $\mathbf{F}(x,y)$ and $\mathbf{T_F}$ is shown in Fig. 2.2

Since the NPT kernel is separable, we can write

$$g(x,y;u,v) = g_R(y,v)g_C(x,u) \tag{2.24a}$$

where $g_R(y,v)$ and $g_C(x,u)$ are row and column transform kernels respectively, given by

$$g_R(y,v) = \alpha\delta_{y,v} + k(1-\alpha)a_R(y,v) \tag{2.24b}$$

for $y,v = 0,1,\ldots,N-1$ and

$$g_C(x,u) = \alpha\delta_{x,u} + k(1-\alpha)a_C(x,u) \tag{2.24c}$$

for $x,u = 0,1,\ldots,N-1$ where $a_R(y,v)$ and $a_C(x,u)$ are respectively the kernels of the normalized row and column symmetric orthogonal transform $\mathbf{A}$; $\delta_{x,u}$ and $\delta_{y,v}$ are kronecker delta functions defined by (2.19).

The two-dimensional NPT of $\mathbf{F}(x,y)$ is obtained by first taking a one-dimensional NPT along the rows of $\mathbf{F}(x,y)$ to give

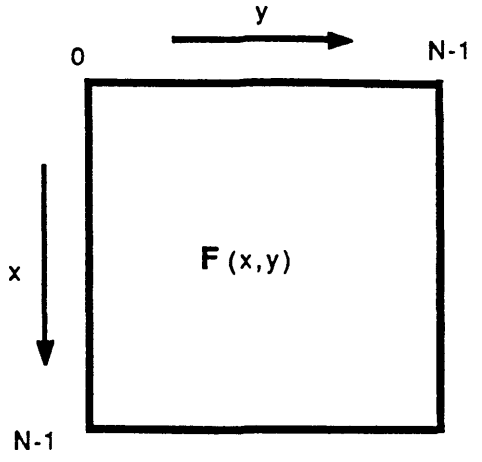
$$\mathbf{T_F}(x,v) = \sum_{y=0}^{N-1} \mathbf{F}(x,y)g_R(y,v) \tag{2.25}$$

$$= \sum_{y=0}^{N-1} \alpha\delta_{y,v}\mathbf{F}(x,y) + \sum_{y=0}^{N-1} k(1-\alpha)a_R(y,v)\mathbf{F}(x,y) \tag{2.26}$$

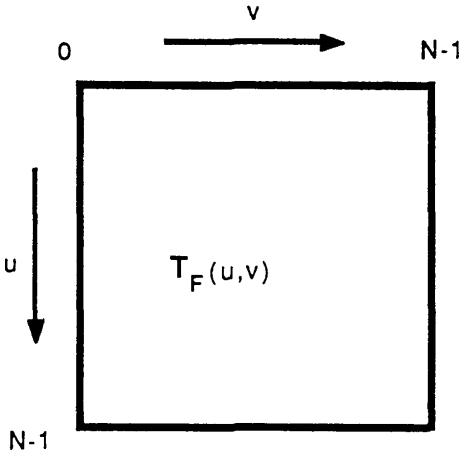
for $x,v = 0,1,\ldots,N-1$ and then performing a one-dimensional NPT along the column of $\mathbf{T_F}(x,v)$ to give

$$\mathbf{T_F}(u,v) = \sum_{x=0}^{N-1} \mathbf{T_F}(x,v)g_C(x,u) \tag{2.27}$$

$$= \sum_{x=0}^{N-1} \alpha\delta_{x,u}\mathbf{T_F}(x,v) + \sum_{x=0}^{N-1} k(1-\alpha)a_C(x,u)\mathbf{T_F}(x,v) \tag{2.28}$$



(a)



(b)

Fig. 2.2 : Notation For The Indices x,y;u,v of The Domains **F** (x,y) and $\mathbf{T_F}$(u,v) ; (a) Data Domain **F**(x,y), (b) Transform Domain $\mathbf{T_F}$ (u,v).

for $u, v = 0, 1, \ldots, N-1$. Substituting (2.26) in (2.28), we obtain

$$\begin{aligned}\mathbf{T_F}(u,v) = &\sum_{x=0}^{N-1}\sum_{y=0}^{N-1} \alpha^2 \delta_{x,u}\delta_{y,v}\mathbf{F}(x,y) \\ &+ \sum_{x=0}^{N-1}\sum_{y=0}^{N-1} \alpha k(1-\alpha)\delta_{x,u}a_R(y,v)\mathbf{F}(x,y) \\ &+ \sum_{x=0}^{N-1}\sum_{y=0}^{N-1} \alpha k(1-\alpha)\delta_{y,v}a_C(x,u)\mathbf{F}(x,y) \\ &+ \sum_{x=0}^{N-1}\sum_{y=0}^{N-1} k^2(1-\alpha)^2 a_R(y,v)a_C(x,u)\mathbf{F}(x,y) \end{aligned} \tag{2.29}$$

for $u, v = 0, 1, \ldots, N-1$, which is the desired series representation. It expresses each point of the transform domain $\mathbf{T_F}(u,v)$ as resulting from the summation of four separate discrete transformations of the data array $\mathbf{F}(x,y)$.

Using theorem 1, the inverse two-dimensional NPT of (2.29) is given in series form by

$$\begin{aligned}\mathbf{F}(x,y) = \frac{1}{\left(\alpha^2 - k^2(1-\alpha^2)\right)^2}\Bigg[&\sum_{u=0}^{N-1}\sum_{v=0}^{N-1} \alpha^2 \delta_{x,u}\delta_{y,v}\mathbf{T_F}(u,v) \\ &- \sum_{u=0}^{N-1}\sum_{v=0}^{N-1} \alpha k(1-\alpha)\delta_{x,u}a_R(y,v)\mathbf{T_F}(u,v) \\ &- \sum_{u=0}^{N-1}\sum_{v=0}^{N-1} \alpha k(1-\alpha)\delta_{y,v}a_C(x,u)\mathbf{T_F}(u,v) \\ &+ \sum_{u=0}^{N-1}\sum_{v=0}^{N-1} k^2(1-\alpha)^2 a_R(y,v)a_C(x,u)\mathbf{T_F}(u,v)\Bigg] \end{aligned} \tag{2.30}$$

for $x, y = 0, 1, \ldots, N-1$.

2.3.3.1.2 Properties of The NPT

(1) Euclidean Norm of The NPT of A Data Sequence

It is an established fact that a linear transformation preserves measure, which includes preservation of the Euclidean norm of a real vector (matrix), if and only if its transformation matrix is orthogonal [6,pp 104]. The general hybrid transform defined by (2.1*a*) is not orthogonal and consequently does not preserve measure. Here, we investigate the effect of the NPT on the energy and length of a data sequence.

An indication of how a transform would affect the energy and length of a data sequence can be obtained from the Euclidean norm of the transformation. The Euclidean norm of an $N \times N$ square matrix $\mathbf{A}$, is by definition

$$\|\mathbf{A}\| = \left[\sum_{i,j} (a_{i,j})^2\right]^{1/2} \tag{2.31}$$

The Euclidean norm is a true norm [12] and satisfies the triangle inequality

$$\|\mathbf{A}_1 + \mathbf{A}_2\| \leq \|\mathbf{A}_1\| + \|\mathbf{A}_2\| \tag{2.32}$$

The Euclidean norm of an $N \times N$ measure-preserving transformation matrix equals $\sqrt{N}$; on the other hand, an $N \times N$ Euclidean norm decreasing (increasing) transformation matrix has an Euclidean norm less than (greater than) $\sqrt{N}$.

First, we consider the Euclidean norm of the data resulting from the application of the general hybrid transform, (2.1*a*), to a data array $\mathbf{F}$. From (2.1*a*), (2.5) and (2.31 – 2.32), it follows that

$$\begin{aligned} \|\psi\{\underline{\alpha}\}\,\mathbf{F}\psi\{\underline{\alpha}\}\| &= \|\sum_{i}^{l}\sum_{j}^{l} \alpha_i\alpha_j \mathbf{A}_i\mathbf{F}\mathbf{A}_j\| \\ &\leq \|\mathbf{F}\|\sum_{i}^{l}\sum_{j}^{l} \alpha_i\alpha_j \end{aligned} \tag{2.33}$$

where we have used the fact that the $\mathbf{A}_i$ are orthogonal. Applying the constraint (2.1*c*), we observe that

$$\|\psi\{\underline{\alpha}\}\,\mathbf{F}\psi\{\underline{\alpha}\}\| \leq \|\mathbf{F}\| \tag{2.34}$$

implying that the Euclidean norm of (2.5) is upperbounded by the Euclidean norm of $\mathbf{F}$. In other words, the energy of the transformed data is upperbounded by the energy in the original data. For the NPT sub-class defined by (2.14), (2.33) gives

$$\|\psi\{\underline{\alpha}\}\,\mathbf{F}\psi\{\underline{\alpha}\}\| \leq \|\mathbf{F}\|\,[\alpha + k(1-\alpha)]^2 \tag{2.35}$$

Next, we make a detailed investigation of the norm of the NPT sub-class defined in section 2.3.3.1 by considering the Hadamard NPT sub-class given by

$$\psi\{\alpha\} = \alpha\mathbf{I} + k(1-\alpha)\mathbf{H}_n \tag{2.36}$$

where $\mathbf{H}_n$ is the normalized natural Hadamard matrix of order $N = 2^n$. The matrix $\mathbf{H}_n$ can be expressed as

$$\mathbf{H}_n = \mathbf{M}^T \begin{bmatrix} \mathbf{I}_{N/2} & \mathbf{0} \\ \mathbf{0} & -\mathbf{I}_{N/2} \end{bmatrix} \mathbf{M} \tag{2.37}$$

where $\mathbf{M}$ is an orthogonal matrix of order 2^n , $\mathbf{I}_{N/2}$ is an identity matrix of order 2^{n-1} and T denotes the transposition operation.Using (2.37), we can re-write (2.36) as

$$\alpha\mathbf{I} + k(1-\alpha)\mathbf{H}_n = \mathbf{M}^T\mathbf{D}\mathbf{M} \tag{2.38a}$$

where $\mathbf{D}$ is the diagonal matrix

$$\mathbf{D} = \begin{bmatrix} (\alpha + k(1-\alpha))\mathbf{I}_{N/2} & \mathbf{0} \\ \mathbf{0} & (\alpha - k(1-\alpha))\mathbf{I}_{N/2} \end{bmatrix} \tag{2.38b}$$

We represent the data array resulting from the application of the two-dimensional Hadamard NPT to a data array $\mathbf{F}$ by $\mathbf{T_F}$. The Euclidean norm of this matrix, using (2.17a), (2.33) and (2.38a) is given by

$$\|\mathbf{T_F}\| = \|\mathbf{M}^T\mathbf{D}\mathbf{M}\mathbf{F}\mathbf{M}^T\mathbf{D}\mathbf{M}\| \tag{2.39}$$

and making use of the fact that

$$\|\mathbf{M}\mathbf{G}\| = \|\mathbf{G}\| \tag{2.40}$$

for $\mathbf{M}$ an orthogonal matrix, it follows that

$$\begin{aligned} \|\mathbf{T_F}\| &= \|\mathbf{D}\mathbf{M}\mathbf{F}\mathbf{M}^T\mathbf{D}\| \\ &\leq \|\mathbf{D}\|\,\|\mathbf{M}\mathbf{F}\mathbf{M}^T\|\,\|\mathbf{D}\| \end{aligned} \tag{2.41}$$

and

$$\|\mathbf{T_F}\| \leq \|\mathbf{D}\|\,\|\mathbf{F}\|\,\|\mathbf{D}\| \tag{2.42}$$

From (2.36) and (2.38a), and making use of (2.40) and (2.31), it can be shown that

$$\|\psi\{\alpha\}\| = \|\mathbf{D}\| = \sqrt{N\left[\alpha^2 + k^2(1-\alpha)^2\right]} \tag{2.43}$$

The norm of the Hadamard NPT given by (2.43) is minimum for $\alpha = \frac{k^2}{1+k^2}$ which gives $\alpha = \frac{1}{2}$ when $k = 1$. Fig. 2.3a is a plot of the Euclidean norm of the Hadamard NPT normalized to that of a normalized measure-preserving transform (i.e. Euclidean norm of the Hadamard NPT divided by $\sqrt{N}$), over the range $-1.2 \leq \alpha \leq 1.2$ with $k = 1$, from which we can deduce that the Hadamard NPT is Euclidean norm reducing (i.e. the normalized Euclidean norm is less than unity) over the interval $0 < \alpha < 1$ and Euclidean norm increasing (i.e. the normalized Euclidean norm is greater than unity) outside this range. The Euclidean norm of the inverse Hadamard NPT can be shown to be given by

$$\|\psi^{-1}\{\alpha\}\| = \frac{\sqrt{N\left[\alpha^2 + k^2(1-\alpha)^2\right]}}{|\alpha^2 - k^2(1-\alpha)^2|} \tag{2.44}$$

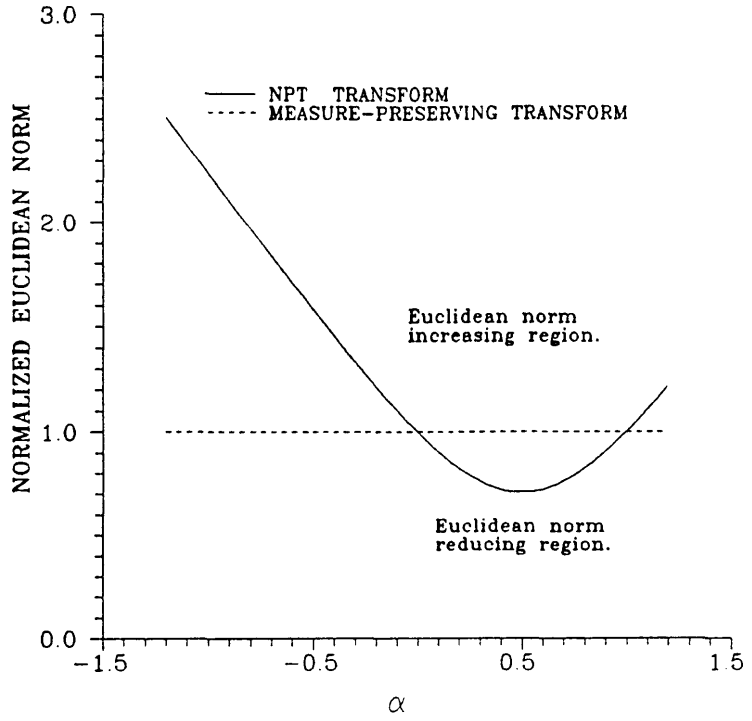


Fig. 2.3a : Normalized Euclidean norm of the Hadamard NPT as a function of α; parameter k=1.

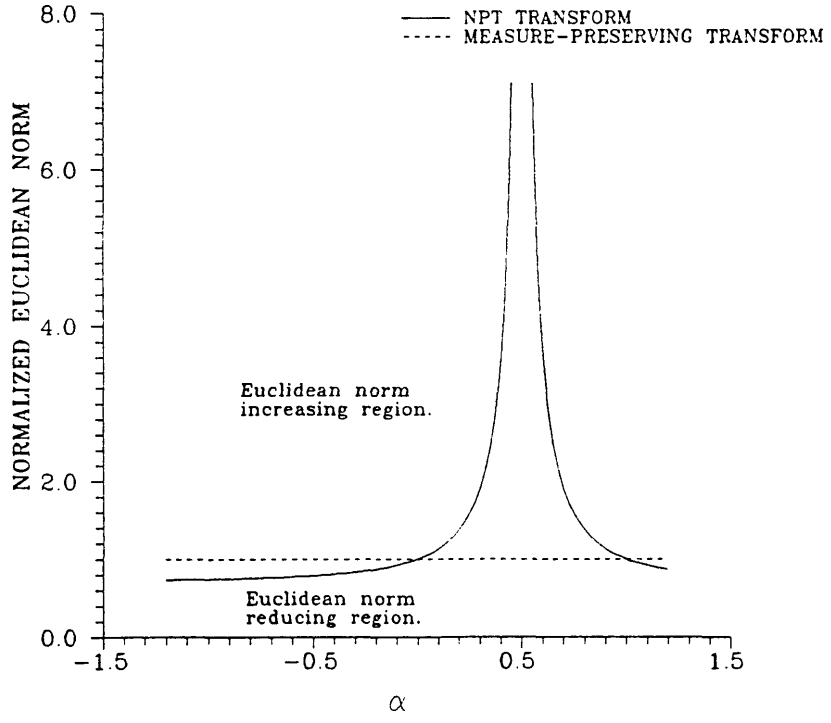


Fig. 2.3b : Normalized Euclidean norm of the inverse Hadamard NPT as a function of α; parameter k=1.

Fig. 2.3b is a plot of the norm of the inverse Hadamard NPT, again normalized to that of a measure-preserving transform over the range $-1.2 \leq \alpha \leq 1.2$ with $k = 1$, which shows that the inverse Hadamard NPT is Euclidean norm increasing over the interval $0 < \alpha < 1$ and Euclidean norm decreasing outside this range.

It can be verified empirically that the norm of the sine NPT and the symmetric cosine NPT sub-classes is also given by (2.43) for the forward transforms and by (2.44) for the inverse transforms ; comments identical to that of the Hadamard NPT apply to the variation of their Euclidean norm with α. It should be noted that the transforms resulting from the choice of parameter $k = 1$ and $\alpha = 0$ or $\alpha = 1$ are measure-preserving.

The norm properties of the NPT have important implications for NPT data compression applications which is the subject of chapter three.

(2) Magnitude of The Coefficients of The NPT of A Data Sequence

Successive application of a transform to a block of input data results in the transformed data having coefficients with larger numerical values than those of the original input data. The DC coefficient is usually the coefficient having the highest magnitude, out of all the coefficients generated by the transform operation (note that this may not be true if a zero-mean or near zero-mean data sequence is transformed). It is obtained by the sequential application of the first rows of the transform matrices to the data and it represents a scaled mean of the original data. For signal processing applications such as coding, it is necessary to ensure that the transform coefficients of interest are retained to the required degree of accuracy. Thus it is useful to be able to determine the maximum value of the coefficients obtained in a transform operation.

As stated earlier, for a data sequence having a mean value whose magnitude is much greater than zero, the magnitude of the DC coefficient is an upper bound on the magnitude of all transform coefficients. The DC coefficient is obtained by effectively scaling the mean of the original data by a factor which we call *Coefficient Magnitude Expansion Factor for DC Values* (this is strictly true for a data sequence having a constant magnitude) and denote by $(CMEF)_{DC}$. A theoretical model for $(CMEF)_{DC}$ can be obtained under the assumption that the original data values take on their maximum possible value ; this would yield the largest possible value of the DC coefficient. For an orthonormal transformation of

order N and dimension c, with a constant DC basis vector, the expansion factor is given by $N^{c/2}$. This result can be derived by following the transform operation leading to the DC coefficient and assuming that the original data take on the same maximum value. A detailed derivation is given in [13] and shall not be considered here.

Using an approach similar to that described above for orthonormal transforms with constant DC basis vectors, it can be shown that for the NPT sub-class of (2.14) comprising a linear combination of a symmetric orthogonal transform **A**, having a constant DC basis vector, the *Coefficient Magnitude Expansion Factor for DC values* $(CMEF)_{DC}$ is approximately given by

$$(CMEF)_{DC} = \left\{\alpha + \sqrt{N}\,k(1-\alpha)\right\}^{c} \tag{2.45}$$

where N, c and k are as previously defined. Figs. 2.4a-c shows some experimental and theoretical evaluations of $(CMEF)_{DC}$ for the two-dimensional Hadamard NPT, symmetric cosine NPT and sine NPT transformed data respectively ; the original data is a two-dimensional Gauss-Markov field generated according to an isotropic model [14] with horizontal and vertical inter-element correlation coefficients of 0.91. The theoretical values were calculated from (2.45). The agreement between the theoretical and experimental values is very good for the Hadamard NPT and the symmetric cosine NPT ; this is due to the Hadamard NPT and symmetric cosine NPT having constant DC basis vectors. However, there is a disparity between the theoretical and experimental $(CMEF)_{DC}$ values for the sine NPT which becomes more marked as the block size increases ; this is due to the non-constancy of the DC basis vectors of the sine transform. From Figs. 2.4a-c, we see that for values of α between 0 and 1, the respective values of $(CMEF)_{DC}$ are between 1 and the value of $(CMEF)_{DC}$ for the classical orthogonal transform component in the NPT kernel. This implies that the DC values given by the NPT are in between those given by the classical orthogonal transform **A** and the mean of the original data. For a two-dimensional NPT transform, (2.45) takes a minimum of zero for values of α given by

$$\alpha_{min} = \frac{k\sqrt{N}}{k\sqrt{N}-1} \tag{2.46}$$

and it is clear that α_{min} approaches unity for large N. There is no stationary point associated with the $(CMEF)_{DC}$ for a one-dimensional transformation. For transformations with dimension $c > 2$, the stationary points associated with $(CMEF)_{DC}$ are points of inflexion which are also given by (2.46).

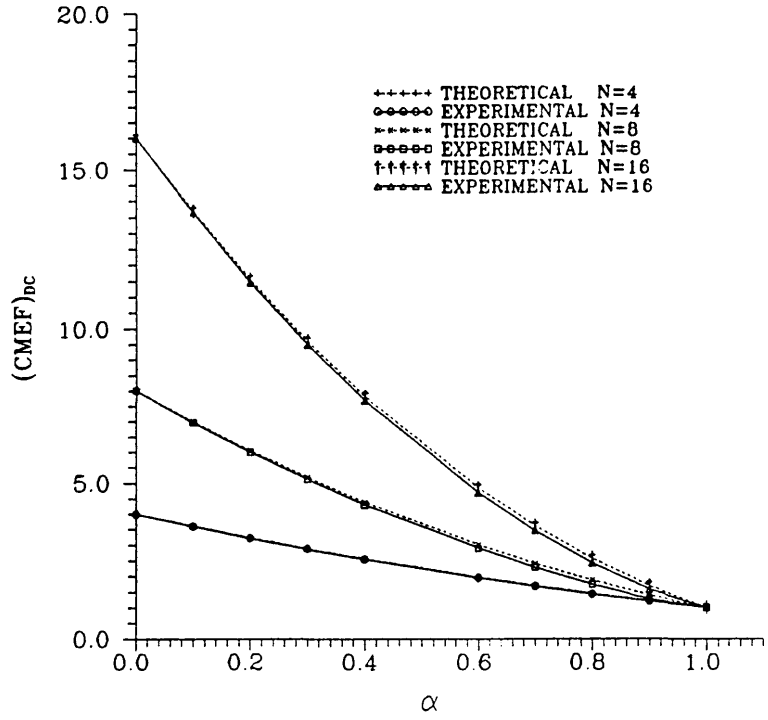


Fig. 2.4a : Two-dimensional Hadamard NPT DC Coefficient Magnitude Expansion Factor as a function of α.

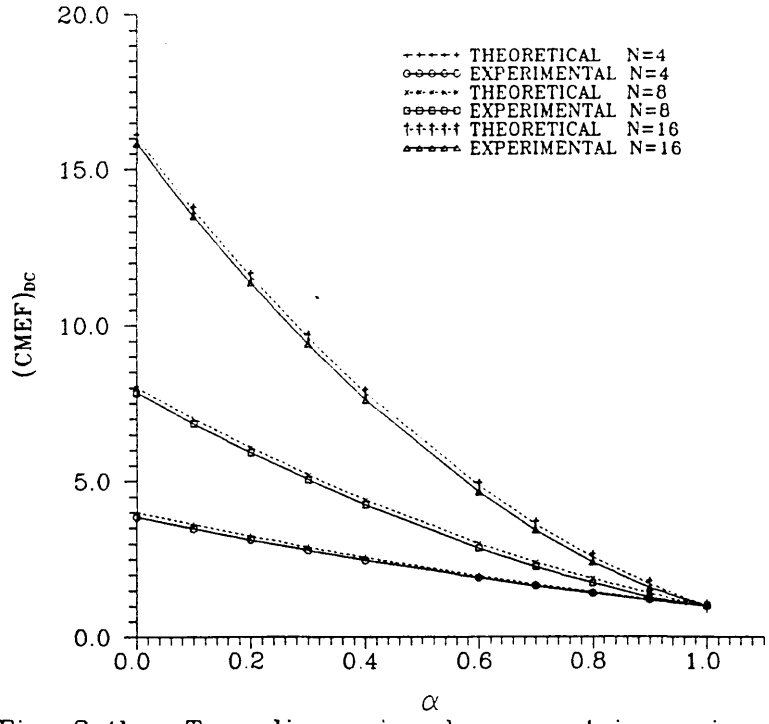


Fig. 2.4b : Two-dimensional symmetric cosine NPT DC Coefficient Magnitude Expansion Factor as a function of α.

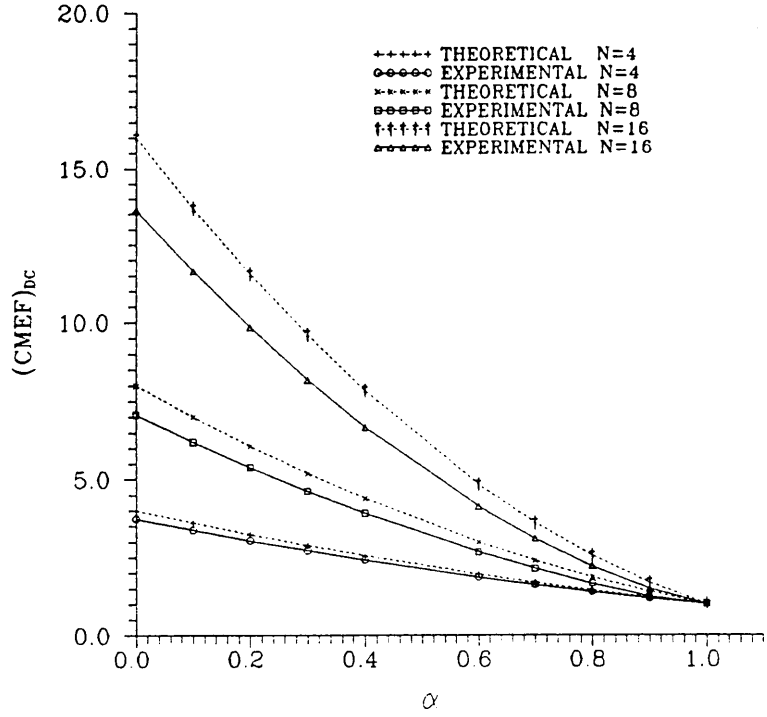


Fig. 2.4c : Two-dimensional sine NPT DC Coefficient Magnitude Expansion Factor as a function of α.

(3) Statistical Properties of An NPT Transformed Data Sequence

An understanding of the properties of a transformed data is very important for applications such as transform data compression. This is because the basic concept of the method relies on the re-distribution of energies (coefficient variances) in the transform domain. Thus, to permit the development of efficient quantization and coding techniques for transformed data samples, a good knowledge of the statistical properties of the transformed data is required. Here, we develop expressions for the mean and covariance matrices of an NPT transformed data.

We assume the original data vector $\mathbf{f}$ to be a sample of a one-dimensional random process. The mean vector of the process, $\bar{\mathbf{f}}$, is given by

$$\bar{\mathbf{f}} = E\{\mathbf{f}\} \tag{2.47}$$

where $E\{\cdot\}$ is the mathematical expectation operation. The covariance matrix of the original data is by definition

$$\mathbf{C_f} = E\{\mathbf{f}\mathbf{f}^T\} - \bar{\mathbf{f}}\bar{\mathbf{f}}^T \tag{2.48}$$

where the T in the exponent denotes the transposition operation.

The NPT of $\mathbf{f}$ is given by

$$\mathbf{t_f} = \psi\{\alpha\}\mathbf{f} \tag{2.49}$$

The mean vector , $\bar{\mathbf{t}}_\mathbf{f}$, of the NPT transformed random process is given by

$$\bar{\mathbf{t}}_\mathbf{f} = E\{\mathbf{t_f}\} \tag{2.50a}$$

$$= E\{\psi\{\alpha\}\mathbf{f}\} \tag{2.50b}$$

$$= \psi\{\alpha\}E\{\mathbf{f}\} \tag{2.50c}$$

$$= \psi\{\alpha\}\bar{\mathbf{f}} \tag{2.50d}$$

The covariance matrix of the NPT transformed random process is given by

$$\mathbf{C_f} = E\{\mathbf{t_f}\mathbf{t_f}^T\} - \bar{\mathbf{t}}_\mathbf{f}\bar{\mathbf{t}}_\mathbf{f}^T \tag{2.51}$$

Substituting (2.49) and (2.50d) in (2.51), we obtain

$$\mathbf{C}_{\mathbf{t_f}} = E\{\psi\{\alpha\}\mathbf{f}\mathbf{f}^T\psi\{\alpha\}\} - \psi\{\alpha\}\bar{\mathbf{f}}\bar{\mathbf{f}}^T\psi\{\alpha\} \tag{2.52a}$$

$$= \psi\{\alpha\}E\{\mathbf{f}\mathbf{f}^T\}\psi\{\alpha\} - \psi\{\alpha\}\bar{\mathbf{f}}\bar{\mathbf{f}}^T\psi\{\alpha\} \tag{2.52b}$$

$$= \psi\{\alpha\}\mathbf{C_f}\psi\{\alpha\} \tag{2.52c}$$

where we have used the fact that the NPT transform $\psi\{\alpha\}$ of interest is symmetric ; (2.50*d*) expresses the fact that the mean vector of the NPT of a one-dimensional data is the NPT of the mean vector of the original data while (2.52*c*) shows that the covariance matrix of the NPT of a one-dimensional data can be obtained by taking the two-dimensional NPT of the covariance matrix of the original data.

For a two-dimensional data array $\mathbf{F}$, it is convenient for the purpose of analysis to convert the array into vector form by column or row scanning $\mathbf{F}$ and abutting the elements to form a long vector [1, pp 128]. We represent the data vector resulting from this stacking operation by $\mathbf{f_F}$. The vector of scanned two-dimensional NPT coefficients is then given by

$$\mathbf{t_F} = \mathbf{W}(\alpha)\mathbf{f_F} \tag{2.53a}$$

where $\mathbf{W}(\alpha)$ is a matrix obtained by forming the cartesian product of $\psi\{\alpha\}$ with itself, i.e.

$$\mathbf{W}(\alpha) = \psi\{\alpha\} \otimes \psi\{\alpha\} \tag{2.53b}$$

and $\otimes$ denotes the cartesian product operation.

By analysis similar to that given above for a one-dimensional process, the mean vector of stacked transform coefficients is given by

$$\bar{\mathbf{t}}_\mathbf{F} = \mathbf{W}(\alpha)\bar{\mathbf{f}}_\mathbf{F} \tag{2.54}$$

and the covariance matrix of the transform coefficients is

$$\mathbf{C_F} = \mathbf{W}(\alpha)\mathbf{C}_{\mathbf{f_F}}\mathbf{W}^T(\alpha) \tag{2.55}$$

where $\bar{\mathbf{f}}_\mathbf{F}$ and $\mathbf{C}_{\mathbf{f_F}}$ are respectively the mean vector and the covariance matrix of the data array $\mathbf{F}$ stacked to form a vector $\mathbf{f_F}$. The variance of the two-dimensional NPT transform coefficients is obtained by arranging the trace of the transform coefficients covariance matrix, given by (2.55), into matrix form.

(4) NPT Identities [3]

The following identities hold for the NPT defined by (2.14) :

(i) $\psi\{1\} = \mathbf{I}$ (2.56*a*)

(ii) $\psi\{0\} = k\mathbf{A}$ (2.56*b*)

(iii) $\psi\{\alpha\} = \alpha\psi\{1\} + (1-\alpha)\psi\{0\}$ (2.56*c*)

(iv) $\psi\{\alpha_1 + \alpha_2\} = \psi\{\alpha_1\} + \psi\{\alpha_2\} - \psi\{0\}$ (2.56*d*)

(v) $\psi\{\alpha_1\alpha_2\} = \alpha_1\psi\{\alpha_2\} + (1-\alpha_1)\psi\{0\}$ (2.56*e*)

The following identities hold in addition when $k = 1$ in (2.14) :

$$(vi)\quad \psi\{\alpha_1\}\psi\{\alpha_2\} = \psi\{\alpha_1\alpha_2 + (1-\alpha_1)(1-\alpha_2)\} \tag{2.56f}$$

$$(vii)\quad \psi\{\alpha\}\psi\left\{\frac{\alpha}{2\alpha-1}\right\} = \psi\{1\} \quad ,\alpha \neq \frac{1}{2} \tag{2.56g}$$

$$(viii)\quad \psi\{\alpha\}\psi\left\{\frac{\alpha-1}{2\alpha-1}\right\} = \psi\{0\} \quad ,\alpha \neq \frac{1}{2} \tag{2.56h}$$

$$(ix)\quad \psi^2\{\alpha\} = \psi\left\{\alpha^2 + (1-\alpha)^2\right\} \tag{2.56i}$$

$$(x)\quad \psi^m\{\alpha\} = \psi\left\{\frac{1+(2\alpha-1)^m}{2}\right\} \tag{2.56j}$$

Identity (i) shows that when $k = 1$, the transform is the identity transform while identity (ii) shows that when $\alpha = 0$, the transform is a scalar multiple of the classical orthogonal transform **A**. Identity (vii) expresses the fact that when $k = 1$, the inverse NPT transform kernel $\psi^{-1}\{\alpha\} = \psi\{\beta\}$ where $\beta = \frac{\alpha}{(2\alpha-1)}$, $\alpha \neq \frac{1}{2}$ which is useful for computation purposes, since in this case α is replaced by β in the forward transform computation algorithm to yield the inverse transform. Identities (vi), (ix) and (x) expresses the fact that the set of all $\psi\{\alpha\}$ derived from (2.14a), when $k = 1$, forms a field under the operation of matrix multiplication.

2.3.3.1.3 Operation Count Required For Computing The NPT of A Data Sequence

The NPT of a data sequence, (2.16b) and (2.17b), can be regarded as a linear combination of orthogonal transforms of the data. The weighted identity transformation of the data does not have a fast computational algorithm; however, the fast computational algorithm of the classical orthogonal transform **A** can be used to compute the component orthogonal transforms of the data and the appropriate results added to yield the NPT of the data.This would in general lead to an operation count higher than that required for data transformation using the classical orthogonal transform **A** . Here, we evaluate the number of operations required to compute the NPT of a data sequence.

One-Dimensional NPT

We represent the number of operations required to transform an $N \times 1$ data vector **f** using a fast transform **A**, by $\mathcal{O}(\mathbf{Af})$ operations where an operation is a multiplication or an addition; the number of operations required for transform coefficient normalization is not included (a total of $\mathcal{O}(\mathbf{Af}) + N$ operations are required , where N operations are due to transform normalization). By including the factor

$k(1-\alpha)$ in the normalization constant, a total of $\mathcal{O}(\mathbf{Af})+N$ operations would be required to transform the data vector $\mathbf{f}$ by the matrix $k(1-\alpha)\mathbf{A}$. Additional $2N$ operations are incurred in obtaining the scaled identity transformation and addition of the components of (2.16*b*) to yield the final result. Thus, the total number of operations required to compute the one-dimensional NPT of an N-length data sequence is

$$\mathcal{O}(\psi\{\alpha\}\mathbf{f}) = 3N + \mathcal{O}(\mathbf{Af}) \tag{2.57}$$

Two-Dimensional NPT

We represent the number of operations required to compute the two-dimensional fast orthogonal transform of an $N \times N$ data array $\mathbf{F}$, including transform normalization, by $\mathcal{O}(\mathbf{AFA})$. It can be shown that

$$\mathcal{O}(\mathbf{AFA}) = N^2 + 2N\cdot\mathcal{O}(\mathbf{Af}) \tag{2.58}$$

where the N^2 term is used for transform normalization.

There are two ways of computing the two-dimensional NPT of a data array. The first approach computes it as a succession of row and column transforms, (2.17*a*). The row (column) NPT requires a total of $2N^2 + N\cdot\mathcal{O}(\mathbf{Af})$ operations and the total number of operations for the two-dimensional transformation becomes

$$\mathcal{O}_1(\psi\{\alpha\}\mathbf{F}\psi\{\alpha\}) = 2(2N^2 + N\cdot\mathcal{O}(\mathbf{Af})) \tag{2.59a}$$

$$= 4N^2 + 2N\cdot\mathcal{O}(\mathbf{Af}) \tag{2.59b}$$

The second approach computes the NPT according to the matrix expansion (2.17*b*). The total number of operations required in this case is

$$\mathcal{O}_2(\psi\{\alpha\}\mathbf{F}\psi\{\alpha\}) = 5N^2 + 3N\cdot\mathcal{O}(\mathbf{Af}) \tag{2.60}$$

2.3.3.2 An Alternative Definition of The NPT

We define an alternative form of the NPT as

$$\psi_{ALT}\{\alpha\} = \frac{1}{(2\alpha-1)}\Big[\alpha\mathbf{I} + (1-\alpha)\mathbf{A}\Big] \tag{2.61a}$$

where we have included the factor $1/(\alpha^2 - k^2(1-\alpha)^2)$, appearing in the inverse transform (2.14*b*), in the forward transform (2.14*a*) and set $k=1$. The inverse transform of this alternative NPT is

$$\psi_{ALT}^{-1}\{\alpha\} = \alpha\mathbf{I} - k(1-\alpha)\mathbf{A} \tag{2.61b}$$

There is an interesting behaviour of the coefficients generated by this transform as α is increased from zero. The *Coefficient Magnitude Expansion Factor for DC values* $(CMEF)_{DC}$ for this transform, when the orthogonal transform **A** has a constant DC basis vector is given by

$$(CMEF)_{DC} = \left\{\frac{1}{(2\alpha - 1)}\left[\alpha + N^{\frac{1}{2}}(1-\alpha)\right]\right\}^{c} \tag{2.62}$$

As α is increased from zero, the transform defined by (2.61*a*) initially gives DC coefficients whose numerical values are larger than those of the transform defined by (2.14*a*), with $k = 1$. However, when the values of α satisfy

$$(CMEF)_{DC} \leq N^{\frac{c}{2}} \tag{2.63}$$

, the DC coefficients of transform (2.61*a*) become identical to those of transform (2.14*a*) with $k = 1$, over the range $0 \leq \alpha \leq 1$. When α is such that (2.63) holds with equality, the DC coefficients of (2.61*a*) and that of the orthonormal transform **A** become identical. Fig. 2.5 shows the theoretical values of $(CMEF)_{DC}$ as a function of α for a two-dimensional alternative NPT, for block sizes of 8 and 16.

For a two-dimensional transformation, by using (2.62) in (2.63), we obtain the inequality

$$2N^{\frac{1}{2}}/(3N^{\frac{1}{2}} - 1) \leq \alpha \leq 1 \tag{2.64}$$

where N is the transform order. The values $\alpha_L = 2N^{\frac{1}{2}}/(3N^{\frac{1}{2}} - 1)$ for which (2.63) holds with equality are tabulated in Table 2.1 for various transform block sizes, N; it is clear that $\alpha_L \rightarrow \frac{2}{3}$ as $N \rightarrow \infty$. For various block sizes, Table 2.1 gives the respective values of α for which the DC coefficients generated from a data sequence by the alternative NPT defined by (2.61*a*) becomes equal to the DC coefficients generated by the classical orthogonal transform component, **A**, in the NPT kernel.

The normalized Euclidean norm of the forward alternative NPT transform is shown in Fig. 2.6a, while the normalized Euclidean norm of the inverse alternative NPT is shown in Fig. 2.6b. From these plots, we deduce that the forward alternative NPT is Euclidean norm increasing while the inverse alternative NPT is Euclidean norm reducing. The alternative NPT could be advantageous for signal transmission through channels subject to additive noise. By transforming the signal information using the alternative NPT prior to transmission through the channel, the Euclidean norm of the noise vector introduced by the channel would be reduced during inverse transformation in the receiver. Hence, the mean-square

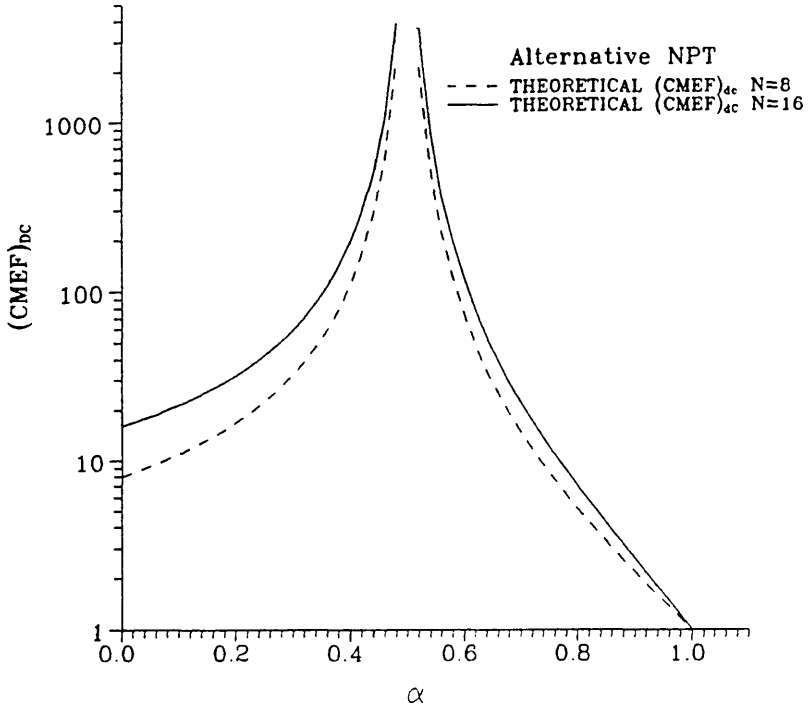


Fig. 2.5 : Theoretical Plot of the Coefficient Magnitude Expansion Factor as a function of α for the altenative NPT.

Table 2.1 : Values of α for which (2.63) holds with equality	
BLOCK SIZE, N	α_L
2	0.87226
4	0.8
8	0.75573
16	0.72727
32	0.70841
64	0.69565
128	0.686905
256	0.68085

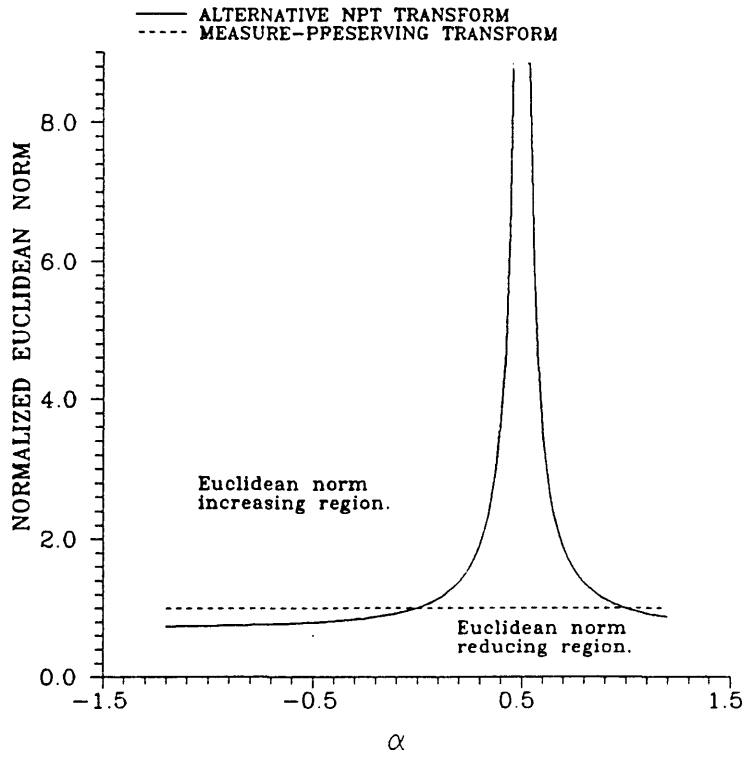


Fig. 2.6a : Normalized Euclidean norm of the alternative Hadamard NPT as a function of α; parameter k=1.

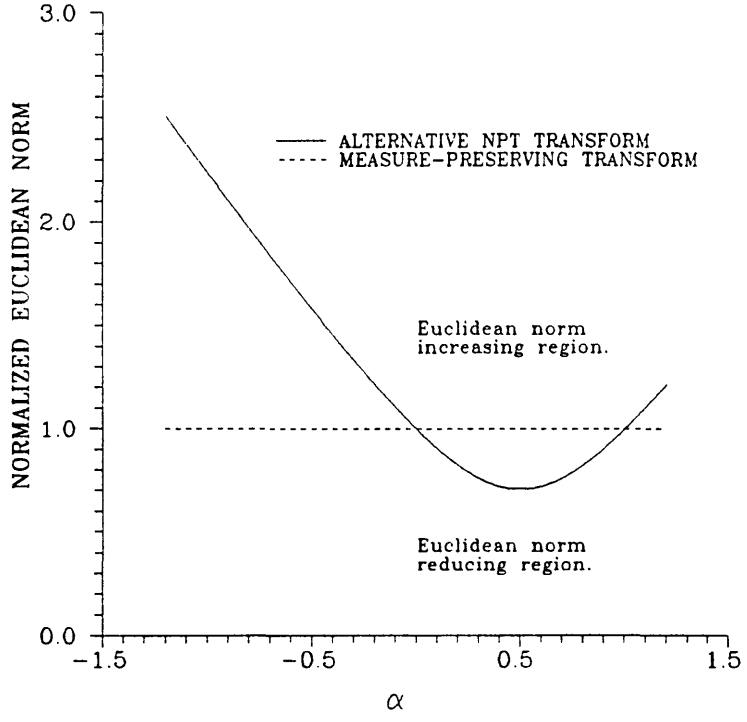


Fig. 2.6b : Normalized Euclidean norm of the inverse alternative Hadamard NPT as a function of α; parameter k=1.

error (MSE) between the original and the received signal, when the alternative NPT is used for transmission would be lower than when the NPT defined by (2.14a) is used.

2.3.4 The Original Pictures Used For Simulation

The original Pictures used for various investigations reported in this thesis are shown in Figs. 2.7–2.11.

2.3.5 Simulation and Results

A computer simulation was conducted to investigate the NPT domain of typical imagery, for various values of the parameter α and some transform block sizes. Both one-dimensional and two- dimensional partitions of the image were considered. The original image used is the 8-bit 256×256 image ALAN shown in Fig. 2.7. The pictorial results presented are clipped magnitude displays of the respective transform domains.

In Figs. 2.12a–c, the effect of the variation of α on the transform domain of the one-dimensional Hadamard NPT transformed image ALAN, using 32×1 partitions of the image, is shown. We observe that features of the original image are visually recognizable from the NPT domains shown at $\alpha = 0.3$ and $\alpha = 0.6$. Figs. 2.13a–b show the transform domains given by the one-dimensional symmetric cosine NPT (SC NPT) at $\alpha = 0.3$ and $\alpha = 0.6$. The variation with α is similar to that of the one-dimensional Hadamard NPT shown in Fig. 2.12. In Fig. 2.14b, the transform domain given by the one-dimensional sine NPT(0.6) is shown. Comparison with the Hadamard NPT(0.6) transform domain shown in Fig. 2.14a indicates that more higher order transform samples are clipped in this case. This is due to the non-constancy of the zero-order basis vector of the sine transform which cause part of the mean energy of the image to 'leak' into the 'AC' transform samples [18].

In Figs. 2.15a–c, the effect of the variation of α on the two-dimensional Hadamard NPT transformed image ALAN, using 8×8 partitions of the image is shown. Again, features of the original image are visually recognizable from the transform domains shown at $\alpha = 0.3$ and $\alpha = 0.6$. Figs. 2.16a–b show the transform domains given by the two-dimensional symmetric cosine NPT at $\alpha = 0.3$ and $\alpha = 0.6$. The effect of the variation of α is similar to that of the two-dimensional Hadamard NPT shown in Fig. 2.15. The transform domain given by the two-dimensional sine NPT(0.6) is shown in Fig. 2.17. This appears visually different



Fig. 2.7 : Original 8-bit, 256×256 Image ALAN.



Fig. 2.8 : Original 8-bit, 256×256 Image CHOIR.

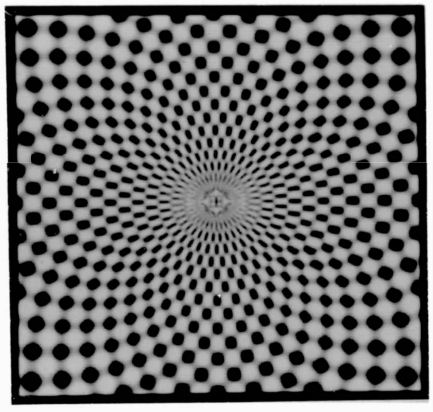


Fig. 2.9 : Original 8-bit, 256×256 Image PATTERN.

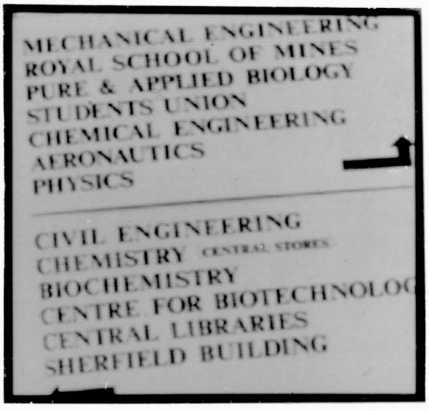


Fig. 2.10 : Original 8-bit, 256×256 Image DOCUMENT.

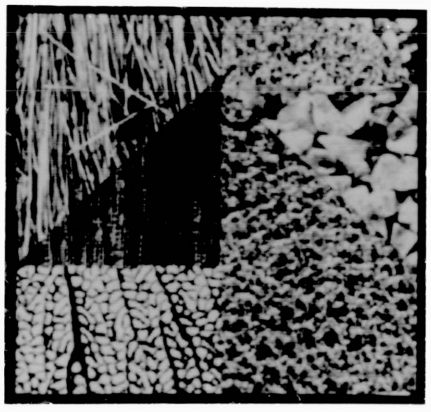


Fig. 2.11 : Original 8-bit, 256×256 Image TEXTURE.

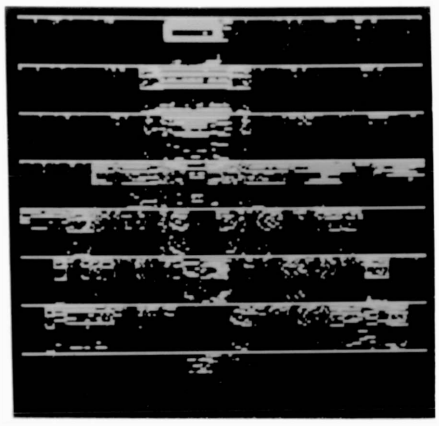


Fig. 2.12a : 32×1 Hadamard Transform ($\alpha=0$) of Image ALAN.



Fig. 2.12b : 32×1 Hadamard NPT(0.3) of Image ALAN.



Fig. 2.12c : 32×1 Hadamard NPT(0.6) of Image ALAN.



Fig. 2.13a : 32×1 Symmetric cosine NPT(0.3) of Image ALAN.



Fig. 2.13b : 32×1 Symmetric cosine NPT(0.6) of Image ALAN.



Fig. 2.14a : 32×1 Hadamard NPT(0.6) of Image ALAN

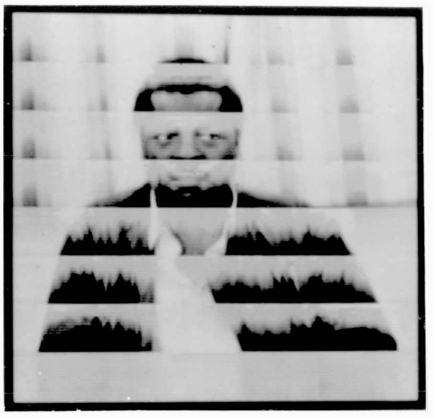


Fig. 2.14b : 32×1 sine NPT(0.6) of Image ALAN.

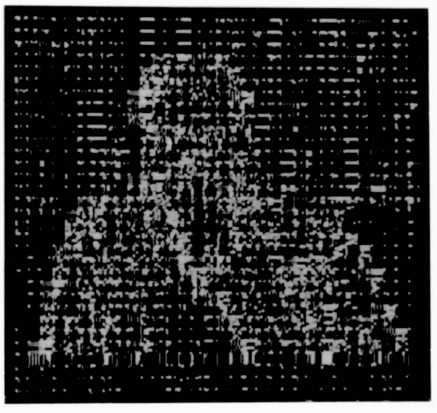


Fig. 2.15a : 8×8 Hadamard Transform ($\alpha=0$) of Image ALAN.

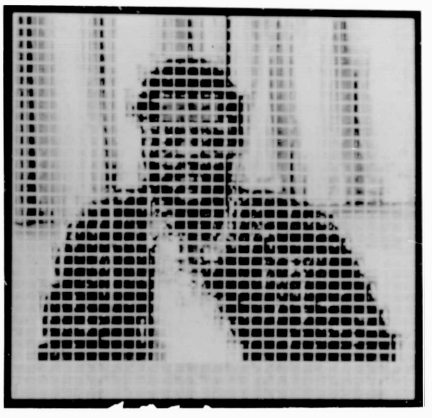


Fig. 2.15b : 8×8 Hadamard NPT(0.3) of Image ALAN.

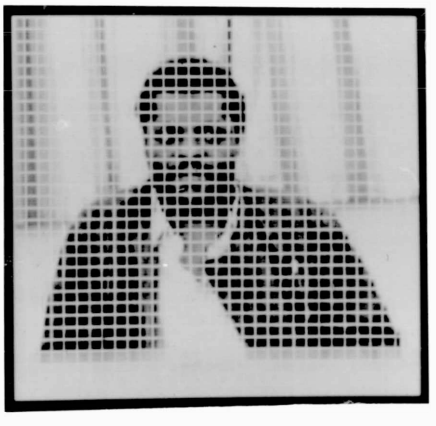


Fig. 2.15c : 8×8 Hadamard NPT(0.6) of Image ALAN.

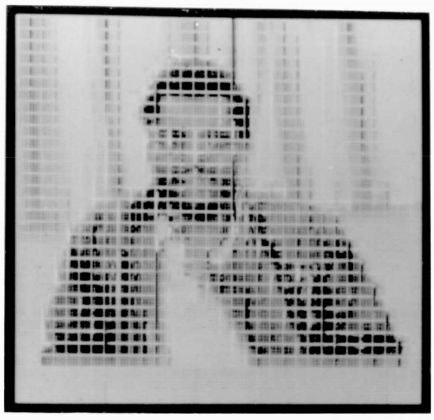


Fig. 2.16a : 8×8 Symmetric cosine NPT(0.3) of Image ALAN.

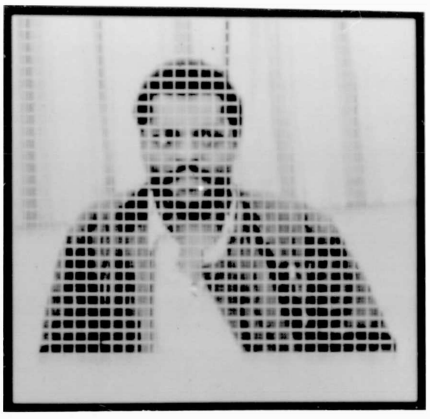


Fig. 2.16b : 8×8 Symmetric cosine NPT(0.6) of Image ALAN.

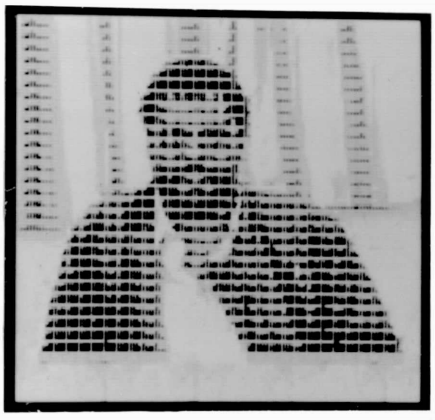


Fig. 2.17 : 8×8 sine NPT(0.6) of Image ALAN.

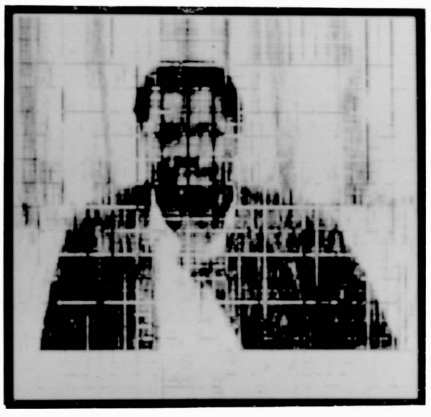


Fig. 2.18a : 256×256 Hadamard NPT(0.49) of Image ALAN.



Fig. 2.18b : 256×256 Hadamard NPT(0.6) of Image ALAN.



Fig. 2.18c : 256×256 Hadamard NPT(0.8) of Image ALAN.

from those of the Hadamard NPT(0.6) and the symmetric cosine NPT(0.6) shown in Fig. 2.15c and Fig. 2.16b respectively. The reason for this is already given above. A further result of the above experiments is that image features are generally comprehensible from NPT transforms of small-size partitions of an image, for $\alpha \geq 0.3$.

The effect of using a very large transform block size is shown in Figs. 2.18a–c. The pictures show the transform domains of the full frame (256×256) Hadamard NPT of the image ALAN at three values of α. These indicate that features of the image are barely intelligible at $\alpha \leq 0.49$; however, the visual comprehensibility improves for $\alpha \geq 0.6$. Thus, the visual perception of image features from its NPT domain at low values of α ($0.25 \leq \alpha < 0.5$) is generally better when small-size partitions of the image are NPT transformed than when a full-frame NPT of the image is taken.

2.4 Summary and Conclusions

Hybrid transforms have been described in this chapter. There are a variety of hybrid transforms resulting from possible linear combinations of orthogonal matrices and we addressed the problem of determining admissible hybrid transforms for signal processing applications. Two theorems, which specify admissible hybrid transforms comprising a linear combination of commuting (anti-commuting) involutory orthogonal matrices, were introduced and derived in appendix I.

The Naturalness-Preserving Transforms (NPT) were shown to be a special case of hybrid transforms when we require that one of the transforms in the linear combination be the identity matrix. Based on the hybrid transform inversion theorems, a parametric family of Naturalness-Preserving Transforms are reported. These comprise a linear combination of the identity matrix and a symmetric orthogonal transform. It was shown that NPT transforms comprising a linear combination of the identity matrix and certain classical transforms which include the discrete cosine transform, Haar transform, Fourier transform, slant transform, the high and low correlation transforms are not admissible for signal processing applications.

A series representation was developed for the defined NPT sub-class. Properties of the NPT, some of which are equivalent to those known for classical orthogonal transforms, have been developed. The non-orthogonal NPT bases were

shown to either reduce or increase the energy content of data, after transformation by the NPT.

An alternative form of the NPT was described. This has the interesting property of giving DC coefficients whose magnitudes are similar to that given by classical orthogonal transforms, when certain bases of the transform are used to transform a data sequence. The alternative NPT offers the possible advantage of being able to achieve a lower overall mean-square error (MSE) of reconstructed signal, when used for transmitting signals through channels subject to additive noise.

Clipped magnitude displays of NPT transformed imagery data were presented which demonstrate the visual comprehensibility of the transform domain of image data transformed by certain NPT bases.

An advantage of the NPT transforms is that they present an infinite number of possible bases that could be exploited for signal processing applications. Moreover, these bases are easily selectable without having to make any changes to the transform implementation algorithm. The component classical orthogonal transform can be selected by appropriate specification of the NPT transform parameters. These bases are investigated in the following chapters for specific signal processing applications.

CHAPTER THREE

NATURALNESS-PRESERVING TRANSFORM IMAGE DATA COMPRESSION

3.1 Introduction

Image data compression techniques [20] address the problem of reducing the number of bits necessary to represent an image subject to a specified fidelity and intelligibility constraint. These have applications primarily in the transmission and storage of information. Image transmission applications include broadcast television, teleconferencing, remote sensing via satellite, radar, sonar, computer communications and facsimile transmission. Image storage applications include image archiving in biomedical applications and the storage of educational and business documents.

In this chapter, image data compression using the NPT transforms is investigated. A brief discussion of the general signal data compression problem is given in section 3.2. Image data compression techniques are reviewed in section 3.3. A unifying description of data compression systems is given in section 3.4.

The work on NPT image data compression is organized into two parts. Part A deals with pure two-dimensional NPT coding of images while part B deals with NPT hybrid coding of images. There is an infinite number of possible bases that can be used for coding a given image or image ensemble. However, the objective of an NPT image coder is to employ the basis giving minimum mean-square error (MSE) for coding a given image or image ensemble.

An algorithm for determining the optimum basis for pure two-dimensional NPT coding of a given image or image ensemble is developed in section 3.5.2, in part A. Results of non-adaptive two-dimensional NPT coding of monochrome images are presented in section 3.5.3. Subsequently, a basis adaptive NPT image coder which features transform basis adaptation according to local image spatial activity is introduced in section 3.5.4. Results of basis adaptive NPT coding of monochrome images using the Hadamard NPT, sine NPT and SC NPT (symmetric cosine NPT) are presented. The effect of errors in the code-word digits used

for representing the transform coefficients, resulting from channel errors, on the subjective quality of reconstructed pictures is also investigated.

Section 3.6, in part B, deals with NPT hybrid coding of images. An algorithm for determining the optimum basis for the hybrid coding of a given image or image sub-array is introduced. Results of simulations of NPT hybrid coding of monochrome images using the Hadamard NPT, sine NPT and SC NPT are presented.

3.2 The Data Compression Problem

The conversion of an analog signal into digital format leads to increased requirements in the bandwidth for transmission and capacity for storage. The digital representation of data offers the advantages of processing flexibility, higher signal-to-noise ratio, easy access to stored data and better immunity to errors but at the price of increased bandwidth and storage requirements. The objective of a data compression system is to minimize this cost subject to a maximum permissible distortion of the original data.

In the digital format of signal representation, a set $B = \{b_1, b_2, \cdots b_N\}$ of information carrying units or bits is associated with the corresponding set $\mathbf{f} = \{f_1, f_2, \cdots f_N\}$ of signal samples, where b_i is the number of bits necessary to represent each signal sample f_i subject to a pre-specified fidelity constraint. The average bit rate resulting from this operation is given by

$$b_{av} = \frac{1}{N} \sum_{i=1}^{N} b_i \tag{3.1}$$

When the elements of the data set $\mathbf{f}$ are to be conveyed to their point of usage via a transmission or storage medium having a limited capacity C, the average information rate of the source signal set must be reduced prior to transmission or storage; this is the problem addressed by data compression or source coding.

The objective of a data compression system is to find another set $\hat{B} = \left\{\hat{b}_1, \hat{b}_2, \cdots \hat{b}_M\right\}$ of information carrying units that would adequately represent the source signal set $\mathbf{f} = \{f_1, f_2, \cdots f_N\}$ subject to the requirement that the distortion between the source set and its reproduction $\hat{\mathbf{f}} = \left\{\hat{f}_1, \hat{f}_2, \cdots \hat{f}_N\right\}$ is within pre-specified fidelity levels and such that the resulting data rate

$$\hat{b}_{av} = \frac{1}{M} \sum_{i=1}^{M} \hat{b}_i < b_{av} = \frac{1}{N} \sum_{i=1}^{N} b_i \tag{3.2}$$

where $M \leq N$. The compression ratio CR is an indication of the amount of compression and is given by

$$CR = b_{av}/\hat{b}_{av} \tag{3.3}$$

The average information content of the source signal set is specified by its entropy which for the sequence of discrete amplitude samples $\mathbf{f} = \{f_1, f_2, \cdots f_N\}$ is defined as

$$H(\mathbf{f}) = -\sum_{i=1}^{L} P(f_i)\, log_2 P(f_i) \tag{3.4}$$

where $P(f_i)$ is the probability that a particular sample f_i would be quantized to one discrete amplitude level out of a total of $L = 2^{b_{av}}$ possible levels and b_{av} is the fixed number of bits used for encoding each level. The source entropy is a useful indicator in image coding. This is because of a fundamental result of the "noiseless coding theorem " [19] of information theory which expresses the fact that it is theoretically possible to code a source of entropy $H(\mathbf{f})$ bits without distortion by using $H(\mathbf{f}) + \delta$ code bits, δ being a positive infinitesimally small quantity; it does imply that it is impossible to code the source with fewer than $H(\mathbf{f})$ bits without distortion. For typical image data $H(\mathbf{f})$ is normally less than b_{av} and data compression is appropriate for removing the redundancy in the data.

3.3 Review of Image Data Compression Techniques

A variety of image data compression techniques have evolved over the years [20,21]. However, these techniques can be classified into the two distinct categories of spatial predictive [1,20] and transform domain techniques [2,20]. There are also hybrid coding schemes [22] which combine the attractive features of the two distinct methods. The basic techniques that are relevant to the work reported in this chapter, are briefly described in the following sub-sections.*

3.3.1 Predictive Coding

In a predictive coding (differential pulse code modulation, DPCM) system, the error incurred in predicting a pixel amplitude value based on a number of previously coded neighbouring pixel amplitude values is coded and transmitted or stored, rather than the actual instantaneous pixel amplitude value. Since typical imagery data is highly correlated, a good prediction is obtainable in practice and the difference signal would be small. By virtue of the degree of correlation existing between neighbouring pixel values, the variance of the difference signal would be

*Vector Quantization (VQ) techniques have also been developed and a brief description of VQ is given on page 250.

considerably smaller than that of the original pixel values. Bandwidth reduction is achieved by coarsely quantizing the difference signal to be transmitted or stored.

A procedure for designing DPCM coders with application to television signals is presented in [23]. A summary of approaches to predictive coding that have been considered, as well as adaptive implementation of these techniques is given in [1,20,24,40]. Other techniques which are related in principle to predictive coding can be found in [25,26,27].

DPCM coding generally gives good results at high bit rates. However, its performance deteriorates considerably at low bit rates. It is also very sensitive to image statistics. Furthermore, the distortion due to quantization is localized at the picture region in question yielding a reconstructed picture that is subjectively annoying. However, its ease of implementation makes it a very attractive technique for image coding.

3.3.2 Transform Coding

Central to a transform coding scheme is the application of an invertible linear transformation to the sub-blocks of the image. The linear transformation maps the set of correlated pixel values into a set of "more independent " coefficients which are subsequently coded and transmitted. Data compression is achieved by coding the transform coefficients in accordance with their information content, subject to the desired fidelity level of reconstructed picture.

The optimum transformation for decorrelating a given data is the Karhunen-Loève (KL) transform [9,28], the transformation kernel of which is made up of the eigenvectors of the data covariance matrix. It also packs the maximum energy in a given number of samples. However, the KL transform is unattractive for practical implementation because it is only unique for a given class of signals specified by its covariance matrix and must be calculated for each different class. Furthermore, there is no known fast algorithmic implementation of the resulting transforms. Consequently, sub-optimal fast transforms such as the Fourier, discrete cosine, Hadamard, Haar, slant, high and low correlation transforms have been investigated as alternatives to the KL transform. Details of these investigations can be found in [2,8,16,28,29,30].

The performance of transform coding systems is generally quite good at moderate bit rates; the coding distortion is distributed in a way that is less objectionable to the human eye. However, at very low bit rates, reconstructed pictures exhibit a so-called "block effect". This effect arises from the fact that each subblock is coded independently leading to discontinuous distortion profiles at block boundaries which makes the boundaries to be visible and objectionable. Some approaches aimed at reducing the "block effect" can be found in [31,32].

Adaptive transform coding schemes generally outperform non-adaptive transform coding schemes. This is because the former adjust the parameters of the coding algorithm according to variations in the local picture statistics and are inherently more efficient than the latter. Possible adaptation parameters include bit allocation, quantizer level spacing and transform basis; some approaches to adaptive transform coding of images can be found in [2].

In part A of this chapter, we shall be developing Naturalness-Preserving transform image coding.

3.3.3 Hybrid Coding

Hybrid coding describes the technique of combining transform coding with DPCM coding. Due to the complexity of implementing two-dimensional transform image coding techniques, the scheme was introduced by Habibi [22] for images and it combines the attractive features of transform coding and predictive coding.

The basic intraframe hybrid coding scheme employs one-dimensional transformations along the rows or columns of the image followed by parallel DPCM coding in the mutually orthogonal direction. The scheme was subsequently extended to interframe coding of images by Roese et al [33]. In this case, two-dimensional transforms are taken followed by predictive coding of transform coefficients at corresponding locations in different frames. Adaptive hybrid coding schemes have also been considered [33,34].

We shall be concerned with Naturalness-Preserving transform hybrid coding of pictorial data in part B of this chapter.

3.4 A Unifying Description of Data Compression Systems

Fig. 3.1 shows a basic data compression system as being made up of three modules viz a pre-processor, a quantizer and a post-processor module.

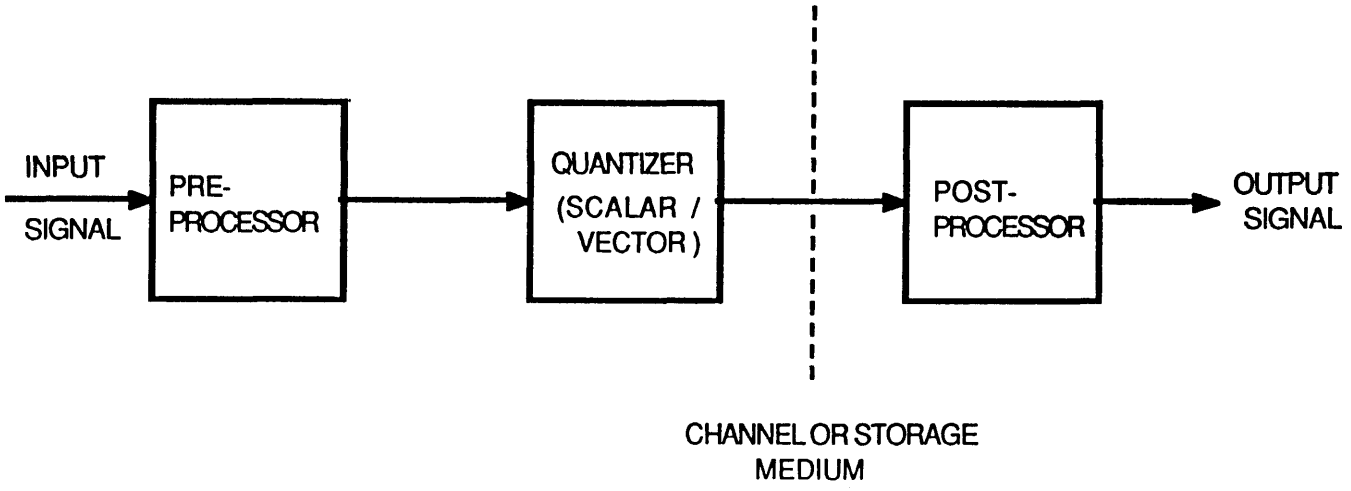


Fig. 3.1 : A Generalized Concept of A Data Compression System.

In a predictive coding system, the pre-processor generates the prediction error signals which are subsequently coded and transmitted or stored while the post-processor performs the reconstruction of an approximation of the original transmitted signal by adding the decoded prediction error signal to the prediction of the corresponding sample value based on previously reconstructed signal samples. The pre- and post- processors in a pure transform coding system are the forward and inverse transformations respectively. The pre-processor in a hybrid coding system performs a transformation (one-dimensional or two-dimensional) on sub-blocks of the image and generates a prediction error sequence from the transform coefficients. The post-processor, on the other hand, generates an approximation of the transform coefficients of the data by adding the decoded prediction errors to the prediction of the corresponding transform coefficients based on previously reconstructed transform coefficients. Subsequently, it performs the inverse transform of the reconstructed transform coefficients to yield an approximation of the original signal.

The characteristics of the quantizer module are usually matched to the probability density function of its input signals and it could either operate on single signal amplitude values at a time (scalar quantizer) or a collection of signal amplitude values at a time (vector quantizer).

Since the use of an appropriate error correcting code and transmission at a rate less than the channel capacity guarantees errorless transmission [19], data compression systems generally assume a noiseless channel and the source coding problem is usually studied separately from the channel coding problem.

PART A : Conventional Pure Transform Coding of Images Using The Naturalness-Preserving Transforms

3.5 Naturalness-Preserving Transform Image Coding

The work reported here represents the pioneering work on the application of the Naturalness-Preserving transform to image coding. A lot of the efforts on transform data compression have concentrated on the application of orthogonal transforms. In chapter two, we defined a parametric family of NPTs which are linear combinations of a classical orthogonal transform and the identity matrix. These transforms are characterized by an infinite set of bases parameterized by α, $-1 < \alpha < 1$.

A very attractive feature of these transforms is that any desired basis can be selected with ease without any modification to the transform implementation algorithm. Consequently, each NPT transform member offers a wide range of possible bases that can be employed for image data compression, the parent classical orthogonal transform still being selectable by a proper choice of transform parameters. Since the objective of a data compression system is to represent a given image data by as small a number of bits as possible subject to a desired minimum fidelity level of reconstructed image, the objective in NPT image coding is to employ the basis or the collection of bases that would yield the highest fidelity level of encoding a given image or image ensemble. Thus, for a given fidelity constraint, an efficient means must be found for determining the optimum basis for encoding a given image or image ensemble.

3.5.1 The Optimum Basis Determination Problem

For simplicity and analytical tractability, we adopt the mean-square error (MSE) between an original and reconstructed picture as the fidelity criterion. The MSE between an $N \times N$ original image $\mathbf{F}$ and its compressed version $\hat{\mathbf{F}}$ is by definition

$$MSE = E\left\{\|\mathbf{F} - \hat{\mathbf{F}}\|^2\right\} \tag{3.5}$$

where $E\{\cdot\}$ is the mathematical expectation operator; this can be estimated in empirical work from

$$MSE = \frac{1}{N^2}\sum_{i=1}^{N}\sum_{j=1}^{N}\left(\mathbf{F}(i,j) - \hat{\mathbf{F}}(i,j)\right)^2 \tag{3.6}$$

The optimum basis determination problem is that of finding the basis or collection of bases that would yield the minimum mean-square error between an original image $\mathbf{F}$ and its encoded version $\hat{\mathbf{F}}$, when used for coding the given image $\mathbf{F}$.

The fact that a fidelity measure compares an original image with its encoded version at first suggests that both the original image and its reconstructed version must be available before a comparison can be made. For an orthogonal transform and an MSE fidelity criterion, the overall MSE of encoding a given picture is conveniently given by the MSE difference between its original and coded transform coefficients. However, as the NPT bases are not orthogonal (only the bases specified by $\alpha = 0$ and $\alpha = 1$ are orthogonal), the MSE between the original and coded transform coefficients of the image would not reflect the overall MSE of

encoding the image and the optimum basis cannot be determined from measures defined on the transform domain alone. Thus, the solution to the optimum basis determination problem is non-trivial.

An exhaustive search through all the possible bases by transform coding at various values of α, measuring the overall MSE of encoding and then determining the basis giving minimum MSE is clearly unacceptable. This is due to the considerable amount of computation involved and the fact that the optimum basis would in general differ for different images and quantization schemes. Thus, for a given image or image ensemble and a specified quantization scheme, an efficient algorithm for determining the optimum basis (in the mean-square error sense) must be found.

3.5.2 Determination of The Optimum NPT Basis [35]

The objective of an NPT coder is to employ the basis or the collection of bases giving minimum MSE for transform coding of a given image or image ensemble. In other words, the NPT image coder must be able to efficiently select a basis different from that given by $\alpha = 0$ when the image statistics dictate. Here, we specify an objective function which is subsequently minimized to yield the optimum basis.

We denote the spatial domain error array (obtained by forming the difference between the original image $\mathbf{F}$ and its coded version $\hat{\mathbf{F}}$) resulting from transform coding an image with the NPT basis specified by α, for a given bit rate and quantization scheme by $\mathbf{E}_S(\alpha, \theta)$. Similarly, we denote the transform domain error array (obtained by forming the difference between the transform coefficients of the original image and their coded version) by $\mathbf{E}_T(\alpha, \theta)$; in both cases, θ is a parameter specifying the dependence on bit rate and quantization scheme. We seek an optimum basis α_{opt} for transform coding such that

$$\alpha_{opt} = \min_{\alpha} \left[E \left\{ ||\mathbf{E}_S(\alpha, \theta)||^2 \right\} \right] \tag{3.7a}$$

or equivalently,

$$\alpha_{opt} = \max_{\alpha} \left[E \left\{ ||\mathbf{E}_S(0, \theta)||^2 \right\} - E \left\{ ||\mathbf{E}_S(\alpha, \theta)||^2 \right\} \right] \tag{3.7b}$$

where $E\{\cdot\}$ is the mathematical expectation operator. In the following development, we derive an explicit functional expression for the objective function given by (3.7).

The error arrays $\mathbf{E}_S(\alpha,\theta)$ and $\mathbf{E}_T(\alpha,\theta)$ satisfy the relation

$$\mathbf{E}_S(\alpha,\theta) = \psi^{-1}\{\alpha\}\,\mathbf{E}_T(\alpha,\theta)\psi^{-1}\{\alpha\} \tag{3.8}$$

from which it follows that

$$E\left\{||\mathbf{E}_S(\alpha,\theta)||^2\right\} = E\left\{||\psi^{-1}\{\alpha\}\,\mathbf{E}_T(\alpha,\theta)\psi^{-1}\{\alpha\}\,||^2\right\} \tag{3.9}$$

Applying Schwartz inequality to (3.9), we obtain

$$E\left\{||\mathbf{E}_S(\alpha,\theta)||^2\right\} \leq ||\psi^{-1}\{\alpha\}\,||^4 \cdot E\left\{||\mathbf{E}_T(\alpha,\theta)||^2\right\} \tag{3.10}$$

We can write

$$E\left\{||\mathbf{E}_S(\alpha,\theta)||^2\right\} = c(\alpha,\theta) \cdot ||\psi^{-1}\{\alpha\}\,||^4 \cdot E\left\{||\mathbf{E}_T(\alpha,\theta)||^2\right\} \tag{3.11}$$

where $c(\alpha,\theta)$ is a function which establishes the equality of (3.10) for all values of α, for a given bit rate and quantization scheme. Making use of the fact that

$$E\left\{||\mathbf{E}_S(0,\theta)||^2\right\} = E\left\{||\mathbf{E}_T(0,\theta)||^2\right\} \tag{3.12}$$

we define

$$c(\alpha,\theta) = b_0 \cdot b(\alpha,\theta) \tag{3.13}$$

where $c(\alpha,\theta) = b(\alpha,\theta) = 1$ when $\alpha = 0$ or $\alpha = 1$. Using (3.13) in (3.11), we obtain

$$b_0 = \frac{1}{||\psi^{-1}\{0\}\,||^4} \tag{3.14}$$

and (3.11) becomes

$$E\left\{||\mathbf{E}_S(\alpha,\theta)||^2\right\} = b(\alpha,\theta) \cdot \frac{||\psi^{-1}\{\alpha\}\,||^4}{||\psi^{-1}\{0\}\,||^4} \cdot E\left\{||\mathbf{E}_T(\alpha,\theta)||^2\right\} \tag{3.15}$$

$$= d(\alpha,\theta) \cdot E\left\{||\mathbf{E}_T(\alpha,\theta)||^2\right\} \tag{3.16}$$

where

$$d(\alpha,\theta) = b(\alpha,\theta) \cdot \frac{||\psi^{-1}\{\alpha\}\,||^4}{||\psi^{-1}\{0\}\,||^4} \tag{3.17}$$

Thus, for a given bit rate and quantization scheme $d(\alpha,\theta)$ is the ratio of the spatial domain MSE to the transform domain MSE at the various values of α and the term $\frac{||\psi^{-1}\{\alpha\}||^4}{||\psi^{-1}\{0\}||^4}$ appearing in (3.15) is a prediction of $d(\alpha,\theta)$; $b(\alpha,\theta)$ is an empirically determined correction factor which accounts for the difference between $d(\alpha,\theta)$ and the prediction given by the norm ratio $\frac{||\psi^{-1}\{\alpha\}||^4}{||\psi^{-1}\{0\}||^4}$. In practice, a suitable representative function for $b(\alpha,\theta)$ would have to be determined for the class of images to be coded. Using (3.15) with our objective function (3.7), we see that
$\alpha_{opt} \neq 0$ iff

$$E\left\{||\mathbf{E}_S(0,\theta)||^2\right\} > b(\alpha,\theta) \cdot \frac{||\psi^{-1}\{\alpha\}\,||^4}{||\psi^{-1}\{0\}\,||^4} \cdot E\left\{||\mathbf{E}_T(\alpha,\theta)||^2\right\} \tag{3.18}$$

The remaining part of our objective function that needs to be specified functionally is the transform domain MSE, $E\left\{||\mathbf{E}_T(\alpha,\theta)||^2\right\}$, which we derive in the following.

The transform domain MSE is given by

$$E\left\{||\mathbf{E}_T(\alpha,\theta)||^2\right\} = \sum_{i=1}^{p}\sum_{j=1}^{p}\sigma^2(i,j;\alpha)\,e(q(i,j;\alpha)) \tag{3.19}$$

where

p = image sub-block size

$\sigma^2(i,j;\alpha)$ = variance of transform coefficients at location (i,j) in the $p \times p$ sub-blocks when the NPT basis given by α is used.

$e(q)$ = quantizer distortion function (MSE for a unit variance signal quantized with a q-level quantizer).

$q(i,j;\alpha)$ = number of quantizer levels used for the transform coefficients at location (i,j) in the $p \times p$ sub-blocks when the NPT basis given by α is used.

The variance of the transform coefficients at location (i,j) within the sub-blocks of the image is found by regarding the (i,j) transform coefficients as sequences of random variables and measuring the variance over the ensemble of sub-blocks, see Fig 3.2. We denote the transform of sub-blocks of the image $\mathbf{F}$ by $\mathbf{T}_{\mathbf{F}_s}$, where $\mathbf{F}_s$ denote the sub-blocks of $\mathbf{F}$. The variance of the (i,j) transform coefficient at a given value of α is given by

$$\sigma^2(i,j;\alpha) = E\left\{\left[\mathbf{T}_{\mathbf{F}_s}(i,j;\alpha)\right]^2\right\} - [\mu(i,j;\alpha)]^2 \qquad 1 \le i,j \le p \tag{3.20}$$

where $\mu(i,j;\alpha)$ is the mean of the (i,j) transform coefficient sequence and is given by

$$\mu(i,j;\alpha) = E\left\{\left[\mathbf{T}_{\mathbf{F}_s}(i,j;\alpha)\right]\right\} \qquad 1 \le i,j \le p \tag{3.21}$$

Using the notation of Fig. 3.2, we can express (3.20) as

$$\sigma^2(i,j;\alpha) = \frac{1}{n_T \times n_T}\sum_{KI=1}^{n_T}\sum_{KJ=1}^{n_T}\left[\mathbf{T}_{\mathbf{F}_s}\Big((KI-1)p+i),(KJ-1)p+j);\alpha\Big)\right]^2 - \left[\mu(i,j;\alpha)\right]^2 \qquad 1 \le i,j \le p \tag{3.22}$$

and

$$\mu(i,j;\alpha) = \frac{1}{n_T \times n_T}\sum_{KI=1}^{n_T}\sum_{KJ=1}^{n_T}\mathbf{T}_{\mathbf{F}_s}\Big((KI-1)p+i),(KJ-1)p+j);\alpha\Big) \qquad 1 \le i,j \le p \tag{3.23}$$

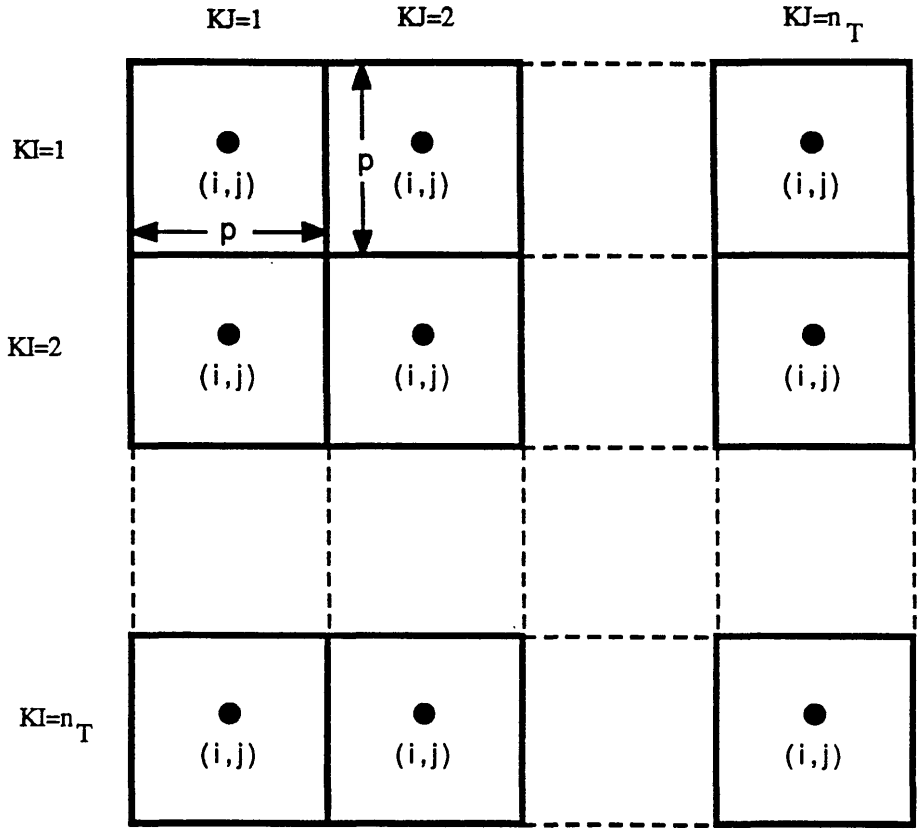


Fig. 3.2 : Notation for The (i,j) Transform Coefficients of The Sub-blocks of Image **F.**

The variance array $\sigma^2(i,j;\alpha)$ and mean array $\mu(i,j;\alpha)$ are dependent on α and we determine explicit expressions for these in terms of α by considering the components of the two-dimensional NPT of an image. We recall from chapter two that this is given by

$$\mathbf{T_F} = \alpha^2\mathbf{F} + k\alpha(1-\alpha)\left[\mathbf{FA} + \mathbf{AF}\right] + k^2(1-\alpha)^2\mathbf{AFA} \tag{3.24a}$$

$$= \alpha^2\mathbf{F} + k\alpha(1-\alpha)\mathbf{X} + k^2(1-\alpha)^2\mathbf{Y} \tag{3.24b}$$

where

$$\mathbf{X} = \mathbf{FA} + \mathbf{AF} \tag{3.24c}$$

and

$$\mathbf{Y} = \mathbf{AFA} \tag{3.24d}$$

, $\mathbf{A}$ is the component orthogonal transform kernel and $\mathbf{F}$ is the image array. Thus, the (i,j) transform coefficients of sub-blocks of $\mathbf{F}$ are given by

$$\mathbf{T_{F_s}}(i,j;\alpha) = \alpha^2\mathbf{F}_s(i,j) + k\alpha(1-\alpha)\mathbf{X}_s(i,j) + k^2(1-\alpha)^2\mathbf{Y}_s(i,j) \tag{3.25}$$

For future use, we adopt the following notation for the mean and covariance (variance) of the (i,j) coefficients of the component arrays in the two-dimensional NPT of $\mathbf{F}$ (refer to (3.24)),

$$\mu_{\mathbf{R}} = E\left\{\mathbf{R}_s(i,j)\right\} \qquad 1 \le i,j \le p \tag{3.26}$$

is the mean array of the (i,j) elements in the sub-blocks of array $\mathbf{R}$ and

$$\sigma^2_{\mathbf{RV}} = E\left\{\mathbf{R}_s(i,j)\mathbf{V}_s(i,j)\right\} - \mu_{\mathbf{R}}\mu_{\mathbf{V}} \quad 1 \le i,j \le p \tag{3.27}$$

is the array of the covariances between the (i,j) elements in the sub-blocks of arrays $\mathbf{R}$ and $\mathbf{V}$. Thus, when $\mathbf{R} = \mathbf{V}$, (3.27) gives the variance, $\sigma^2_{\mathbf{RR}}$, of the (i,j) elements in the sub-blocks of the array $\mathbf{R}$. Dropping the (i,j) indices on the right hand side of (3.25), we write

$$\mathbf{T_{F_s}}(i,j;\alpha) = \gamma_0\mathbf{F}_s + \gamma_1\mathbf{X}_s + \gamma_2\mathbf{Y}_s \tag{3.28}$$

where

$$\gamma_0 = \alpha^2 \tag{3.29a}$$

$$\gamma_1 = k\alpha(1-\alpha) \tag{3.29b}$$

$$\gamma_2 = k^2(1-\alpha)^2 \tag{3.29c}$$

Using (3.28) in (3.21), we have

$$\mu(i,j;\alpha) = E\{\gamma_0 \mathbf{F}_s + \gamma_1 \mathbf{X}_s + \gamma_2 \mathbf{Y}_s\} \tag{3.30a}$$

$$= \gamma_0 E\{\mathbf{F}_s\} + \gamma_1 E\{\mathbf{X}_s\} + \gamma_2 E\{\mathbf{Y}_s\} \tag{3.30b}$$

$$= \gamma_0 \mu_{\mathbf{F}} + \gamma_1 \mu_{\mathbf{X}} + \gamma_2 \mu_{\mathbf{Y}} \tag{3.30c}$$

Substituting the values of γ_0, γ_1 and γ_2 from (3.29$a-c$), we obtain

$$\mu(i,j;\alpha) = \left(\mu_{\mathbf{F}} - k\mu_{\mathbf{X}} + k^2\mu_{\mathbf{Y}}\right)\alpha^2 + \left(k\mu_{\mathbf{X}} - 2k^2\mu_{\mathbf{Y}}\right)\alpha + k^2\mu_{\mathbf{Y}} \tag{3.31}$$

which is a second order polynomial in α with coefficients which depend on the image statistics and the classical orthogonal transform used in the NPT kernel.

$$E\left\{[\mathbf{T}_{\mathbf{F}_s}(i,j;\alpha)]^2\right\} = E\left\{\left(\gamma_0 \mathbf{F}_s + \gamma_1 \mathbf{X}_s + \gamma_2 \mathbf{Y}_s\right)^2\right\} \tag{3.32a}$$

$$= \gamma_0^2 E\{\mathbf{F}_s^2\} + \gamma_1^2 E\{\mathbf{X}_s^2\} + \gamma_2^2 E\{\mathbf{Y}_s^2\} + 2\gamma_0\gamma_1 E\{\mathbf{F}_s\mathbf{X}_s\}$$
$$+ 2\gamma_0\gamma_2 E\{\mathbf{F}_s\mathbf{Y}_s\} + 2\gamma_1\gamma_2 E\{\mathbf{X}_s\mathbf{Y}_s\} \tag{3.32b}$$

$$[\mu(i,j;\alpha)]^2 = \left(\gamma_0\mu_{\mathbf{F}} + \gamma_1\mu_{\mathbf{X}} + \gamma_2\mu_{\mathbf{Y}}\right)^2 \tag{3.33a}$$

$$= \gamma_0^2\mu_{\mathbf{F}}^2 + \gamma_1^2\mu_{\mathbf{X}}^2 + \gamma_2^2\mu_{\mathbf{Y}}^2 + 2\gamma_0\gamma_1\mu_{\mathbf{F}}\mu_{\mathbf{X}}$$
$$+ 2\gamma_0\gamma_2\mu_{\mathbf{F}}\mu_{\mathbf{Y}} + 2\gamma_1\gamma_2\mu_{\mathbf{X}}\mu_{\mathbf{Y}} \tag{3.33b}$$

Using (3.32b) and (3.33b) in (3.20), we obtain

$$\sigma^2(i,j;\alpha) = \gamma_0^2\left(E\{\mathbf{F}_s^2\} - \mu_{\mathbf{F}}^2\right) + \gamma_1^2\left(E\{\mathbf{X}_s^2\} - \mu_{\mathbf{X}}^2\right) + \gamma_2^2\left(E\{\mathbf{Y}_s^2\} - \mu_{\mathbf{Y}}^2\right)$$
$$+ 2\gamma_0\gamma_1\left(E\{\mathbf{F}_s\mathbf{X}_s\} - \mu_{\mathbf{F}}\mu_{\mathbf{X}}\right) + 2\gamma_0\gamma_2\left(E\{\mathbf{F}_s\mathbf{Y}_s\} - \mu_{\mathbf{F}}\mu_{\mathbf{Y}}\right)$$
$$+ 2\gamma_1\gamma_2\left(E\{\mathbf{X}_s\mathbf{Y}_s\} - \mu_{\mathbf{X}}\mu_{\mathbf{Y}}\right) \tag{3.34}$$

and based on the notation of (3.27), we write

$$\sigma^2(i,j;\alpha) = \gamma_0^2\sigma_{\mathbf{FF}}^2 + \gamma_1^2\sigma_{\mathbf{XX}}^2 + \gamma_2^2\sigma_{\mathbf{YY}}^2$$
$$+ 2\gamma_0\gamma_1\sigma_{\mathbf{FX}}^2 + 2\gamma_0\gamma_2\sigma_{\mathbf{FY}}^2 + 2\gamma_1\gamma_2\sigma_{\mathbf{XY}}^2 \tag{3.35}$$

Substituting the values of γ_0, γ_1 and γ_2 from (3.29$a-c$) into (3.35) and collecting terms of the same power in α, we obtain

$$\sigma^2(i,j;\alpha) = k^4\sigma_{\mathbf{YY}}^2 + \left(2k^3\sigma_{\mathbf{XY}}^2 - 4k^4\sigma_{\mathbf{YY}}^2\right)\alpha$$
$$+ \left(k^2\sigma_{\mathbf{XX}}^2 + 6k^4\sigma_{\mathbf{YY}}^2 + 2k^2\sigma_{\mathbf{FY}}^2 - 6k^3\sigma_{\mathbf{XY}}^2\right)\alpha^2$$
$$+ \left(2k\sigma_{\mathbf{FX}}^2 + 6k^3\sigma_{\mathbf{XY}}^2 - 2k^2\sigma_{\mathbf{XX}}^2 - 4k^4\sigma_{\mathbf{YY}}^2 - 4k^2\sigma_{\mathbf{FY}}^2\right)\alpha^3$$
$$+ \left(\sigma_{\mathbf{FF}}^2 + k^2\sigma_{\mathbf{XX}}^2 + k^4\sigma_{\mathbf{YY}}^2 + 2k^2\sigma_{\mathbf{FY}}^2 - 2k\sigma_{\mathbf{FX}}^2 - 2k^3\sigma_{\mathbf{XY}}^2\right)\alpha^4 \tag{3.36}$$

which can be written as

$$\sigma^2(i,j;\alpha) = \mathbf{G}_0(i,j) + \mathbf{G}_1(i,j)\alpha + \mathbf{G}_2(i,j)\alpha^2 + \mathbf{G}_3(i,j)\alpha^3 + \mathbf{G}_4(i,j)\alpha^4 \tag{3.37}$$

where

$$\mathbf{G}_0(i,j) = k^4\sigma^2_{\mathbf{YY}} \tag{3.38a}$$

$$\mathbf{G}_1(i,j) = 2k^3\sigma^2_{\mathbf{XY}} - 4k^4\sigma^2_{\mathbf{YY}} \tag{3.38b}$$

$$\mathbf{G}_2(i,j) = k^2\sigma^2_{\mathbf{XX}} + 6k^4\sigma^2_{\mathbf{YY}} + 2k^2\sigma^2_{\mathbf{FY}} - 6k^3\sigma^2_{\mathbf{XY}} \tag{3.38c}$$

$$\mathbf{G}_3(i,j) = 2k\sigma^2_{\mathbf{FX}} + 6k^3\sigma^2_{\mathbf{XY}} - 2k^2\sigma^2_{\mathbf{XX}} - 4k^4\sigma^2_{\mathbf{YY}} - 4k^2\sigma^2_{\mathbf{FY}} \tag{3.38d}$$

$$\mathbf{G}_4(i,j) = \sigma^2_{\mathbf{FF}} + k^2\sigma^2_{\mathbf{XX}} + k^4\sigma^2_{\mathbf{YY}} + 2k^2\sigma^2_{\mathbf{FY}} - 2k\sigma^2_{\mathbf{FX}} - 2k^3\sigma^2_{\mathbf{XY}} \tag{3.38e}$$

We note that the variance of the (i,j) NPT transform samples given by (3.37) is a fourth order polynomial in α whose coefficients $\mathbf{G}_t(i,j)$, $t = 0, 1, \ldots 4$ vary with image statistics and the classical orthogonal transform employed. Thus, for a given image and given classical transform, (3.37) is a fourth order polynomial in α with constant coefficients $\mathbf{G}_t(i,j)$, $t = 0, 1, \ldots 4$. Hence, we refer to the $\mathbf{G}_t(i,j)$, $t = 0, 1, \ldots 4$ as the *"two-dimensional NPT statistic functions"* since they are primarily determined by the statistics of the image. Substituting (3.37) into (3.19), we obtain the transform domain MSE as

$$E\left\{||\mathbf{E_T}(\alpha,\theta)||^2\right\} = d_0 + d_1\alpha + d_2\alpha^2 + d_3\alpha^3 + d_4\alpha^4 \tag{3.39}$$

where

$$d_t = \sum_{i=1}^{p}\sum_{j=1}^{p} \mathbf{G}_t(i,j)e\left(q(i,j;\alpha)\right), \quad t = 0, 1, \ldots 4 \tag{3.40}$$

which is a fourth order polynomial in α whose coefficients d_t, $t = 0, 1, \ldots 4$ are a summation of the respective NPT statistic weighted distortion functions. The distortion functions $e\left(q\left(i,j;\alpha\right)\right)$ in (3.40) are constants which depend on the number of bits assigned to the (i,j) transform coefficients and the quantizer used. From (3.36), we observe that an identical functional relationship holds for the variation of the variance of each (i,j) transform sample with α. Furthermore, for $k = 1$ and $|\alpha| << 1$, the contribution to the variance due to the terms in α^2 and higher powers would be negligible [1] and the magnitude of the variances of the transform samples in relation to one another will not change as α is varied. By assigning bits in

[1] It should be noted that if the (i,j) entries of $\mathbf{F}_s$, $\mathbf{X}_s$ and $\mathbf{Y}_s$ are mutually uncorrelated, the cross-variance terms in (3.36) become zero. In practice, one would expect any mutual correlation between the corresponding (i,j) entries of $\mathbf{F}_s$, $\mathbf{X}_s$ and $\mathbf{Y}_s$ to be very small due to the decorrelation properties of classical orthogonal transforms and their contribution to the overall variance can be neglected.

proportion to the variance of the transform samples, the bit assignment will not change very much with α and it need not be re-determined as α is varied. Hence, (3.39) becomes a fourth order polynomial in α with constant coefficients.

Substituting (3.39) into (3.15), we obtain the functional expression for the spatial domain MSE as

$$E\left\{||\mathbf{E}_S(\alpha,\theta)||^2\right\} = b(\alpha,\theta)\cdot\frac{||\psi^{-1}\{\alpha\}||^4}{||\psi^{-1}\{0\}||^4}\cdot(d_0+d_1\alpha+d_2\alpha^2+d_3\alpha^3+d_4\alpha^4) \tag{3.41}$$

$$= b(\alpha,\theta)\cdot\frac{\left[\alpha^2+k^2(1-\alpha)^2\right]^2}{\left[\alpha^2-k^2(1-\alpha)^2\right]^4}\cdot(d_0+d_1\alpha+d_2\alpha^2+d_3\alpha^3+d_4\alpha^4) \tag{3.42}$$

As stated earlier, $b(\alpha,\theta)$ is an empirically determined correction function. Once representative functions for the classes of images to be coded have been obtained, all the terms of (3.42) are completely specified and the optimum basis can be determined by numerically minimizing (3.42) with respect to α. Suitable algorithms for solving (3.42) can be found in [38,39].

3.5.3 Simulation, Results and Discussion of Non-Adaptive NPT Image Coding

A variety of simulations was conducted in order to investigate various aspects of NPT image coding. In the simulations, $p \times p$ small-size partitions of 256×256 monochrome images were NPT transformed. Bit allocation and quantization was carried out within the framework of conventional transform coding techniques. Details of these investigations are described in the following sub-sections.

3.5.3.1 Bit Allocation

A computational approach of bit assignment [20,40] which is based on the marginal analysis technique [41] was adopted for allocating coding bits $b_{i,j}$ to the (i,j) transform sample within the $p \times p$ NPT transformed sub-blocks. In this approach, the total number of available bits are allocated to the transformed samples on a bit - by - bit basis. The procedure is briefly described in the following.

We represent the accumulated number of bits assigned to the (i,j) transform sample at the instance of assigning the m^{th} bit by $b_{i,j}^m$. Initially, we set $m=1$ and $b_{i,j}^m = 0$ for $i,j = 1,2,\ldots p$. Subsequently, the marginal returns defined by

$$\Delta_{i,j} = \sigma^2(i,j;\alpha)\left[e\left(b_{i,j}^{m-1}\right) - e\left(b_{i,j}^{m-1}+1\right)\right] \tag{3.43}$$

are calculated for all (i,j) transform samples, where $\sigma^2(i,j;\alpha)$ is the variance of the (i,j) transform sample when the NPT basis specified by α is used and $e(b)$ is the mean square quantization error of a b-bit quantizer, for a unit variance source. One bit is then allocated to the sample having the largest marginal return and the counter m is incremented by 1. The procedure is repeated until all the available bits have been allocated.

Other bit assignment procedures are reported in [42,43,44] but these have the drawback that the optimally assigned bits are not necessarily integers and may even be negative. Rounding off to the nearest positive integer or zero is then required, which may lead to the total number of bits assigned becoming greater than the total number of available bits. In the event of this, the bit allocation is then adjusted, usually in an arbitrary fashion, until the required number of available bits is achieved, which may offset the optimality of the bit assignment. These approaches are inferior to the computational approach described above since in the latter case, there is is no roundoff error in bit assignment. Furthermore, the assumption of a shannon quantizer is implicit in the procedures described in [43] and [44], but in practice, it is the pdf-optimized quantizers that are used and this is not accounted for in these bit assignment algorithms. The effect of non-shannon quantization error can be easily incorporated into the computational approach by replacing the shannon quantization error with the quantization error of the pdf-optimized quantizer, in the marginal returns calculation; it has been shown [45] that this leads to a superior performance for block quantization schemes. The main drawback of the computational approach is its computational load, however, a fast algorithm described in [45] reduces the amount of computation considerably and this was used in the simulations.

3.5.3.2 Variation of The Mean-square Error of NPT Image Coding With Transform Basis

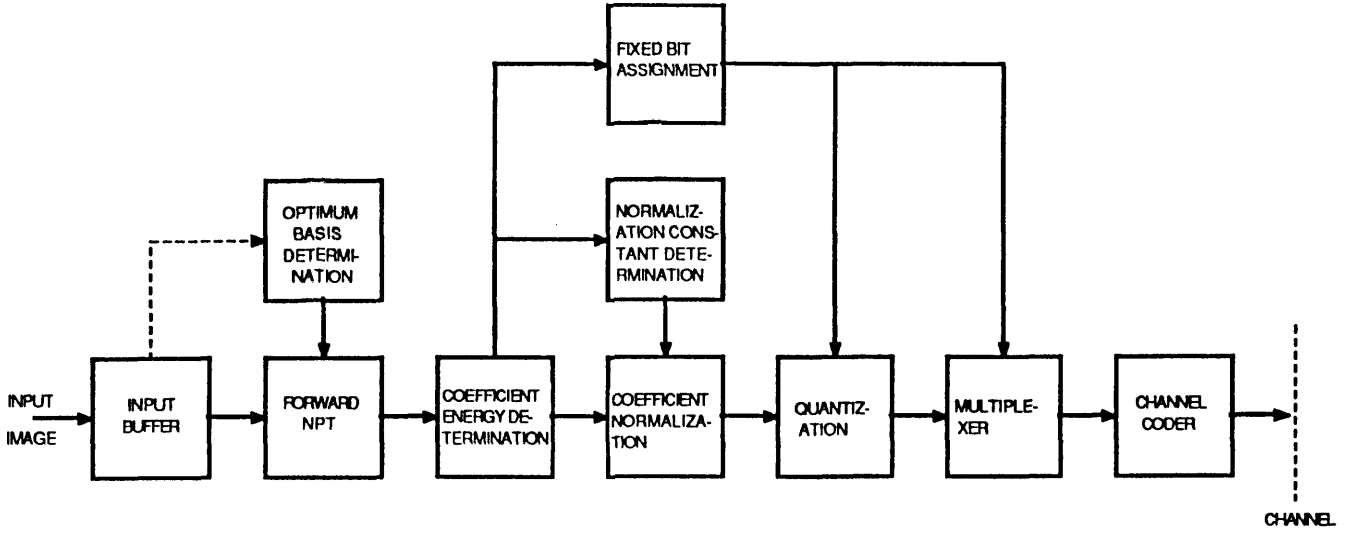
In chapter two, we specified the range of values of the transform basis parameter α to be $|\alpha| \leq 1$. As we stated earlier in section 3.5.2, the objective of an NPT image coder is to employ the basis or the collection of bases giving minimum MSE for coding an image or image ensemble. Thus, a good understanding of the MSE behaviour as a function of the transform basis is necessary in order to facilitate the determination of the optimum basis for coding an image or image ensemble.

Specifically, a knowledge of the possible range of values of α at which the minimum MSE can be located would permit a faster determination of the optimum basis.

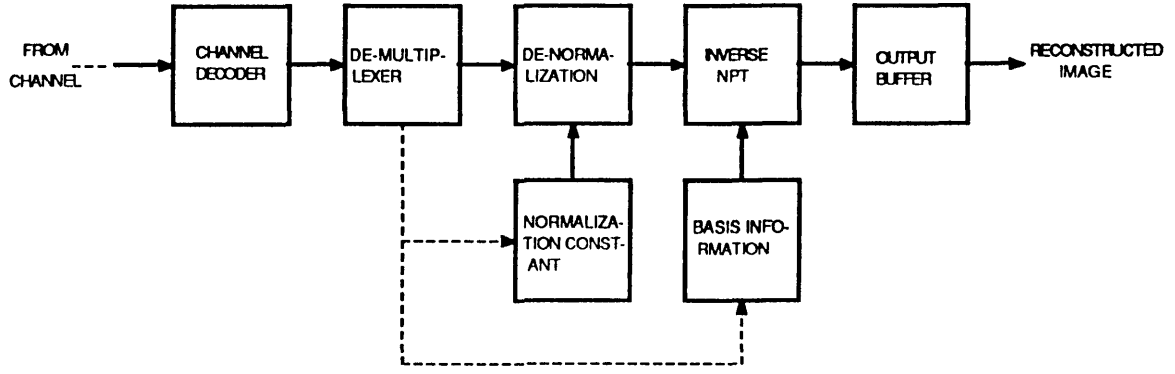
An experimental investigation was conducted in which a number of monochrome images were coded at various bit rates using a non-adaptive NPT image coder, the block diagram of which is shown in Fig. 3.3; the NPT transforms used are the Hadamard NPT, the sine NPT and the SC NPT. Since each NPT sample in a block is obtained by a linear summation of all the pixel values within the original image sub-block, the central limit theorem [46] indicates that the probability density of the transform coefficients can be modelled approximately by a Gaussian distribution; hence an optimum Gaussian Max [47] quantizer was used for quantizing the transform coefficients. Based on these investigations, it was found that the minimum MSE is generally obtained at a value of α lying within the range $|\alpha| \leq 0.2$. Hence, only these values of α would be considered in our further investigations.

The errors in a transform coding operation are due to coefficient deletion, coefficient quantization, finite computational accuracy and errors introduced into the channel or storage medium. As mentioned in section 3.4, errorless transmission through the channel can be achieved in practice and we shall ignore the effect of this in the present investigation. We shall also assume that the transform coefficients are held to a very high degree of accuracy and ignore the errors due to finite computational accuracy. For the NPT, there is an additional source of error and this is due to inverse transformation. We showed in section 3.5.2 that the effect of this error manifests as a factor multiplying the transform domain MSE during inverse transformation. Thus, it is desirable in NPT image coding to reduce the transform domain MSE as much as possible.

The mean and variance arrays at three values of α viz $\alpha = -0.1$, $\alpha = 0$ and $\alpha = 0.1$ for the 4×4 Hadamard NPT transformed image ALAN (the original image is shown in Fig. 2.7) are shown in Tables 3.1a-b, Tables 3.2a-b and Tables 3.3a-b respectively. We can observe that there is some energy residing in the mean of the 'AC' transform coefficients, especially for $\alpha \neq 0$; the magnitude of this energy increases as α is increased or decreased from zero. Furthermore, the symmetry of the NPT kernel gives rise to some structure in the mean array. The deletion



(a)



(b)

Fig. 3.3 : Non-Adaptive NPT Coding of Images; (a) Coder and (b) Decoder.

of an 'AC' transform coefficient increases the error incurred in the transform domain by the variance of the transform coefficient as well as by its mean energy.

Table 3.1a : Mean Array For The 4 x 4 Hadamard NPT Transformed Image ALAN, $\alpha = -0.1$.

860.175	-14.2853	-42.115	-41.460
-40.692	1.951	2.004	1.973
-40.839	1.949	2.017	1.948
-41.194	1.981	2.022	1.992

Table 3.1b : Variance Array For The 4 x 4 Hadamard NPT Transformed Image ALAN, $\alpha = -0.1$.

37279.938	506.428	242.697	293.094
963.386	54.972	10.472	18.236
315.190	27.808	5.822	8.713
318.475	16.189	3.904	5.624

Table 3.2a : Mean Array For The 4 x 4 Hadamard NPT Transformed Image ALAN, $\alpha = 0$.

780.131	-0.231	-0.968	-0.449
0.251	-0.002	0.009	0.010
0.081	-0.009	0.013	-0.015
-0.200	0.003	0.004	0.004

Table 3.2b : Variance Array For The 4 x 4 Hadamard NPT Transformed Image ALAN, $\alpha = 0$.

30614.500	306.593	100.772	129.413
687.037	39.364	3.996	8.807
132.320	15.998	2.039	3.387
135.313	8.389	1.203	1.899

Table 3.3a : Mean Array For The 4 x 4 Hadamard NPT Transformed Image ALAN, $\alpha = 0.1$.

703.998	36.915	36.266	36.659
37.285	1.952	1.928	1.951
37.096	1.938	1.920	1.922
36.883	1.936	1.903	1.922

Table 3.3b : Variance Array For The 4 x 4 Hadamard NPT Transformed Image ALAN, $\alpha = 0.1$.

24890.938	285.545	128.538	142.486
600.192	31.968	3.307	6.165
134.315	10.112	1.202	1.805
136.735	5.392	0.958	1.231

We can observe from the mean arrays shown in Tables 3.1-3.3 that the contribution of the mean energy to the transform domain error and consequently the spatial domain error, would increase as α is increased or decreased from zero. Based on empirical investigations, we found that the contribution of this error to the overall MSE resulting from the transform coding operation can be reduced by

replacing a deleted coefficient by its mean value. For example, at $\alpha = 0.1$, for 4×4 Hadamard NPT coding of image ALAN at 1.5 bits/pixel, using the optimum Gaussian Max quantizer, an MSE of 31.46 was obtained. However, when deleted transform coefficients were replaced by their mean values at the receiver, an MSE of 27.983 was obtained. The bit assignment for the transform coefficients is shown in Table 3.4.

Table 3.4 : Bit Assignment For The 4×4 Hadamard NPT Transformed Image ALAN, Rate = 1.5 bits/pixel, $\alpha = 0.1$			
7	3	2	3
4	1	0	0
2	0	0	0
2	0	0	0

An interesting result of the experiments is that the mean of the 'AC' coefficients do not need to be known accurately. Thus, we can exploit the structure in the mean array in order to reduce the number of bits for transmitting the mean information. We found that replacing the respective means of the 'AC' coefficients along the first row and column of the mean array by their average value and the respective means of the remaining 'AC' coefficients by their average value provides a very good approximation of the mean of the 'AC' coefficients, with a negligible increase in MSE. In this way, only two values are used to represent the mean of the 'AC' coefficients instead of fifteen. For the 4×4 Hadamard NPT coding of image ALAN, an MSE of 27.98311 was obtained by using the approximation of the mean of the 'AC' coefficients instead of the actual mean values; the MSE value is practically the same as when the actual mean values were used.

In Fig. 3.4a, both the transform domain MSE and the spatial domain MSE resulting from the 4×4 Hadamard NPT coding of image ALAN (the original image is shown in Fig. 2.7) at a bit rate of 1.5 bits/pixel, using a block size of 4 and optimum Gaussian Max quantization of the transform samples, is plotted as a function of α. From the plot, we observe that for $\alpha < 0.0$, the spatial domain MSE is less than the transform domain MSE. This is a consequence of the Euclidean norm properties of the NPT which was dealt with in chapter two. The minimum

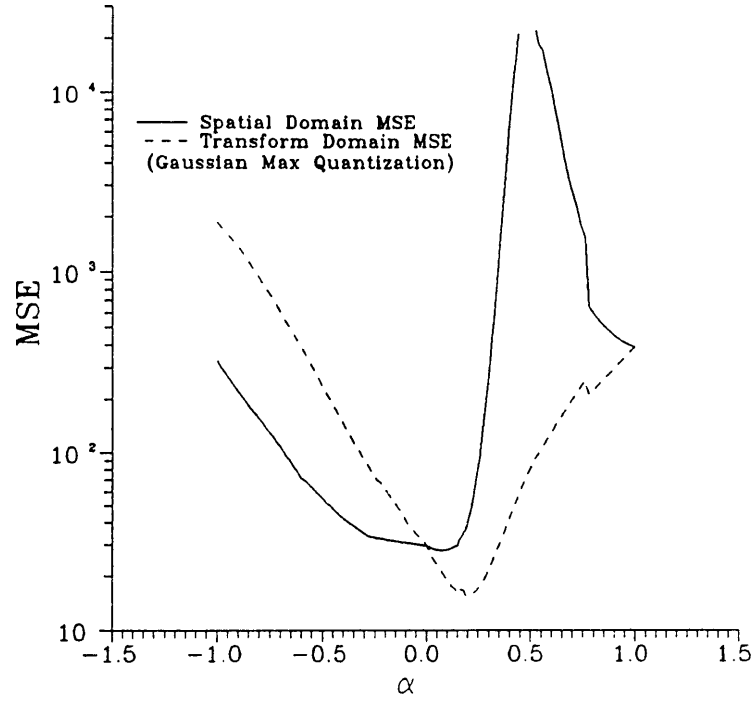


Fig. 3.4a : Spatial and Transform domain MSE as a function of α; Hadamard NPT coding of image ALAN at 1.5 Bits/pixel, using a block size of 4.

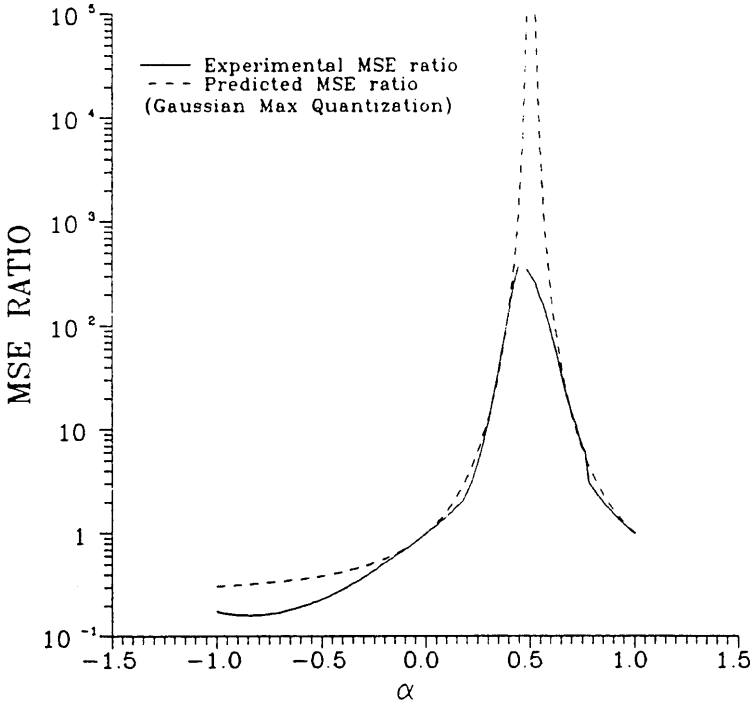


Fig. 3.4b : Experimental and Predicted Spatial/Transform domain MSE ratio as a function of α; Hadamard NPT coding of image ALAN at 1.5 bits/pixel, using a block size of 4.

spatial domain MSE is obtained at approximately $\alpha = 0.07$, while the minimum of the transform domain MSE is obtained at $\alpha = 0.2$; however, a higher overall spatial domain MSE is obtained at $\alpha = 0.2$ due to the transform domain MSE being increased by a higher factor during the inverse NPT transformation. It was shown in section 3.5.2 that the spatial domain MSE and the transform domain MSE are related by a multiplicative factor which is proportional to the fourth power of the ratio of the norm of the inverse NPT to the norm of an orthogonal transform. In Fig. 3.4b, the ratio of the spatial domain MSE to the transform domain MSE is plotted as a function of α, for the Hadamard NPT coding of image ALAN at a bit rate of 1.5 bits/pixel, using a block size of 4 and optimum Gaussian Max quantization of the transform samples. The prediction of this ratio given by the norm ratio $\frac{||\psi^{-1}\{\alpha\}||^4}{||\psi^{-1}\{0\}||^4}$ appearing in the right hand side of (3.15) is also plotted. We can observe that the prediction given by the norm ratio is very good for the values of α approximately in the ranges $-0.15 \leq \alpha \leq 0.05$, $0.28 < \alpha < 0.45$ and $0.65 < \alpha < 0.75$. As we pointed out earlier, an empirically determined correction factor would need to be applied in order to correct the prediction of the Spatial/Transform domain MSE ratio, given by the norm ratio. The sine NPT and the SC NPT show a similar behaviour.

In the following section, we investigate the form of the correction factor applicable for the transform bases in the range $|\alpha| \leq 0.2$, as well as its dependence on various parameters of importance in NPT image coding such as bit rate, block size, image content, quantization scheme and the type of NPT transform used.

3.5.3.3 Investigations on NPT Image Coding Correction Factor

1) Variation of The Correction Factor with Bit Rate

The image ALAN was coded at various bit rates, for a given NPT transform type, given block size and optimum Gaussian Max quantization scheme, for values of α in the range $|\alpha| \leq 0.2$. Fig. 3.5a shows the ratio of the spatial domain MSE to the transform domain MSE at bit rates of 0.5, 1.0, 1.5 and 2.0 bits/pixel respectively, for the 4×4 Hadamard NPT coding of image ALAN. The prediction given by the norm ratio is also plotted. We observe that the prediction given by the norm ratio is only markedly different from the experimental values for $\alpha > 0.04$. A slight increase in the MSE ratio with bit rate can be observed when $\alpha > 0.0$ while a slight decrease in MSE ratio with bit rate can be observed when $\alpha < 0.0$. The corresponding correction factors as a function of α are shown in Fig. 3.5b. We observe

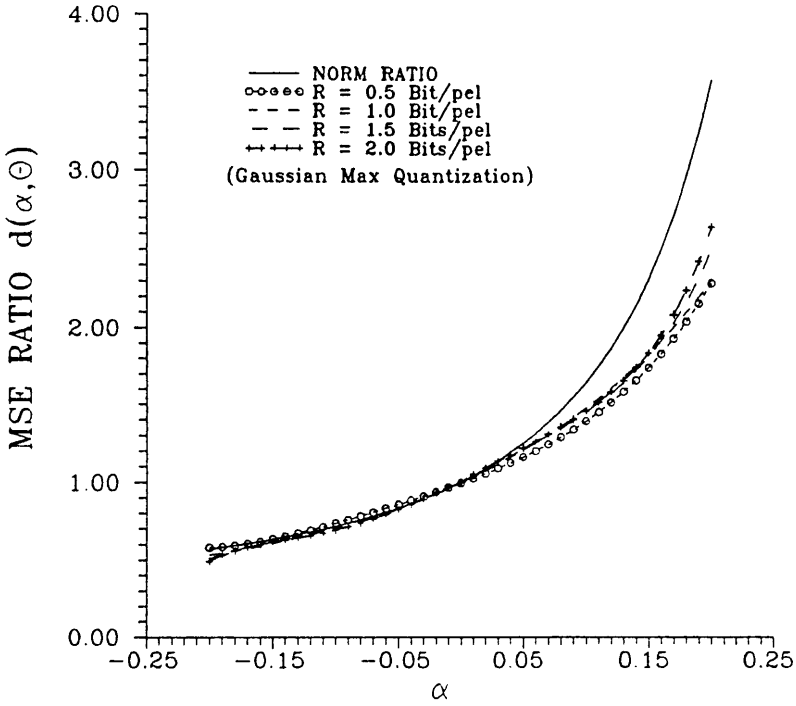


Fig. 3.5a : Spatial/Transform domain MSE ratio as a function of α ; 4 x 4 Hadamard NPT coding of image ALAN.

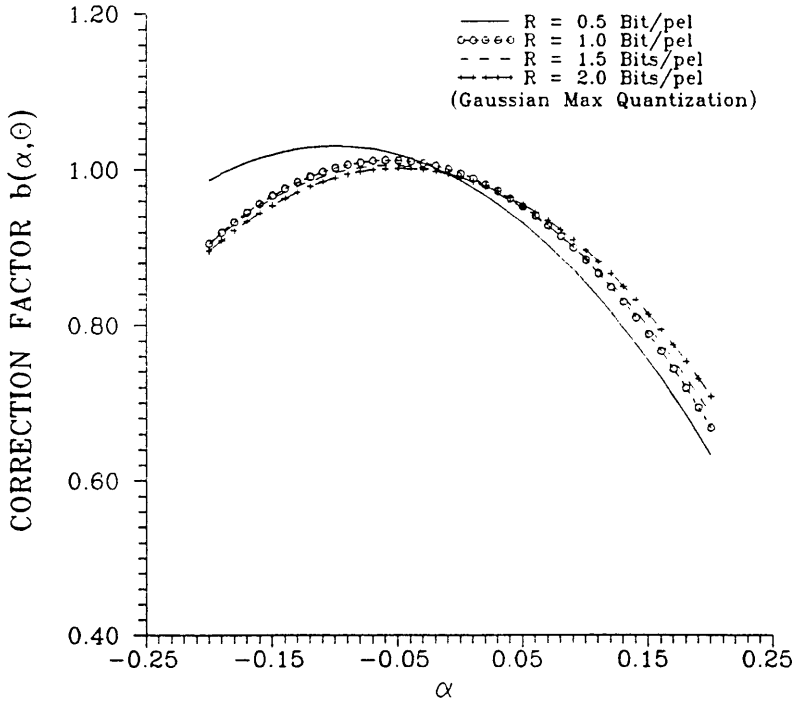


Fig. 3.5b : Hadamard NPT correction factor as a function of α; 4 x 4 Hadamard NPT coding of image ALAN.

that the correction factor increases with bit rate for $\alpha > 0.0$ and decreases with bit rate for $\alpha < 0.0$. Furthermore, we note that the change in correction factor as the bit rate is increased from 0.5 bit/pixel to 1 bit/pixel is greater than the subsequent changes in the correction factor as the bit rate is increased to 1.5 bits/pixel and 2.0 bits/pixel respectively. The correction factor is well approximated by a second order polynomial in α with constant coefficients. The correction factors for the sine NPT and the SC NPT show a similar behaviour.

2) Variation of The Correction Factor with Image Content

The behaviour of the correction factor in relation to the content of images was investigated. In Fig. 3.6a, the correction factors for five stationary first order Gauss-Markov images having horizontal (ρ_H) and vertical (ρ_V) inter-element correlation coefficients ranging from 0.55 to 0.95 are plotted. The images were generated using an isotropic white noise driven model [14], and were coded using a 4×4 Hadamard NPT with optimum Gaussian Max quantization of the transform samples. For $\alpha > 0.0$, an increase in the correction factor with decreasing inter-element correlation can be observed. This implies that the prediction given by the norm ratio gets closer to the actual MSE ratio with decreasing inter-element correlation. However, for $\alpha < 0.0$, no general statement can be made about the variation of the correction factor with inter-element correlation coefficient, other than the fact that the correction factor is highest for $\rho_H = \rho_V = 0.95$ meaning that the prediction given by the norm ratio is more accurate for this value of horizontal and vertical inter-element correlation coefficient, when $\alpha < 0.0$. Fig. 3.6b is a plot of the correction factor as a function of α for the monochrome images ALAN, CHOIR, PATTERN and DOCUMENT. We can observe that the magnitude of the correction factors for the ALAN ($\rho_H = 0.987, \rho_V = 0.962$) and CHOIR ($\rho_H = 0.955, \rho_V = 0.898$) images are very close in value. The slight difference between the magnitude of the correction factors can be attributed to a difference in the statistics of the two images, an indication of which is provided by the differences in the values of the vertical and horizontal inter-element correlation coefficients of the two images. It is also observed that the correction factors for the PATTERN ($\rho_H = 0.881, \rho_V = 0.881$) and DOCUMENT ($\rho_H = 0.84, \rho_V = 0.812$) images are very much different from those of the ALAN and CHOIR images; this can also be attributed to the differences in the statistics of the images. In practice, images of similar statistical properties can be grouped into classes and a representative correction factor can then be

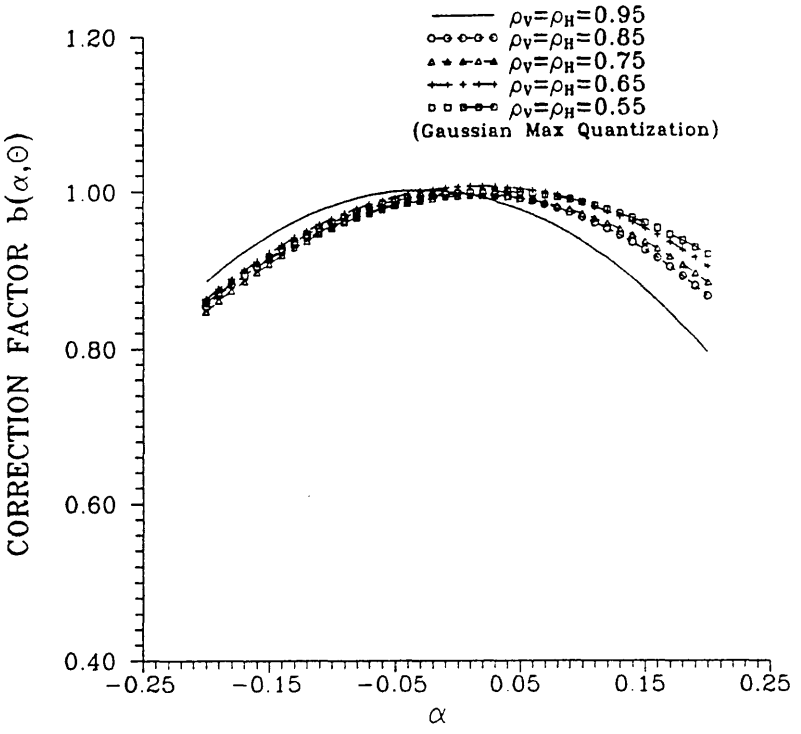


Fig. 3.6a : Hadamard NPT correction factor as a function of α for first order Gauss-Markov images; 4 x 4 Hadamard NPT coding at 1.5 bits/pixel.

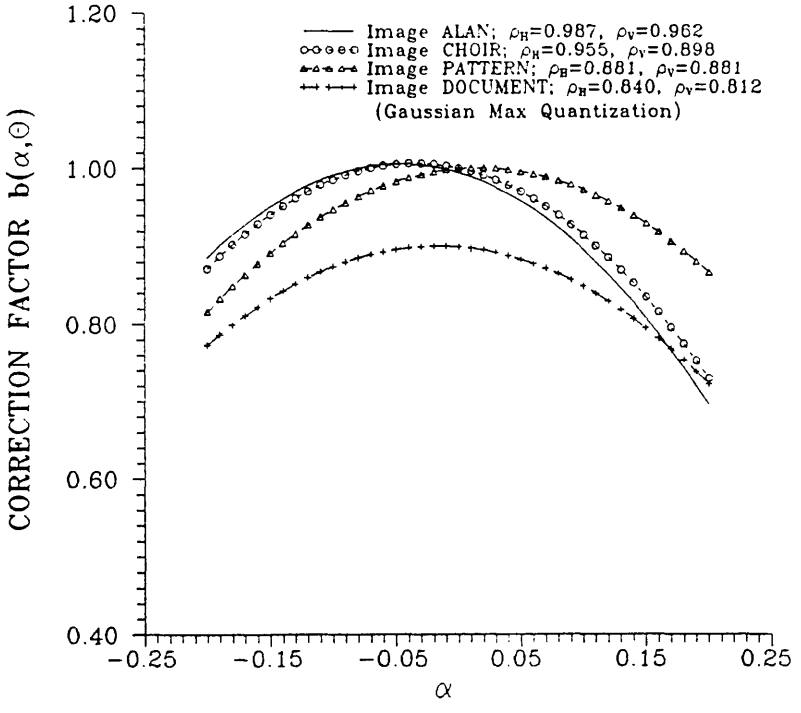


Fig. 3.6b : Hadamard NPT correction factor as a function of α for the monochrome images ALAN, CHOIR, PATTERN and DOCUMENT; 4 x 4 Hadamard NPT coding at 1.5 bits/pixel.

determined for each class; for example, a representative correction factor can be determined for the images ALAN and CHOIR.

3) Variation of The Correction Factor with Quantization Scheme

Fig. 3.7 is a plot of the correction factor as a function of α for 4×4 Hadamard NPT coding of the image ALAN, using Gaussian, Laplacian and Gamma quantizers for quantizing the transform coefficients. We can observe that the correction factor is not very sensitive to the particular quantizer used for quantizing the transform coefficients. The difference in the magnitude of the correction factors is mainly significant for $\alpha > 0.06$, where we can observe that the prediction of the Spatial/Transform domain MSE ratio, given by the norm ratio, is more accurate for the Gamma quantization scheme.

4) Variation of The Correction Factor with Transform Block Size

In Fig. 3.8, the correction factor as a function of α is plotted for the Hadamard NPT coding of image ALAN at a bit rate of 1.5 bits/pixel, using block sizes of 4, 8 and 16 respectively. We can observe that the correction factors obtained when block sizes of 4 and 8 are used, are close in magnitude. However, there is an increase in the correction factor when the block size is increased to 16, for $\alpha > 0.0$, while there is a decrease in the correction factor when the block size is increased to 16 for $\alpha < 0.0$. In practice, once a block size has been chosen, the correction factor need only be determined for the block size specified.

5) Variation of The Correction Factor with The NPT Transform Used

Fig. 3.9a is a plot of the respective correction factors as a function of α for the Hadamard NPT, sine NPT and SC NPT coding of image ALAN at a bit rate of 1.5 bits/pixel, using a block size of 4 and optimum Gaussian Max quantization of the transform samples. Fig. 3.9b is a plot of the correction factors obtained in a similar scheme to that of Fig. 3.9a but using a block size of 8. We can observe that for a block size of 4, the correction factors for the sine NPT and the SC NPT are very close in magnitude; they are in general higher than that of the Hadamard NPT for most values of α. For a block size of 8, the magnitude of the correction factors for the three transforms are very close for $\alpha > -0.05$. However, for $\alpha < -0.05$, the difference between the magnitude of the correction factors for the respective NPT transforms increases with decreasing α. In practice, once a particular NPT

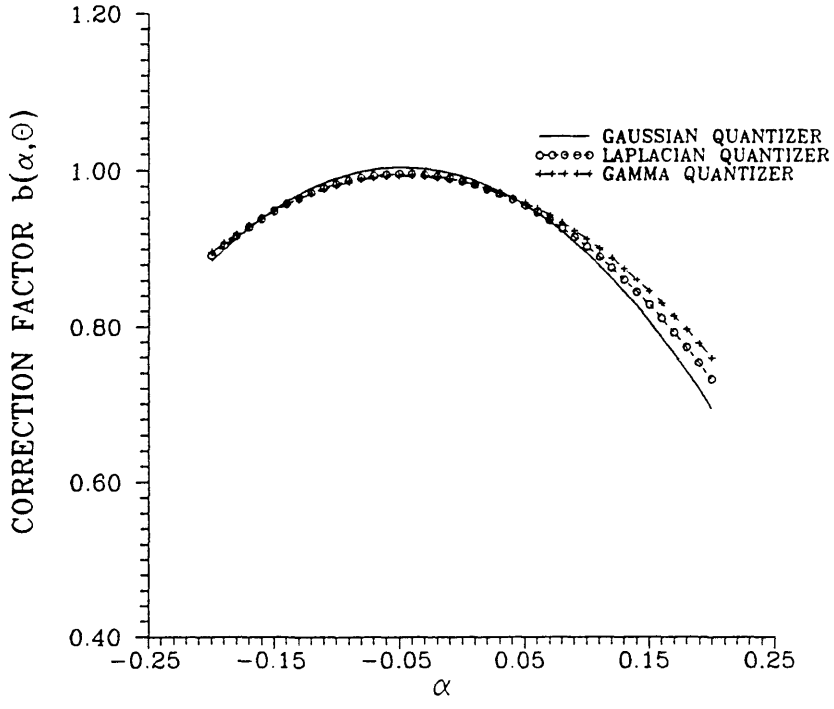


Fig. 3.7 : Hadamard NPT correction factor as a function of α for Gaussian, Laplacian and Gamma quantization schemes; 4 x 4 Hadamard NPT coding of image ALAN at 1.5 bits/pixel.

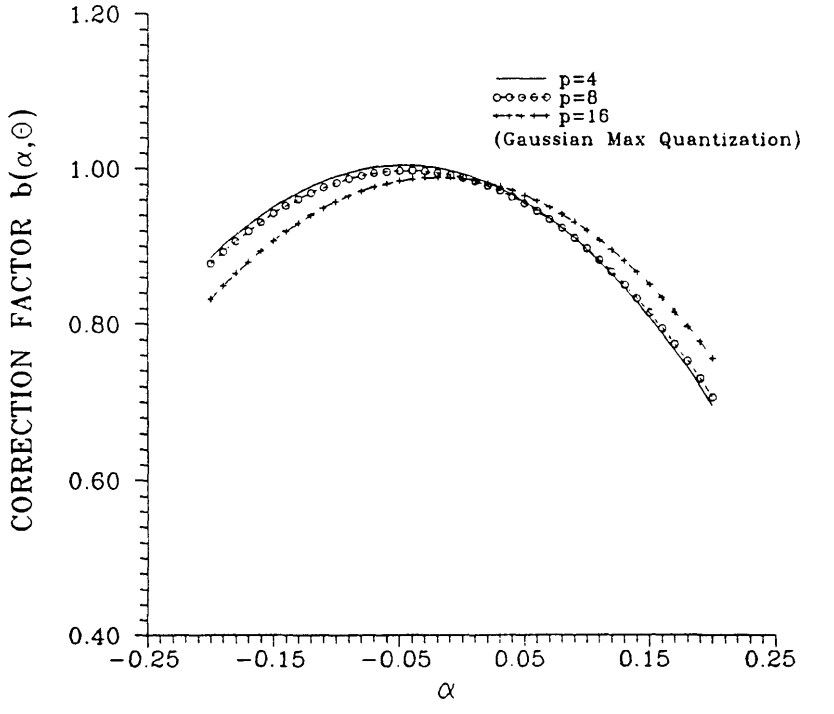


Fig. 3.8 : Hadamard NPT correction factor as a function of α ; Hadamard NPT coding of image ALAN at 1.5 bits/pel using block sizes of 4,8 and 16.

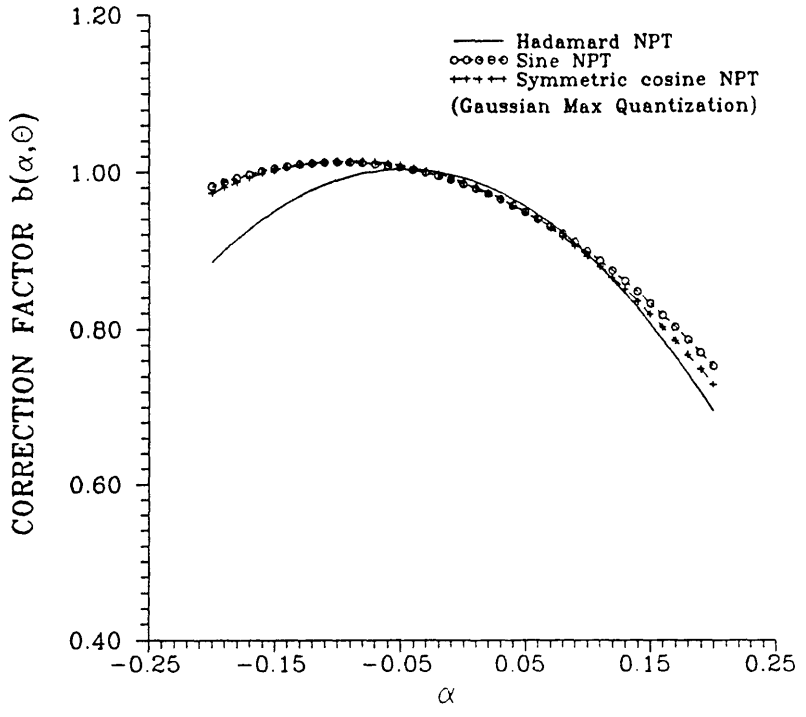


Fig. 3.9a : Correction factor as a function of α for the Hadamard NPT, sine NPT and SC NPT respectively coding of image ALAN at 1.5 bits/pel., using a block size of 4.

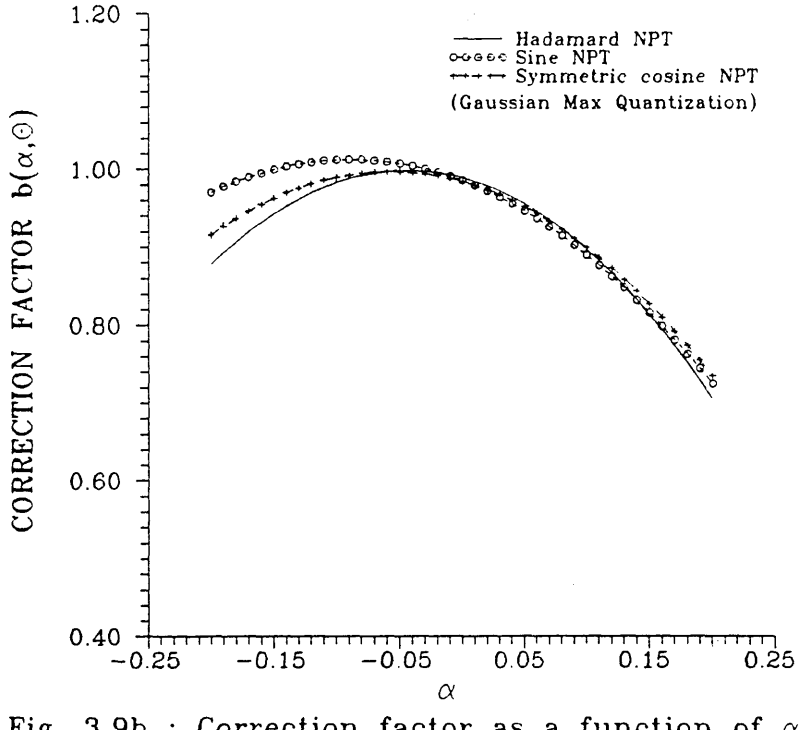


Fig. 3.9b : Correction factor as a function of α for the Hadamard NPT, sine NPT and SC NPT respectively coding of image ALAN at 1.5 bits/pel., using a block size of 8.

transform has been chosen, the correction factor need only be determined for this transform.

Discussion

The correction factor, by definition, establishes the correct relationship between the transform domain MSE and the spatial domain MSE for NPT image coding. An accurate determination of the optimum basis for an NPT image coding scheme depends on a good knowledge of the correction factor that is applicable. From (3.15), we can see that an error in the correction factor applied would result in an error in the spatial domain MSE obtained; the error in the spatial domain MSE would be a multiple of the transform domain MSE. Thus, the effect of an error in the correction factor at a high MSE level (low bit rate) would be greater than at a low MSE level (high bit rate).

Out of all the parameters considered above for the correction factor, the transform basis, bit rate and image content are of greater importance. This is because the effect of the other parameters can be eliminated in practice, for example, the coder can be designed for a given NPT transform, block size and quantizer. The correction factor as a function of α can then be determined for this choice of parameters. However, the variation with respect to the bit rate must be adequately accounted for so as to permit variable bit rate coding, since this has a great deal of effect on the MSE level. Fig. 3.5b shows that it is possible to determine representative correction factors which are applicable over a range of bit rates. From Fig. 3.6b, we can see that an accurate determination of the correction factor with respect to image content is necessary. In practice, representative correction factors can be determined for the respective classes of images to be coded.

3.5.3.4 Further Results on Non-Adaptive NPT Image Coding

The first step in an NPT coding scheme is the determination of the optimum basis for coding a given image or image ensemble. In section 3.5.2, an algorithm for determining the optimum basis was introduced. We determined the optimum basis for coding the image ALAN, using 4×4 Hadamard NPT at a bit rate of 1.5 bits/pixel and an optimum Gaussian Max quantizer, via this algorithm. The empirically determined correction factor was $0.9932670 - 0.4750328\alpha - 5.069712\alpha^2$, $|\alpha| \leq 0.2$, and the minimization of (3.42) was carried out using the one-dimensional Golden section search algorithm [39, pg. 277]. The bit assignment used in the optimum

basis determination algorithm was fixed at that for the transform coefficients generated by an NPT transform at a value of α very close to zero; the only variation in bit assignment that we observed in practice consisted of a transfer of bits between transform coefficients having nearly equal variances and this has a negligible effect on the MSE. The optimum basis obtained was 0.0204 and the corresponding MSE was 29.05. However, the optimum basis obtained via an alternative search procedure which involved trial transform coding at some selected values of α was 0.0730 and the corresponding MSE was 27.712; the MSE given by the Hadamard transform was 29.896. The error in the optimum basis determined can be attributed to possible mismatches in the correction factors for some sub-blocks of the image. This is a direct consequence of the fact that a non-adaptive image coder assumes that the image is stationary but real images are in general non-stationary. In addition, some errors are also introduced during the approximation of the empirically determined correction factors by a polynomial function, but these errors are usually very small in magnitude. The implication of this for non-adaptive NPT image coding is that the optimum basis determined by the algorithm would have to be confirmed by actual coding with possible refinements to the value obtained. The optimum basis determination algorithm however is useful for obtaining an approximate value of the optimum basis parameter for non-adaptive image coding.

Fig. 3.10 summarizes the results of 4×4 Hadamard NPT coding of image ALAN at bit rates of 0.5, 1.0, 1.5, 2.0 and 2.5 bits/pixel respectively, using an optimum Gaussian Max quantizer for quantizing the transform coefficients; the respective optimum bases at the bit rates are indicated in the figure. We can observe that a performance superior to that of the Hadamard transform is obtained by using the Hadamard NPT at all the bit rates. Furthermore, the optimum basis is dependent on the bit rate. Fig. 3.11 summarizes the results of 4×4 Hadamard NPT coding of image CHOIR (the original image is shown in Fig. 2.8) for a similar scheme to that of Fig. 3.10. A superior performance to that of the Hadamard transform is also obtained at all the bit rates with the respective optimum bases being dependent on the bit rate. In addition, the optimum bases at the respective bit rates for the two images are different which implies that the optimum basis is also dependent on the image content.

In Fig. 3.12, the effect of using different transform block sizes in NPT image coding is shown for the Hadamard NPT coding of image ALAN at a bit rate of

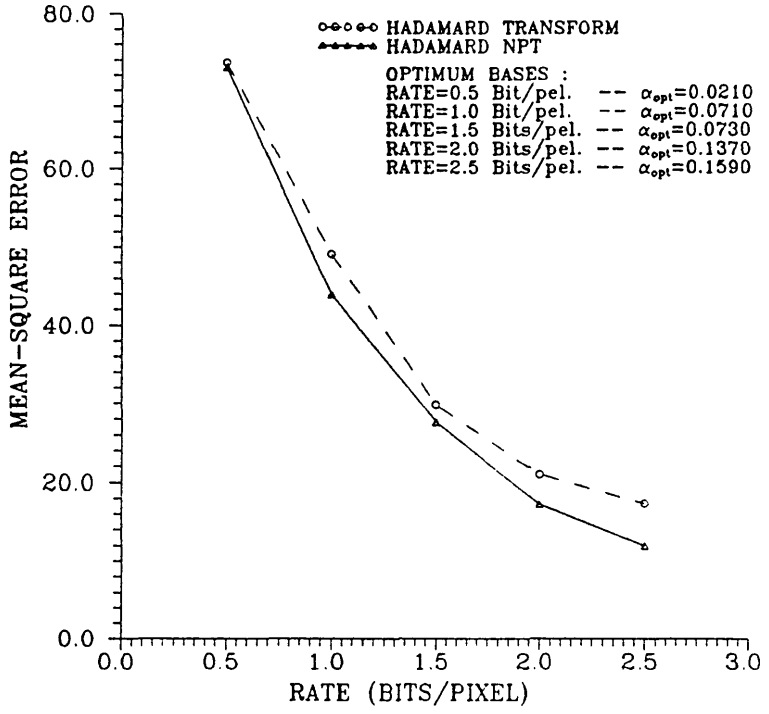


Fig. 3.10 : Mean-square error as a function of bit rate for the 4 x 4 Hadamard NPT coding of image ALAN, using Gaussian Max quantization for the transform samples.

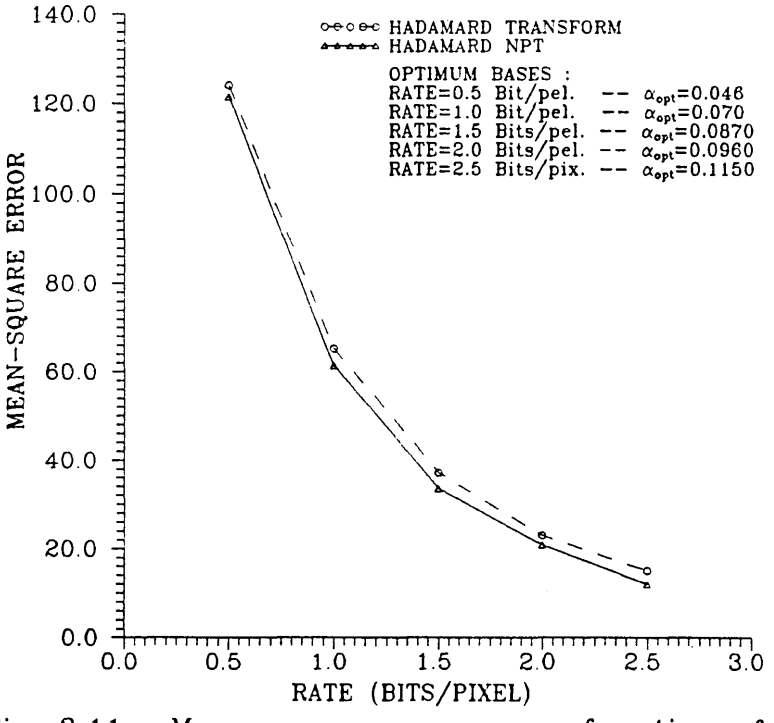


Fig. 3.11 : Mean-square error as a function of bit rate for the 4 x 4 Hadamard NPT coding of image CHOIR, using Gaussian Max quantization for the transform samples.

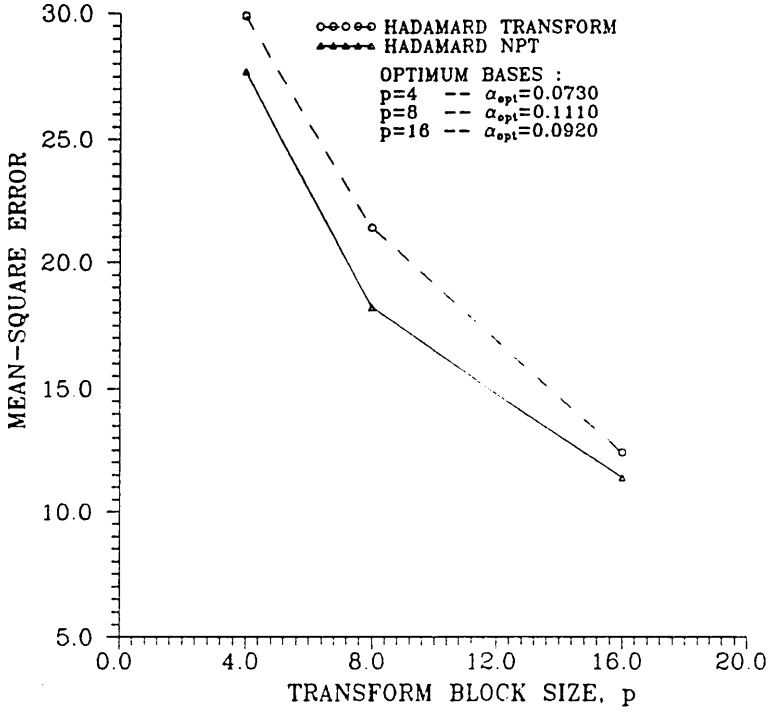


Fig. 3.12 : Mean-square error as a function of transform block size for the Hadamard NPT coding of image ALAN at a bit rate of 1.5 bits/pel, using Gaussian Max quantization.

1.5 bits/pixel; an optimum Gaussian Max quantizer was used for quantizing the transform samples. It is observed that the optimum basis is dependent on the block size. In addition, the improvement in MSE obtained by using the NPT basis is lowest at the biggest block size. Table 3.5 summarizes the relative performance of the Hadamard NPT, sine NPT and SC NPT when used for coding an image. The result was obtained using a block size of 8 and optimum Gaussian Max quantization for the transform coefficients, at a bit rate of 1.5 bits/pixel. The optimum bases for the sine NPT and SC NPT correspond to negative values of α. The SC NPT has the best performance, however, the improvement in MSE is highest for the Hadamard NPT. The pictorial results corresponding to Table 3.5 are shown in Figs. 3.13a-f.

Table 3.5 : Results of The 8×8 Coding of Image ALAN at 1.5 bits/pixel Using The Hadamard NPT, sine NPT and SC NPT Respectively.

		MSE	
TRANSFORM	OPTIMUM BASIS	NPT BASIS	ORTHOGONAL BASIS
HADAMARD NPT	0.1110	18.203	21.378
SINE NPT	-0.0650	18.144	18.925
SC NPT	-0.0490	16.433	16.948

Discussion

For a given transform block size and quantization scheme, the optimum NPT basis for coding images is dependent on the bit rate and image content. A non-adaptive coder which treats all the image regions in the same way is inherently inefficient.This is because the variations in picture detail from one image to another dictates that the parameters of the coder be adjusted to account for the changes in statistics. Since the NPT optimum basis differ for different images, we would expect that the bases for coding regions of the image having different statistics would be different. Empirical investigations confirm this fact and we propose NPT image coders which feature NPT basis adaptation according to local image content. These coders which we shall refer to as *Basis Adaptive NPT Coders (BANPTC)* are developed in the next section. It should be noted that the non-adaptive NPT coder considered in this section is basis adaptive over an ensemble of images. However, since the coder uses the same basis and bit allocation for



Fig. 3.13a : Non-Adaptive, 8×8 Hadamard Transform Coding of ALAN at 1.5 Bits/pel. ; $\alpha=0$.



Fig. 3.13b : Non-Adaptive, 8×8 Hadamard NPT Coding of ALAN at 1.5 Bits/pel. ; $\alpha=0.1110$.



Fig. 3.13c : Non-Adaptive, 8×8 sine Transform coding of ALAN at 1.5 Bits/pel. ; $\alpha=0$.



Fig. 3.13d : Non-Adaptive, 8×8 sine NPT Coding of ALAN at 1.5 Bits/pel. ; $\alpha=-0.0650$.



Fig. 3.13e : Non-Adaptive, 8×8 SC Transform Coding of ALAN at 1.5 Bits/pel. ; $\alpha=0$.



Fig. 3.13f : Non-Adaptive, 8×8 SC NPT Coding of ALAN at 1.5 Bits/pel. ; $\alpha=-0.0490$.

all the sub-blocks of a given image, we shall regard this as a non-adaptive NPT coder.

3.5.4 Basis Adaptive NPT Image Coding

3.5.4.1 Introduction and Description of The Basis Adaptive NPT Image Coder (BANPTC)

Adaptive transform coding schemes [2,24] adjust the parameters of the coder in accordance with the local statistical changes within an image or image ensemble. Typical adaptation parameters include sample selection, bit allocation and quantizer level spacing. Adaptation of the transform basis is also possible, but this is the most expensive. For example, in the case of the optimal KL transform, new transform basis vectors have to be determined and transmitted for significant changes in input image statistics. Moreover, the KL transform does not have a fast computational algorithm.

The results of the previous section on non-adaptive NPT image coding show that the optimum basis for image coding varies with the parameters of the coder and image content. Furthermore, we pointed out in chapter two that a change from one NPT basis to another can be accomplished simply by setting the transform basis parameter α to a new value in the transform implementation algorithm. Consequently, for effective adaptation of the NPT bases to the non-stationary nature of typical imagery data, we propose an adaptive transform coder which features NPT basis adaptation in addition to conventional adaptation techniques (adaptive bit allocation/quantization).

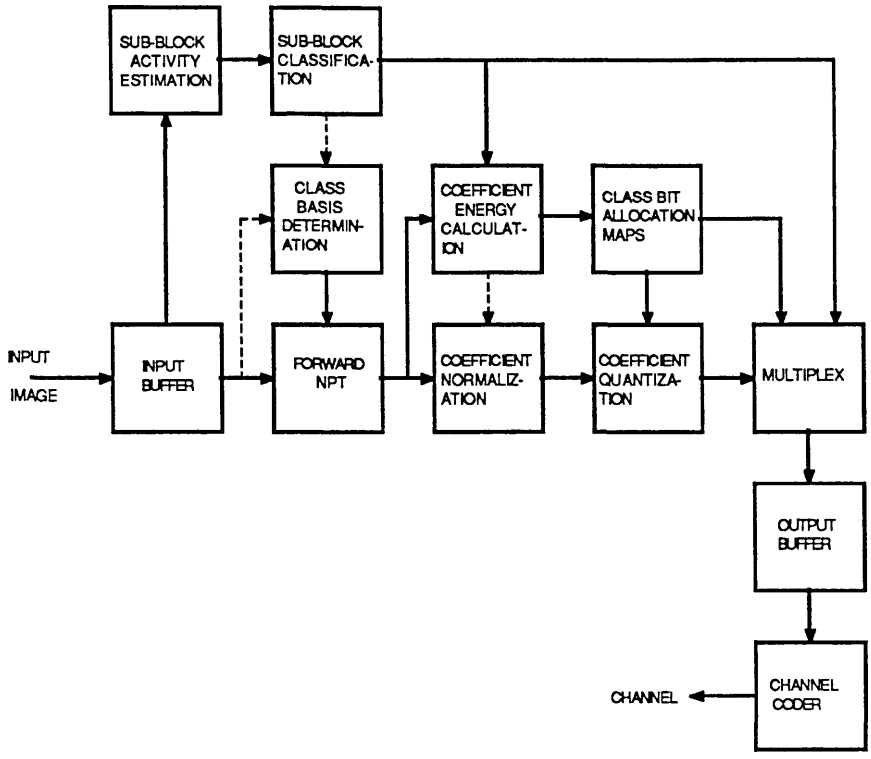
The Basis Adaptive NPT Coder (BANPTC) is a block classification adaptive transform coder which adjusts the transform basis and bit allocation according to local image activity. A spatial activity index measure [48] which is defined as the sum of the horizontal and vertical mean square differences ΔH, ΔV between adjacent pixels within each $p \times p$ sub-block of the image, i.e.

$$\Delta H = \frac{1}{p(p-1)} \sum_{i=1}^{p} \sum_{j=1}^{p} (F(i,j) - F(i,j+1))^2 \tag{3.44}$$

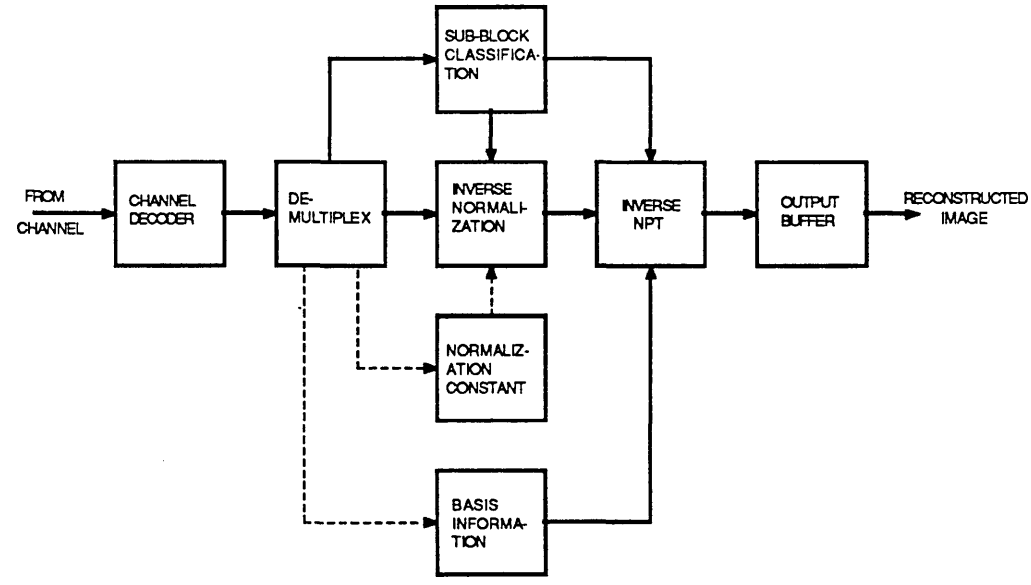
and

$$\Delta V = \frac{1}{p(p-1)} \sum_{i=1}^{p} \sum_{j=1}^{p} (F(i,j) - F(i+1,j))^2 \tag{3.45}$$

was used for classifying image sub-blocks into activity classes. The division of sub-blocks into activity classes was based on fixed activity index thresholds, which



(a) Coder



(b) Decoder

Fig. 3.14 : Detailed Block Diagram of The Basis Adaptive NPT Coder (BANPTC).

were set based on the activity index distributions of the ensemble of images to be coded. The use of fixed thresholds, as opposed to floating thresholds [49], permits the unique classification of sub-blocks of an image ensemble into activity classes, thereby ensuring a unique match of basis to local image activity. The basis adaptation was realized by computing the optimum basis for each class using the minimization technique described in section 3.5.2. The sub-block classification map provides the switching information for basis adaptation. However, information about the basis used for each class needs to be transmitted to the decoder; this minimal overhead can be avoided by determining the class optimum basis a priori over the image ensemble and making this information available at both the coder and decoder. The bit rates for coding the respective classes was obtained by specifying the rates for the respective classes of the most active image in the ensemble, necessary for achieving a desired maximum transmission rate. This strategy leads to less active images being coded with fewer bits. A detailed block diagram of the BANPTC is shown in Fig. 3.14.

3.5.4.2 Simulation and Results of Basis Adaptive NPT Image Coding

Figs. 3.15a-b show the activity distributions for 4×4 and 8×8 sub-blocks respectively , of the monochrome images ALAN, CHOIR, PATTERN, DOCUMENT and TEXTURE which are shown in Figs. 2.7-2.11 respectively. Based on these distributions, the sub-blocks of the images were classified into four unequally populated classes using the thresholds specified in Table 3.6. The 8×8 activity index threshold for class 1 was set at 55 since only a relatively few sub-blocks of the less active images ALAN, CHOIR and DOCUMENT have an activity index greater than 30.

Table 3.6 : Activity Index Thresholds Used For Sub-block Classification.

CLASS	ACTIVITY INDEX RANGE	
	4×4	8×8
1	45 and above	55 and above
2	30-44	25-54
3	15-29	15-24
4	0-14	0-14

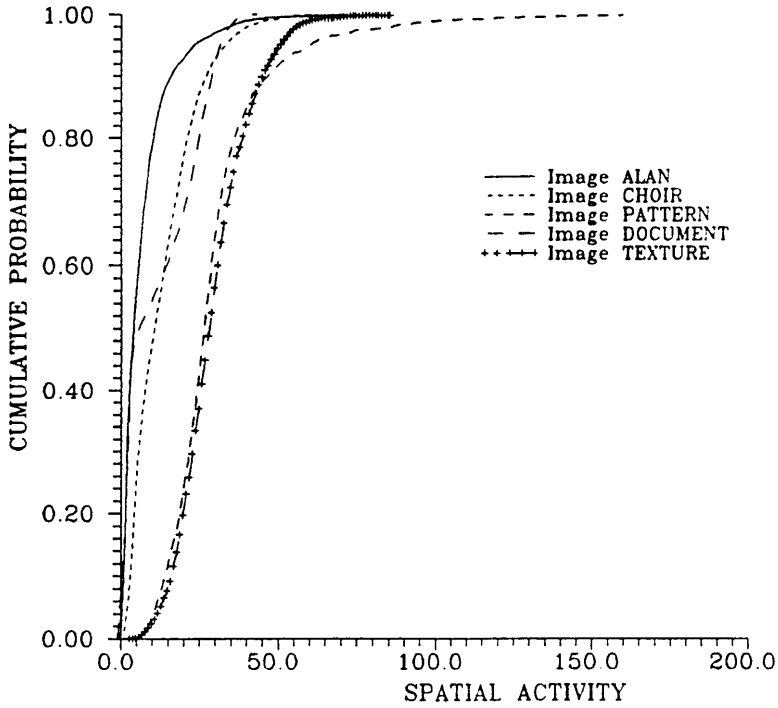


Fig. 3.15a : Cumulative Probability distributions of spatial activity for 4 x 4 sub-blocks of the images ALAN, CHOIR, PATTERN, DOCUMENT AND TEXTURE.

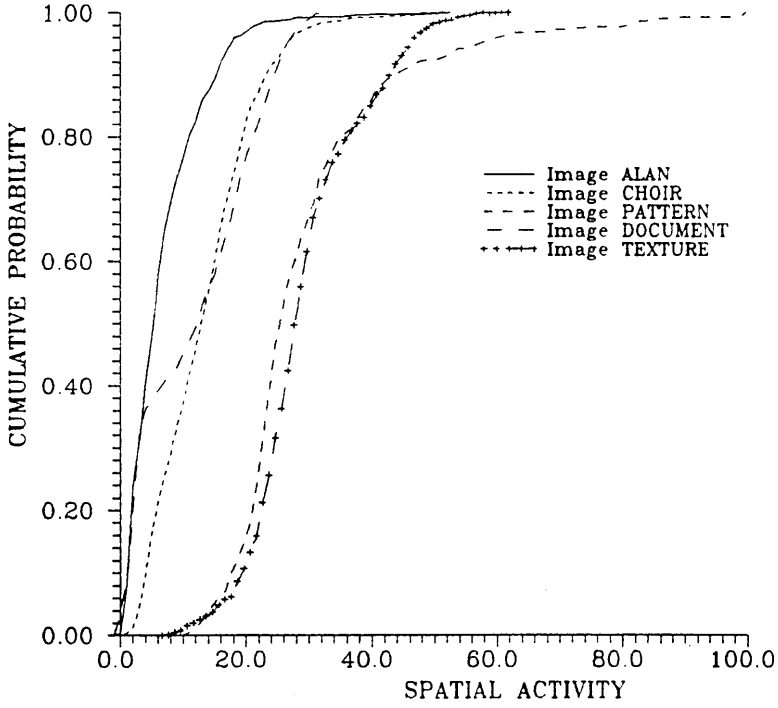


Fig. 3.15b : Cumulative Probability distributions of spatial activity for 8 x 8 sub-blocks of the images ALAN, CHOIR, PATTERN, DOCUMENT and TEXTURE.

The 4×4 Hadamard NPT correction factors applicable for the respective classes of the image CHOIR are shown in Fig. 3.16a and Fig. 3.16b for bit rates of 0.5 bit/pixel and 2.0 bits/pixel respectively. The number of sub-blocks in the various activity classes are class 1 :- 42 blocks, class 2 :- 246 blocks, class 3 :- 1202 blocks and class 4 :- 2606 blocks. It is observed that the correction factors for classes 2-4 are close in magnitude. The correction factor for class 1 of the image is close in magnitude to that of the remaining classes for $\alpha < 0.0$ but higher in magnitude for $\alpha > 0.0$. The results show that different correction factors are applicable at different bit rates, however, the results of Fig. 3.5b in section 3.5.3.3 implies the possibility of determining correction factors which are applicable over a range of bit rates.

We simulated the basis adaptive NPT coding of the images CHOIR, PATTERN, DOCUMENT and ALAN; the original images are shown in Figs. 2.7-2.10 respectively. The rates for coding each class were set so as to achieve an overall rate of 1.5 bits/pixel over the more active image PATTERN. This correspond to rates of 2.5 bits/pixel, 1.875 bits/pixel, 1.25 bits/pixel and 0.9375 bits/pixel for classes 1,2,3 and 4 respectively, for 4×4 coding and rates of 2.4375 bits /pixel, 1.8125 bits/pixel, 1.125 bits/pixel and 0.78125 bits/pixel for classes 1,2,3 and 4 respectively, for 8×8 coding. However, an overhead of 2 bits/block was subtracted for transmitting the sub-block classification maps. Fig. 3.17 shows the result of 4×4 coding of image CHOIR. It is observed that superior performance to that of the Hadamard transform is given by the Hadamard NPT, especially over the more active sub-blocks of the image. The overall rate achieved was 1.102 bits/pixel. The MSE values shown were measured separately for each class. The optimum bases obtained via minimization of (3.42) are 0.037, 0.069, 0.065 and 0.009 for classes 1,2,3 and 4 respectively. The corresponding MSE values are 37.27, 50.88, 56.32 and 18.60 respectively. The optimum bases obtained with refinements to the initial values stated above are 0.011, 0.07, 0.07 and 0.0180 for classes 1,2,3 and 4 respectively. The corresponding MSE values are 36.42, 50.82, 56.28 and 18.54 respectively. The MSE values given by the Hadamard transform are 36.92, 54.29, 59.18 and 18.73 for classes 1,2,3 and 4 respectively. The errors in the optimum bases determined via the minimization of (3.42) can be attributed to the approximation of the empirically determined correction factors by a polynomial function. However, it is only in the case of class 1 that the MSE value given by the basis obtained via the minimization of (3.42) is higher than that of the Hadamard transform but the effect of

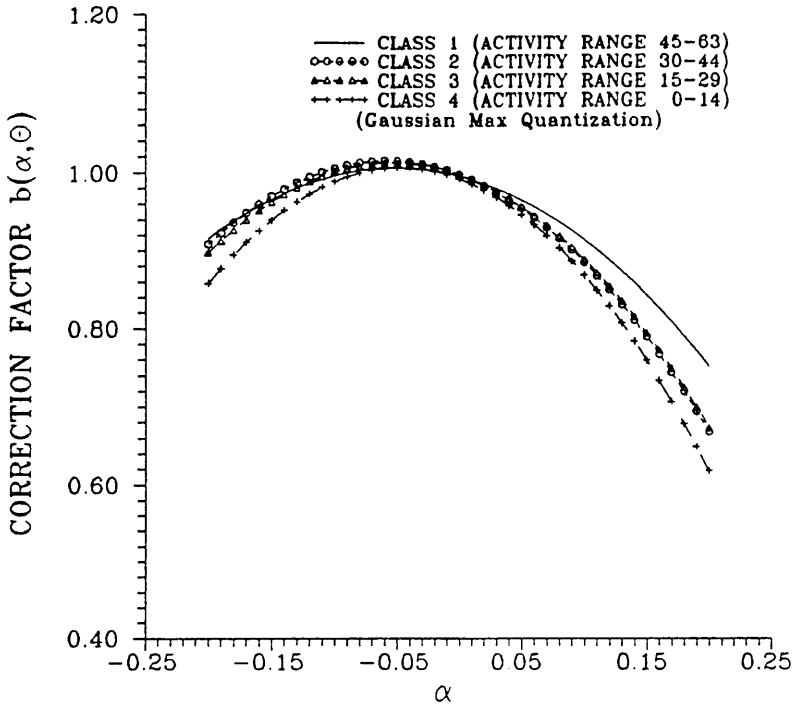


Fig. 3.16a : Correction factor as a function of α for the Hadamard NPT coding of the respective activity classes of the image CHOIR at 0.5 bit/pel., using a block size of 4.

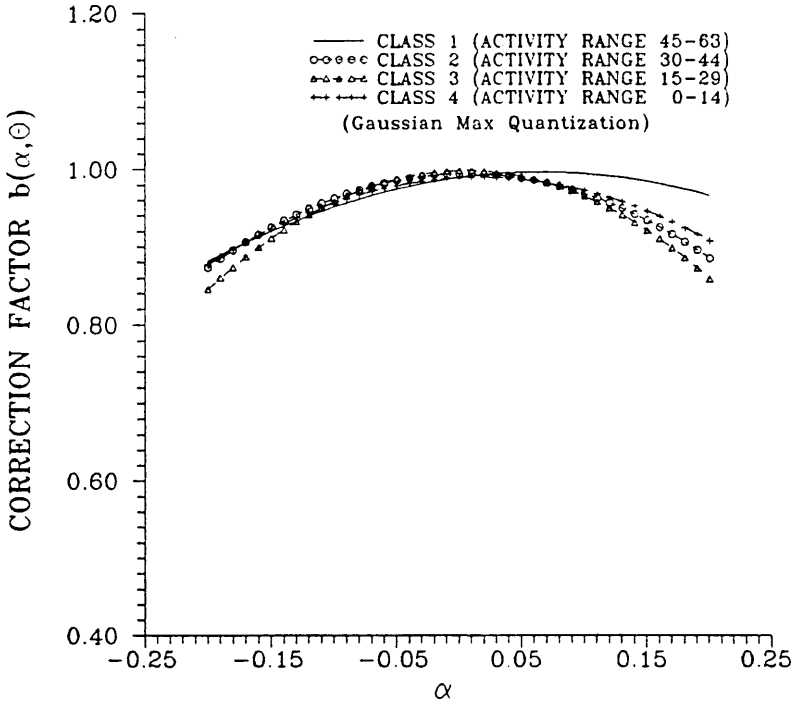


Fig. 3.16b : Correction factor as a function of α for the Hadamard NPT coding of the respective activity classes of the image CHOIR at 2.0 bits/pel., using a block size of 4.

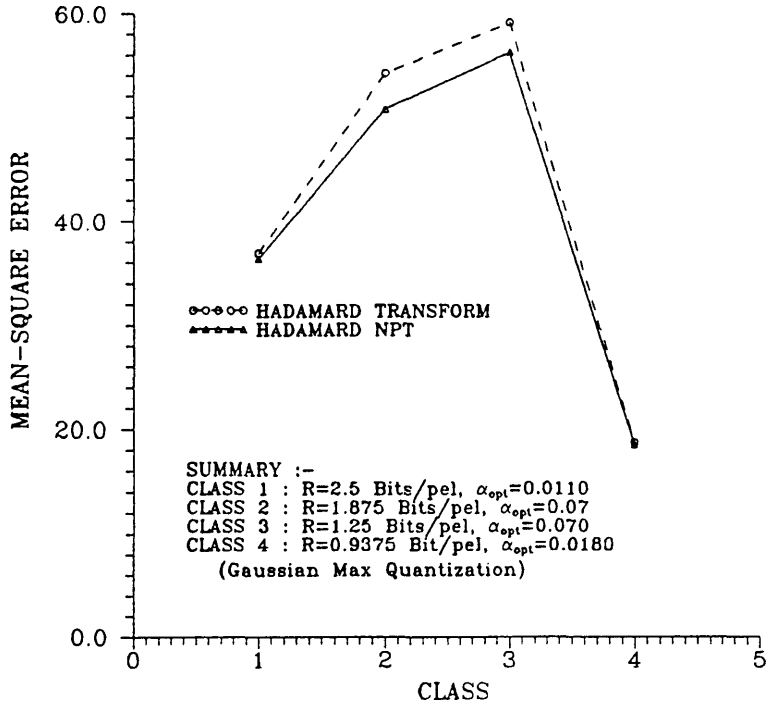


Fig. 3.17 : Result of the basis adaptive Hadamard NPT coding of image CHOIR, using a block size of 4 at an overall rate of 1.102 bits/pel.

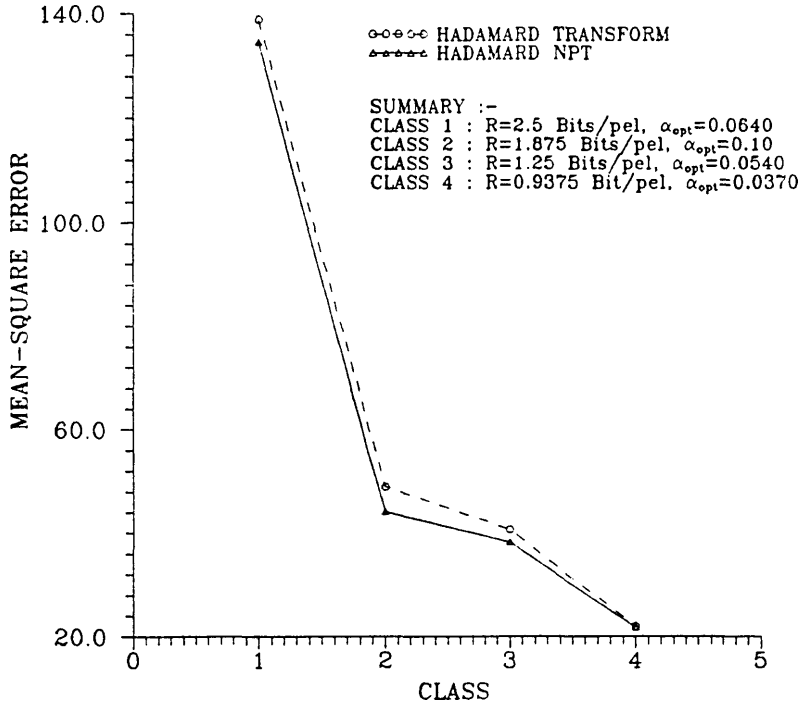


Fig. 3.18 : Result of the basis adaptive Hadamard NPT coding of image PATTERN, using a block size of 4 at an overall rate of 1.498 bits/pel.

this is small. In another investigation, the possibility of using correction factors that are representative of the respective activity classes of a collection of images was considered. Representative correction factors determined for classes 2 and 3 of the images CHOIR and ALAN were used to compute the optimum bases for coding classes 2 and 3 of image CHOIR. The optimum bases obtained are 0.0671 and 0.0653 for classes 2 and 3 respectively. The corresponding MSE values are 50.92 and 56.307 respectively. The results compare very well with that obtained when the correction factor determined separately for image CHOIR was used for computing the optimum bases. However, considerations as to whether the spatial activity index is a sufficient criterion for grouping sub-blocks of an image ensemble together for the purpose of determining the representative correction factors that would be applicable for the activity classes of the images is a matter for further investigation.

Fig. 3.18 shows the result of 4×4 Hadamard NPT coding of the respective activity classes of image PATTERN at an overall rate of 1.498 bits/pixel. A superior performance to that of the Hadamard transform is given by the Hadamard NPT. The improvement in MSE is higher for the more active sub-blocks of the image. Fig. 3.19 shows the result of 4×4 Hadamard NPT coding of image DOCUMENT, at an overall rate of 1.107 bits/pixel. Only three classes were obtained for this image. Superior performance to that of the Hadamard transform is given by the Hadamard NPT, with a higher improvement in MSE being obtained over the more active sub-blocks of the image. Fig. 3.20 shows the result of 4×4 Hadamard NPT coding of image ALAN at an overall rate of 0.9937 bit/pixel. In this case, superior performance to that of the Hadamard transform is given by the Hadamard NPT, however, the performances of the Hadamard NPT and the Hadamard transform are very close for classes 2 and 4.

The effect of using different NPT transforms is shown in Figs. 3.20-3.22 for the 4×4 coding of image ALAN. Fig. 3.21 shows the result of 4×4 sine NPT coding of image ALAN. It is observed that a superior performance to that of the sine transform is given by the sine NPT; the improvement in MSE is higher over the more active sub-blocks of the image. Fig. 3.22 shows the result of 4×4 SC NPT coding of image ALAN. It is observed that a superior performance to that of the SC transform is given by the SC NPT; however, the improvement in MSE in this case is higher over the less active sub-blocks of the image. The corresponding result of 4×4 Hadamard NPT coding of image ALAN is shown in Fig. 3.20.

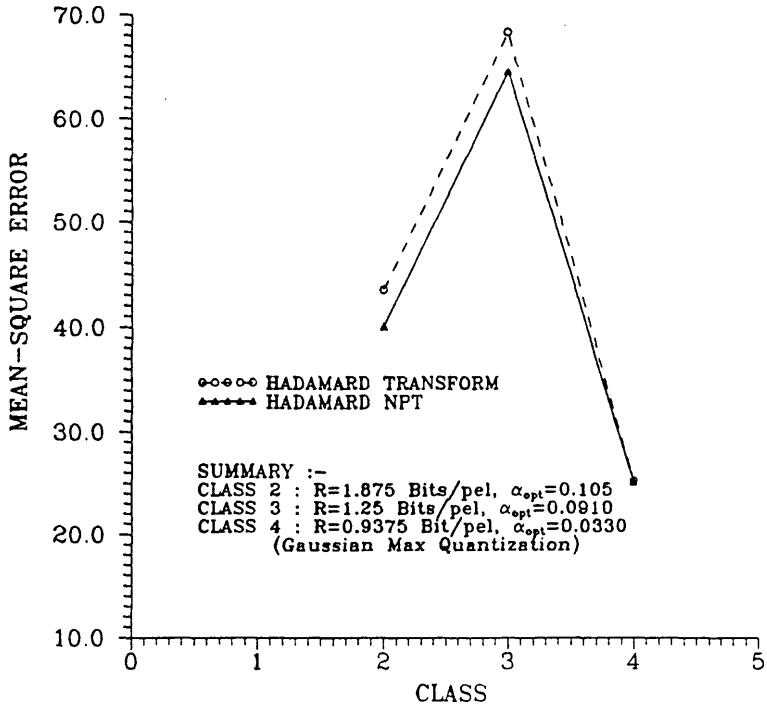


Fig. 3.19 : Result of the basis adaptive Hadamard NPT coding of image DOCUMENT, using a block size of 4 at an overall rate of 1.107 bits/pel.

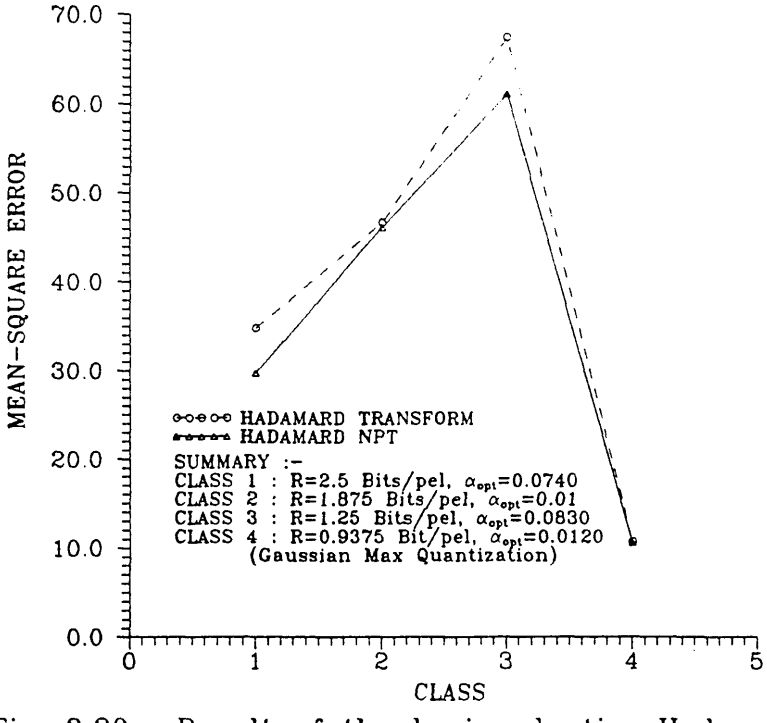


Fig. 3.20 : Result of the basis adaptive Hadamard NPT coding of image ALAN, using a block size of 4 at an overall rate of 0.9937 bit/pel.

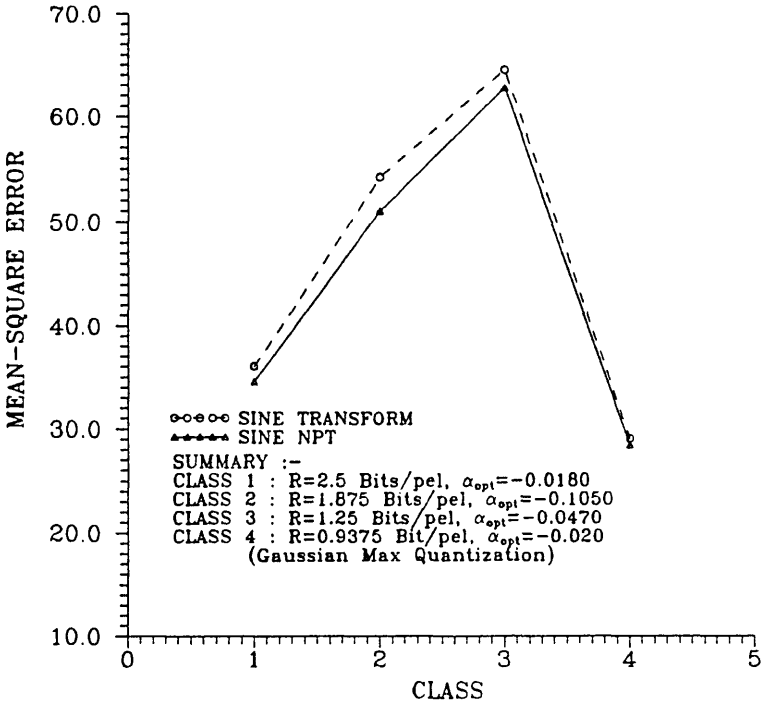


Fig. 3.21 : Result of the basis adaptive sine NPT coding of image ALAN, using a block size of 4 at an overall rate of 0.9937 bit/pel.

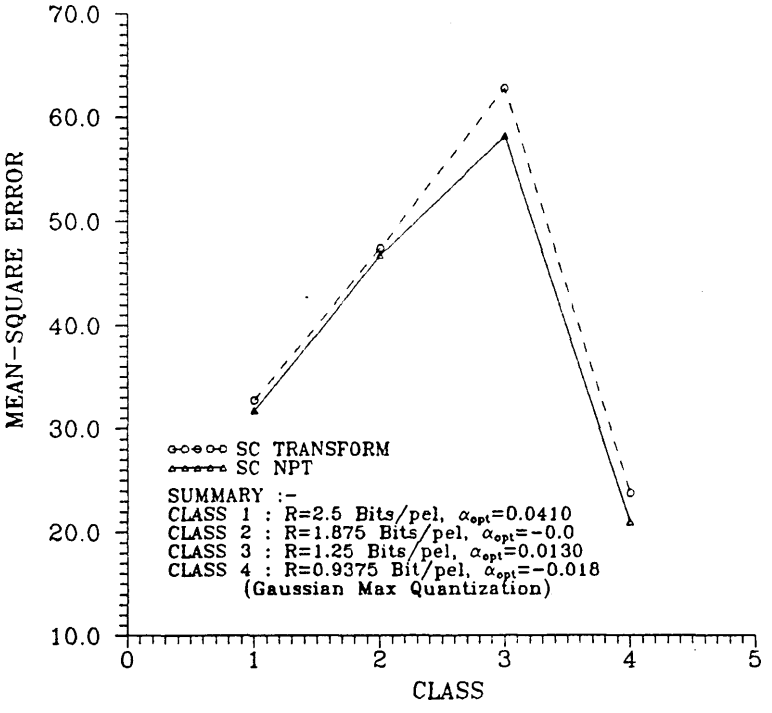


Fig. 3.22 : Result of the basis adaptive SC NPT coding of image ALAN, using a block size of 4 at an overall rate of 0.9937 bit/pel.

A summary of the number of sub-blocks in the respective activity classes of the images CHOIR, PATTERN, DOCUMENT and ALAN is given in Table 3.7. The pictorial results of the 4 x 4 Hadamard NPT coding of the images CHOIR, PATTERN, DOCUMENT and ALAN are shown respectively in Figs. 3.23-3.26. The pictorial results of the 4 x 4 sine NPT and the 4 x 4 SC NPT coding of image ALAN are shown in Fig. 3.27 and Fig. 3.28 respectively.

Table 3.7 : The Number of 4 x 4 Sub-blocks in The Respective Activity Classes of The Images CHOIR, PATTERN, DOCUMENT and ALAN

CLASS	NUMBER OF BLOCKS			
	CHOIR	PATTERN	DOCUMENT	ALAN
1	42	442	0	26
2	246	982	306	95
3	1202	2192	1307	322
4	2606	480	2483	3653

Fig. 3.29 shows the result of 8 x 8 Hadamard NPT coding of image ALAN at an overall bit rate of 0.827 bit/pixel. Only three classes were obtained and the improvement in MSE due to a change of basis from that of the Hadamard transform to that of the Hadamard NPT is very small. This was observed to be a general result for low activity images. Figs. 3.30-3.32 respectively show the results of 8 x 8 Hadamard NPT, 8 x 8 sine NPT and 8 x 8 SC NPT coding of image PATTERN (original image is shown in Fig. 2.9) at an overall rate of 1.4993 bits/pixel. In the case of the 8 x 8 Hadamard NPT coding, a superior performance to that of the Hadamard transform is given by the Hadamard NPT for all the four classes. However, for the 8 x 8 sine NPT coding, an improvement in MSE due to a change of basis was only obtained for classes 1 and 2. For the 8 x 8 SC NPT coding, a superior performance to that of the SC transform is given by the SC NPT for all the four classes.

For the three transforms, it was observed that the improvement in MSE due to a change of basis is generally higher for 4 x 4 coding than that for 8 x 8 coding. Furthermore, the MSE improvement in the case of 8 x 8 coding decreases with decreasing image activity. Table 3.8 show the number of 8 x 8 sub-blocks in the



Fig. 3.23a : Four Class Adaptive, 4×4 Hadamard Transform Coded Version of CHOIR; 1.102 Bits/pel.



Fig. 3.23b : Four Class Basis Adaptive, 4×4 Hadamard NPT Coded Version of CHOIR; 1.102 Bits/pel.

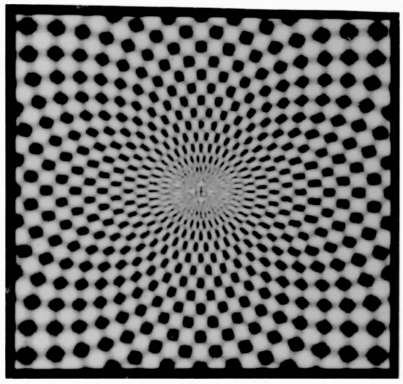


Fig. 3.24a : Four Class Adaptive, 4×4 Hadamard Transform Coded Version of PATTERN; 1.498 Bits/pel.

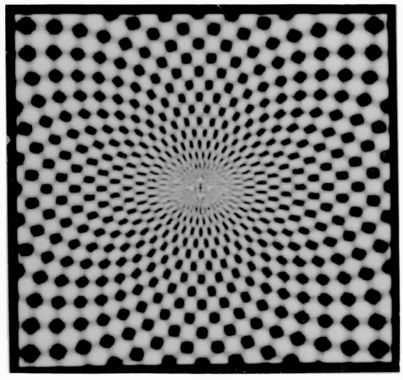


Fig.3.24b : Four Class Basis Adaptive, 4×4 Hadamard NPT Coded Version of PATTERN; 1.498 Bits/pel.

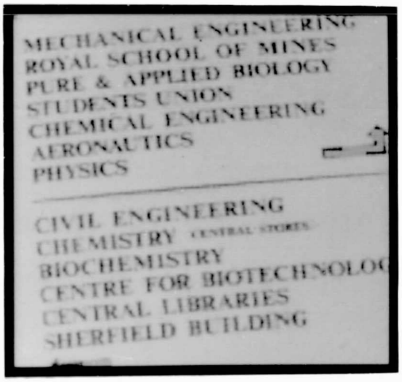


Fig. 3.25a : Four Class Adaptive, 4×4 Hadamard Transform Coded Version of DOCUMENT; 1.107 Bits/pel.

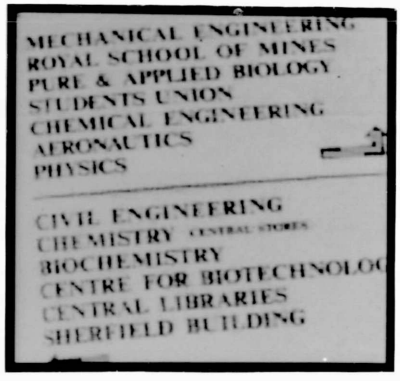


Fig. 3.25b : Four Class Basis Adaptive, 4×4 Hadamard NPT Coded Version of DOCUMENT; 1.107 Bits/pel.



Fig. 3.26a : Four Class Adaptive, 4×4 Hadamard Transform Coded Version of ALAN ; 0.9937 Bit/pel.



Fig. 3.26b : Four Class Basis Adaptive, 4×4 Hadamard NPT Coded Version of ALAN ; 0.9937 Bit/pel.



Fig. 3.27a : Four Class Adaptive, 4×4 sine Transform Coded Version of ALAN ; 0.9937 Bit/pel.



Fig. 3.27b : Four Class Basis Adaptive, 4×4 sine NPT Coded Version of ALAN ; 0.9937 Bit/pel.



Fig. 3.28a : Four Class Adaptive, 4×4 SC Transform Coded Version of ALAN ; 0.9937 Bit/pel.



Fig. 3.28b : Four Class Basis Adaptive, 4×4 SC NPT Coded Version of ALAN ; 0.9937 Bit/pel.

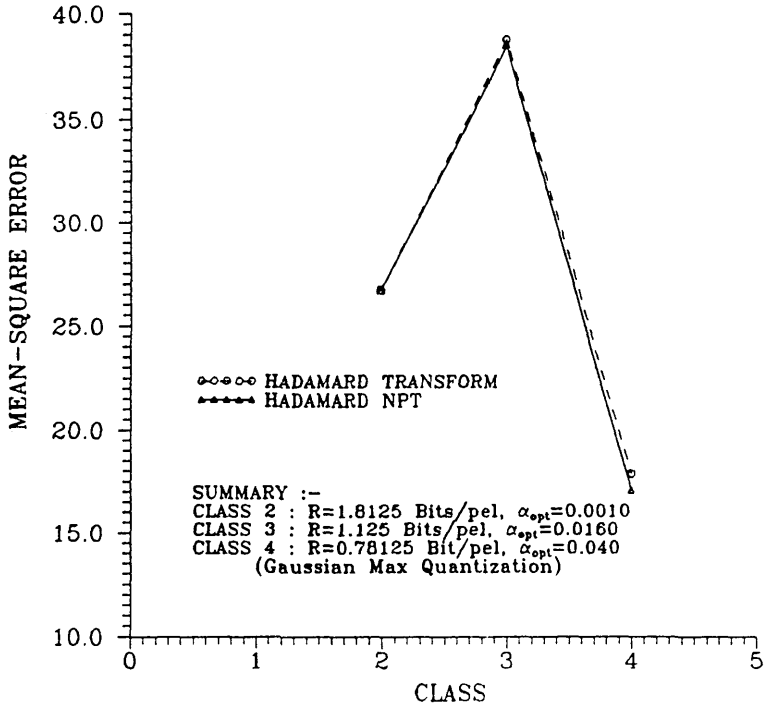


Fig. 3.29 : Result of the basis adaptive Hadamard NPT coding of image ALAN, using a block size of 8 at an overall rate of 0.827 bit/pel.

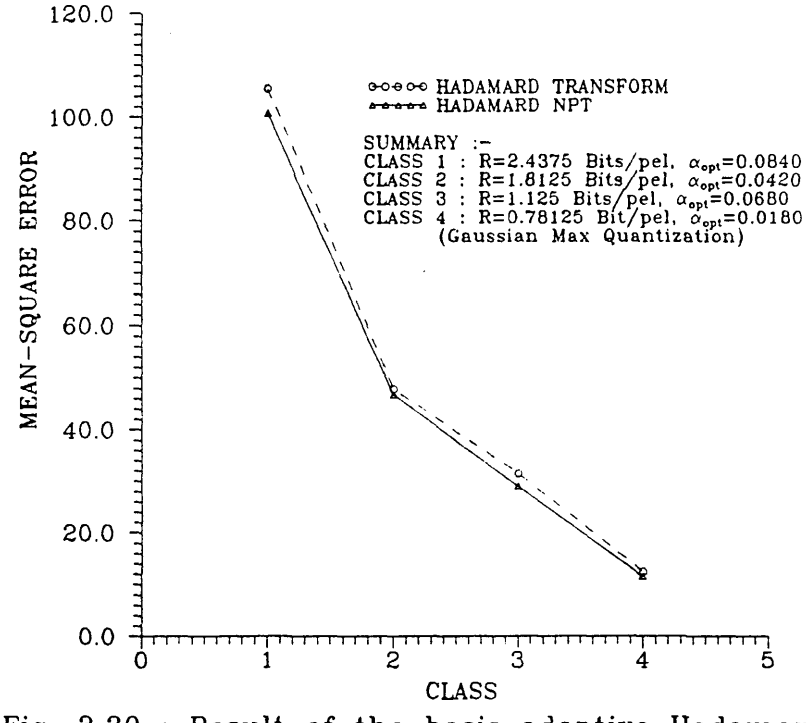


Fig. 3.30 : Result of the basis adaptive Hadamard NPT coding of image PATTERN, using a block size of 8 at an overall rate of 1.4993 bits/pel.

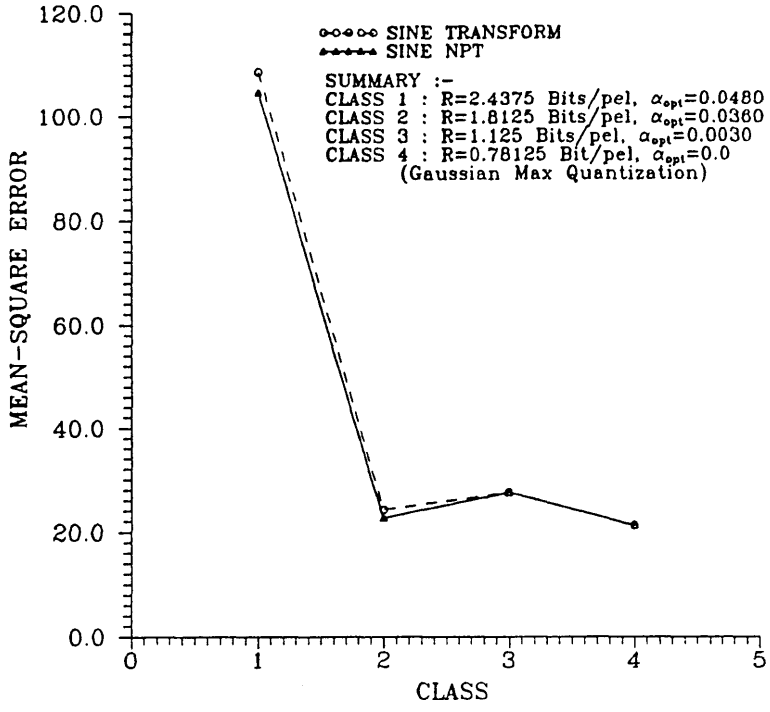


Fig. 3.31 : Result of the basis adaptive sine NPT coding of image PATTERN, using a block size of 8 at an overall rate of 1.4993 bits/pel.

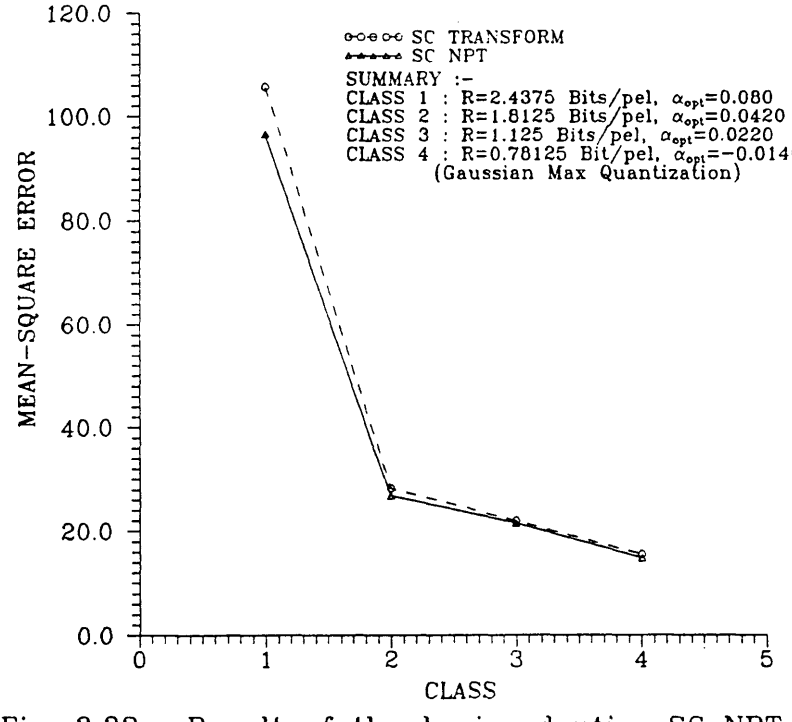


Fig. 3.32 : Result of the basis adaptive SC NPT coding of image PATTERN, using a block size of 8 at an overall rate of 1.4993 bits/pel.

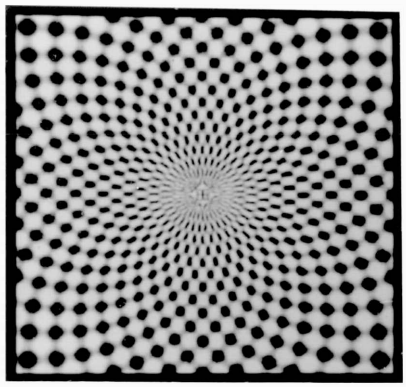


Fig. 3.33a : Four Class Adaptive, 8×8 Hadamard Transform Coded Version of PATTERN ; 1.4993 Bits/pel.

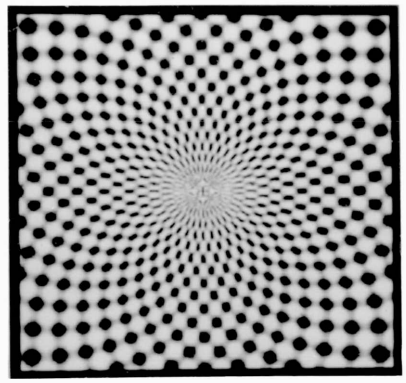


Fig. 3.33b : Four Class Basis Adaptive, 8×8 Hadamard NPT Coded Version of PATTERN 1.4993 Bits/pel.

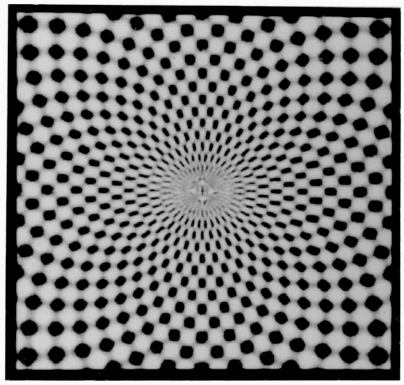


Fig. 3.34a : Four Class Adaptive, 8×8 sine Transform Coded Version of PATTERN; 1.4993 Bits/pel.

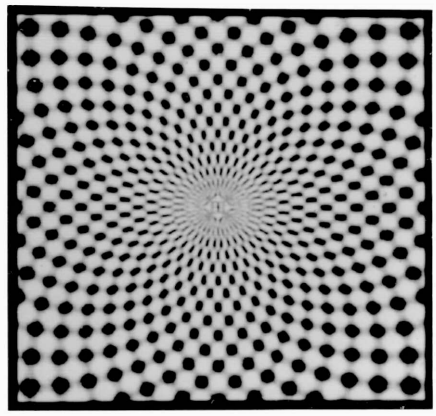


Fig. 3.34b : Four Class Basis Adaptive, 8×8 sine NPT Coded Version of PATTERN; 1.4993 Bits/pel.

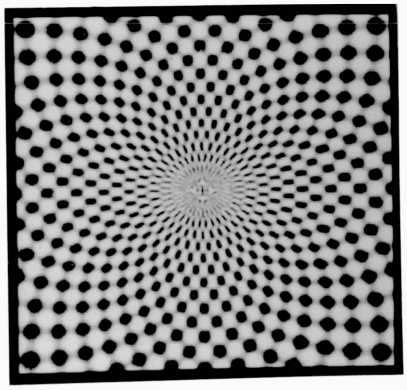


Fig. 3.35a : Four Class Adaptive, 8×8 SC Transform Coded Version of PATTERN; 1.4993 Bits/pel.

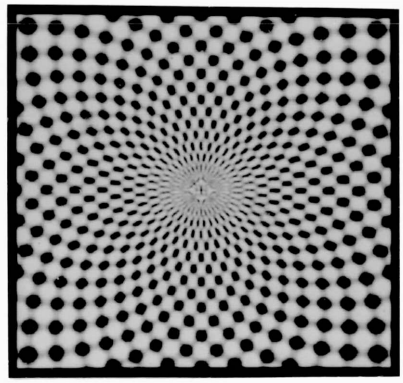


Fig. 3.35b : Four Class Basis Adaptive, 8×8 SC NPT Coded Version of PATTERN; 1.4993 Bits/pel.

respective activity classes of the images ALAN and PATTERN. The pictorial results of 8×8 Hadamard NPT coding, 8×8 sine NPT coding and the 8×8 SC NPT coding of image PATTERN are shown in Figs. 3.33-3.35 respectively.

Table 3.8 : The Number of 8×8 Sub-blocks in The Respective Activity Classes of The Images ALAN and PATTERN

CLASS	NUMBER OF BLOCKS	
	ALAN	PATTERN
1	0	60
2	13	469
3	96	443
4	915	52

3.5.4.3 The Effect of Channel Errors

The effect of channel errors on two-dimensional transform coded pictures is traditionally investigated by assuming a binary symmetric channel. In this context, a channel error is the inversion of an individual code-word digit, i.e. changing a '0' into a '1', and vice versa. An error in the code words used for representing the overhead information can lead to catastrophic errors [49]. Hence, in our investigations, we regard these as having been adequately error protected and we consider the effect of errors in the code words used for representing the transform coefficients.

Fig. 3.36a shows the reconstructed picture for the four-class adaptive, 4×4 Hadamard transform coding of image ALAN at an overall rate of 0.9937 bit/pixel and a BER (bit-error-rate) of 10^{-4}. Fig. 3.36b shows the reconstructed pictures for the four-class basis adaptive, 4×4 Hadamard NPT coding of image ALAN at an overall rate of 0.9937 bit/pixel and a BER of 10^{-4}. The no-error results for these schemes correspond to Fig. 3.26a and Fig. 3.26b respectively. There is no noticeable effect in the coded pictures, of the errors in the code-word digits used for representing the transform coefficients. Fig. 3.37a shows the reconstructed picture for the four-class adaptive, 4×4 Hadamard transform coding of image ALAN at an overall rate of 0.9937 bit/pixel and a BER of 10^{-3}. We can observe the effect



Fig. 3.36a : Four Class Adaptive, 4×4 Hadamard Transform Coding of ALAN ; 0.9937 Bit/pel. , BER=10^{-4}.



Fig. 3.36b : Four Class Basis Adaptive, 4×4 Hadamard NPT Coding of ALAN ; 0.9937 Bit/pel. , BER=10^{-4}.



Fig. 3.37a : Four Class Adaptive, 4×4 Hadamard Transform Coding of ALAN ; 0.9937 Bit/pel. , BER=10^{-3}.



Fig. 3.37b : Four Class Basis Adaptive, 4×4 Hadamard NPT Coding of ALAN ; 0.9937 Bit/pel. , BER=10^{-3}.

of incorrect basis picture contributions in the coded picture. Fig. 3.37b shows the reconstructed picture for the four-class basis adaptive, 4×4 Hadamard NPT coding of image ALAN at an overall rate of 0.9937 bit/pixel and a BER of 10^{-3}. The effect of incorrect basis picture contributions is also noticeable in the reconstructed picture. For a higher BER of 10^{-2}, the effect of incorrect basis picture contributions is much higher. The results for the sine NPT and the SC NPT are similar to that of the Hadamard NPT. In all cases, the signal-to-noise ratio for the coded pictures in the presence of channel errors using the basis adaptive NPT coding scheme was better than that obtained for the four-class adaptive, classical orthogonal transform coding scheme.

PART B : Predictive Naturalness-Preserving Transform Coding of Images

Introduction

In part A of this chapter, we developed conventional pure transform coding systems based on the NPT and proposed basis adaptive NPT coders which feature transform basis adaptation according to local image content and conventional adaptation techniques (adaptive bit allocation/quantization). Here, we investigate intraframe Hybrid NPT coding of images. As mentioned earlier in this chapter, hybrid coding schemes combine the attractive features of transform domain techniques and predictive (DPCM) techniques, and their relative ease of implementation compared with pure two-dimensional transform coding schemes have made them very attractive for practical image coding applications.

The hybrid coding scheme we shall consider, employ one-dimensional NPTs and a bank of DPCM operators; the description and analysis of this scheme are presented in the following sections.

3.6 The Intraframe NPT Hybrid Image Coding Scheme

In this scheme, the $N \times N$ image array $\mathbf{F}$, is divided into sub-arrays of $N \times p$ pixels and one-dimensional $(1 \times p)$ NPTs are then taken along each row of the sub-array. The one-dimensional forward row NPTs of the image sub-array $\mathbf{F}_w$, are modelled by

$$\mathbf{T}_w(x, v; \alpha) = \sum_{y=1}^{p} \mathbf{F}_w(x, y)\psi(y, v; \alpha) \tag{3.46}$$

for $v = 1,2,\ldots p$, $x = 1,2,\ldots N$, and $w = 1,2,\ldots \frac{N}{p}$ where $\psi(y,v;\alpha)$ are forward NPT basis elements. A bank of DPCM operators are then applied to the columns of the transformed array $\mathbf{T}_w(x,v;\alpha)$.

In the v^{th} DPCM coder, an n^{th} order prediction of transform coefficients in the v^{th} column of the sub-array $\mathbf{T}_w(x,v;\alpha)$ based on a history of coded transform coefficients in the same column is obtained according to

$$\hat{\mathbf{T}}_w(x,v;\alpha) = \sum_{i=1}^{n} a_i(v)\tilde{\mathbf{T}}_w(x-i,v;\alpha) \tag{3.47}$$

for $v = 1,2,\ldots p$, $x = 1,2,\ldots N$, and $w = 1,2,\ldots \frac{N}{p}$ where $\tilde{\mathbf{T}}_w(x,v;\alpha)$ is the coded version of $\mathbf{T}_w(x,v;\alpha)$ and the $a_i(v)$ are the predictor coefficients. The differential signals

$$\mathbf{D}_w(x,v;\alpha) = \mathbf{T}_w(x,v;\alpha) - \hat{\mathbf{T}}_w(x,v;\alpha) \tag{3.48}$$

are then coded and transmitted or stored. The predictor coefficients $a_i(v)$ are chosen to minimize the mean-square prediction error difference $E\{\mathbf{D}^2(x,v;\alpha)\}$. It should be noted that the coded transform coefficients $\tilde{\mathbf{T}}_w(x-i,v;\alpha), \quad i = 1,2,\ldots n$ used in the prediction process described by (3.47) each satisfy

$$\tilde{\mathbf{T}}_w(x-i,v;\alpha) = \hat{\mathbf{T}}_w(x-i,v;\alpha) + \tilde{\mathbf{D}}_w(x-i,v;\alpha) \tag{3.49}$$

where $\tilde{\mathbf{D}}_w(x-i,v;\alpha)$ is the coded differential signal at instant $x-i$ along the v^{th} column of the w^{th} sub-array of transform coefficients, which permits the decoder to make a prediction of transform coefficients similar to that in the coder. At the decoder, the decoded differential signals are added to the predicted transform coefficients (derived at the decoder) to yield the reconstructed transform coefficients $\tilde{\mathbf{T}}_w(x,v;\alpha)$, i.e.

$$\tilde{\mathbf{T}}_w(x,v;\alpha) = \hat{\mathbf{T}}_w(x,v;\alpha) + \tilde{\mathbf{D}}_w(x,v;\alpha) \tag{3.50}$$

An inverse transformation of the reconstructed transform coefficients, described by

$$\hat{\mathbf{F}}_w(x,y) = \sum_{v=1}^{p} \tilde{\mathbf{T}}_w(x,v;\alpha)\psi^{-1}(y,v;\alpha) \tag{3.51}$$

for $y = 1,2,\ldots p$, $x = 1,2,\ldots N$, and $w = 1,2,\ldots \frac{N}{p}$ where $\psi^{-1}(y,v;\alpha)$ are the inverse NPT basis elements, yields the coded version of the original transmitted image sub-array. A block diagram of the complete codec is shown in Fig. 3.38.

As was pointed out in part A, the NPT offers an infinite set of possible basis, most of which are not orthogonal, that could be employed for coding an image

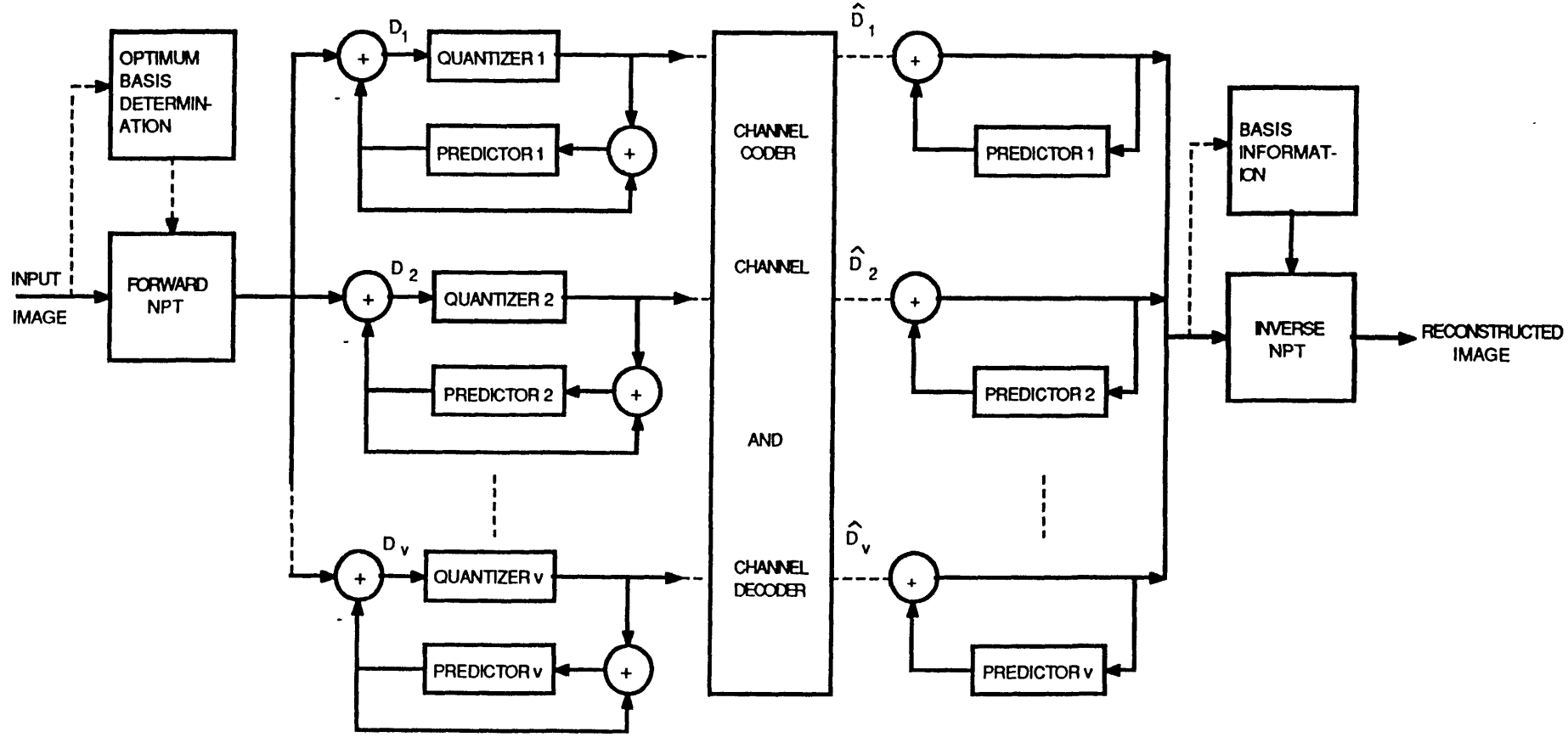


Fig. 3.38 : Hybrid Coding System Using A Cascade of 1-D NPT Transforms and a Bank of DPCM Systems.

or image ensemble. Of interest, however, is the basis or collection of bases that would yield the highest fidelity level of reconstructed image, when the NPT is used for hybrid image coding. For a mean-square error fidelity criterion, the statement of this problem is similar to that for conventional pure transform coding given in section 3.5.1 and the algorithm for determining the optimum basis for hybrid NPT image coding is developed in the next section.

3.6.1 Determination of The Optimum NPT Basis for Hybrid Coding of Images

The objective of an NPT hybrid coder [36] is to employ the basis or collection of bases giving minimum MSE for coding a given image sub-array or image array. This is equivalent to requiring that the coder must be able to select a basis or a collection of bases different from that specified by $\alpha = 0$ for hybrid coding of a given image sub-array or image array, when the image statistics dictate. For efficient adaptation of the NPT bases to the non-stationary nature of typical imagery data, an algorithm for determining the optimum basis is developed in this section. Essentially, we specify an objective function, which is subsequently minimized to yield the optimum basis.

At this point, it is worthwhile mentioning that the development of the optimum basis determination algorithm for hybrid image coding is very similar to that for pure two-dimensional NPT coding, which was given in section 3.5.2. Hence, if desired, the material from the next paragraph up to equation (3.89) may be omitted without seriously affecting the understanding of the subsequent materials in the chapter. A detailed derivation of the algorithm has been given for completeness.

We denote the spatial domain error array (obtained by forming the difference between the original image sub-array $\mathbf{F}_w$ and its coded version $\hat{\mathbf{F}}_w$) resulting from NPT hybrid coding of an image sub-array with the NPT basis specified by α, for a given bit rate and quantization scheme by $\mathbf{E}_S(\alpha, \theta)$. Similarly, we denote the transform domain error array (obtained by forming the difference between the transform coefficients of the original image sub-array and their coded version) by $\mathbf{E}_T(\alpha, \theta)$; in both cases, θ specifies the dependence on bit rate and quantization scheme.

The optimum basis is given by

$$\alpha_{opt} = \min_{\alpha} \left[E \left\{ ||\mathbf{E}_S(\alpha, \theta)||^2 \right\} \right] \tag{3.52a}$$

or equivalently,

$$\alpha_{opt} = \max_{\alpha} \left[E\left\{ ||\mathbf{E}_S(0,\theta)||^2 \right\} - E\left\{ ||\mathbf{E}_S(\alpha,\theta)||^2 \right\} \right] \tag{3.52b}$$

where $E\{\cdot\}$ is the mathematical expectation operator. An explicit functional expression for the objective function, given by (3.52) is derived in the following way.

Noting that the error arrays $\mathbf{E}_S(\alpha,\theta)$ and $\mathbf{E}_T(\alpha,\theta)$ are related by

$$\mathbf{E}_S(\alpha,\theta) = \mathbf{E}_T(\alpha,\theta)\psi^{-1}\{\alpha\} \tag{3.53}$$

, it follows that

$$E\left\{ ||\mathbf{E}_S(\alpha,\theta)||^2 \right\} = E\left\{ ||\mathbf{E}_T(\alpha,\theta)\psi^{-1}\{\alpha\}||^2 \right\} \tag{3.54}$$

Applying Schwartz inequality to (3.54), we obtain

$$E\left\{ ||\mathbf{E}_S(\alpha,\theta)||^2 \right\} \leq ||\psi^{-1}\{\alpha\}||^2 E\left\{ ||\mathbf{E}_T(\alpha,\theta)||^2 \right\} \tag{3.55}$$

from which we can write

$$E\left\{ ||\mathbf{E}_S(\alpha,\theta)||^2 \right\} = c(\alpha,\theta)||\psi^{-1}\{\alpha\}||^2 E\left\{ ||\mathbf{E}_T(\alpha,\theta)||^2 \right\} \tag{3.56}$$

where $c(\alpha,\theta)$ is a function which establishes the equality of (3.54) for all values of α, for a given bit rate and quantization scheme. Making use of the fact that

$$E\left\{ ||\mathbf{E}_S(0,\theta)||^2 \right\} = E\left\{ ||\mathbf{E}_T(0,\theta)||^2 \right\} \tag{3.57}$$

we define

$$c(\alpha,\theta) = b_0 \cdot b(\alpha,\theta) \tag{3.58}$$

where $c(\alpha,\theta) = b(\alpha,\theta) = 1$ when $\alpha = 0$ or $\alpha = 1$. Using (3.58) in (3.56) and making use of (3.57), we obtain

$$b_0 = \frac{1}{||\psi^{-1}\{0\}||^2} \tag{3.59}$$

and (3.56) becomes

$$E\left\{ ||\mathbf{E}_S(\alpha,\theta)||^2 \right\} = d(\alpha,\theta) \cdot E\left\{ ||\mathbf{E}_T(\alpha,\theta)||^2 \right\} \tag{3.60}$$

where

$$d(\alpha,\theta) = b(\alpha,\theta) \cdot \frac{||\psi^{-1}\{\alpha\}||^2}{||\psi^{-1}\{0\}||^2} \tag{3.61}$$

for a given bit rate and quantization scheme. Hence, $d(\alpha,\theta)$ is the ratio of the spatial domain MSE to the transform domain MSE as a function of α and the term $\frac{||\psi^{-1}\{\alpha\}||^2}{||\psi^{-1}\{0\}||^2}$ appearing in (3.61) is a prediction of $d(\alpha,\theta)$; $b(\alpha,\theta)$ is an empirically determined correction factor which accounts for the difference between $d(\alpha,\theta)$ and

the prediction given by the norm ratio $\frac{||\psi^{-1}\{\alpha\}||^2}{||\psi^{-1}\{0\}||^2}$. In practice, a suitable representative function would have to be determined for the class of images to be coded. Using (3.60) in the objective function (3.52), it is clear that $\alpha_{opt} \neq 0$ iff

$$E\left\{||\mathbf{E}_S(0,\theta)||^2\right\} > d(\alpha,\theta) \cdot E\left\{||\mathbf{E}_T(\alpha,\theta)||^2\right\} \tag{3.62}$$

The remaining term in (3.60) that needs to be specified functionally is the transform domain MSE $E\left\{||\mathbf{E}_T(\alpha,\theta)||^2\right\}$, which we derive in the following.

The transform domain MSE is given by

$$E\left\{||\mathbf{E}_T(\alpha,\theta)||^2\right\} = \sum_{v=1}^{p} e^2(v;\alpha)\, r\left(q(v;\alpha)\right) \tag{3.63}$$

where

$e^2(v;\alpha)$ = variance of the differential signal in the v^{th} DPCM system.

p = one-dimensional transform order.

$r(q)$ = MSE for a unit-variance signal quantized with a q- level quantizer.

$q(v;\alpha)$ = number of quantizer levels used for quantizing the differential signal in the v^{th} DPCM system, when the NPT basis specified at α is used.

The variance of the differential signal in the v^{th} DPCM system using an n^{th} order predictor is given by [23]

$$e^2(v;\alpha) = R_{00}(v;\alpha) - \sum_{i=1}^{n} a_i(v;\alpha) R_{0i}(v;\alpha) \tag{3.64}$$

where $R_{00}(v;\alpha)$ is the variance, $\sigma^2(v;\alpha)$, of the transform coefficients in the v^{th} column of the image sub-array and the $a_i(v;\alpha)$ are the optimum predictor coefficients which are related to the $R_{0i}(v;\alpha)$ by a set of n simultaneous equations.

For an image of moderate detail, it has been shown [37] that a negligible improvement in the performance of hybrid coding systems is obtained when a predictor of order higher than one is used. Thus, we limit the predictor order to unity and the variance of the differential signal for first order prediction becomes

$$e^2(v;\alpha) = \sigma^2(v;\alpha)\left(1 - a_1^2(v;\alpha)\right) \tag{3.65}$$

The variance of the differential signal in each DPCM channel given by (3.65) is dependent on α and we can obtain an explicit expression for it as a function of α by developing explicit expressions for the variance of transform coefficients

$\sigma^2(v;\alpha)$, and the first order predictor coefficients $a_1(v;\alpha)$, respectively in terms of α and using these in (3.65).

First, we develop an expression for the variance of the transform coefficients $\sigma^2(v;\alpha)$, in terms of α. The variance of the transform coefficients in the v^{th} column of the transformed sub-array is given by

$$\sigma^2(v;\alpha) = E\left\{[\mathbf{T}_w(i,v;\alpha)]^2\right\} - [\mu(v;\alpha)]^2 \qquad 1 \le v \le p \tag{3.66}$$

which can be expressed as

$$\sigma^2(v;\alpha) = \left(\frac{1}{N}\sum_{i=1}^{N}[\mathbf{T}_w(i,v;\alpha)]^2\right) - [\mu(v;\alpha)]^2 \qquad 1 \le v \le p \tag{3.67}$$

where $\mu(v;\alpha)$ is the mean of the transform coefficients in the v^{th} column of the transformed sub-array $\mathbf{T}_w$ and is given by

$$\mu(v;\alpha) = E\{\mathbf{T}_w(i,v;\alpha)\} \qquad 1 \le v \le p \tag{3.68}$$

or equivalently,

$$\mu(v;\alpha) = \frac{1}{N}\sum_{i=1}^{N}\mathbf{T}_w(i,v;\alpha) \qquad 1 \le v \le p \tag{3.69}$$

An explicit expression for $\sigma^2(v;\alpha)$ in terms of α can be derived by considering the components of the one-dimensional row NPT of the image sub-array. We can express the one-dimensional row NPT of an array $\mathbf{F}$ as

$$\mathbf{T} = \alpha\mathbf{F} + k(1-\alpha)\mathbf{FA} \tag{3.70a}$$

$$= \alpha\mathbf{F} + k(1-\alpha)\mathbf{Y} \tag{3.70b}$$

where $\mathbf{Y} = \mathbf{FA}$ and $\mathbf{A}$ is the component classical orthogonal transform used in the NPT kernel. Thus, the transform coefficients at location (i,v) of the sub-array $\mathbf{T}_w$ can be expressed as

$$\mathbf{T}_w(i,v;\alpha) = \alpha\mathbf{F}_w(i,v) + k(1-\alpha)\mathbf{Y}_w(i,v) \tag{3.71}$$

Using (3.71) in (3.68), we obtain the mean of the (i,v) transform components as

$$\mu(v;\alpha) = \alpha E\{\mathbf{F}_w(i,v)\} + k(1-\alpha)E\{\mathbf{Y}_w(i,v)\} \tag{3.72}$$

and defining

$$\mu_R = E\{\mathbf{R}_w(i,v)\} \qquad 1 \le v \le p \tag{3.73}$$

we can re-write (3.72) as

$$\mu(v;\alpha) = (\mu_{\mathbf{F}} - k\mu_{\mathbf{Y}})\,\alpha + k\mu_{\mathbf{Y}} \tag{3.74}$$

which is a first-order polynomial in α whose coefficients depend on the statistics of the image and the component classical orthogonal transform $\mathbf{A}$, used in the NPT kernel. Dropping the (i,v) indices on the right hand side of (3.71), we can write

$$E\left\{[\mathbf{T}_w(i,v;\alpha)]^2\right\} = E\left\{[\alpha\mathbf{F}_w + k(1-\alpha)\mathbf{Y}_w]^2\right\} \tag{3.75a}$$

or

$$E\left\{[\mathbf{T}_w(i,v;\alpha)]^2\right\} = \alpha^2 E\left\{\mathbf{F}_w^2\right\} + 2\alpha k(1-\alpha)E\left\{\mathbf{F}_w\mathbf{Y}_w\right\} + k^2(1-\alpha)^2 E\left\{\mathbf{Y}_w^2\right\} \tag{3.75b}$$

Using (3.75b) and (3.74) in (3.66), we obtain

$$\begin{aligned}\sigma^2(v;\alpha) = {} & \alpha^2\left(E\left\{\mathbf{F}_w^2\right\} - \mu_{\mathbf{F}}^2\right) + 2\alpha k(1-\alpha)\left(E\left\{\mathbf{F}_w\mathbf{Y}_w\right\} - \mu_{\mathbf{F}}\mu_{\mathbf{Y}}\right) \\ & + k^2(1-\alpha)^2\left(E\left\{\mathbf{Y}_w^2\right\} - \mu_{\mathbf{Y}}^2\right)\end{aligned} \tag{3.76}$$

Defining

$$\sigma_{\mathbf{RX}}^2 = E\left\{\mathbf{R}_w(i,v)\mathbf{X}_w(i,v)\right\} - \mu_{\mathbf{R}}\mu_{\mathbf{X}} \tag{3.77}$$

we can re-write (3.76) as

$$\sigma^2(v;\alpha) = \alpha^2\sigma_{\mathbf{FF}}^2 + 2\alpha k(1-\alpha)\sigma_{\mathbf{FY}}^2 + k^2(1-\alpha)^2\sigma_{\mathbf{YY}}^2 \tag{3.78}$$

and collecting terms of similar powers in α, we obtain

$$\sigma^2(v;\alpha) = h_0(v) + h_1(v)\alpha + h_2(v)\alpha^2 \tag{3.79}$$

where

$$h_0(v) = k^2\sigma_{\mathbf{YY}}^2 \tag{3.80a}$$

$$h_1(v) = 2k\sigma_{\mathbf{FY}}^2 - 2k^2\sigma_{\mathbf{YY}}^2 \tag{3.80b}$$

$$h_2(v) = \sigma_{\mathbf{FF}}^2 - 2k\sigma_{\mathbf{FY}}^2 + k^2\sigma_{\mathbf{YY}}^2 \tag{3.80c}$$

Thus, the variance of the NPT coefficients in the v^{th} column of the sub-array $\mathbf{T}_w$ is a second order polynomial in α whose coefficients $h_j(v)$, $j = 0,1,2$ vary with the statistics of the image and the classical orthogonal transform used in the NPT kernel. For a given image and classical orthogonal transform, (3.79) is a second order polynomial in α with constant coefficients h_j, $j = 0,1,2$; parallel to the two-dimensional NPT case, we refer to the coefficients h_j, $j = 0,1,2$ as the *"one-dimensional NPT statistic functions "*.

A functional expression for the first order predictor coefficients $a_1(v;\alpha)$, in terms of α is now derived. Under the assumption of a zero-mean random process in each column, the optimum predictor coefficients are given by

$$a_1(v;\alpha) = \frac{E\left\{\mathbf{T}_w(i,v;\alpha)\mathbf{T}_w(i-1,v;\alpha)\right\}}{\sigma^2(v;\alpha)} \tag{3.81}$$

Using (3.71) in (3.81), we obtain

$$a_1(v;\alpha) = \frac{E\left\{[\alpha \mathbf{F}_w(i,v) + k(1-\alpha)\mathbf{Y}_w(i,v)]\,[\alpha \mathbf{F}_w(i-1,v) + k(1-\alpha)\mathbf{Y}_w(i-1,v)]\right\}}{\sigma^2(v;\alpha)} \tag{3.82}$$

Defining

$$\tilde{\rho}_{\mathbf{AB}} = E\left\{\mathbf{A}(i,v)\mathbf{B}(i-1,v)\right\} \tag{3.83}$$

we can express (3.82) as

$$a_1(v;\alpha) = \Big[\left(\tilde{\rho}_{\mathbf{FF}} - k\tilde{\rho}_{\mathbf{FY}} - k\tilde{\rho}_{\mathbf{YF}} + k^2\tilde{\rho}_{\mathbf{YY}}\right)\alpha^2 + \left(k\tilde{\rho}_{\mathbf{FY}} + k\tilde{\rho}_{\mathbf{YF}} - 2k^2\tilde{\rho}_{\mathbf{YY}}\right)\alpha + k^2\tilde{\rho}_{\mathbf{YY}}\Big]/\sigma^2(v;\alpha) \tag{3.84}$$

or

$$a_1(v;\alpha) = \frac{c_0(v) + c_1(v)\alpha + c_2(v)\alpha^2}{h_0(v) + h_1(v)\alpha + h_2(v)\alpha^2} \tag{3.85}$$

where

$$c_0(v) = k^2\tilde{\rho}_{\mathbf{YY}} \tag{3.86a}$$

$$c_1(v) = k\left(\tilde{\rho}_{\mathbf{FY}} + \tilde{\rho}_{\mathbf{YF}}\right) - 2k^2\tilde{\rho}_{\mathbf{YY}} \tag{3.86b}$$

$$c_2(v) = \tilde{\rho}_{\mathbf{FF}} - k\left(\tilde{\rho}_{\mathbf{FY}} + \tilde{\rho}_{\mathbf{YF}}\right) + k^2\tilde{\rho}_{\mathbf{YY}} \tag{3.86c}$$

and $h_0(v)$, $h_1(v)$ and $h_2(v)$ are as previously defined in (3.80). Substituting (3.79) and (3.85) in (3.65) we obtain the variance of the differential signals as

$$e^2(v;\alpha) = \sigma^2(v;\alpha)\left[1 - \frac{\left(c_0(v) + c_1(v)\alpha + c_2(v)\alpha^2\right)^2}{\sigma^4(v;\alpha)}\right] \tag{3.87a}$$

$$= \frac{\left(h_0(v) + h_1(v)\alpha + h_2(v)\alpha^2\right)^2 - \left(c_0(v) + c_1(v)\alpha + c_2(v)\alpha^2\right)^2}{h_0(v) + h_1(v)\alpha + h_2(v)\alpha^2} \tag{3.87b}$$

which after algebraic manipulations yield

$$e^2(v;\alpha) = d_0(v;\alpha) + d_1(v;\alpha)\alpha + d_2(v;\alpha)\alpha^2 + d_3(v;\alpha)\alpha^3 + d_4(v;\alpha)\alpha^4 \tag{3.88}$$

where

$$d_0(v;\alpha) = \left(h_0^2(v) - c_0^2(v)\right)\cdot\left(h_0(v) + h_1(v)\alpha + h_2(v)\alpha^2\right)^{-1} \tag{3.89a}$$

$$d_1(v;\alpha) = 2\left(h_0(v)h_1(v) - c_0(v)c_1(v)\right)\cdot\left(h_0(v) + h_1(v)\alpha + h_2(v)\alpha^2\right)^{-1} \tag{3.89b}$$

$$d_2(v;\alpha) = \left(2h_0(v)h_2(v) + h_1^2(v) - 2c_0(v)c_2(v) - c_1^2(v)\right)\cdot \left(h_0(v) + h_1(v)\alpha + h_2(v)\alpha^2\right)^{-1} \tag{3.89c}$$

$$d_3(v;\alpha) = 2\left(h_1(v)h_2(v) - c_1(v)c_2(v)\right)\cdot\left(h_0(v) + h_1(v)\alpha + h_2(v)\alpha^2\right)^{-1} \tag{3.89d}$$

$$d_4(v;\alpha) = \left(h_2^2(v) - c_2^2(v)\right)\cdot\left(h_0(v) + h_1(v)\alpha + h_2(v)\alpha^2\right)^{-1} \tag{3.89e}$$

Thus, the differential signal variance is a polynomial in α whose coefficients $d_j(v;\alpha)$, $j = 0, 1, \ldots, 4$ are dependent on α, the statistics of the image, the classical orthogonal transform used in the NPT kernel and the characteristics of the

predictor. We refer to the coefficients $d_j(v;\alpha)$, $j = 0,1,\ldots,4$ as *"predictive one-dimensional NPT statistic functions"*. Substituting (3.88) into (3.63), we obtain the transform domain MSE for predictive NPT image coding as

$$E\left\{||\mathbf{E}_T(\alpha,\theta)||^2\right\} = g_0(\alpha) + g_1(\alpha)\alpha + g_2(\alpha)\alpha^2 + g_3(\alpha)\alpha^3 + g_4(\alpha)\alpha^4 \tag{3.90}$$

where

$$g_t(\alpha) = \sum_{v=1}^{p} d_t(v;\alpha) r\left(q(v;\alpha)\right) \qquad t = 0,1,\ldots,4 \tag{3.91}$$

which is a nonlinear polynomial in α whose coefficients are a summation of the respective predictive one-dimensional NPT statistic weighted distortion functions. The quantizer distortion functions $r\left(q(v;\alpha)\right)$ in (3.91) are constants that depend on the number of bits assigned to the differential signals in the v^{th} column and the quantizer characteristics. Since an identical functional relationship holds for the variation of the differential signal variance with α, it implies that the magnitude of the variances of the differential signals in the respective columns of the sub-array, in relation to each other, would not change as α is varied. Hence, by assigning bits in proportion to the variance of the differential signals, the variation of bit assignment with α will be negligible and the bit assignment need only be determined once.

Substituting (3.90) into (3.60), we obtain the functional expression for the spatial domain MSE, resulting from the hybrid NPT coding of an image sub-array as

$$E\left\{||\mathbf{E}_S(\alpha,\theta)||^2\right\} = b(\alpha,\theta)\cdot\frac{||\psi^{-1}\{\alpha\}||^2}{||\psi^{-1}\{0\}||^2}\cdot \left(g_0(\alpha) + g_1(\alpha)\alpha + g_2(\alpha)\alpha^2 + g_3(\alpha)\alpha^3 + g_4(\alpha)\alpha^4\right) \tag{3.92}$$

As previously stated, $b(\alpha,\theta)$ is an empirically determined correction function and representative functions can be obtained for the various classes of images to be coded. In this way, all the terms of (3.92) are completely specified and the optimum basis can be obtained by numerically minimizing (3.92) with respect to α. Suitable algorithms for solving (3.92) can be found in [38,39].

3.6.2 Simulation, Results and Discussion

The hybrid coding scheme described in the previous section is an adaptive hybrid coding scheme which uses different transform basis, transform coefficient statistics and bit allocation for the respective image sub-arrays. The hybrid coding

scheme was simulated for NPT hybrid coding of some monochrome images. In the simulations, the images were partitioned into 256×64 sub-arrays and the optimum basis for each sub-array was determined. Bits were assigned to the differential signals using the marginal analysis approach [41,45]. The differential signals were quantized using the optimum Laplacian quantizer.

As indicated in the developments of the previous section, the optimum basis determination algorithm requires a correction factor to correct the prediction of the spatial/transform domain MSE ratio by the norm ratio $\frac{||\psi^{-1}\{\alpha\}||^2}{||\psi^{-1}\{0\}||^2}$. Fig. 3.39a shows the ratio of the spatial domain MSE to the transform domain MSE as a function of α, at bit rates of 0.5 bit/pixel, 1.0 bit/pixel, 1.5 bits/pixel and 2.0 bits/pixel respectively, for one of the 256×64 sub-arrays of image ALAN (the original picture is shown in Fig. 2.7). The norm ratio is also plotted. It is observed that the norm ratio is a good approximation of the spatial/transform domain MSE ratio over the range $-0.15 < \alpha < 0.06$. Furthermore, the MSE ratio increases with bit rate. The corresponding correction factors are shown in Fig. 3.39b. The behaviour of the correction factors is similar to that for two-dimensional transform coding where we observed that the correction factors for bit rates above 1.0 bit/pixel are close in magnitude, with that at a bit rate of 0.5 bit/pixel being of lower magnitude. Fig. 3.40 shows the variation of the correction factor with image sub-array; the sub-arrays are numbered starting from the left hand side of the picture. It is observed that the differences in the magnitudes of the correction factors is highest for $\alpha > 0$. However, the magnitudes of the correction factors for sub-arrays 2 and 3 are very similar for $\alpha > 0$. Fig. 3.41 shows the respective correction factors for the Hadamard NPT, sine NPT and SC NPT hybrid coding of a 256×64 sub-array of image ALAN, at a bit rate of 1.5 bits/pixel. The greatest variation in the correction factors is obtained at $\alpha > 0$. By specifying an NPT transform type and bit rate, the correction factors become only dependent on the transform basis parameter α and image sub-array statistics. The variation with image sub-array statistics can be accounted for in a practical coding application by determining the respective correction factors that are representative for the image sub-arrays in the ensemble of images to be coded. The effect of the variation in the correction factors has greater significance at high MSE levels (low bit rate) than at low MSE levels (high bit rate).

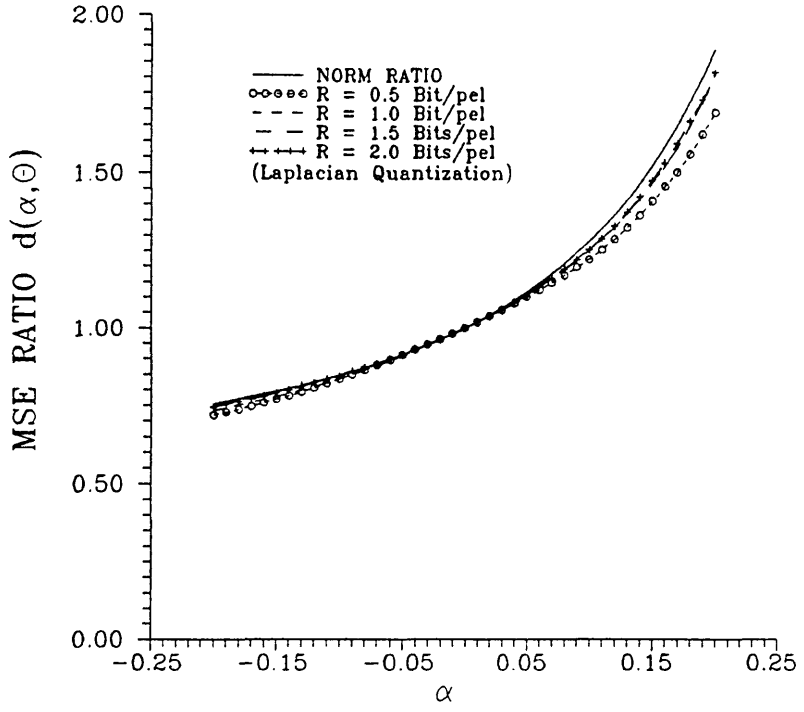


Fig. 3.39a : Spatial/Transform domain MSE ratio as a function of α; Hadamard NPT hybrid coding of a 256 x 64 sub-array of image ALAN.

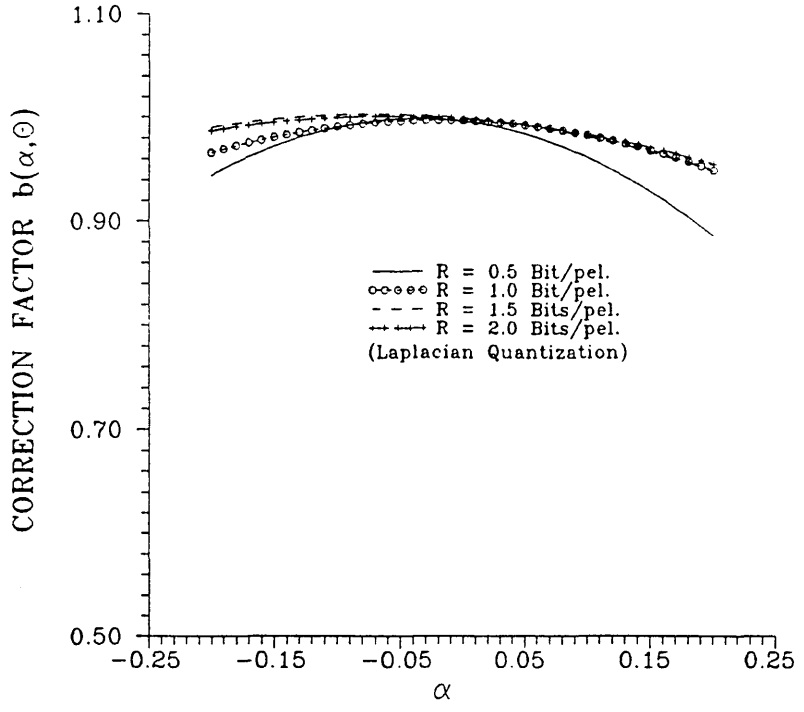


Fig. 3.39b : Hadamard NPT correction factor as a function of α; Hadamard NPT hybrid coding of a 256 x 64 sub-array of image ALAN.

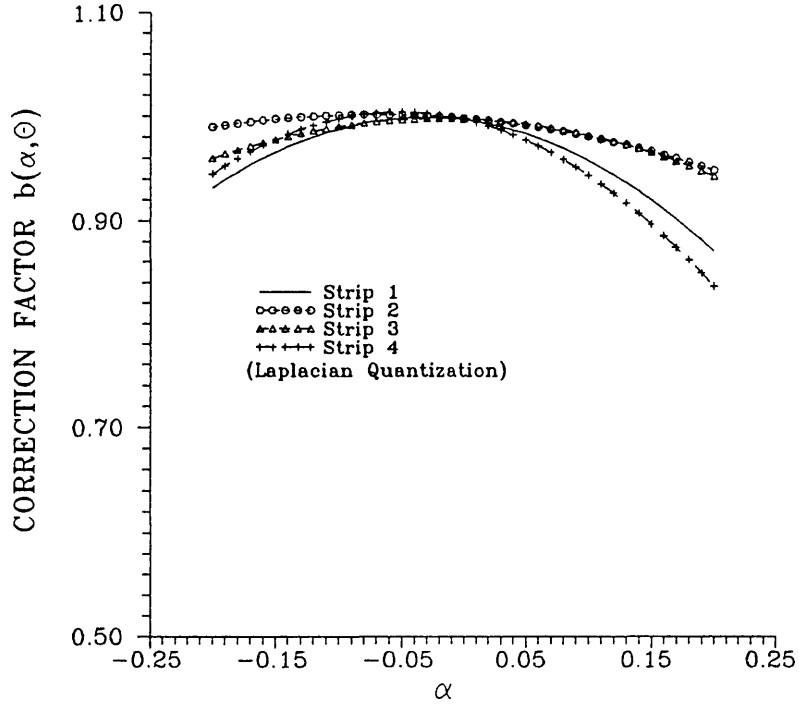


Fig. 3.40 : Hadamard NPT correction factors as a function of α, for the Hadamard NPT hybrid coding of the respective 256 x 64 sub-arrays of image ALAN at a rate of 1.5 bits/pel.

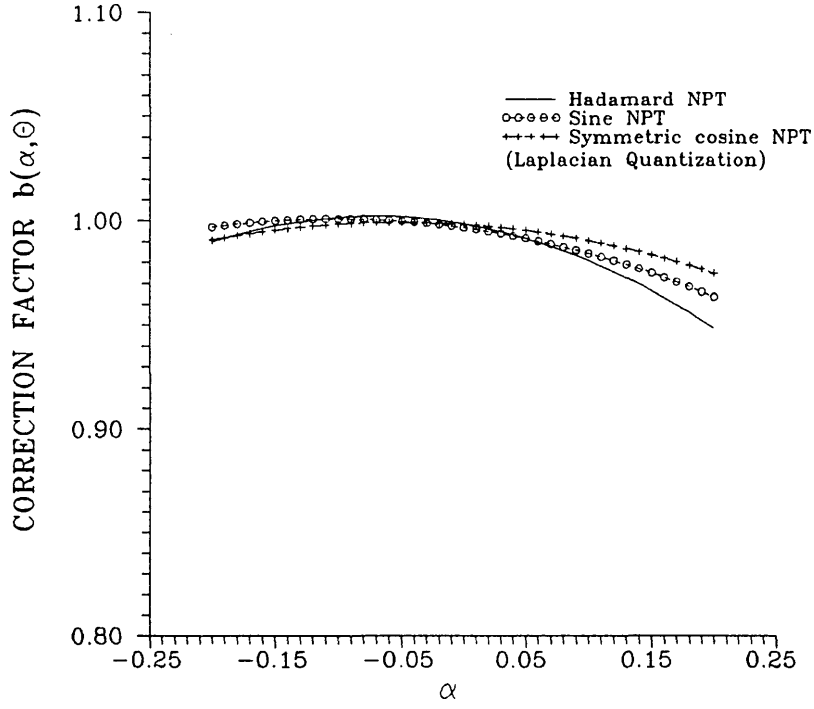


Fig. 3.41 : Correction factor as a function of α for the respective Hadamard NPT, sine NPT and SC NPT hybrid coding of a 256 x 64 sub-array of image ALAN at 1.5 bits/pel.

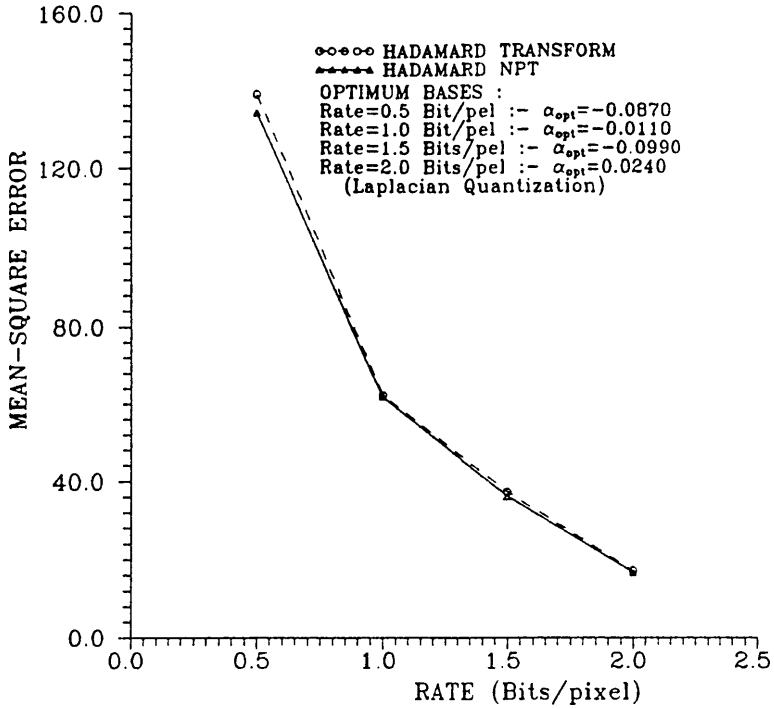


Fig. 3.42 : Mean-square error as a function of bit rate for the Hadamard NPT hybrid coding of a 256 x 64 sub-array of image DOCUMENT.

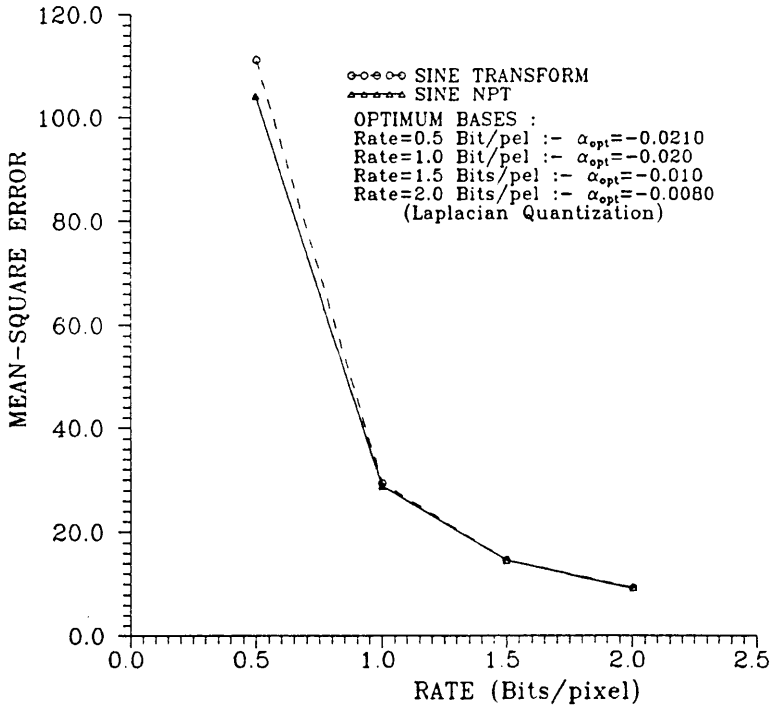


Fig. 3.43 : Mean-square error as a function of bit rate for the sine NPT hybrid coding of a 256 x 64 sub-array of image DOCUMENT.

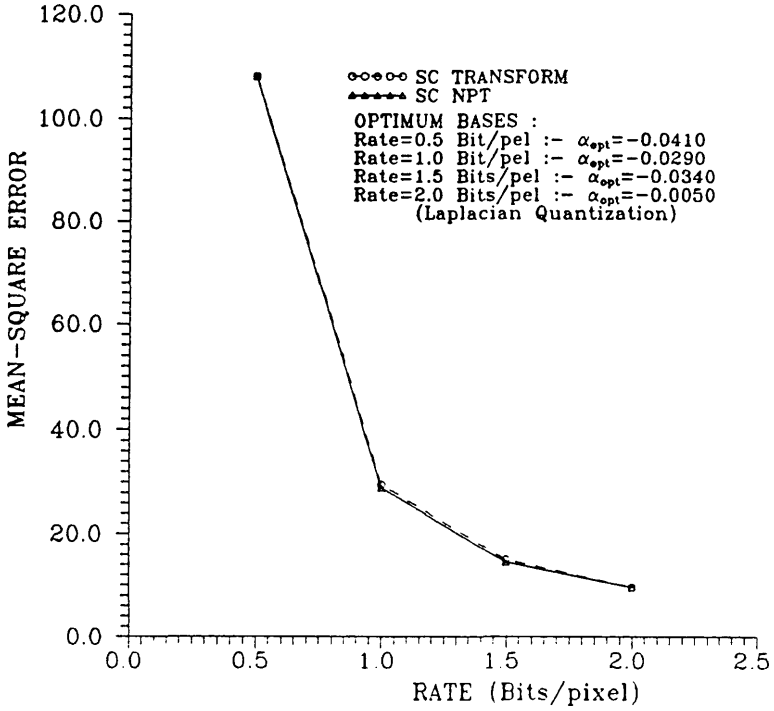


Fig. 3.44 : Mean-square error as a function of bit rate for the SC NPT hybrid coding of a 256 x 64 sub-array of image DOCUMENT.

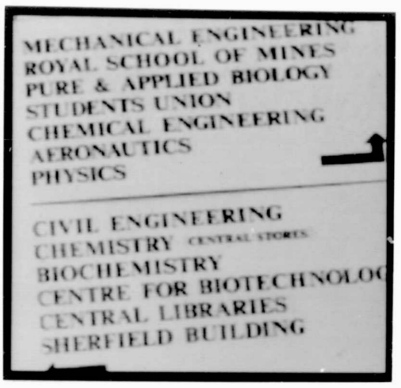


Fig. 3.45a : 1×64 Hadamard Transform Hybrid Coding of DOCUMENT ; 2.0 Bits/pel.

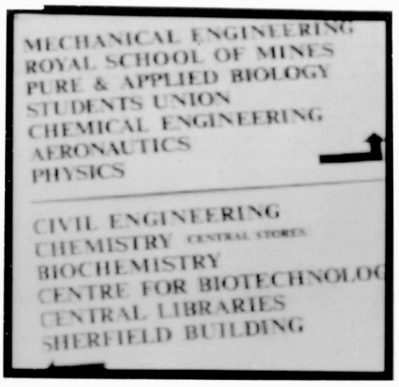


Fig. 3.45b : 1×64 Hadamard NPT(0.1) Hybrid Coding of DOCUMENT ; 2.0 Bits/pel.

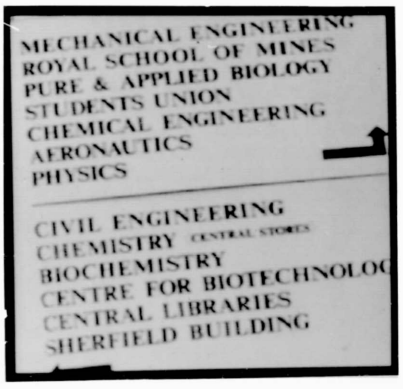


Fig. 3.46a : 1×64 sine Transform Hybrid Coding of DOCUMENT ; 2.0 Bits/pel.

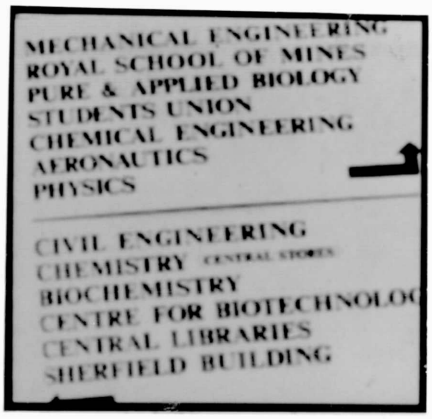


Fig. 3.46b : 1×64 sine NPT(0.1) Hybrid Coding of DOCUMENT ; 2.0 Bits/pel.

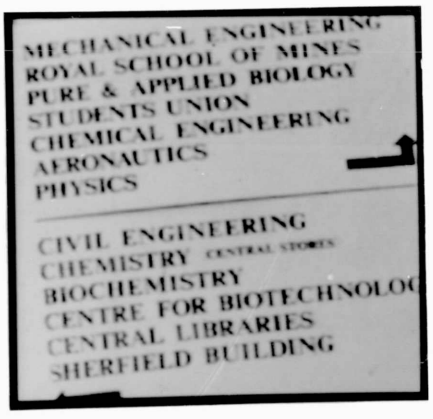


Fig. 3.47a : 1×64 SC Transform Hybrid Coding of DOCUMENT ; 2.0 Bits/pel.

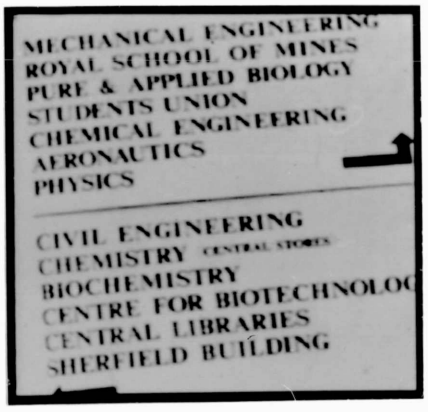


Fig. 3.47b : 1×64 SC NPT(0.1) Hybrid Coding of DOCUMENT ; 2.0 Bits/pel.

The NPT hybrid coding of the images ALAN, CHOIR, PATTERN and DOCUMENT was simulated. For the sub-arrays of the image ALAN, very little improvement in MSE was obtained when the optimum NPT basis was used, compared to when the corresponding orthogonal transform basis ($\alpha = 0$) was used. For the remaining images, an improvement in MSE was obtained for some sub-arrays of the images but the improvement in MSE was higher at low bit rates. Figs. 3.42-3.44 respectively show the results of the Hadamard NPT, sine NPT and the SC NPT hybrid coding of a sub-array of the image DOCUMENT. An improvement in MSE is obtained for the Hadamard NPT and sine NPT hybrid coding of the image sub-array at a bit rate of 0.5 bit/pixel, while at higher bit rates, little or no improvement was obtained by using the NPT bases. The SC NPT show negligible improvement in MSE at all bit rates.

The conclusion that can be drawn from the MSE results above and that presented in [36] is that the improvement in MSE by using the Hadamard NPT and the sine NPT for hybrid coding is higher at low bit rates than at high bit rates. The SC NPT bases show negligible improvement over the SC transform basis for hybrid coding of the images considered. An additional observation is that a higher MSE improvement is obtained by using the NPT bases for pure two-dimensional transform coding than for hybrid coding using one-dimensional NPT transforms.

Fig. 3.45a, Fig. 3.46a and Fig. 3.47a respectively show the pictorial results of the Hadamard transform hybrid coding, sine transform hybrid coding and the SC transform hybrid coding of image DOCUMENT at a bit rate of 2.0 bits/pixel, using a block size of 64. Fig. 3.45b, Fig. 3.46b and Fig. 3.47b respectively show the corresponding pictorial results of the Hadamard NPT hybrid coding, sine NPT hybrid coding and the SC NPT hybrid coding of image DOCUMENT at a bit rate of 2.0 bits/pixel , using the NPT basis specified at $\alpha = 0.1$. There is little noticeable difference between the subjective quality of the respective pictures coded using the orthogonal transform basis ($\alpha = 0$) and the NPT basis specified at $\alpha = 0.1$.

3.7 Summary and Conclusion

The focus of this chapter has been on image data compression using the NPT transforms. The NPT has been investigated within the framework of pure two-dimensional transform coding in part A of the chapter. The NPT transforms offer an infinite number of possible basis for encoding a given picture or picture ensemble. Consequently, the problem of determining the basis (or collection of

bases) giving minimum mean-square error for coding a given picture (or picture ensemble) has been addressed. An algorithm for determining the optimum basis for coding a given picture has been introduced. The algorithm requires the specification of an empirically determined correction factor which corrects for the representation of the ratio of the spatial domain MSE to the transform domain MSE by the fourth power of the ratio of the norm of the inverse NPT matrix to the norm of an orthogonal transform matrix. The correction factor has been modelled by a second order polynomial in the basis parameter α, with constant coefficients. The correction factor has been found to be mainly dependent on the basis parameter α, but has some variations with the transform order, bit rate, NPT transform type, quantization scheme and image content. However, specifying a block size, bit rate, NPT transform and quantization scheme effectively reduces the number of parameters to be considered in the determination of the correction factors.

Non-adaptive NPT image coding has been investigated. The non-adaptive NPT coder is basis adaptive over an ensemble of images, since it uses a different basis for coding the respective images in the ensemble. Superior MSE performance to that of the parent classical orthogonal transform ($\alpha = 0$) has been obtained by using the optimum NPT basis for image coding. The optimum basis for coding an image has been found to vary with the bit rate, block size, NPT transform type and image content.

For effective adaptation of the NPT bases to the non-stationary nature of typical imagery data, a basis adaptive NPT coding scheme has been proposed. The Basis Adaptive NPT Coder (BANPTC) is a block classification adaptive transform coding system which features transform basis adaptation according to local image content. Superior MSE performance to that of the classical orthogonal transform basis ($\alpha = 0$) based scheme has been obtained by adapting the NPT bases to the local image spatial activity. The MSE improvement has been shown to be higher when a small block size of 4 is used than when a larger block size of 8 is used.

Errors in the code-word digits used for representing the transform coefficients (resulting from channel errors) has been shown to have no noticeable effect on the subjective quality of the coded pictures at a BER of 10^{-4} and less. However, incorrect basis picture contributions to the reconstructed picture has been shown

to have a noticeable effect on the subjective quality of coded pictures at a BER of 10^{-3} and above.

NPT hybrid coding of images has been investigated in part B of this chapter. An algorithm for determining the optimum NPT basis for coding a given image or image sub-array has been introduced. The algorithm also requires the specification of an empirically determined correction factor which corrects for the representation of the spatial to transform domain MSE ratio by the second power of the ratio of the norm of the inverse NPT matrix to the norm of the orthogonal transform matrix. The correction factor has been found to be dependent on the bit rate, image sub-array statistics and NPT transform type, and has been modelled by a second order polynomial in the basis parameter α, with constant coefficients.

The NPT hybrid image coder is an adaptive hybrid coder which uses a different transform basis, transform coefficients statistics and bit allocation for coding the respective sub-arrays of the image or image ensemble. The MSE improvement that is achieved when the optimum NPT basis is used for hybrid coding, as opposed to when the parent classical orthogonal transform basis ($\alpha = 0$) is used, has been shown to be higher at low bit rates than at high bit rates. However, the degree of MSE improvement has been shown to vary from one image sub-array to another; in some instances, no MSE improvement has been obtained by using the NPT basis. The MSE improvement for pure two-dimensional NPT transform coding is higher than that for NPT hybrid coding using one-dimensional NPT transforms, when the respective schemes are compared to the equivalent ones using the parent classical orthogonal transform basis ($\alpha = 0$).

CHAPTER FOUR

RATE-DISTORTION THEORETIC ANALYSIS FOR NPT IMAGE CODERS

4.1 Introduction

In chapter three of this thesis, we examined the application of the NPT transforms in image data compression. For a given transmission rate, our main concern was to be able to use the basis giving minimum mean-square error for encoding an image (or image ensemble). A pertinent question, however, is that for a given NPT transform basis (or collection of bases), what is the minimum rate required to transmit or store an image, in order to achieve a desired level of reconstructed picture ?. Rate-distortion theory provides an answer to this question by enabling us to specify a rate-distortion function, which gives the minimum source coder output rate as a function of the desired average distortion level.

This chapter concentrates on the determination of such a function for the NPT based image coders. Some fundamental ideas of rate-distortion theory are presented in section 4.2. A brief discussion of the areas in which the results of rate-distortion theory have been applied to transform image coding is given. Section 4.3 deals with the problem of determining the rate-distortion function for NPT image coders. An equivalent model of an NPT image data compression system is described. A clear mathematical statement of the problem of determining the rate-distortion function for NPT image coders is given. In section 4.4, we restate the NPT image coder rate-distortion function determination problem as that of minimizing the rate necessary to code a sequence of statistically independent samples subject to a weighted MSE (mean-square error) distortion criterion. Employing the optimal Karhunen-Loève transform to convert the NPT samples of the information to a sequence of Gaussian distributed and statistically independent samples, we obtain a rate-distortion function which is effectively an upper bound for the minimum information rate required for coding image data with known second order statistics, using NPT based image coders.

The bounds given by the rate-distortion function are empirically evaluated in section 4.5. In section 4.6, the results of practical NPT coding of a stationary

first order Gauss-Markov image are compared with the theoretical rate-distortion bound for two-dimensional unconstrained complexity coding of stationary first order Gauss-Markov images.

4.2 Fundamentals of Rate-Distortion Theory

Fig. 4.1 describes a basic data compression scheme in which a space or time discrete random vector sequence $\{\mathbf{f}\}$ is mapped into a compressed sequence $\{\hat{\mathbf{f}}\}$. Assuming that the source vectors $\{\mathbf{f}\}$ and sink vectors $\{\hat{\mathbf{f}}\}$ belong to an N-dimensional vector space $\mathcal{V}^N$, then the average information rate (mutual information) $M_N(\mathbf{f},\hat{\mathbf{f}})$ between the vectors, when the vector components are of continuous amplitude, is defined as [44,51]

$$M_N(f,\hat{f}) = \iint_{\mathcal{V}^N} P(\mathbf{f})\, Q(\hat{\mathbf{f}}/\mathbf{f}) log \frac{Q(\hat{\mathbf{f}}/\mathbf{f})}{Q(\hat{\mathbf{f}})} d\mathbf{f}\, d\hat{\mathbf{f}} \tag{4.1}$$

where $P(\mathbf{f})$ is the apriori joint probability density function (pdf) of the input vector sequence and $Q(\hat{\mathbf{f}})$ is the marginal joint probability density function of the output vector sequence. The marginal joint pdf is given by

$$Q(\hat{\mathbf{f}}) = \int_{\mathcal{V}^N} P(\mathbf{f})\, Q(\hat{\mathbf{f}}/\mathbf{f}) d\mathbf{f} \tag{4.2}$$

Associated with every conditional density $Q(\hat{\mathbf{f}}/\mathbf{f})$ is the mutual information $M_N(\mathbf{f},\hat{\mathbf{f}})$ given by (4.1) and an average distortion

$$d(Q) = \iint_{\mathcal{V}^N} \Theta(\mathbf{f},\hat{\mathbf{f}}) d\mathbf{f}\, d\hat{\mathbf{f}} \tag{4.3}$$

where $\Theta(\mathbf{f},\hat{\mathbf{f}})$ is a fidelity criterion to be specified. It is the transition probability density function $Q(\hat{\mathbf{f}}/\mathbf{f})$ which characterizes the compression scheme. An N-block rate-distortion function for the given source is defined as [44,51]

$$R_N(D) = \inf_{Q \in Q_D} \frac{1}{N} M_N(\mathbf{f},\hat{\mathbf{f}}) \tag{4.4}$$

where $R_N(D)$ is the normalized minimum information rate and Q_D is the D-admissible set of conditional densities $Q(\hat{\mathbf{f}}/\mathbf{f})$. This set of densities is given by

$$Q_D = \{Q(\hat{\mathbf{f}}/\mathbf{f}) : d(Q) \leq D\} \tag{4.5}$$

Thus $d(Q)$ is upper bounded by D.

The limiting value of the N-block rate-distortion function is called the rate-distortion function $R(D)$ and is defined as

$$R(D) = \lim_{N \to \infty} R_N(D) \tag{4.6}$$

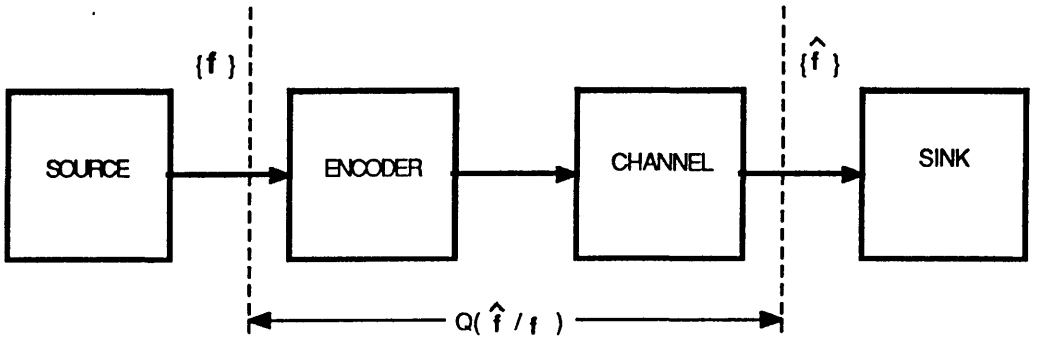


Fig. 4.1 : Basic Data Compression Scheme Specified by Q($\hat{f}$ / f).

In general, there is an increase in the storage or transmission requirement, as a result of using finite N-dimensional blocks of data for compression. This increase in the required rate is given by

$$\Delta R = R_N(D) - R(D) \tag{4.7}$$

Thus, (4.7) implies that $R(D)$ is the minimum rate achievable by an arbitrary complex encoding scheme [52].

There are many forms that the fidelity criterion $\Theta(\mathbf{f}, \hat{\mathbf{f}})$ may take. The so-called 'difference' distortion measures which have the form

$$\Theta(\mathbf{f}, \hat{\mathbf{f}}) = ||\mathbf{f} - \hat{\mathbf{f}}||^2 \tag{4.8a}$$

$$= (\mathbf{f} - \hat{\mathbf{f}})^T(\mathbf{f} - \hat{\mathbf{f}}) \tag{4.8b}$$

or

$$\Theta(\mathbf{f}, \hat{\mathbf{f}}) = |\mathbf{f} - \hat{\mathbf{f}}| \tag{4.9}$$

have received a lot of attention. In particular, the square error distortion given by (4.8) has been extensively used and a mathematically tractable result can be obtained when the information rate minimization is carried out with respect to this fidelity constraint. Discussions on other types of distortion measures such as the maximum distortion criterion and the frequency weighted distortion criterion can be found in [44,51,53].

If the discrete time or space source information is considered to be statistically independent and identically distributed (i.e. memoryless), the minimization of the information rate can be carried out analytically, for many types of distributions (e.g. Gaussian, Gamma, Rayleigh, Laplacian etc.) with respect to a variety of fidelity constraints [51]. In practice, it is for sources with memory (i.e. sources generating information with large redundancy) that optimum encoding produces the greatest gains. For these sources, the rate optimization is usually carried out for information that is assumed to have Gaussian statistics [51], under an MSE fidelity constraint. Combinations of other distribution types and fidelity criteria do not yield analytical results. However, of importance is the fact that the rate-distortion function for a Gaussian source and MSE criterion is an upper bound on the achievable performance for any source with specified second order statistics [51]. This is linked to the fact that the entropy of a Gaussian source is the maximum for all types of distributions [51,pg. 108]. Thus, the solution for a

Gaussian source is useful in the development of practical systems and it gives an idea of the bound on achievable system performance, when the system is used for coding non-Gaussian sources.

4.2.1 Rate-Distortion Theory and Transform Image Coding

Fig. 4.2 is a block diagram of a typical transform data compression system. Here, a forward transform operation specified by $\tau(\mathbf{T_F}/\mathbf{F})$ is performed on the correlated samples of the image source $\{\mathbf{F}\}$ to yield another data sequence $\{\mathbf{T_F}\}$. The transforms used in practice are sub-optimal in the sense of complete decorrelation of data and a certain degree of memory exists in the transformed sequence $\{\mathbf{T_F}\}$. However, the samples of $\{\mathbf{T_F}\}$ are coded in a memoryless fashion which results in a higher rate for the sequence $\{\mathbf{T_F}\}$ than if the memory between the samples of the sequence were taken into account [51,pg. 115]. An inverse transform operation specified by $\tau^{-1}(\hat{\mathbf{F}}/\hat{\mathbf{T}}_\mathbf{F})$ yields the reconstructed compressed image. If the transform kernel is orthogonal, no further MSE is introduced as a result of the inverse transformation and the rate-distortion function can be obtained by considering the sequences $\{\mathbf{T_F}\}$ and $\{\hat{\mathbf{T}}_\mathbf{F}\}$ as the input and output sequences respectively, of the image transmission or storage system.

An upper bound of the rate-distortion function can be obtained by replacing the sub-optimal transformation with the optimal Karhunen-Loève (KL) transform, which produces a sequence $\{\mathbf{T'_F}\}$ of statistically independent (memoryless) samples. The rate requirement for this sequence is the same as that for the original image source $\{\mathbf{F}\}$, since the mutual information is not affected by the transformation. Since the samples of $\{\mathbf{T'_F}\}$ are statistically independent, the result of the rate-distortion function for memoryless sources applies [44,51], which yields the upper bound for the rate-distortion function for an orthogonal transform coder.

There are three main areas that the results of rate-distortion theory have been of relevance to transform image coding. These are

(i) Comparison of transforms on the basis of the rates needed for coding the individual transform coefficient sequences

(ii) Quantizer design and a comparison of the performance of quantizers with the theoretical limits provided by the theory and

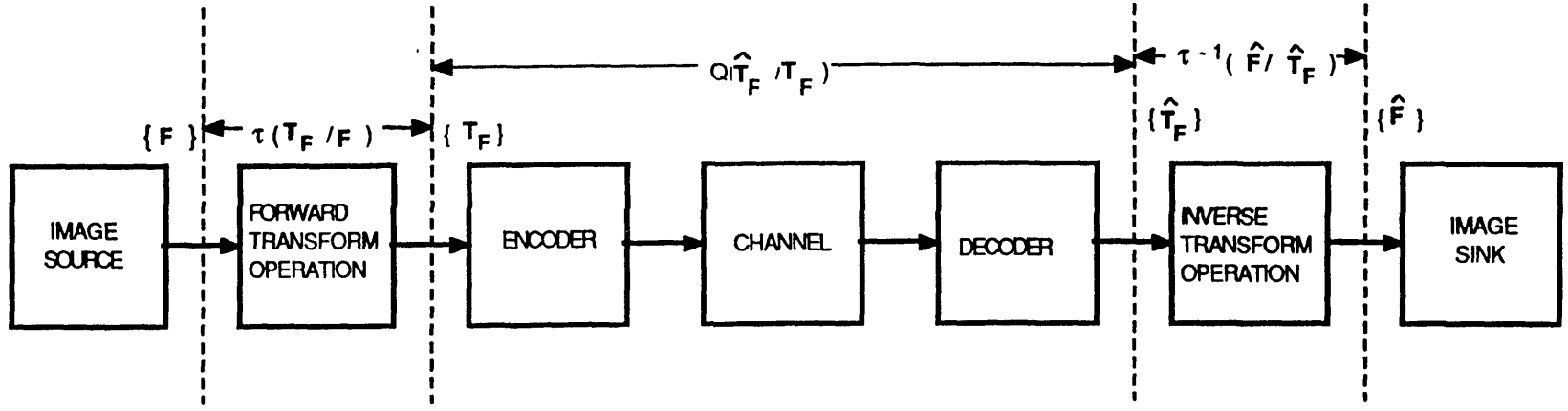


Fig. 4.2 : Basic Transform Coding System.

(iii) Bit allocation where the rate-distortion function for a memoryless Gaussian source is widely used for assigning coding capacity to the individual transform samples.

The main thrust of the work reported here is on the first area mentioned above and precisely, in relation to the NPT transforms, we seek to determine a function which gives us an idea of the rate needed to achieve a desired MSE distortion level when a given NPT basis is used for coding an image.

4.3 Determination of The Rate-Distortion Function for NPT Image Coders

We stated in chapters two and three that the NPT bases are not orthogonal. Specifically, we showed in chapter two that the forward NPT transform kernel considered in this thesis is Euclidean norm reducing while the inverse NPT kernel is Euclidean norm increasing. The implication of these facts is that the inverse of the pre-whitening transformation in the model of Fig. 4.2, i.e. $\tau^{-1}(\hat{\mathbf{F}}/\hat{\mathbf{T}}_{\mathbf{F}})$, introduces some additional MSE distortion. It is in this respect that the rate-distortion analysis for NPT image coders differs significantly from the traditional approaches carried out for orthogonal transforms. The main problem lies in being able to incorporate the effect of the change in MSE due to inverse transformation in the derivation of the rate-distortion function.

In chapter three, we showed that the overall MSE distortion when an NPT transform is used for coding an image can be obtained by multiplying the MSE distortion between the original and coded transform samples by a factor which is determined by the norm of the NPT transform matrix and the norm of the classical orthogonal transform matrix component in the NPT kernel. Based on this decomposition, we can represent the NPT data compression system by the model shown in Fig. 4.3.

Here, we have replaced the inverse NPT transform by two transforms viz an 'ideal' inverse NPT transform which produces the data sequence $\{\mathbf{F}'\}$ such that

$$E\left\{\|\hat{\mathbf{T}}_{\mathbf{F}} - \mathbf{T}_{\mathbf{F}}\|^2\right\} = E\left\{\|\mathbf{F}' - \mathbf{F}\|^2\right\} \tag{4.10}$$

where $E\{\cdot\}$ is the mathematical expectation operator, and a conceptual noisy transformation which produces the final compressed image data sequence $\{\hat{\mathbf{F}}\}$ such

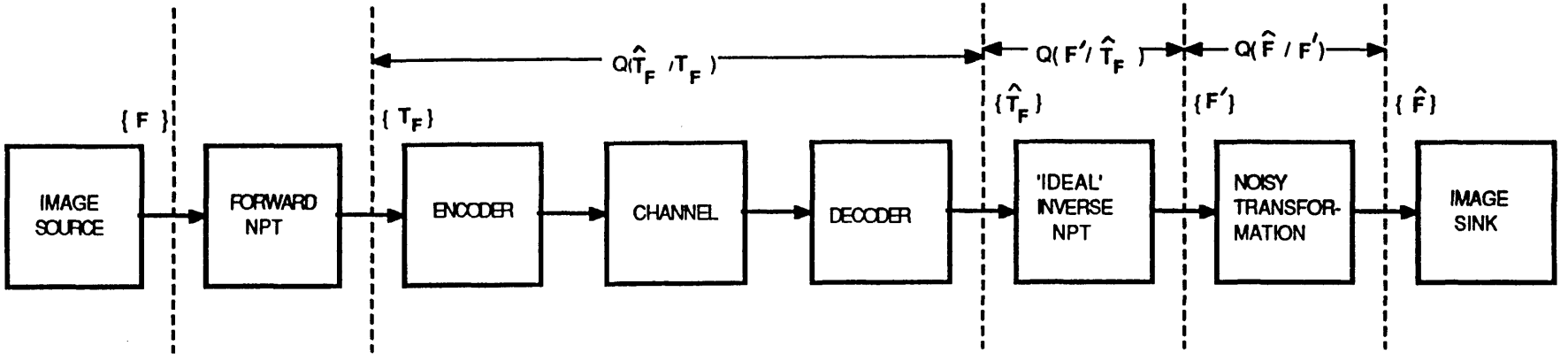


Fig. 4.3 : Model of An NPT Image Data Compression System.

that

$$E\left\{\|\hat{\mathbf{F}}-\mathbf{F}\|^2\right\} = c(\alpha)\cdot E\left\{\|\mathbf{F}'-\mathbf{F}\|^2\right\} \tag{4.11}$$

where $c(\alpha)$ is the factor by which the transform domain MSE changes, due to inverse NPT transformation and α is the NPT basis parameter.

4.3.1 Problem Statement

Having characterized the NPT data compression system by the model of Fig. 4.3, the problem of minimizing the rate necessary to transmit or store the source information $\{\mathbf{F}\}$ subject to a specified level of total distortion is to be solved. This problem is equivalent to that of minimizing the rate necessary to transmit or store the information in the transformed data sequence $\{\mathbf{T_F}\}$ subject to a specified level of total distortion between the spatial domain source information $\{\mathbf{F}\}$ and the final compressed version $\{\hat{\mathbf{F}}\}$. We represent the spatial domain allowable distortion by D_{sp} and specify this as the MSE between the spatial domain information $\{\mathbf{F}\}$ and the compressed version $\{\hat{\mathbf{F}}\}$ i.e.,

$$D_{sp} = E\left\{\|\hat{\mathbf{F}}-\mathbf{F}\|^2\right\} \tag{4.12}$$

Based on the model of Fig. 4.3 and the development in section 3.5.2, we can express the total spatial domain distortion as the product of the encoding distortion in the transform domain D_{tr} and a factor D_I which accounts for the effect of the inverse transformation such that

$$D_{sp} = D_{tr}\cdot D_I \leq D_{max} \tag{4.13}$$

where D_{max} is a specified maximum permissible distortion.

This problem can be approached via variational calculus. Specifically, for mutual information $M_N(\mathbf{T_F},\hat{\mathbf{T}}_\mathbf{F})$ between $\{\mathbf{T_F}\}$ and $\{\hat{\mathbf{T}}_\mathbf{F}\}$, we wish to minimize the function

$$J(\mathbf{T_F},\hat{\mathbf{T}}_\mathbf{F};\lambda) = M_N(\mathbf{T_F},\hat{\mathbf{T}}_\mathbf{F}) + \lambda(D_{tr}\cdot D_I) \tag{4.14}$$

where λ is a Lagrange multiplier, to obtain a rate-distortion function

$$R(D_T) = \inf_{Q(\hat{\mathbf{T}}_\mathbf{F}/\mathbf{T_F})\in Q_{D_{sp}}} M_N(\mathbf{T_F},\hat{\mathbf{T}}_\mathbf{F}) \tag{4.15}$$

where $Q_{D_{sp}}$ is the D_{sp}-admissible set of conditional density functions or compressors that each produce a distortion level D_{sp} satisfying the constraint of (4.13).

4.4 An Upper Bound of The Rate-Distortion Function for NPT Image Coders

In the NPT coding schemes of chapter 3, we coded each NPT sample in a memoryless fashion. However, the samples of the transformed sequence $\{\mathbf{T_F}(i,j)\}$ generated by an NPT transform are not memoryless, especially for high values of the basis parameter α. The rate-distortion function obtained in this scenario would be an upper bound on that achievable if memory were taken into account. This upper bound of the rate-distortion function can be derived in the following way.

Fig. 4.4 shows a modified model of an NPT image coder. Here, the forward NPT transformation of the input data sequence is followed by a KL transformation which produces a sequence of statistically independent, Gaussian distributed samples $\{\mathbf{T'_F}(i,j)\}$. It is the samples of the sequence $\{\mathbf{T'_F}(i,j)\}$ that are individually coded and transmitted. An inverse KL transform yields the coded NPT transform sequence $\{\hat{\mathbf{T}}_\mathbf{F}\}$, and inverse NPT transformation of this sequence yields the compressed image. Since the rate requirement for the KL transformed sequence $\{\mathbf{T'_F}(i,j)\}$ is the same as that required for coding the NPT transformed sequence $\{\mathbf{T_F}(i,j)\}$, the rate-distortion function can be obtained by considering the problem of minimizing the rate necessary to code the statistically independent samples of $\{\mathbf{T'_F}(i,j)\}$ subject to a maximum allowable distortion of the final reconstructed image $\{\hat{\mathbf{F}}\}$. Since the rate-distortion function for the Gaussian source under an MSE criterion is an upper bound for that of those sources having different distributions but of equal variance, the NPT coder rate-distortion function obtained in this way would give an idea of the bound on the achievable performance of practical NPT coding systems.

The rate-distortion function for a source generating a sequence of Gaussian distributed statistically independent samples, having variances σ^2 is given by

$$R(\zeta) = \begin{cases} \frac{1}{2} log\left(\frac{\sigma^2}{\zeta}\right) & 0 \leq \zeta < \sigma^2 \\ 0 & \sigma^2 \leq \zeta \end{cases} \tag{4.16}$$

The above result will not be derived here since this is already given in [51]. We shall make use of this result bearing in mind that the σ^2 in (4.16) refers to the variance of the KL transform samples of the sequence $\{\mathbf{T'_F}(i,j)\}$ and ζ is a distortion parameter which represents the maximum allowable distortion of coding

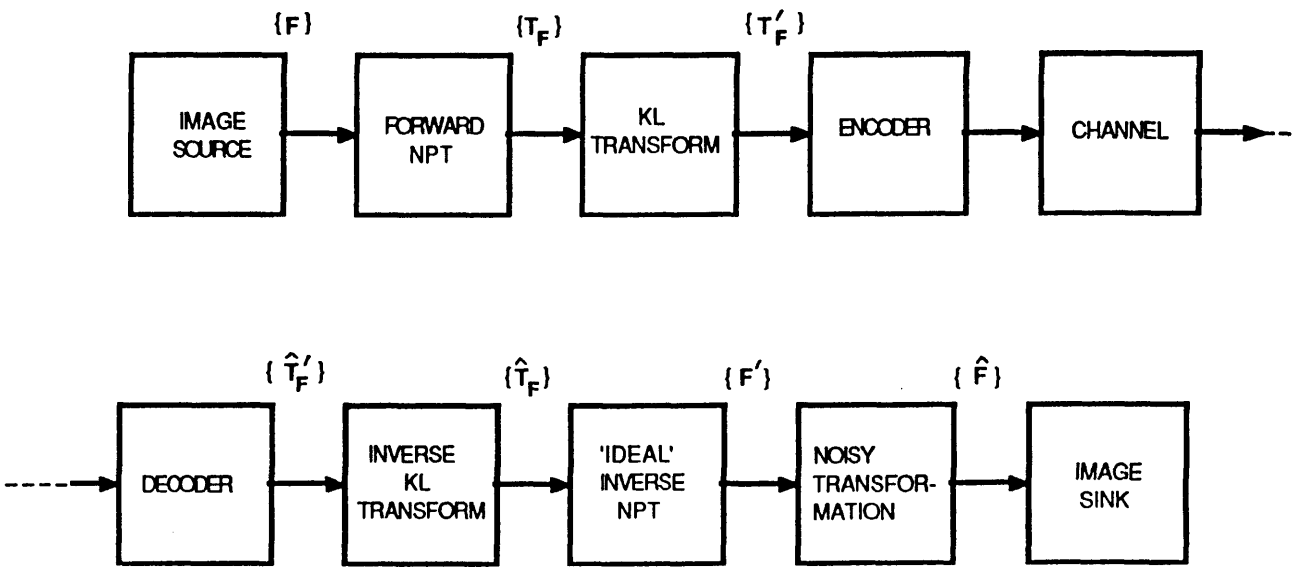


Fig. 4.4 : An Equivalent Model of An NPT Image Data Compression System.

each transform sample. The block average distortion due to coding the transform samples is

$$D(\zeta) = \frac{1}{N}\sum_{i=1}^{N} min(\zeta, \sigma_i^2) \tag{4.17}$$

and the average rate is

$$R_N(D) = \frac{1}{2N}\sum_{i=1}^{N} max\left(0, log\left(\sigma_i^2/\zeta\right)\right) \tag{4.18}$$

Since the KL transform is orthogonal, (4.18) gives the average rate required to achieve a maximum allowable MSE distortion D between the original and coded NPT transform samples. However, our interest lies in obtaining the rate as a function of the allowable total distortion in the spatial domain. We can obtain this by considering the alternative problem of minimizing the rate necessary to code the statistically independent samples $\{\mathbf{T'_F}(i,j)\}$ subject to a weighted MSE distortion criterion.

The rate-distortion function in this case, has a similar form to (4.18) and is obtained as follows. For a specified NPT coding system, the MSE distortion in the transform domain D_{tr} and the MSE distortion in the spatial domain D_{sp} are related by (refer to section 3.5.2 of this thesis)

$$D_{sp} = c(\alpha) D_{tr} \tag{4.19}$$

where

$$c(\alpha) = b(\alpha)\frac{||\psi^{-1}\{\alpha\}||^4}{||\psi\{0\}||^4} \tag{4.20}$$

Note that in (4.20), we have dropped the parameter θ which specifies the coding parameters; $b(\alpha)$ has a similar significance to the correction factor introduced in chapter three. Thus, it implies that the factor D_I in (4.13) equals $c(\alpha)$. Analogous to the distortion parameter ζ in the transform domain, we introduce the distortion parameter γ in the spatial domain which is related to the distortion parameter in the transform domain by

$$\gamma(\alpha) = c(\alpha)\zeta \tag{4.21}$$

We can regard $\gamma(\alpha)$ as the maximum allowable distortion of each reconstructed spatial signal sample. Using (4.17), (4.19), and (4.21), we can express the average distortion in the spatial domain as

$$D_{sp}(\alpha, \gamma) = \frac{1}{N}\sum_{i=1}^{N} c(\alpha)\, min\left(\frac{\gamma(\alpha)}{c(\alpha)}, \sigma_i^2\right) \tag{4.22}$$

The individual rate needed for coding each transform sample in order to achieve the average distortion $D_{sp} \leq D_{max}$ in the spatial domain is given by

$$R(\gamma,\alpha) = \begin{cases} \frac{1}{2} log\left(\frac{\sigma_i^2}{[\gamma(\alpha)/c(\alpha)]}\right) & 0 \leq \frac{\gamma(\alpha)}{c(\alpha)} < \sigma_i^2 \\ 0 & \sigma_i^2 \leq \frac{\gamma(\alpha)}{c(\alpha)} \end{cases} \tag{4.23}$$

and the average rate is

$$R_N(\gamma,\alpha) = \frac{1}{2N}\sum_{i=1}^{N} max\left(0, log\left(\frac{\sigma_i^2}{[\gamma(\alpha)/c(\alpha)]}\right)\right) \tag{4.24}$$

or

$$R_N(\gamma,\alpha) = \frac{1}{2N}\sum_{i=1}^{N} log\left(\frac{\sigma_i^2}{min\,[\sigma_i^2, \gamma(\alpha)/c(\alpha)]}\right) \tag{4.25}$$

where D_{max} is the maximum allowable total MSE distortion between the original image $\{\mathbf{F}\}$ and the reconstructed version $\{\hat{\mathbf{F}}\}$.

4.5 Evaluation of The Rate-Distortion Bounds for NPT Image Coders

In this section, we evaluate the theoretical N-block rate-distortion bounds for an NPT transform image coder, given by (4.22) and (4.25). As we stated earlier, our interest lies in being able to obtain an idea of the rate necessary to achieve a specified total distortion in the reconstructed image, when a given NPT transform basis is used to code a given image or image ensemble. Hence, we shall be concerned with the bit rate of compression as a function of the compression distortion in the spatial domain, D_{sp}.

In evaluating the bounds, we have employed a stationary first order Gauss-Markov image having horizontal (ρ_H) and vertical (ρ_V) inter-element correlation coefficient of 0.9 which was generated using a causal minimum variance model [14]. Using (4.22), the value of $\gamma(\alpha)$ giving rise to a specified total distortion in the spatial domain was obtained. Subsequently, the value of $\gamma(\alpha)$ was used to obtain the required average rate from (4.24). The correction factor term $c(\alpha)$ and the variances σ_i^2 appearing in (4.22) and (4.25) were determined empirically.

Fig. 4.5 is a plot of the rate as a function of the distortion that is obtained from (4.22) and (4.25) for the Hadamard NPT, using a block size of 8. The transform bases considered are specified at $\alpha = -0.15$, $\alpha = 0.0$, $\alpha = 0.05$, $\alpha = 0.1$, and $\alpha = 0.15$. We can observe that the bounds obtained for the bases $\alpha = 0.0$ and $\alpha = 0.05$ are practically the same. In general, the rate requirement can be said to increase by up to 0.3 bits as α is increased or decreased from zero, when the normalized

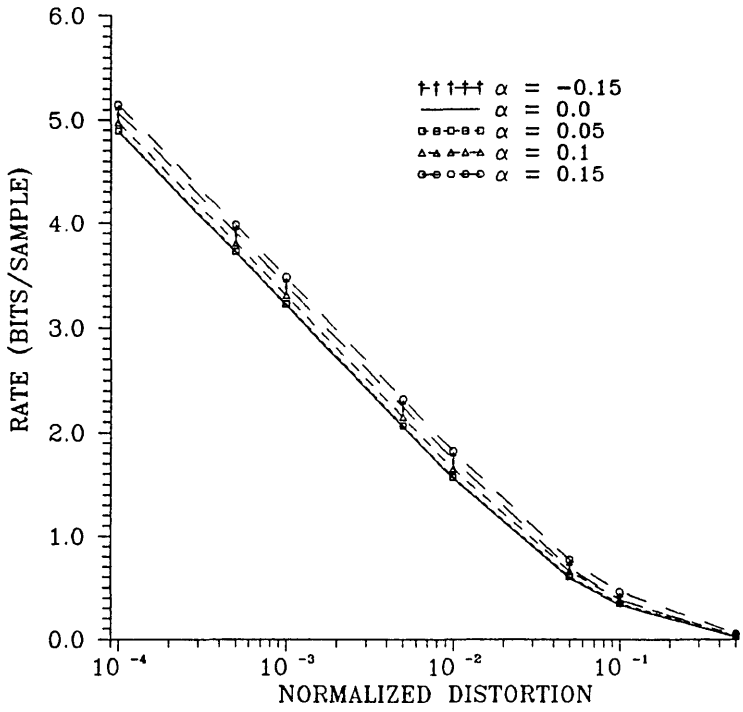


Fig. 4.5 : Theoretical N-block Rate-Distortion bounds for the 8 x 8 Hadamard NPT coder; the input image is a stationary first order Gauss-Markov image with $\rho_H=\rho_V=0.9$.

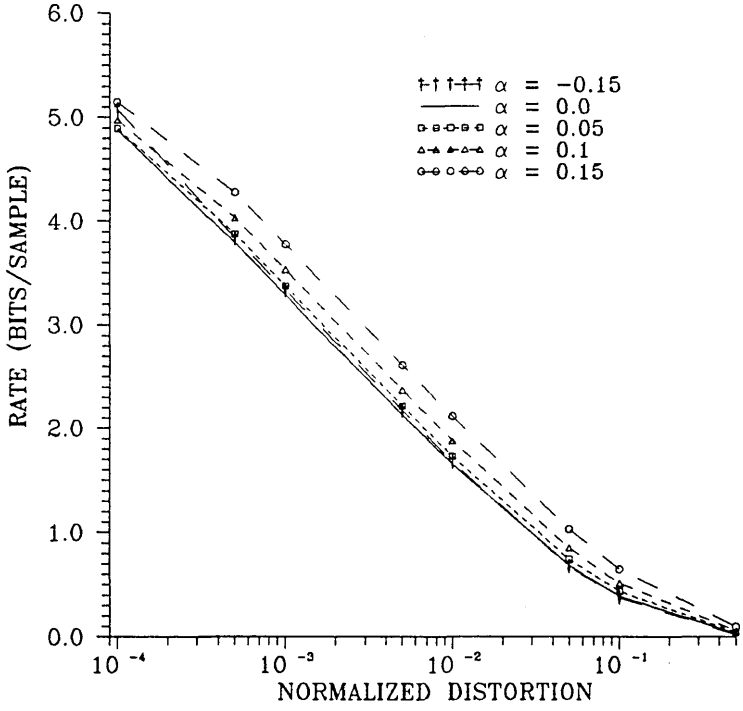


Fig. 4.6 : Theoretical N-block Rate-Distortion bounds for the 8 x 8 sine NPT coder; the input image is a stationary first order Gauss-Markov image with $\rho_H=\rho_V=0.9$.

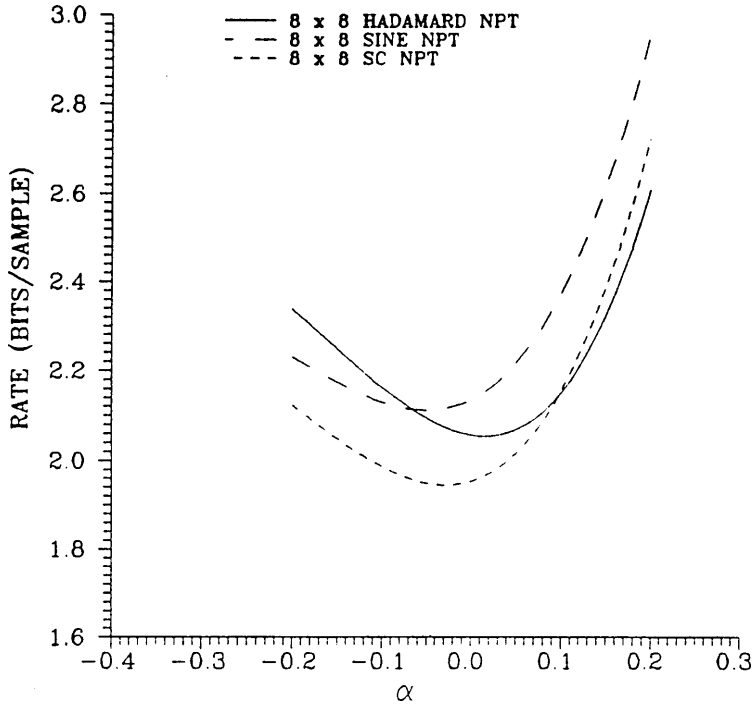


Fig. 4.7 : The Rate as a function of α , necessary to achieve a normalized distortion of 5 x 10^{-3}, for the respective NPT transform coding of a stationary first order Gauss-Markov (ρ_H=ρ_V=0.9) image.

distortion is less than or equal to 10^{-2}; for higher distortion levels, the increase in rate requirement is lower. Fig. 4.6 shows the corresponding bounds obtained for the sine NPT. In this case, we observe that the rate requirements at $\alpha = -0.15$ and $\alpha = 0.0$ are very close, and in fact the performance of the basis $\alpha = -0.15$ is superior to that of the basis $\alpha = 0.0$, for normalized distortion in the region of 10^{-1}. This result is consistent with that obtained in chapter 3 where we noted that a sine NPT basis specified at negative values of α can perform better than the sine transform.

Fig. 4.7 is a plot of the rate necessary to achieve a normalized distortion of 5×10^{-3} as a function of the transform basis parameter α, $|\alpha| \leq 0.2$, for the Hadamard NPT, the sine NPT and the symmetric cosine NPT. We observe that the minimum rates are achieved at $\alpha = -0.03$, $\alpha = 0.02$ and $\alpha = -0.05$ for the SC NPT, the Hadamard NPT and the sine NPT respectively. Furthermore, the rate required for the optimum SC NPT basis is the lowest followed by that of the optimum Hadamard NPT basis, with the rate required by the optimum sine NPT being the highest. Fig. 4.7 also gives an indication of the relative performance of the respective NPT transforms, at various values of the basis parameter in the range $|\alpha| \leq 0.2$, for the non-adaptive coding of images having statistics that can be modelled by that of a stationary first order Gauss-Markov image. For example, we can expect the best performance to be given by the Hadamard NPT when $\alpha > 0.1$ while for $\alpha < 0.1$, we can expect the performance of the SC NPT to be the best. However, it must be noted that the result of this comparison may not be the same for real images since a stationary first order Gauss-Markov image best represents the gross characteristics of real images.

4.6 Comparison of The Theoretical Bounds With The Performance of Sub-optimal NPT Compressors

The rate-distortion bound for the unconstrained complexity (infinite block length) coding of a stationary first order Gauss-Markov image, in the low distortion region is given by [1,pg. 192]

$$R(D_{sp}) = \frac{1}{2} log_2 \left[\frac{(1-\rho_H^2)(1-\rho_V^2)}{D_{sp}} \right] \tag{4.26}$$

where D_{sp} is the normalized distortion in the spatial domain. However, because of the practical need for constraining the complexity of compression schemes, the bound of (4.26) cannot be achieved in practice. Here, we compare the performance

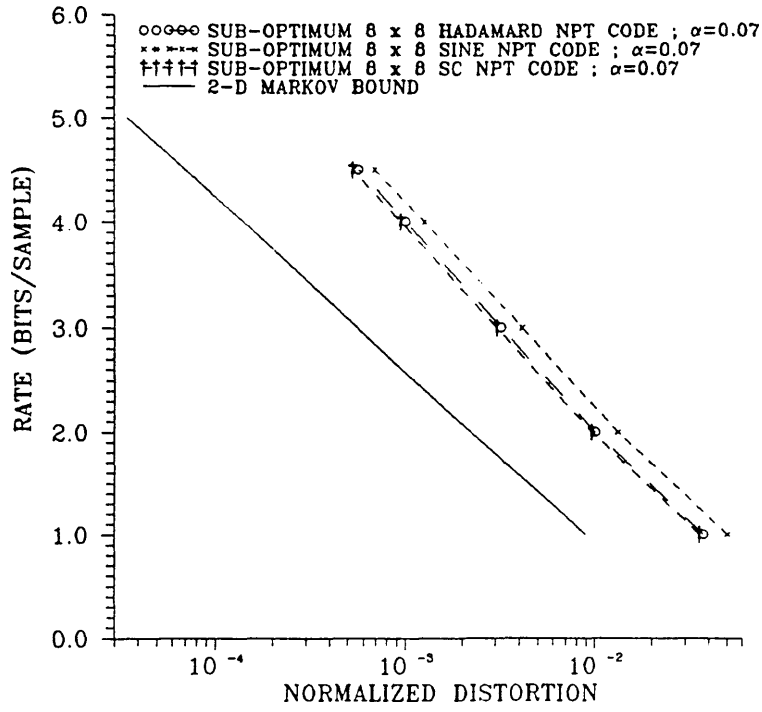


Fig. 4.8 : Performance comparison of two-dimensional practical NPT coders employing the basis α=0.07, with the two-dimensional theoretical bound.

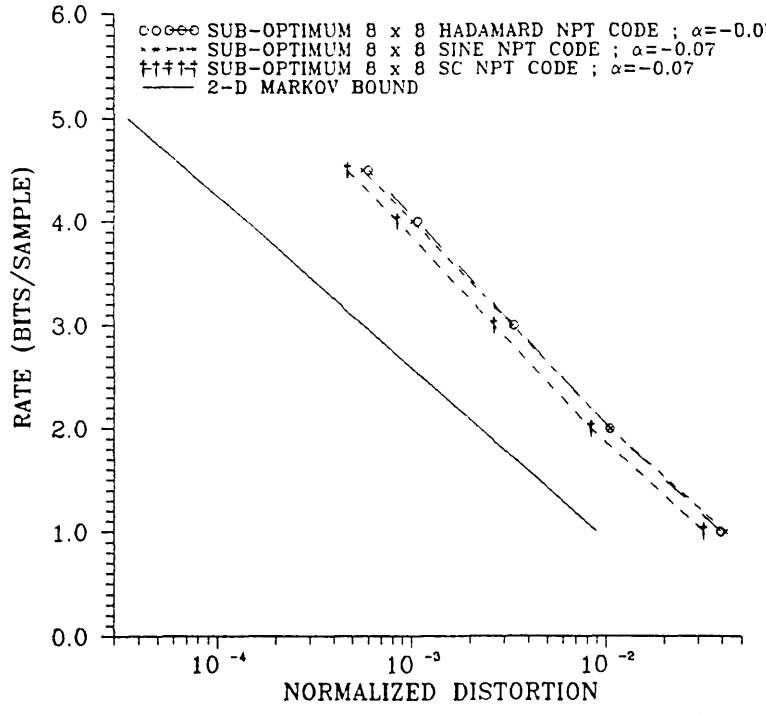


Fig. 4.9 : Performance comparison of two-dimensional practical NPT coders employing the basis α=-0.07, with the two-dimensional theoretical bound.

of sub-optimum two-dimensional NPT compression schemes with the optimum theoretical performance obtained under unconstrained complexity conditions.

Fig. 4.8 shows the practical rate-distortion performance for 8×8 block coding of the Gauss-Markov image ($\rho_H = \rho_V = 0.9$), using the respective NPT transforms at $\alpha = 0.07$. The theoretical Markov bound, given by (4.26) is also plotted. We can observe that the increase in rate as a result of constraining the complexity of the coder is at least 1 bit/sample and in addition, the difference between the practical performance of the respective NPT coders and the Markov bound increases with bit rate. The practical performance plots indicate that the best performance is obtained for the SC NPT coder, which is closely followed by that of the Hadamard NPT coder, with the performance of the sine NPT being the worst; the practical relative performance of the coders for a distortion of 5×10^{-3} is in agreement with the theoretical prediction given by Fig. 4.7. Fig. 4.9 shows the plots of the practical performance of the NPT coders at $\alpha = -0.07$. The Gauss-Markov bound is also plotted for comparison. Again, we observe that the difference between the Gauss-Markov bound and the practical performance increases with bit rate. The respective performances of the sine NPT and the Hadamard NPT are very close but the sine NPT performs better than the Hadamard NPT at high bit rates while the Hadamard NPT performs better than the sine NPT at low bit rates; the SC NPT has a better performance than the sine and Hadamard NPTs for this choice of α. For a normalized distortion of 5×10^{-3} , we can observe that the practical relative performance of the NPT transforms is in agreement with the prediction given by Fig. 4.7.

4.7 Summary and Conclusion

A rate-distortion theoretic analysis for NPT coders has been presented. The emphasis has been on ascertaining the rate necessary to achieve a desired level of total distortion in the reconstructed image, when a specified NPT basis is used for coding an image or image ensemble. An upper bound of the compression rate subject to a mean-square error (MSE) fidelity constraint has been derived. This bound has been evaluated for a first order Gauss-Markov image and has been used to predict the relative performance of the respective NPT transforms, for various choices of the transform basis parameter α, $|\alpha| \leq 0.2$. The agreement between the practical relative performance and the prediction of the relative performance that is obtained from the rate-distortion bound has been demonstrated.

The performance of practical two-dimensional NPT coders when used for coding a stationary first order Gauss-Markov image has been compared with the bound obtained for two-dimensional unconstrained complexity coding of stationary first order Gauss-Markov images. There is an increase in rate of at least 1 bit/sample as a result of using a finite block size ($N = 8$) for block coding.

PART II
ITERATIVE HADAMARD NATURALNESS-PRESERVING TRANSFORM PROCESSING OF SIGNALS

CHAPTER FIVE

ITERATIVE ONE-DIMENSIONAL HADAMARD NATURALNESS-PRESERVING TRANSFORM RECONSTRUCTION OF SIGNALS DEGRADED BY NON-STATIONARY NOISE PROCESSES OR JAMMING

5.1 Introduction

5.1.1 Problem Statement

The basic problem addressed in this chapter can be stated as follows : We transmit a signal, and, as a result of non-stationary channel noise, segments of the transmission are rendered unusable due to unacceptable error levels. We develop pre-/post-transmission signal processing techniques that would permit the reconstruction of a useful version of the original transmitted signal.

Hadamard NPT pre-processing is considered, for signal transmission under this scenario. Signal degradation is modelled as a complete loss of segments of the transmitted signal and thus, we address the problem of reconstructing a signal from segments of its one-dimensional Hadamard NPT.

5.1.2 Background to The Reconstruction Problem and Practical Applications of Hadamard NPT Signal Reconstruction

Under adverse channel signalling conditions, segments of a transmitted signal could be rendered unusable. In tactical communications where the signal must pass through channels whose qualities and characteristics are unpredictable due to non-stationary noise processes or jamming, segments of the transmission could be excised or rendered unusable as a result of "blocking " by the opposition [3]. In other instances, this could be caused either by crowding of the frequency spectrum in times of crisis activity or failure of the error correcting code [54]. In packetized

information-lossy transfer networks, packet loss which could be due to heavy loading of the network or corruption of the address of a packet, can lead to the loss of segments of a transmitted signal.

Hadamard NPT signal reconstruction has applications in these signal transmission scenario. In addition, for signal transmission over a disruption-prone communication link, the selective transmission of the Hadamard NPT segments of the signal with reconstruction at the receiver would minimize delay.

5.1.3 Scope of Research

The main focus of the work reported here is on the reconstruction of a signal from the received segments of its Hadamard NPT. Specifically, we develop techniques for the reconstruction of a signal from various formats of its Hadamard NPT segments. A related problem however, is that of determining which segments of the signal have been rendered unusable but this is not within the scope of the present investigation.

The method of solution of the latter problem depends very much on the application. Some applications like military communications may require a sophisticated approach which for example may involve the construction of special error correcting codes while others may require a simple solution. For example, in packetized information-lossy transfer networks, the labels of missing packets could be used to determine the unavailable Hadamard NPT segments.

5.1.4 Chapter Organization

The chapter commences with a discussion of Hadamard NPT pre-processing in section 5.2.1. The theoretical basis for the solution of the reconstruction problem is given. An appraisal of classical solutions to the reconstruction problem is given in section 5.2.2. Section 5.2.3 deals with iterative Hadamard NPT reconstruction. Examples of iterative one-dimensional Hadamard NPT reconstruction formats are discussed.

The reconstruction algorithm is applied to stationary first order Gauss-Markov and speech signals in section 5.3. An intraframe image packet transmission scheme which is based on Hadamard NPT reconstruction is introduced in section 5.4.

5.2 Signal Reconstruction From Hadamard NPT Segments

5.2.1 Hadamard NPT Pre-Processing

The Hadamard NPT, which we consider, is defined by

$$\psi\{\alpha\} = \alpha\mathbf{I} + (1-\alpha)\mathbf{H}_n \qquad |\alpha| < 1 \tag{5.1a}$$

with the inverse given by

$$\psi^{-1}\{\alpha\} = \frac{1}{(2\alpha-1)}[\alpha\mathbf{I} - (1-\alpha)\mathbf{H}_n] \qquad \alpha \neq \frac{1}{2} \tag{5.1b}$$

where $\mathbf{H}_n$ is the normalized natural Hadamard matrix [8] of order 2^n.

We represent an N-length segment of a one-dimensional time-dependent signal $S(t)$ by a data vector S^q, given by

$$S^q = [s_i \quad s_{i+1} \quad s_{i+2} \quad \cdots \quad s_{i+N-1}]^T \tag{5.2}$$

where the superscript T denotes transposition and i is the time index representing the beginning of the q^{th} segment. $S(t)$ is thus given by

$$S(t) = \{S^q \;;\; q = 1,2,\ldots n_D\} \tag{5.3}$$

where n_D is the total number of segments.

Using (5.1a), the one-dimensional Hadamard NPT of the data vector S^q is given by

$$R^q = \psi\{\alpha\}\, S^q = \alpha S^q + (1-\alpha)\mathbf{H}_n S^q \tag{5.4}$$

where R^q is a vector defined as

$$R^q = [r_i \quad r_{i+1} \quad r_{i+2} \quad \cdots \quad r_{i+N-1}]^T \tag{5.5}$$

From (5.1b), S^q is given by

$$S^q = \psi^{-1}\{\alpha\}\, R^q \tag{5.6}$$

Equation (5.4) defines R^q as the sum of two component vectors, viz αS^q, which is a weighting of the original signal, and $(1-\alpha)\mathbf{H}_n S^q$, which is a weighting of the Hadamard transform of the signal. Since the Hadamard transform achieves a certain degree of decorrelation of S^q, the components of vector $(1-\alpha)\mathbf{H}_n S^q$ are less correlated than those of vector S^q. However, because the Hadamard transform is not the optimal transform for decorrelating S^q, there still remains some residual

correlation within $(1-\alpha)\mathbf{H}_n S^q$. For stationary Markov-1 signals, it was shown in [76] that the residual correlation cannot be removed by increasing the block size.

In a typical scenario, we transmit R^q and we receive a truncated vector $\tilde{R}^q$, which is R^q with some segments excised. Since the two components of this vector are uncorrelated, we can exploit the fact that the correlation range of the original signal component αS^q is longer than that of the transform component $(1-\alpha)\mathbf{H}_n S^q$ to derive an estimate of the original signal amplitude over the correctly received segments; we can then use the estimate derived to solve for an approximation of the lost signal information.

The reconstruction problem is thus made up of two sub-problems, viz

(i) an estimation problem,

(ii) developing techniques for reconstructing a signal from segments of its Hadamard NPT.

Solutions to these problems are derived in the following sections.

5.2.2 Classical Solution

The Hadamard NPT is a linear transformation and (5.4) expresses each entry of R^q as a linear combination of all the entries of S^q, where R^q and S^q are $N \times 1$ vectors. For convenience, we represent the forward Hadamard NPT matrix, given by (5.1*a*), by the matrix $\mathbf{P}$ and the inverse Hadamard NPT matrix, given by (5.1*b*), by the matrix $\mathbf{Q}$. We represent the number of unknown samples from the vectors R^q and S^q by n_u, and represent the number of known samples from the vectors R^q and S^q by n_k, such that

$$N = n_k + n_u \tag{5.7}$$

We can express (5.4) as

$$\begin{bmatrix} R_k \\ R_u \end{bmatrix} = \begin{bmatrix} \mathbf{P}_{k1} & \mathbf{P}_{u1} \\ \mathbf{P}_{k2} & \mathbf{P}_{u2} \end{bmatrix} \begin{bmatrix} S_k \\ S_u \end{bmatrix} \tag{5.8}$$

and similarly, (5.6) becomes

$$\begin{bmatrix} S_k \\ S_u \end{bmatrix} = \begin{bmatrix} \mathbf{Q}_{k1} & \mathbf{Q}_{u1} \\ \mathbf{Q}_{k2} & \mathbf{Q}_{u2} \end{bmatrix} \begin{bmatrix} R_k \\ R_u \end{bmatrix} \tag{5.9}$$

where R_k and R_u are vectors of the known and the unknown components respectively, derived from R^q; similarly, S_k and S_u are vectors of the known and the unknown components respectively, derived from S^q. R_k and S_k are of dimension

$n_k \times 1$ while R_u and S_u are of dimension $n_u \times 1$. $\mathbf{P}_{k1}$, $\mathbf{P}_{k2}$, $\mathbf{P}_{u1}$ and $\mathbf{P}_{u2}$ are sub-matrices derived from $\mathbf{P}$ in order to determine R_k and R_u in terms of S_k and S_u. Similarly, $\mathbf{Q}_{k1}$, $\mathbf{Q}_{k2}$, $\mathbf{Q}_{u1}$ and $\mathbf{Q}_{u2}$ are sub-matrices derived from $\mathbf{Q}$ in order to express S_k and S_u in terms of R_k and R_u. $\mathbf{P}_{k1}$ and $\mathbf{Q}_{k1}$ are of dimension $n_k \times n_k$, $\mathbf{P}_{k2}$ and $\mathbf{Q}_{k2}$ are of dimension $n_u \times n_k$, $\mathbf{P}_{u1}$ and $\mathbf{Q}_{u1}$ are of dimension $n_k \times n_u$ while $\mathbf{P}_{u2}$ and $\mathbf{Q}_{u2}$ are of dimension $n_u \times n_u$.

Using (5.8), we can write

$$R_k = \mathbf{P}_{k1} S_k + \mathbf{P}_{u1} S_u \tag{5.10a}$$

and

$$R_u = \mathbf{P}_{k2} S_k + \mathbf{P}_{u2} S_u \tag{5.10b}$$

Equation (5.10a) expresses the n_u desired (but unknown) entries of S^q as a function of the known entries of R^q and S^q. The components of the desired (but unknown) vector S_u can be obtained by solving the system of equations

$$\mathbf{P}_{u1} S_u = y_k \tag{5.11a}$$

where

$$y_k = R_k - \mathbf{P}_{k1} S_k \tag{5.11b}$$

; the n_u unknown components of vector S_u are related by n_k equations.

The system of equations, (5.11a), can be solved using classical methods, however, the following comments concerning the existence of the solution of (5.11a) should be noted.

(i) If $n_k = n_u$, then there are as many equations as unknowns and a unique solution for S_u exist provided that the set of equations is not degenerate. For the non-singular case, (5.14a) can be solved using Gauss-Jordan elimination method or LU decomposition method. The operation count for these methods are respectively $(n_k^3 + n_k^2 n_u)$ and $(\frac{1}{3}n_k^3 + n_k^2)$, additions and multiplications **, which works out to be $\frac{N^3}{4}$ and $\frac{N^3}{24} + \frac{N^2}{4}$ multiplications and additions, respectively (obtained by setting $n_k = n_u = \frac{N}{2}$).

(ii) If $n_k < n_u$ or if $n_k = n_u$ but the equations are degenerate, then there are effectively fewer equations than unknowns. In this case, there can either be

** It should be noted that this does not include the number of operations required to set up (5.11a)

no solution or else more than one solution vector, S_u. In the latter situation, the solution space consists of a particular solution S_{up} added to any linear combination of (typically) $n_u - n_k$ vectors, which are said to be in the nullspace of the matrix $\mathbf{P}_{u1}$.

(iii) If $n_k > n_u$, there are more equations than unknowns. In this case, there is, in general, no solution vector S_u to (5.11*a*), and the equations are said to be overdetermined. Usually, a best "compromise " solution, which comes closest to satisfying all equations simultaneously, is sought. Defining closeness in the least squares sense, the overdetermined linear problem reduces to the linear least squares problem.

In practice, it is the estimate, $\hat{S}_k$, of S_k (derived from the known transform segment R_k) that is used in (5.11*a*). The approximate version of S_u, i.e. $\hat{S}_u$, thus satisfy the system of equations

$$\mathbf{P}_{u1}\hat{S}_u = R_k - \mathbf{P}_{k1}\hat{S}_k \tag{5.12}$$

Solution via classical approaches is unattractive for two reasons. Firstly, the operation count is high; this is of the order of N^3 multiplications and additions. Secondly, setting up the system of equations (5.12) is cumbersome, since transform segments could be lost in a variety of formats.

In the following section, we introduce an iterative one-dimensional Hadamard NPT reconstruction algorithm which requires a considerably less number of operations than classical methods such as LU decomposition or Gauss-Jordan elimination.

5.2.3 Iterative One-Dimensional Hadamard NPT Reconstruction

We first introduce some important notation and operators.

Notation :

We shall drop the index q and refer to S^q simply as S, and also refer to R^q as R.

S = original signal vector.

R = $\psi\{\alpha\}S$; NPT of S.

$\tilde{R}$ = truncated R; NPT of S with some segments (defined by an index ID) excised.

$\tilde{S}$ = $\psi^{-1}\{\alpha\}\,\tilde{R}$; inverse NPT of truncated R.

$\hat{S}^W$ = estimate of the original signal, derived from $\tilde{R}$ - the components of $\hat{S}^W$ are zero at locations corresponding to the truncated samples of R and contain an estimate of the original signal amplitude over the known segments of R.

$\hat{S}_m$ = reconstruction of S at the m^{th} iteration.

$\hat{R}_m$ = reconstruction of R at the m^{th} iteration.

Operators :

$F(\cdot)$ = estimation operator.

ϕ_{ID} = replacement operator, where ID is a vector of indices. For example, the operation $A\phi_{ID}B$ where $ID = [j_1\ j_2]^T$ replaces the components of vector A, from locations j_1 to j_2 with the corresponding components of vector B.

The estimation of signal amplitude over the correctly received segments of R is then modelled by

$$\hat{S}^W = F\left(\tilde{R}\right) \tag{5.13}$$

The reconstruction, $\hat{S}_m$, of S at the m^{th} iteration is given by

$$\hat{S}_m = \left[\psi^{-1}\{\alpha\}\left(\hat{R}_m\phi_{ID}\tilde{R}\right)\right]\phi_{ID}\hat{S}^W \quad m = 1, 2, \ldots p \tag{5.14a}$$

where

$$\hat{R}_m = \begin{cases} \psi\{\alpha\}\left(\hat{S}_0\phi_{ID}\hat{S}^W\right) & m = 1 \\ \psi\{\alpha\}\,\hat{S}_{m-1} & m = 2, 3, \ldots p \end{cases} \tag{5.14b}$$

and

$$\hat{S}_0 = \psi^{-1}\{\alpha\}\,\tilde{R} \tag{5.14c}$$

Fig. 5.1 is a simplified block diagram of the iterative Hadamard NPT reconstructor. The processor is made up of three main modules, viz

(i) an "INITIALIZATION " module which implements equations (5.13) and (5.14c),

(ii) a "REPLACEMENT PROCESSOR " module (RPM) which carries out the replacement operations, and

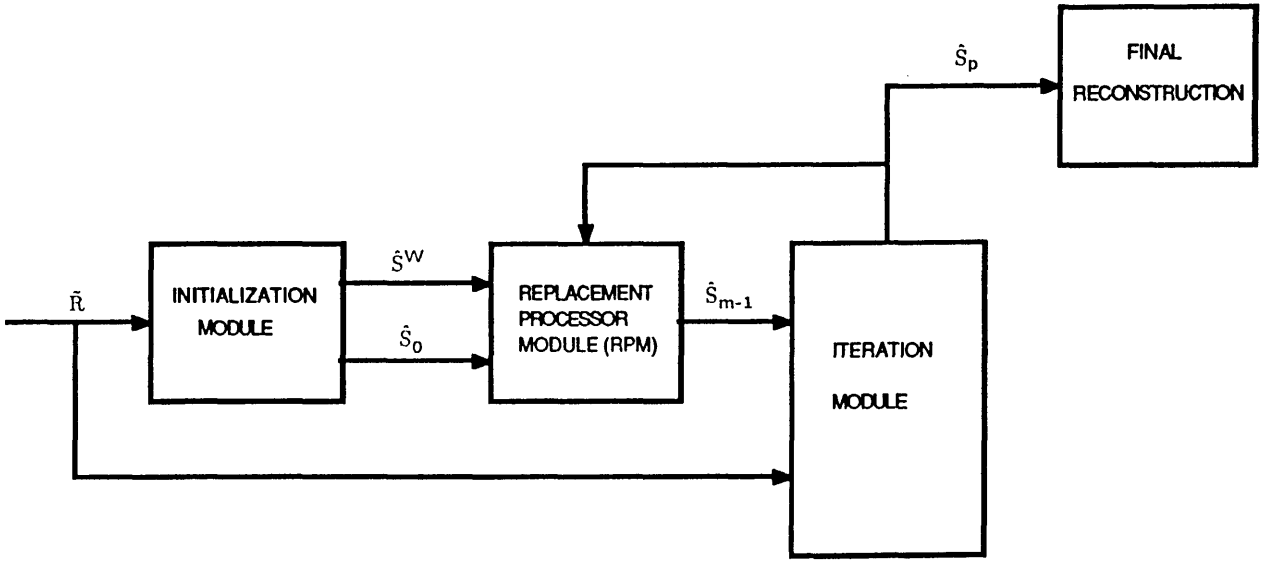


Fig. 5.1: Simplified Block Diagram of Iterative Hadamard NPT Reconstruction .

(iii) an "ITERATION " module which basically implements the iterative reconstruction.

Fig. 5.2 is a more detailed block diagram of the processor. The replacement processor module is a general purpose one, the correct replacement is done by routing the signals through the correct ports. Port A in the RPM module is essentially a gated port which allows the signal $\hat{S}_0$ from the initialization module to be used for replacement at the beginning of the iteration and the signal $\hat{S}_m$ from the output of the iteration module to be used for replacement at subsequent iterations.

Defining

$$D^{(m)} = d\left(\tilde{R}, \hat{R}_m\right)_{ID} \tag{5.15}$$

as a measure of the difference between the components of vectors $\tilde{R}$ and $\hat{R}_m$ at the locations specified by ID, the vector segment comparator terminates the reconstruction when

$$|D^{(m+1)} - D^{(m)}| < \epsilon \tag{5.16}$$

subject to a maximum permissible number of iterations, where ϵ is a threshold specified by the user. We define $D^{(m)}$ as the mean-square error difference measure and set $\epsilon \leq 1.0 \times 10^{-2}$.

The iterative reconstruction algorithm described by (5.14) converges for $\alpha \leq 0.464$; the proof of convergence is given in appendix II. For m iterations, the scheme requires $2m(N log_2 N + 3N)$ operations; conventional methods such as LU decomposition need of the order of N^3 operations.

5.2.3.1 Examples of Iterative One-Dimensional Hadamard NPT Reconstruction Formats

We now investigate in detail, the iterative reconstruction from specific formats of Hadamard NPT segments. In the following examples, we consider an N-length data vector and partition this into n_s segments, each of length l_s such that

(i) n_s is an integral power of 2,

(ii) l_s is an integral power of 2,

(iii) segments are assigned subscripts j, $j = 1, 2, \ldots n_s$, with the subscripts increasing with the vector index.

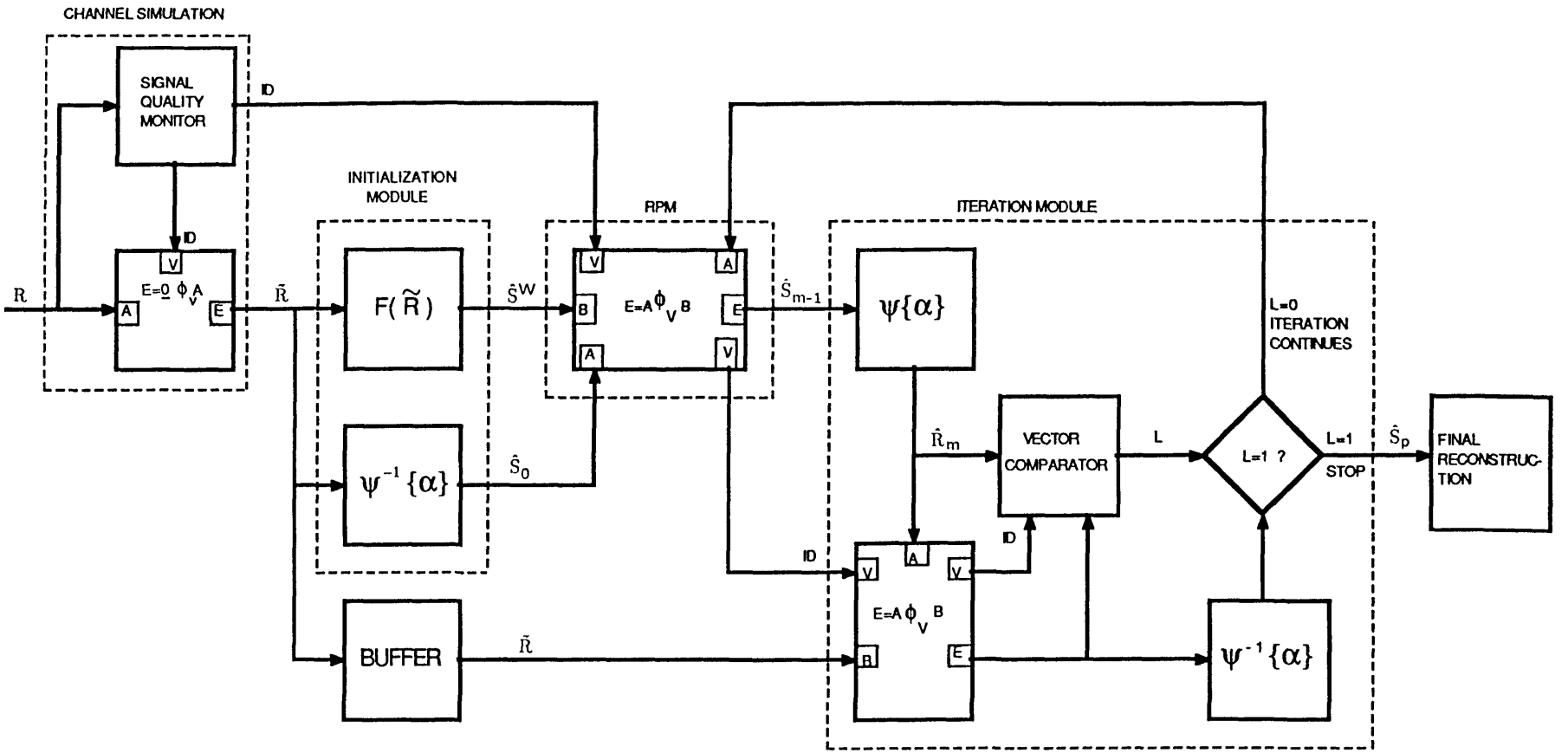


Fig. 5.2 : Detailed Block Diagram of Iterative One-Dimensional Hadamard NPT Reconstruction Processor.

The original signal vector is thus given by the partitioned vector

$$S = [\underline{s}_1 \,|\, \underline{s}_2 \,|\, \underline{s}_3 \,|\, \cdots \,|\, \underline{s}_{n_s}]^T \tag{5.17}$$

while the Hadamard NPT of S is given by

$$R = [\underline{r}_1 \,|\, \underline{r}_2 \,|\, \underline{r}_3 \,|\, \cdots \,|\, \underline{r}_{n_s}]^T \tag{5.18}$$

where $\underline{s}_j$ and $\underline{r}_j$ are vectors of length l_s

We define an error vector E as

$$E = [\underline{e}_1 \,|\, \underline{e}_2 \,|\, \underline{e}_3 \,|\, \cdots \,|\, \underline{e}_{n_s}]^T \tag{5.19}$$

where $\underline{e}_j$ is the error incurred in the estimation of the original signal segment $\underline{s}_j$. In addition, we express the iteration vectors $\hat{S}_m$ and $\hat{R}_m$ as the partitioned vectors

$$\hat{S}_m = \left[\hat{\underline{s}}_1^{(m)} \,|\, \hat{\underline{s}}_2^{(m)} \,|\, \hat{\underline{s}}_3^{(m)} \,|\, \cdots \,|\, \hat{\underline{s}}_{n_s}^{(m)}\right]^T \tag{5.20}$$

and

$$\hat{R}_m = \left[\hat{\underline{r}}_1^{(m)} \,|\, \hat{\underline{r}}_2^{(m)} \,|\, \hat{\underline{r}}_3^{(m)} \,|\, \cdots \,|\, \hat{\underline{r}}_{n_s}^{(m)}\right]^T \tag{5.21}$$

respectively.

1) Odd-Index Vector Reconstruction

The formats are shown in Fig. 5.3 where the hatched segments are unknown. They correspond to the loss of the "dc " sample and some dominant transform samples.

Case 1

This is depicted in Fig. 5.3a. The original signal vector is given by

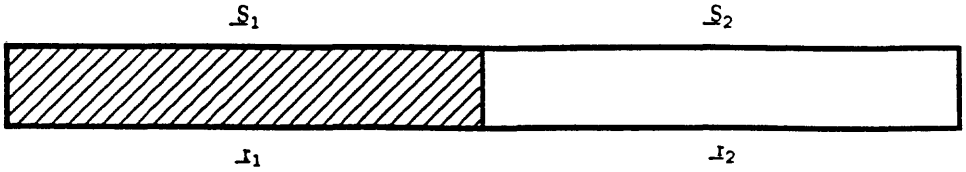
$$S = [\underline{s}_1 \,|\, \underline{s}_2]^T \tag{5.22}$$

while the NPT of S is given by

$$R = [\underline{r}_1 \,|\, \underline{r}_2]^T \tag{5.23}$$

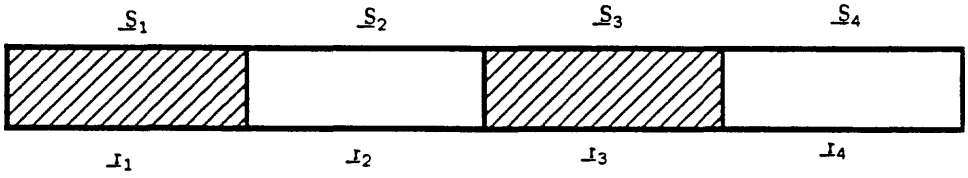
Using (5.1) and the recursive definition of a normalized natural Hadamard matrix of order N, i.e.

$$\mathbf{H}_N = \frac{1}{\sqrt{2}} \begin{bmatrix} \mathbf{H}_{\frac{N}{2}} & \mathbf{H}_{\frac{N}{2}} \\ \mathbf{H}_{\frac{N}{2}} & -\mathbf{H}_{\frac{N}{2}} \end{bmatrix} \tag{5.24}$$



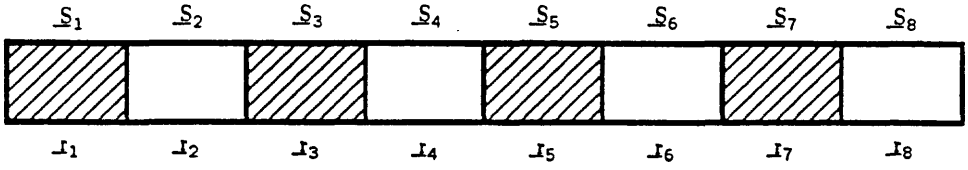
$\underline{S}_1$ = desired (but unknown) signal segment
$\underline{S}_2$ = known signal segment
$\underline{I}_1$ = desired (but unknown) transform segment
$\underline{I}_2$ = known transform segment.

Fig. 5.3a : Case 1



$\underline{S}_1$, $\underline{S}_3$ = desired (but unknown) signal segments
$\underline{S}_2$, $\underline{S}_4$ = known signal segments
$\underline{I}_1$, $\underline{I}_3$ = desired (but unknown) transform segments
$\underline{I}_2$, $\underline{I}_4$ = known transform segments.

Fig. 5.3b : Case 2



$\underline{S}_1$, $\underline{S}_3$, $\underline{S}_5$, $\underline{S}_7$ = desired (but unknown) signal segments
$\underline{S}_2$, $\underline{S}_4$, $\underline{S}_6$, $\underline{S}_8$ = known signal segments
$\underline{I}_1$, $\underline{I}_3$, $\underline{I}_5$, $\underline{I}_7$ = desired (but unknown) transform segments
$\underline{I}_2$, $\underline{I}_4$, $\underline{I}_6$, $\underline{I}_8$ = known transform segments.

Fig. 5.3c : Case 3

Fig. 5.3 : Loss of Odd-Index Vectors.

we can relate the transform segments $\underline{r}_j$ in (5.23) to the original signal segments as follows:

$$\underline{r}_1 = \left(\alpha \mathbf{I}_{\frac{N}{2}} + c_1 \mathbf{H}_{\frac{N}{2}}\right) \underline{s}_1 + c_1 \mathbf{H}_{\frac{N}{2}} \underline{s}_2 \tag{5.25a}$$

$$\underline{r}_2 = c_1 \mathbf{H}_{\frac{N}{2}} \underline{s}_1 - \left(\alpha \mathbf{I}_{\frac{N}{2}} - c_1 \mathbf{H}_{\frac{N}{2}}\right) \underline{s}_2 \tag{5.25b}$$

where

$$c_1 = \frac{(1-\alpha)}{\sqrt{2}} \tag{5.25c}$$

$\mathbf{I}_{\frac{N}{2}}$ is an identity matrix of order $\frac{N}{2}$ and $\mathbf{H}_{\frac{N}{2}}$ is a normalized natural Hadamard matrix of order $\frac{N}{2}$.

Similarly, the original signal segments $\underline{s}_j$ in (5.22) are related to the transform segments as follows:

$$\underline{s}_1 = \frac{1}{2\alpha - 1} \left\{ \left(\alpha \mathbf{I}_{\frac{N}{2}} - c_1 \mathbf{H}_{\frac{N}{2}}\right) \underline{r}_1 - c_1 \mathbf{H}_{\frac{N}{2}} \underline{r}_2 \right\} \tag{5.26a}$$

$$\underline{s}_2 = \frac{1}{2\alpha - 1} \left\{ -c_1 \mathbf{H}_{\frac{N}{2}} \underline{r}_1 + \left(\alpha \mathbf{I}_{\frac{N}{2}} + c_1 \mathbf{H}_{\frac{N}{2}}\right) \underline{r}_2 \right\} \tag{5.26b}$$

The truncated NPT vector, $\tilde{R}$, for this scenario is given by

$$\tilde{R} = [\underline{0} \,|\, \underline{r}_2]^T \tag{5.27}$$

The estimate, $\hat{S}^W$, of the signal amplitude over the known transform segments (derived from $\tilde{R}$), can be expressed as

$$\hat{S}^W = [\underline{0} \,|\, \hat{\underline{s}}_2]^T \tag{5.28a}$$

$$= [\underline{0} \,|\, \underline{s}_2 + \underline{e}_2]^T \tag{5.28b}$$

Iterates from (5.14), for the format of Fig. 5.3a, are evaluated as follows. The iteration vectors $\hat{S}_m$ and $\hat{R}_m$ are given respectively by

$$\hat{S}_m = \left[\hat{\underline{s}}_1^{(m)} \,|\, \hat{\underline{s}}_2^{(m)}\right]^T \tag{5.29}$$

and

$$\hat{R}_m = \left[\hat{\underline{r}}_1^{(m)} \,|\, \hat{\underline{r}}_2^{(m)}\right]^T \tag{5.30}$$

Initialization

Perform the inverse Hadamard NPT of $\tilde{R}$ (defined in (5.27)) to obtain the vector $\hat{S}_0$. The segments of $\hat{S}_0$ are given by (these are obtained by setting $\underline{r}_1 = \underline{0}$ in (5.26))

$$\hat{\underline{s}}_1^{(0)} = \frac{1}{2\alpha - 1} \left\{ -c_1 \mathbf{H}_{\frac{N}{2}} \underline{r}_2 \right\} \tag{5.31a}$$

and

$$\hat{\underline{s}}_2^{(0)} = \frac{1}{2\alpha - 1}\left\{\left(\alpha \mathbf{I}_{\frac{N}{2}} + c_1 \mathbf{H}_{\frac{N}{2}}\right)\underline{r}_2\right\} \tag{5.31b}$$

Replace the vector $\hat{\underline{s}}_2^{(0)}$ in $\hat{S}_0$ with the estimate of $\underline{s}_2$, i.e. $\hat{\underline{s}}_2$, to obtain a vector $\hat{S}_0'$ whose segments are

$$\check{\underline{s}}_1^{(0)} = \hat{\underline{s}}_1^{(0)} = \frac{1}{2\alpha - 1}\left\{-c_1 \mathbf{H}_{\frac{N}{2}}\underline{r}_2\right\} \tag{5.32a}$$

and

$$\check{\underline{s}}_2^{(0)} = \hat{\underline{s}}_2 = \frac{1}{2\alpha - 1}\left\{-c_1 \mathbf{H}_{\frac{N}{2}}\underline{r}_1 + \left(\alpha \mathbf{I}_{\frac{N}{2}} + c_1 \mathbf{H}_{\frac{N}{2}}\right)\underline{r}_2\right\} + \underline{e}_2 \tag{5.32b}$$

Iteration 1

Forward Hadamard NPT

Perform the forward Hadamard NPT of the vector whose segments are given by (5.32) to obtain the respective segments of $\hat{R}_1$. Thus, we have

$$\hat{\underline{r}}_1^{(1)} = \left[\left(\alpha \mathbf{I}_{\frac{N}{2}} + c_1 \mathbf{H}_{\frac{N}{2}}\right)\hat{\underline{s}}_1^{(0)}\right] + \left[c_1 \mathbf{H}_{\frac{N}{2}}\hat{\underline{s}}_2\right] \tag{5.33a}$$

$$= \left[\frac{1}{2\alpha - 1}\left\{-\alpha c_1 \mathbf{H}_{\frac{N}{2}}\underline{r}_2 - c_1^2\underline{r}_2\right\}\right] + \left[\frac{1}{2\alpha - 1}\left\{-c_1^2\underline{r}_1 + \alpha c_1 \mathbf{H}_{\frac{N}{2}}\underline{r}_2 + c_1^2\underline{r}_2\right\} + c_1 \mathbf{H}_{\frac{N}{2}}\underline{e}_2\right] \tag{5.33b}$$

$$= \frac{1}{2\alpha - 1}\left\{-c_1^2\underline{r}_1\right\} + c_1 \mathbf{H}_{\frac{N}{2}}\underline{e}_2 \tag{5.33c}$$

$$\hat{\underline{r}}_2^{(1)} = \left[c_1 \mathbf{H}_{\frac{N}{2}}\hat{\underline{s}}_1^{(0)}\right] + \left[\left(\alpha \mathbf{I}_{\frac{N}{2}} - c_1 \mathbf{H}_{\frac{N}{2}}\right)\hat{\underline{s}}_2\right] \tag{5.34a}$$

$$= \left[\frac{1}{2\alpha - 1}\left\{-c_1^2\underline{r}_2\right\}\right] + \left[\frac{1}{2\alpha - 1}\left\{-\alpha c_1 \mathbf{H}_{\frac{N}{2}}\underline{r}_1 + c_1^2\underline{r}_1 + \left(\alpha^2 - c_1^2\right)\underline{r}_2\right\} + \alpha\underline{e}_2 - c_1 \mathbf{H}_{\frac{N}{2}}\underline{e}_2\right] \tag{5.34b}$$

$$= \underline{r}_2 + \frac{1}{2\alpha - 1}\left\{c_1^2\underline{r}_1 - \alpha c_1 \mathbf{H}_{\frac{N}{2}}\underline{r}_1\right\} + \alpha\underline{e}_2 - c_1 \mathbf{H}_{\frac{N}{2}}\underline{e}_2 \tag{5.34c}$$

Replace the vector $\hat{\underline{r}}_2^{(1)}$ in $\hat{R}_1$ with $\underline{r}_2$ (obtained from $\tilde{R}$) to yield a vector $\hat{R}_1'$ whose segments are

$$\check{\underline{r}}_1^{(1)} = \hat{\underline{r}}_1^{(1)} = \frac{1}{2\alpha - 1}\left\{-c_1^2\underline{r}_1\right\} + c_1 \mathbf{H}_{\frac{N}{2}}\underline{e}_2 \tag{5.35a}$$

$$\check{\underline{r}}_2^{(1)} = \underline{r}_2 \tag{5.35b}$$

At this point, we make the following observation : (5.35a) expresses the sub-vector $\hat{\underline{r}}_1^{(1)}$ in terms of the desired (but unknown) transform segment $\underline{r}_1$. If the

estimation error vector $\underline{e}_2$ is a null vector (errorless estimation of the original signal segment $\underline{s}_2$), multiplying the segment $\check{\underline{r}}_1^{(1)}$ of $\hat{R}_1'$ by $-\frac{(2\alpha-1)}{c^2}$ and inverse transforming the resulting vector would yield a perfectly reconstructed original transmitted signal, S.

We continue with the iterative reconstruction process in the following way. For convenience, we re-write (5.35) as

$$\check{\underline{r}}_1^{(1)} = g_1 \underline{r}_1 + v_1 \mathbf{H}_{\frac{N}{2}} \underline{e}_2 \tag{5.36a}$$

$$\check{\underline{r}}_2^{(1)} = \underline{r}_2 \tag{5.36b}$$

where

$$g_1 = \frac{-c_1^2}{2\alpha - 1} \tag{5.36c}$$

and

$$v_1 = c_1 = \frac{1-\alpha}{\sqrt{2}} \tag{5.36d}$$

Inverse Hadamard NPT

The inverse Hadamard NPT of the vector whose segments are given by (5.36*a*) and (5.36*b*) yields the vector $\hat{S}_1'$ whose segments are given by

$$\check{\underline{s}}_1^{(1)} = \frac{1}{2\alpha - 1} \left\{ \left(\alpha \mathbf{I}_{\frac{N}{2}} - c_1 \mathbf{H}_{\frac{N}{2}} \right) \check{\underline{r}}_1^{(1)} - c_1 \mathbf{H}_{\frac{N}{2}} \underline{r}_2 \right\} \tag{5.37a}$$

$$= \frac{1}{2\alpha - 1} \left\{ g_1 \left(\alpha \mathbf{I}_{\frac{N}{2}} - c_1 \mathbf{H}_{\frac{N}{2}} \right) \underline{r}_1 - c_1 \mathbf{H}_{\frac{N}{2}} \underline{r}_2 - c_1 v_1 \underline{e}_2 + \alpha v_1 \mathbf{H}_{\frac{N}{2}} \underline{e}_2 \right\} \tag{5.37b}$$

and

$$\check{\underline{s}}_2^{(1)} = \frac{1}{2\alpha - 1} \left\{ -c_1 \mathbf{H}_{\frac{N}{2}} \check{\underline{r}}_1^{(1)} + \left(\alpha \mathbf{I}_{\frac{N}{2}} + c_1 \mathbf{H}_{\frac{N}{2}} \right) \underline{r}_2 \right\} \tag{5.38a}$$

$$= \frac{1}{2\alpha - 1} \left\{ -g_1 c_1 \mathbf{H}_{\frac{N}{2}} \underline{r}_1 + \left(\alpha \mathbf{I}_{\frac{N}{2}} + c_1 \mathbf{H}_{\frac{N}{2}} \right) \underline{r}_2 - c_1 v_1 \underline{e}_2 \right\} \tag{5.38b}$$

We obtain the iteration vector $\hat{S}_1$ by replacing the vector $\check{\underline{s}}_2^{(1)}$ in $\hat{S}_1'$ with $\hat{\underline{s}}_2$; the segments of $\hat{S}_1$ are then given by

$$\hat{\underline{s}}_1^{(1)} = \check{\underline{s}}_1^{(1)} = \frac{1}{2\alpha - 1} \left\{ g_1 \left(\alpha \mathbf{I}_{\frac{N}{2}} - c_1 \mathbf{H}_{\frac{N}{2}} \right) \underline{r}_1 - c_1 \mathbf{H}_{\frac{N}{2}} \underline{r}_2 - c_1 v_1 \underline{e}_2 + \alpha v_1 \mathbf{H}_{\frac{N}{2}} \underline{e}_2 \right\} \tag{5.39a}$$

and

$$\hat{\underline{s}}_2^{(1)} = \hat{\underline{s}}_2 = \frac{1}{2\alpha - 1} \left\{ -c_1 \mathbf{H}_{\frac{N}{2}} \underline{r}_1 + \left(\alpha \mathbf{I}_{\frac{N}{2}} + c_1 \mathbf{H}_{\frac{N}{2}} \right) \underline{r}_2 \right\} + \underline{e}_2 \tag{5.39b}$$

Iteration 2

Forward Hadamard NPT

Perform the forward Hadamard NPT of the vector $\hat{S}_1$ whose segments are given by (5.39), to obtain the vector $\hat{R}_2$ whose segments are

$$\hat{\underline{r}}_1^{(2)} = \left[\left(\alpha \mathbf{I}_{\frac{N}{2}} + c_1 \mathbf{H}_{\frac{N}{2}}\right) \hat{\underline{s}}_1^{(1)}\right] + \left[c_1 \mathbf{H}_{\frac{N}{2}} \hat{\underline{s}}_2\right] \tag{5.40a}$$

$$= \left[\frac{1}{2\alpha - 1}\left\{g_1 \left(\alpha^2 - c_1^2\right) \underline{r}_1 - \alpha c_1 \mathbf{H}_{\frac{N}{2}} \underline{r}_2 - c_1^2 \underline{r}_2 + \alpha^2 v_1 \mathbf{H}_{\frac{N}{2}} \underline{e}_2 + \alpha c_1 v_1 \underline{e}_2 - \alpha c_1 v_1 \underline{e}_2 - c_1^2 v_1 \mathbf{H}_{\frac{N}{2}} \underline{e}_2\right\}\right] + \left[\frac{1}{2\alpha - 1}\left\{-c_1^2 \underline{r}_1 + \alpha c_1 \mathbf{H}_{\frac{N}{2}} \underline{r}_2 + c_1^2 \underline{r}_2\right\} + c_1 \mathbf{H}_{\frac{N}{2}} \underline{e}_2\right] \tag{5.40b}$$

$$= \frac{1}{2\alpha - 1}\left\{\left(g_1 \left(\alpha^2 - c_1^2\right) - c_1^2\right) \underline{r}_1 + \left(v_1 \left(\alpha^2 - c_1^2\right) + (2\alpha - 1) c_1\right) \mathbf{H}_{\frac{N}{2}} \underline{e}_2\right\} \tag{5.40c}$$

and

$$\hat{\underline{r}}_2^{(2)} = \left[c_1 \mathbf{H}_{\frac{N}{2}} \hat{\underline{s}}_1^{(1)}\right] + \left[\left(\alpha \mathbf{I}_{\frac{N}{2}} - c_1 \mathbf{H}_{\frac{N}{2}}\right) \hat{\underline{s}}_2\right] \tag{5.41a}$$

$$= \left[\frac{1}{2\alpha - 1}\left\{\alpha g_1 c_1 \mathbf{H}_{\frac{N}{2}} \underline{r}_1 - g_1 c_1^2 \underline{r}_1 - c_1^2 \underline{r}_2 + \alpha c_1 v_1 \underline{e}_2 - c_1^2 v_1 \mathbf{H}_{\frac{N}{2}} \underline{e}_2\right\}\right] + \left[\frac{1}{2\alpha - 1}\left\{-\alpha c_1 \mathbf{H}_{\frac{N}{2}} \underline{r}_1 + c_1^2 \underline{r}_1 + \left(\alpha^2 - c_1^2\right) \underline{r}_2\right\} + \alpha \underline{e}_2 - c_1 \mathbf{H}_{\frac{N}{2}} \underline{e}_2\right] \tag{5.41b}$$

$$= \underline{r}_2 + \frac{1}{2\alpha - 1}\left\{(1 - g_1)\left(c_1^2 \underline{r}_1 - \alpha c_1 \mathbf{H}_{\frac{N}{2}} \underline{r}_1\right) + (c_1 v_1 + 2\alpha - 1)\left(\alpha \underline{e}_2 - c_1 \mathbf{H}_{\frac{N}{2}} \underline{e}_2\right)\right\} \tag{5.41c}$$

We replace the vector $\hat{\underline{r}}_2^{(2)}$ in $\hat{R}_2$ with $\underline{r}_2$ (obtained from $\tilde{R}$) to yield a vector $\hat{R}_2'$ whose segments are

$$\check{\underline{r}}_1^{(2)} = \hat{\underline{r}}_1^{(2)} = g_2 \underline{r}_1 + v_2 \mathbf{H}_{\frac{N}{2}} \underline{e}_2 \tag{5.42a}$$

and

$$\check{\underline{r}}_2^{(2)} = \underline{r}_2 \tag{5.42b}$$

where

$$g_2 = \frac{1}{2\alpha - 1}\left(g_1 \left(\alpha^2 - c_1^2\right) - c_1^2\right) \tag{5.42c}$$

and

$$v_2 = \frac{1}{2\alpha - 1}\left(c_1 v_1 + 2\alpha - 1\right) \tag{5.42d}$$

; g_1 and v_1 are already defined in (5.36c) and (5.36d) respectively.

Inverse Hadamard NPT

By comparing (5.42a) and (5.42b) with (5.36a) and (5.36b) respectively, it is clear that performing the inverse Hadamard NPT of the vector $\hat{R}_2'$ whose segments

are given by (5.42*a*) and (5.42*b*), would yield a vector $\hat{S}'_2$ whose segments can be obtained by replacing g_1 and v_1 in (5.37*b*) and (5.38*b*), with g_2 and v_2 respectively. Replacement of $\underline{\check{s}}_2^{(2)}$ in $\hat{S}'_2$ with $\underline{\hat{s}}_2$ (obtained from $\hat{S}^W$) yields the iteration vector $\hat{S}_2$, whose segments are given by

$$\underline{\hat{s}}_1^{(2)} = \underline{\check{s}}_1^{(2)} = \frac{1}{2\alpha - 1}\Big\{ g_2 \left(\alpha \mathbf{I}_{\frac{N}{2}} - c_1 \mathbf{H}_{\frac{N}{2}}\right) \underline{r}_1 - c_1 \mathbf{H}_{\frac{N}{2}} \underline{r}_2 + \alpha v_2 \mathbf{H}_{\frac{N}{2}} \underline{e}_2 - c_1 v_2 \underline{e}_2 \Big\} \tag{5.43a}$$

and

$$\underline{\hat{s}}_2^{(2)} = \underline{\hat{s}}_2 = \frac{1}{2\alpha - 1}\Big\{ -c_1 \mathbf{H}_{\frac{N}{2}} \underline{r}_1 + \left(\alpha \mathbf{I}_{\frac{N}{2}} + c_1 \mathbf{H}_{\frac{N}{2}}\right) \underline{r}_2 \Big\} + \underline{e}_2 \tag{5.43b}$$

Iteration m

We can infer, based on the results of the previous two iterations, that by continuing the iterative Hadamard NPT reconstruction process to the m^{th} ($m \geq 1$) iteration stage, the segments of the iteration vector $\hat{R}_m$ that is obtained are given by

$$\underline{\hat{r}}_1^{(m)} = g_m \underline{r}_1 + v_m \mathbf{H}_{\frac{N}{2}} \underline{e}_2 \tag{5.44a}$$

and

$$\underline{\hat{r}}_2^{(m)} = \underline{r}_2 + \frac{1}{2\alpha - 1}\Big\{ (1 - g_{m-1}) \left(c_1^2 \underline{r}_1 - \alpha c_1 \mathbf{H}_{\frac{N}{2}} \underline{r}_1\right) + (c_1 v_{m-1} + 2\alpha - 1) \left(\alpha \underline{e}_2 - c_1 \mathbf{H}_{\frac{N}{2}} \underline{e}_2\right) \Big\} \tag{5.44b}$$

where g_m is the convergence factor and v_m is the error vector multiplying factor; g_m and v_m are given recursively by

$$g_m = \frac{\left[g_{m-1}\left(\alpha^2 - \beta_0\right) - \beta_0\right]}{2\alpha - 1} \qquad m > 1;$$
$$g_0 = 0, \quad g_1 = \frac{-(1-\alpha)^2}{2(2\alpha - 1)}, \quad \beta_0 = c_1^2 \tag{5.45}$$

and

$$v_m = \frac{\left[v_{m-1}\left(\alpha^2 - \beta_0\right) + (2\alpha - 1)\, c_1\right]}{2\alpha - 1} \qquad m > 1;$$
$$v_0 = 0, \quad v_1 = c_1 = \frac{1 - \alpha}{\sqrt{2}} \tag{5.46}$$

respectively.

Replacing the vector $\underline{\hat{r}}_2^{(m)}$ in $\hat{R}_m$ with $\underline{r}_2$ (obtained from $\tilde{R}$) to yield the vector $\hat{R}'_m$ and performing the inverse Hadamard NPT of $\hat{R}'_m$, we obtain a vector $\hat{S}'_m$ whose

segments are given by

$$\underline{\check{s}}_1^{(m)} = \frac{1}{2\alpha - 1}\Big\{ g_m \left(\alpha \mathbf{I}_{\frac{N}{2}} - c_1 \mathbf{H}_{\frac{N}{2}}\right) \underline{r}_1 - c_1 \mathbf{H}_{\frac{N}{2}} \underline{r}_2 + \alpha v_m \mathbf{H}_{\frac{N}{2}} \underline{e}_2 - c_1 v_m \underline{e}_2 \Big\} \tag{5.47a}$$

and

$$\underline{\check{s}}_2^{(m)} = \frac{1}{2\alpha - 1}\Big\{ -g_m c_1 \mathbf{H}_{\frac{N}{2}} \underline{r}_1 + \left(\alpha \mathbf{I}_{\frac{N}{2}} + c_1 \mathbf{H}_{\frac{N}{2}}\right) \underline{r}_2 - c_1 v_m \underline{e}_2 \Big\} \tag{5.47b}$$

Results of Empirical Investigations of The Behaviour of g_m and v_m

For convergence, the factor g_m in (5.44a) must tend to unity as iteration progresses; the error multiplying factor should also converge to a finite constant, with a low magnitude. Fig. 5.4a shows the convergence parameter g_m as a function of the number of iterations for four values of α, $\alpha \leq 0.4$. The corresponding error multiplying factors v_m are shown in Fig. 5.4b. We can observe that g_m converges to unity with increasing number of iterations and v_m converges to a finite constant which we have shown to be given by $\frac{\sqrt{2}(1-2\alpha)}{1-\alpha}$. Thus, convergence obtains for these values of α, $\alpha \leq 0.4$, with the fastest rate of convergence being obtained at $\alpha = 0.4$; depending on the value of α, between 3 and 7 iterations are required for convergence.

Fig. 5.5a and Fig. 5.5b respectively show the behaviour of the convergence parameter g_m and the error multiplying factor v_m as the singularity at $\alpha = \frac{1}{2}$ is approached from the left. We can observe oscillations in the values of g_m and v_m as iteration progresses, for values of α in the range $0.45 \leq \alpha \leq 0.464$; it should be noted that the points for g_m and v_m when $\alpha = 0.464$ are not joined by a continuous line in the plots. Furthermore, the amplitude of the bounded oscillations increase with increasing values of α in this range, and the amplitude of the oscillation decrease with iteration. The oscillations eventually get damped out and convergence obtains, but the number of iterations required increases with increasing values of α. For $0.464 < \alpha < 0.5$, the amplitude of the oscillations increase with iteration and eventually become unbounded. Thus, convergence is not obtained for values of α in the range $0.464 < \alpha < 0.5$.

Fig. 5.6a and Fig. 5.6b respectively show the behaviour of g_m and v_m for three values of α, $\alpha > 0.5$. It is observed that both g_m and v_m diverge. The conclusion that can be drawn from the empirical investigations of the behaviour of g_m and v_m with

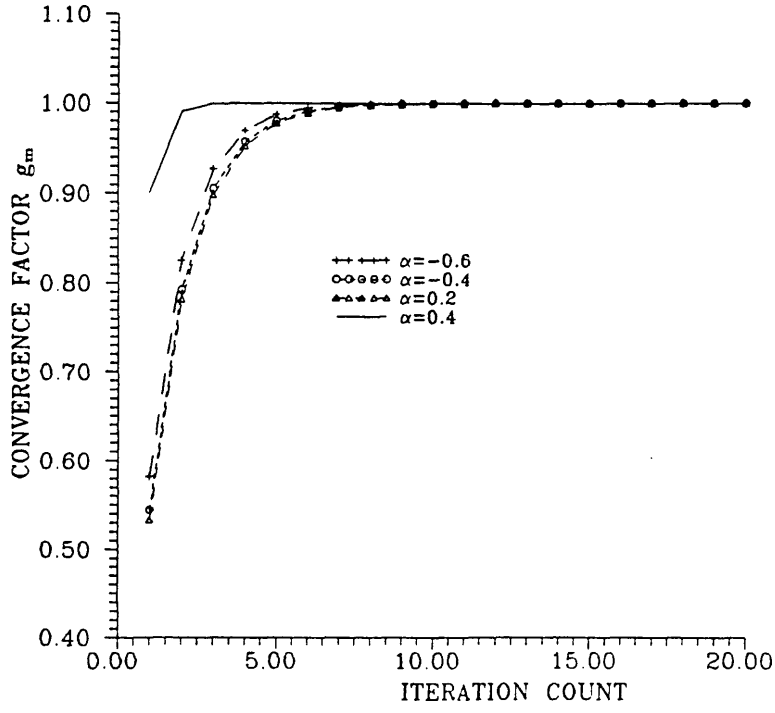


Fig. 5.4a : Convergence factor g_m as a function of iteration count; iterative one-dimensional Hadamard NPT reconstruction at $\alpha < 0.45$.

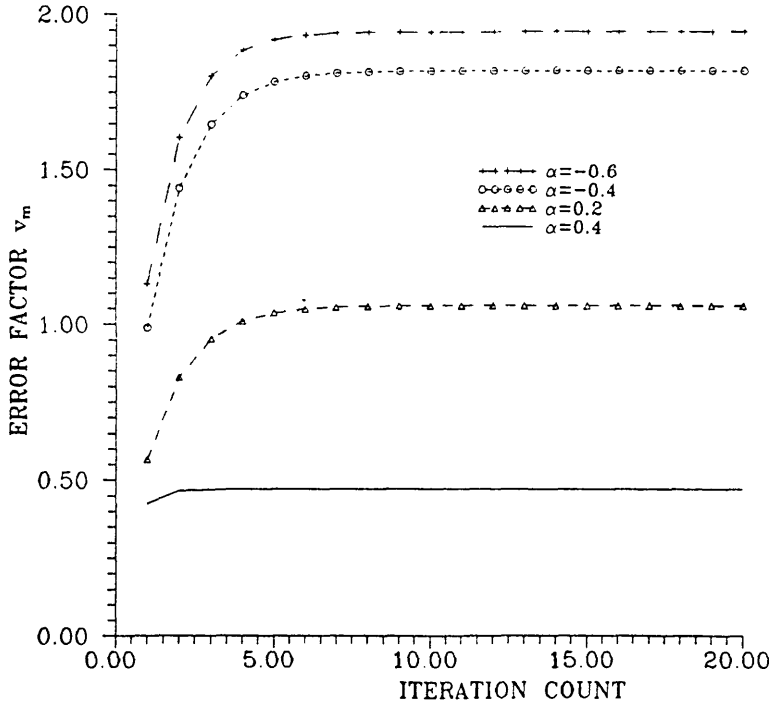


Fig. 5.4b : Error multiplying factor v_m as a function of iteration count; iterative one-dimensional Hadamard NPT reconstruction at $\alpha < 0.45$.

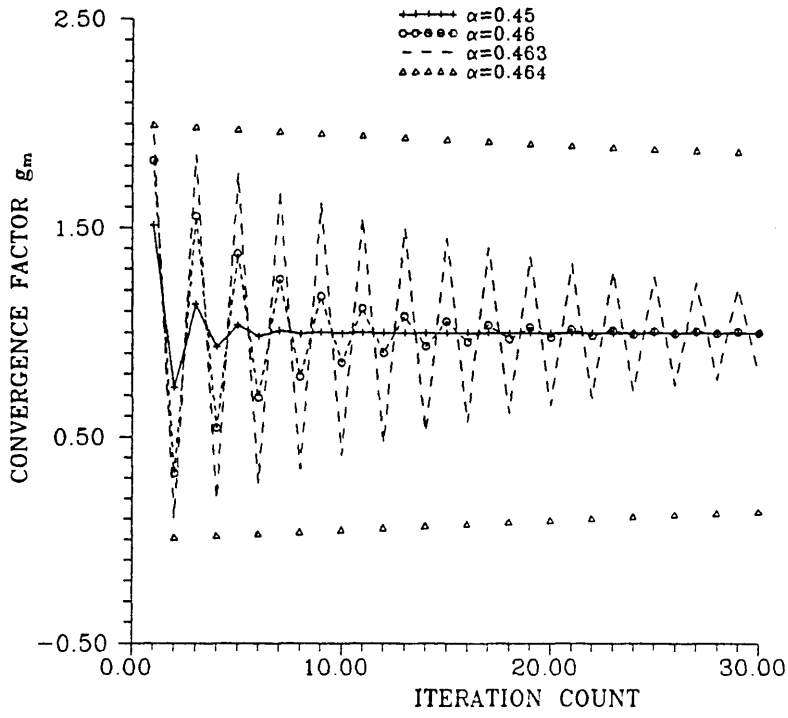


Fig. 5.5a : Convergence factor g_m as a function of iteration count; iterative one-dimensional Hadamard NPT reconstruction at $0.45 \leq \alpha < 0.49$.

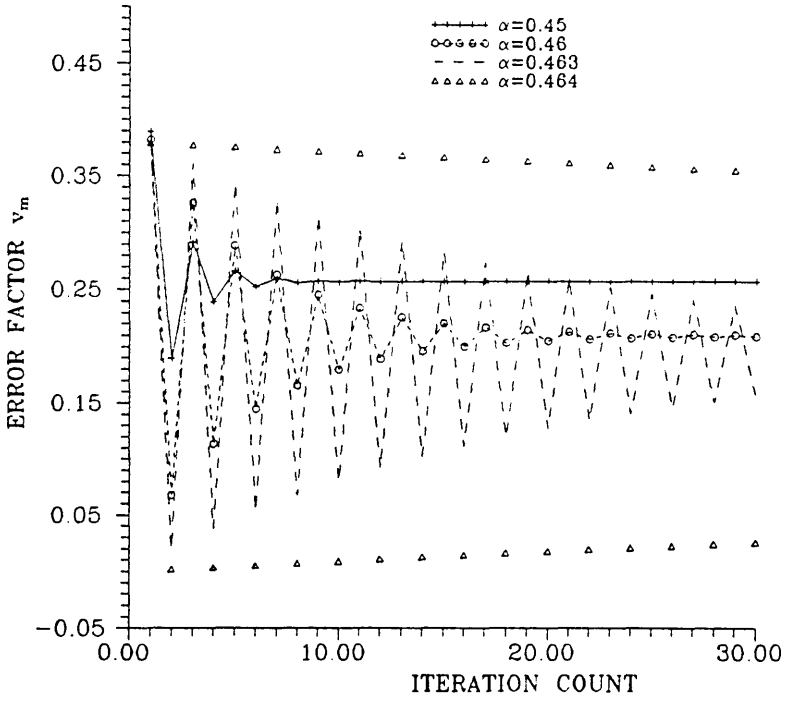


Fig. 5.5b : Error multiplying factor v_m as a function of iteration count; iterative one-dimensional Hadamard NPT reconstruction at $0.45 \leq \alpha < 0.49$.

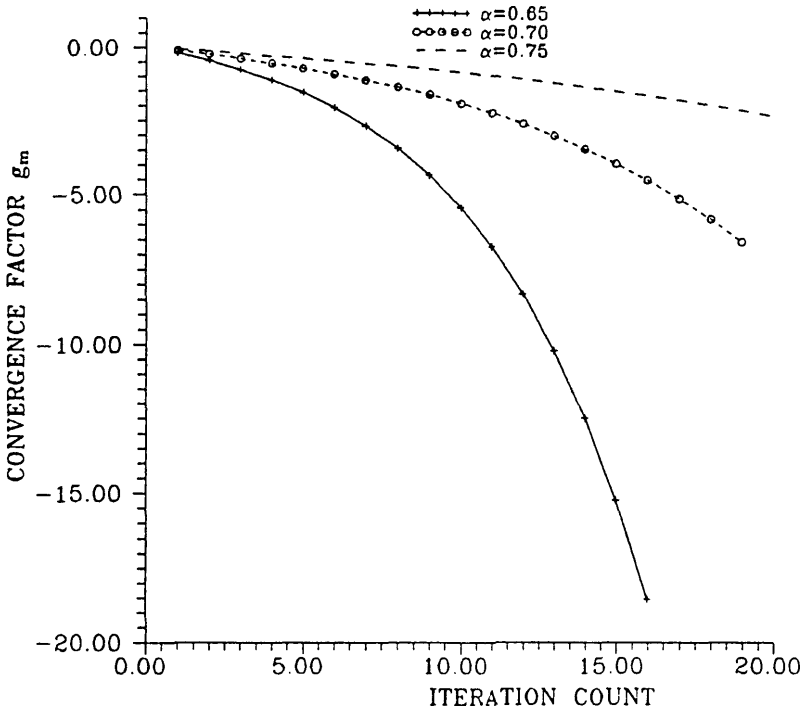


Fig. 5.6a : Convergence factor g_m as a function of iteration count; iterative one-dimensional Hadamard NPT reconstruction at $\alpha > 0.5$.

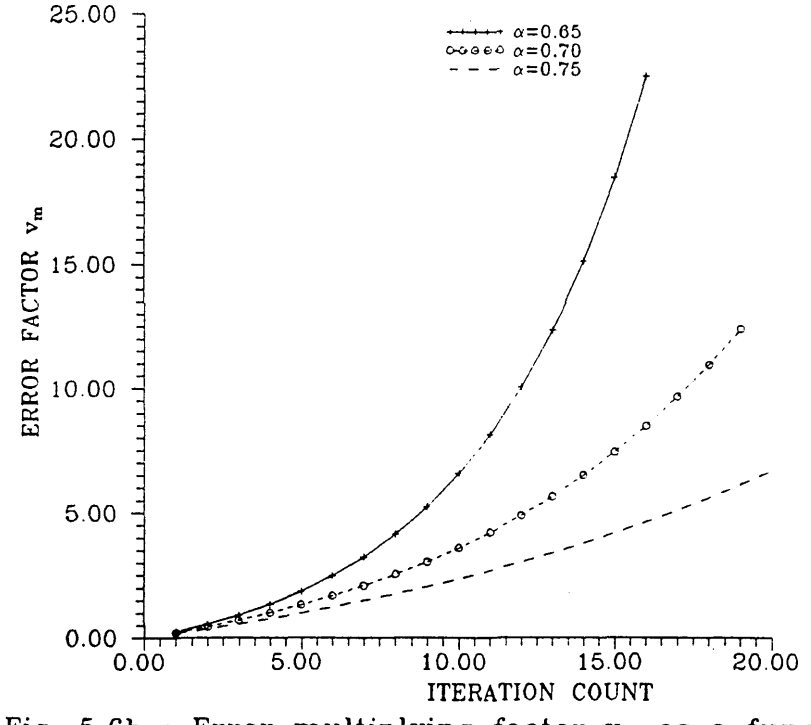


Fig. 5.6b : Error multiplying factor v_m as a function of iteration count; iterative one-dimensional Hadamard NPT reconstruction at $\alpha > 0.5$.

increasing number of iterations is that the iterative Hadamard NPT reconstruction algorithm converges for $\alpha \leq 0.464$.

Case 2

This is depicted in Fig. 5.3b. The original signal vector is given by

$$S = [\underline{s}_1 \,|\, \underline{s}_2 \,|\, \underline{s}_3 \,|\, \underline{s}_4]^T \tag{5.48}$$

while the NPT of S is given by

$$R = [\underline{r}_1 \,|\, \underline{r}_2 \,|\, \underline{r}_3 \,|\, \underline{r}_4]^T \tag{5.49}$$

Using (5.1) and (5.24), we can relate the transform segments $\underline{r}_j$ in (5.49) to the original signal segments as follows :

$$\underline{r}_1 = \left(\alpha \mathbf{I}_{\frac{N}{4}} + c_2 \mathbf{H}_{\frac{N}{4}}\right) \underline{s}_1 + c_2 \mathbf{H}_{\frac{N}{4}} \underline{s}_2 + c_2 \mathbf{H}_{\frac{N}{4}} \underline{s}_3 + c_2 \mathbf{H}_{\frac{N}{4}} \underline{s}_4 \tag{5.50a}$$

$$\underline{r}_2 = c_2 \mathbf{H}_{\frac{N}{4}} \underline{s}_1 + \left(\alpha \mathbf{I}_{\frac{N}{4}} - c_2 \mathbf{H}_{\frac{N}{4}}\right) \underline{s}_2 + c_2 \mathbf{H}_{\frac{N}{4}} \underline{s}_3 - c_2 \mathbf{H}_{\frac{N}{4}} \underline{s}_4 \tag{5.50b}$$

$$\underline{r}_3 = c_2 \mathbf{H}_{\frac{N}{4}} \underline{s}_1 + c_2 \mathbf{H}_{\frac{N}{4}} \underline{s}_2 + \left(\alpha \mathbf{I}_{\frac{N}{4}} - c_2 \mathbf{H}_{\frac{N}{4}}\right) \underline{s}_3 - c_2 \mathbf{H}_{\frac{N}{4}} \underline{s}_4 \tag{5.50c}$$

$$\underline{r}_4 = c_2 \mathbf{H}_{\frac{N}{4}} \underline{s}_1 - c_2 \mathbf{H}_{\frac{N}{4}} \underline{s}_2 - c_2 \mathbf{H}_{\frac{N}{4}} \underline{s}_3 + \left(\alpha \mathbf{I}_{\frac{N}{4}} + c_2 \mathbf{H}_{\frac{N}{4}}\right) \underline{s}_4 \tag{5.50d}$$

where

$$c_2 = \frac{1-\alpha}{2} \tag{5.50e}$$

$\mathbf{I}_{\frac{N}{4}}$ is an identity matrix of order $\frac{N}{4}$ and $\mathbf{H}_{\frac{N}{4}}$ is a normalized natural Hadamard matrix of order $\frac{N}{4}$.

Similarly, the original signal segments $\underline{s}_j$ in (5.48) are related to the transform segments as follows :

$$\underline{s}_1 = \frac{1}{2\alpha - 1}\left\{\left(\alpha \mathbf{I}_{\frac{N}{4}} - c_2 \mathbf{H}_{\frac{N}{4}}\right) \underline{r}_1 - c_2 \mathbf{H}_{\frac{N}{4}} \underline{r}_2 - c_2 \mathbf{H}_{\frac{N}{4}} \underline{r}_3 - c_2 \mathbf{H}_{\frac{N}{4}} \underline{r}_4\right\} \tag{5.51a}$$

$$\underline{s}_2 = \frac{1}{2\alpha - 1}\left\{-c_2 \mathbf{H}_{\frac{N}{4}} \underline{r}_1 + \left(\alpha \mathbf{I}_{\frac{N}{4}} + c_2 \mathbf{H}_{\frac{N}{4}}\right) \underline{r}_2 - c_2 \mathbf{H}_{\frac{N}{4}} \underline{r}_3 + c_2 \mathbf{H}_{\frac{N}{4}} \underline{r}_4\right\} \tag{5.51b}$$

$$\underline{s}_3 = \frac{1}{2\alpha - 1}\left\{-c_2 \mathbf{H}_{\frac{N}{4}} \underline{r}_1 - c_2 \mathbf{H}_{\frac{N}{4}} \underline{r}_2 + \left(\alpha \mathbf{I}_{\frac{N}{4}} + c_2 \mathbf{H}_{\frac{N}{4}}\right) \underline{r}_3 + c_2 \mathbf{H}_{\frac{N}{4}} \underline{r}_4\right\} \tag{5.51c}$$

$$\underline{s}_4 = \frac{1}{2\alpha - 1}\left\{-c_2 \mathbf{H}_{\frac{N}{4}} \underline{r}_1 + c_2 \mathbf{H}_{\frac{N}{4}} \underline{r}_2 + c_2 \mathbf{H}_{\frac{N}{4}} \underline{r}_3 + \left(\alpha \mathbf{I}_{\frac{N}{4}} - c_2 \mathbf{H}_{\frac{N}{4}}\right) \underline{r}_4\right\} \tag{5.51d}$$

The truncated NPT vector, $\tilde{R}$, for this case is given by

$$\tilde{R} = [\underline{0} \,|\, \underline{r}_2 \,|\, \underline{0} \,|\, \underline{r}_4]^T \tag{5.52}$$

The estimate, $\hat{S}^W$, of the signal amplitude over the known transform segments (derived from $\tilde{R}$) can be expressed as

$$\hat{S}^W = [\underline{0} \,|\, \underline{\hat{s}}_2 \,|\, \underline{0} \,|\, \underline{\hat{s}}_4]^T \tag{5.53a}$$

$$= [\underline{0} \,|\, \underline{s}_2 + \underline{e}_2 \,|\, \underline{0} \,|\, \underline{s}_4 + \underline{e}_4]^T \tag{5.53b}$$

Iterates from (5.14), for this format, are evaluated as follows. The iteration vectors $\hat{S}_m$ and $\hat{R}_m$ are respectively given by

$$\hat{S}_m = \left[\underline{\hat{s}}_1^{(m)} \,|\, \underline{\hat{s}}_2^{(m)} \,|\, \underline{\hat{s}}_3^{(m)} \,|\, \underline{\hat{s}}_4^{(m)}\right]^T \tag{5.54}$$

and

$$\hat{R}_m = \left[\underline{\hat{r}}_1^{(m)} \,|\, \underline{\hat{r}}_2^{(m)} \,|\, \underline{\hat{r}}_3^{(m)} \,|\, \underline{\hat{r}}_4^{(m)}\right]^T \tag{5.55}$$

Initialization

Perform the inverse Hadamard NPT of $\tilde{R}$ to obtain the vector $\hat{S}_0$. The segments of $\hat{S}_0$ can be obtained by setting $\underline{r}_1 = \underline{r}_3 = \underline{0}$ in (5.51) to yield

$$\underline{\hat{s}}_1^{(0)} = \frac{1}{2\alpha - 1}\left\{-c_2 \mathbf{H}_{\frac{N}{4}} \underline{r}_2 - c_2 \mathbf{H}_{\frac{N}{4}} \underline{r}_4\right\} \tag{5.56a}$$

$$\underline{\hat{s}}_2^{(0)} = \frac{1}{2\alpha - 1}\left\{\left(\alpha \mathbf{I}_{\frac{N}{4}} + c_2 \mathbf{H}_{\frac{N}{4}}\right) \underline{r}_2 + c_2 \mathbf{H}_{\frac{N}{4}} \underline{r}_4\right\} \tag{5.56b}$$

$$\underline{\hat{s}}_3^{(0)} = \frac{1}{2\alpha - 1}\left\{-c_2 \mathbf{H}_{\frac{N}{4}} \underline{r}_2 + c_2 \mathbf{H}_{\frac{N}{4}} \underline{r}_4\right\} \tag{5.56c}$$

$$\underline{\hat{s}}_4^{(0)} = \frac{1}{2\alpha - 1}\left\{c_2 \mathbf{H}_{\frac{N}{4}} \underline{r}_2 + \left(\alpha \mathbf{I}_{\frac{N}{4}} - c_2 \mathbf{H}_{\frac{N}{4}}\right) \underline{r}_4\right\} \tag{5.56d}$$

Replace the vectors $\underline{\hat{s}}_2^{(0)}$ and $\underline{\hat{s}}_4^{(0)}$ in $\hat{S}_0$ with $\underline{\hat{s}}_2$ and $\underline{\hat{s}}_4$ (derived from $\hat{S}^W$) to obtain a vector $\hat{S}_0'$, whose segments are

$$\underline{\check{s}}_1^{(0)} = \underline{\hat{s}}_1^{(0)} = \frac{1}{2\alpha - 1}\left\{-c_2 \mathbf{H}_{\frac{N}{4}} \underline{r}_2 - c_2 \mathbf{H}_{\frac{N}{4}} \underline{r}_4\right\} \tag{5.57a}$$

$$\underline{\check{s}}_2^{(0)} = \underline{\hat{s}}_2 = \frac{1}{2\alpha - 1}\left\{-c_2 \mathbf{H}_{\frac{N}{4}} \underline{r}_1 + \left(\alpha \mathbf{I}_{\frac{N}{4}} + c_2 \mathbf{H}_{\frac{N}{4}}\right) \underline{r}_2 - c_2 \mathbf{H}_{\frac{N}{4}} \underline{r}_3 + c_2 \mathbf{H}_{\frac{N}{4}} \underline{r}_4\right\} + \underline{e}_2 \tag{5.57b}$$

$$\underline{\check{s}}_3^{(0)} = \underline{\hat{s}}_3^{(0)} = \frac{1}{2\alpha - 1}\left\{-c_2 \mathbf{H}_{\frac{N}{4}} \underline{r}_2 + c_2 \mathbf{H}_{\frac{N}{4}} \underline{r}_4\right\} \tag{5.57c}$$

$$\underline{\check{s}}_4^{(0)} = \underline{\hat{s}}_4 = \frac{1}{2\alpha - 1}\left\{-c_2 \mathbf{H}_{\frac{N}{4}} \underline{r}_1 + c_2 \mathbf{H}_{\frac{N}{4}} \underline{r}_2 + c_2 \mathbf{H}_{\frac{N}{4}} \underline{r}_3 + \left(\alpha \mathbf{I}_{\frac{N}{4}} - c_2 \mathbf{H}_{\frac{N}{4}}\right) \underline{r}_4\right\} + \underline{e}_4 \tag{5.57d}$$

Iteration 1

Perform the forward Hadamard NPT of the vector whose segments are given by (5.57) to obtain the respective segments of $\hat{R}_1$ as follows :

$$\underline{\hat{r}}_1^{(1)} = \left[\left(\alpha \mathbf{I}_{\frac{N}{4}} + c_2 \mathbf{H}_{\frac{N}{4}}\right) \underline{\hat{s}}_1^{(0)}\right] + \left[c_2 \mathbf{H}_{\frac{N}{4}} \underline{\hat{s}}_2\right] + \left[c_2 \mathbf{H}_{\frac{N}{4}} \underline{\hat{s}}_3^{(0)}\right] + \left[c_2 \mathbf{H}_{\frac{N}{4}} \underline{\hat{s}}_4\right] \tag{5.58a}$$

$$= \left[\frac{1}{2\alpha - 1}\left\{-\alpha c_2 \mathbf{H}_{\frac{N}{4}} \underline{r}_2 - c_2^2 \underline{r}_2 - \alpha c_2 \mathbf{H}_{\frac{N}{4}} \underline{r}_4 - c_2^2 \underline{r}_4\right\}\right] + \left[\frac{1}{2\alpha - 1}\left\{-c_2^2 \underline{r}_1 + \alpha c_2 \mathbf{H}_{\frac{N}{4}} \underline{r}_2 + c_2^2 \underline{r}_2 - c_2^3 \underline{r}_3 + c_2^2 \underline{r}_4\right\} + c_2 \mathbf{H}_{\frac{N}{4}} \underline{e}_2\right] + \left[\frac{1}{2\alpha - 1}\left\{-c_2^2 \underline{r}_2 + c_2^2 \underline{r}_4\right\}\right] + \left[\frac{1}{2\alpha - 1}\left\{-c_2^2 \underline{r}_1 + c_2^2 \underline{r}_2 + c_2^2 \underline{r}_3 + \alpha c_2 \mathbf{H}_{\frac{N}{4}} \underline{r}_4 - c_2^2 \underline{r}_4\right\} + c_2 \mathbf{H}_{\frac{N}{4}} \underline{e}_4\right] \tag{5.58b}$$

$$= \frac{1}{2\alpha - 1}\left\{-2c_2^2 \underline{r}_1\right\} + c_2 \mathbf{H}_{\frac{N}{4}} \underline{e}_2 + c_2 \mathbf{H}_{\frac{N}{4}} \underline{e}_4 \tag{5.58c}$$

$$\underline{\hat{r}}_2^{(1)} = \left[c_2 \mathbf{H}_{\frac{N}{4}} \underline{\hat{s}}_1^{(0)}\right] + \left[\left(\alpha \mathbf{I}_{\frac{N}{4}} - c_2 \mathbf{H}_{\frac{N}{4}}\right) \underline{\hat{s}}_2\right] + \left[c_2 \mathbf{H}_{\frac{N}{4}} \underline{\hat{s}}_3^{(0)}\right] + \left[-c_2 \mathbf{H}_{\frac{N}{4}} \underline{\hat{s}}_4\right] \tag{5.59a}$$

$$= \left[\frac{1}{2\alpha - 1}\left\{-c_2^2 \underline{r}_2 - c_2^2 \underline{r}_4\right\}\right] + \left[\frac{1}{2\alpha - 1}\left\{-\alpha c_2 \mathbf{H}_{\frac{N}{4}} \underline{r}_1 + c_2^2 \underline{r}_1 + \left(\alpha^2 - c_2^2\right) \underline{r}_2 - \alpha c_2 \mathbf{H}_{\frac{N}{4}} \underline{r}_3 + c_2^2 \underline{r}_3 + \alpha c_2 \mathbf{H}_{\frac{N}{4}} \underline{r}_4 - c_2^2 \underline{r}_4\right\} + \alpha \underline{e}_2 - c_2 \mathbf{H}_{\frac{N}{4}} \underline{e}_2\right] + \left[\frac{1}{2\alpha - 1}\left\{-c_2^2 \underline{r}_2 + c_2^2 \underline{r}_4\right\}\right] + \left[\frac{1}{2\alpha - 1}\left\{c_2^2 \underline{r}_1 - c_2^2 \underline{r}_2 - c_2^2 \underline{r}_3 - \alpha c_2 \mathbf{H}_{\frac{N}{4}} \underline{r}_4 + c_2^2 \underline{r}_4\right\} - c_2 \mathbf{H}_{\frac{N}{4}} \underline{e}_4\right] \tag{5.59b}$$

$$= \underline{r}_2 + \frac{1}{2\alpha - 1}\left\{2c_2^2 \underline{r}_1 - \alpha c_2 \mathbf{H}_{\frac{N}{4}} \underline{r}_1 - \alpha c_2 \mathbf{H}_{\frac{N}{4}} \underline{r}_3\right\} + \alpha \underline{e}_2 - c_2 \mathbf{H}_{\frac{N}{4}} \underline{e}_2 - c_2 \mathbf{H}_{\frac{N}{4}} \underline{e}_4 \tag{5.59c}$$

$$\underline{\hat{r}}_3^{(1)} = \left[c_2 \mathbf{H}_{\frac{N}{4}} \underline{\hat{s}}_1^{(0)}\right] + \left[c_2 \mathbf{H}_{\frac{N}{4}} \underline{\hat{s}}_2\right] + \left[\left(\alpha \mathbf{I}_{\frac{N}{4}} - c_2 \mathbf{H}_{\frac{N}{4}}\right) \underline{\hat{s}}_3^{(0)}\right] + \left[-c_2 \mathbf{H}_{\frac{N}{4}} \underline{\hat{s}}_4\right] \tag{5.60a}$$

$$= \left[\frac{1}{2\alpha - 1}\left\{-c_2^2 \underline{r}_2 - c_2^2 \underline{r}_4\right\}\right] + \left[\frac{1}{2\alpha - 1}\left\{-c_2^2 \underline{r}_1 + \alpha c_2 \mathbf{H}_{\frac{N}{4}} \underline{r}_2 + c_2^2 \underline{r}_2 - c_2^2 \underline{r}_3 + c_2^2 \underline{r}_4\right\} + c_2 \mathbf{H}_{\frac{N}{4}} \underline{e}_2\right] + \left[\frac{1}{2\alpha - 1}\left\{-\alpha c_2 \mathbf{H}_{\frac{N}{4}} \underline{r}_2 + c_2^2 \underline{r}_2 + \alpha c_2 \mathbf{H}_{\frac{N}{4}} \underline{r}_4 - c_2^2 \underline{r}_4\right\}\right] + \left[\frac{1}{2\alpha - 1}\left\{c_2^2 \underline{r}_1 - c_2^2 \underline{r}_2 - c_2^2 \underline{r}_3 - \alpha c_2 \mathbf{H}_{\frac{N}{4}} \underline{r}_4 + c_2^2 \underline{r}_4\right\} - c_2 \mathbf{H}_{\frac{N}{4}} \underline{e}_4\right] \tag{5.60b}$$

$$= \frac{1}{2\alpha - 1}\left\{-2c_2^2 \underline{r}_3\right\} + c_2 \mathbf{H}_{\frac{N}{4}} \underline{e}_2 - c_2 \mathbf{H}_{\frac{N}{4}} \underline{e}_4 \tag{5.60c}$$

$$\underline{\hat{r}}_4^{(1)} = \left[c_2 \mathbf{H}_{\frac{N}{4}} \underline{\hat{s}}_1^{(0)}\right] + \left[-c_2 \mathbf{H}_{\frac{N}{4}} \underline{\hat{s}}_2\right] + \left[-c_2 \mathbf{H}_{\frac{N}{4}} \underline{\hat{s}}_3^{(0)}\right] + \left[\left(\alpha \mathbf{I}_{\frac{N}{4}} + c_2 \mathbf{H}_{\frac{N}{4}}\right) \underline{\hat{s}}_4\right] \tag{5.61a}$$

$$= \left[\frac{1}{2\alpha - 1}\left\{-c_2^2 \underline{r}_2 - c_2^2 \underline{r}_4\right\}\right] + \left[\frac{1}{2\alpha - 1}\left\{c_2^2 \underline{r}_1 - \alpha c_2 \mathbf{H}_{\frac{N}{4}} \underline{r}_2 - c_2^2 \underline{r}_2 + c_2^2 \underline{r}_3 - c_2^2 \underline{r}_4\right\} - c_2 \mathbf{H}_{\frac{N}{4}} \underline{e}_2\right] + \left[\frac{1}{2\alpha - 1}\left\{c_2^2 \underline{r}_2 - c_2^2 \underline{r}_4\right\}\right] + \left[\frac{1}{2\alpha - 1}\left\{-\alpha c_2 \mathbf{H}_{\frac{N}{4}} \underline{r}_1 - c_2^2 \underline{r}_1 + \alpha c_2 \mathbf{H}_{\frac{N}{4}} \underline{r}_2 + c_2^2 \underline{r}_2 + \alpha c_2 \mathbf{H}_{\frac{N}{4}} \underline{r}_3 + c_2^2 \underline{r}_3 + \left(\alpha^2 - c_2^2\right) \underline{r}_4\right\}\right.$$

$$+ \alpha \underline{e}_4 + c_2 \mathbf{H}_{\frac{N}{4}} \underline{e}_4 \Big] \tag{5.61b}$$

$$= \underline{r}_4 + \frac{1}{2\alpha - 1} \Big\{ 2c_2^2 \underline{r}_3 - \alpha c_2 \mathbf{H}_{\frac{N}{4}} \underline{r}_1 + \alpha c_2 \mathbf{H}_{\frac{N}{4}} \underline{r}_3 \Big\} - c_2 \mathbf{H}_{\frac{N}{4}} \underline{e}_2 + \alpha \underline{e}_4$$
$$+ c_2 \mathbf{H}_{\frac{N}{4}} \underline{e}_4 \tag{5.61c}$$

Replace the vectors $\hat{\underline{r}}_2^{(1)}$ and $\hat{\underline{r}}_4^{(1)}$ in $\hat{R}_1$ with the vectors $\underline{r}_2$ and $\underline{r}_4$ (these were correctly received) to yield a vector $\hat{R}_1'$ whose segments are

$$\check{\underline{r}}_1^{(1)} = \hat{\underline{r}}_1^{(1)} = g_1 \underline{r}_1 + v_1 \mathbf{H}_{\frac{N}{4}} (\underline{e}_2 + \underline{e}_4) \tag{5.62a}$$

$$\check{\underline{r}}_2^{(1)} = \underline{r}_2 \tag{5.62b}$$

$$\check{\underline{r}}_3^{(1)} = \hat{\underline{r}}_3^{(1)} = g_1 \underline{r}_3 + v_1 \mathbf{H}_{\frac{N}{4}} (\underline{e}_2 - \underline{e}_4) \tag{5.62c}$$

$$\check{\underline{r}}_4^{(1)} = \underline{r}_4 \tag{5.62d}$$

where

$$g_1 = \frac{-2c_2^2}{2\alpha - 1} \tag{5.63a}$$

and

$$v_1 = c_2 = \frac{1 - \alpha}{2} \tag{5.63b}$$

We note that (5.62*a*) and (5.62*c*) respectively express the sub-vectors $\hat{\underline{r}}_1^{(1)}$ and $\hat{\underline{r}}_3^{(1)}$ in terms of the desired (but unknown) transform segments $\underline{r}_1$ and $\underline{r}_3$.

Inverse Hadamard NPT

We proceed with the iterative reconstruction process by performing the inverse Hadamard NPT of $\hat{R}_1'$ to obtain a vector $\hat{S}_1'$ whose segments are given by

$$\check{\underline{s}}_1^{(1)} = \frac{1}{2\alpha - 1} \Big\{ \Big(\alpha \mathbf{I}_{\frac{N}{4}} - c_2 \mathbf{H}_{\frac{N}{4}} \Big) \check{\underline{r}}_1^{(1)} - c_2 \mathbf{H}_{\frac{N}{4}} \underline{r}_2 - c_2 \mathbf{H}_{\frac{N}{4}} \check{\underline{r}}_3^{(1)} - c_2 \mathbf{H}_{\frac{N}{4}} \underline{r}_4 \Big\} \tag{5.64a}$$

$$= \frac{1}{2\alpha - 1} \Big\{ g_1 \Big(\alpha \mathbf{I}_{\frac{N}{4}} - c_2 \mathbf{H}_{\frac{N}{4}} \Big) \underline{r}_1 - c_2 \mathbf{H}_{\frac{N}{4}} \underline{r}_2 - g_1 c_2 \mathbf{H}_{\frac{N}{4}} \underline{r}_3 - c_2 \mathbf{H}_{\frac{N}{4}} \underline{r}_4$$
$$- 2c_2 v_1 \underline{e}_2 + \alpha v_1 \mathbf{H}_{\frac{N}{4}} (\underline{e}_2 + \underline{e}_4) \Big\} \tag{5.64b}$$

$$\check{\underline{s}}_2^{(1)} = \frac{1}{2\alpha - 1} \Big\{ -c_2 \mathbf{H}_{\frac{N}{4}} \check{\underline{r}}_1^{(1)} + \Big(\alpha \mathbf{I}_{\frac{N}{4}} + c_2 \mathbf{H}_{\frac{N}{4}} \Big) \underline{r}_2 - c_2 \mathbf{H}_{\frac{N}{4}} \check{\underline{r}}_3^{(1)} + c_2 \mathbf{H}_{\frac{N}{4}} \underline{r}_4 \Big\} \tag{5.65a}$$

$$= \frac{1}{2\alpha - 1} \Big\{ -g_1 c_2 \mathbf{H}_{\frac{N}{4}} \underline{r}_1 + \Big(\alpha \mathbf{I}_{\frac{N}{4}} + c_2 \mathbf{H}_{\frac{N}{4}} \Big) \underline{r}_2 - g_1 c_2 \mathbf{H}_{\frac{N}{4}} \underline{r}_3 + c_2 \mathbf{H}_{\frac{N}{4}} \underline{r}_4$$
$$- 2c_2 v_1 \underline{e}_2 \Big\} \tag{5.65b}$$

$$\check{\underline{s}}_3^{(1)} = \frac{1}{2\alpha - 1} \Big\{ -c_2 \mathbf{H}_{\frac{N}{4}} \check{\underline{r}}_1^{(1)} - c_2 \mathbf{H}_{\frac{N}{4}} \underline{r}_2 + \Big(\alpha \mathbf{I}_{\frac{N}{4}} + c_2 \mathbf{H}_{\frac{N}{4}} \Big) \check{\underline{r}}_3^{(1)} + c_2 \mathbf{H}_{\frac{N}{4}} \underline{r}_4 \Big\} \tag{5.66a}$$

$$= \frac{1}{2\alpha - 1} \Big\{ -g_1 c_2 \mathbf{H}_{\frac{N}{4}} \underline{r}_1 - c_2 \mathbf{H}_{\frac{N}{4}} \underline{r}_2 + g_1 \Big(\alpha \mathbf{I}_{\frac{N}{4}} + c_2 \mathbf{H}_{\frac{N}{4}} \Big) \underline{r}_3 + c_2 \mathbf{H}_{\frac{N}{4}} \underline{r}_4$$
$$- 2c_2 v_1 \underline{e}_4 + \alpha v_1 \mathbf{H}_{\frac{N}{4}} (\underline{e}_2 - \underline{e}_4) \Big\} \tag{5.66b}$$

$$\check{\underline{s}}_4^{(1)} = \frac{1}{2\alpha-1}\Big\{-c_2\mathbf{H}_{\frac{N}{4}}\check{\underline{r}}_1^{(1)} + c_2\mathbf{H}_{\frac{N}{4}}\underline{r}_2 + c_2\mathbf{H}_{\frac{N}{4}}\check{\underline{r}}_3^{(1)} + \left(\alpha\mathbf{I}_{\frac{N}{4}} - c_2\mathbf{H}_{\frac{N}{4}}\right)\underline{r}_4\Big\} \tag{5.67a}$$

$$= \frac{1}{2\alpha-1}\Big\{-g_1c_2\mathbf{H}_{\frac{N}{4}}\underline{r}_1 - c_2\mathbf{H}_{\frac{N}{4}}\underline{r}_2 + g_1c_2\mathbf{H}_{\frac{N}{4}}\underline{r}_3 + \left(\alpha\mathbf{I}_{\frac{N}{4}} - c_2\mathbf{H}_{\frac{N}{4}}\right)\underline{r}_4 - 2c_2v_1\underline{e}_4\Big\} \tag{5.67b}$$

We obtain the iteration vector $\hat{S}_1$ by replacing the sub-vectors $\check{\underline{s}}_2^{(1)}$ and $\check{\underline{s}}_4^{(1)}$ in $\hat{S}_1'$ with $\hat{\underline{s}}_2$ and $\hat{\underline{s}}_4$ respectively; the segments of $\hat{S}_1$ are then given by

$$\hat{\underline{s}}_1^{(1)} = \check{\underline{s}}_1^{(1)} = \frac{1}{2\alpha-1}\Big\{g_1\left(\alpha\mathbf{I}_{\frac{N}{4}} - c_2\mathbf{H}_{\frac{N}{4}}\right)\underline{r}_1 - c_2\mathbf{H}_{\frac{N}{4}}\underline{r}_2 - g_1c_2\mathbf{H}_{\frac{N}{4}}\underline{r}_3 - c_2\mathbf{H}_{\frac{N}{4}}\underline{r}_4 - 2c_2v_1\underline{e}_2 + \alpha v_1\mathbf{H}_{\frac{N}{4}}(\underline{e}_2 + \underline{e}_4)\Big\} \tag{5.68a}$$

$$\hat{\underline{s}}_2^{(1)} = \hat{\underline{s}}_2 = \frac{1}{2\alpha-1}\Big\{-c_2\mathbf{H}_{\frac{N}{4}}\underline{r}_1 + \left(\alpha\mathbf{I}_{\frac{N}{4}} + c_2\mathbf{H}_{\frac{N}{4}}\right)\underline{r}_2 - c_2\mathbf{H}_{\frac{N}{4}}\underline{r}_3 + c_2\mathbf{H}_{\frac{N}{4}}\underline{r}_4\Big\} + \underline{e}_2 \tag{5.68b}$$

$$\hat{\underline{s}}_3^{(1)} = \check{\underline{s}}_3^{(1)} = \frac{1}{2\alpha-1}\Big\{-g_1c_2\mathbf{H}_{\frac{N}{4}}\underline{r}_1 - c_2\mathbf{H}_{\frac{N}{4}}\underline{r}_2 + g_1\left(\alpha\mathbf{I}_{\frac{N}{4}} + c_2\mathbf{H}_{\frac{N}{4}}\right)\underline{r}_3 + c_2\mathbf{H}_{\frac{N}{4}}\underline{r}_4 - 2c_2v_1\underline{e}_4 + \alpha v_1\mathbf{H}_{\frac{N}{4}}(\underline{e}_2 - \underline{e}_4)\Big\} \tag{5.68c}$$

$$\hat{\underline{s}}_4^{(1)} = \hat{\underline{s}}_4 = \frac{1}{2\alpha-1}\Big\{-c_2\mathbf{H}_{\frac{N}{4}}\underline{r}_1 + c_2\mathbf{H}_{\frac{N}{4}}\underline{r}_2 + c_2\mathbf{H}_{\frac{N}{4}}\underline{r}_3 + \left(\alpha\mathbf{I}_{\frac{N}{4}} - c_2\mathbf{H}_{\frac{N}{4}}\right)\underline{r}_4\Big\} + \underline{e}_4 \tag{5.68d}$$

Iteration 2

Forward Hadamard NPT

Perform the forward Hadamard NPT of the vector $\hat{S}_1$, whose segments are given by (5.68), to obtain the vector $\hat{R}_2$ whose segments are

$$\hat{\underline{r}}_1^{(2)} = \left[\left(\alpha\mathbf{I}_{\frac{N}{4}} + c_2\mathbf{H}_{\frac{N}{4}}\right)\hat{\underline{s}}_1^{(1)}\right] + \left[c_2\mathbf{H}_{\frac{N}{4}}\hat{\underline{s}}_2\right] + \left[c_2\mathbf{H}_{\frac{N}{4}}\hat{\underline{s}}_3^{(1)}\right] + \left[c_2\mathbf{H}_{\frac{N}{4}}\hat{\underline{s}}_4\right] \tag{5.69a}$$

$$= \Big[\frac{1}{2\alpha-1}\Big\{g_1(\alpha^2 - c_2^2)\underline{r}_1 - \alpha c_2\mathbf{H}_{\frac{N}{4}}\underline{r}_2 - c_2^2\underline{r}_2 - g_1\alpha c_2\mathbf{H}_{\frac{N}{4}}\underline{r}_3 - g_1c_2^2\underline{r}_3 - \alpha c_2\mathbf{H}_{\frac{N}{4}}\underline{r}_4 - c_2^2\underline{r}_4 - 2\alpha c_2v_1\underline{e}_2 - 2c_2^2v_1\mathbf{H}_{\frac{N}{4}}\underline{e}_2 + \alpha^2v_1\mathbf{H}_{\frac{N}{4}}\underline{e}_2 + \alpha c_2v_1\underline{e}_2 + \alpha^2v_1\mathbf{H}_{\frac{N}{4}}\underline{e}_4 + \alpha c_2v_1\underline{e}_4\Big\}\Big] + \Big[\frac{1}{2\alpha-1}\Big\{-c_2^2\underline{r}_1 + \alpha c_2\mathbf{H}_{\frac{N}{4}}\underline{r}_2 + c_2^2\underline{r}_2 - c_2^2\underline{r}_3 + c_2^2\underline{r}_4\Big\} + c_2\mathbf{H}_{\frac{N}{4}}\underline{e}_2\Big] + \Big[\frac{1}{2\alpha-1}\Big\{-g_1c_2^2\underline{r}_1 - c_2^2\underline{r}_2 + g_1\alpha c_2\mathbf{H}_{\frac{N}{4}}\underline{r}_3 + g_1c_2^2\underline{r}_3 + c_2^2\underline{r}_4 - 2c_2^2v_1\mathbf{H}_{\frac{N}{4}}\underline{e}_4 + \alpha c_2v_1\underline{e}_2 - \alpha c_2v_1\underline{e}_4\Big\}\Big] + \Big[\frac{1}{2\alpha-1}\Big\{-c_2^2\underline{r}_1 + c_2^2\underline{r}_2 + c_2^2\underline{r}_3 + \alpha c_2\mathbf{H}_{\frac{N}{4}}\underline{r}_4 - c_2^2\underline{r}_4\Big\} + c_2\mathbf{H}_{\frac{N}{4}}\underline{e}_4\Big] \tag{5.69b}$$

$$= \frac{1}{2\alpha-1}\Big\{\Big[g_1\left(\alpha^2-2c_2^2\right)-2c_2^2\Big]\underline{r}_1+\Big[v_1\left(\alpha^2-2c_2^2\right)+(2\alpha-1)\,c_2\Big]\mathbf{H}_{\underline{N}}\left(\underline{e}_2+\underline{e}_4\right)\Big\} \quad (5.69c)$$

$$= g_2\underline{r}_1+v_2\mathbf{H}_{\underline{N}}\left(\underline{e}_2+\underline{e}_4\right) \quad (5.69d)$$

where

$$g_2=\frac{1}{2\alpha-1}\left[g_1\left(\alpha^2-2c_2^2\right)-2c_2^2\right] \qquad ;\; g_1=\frac{-2c_2^2}{2\alpha-1} \quad (5.70a)$$

and

$$v_2=\frac{1}{2\alpha-1}\left[v_1\left(\alpha^2-2c_2^2\right)+(2\alpha-1)\,c_2\right] \qquad ;\; v_1=c_2 \quad (5.70b)$$

$$\hat{\underline{r}}_2^{(2)}=\Big[c_2\mathbf{H}_{\underline{N}}\hat{\underline{s}}_1^{(1)}\Big]+\Big[\Big(\alpha\mathbf{I}_{\underline{N}}-c_2\mathbf{H}_{\underline{N}}\Big)\hat{\underline{s}}_2\Big]+\Big[c_2\mathbf{H}_{\underline{N}}\hat{\underline{s}}_3^{(1)}\Big]+\Big[-c_2\mathbf{H}_{\underline{N}}\hat{\underline{s}}_4\Big] \quad (5.71a)$$

$$\begin{aligned}
&= \Big[\frac{1}{2\alpha-1}\Big\{g_1\alpha c_2\mathbf{H}_{\underline{N}}\underline{r}_1-g_1c_2^2\underline{r}_1-c_2^2\underline{r}_2-g_1c_2^2\underline{r}_3-c_2^2\underline{r}_4-2c_2^2v_1\mathbf{H}_{\underline{N}}\underline{e}_2\\
&\quad+\alpha c_2v_1\underline{e}_2+\alpha c_2v_1\underline{e}_4\Big\}\Big]+\Big[\frac{1}{2\alpha-1}\Big\{-\alpha c_2\mathbf{H}_{\underline{N}}\underline{r}_1+c_2^2\underline{r}_1+\left(\alpha^2-c_2^2\right)\underline{r}_2\\
&\quad-\alpha c_2\mathbf{H}_{\underline{N}}\underline{r}_3+c_2^2\underline{r}_3+\alpha c_2\mathbf{H}_{\underline{N}}\underline{r}_4-c_2^2\underline{r}_4\Big\}+\alpha\underline{e}_2-c_2\mathbf{H}_{\underline{N}}\underline{e}_2\Big]\\
&\quad+\Big[\frac{1}{2\alpha-1}\Big\{-g_1c_2^2\underline{r}_1-c_2^2\underline{r}_2+g_1\alpha c_2\mathbf{H}_{\underline{N}}\underline{r}_3+g_1c_2^2\underline{r}_3+c_2^2\underline{r}_4-2c_2^2v_1\mathbf{H}_{\underline{N}}\underline{e}_4\\
&\quad+\alpha c_2v_1\underline{e}_2-\alpha c_2v_1\underline{e}_4\Big\}\Big]+\Big[\frac{1}{2\alpha-1}\Big\{c_2^2\underline{r}_1-c_2^2\underline{r}_2-c_2^2\underline{r}_3\\
&\quad-\alpha c_2\mathbf{H}_{\underline{N}}\underline{r}_4+c_2^2\underline{r}_4\Big\}-c_2\mathbf{H}_{\underline{N}}\underline{e}_4\Big]
\end{aligned} \quad (5.71b)$$

$$\begin{aligned}
&= \underline{r}_2+\frac{1}{2\alpha-1}\Big\{(1-g_1)\Big[2c_2^2\underline{r}_1-\alpha c_2\mathbf{H}_{\underline{N}}\underline{r}_1-\alpha c_2\mathbf{H}_{\underline{N}}\underline{r}_3\Big]\\
&\quad+(2c_2v_1+2\alpha-1)\Big[\alpha\underline{e}_2-c_2\mathbf{H}_{\underline{N}}\underline{e}_2-c_2\mathbf{H}_{\underline{N}}\underline{e}_4\Big]\Big\}
\end{aligned} \quad (5.71c)$$

$$\hat{\underline{r}}_3^{(2)}=\Big[c_2\mathbf{H}_{\underline{N}}\hat{\underline{s}}_1^{(1)}\Big]+\Big[c_2\mathbf{H}_{\underline{N}}\hat{\underline{s}}_2\Big]+\Big[\Big(\alpha\mathbf{I}_{\underline{N}}-c_2\mathbf{H}_{\underline{N}}\Big)\hat{\underline{s}}_3^{(1)}\Big]+\Big[-c_2\mathbf{H}_{\underline{N}}\hat{\underline{s}}_4\Big] \quad (5.72a)$$

$$\begin{aligned}
&= \Big[\frac{1}{2\alpha-1}\Big\{g_1\alpha c_2\mathbf{H}_{\underline{N}}\underline{r}_1-g_1c_2^2\underline{r}_1-c_2^2\underline{r}_2-g_1c_2^2\underline{r}_3-c_2^2\underline{r}_4-2c_2^2v_1\mathbf{H}_{\underline{N}}\underline{e}_2\\
&\quad+\alpha c_2v_1\underline{e}_2+\alpha c_2v_1\underline{e}_4\Big\}\Big]+\Big[\frac{1}{2\alpha-1}\Big\{-c_2^2\underline{r}_1+\alpha c_2\mathbf{H}_{\underline{N}}\underline{r}_2+c_2^2\underline{r}_2-c_2^2\underline{r}_3+c_2^2\underline{r}_4\Big\}\\
&\quad+c_2\mathbf{H}_{\underline{N}}\underline{e}_2\Big]+\Big[\frac{1}{2\alpha-1}\Big\{-g_1\alpha c_2\mathbf{H}_{\underline{N}}\underline{r}_1+g_1c_2^2\underline{r}_1-\alpha c_2\mathbf{H}_{\underline{N}}\underline{r}_2+c_2^2\underline{r}_2+g_1\left(\alpha^2-c_2^2\right)\underline{r}_3\\
&\quad+\alpha c_2\mathbf{H}_{\underline{N}}\underline{r}_4-c_2^2\underline{r}_4-2\alpha c_2v_1\underline{e}_4+2c_2^2v_1\mathbf{H}_{\underline{N}}\underline{e}_4+\alpha^2v_1\mathbf{H}_{\underline{N}}\underline{e}_2-\alpha c_2v_1\underline{e}_2\\
&\quad-\alpha^2v_1\mathbf{H}_{\underline{N}}\underline{e}_4+\alpha c_2v_1\underline{e}_4\Big\}\Big]+\Big[\frac{1}{2\alpha-1}\Big\{c_2^2\underline{r}_1-c_2^2\underline{r}_2-c_2^2\underline{r}_3-\alpha c_2\mathbf{H}_{\underline{N}}\underline{r}_4\\
&\quad+c_2^2\underline{r}_4\Big\}-c_2\mathbf{H}_{\underline{N}}\underline{e}_4\Big]
\end{aligned} \quad (5.72b)$$

$$= \frac{1}{2\alpha-1}\Big\{\Big[g_1\left(\alpha^2-2c_2^2\right)-2c_2^2\Big]\underline{r}_3+\Big[v_1\left(\alpha^2-2c_2^2\right)+(2\alpha-1)\,c_2\Big]\mathbf{H}_{\frac{N}{4}}\left(\underline{e}_2-\underline{e}_4\right) \tag{5.72c}$$

$$= g_2\underline{r}_3+v_2\mathbf{H}_{\frac{N}{4}}\left(\underline{e}_2-\underline{e}_4\right) \tag{5.72d}$$

$$\hat{\underline{r}}_4^{(2)} = \Big[c_2\mathbf{H}_{\frac{N}{4}}\hat{\underline{s}}_1^{(1)}\Big]+\Big[-c_2\mathbf{H}_{\frac{N}{4}}\hat{\underline{s}}_2\Big]+\Big[-c_2\mathbf{H}_{\frac{N}{4}}\hat{\underline{s}}_3^{(1)}\Big]+\Big[\Big(\alpha\mathbf{I}_{\frac{N}{4}}+c_2\mathbf{H}_{\frac{N}{4}}\Big)\hat{\underline{s}}_4\Big] \tag{5.73a}$$

$$\begin{aligned}
&= \Big[\frac{1}{2\alpha-1}\Big\{g_1\alpha c_2\mathbf{H}_{\frac{N}{4}}\underline{r}_1-g_1c_2^2\underline{r}_1-c_2^2\underline{r}_2-g_1c_2^2\underline{r}_3-c_2^2\underline{r}_4-2c_2^2v_1\mathbf{H}_{\frac{N}{4}}\underline{e}_2\\
&\quad+\alpha c_2v_1\underline{e}_2+\alpha c_2v_1\underline{e}_4\Big\}\Big]+\Big[\frac{1}{2\alpha-1}\Big\{c_2^2\underline{r}_1-\alpha c_2\mathbf{H}_{\frac{N}{4}}\underline{r}_2-c_2^2\underline{r}_2+c_2^2\underline{r}_3\\
&\quad-c_2^2\underline{r}_4\Big\}-c_2\mathbf{H}_{\frac{N}{4}}\underline{e}_2\Big]+\Big[\frac{1}{2\alpha-1}\Big\{g_1c_2^2\underline{r}_1+c_2^2\underline{r}_2-g_1\alpha c_2\mathbf{H}_{\frac{N}{4}}\underline{r}_3-g_1c_2^2\underline{r}_3\\
&\quad-c_2^2\underline{r}_4+2c_2^2v_1\mathbf{H}_{\frac{N}{4}}\underline{e}_4-\alpha c_2v_1\underline{e}_2+\alpha c_2v_1\underline{e}_4\Big\}\Big]+\Big[\frac{1}{2\alpha-1}\Big\{-\alpha c_2\mathbf{H}_{\frac{N}{4}}\underline{r}_1\\
&\quad-c_2^2\underline{r}_1+\alpha c_2\mathbf{H}_{\frac{N}{4}}\underline{r}_2+c_2^2\underline{r}_2+\alpha c_2\mathbf{H}_{\frac{N}{4}}\underline{r}_3+c_2^2\underline{r}_3+\left(\alpha^2-c_2^2\right)\underline{r}_4\Big\}\\
&\quad+\alpha\underline{e}_4+c_2\mathbf{H}_{\frac{N}{4}}\underline{e}_4\Big]
\end{aligned} \tag{5.73b}$$

$$\begin{aligned}
&= \underline{r}_4+\frac{1}{2\alpha-1}\Big\{(1-g_1)\Big[-\alpha c_2\mathbf{H}_{\frac{N}{4}}\underline{r}_1+2c_2^2\underline{r}_3+\alpha c_2\mathbf{H}_{\frac{N}{4}}\underline{r}_3\Big]\\
&\quad+(2c_2v_1+2\alpha-1)\Big[-c_2\mathbf{H}_{\frac{N}{4}}\underline{e}_2+\alpha\underline{e}_4+c_2\mathbf{H}_{\frac{N}{4}}\underline{e}_4\Big]\Big\}
\end{aligned} \tag{5.73c}$$

Replace the vectors $\hat{\underline{r}}_2^{(2)}$ and $\hat{\underline{r}}_4^{(2)}$ in $\hat{R}_2$ with $\underline{r}_2$ and $\underline{r}_4$ (obtained from $\tilde{R}$) to yield the vector $\hat{R}_2'$ whose segments are

$$\check{\underline{r}}_1^{(2)} = \hat{\underline{r}}_1^{(2)} = g_2\underline{r}_1+v_2\mathbf{H}_{\frac{N}{4}}\left(\underline{e}_2+\underline{e}_4\right) \tag{5.74a}$$

$$\check{\underline{r}}_2^{(2)} = \underline{r}_2 \tag{5.74b}$$

$$\check{\underline{r}}_3^{(2)} = \hat{\underline{r}}_3^{(2)} = g_2\underline{r}_3+v_2\mathbf{H}_{\frac{N}{4}}\left(\underline{e}_2-\underline{e}_4\right) \tag{5.74c}$$

$$\check{\underline{r}}_4^{(2)} = \underline{r}_4 \tag{5.74d}$$

Inverse Hadamard NPT

By comparing (5.74) with (5.62) it is clear that performing the inverse Hadamard NPT of the vector $\hat{R}_2'$ whose segments are given by (5.74), would yield a vector $\hat{S}_2'$, whose segments can be obtained by replacing g_1 and v_1 in (5.64*b*), (5.65*b*), (5.66*b*) and (5.67*b*) with g_2 and v_2 respectively. Replacement of the vectors $\check{\underline{s}}_2^{(2)}$ and $\check{\underline{s}}_4^{(2)}$ in $\hat{S}_2'$ with $\hat{\underline{s}}_2$ and $\hat{\underline{s}}_4$ respectively (derived from $\hat{S}^W$) yields the iteration vector $\hat{S}_2$ whose segments are given by

$$\begin{aligned}
\hat{\underline{s}}_1^{(2)} = \check{\underline{s}}_1^{(2)} = \frac{1}{2\alpha-1}\Big\{&g_2\left(\alpha\mathbf{I}_{\frac{N}{4}}-c_2\mathbf{H}_{\frac{N}{4}}\right)\underline{r}_1-c_2\mathbf{H}_{\frac{N}{4}}\underline{r}_2-g_2c_2\mathbf{H}_{\frac{N}{4}}\underline{r}_3-c_2\mathbf{H}_{\frac{N}{4}}\underline{r}_4\\
&-2c_2v_2\underline{e}_2+\alpha v_2\mathbf{H}_{\frac{N}{4}}\left(\underline{e}_2+\underline{e}_4\right)\Big\}
\end{aligned} \tag{5.75a}$$

$$\hat{\underline{s}}_2^{(2)} = \hat{\underline{s}}_2 = \frac{1}{2\alpha-1}\Big\{-c_2\mathbf{H}_{\frac{N}{4}}\underline{r}_1 + \left(\alpha\mathbf{I}_{\frac{N}{4}} + c_2\mathbf{H}_{\frac{N}{4}}\right)\underline{r}_2 - c_2\mathbf{H}_{\frac{N}{4}}\underline{r}_3 + c_2\mathbf{H}_{\frac{N}{4}}\underline{r}_4\Big\} + \underline{e}_2 \tag{5.75b}$$

$$\hat{\underline{s}}_3^{(2)} = \check{\underline{s}}_3^{(2)} = \frac{1}{2\alpha-1}\Big\{-g_2c_2\mathbf{H}_{\frac{N}{4}}\underline{r}_1 - c_2\mathbf{H}_{\frac{N}{4}}\underline{r}_2 + g_2\left(\alpha\mathbf{I}_{\frac{N}{4}} + c_2\mathbf{H}_{\frac{N}{4}}\right)\underline{r}_3 + c_2\mathbf{H}_{\frac{N}{4}}\underline{r}_4 - 2c_2v_2\underline{e}_4 + \alpha v_2\mathbf{H}_{\frac{N}{4}}(\underline{e}_2 - \underline{e}_4)\Big\} \tag{5.75c}$$

$$\hat{\underline{s}}_4^{(2)} = \hat{\underline{s}}_4 = \frac{1}{2\alpha-1}\Big\{-c_2\mathbf{H}_{\frac{N}{4}}\underline{r}_1 + c_2\mathbf{H}_{\frac{N}{4}}\underline{r}_2 + c_2\mathbf{H}_{\frac{N}{4}}\underline{r}_3 + \left(\alpha\mathbf{I}_{\frac{N}{4}} - c_2\mathbf{H}_{\frac{N}{4}}\right)\underline{r}_4\Big\} + \underline{e}_4 \tag{5.75d}$$

Iteration m

We can infer, based on the results of the previous iterations, that by continuing the iterative Hadamard NPT reconstruction process to the m^{th} $(m \geq 1)$ iteration stage, the segments of the iteration vector $\hat{R}_m$ that is obtained are given by

$$\hat{\underline{r}}_1^{(m)} = g_m\underline{r}_1 + v_m\mathbf{H}_{\frac{N}{4}}(\underline{e}_2 + \underline{e}_4) \tag{5.76a}$$

$$\hat{\underline{r}}_2^{(m)} = \underline{r}_2 + \frac{1}{2\alpha-1}\Big\{(1-g_{m-1})\left[2c_2^2\underline{r}_1 - \alpha c_2\mathbf{H}_{\frac{N}{4}}\underline{r}_1 - \alpha c_2\mathbf{H}_{\frac{N}{4}}\underline{r}_3\right] + (2c_2v_{m-1} + 2\alpha - 1)\left[\alpha\underline{e}_2 - c_2\mathbf{H}_{\frac{N}{4}}\underline{e}_2 - c_2\mathbf{H}_{\frac{N}{4}}\underline{e}_4\right]\Big\} \tag{5.76b}$$

$$\hat{\underline{r}}_3^{(m)} = g_m\underline{r}_3 + v_m\mathbf{H}_{\frac{N}{4}}(\underline{e}_2 - \underline{e}_4) \tag{5.76c}$$

$$\hat{\underline{r}}_4^{(m)} = \underline{r}_4 + \frac{1}{2\alpha-1}\Big\{(1-g_{m-1})\left[-\alpha c_2\mathbf{H}_{\frac{N}{4}}\underline{r}_1 + 2c_2^2\underline{r}_3 + \alpha c_2\mathbf{H}_{\frac{N}{4}}\underline{r}_3\right] + (2c_2v_{m-1} + 2\alpha - 1)\left[-c_2\mathbf{H}_{\frac{N}{4}}\underline{e}_2 + \alpha\underline{e}_4 + c_2\mathbf{H}_{\frac{N}{4}}\underline{e}_4\right]\Big\} \tag{5.76d}$$

where g_m is the convergence factor and v_m is the error multiplying factor; g_m and v_m are also recursively given by (5.45) and (5.46) respectively but with the substitutions $c_1 = c_2$, $\beta_0 = 2c_2^2$ and $v_1 = c_2 = \frac{1-\alpha}{2}$ in these equations.

Replacing the vectors $\hat{\underline{r}}_2^{(m)}$ and $\hat{\underline{r}}_4^{(m)}$ in $\hat{R}_m$ with $\underline{r}_2$ and $\underline{r}_4$ respectively (obtained from $\tilde{R}$) to yield the vector $\hat{R}'_m$ and performing the inverse Hadamard NPT of $\hat{R}'_m$, we obtain a vector $\hat{S}'_m$ whose segments are given by

$$\check{\underline{s}}_1^{(m)} = \frac{1}{2\alpha-1}\Big\{g_m\left(\alpha\mathbf{I}_{\frac{N}{4}} - c_2\mathbf{H}_{\frac{N}{4}}\right)\underline{r}_1 - c_2\mathbf{H}_{\frac{N}{4}}\underline{r}_2 - g_mc_2\mathbf{H}_{\frac{N}{4}}\underline{r}_3 - c_2\mathbf{H}_{\frac{N}{4}}\underline{r}_4 - 2c_2v_m\underline{e}_2 + \alpha v_m\mathbf{H}_{\frac{N}{4}}(\underline{e}_2 + \underline{e}_4)\Big\} \tag{5.77a}$$

$$\check{\underline{s}}_2^{(m)} = \frac{1}{2\alpha-1}\Big\{-g_mc_2\mathbf{H}_{\frac{N}{4}}\underline{r}_1 + \left(\alpha\mathbf{I}_{\frac{N}{4}} + c_2\mathbf{H}_{\frac{N}{4}}\right)\underline{r}_2 - g_mc_2\mathbf{H}_{\frac{N}{4}}\underline{r}_3 + c_2\mathbf{H}_{\frac{N}{4}}\underline{r}_4 - 2c_2v_m\underline{e}_2\Big\} \tag{5.77b}$$

$$\check{s}_3^{(m)} = \frac{1}{2\alpha - 1}\Big\{-g_m c_2 \mathbf{H}_{\frac{N}{4}} \underline{r}_1 - c_2 \mathbf{H}_{\frac{N}{4}} \underline{r}_2 + g_m \left(\alpha \mathbf{I}_{\frac{N}{4}} + c_2 \mathbf{H}_{\frac{N}{4}}\right) \underline{r}_3 + c_2 \mathbf{H}_{\frac{N}{4}} \underline{r}_4 - 2c_2 v_m \underline{e}_4 + \alpha v_m \mathbf{H}_{\frac{N}{4}} (\underline{e}_2 - \underline{e}_4)\Big\} \tag{5.77c}$$

$$\check{s}_4^{(m)} = \frac{1}{2\alpha - 1}\Big\{-g_m c_2 \mathbf{H}_{\frac{N}{4}} \underline{r}_1 - c_2 \mathbf{H}_{\frac{N}{4}} \underline{r}_2 + g_m c_2 \mathbf{H}_{\frac{N}{4}} \underline{r}_3 + \left(\alpha \mathbf{I}_{\frac{N}{4}} - c_2 \mathbf{H}_{\frac{N}{4}}\right) \underline{r}_4 - 2c_2 v_m \underline{e}_4\Big\} \tag{5.77d}$$

As we stated in the previous example, for convergence, the factor g_m in (5.76) must tend to unity with increasing number of iterations; the error multiplying factor v_m should also converge to a finite constant with a low magnitude. The plot of g_m as a function of α for this case is identical to that shown in Fig. 5.4a. The behaviour of v_m as a function of iteration is also similar to that shown in Fig. 5.4b except that v_m converges to $\frac{1-2\alpha}{1-\alpha}$ with increasing number of iterations.

Case 3

This is depicted in Fig. 5.3c. By an analysis similar to that carried out above for cases 1 and 2, from (5.14), we can express the reconstruction of the missing transform segments at the m^{th} iteration, in terms of the desired (but unknown) transform segments, as

$$\hat{\underline{r}}_1^{(m)} = g_m \underline{r}_1 + v_m \mathbf{H}_{\frac{N}{8}} (\underline{e}_2 + \underline{e}_4 + \underline{e}_6 + \underline{e}_8) \tag{5.78}$$

$$\hat{\underline{r}}_3^{(m)} = g_m \underline{r}_3 + v_m \mathbf{H}_{\frac{N}{8}} (\underline{e}_2 - \underline{e}_4 + \underline{e}_6 - \underline{e}_8) \tag{5.79}$$

$$\hat{\underline{r}}_5^{(m)} = g_m \underline{r}_5 + v_m \mathbf{H}_{\frac{N}{8}} (\underline{e}_2 + \underline{e}_4 - \underline{e}_6 - \underline{e}_8) \tag{5.80}$$

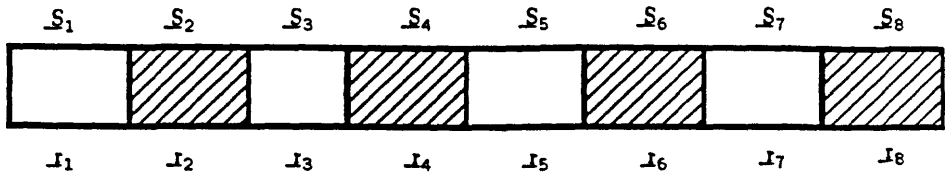
and

$$\hat{\underline{r}}_7^{(m)} = g_m \underline{r}_7 + v_m \mathbf{H}_{\frac{N}{8}} (\underline{e}_2 - \underline{e}_4 - \underline{e}_6 + \underline{e}_8) \tag{5.81}$$

The recursive expressions for g_m and v_m have the same form as (5.45) and (5.46) respectively, but with the substitutions $c_1 = c_3$, $\beta_0 = 4c_3^2$ and $v_1 = c_3 = \frac{1-\alpha}{2^{3/2}}$ in these equations.

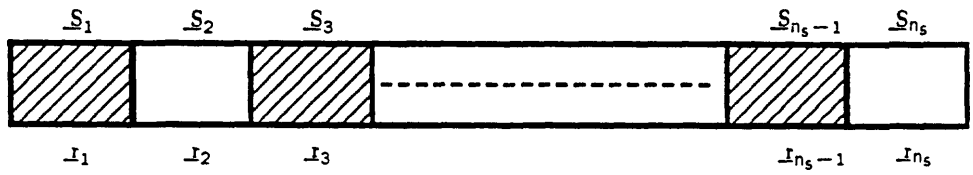
2) Even-Index Vector Reconstruction

For these formats, the expressions for the reconstruction of the lost transform segments at the m^{th} iteration, in terms of the desired (but unknown) transform segments, have a similar form to those for the cases of losing odd-index vectors. These correspond to receiving the "dc " sample and some other "ac " samples; the format of Fig. 5.7 illustrates this situation. Using a similar approach to that



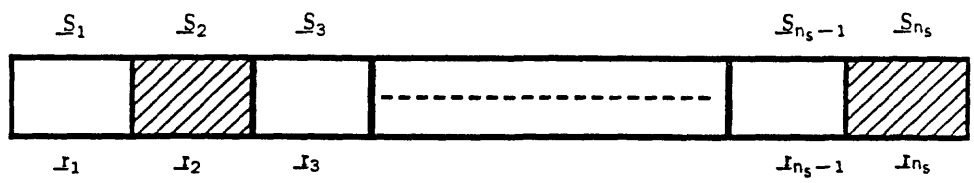
$\underline{S}_2, \underline{S}_4, \underline{S}_6, \underline{S}_8$ = desired (but unknown) signal segments
$\underline{S}_1, \underline{S}_3, \underline{S}_5, \underline{S}_7$ = known signal segments
$\underline{I}_2, \underline{I}_4, \underline{I}_6, \underline{I}_8$ = desired (but unknown) transform segments
$\underline{I}_1, \underline{I}_3, \underline{I}_5, \underline{I}_7$ = known transform segments.

Fig. 5.7 : Loss of Even-Index Vectors .



$\underline{S}_1, \underline{S}_3, \ldots\ldots \underline{S}_{n_s-1}$ = desired (but unknown) signal segments
$\underline{S}_2, \underline{S}_4, \ldots\ldots \underline{S}_{n_s}$ = known signal segments
$\underline{I}_1, \underline{I}_3, \ldots\ldots \underline{I}_{n_s-1}$ = desired (but unknown) transform segments
$\underline{I}_2, \underline{I}_4, \ldots\ldots \underline{I}_{n_s}$ = known transform segments.

Fig. 5.8a : Loss of Odd-Index Vectors .



$\underline{S}_2, \underline{S}_4, \ldots\ldots \underline{S}_{n_s}$ = desired (but unknown) signal segments
$\underline{S}_1, \underline{S}_3, \ldots\ldots \underline{S}_{n_s-1}$ = known signal segments
$\underline{I}_2, \underline{I}_4, \ldots\ldots \underline{I}_{n_s}$ = desired (but unknown) transform segments
$\underline{I}_1, \underline{I}_3, \ldots\ldots \underline{I}_{n_s-1}$ = known transform segments.

Fig. 5.8b : Loss of Even-Index Vectors .

Fig. 5.8 : General Case .

described above for odd-index vector reconstruction, from (5.14), we can express the reconstruction of the lost transform segments at the m^{th} iteration, in terms of the desired (but unknown) transform segments, as

$$\hat{\underline{r}}_2^{(m)} = g_m \underline{r}_2 + v_m \mathbf{H}_{\frac{N}{8}} (\underline{e}_1 + \underline{e}_3 + \underline{e}_5 + \underline{e}_7) \tag{5.82}$$

$$\hat{\underline{r}}_4^{(m)} = g_m \underline{r}_4 + v_m \mathbf{H}_{\frac{N}{8}} (\underline{e}_1 - \underline{e}_3 + \underline{e}_5 - \underline{e}_7) \tag{5.83}$$

$$\hat{\underline{r}}_6^{(m)} = g_m \underline{r}_6 + v_m \mathbf{H}_{\frac{N}{8}} (\underline{e}_1 + \underline{e}_3 - \underline{e}_5 - \underline{e}_7) \tag{5.84}$$

and

$$\hat{\underline{r}}_8^{(m)} = g_m \underline{r}_8 + v_m \mathbf{H}_{\frac{N}{8}} (\underline{e}_1 - \underline{e}_3 - \underline{e}_5 + \underline{e}_7) \tag{5.85}$$

3) General Case

The general case is depicted in Fig. 5.8. We have shown that, using (5.14), we can express the reconstruction of the lost transform segments at the m^{th} iteration, in terms of the desired (but unknown) transform segments, as

$$\hat{\underline{r}}_{j(u)}^{(m)} = g_m \underline{r}_{j(u)} + v_m \mathbf{H}_{l_s} \sum_{x=0}^{\frac{n_s}{2}-1} (-1)^{\gamma(x,u)} \underline{e}_{w(x)} \tag{5.86}$$

where

$$j(u) = \begin{cases} 2u+1 & \text{odd index vectors} \\ 2u+2 & \text{even index vectors} \end{cases} \tag{5.87a}$$

for $u = 0, 1, \ldots \frac{n_s}{2} - 1$,

$$w(x) = \begin{cases} 2x+2 & \text{odd index vectors} \\ 2x+1 & \text{even index vectors} \end{cases} \tag{5.87b}$$

$$, \ \gamma(x,u) = \sum_{y=0}^{\frac{n_s}{2}-1} b_y(x) b_y(u) \tag{5.87c}$$

$$, \ g_m = \frac{\left[g_{m-1}\left(\alpha^2 - \frac{n_s}{2}c_i^2\right) - \frac{n_s}{2}c_i^2\right]}{2\alpha - 1} \qquad m > 1 \ ;$$

$$g_0 = 0 \ , \quad g_1 = \frac{-n_s c_i^2}{2(2\alpha - 1)} \ , \quad c_i = \frac{1-\alpha}{\sqrt{n_s}} \tag{5.87d}$$

and

$$v_m = \frac{\left[v_{m-1}\left(\alpha^2 - \frac{n_s}{2}c_i^2\right) + (2\alpha - 1)\, c_i\right]}{2\alpha - 1} \qquad m > 1 \ ;$$

$$v_0 = 0 \ , v_1 = c_i \tag{5.87e}$$

The summation in the exponent in (5.86) given by (5.87c) is performed in modulo 2 arithmetic; the terms $b_y(x)$ and $b_y(u)$ are the bit states of the binary representation of x and u respectively. $\mathbf{H}_{l_s}$ is a normalized natural ordered Hadamard matrix of order l_s and $\underline{e}_{w(x)}$ is the estimation error vector of segment $w(x)$.

5.2.3.2 Fast Reconstruction Algorithms

This set of algorithms provides the required solutions in a single iteration and they are only valid for the examples discussed in the previous section.

Scheme 1

This is based on dividing the reconstruction of lost transform segments, at the first iteration, by the convergence parameter

$$g_1 = \frac{-(1-\alpha)^2}{2(2\alpha-1)} \tag{5.88}$$

Replacement with known segments from $\tilde{R}$ and subsequent inverse Hadamard NPT yields the required solution. For the general format depicted in Fig. 5.8, the solution given by the fast reconstruction scheme, for the signal segments with indices corresponding to the lost transform segments, is

$$\underline{\hat{s}}_{j(u)} = \underline{s}_{j(u)} + \underline{e}_{z(u)} - \frac{\alpha}{1-\alpha}\mathbf{H}_{l_s} \sum_{x=0}^{\frac{n_s}{2}-1} (-1)^{\gamma(x,u)} \underline{e}_{w(x)} \tag{5.89}$$

for $u = 0, 1, \ldots \frac{n_s}{2} - 1$, where

$$z(u) = \begin{cases} 2u+2 & \text{odd index } j(u) \\ 2u+1 & \text{even index } j(u) \end{cases} \tag{5.90}$$

$\gamma(x,u)$ is given by (5.87c), and $j(u)$, $w(x)$, $b_y(x)$ and $b_y(u)$ are as previously defined in section 5.2.3.1, under the general reconstruction format example. The solution obtained for the signal segments with indices corresponding to the known transform segments is

$$\underline{\hat{s}}_{z(u)} = \underline{s}_{z(u)} + \underline{e}_{z(u)} \tag{5.91}$$

Scheme 2

This is based on following the procedure outlined in the flow-chart of Fig. 5.9 and the solution obtained is the same as that for scheme 1.

Operation Count

After the reconstructed transform domain at the first iteration has been obtained, scheme 1 requires an additional $(N log_2 N + \frac{7N}{2})$ operations, while scheme 2 requires an additional $3N$ operations.

The iterative scheme given by (5.14) converges to the solution given by the fast schemes, and m iterations of the algorithm requires $2m\,(N log_2 N + 3N)$ operations.

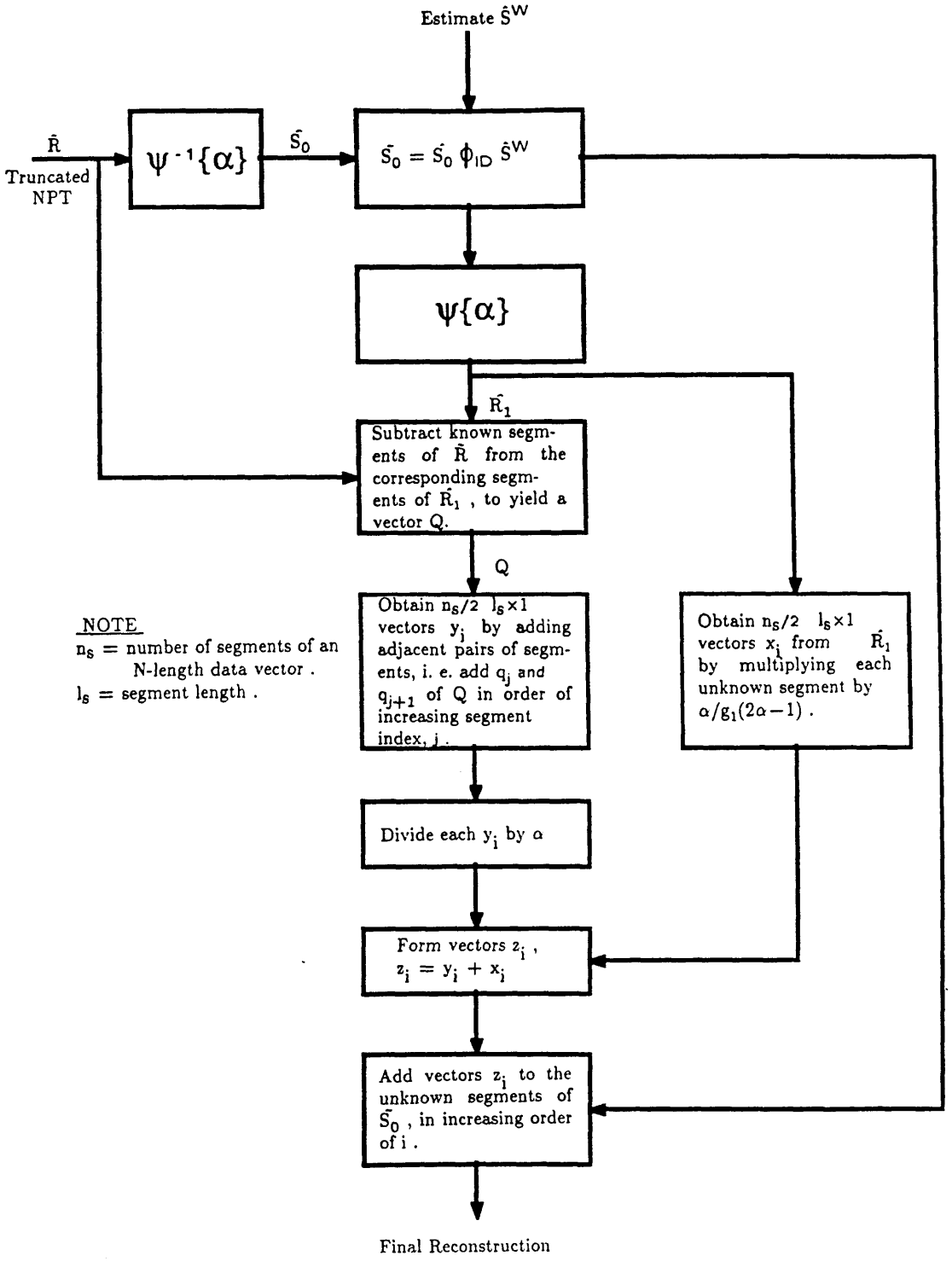


Fig. 5.9 : Fast Reconstruction Scheme 2 .

5.2.3.3 Degenerate Formats

Two formats correspond to a degenerate system of equations and these are shown in Fig. 5.10. For these formats, the iterative Hadamard NPT reconstruction algorithm do not yield the required solutions.

Case 1

The format is depicted in Fig. 5.10a. We have shown that using (5.14), we can express the reconstruction of the transform segments at the m^{th} iteration (i.e. the segments of the iteration vector $\hat{R}_m$), in terms of the desired (but unknown) transform segments, as

$$\hat{\underline{r}}_1^{(m)} = g_m\,(\underline{r}_1 - \underline{r}_4) + v_m \mathbf{H}_{\frac{N}{4}}\,(\underline{e}_2 + \underline{e}_3) \tag{5.92a}$$

$$\begin{aligned}\hat{\underline{r}}_2^{(m)} = \underline{r}_2 + \frac{1}{2\alpha-1}\Big\{&\alpha c_2\,(2g_{m-1}-1)\,\mathbf{H}_{\frac{N}{4}}\,(\underline{r}_1 - \underline{r}_4)\\ &+ \alpha\,(2v_{m-1}c_2 + 2\alpha - 1)\,\underline{e}_2 - (2\alpha-1)\,c_2\mathbf{H}_{\frac{N}{4}}\underline{e}_2 + 2\alpha v_{m-1}c_2\underline{e}_3\\ &+ (2\alpha-1)\,c_2\mathbf{H}_{\frac{N}{4}}\underline{e}_3\Big\}\end{aligned} \tag{5.92b}$$

$$\begin{aligned}\hat{\underline{r}}_3^{(m)} = \underline{r}_3 + \frac{1}{2\alpha-1}\Big\{&\alpha c_2\,(2g_{m-1}-1)\,\mathbf{H}_{\frac{N}{4}}\,(\underline{r}_1 - \underline{r}_4) + 2\alpha v_{m-1}c_2\underline{e}_2\\ &+ (2\alpha-1)\,c_2\mathbf{H}_{\frac{N}{4}}\underline{e}_2 + \alpha\,(2v_{m-1}c_2 + 2\alpha - 1)\,\underline{e}_3 - (2\alpha-1)\,c_2\mathbf{H}_{\frac{N}{4}}\underline{e}_3\Big\}\end{aligned} \tag{5.92c}$$

$$\hat{\underline{r}}_4^{(m)} = -g_m\,(\underline{r}_1 - \underline{r}_4) - v_m \mathbf{H}_{\frac{N}{4}}\,(\underline{e}_2 + \underline{e}_3) \tag{5.92d}$$

where

$$\begin{aligned} g_m &= \frac{1}{2\alpha-1}\left\{(\alpha^2 g_{m-1} - 2c_2^2)\right\} \qquad m > 1\ ;\\ g_0 &= 0\ ,\quad g_1 = \frac{-(1-\alpha)^2}{2(2\alpha-1)}\ ,\quad c_2 = \frac{1-\alpha}{2}\end{aligned} \tag{5.93a}$$

and

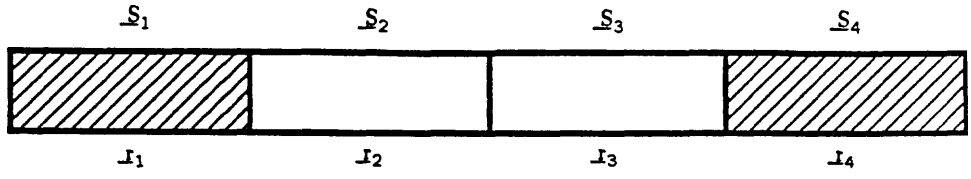
$$\begin{aligned} v_m &= \frac{1}{2\alpha-1}\left\{(\alpha^2 v_{m-1} + (2\alpha-1)c_2)\right\} \qquad m > 1\ ;\\ v_0 &= 0\ ,\quad v_1 = c_2 = \frac{1-\alpha}{2}\end{aligned} \tag{5.93b}$$

Replacing $\hat{\underline{r}}_2^{(m)}$ and $\hat{\underline{r}}_3^{(m)}$ with $\underline{r}_2$ and $\underline{r}_3$ (obtained from $\tilde{R}$) and performing the inverse Hadamard NPT of the resulting vector $\hat{R}'_m$, we obtain

$$\begin{aligned}\check{\underline{s}}_1^{(m)} = \frac{1}{2\alpha-1}\Big\{&g_m\alpha\underline{r}_1 - c_2\mathbf{H}_{\frac{N}{4}}\underline{r}_2 - c_2\mathbf{H}_{\frac{N}{4}}\underline{r}_3 - g_m\alpha\underline{r}_4\\ &+ \alpha v_m\mathbf{H}_{\frac{N}{4}}\,(\underline{e}_2 + \underline{e}_3)\Big\}\end{aligned} \tag{5.94a}$$

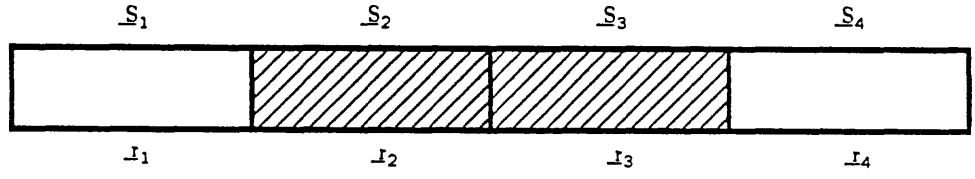
$$\begin{aligned}\check{\underline{s}}_2^{(m)} = \frac{1}{2\alpha-1}\Big\{&-2g_m c_2\mathbf{H}_{\frac{N}{4}}\underline{r}_1 + \left(\alpha\mathbf{I}_{\frac{N}{4}} + c_2\mathbf{H}_{\frac{N}{4}}\right)\underline{r}_2 - c_2\mathbf{H}_{\frac{N}{4}}\underline{r}_3\\ &+ 2g_m c_2\mathbf{H}_{\frac{N}{4}}\underline{r}_4 - 2c_2 v_m\,(\underline{e}_2 + \underline{e}_3)\Big\}\end{aligned} \tag{5.94b}$$

$$\check{\underline{s}}_3^{(m)} = \frac{1}{2\alpha-1}\Big\{-2g_m c_2\mathbf{H}_{\frac{N}{4}}\underline{r}_1 - c_2\mathbf{H}_{\frac{N}{4}}\underline{r}_2 + \left(\alpha\mathbf{I}_{\frac{N}{4}} + c_2\mathbf{H}_{\frac{N}{4}}\right)\underline{r}_3$$



$\underline{S}_1$, $\underline{S}_4$ = desired (but unknown) signal segments
$\underline{S}_2$, $\underline{S}_3$ = known signal segments
$\underline{I}_1$, $\underline{I}_4$ = desired (but unknown) transform segments
$\underline{I}_2$, $\underline{I}_3$ = known transform segments.

Fig. 5.10a : Case 1



$\underline{S}_2$, $\underline{S}_3$ = desired (but unknown) signal segments
$\underline{S}_1$, $\underline{S}_4$ = known signal segments
$\underline{I}_2$, $\underline{I}_3$ = desired (but unknown) transform segments
$\underline{I}_1$, $\underline{I}_4$ = known transform segments.

Fig. 5.10b : Case 2

Fig. 5.10 : Degenerate Formats of Lost/Received Hadamard NPT Segments of A Signal.

$$+ 2g_m c_2 \mathbf{H}_{\frac{N}{4}} \underline{r}_4 - 2c_2 v_m (\underline{e}_2 + \underline{e}_3)\Big\} \tag{5.94c}$$

$$\check{\underline{s}}_4^{(m)} = \frac{1}{2\alpha - 1}\Big\{-g_m \alpha \underline{r}_1 + c_2 \mathbf{H}_{\frac{N}{4}} \underline{r}_2 + c_2 \mathbf{H}_{\frac{N}{4}} \underline{r}_3 + g_m \alpha \underline{r}_4 - \alpha v_m \mathbf{H}_{\frac{N}{4}} (\underline{e}_2 + \underline{e}_3)\Big\} \tag{5.94d}$$

We can observe that (5.92*a*) and (5.92*d*) respectively express the sub-vectors $\hat{\underline{r}}_1^{(m)}$ and $\hat{\underline{r}}_4^{(m)}$ in terms of the two desired (but unknown) transform segments $\underline{r}_1$ and $\underline{r}_4$. Furthermore, these vectors are present in the same linear combination in the two equations, at progressive stages of the iterative reconstruction process. This implies that the Hadamard NPT reconstruction algorithm would not yield the true solution for this scenario.

Case 2

This is depicted in Fig. 5.10b. The reconstructed transform segments at the first iteration are given by

$$\hat{\underline{r}}_1^{(1)} = \underline{r}_1 + \frac{1}{2\alpha - 1}\Big\{-\alpha c_2 \mathbf{H}_{\frac{N}{4}} (\underline{r}_2 + \underline{r}_3)\Big\} + \alpha \underline{e}_1 + c_2 \mathbf{H}_{\frac{N}{4}} (\underline{e}_1 + \underline{e}_4) \tag{5.95a}$$

$$\hat{\underline{r}}_2^{(1)} = \frac{1}{2\alpha - 1}\{-2c_2^2 (\underline{r}_2 + \underline{r}_3)\} + c_2 \mathbf{H}_{\frac{N}{4}} (\underline{e}_1 - \underline{e}_4) \tag{5.95b}$$

$$\hat{\underline{r}}_3^{(1)} = \frac{1}{2\alpha - 1}\{-2c_2^2 (\underline{r}_2 + \underline{r}_3)\} + c_2 \mathbf{H}_{\frac{N}{4}} (\underline{e}_1 - \underline{e}_4) \tag{5.95c}$$

$$\hat{\underline{r}}_4^{(1)} = \underline{r}_4 + \frac{1}{2\alpha - 1}\Big\{\alpha c_2 \mathbf{H}_{\frac{N}{4}} (\underline{r}_2 + \underline{r}_3)\Big\} + \alpha \underline{e}_4 + c_2 \mathbf{H}_{\frac{N}{4}} (\underline{e}_1 + \underline{e}_4) \tag{5.95d}$$

We observe that the desired (but unknown) transform segments $\underline{r}_2$ and $\underline{r}_3$ are coupled together in (5.95*b*) and (5.95*c*), and since the same linear combination of $\underline{r}_2$ and $\underline{r}_3$ is present in these equations, it follows from the result of case 1, that the iterative Hadamard NPT reconstruction algorithm would not yield the true solution for this format.

5.2.3.4 Signal Estimation From One-Dimensional Hadamard NPT Segments

The Hadamard NPT reconstruction algorithm presented earlier requires an estimate of the signal amplitude over the available transform segments. It must be emphasized that the quality of the final reconstruction depends on how well we can estimate the original signal amplitude from the known transform segments. Based on the correlation properties of the components of the one-dimensional Hadamard NPT of a signal, we employ an adaptive Wiener filtering approach; specifically an adaptive line enhancer (ALE) [58].

The adaptive line enhancer is a special case of an adaptive noise canceller [59], where a delayed version of the noisy signal is used as the reference input to the noise canceller, as shown in Fig. 5.11.

We can express the entries $\tilde{r}_j$ of the truncated Hadamard NPT vector $\tilde{R}$ as

$$\tilde{r}_j = \begin{cases} \alpha s_j + (1-\alpha)p_j \; ; \quad p_j = \sum_{i=1}^{N} a_{ji} s_i & j \in ID \\ 0 & j \notin ID \end{cases} \tag{5.96}$$

where a_{ji} are basis elements derived from the normalized natural ordered Hadamard matrix of order N. The application of adaptive line enhancing techniques to the estimation of the signal samples s_j corresponding to the known samples of the truncated Hadamard NPT vector $\tilde{R}$, i.e. $\tilde{r}_j$, $j \in ID$, is described in Fig. 5.12. This arrangement treats the signal component αs_j as "noise "; thus, the primary input consists of the signal $(1-\alpha)p_j$, $j \in ID$, and an additive "noise " component αs_j, $j \in ID$. The reference input is obtained by passing the "noise " component αs_j through the filter with transfer function $H_2(Z) = Z^{-\Delta}$, where Δ is the number of delay elements. A signal component $(1-\alpha)p_j * h_1(j)$ is also present in the reference input, where $h_1(j)$ is the impulse response of the channel whose transfer function is $H_1(Z) = Z^{-\Delta}$. By selecting the delay Δ to be longer than the effective correlation length of the component $(1-\alpha)p_j$, and shorter than the correlation length of αs_j, the adaptive Wiener filter will respond to cancel an estimate of the αs_j component from the output, as shown in Fig. 5.12. It is these estimates of αs_j that are used to generate the components of the estimation vector $\hat{S}^W$.

The adaptive filter weights are iteratively adjusted according to the relation

$$w(i+1) = w(i) + \Delta w(i) \tag{5.97}$$

where $\Delta w(i)$ is the correction term at instant i, determined by using an adaptive algorithm so as to minimize the expected error signal power. A detailed description of the LMS adaptive filter algorithm and the recursive least-squares adaptive filter algorithm is given respectively in [58] and [59].

The steady-state Wiener filter weights are given by $\mathbf{w} = \mathbf{C}^{-1}\underline{b}$. The matrix $\mathbf{C}$ is given in terms of the autocorrelation of the signal $\tilde{r}_j$ as follows :

$$\mathbf{C}_{u,v,i} = E\{y_{i-u}y_{i-v}\} \tag{5.98}$$

or

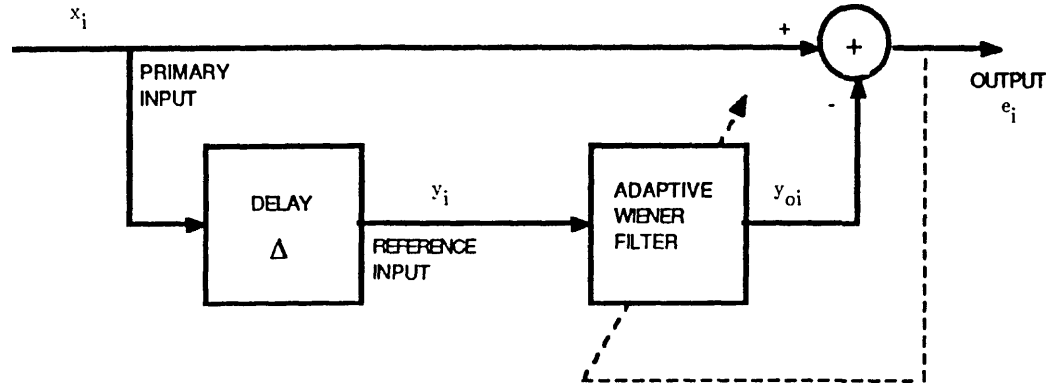


Fig. 5.11 : Basic Block Diagram of An Adaptive Line Enhancer .

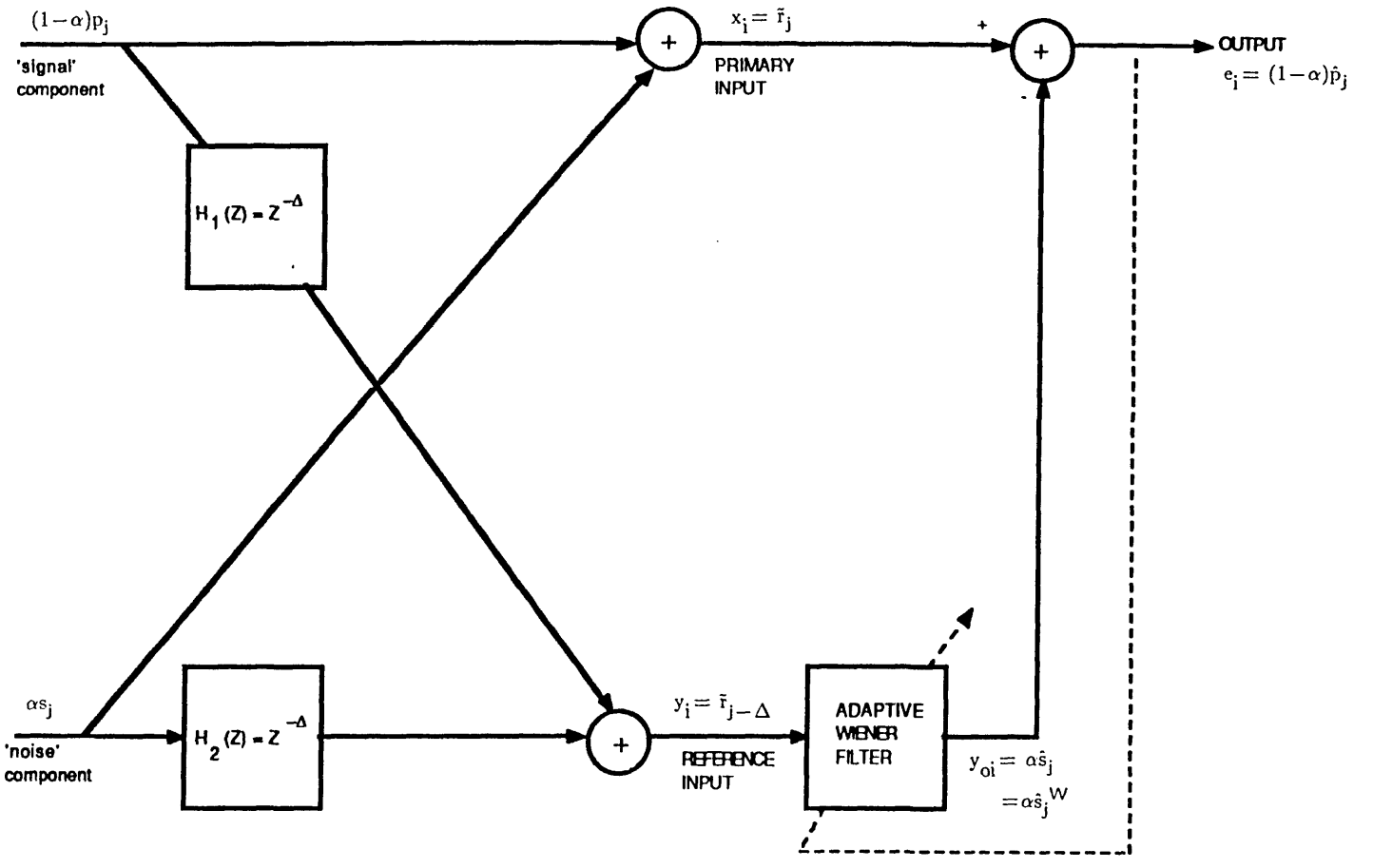


Fig. 5.12 : Adaptive Line Enhancer Estimation of Signal Vector From The Truncated Hadamard NPT Vector ; $j \in ID$.

$$\mathbf{C}_{\tilde{r}\tilde{r}}(j,\Delta,u,v) = E\{\tilde{r}_{j-\Delta-u}\tilde{r}_{j-\Delta-v}\} \tag{5.99}$$

and in terms of the autocorrelation of the component signals s_j and p_j by

$$\begin{aligned}\mathbf{C}_{PP;SS}(j,\Delta,u,v) &= E\{(\alpha s_{j-\Delta-u} + (1-\alpha)p_{j-\Delta-u})(\alpha s_{j-\Delta-v} \\ &\quad + (1-\alpha)p_{j-\Delta-v})\} \qquad (5.100)\\ &= \alpha^2\mathbf{C}_{SS}(j,\Delta,u,v) + (1-\alpha)^2\mathbf{C}_{PP}(j,\Delta,u,v) \qquad (5.101)\end{aligned}$$

where we have made use of the fact that the components of S and P are mutually uncorrelated, for all practical purposes.

Similarly, the vector $\underline{b}$ is given in terms of the autocorrelation of the signal $\tilde{r}_j$ by

$$\begin{aligned}\underline{b}_u &= E\{x_i y_{i-u}\} \qquad (5.102)\\ &= E\{\tilde{r}_j\tilde{r}_{j-\Delta-u}\} = \underline{c}_{\tilde{r}\tilde{r}}(j,\Delta,u) \qquad (5.103)\end{aligned}$$

and in terms of the autocorrelation of the component signals s_j and p_j by

$$\begin{aligned}\underline{b}_u &= E\{(\alpha s_j + (1-\alpha)p_j)(\alpha s_{j-\Delta-u} + (1-\alpha)p_{j-\Delta-u})\} \qquad (5.104)\\ &= \alpha^2\underline{c}_{SS}(j,\Delta,u) + (1-\alpha)^2\underline{c}_{PP}(j,\Delta,u) \qquad (5.105)\end{aligned}$$

For a stationary signal S, (5.101) and (5.105) reduce to

$$\mathbf{C}_{PP;SS}(j,\Delta,u,v) = \alpha^2\mathbf{C}_{SS}(u-v) + (1-\alpha)^2\mathbf{C}_{PP}(j,\Delta,u,v) \tag{5.106}$$

and

$$\underline{b}_u = \alpha^2\underline{c}_{SS}(u+\Delta) + (1-\alpha)^2\underline{c}_{PP}(j,\Delta,u) \tag{5.107}$$

respectively, where the dependence on j,Δ,u and v of the matrix $\mathbf{C}_{PP}$, and the dependence on j,Δ and u of the vector $\underline{c}_{PP}$ on the right hand sides of (5.106) and (5.107) respectively, account for the fact that the Hadamard transform of a stationary signal is in general non-stationary [2, pg. 90]. However, the adaptive filter is able to track non-stationarities in the signal to be filtered [60].

5.3 Simulation, Results and Discussion

The reconstruction algorithm described in the previous section was simulated for some formats of received Hadamard NPT samples of some typical signals. A recursive least-squares adaptive filter was used in the ALE algorithm described in

Fig. 5.12. In the simulations, we consider that the number of known transform samples is greater than or equal to the number of unknown transform samples.

5.3.1 Reconstruction of Stationary First Order Gauss-Markov Signals

Fig. 5.13 is a plot of 512 samples of a stationary first order Gauss-Markov signal having a high inter-element correlation coefficient of 0.9. Fig. 5.14 is a plot of the autocorrelation function of the Gauss-Markov signal and that of its Hadamard transform. Thus, only one delay element is needed to generate the reference signal for the ALE estimation algorithm described in Fig. 5.12. In the simulation of the reconstruction of first order Gauss-Markov signals from formats of received Hadamard NPT segments discussed in the following, a two-tap adaptive filter was used in the ALE algorithm and the weights were adapted using the recursive least-squares algorithm.

1) The reconstruction from the received Hadamard NPT segment corresponding to the format of Fig. 5.3a was simulated. For this format, the transform samples at locations 1 to 256 were lost. Fig. 5.15a is a plot of the reconstructed signal, obtained by taking the inverse Hadamard NPT(0.4) of the received samples (From notation introduced in chapter two, Hadamard NPT(0.4) means a Hadamard NPT basis specified by $\alpha = 0.4$). For the purpose of display, the samples of the reconstructed signal were clipped to between -600 and 600. Fig. 5.15b shows the reconstructed signal obtained by application of the fast reconstruction algorithm to the received samples; the required solution was obtained in a single iteration. The required solution can also be obtained by using the iterative reconstruction scheme. However, the number of iterations required for convergence depends on the threshold ϵ specified by the user. For $\epsilon = 1 \times 10^{-2}$, convergence was obtained in five iterations; a lower value of ϵ would require a higher number of iterations. Empirical investigations show that there is only a negligible improvement in the quality of the reconstructed signal for $\epsilon < 1 \times 10^{-2}$.

It is observed that there is a great deal of improvement in the reconstructed signal, although it is characterized by spikes in a number of places. The quality of the reconstructed signal can be improved by pre-filtering the estimates derived from the received segments, before using these in the reconstruction algorithm. The aim of this is to remove the spikes in the estimate which would contribute to errors in the reconstructed segment. Fig. 5.15c shows the reconstructed signal, with pre-reconstruction filtering of the estimate, using a median-threshold-decision

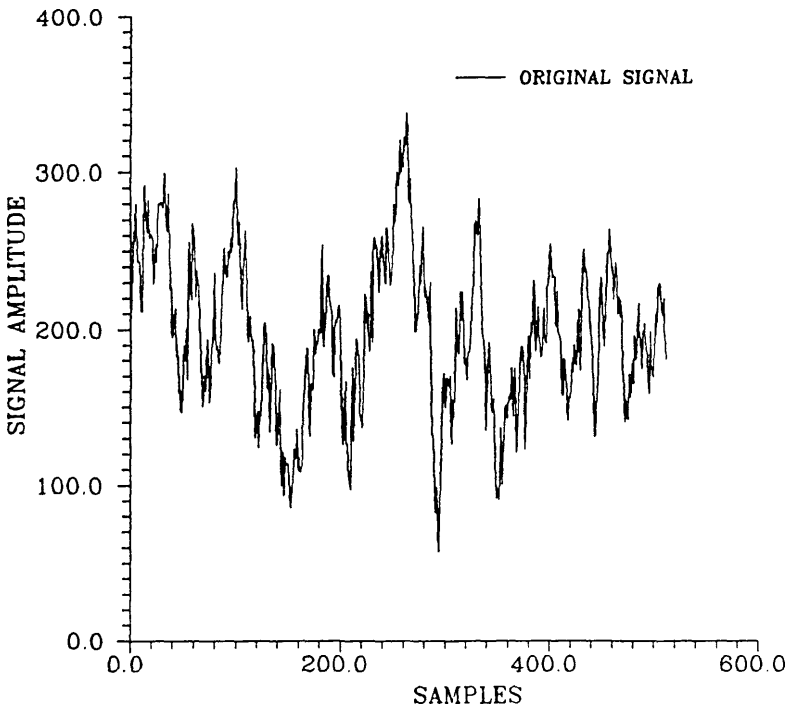


Fig. 5.13 : Original stationary first order Gauss-Markov signal, ρ=0.9.

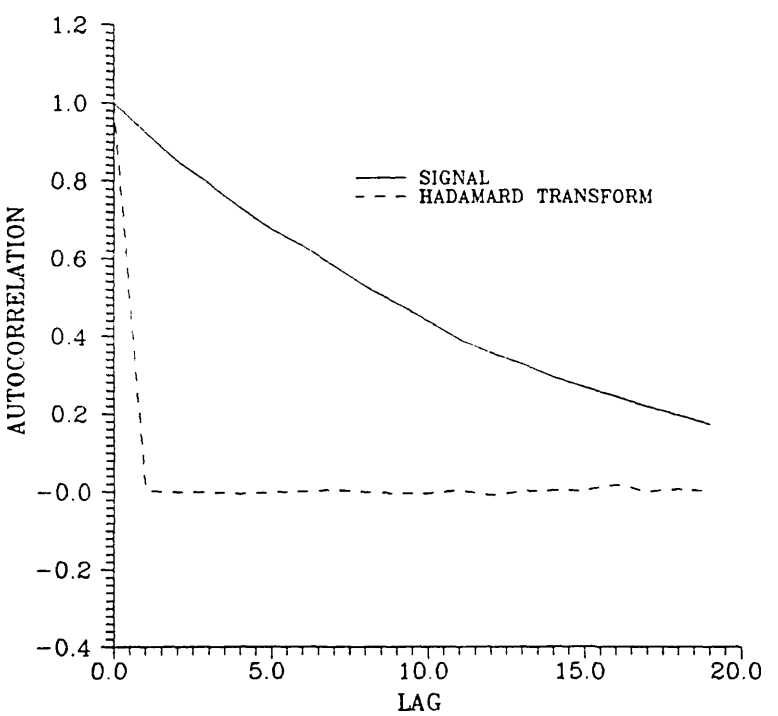


Fig. 5.14 : Autocorrelation function of the components of the Hadamard NPT of the stationary first order Gauss-Markov signal (ρ = 0.9) shown in Fig. 5.13.

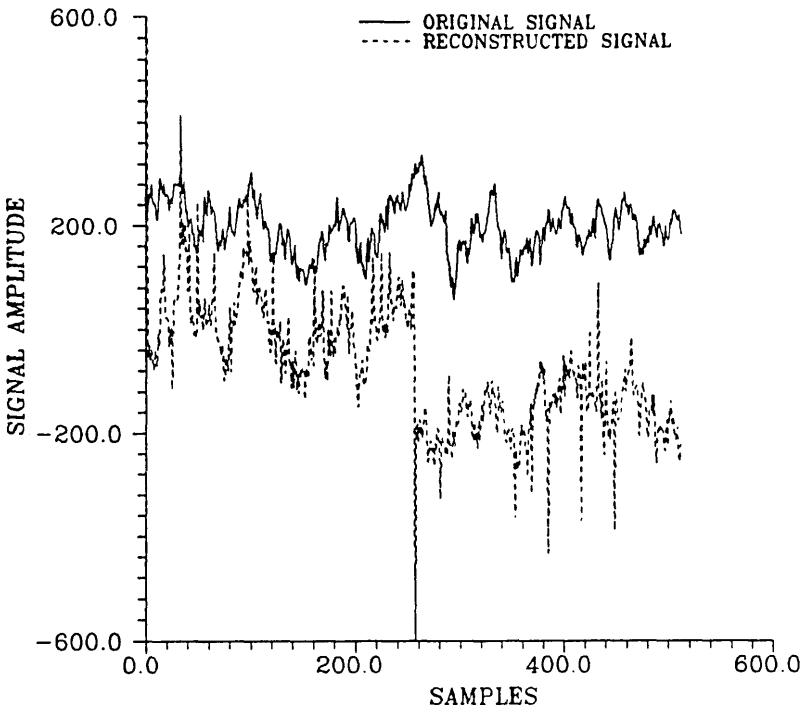


Fig. 5.15a : Result of inverse Hadamard NPT of received samples corresponding to the format of Fig. 5.3a at α=0.4; the original signal is a first order Gauss-Markov signal, ρ=0.9.

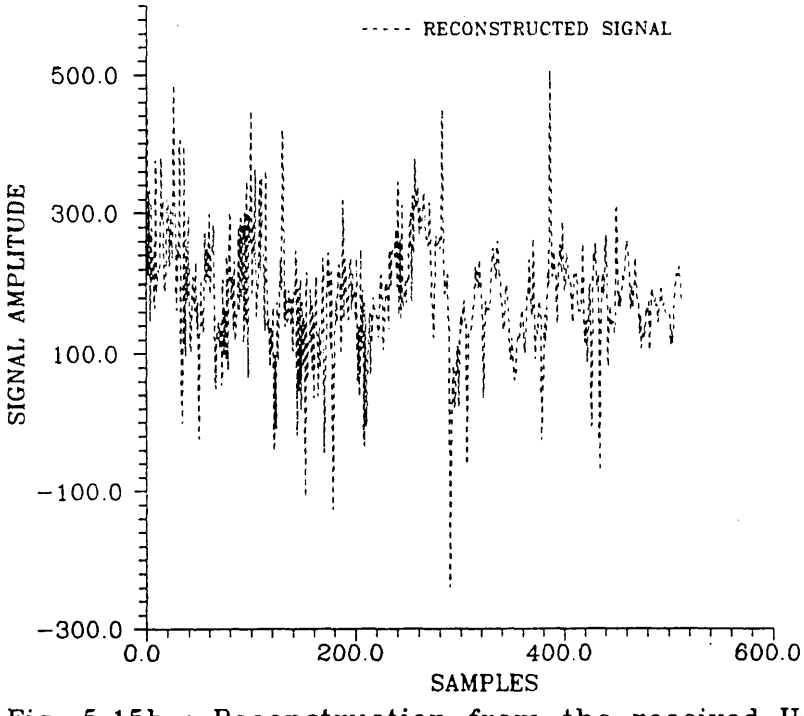


Fig. 5.15b : Reconstruction from the received Hadamard NPT segment corresponding to the format of Fig. 5.3a at α=0.4, with no pre-/ post-reconstruction filtering; original signal is shown in Fig. 5.13.

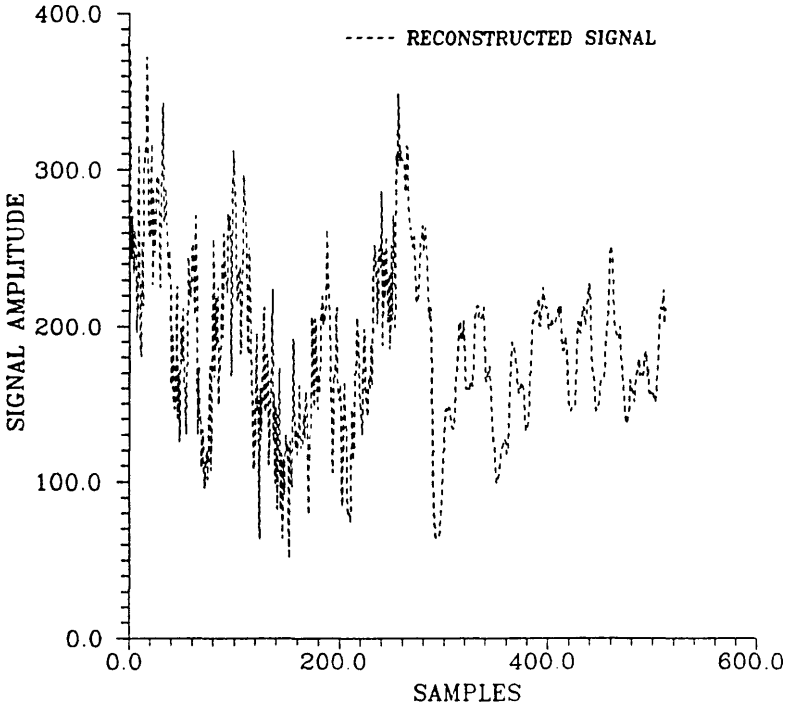


Fig. 5.15c : Reconstruction from the received Hadamard NPT segment corresponding to the format of Fig. 5.3a at α=0.4, with pre-reconstruction filtering; original signal is shown in Fig. 5.13.

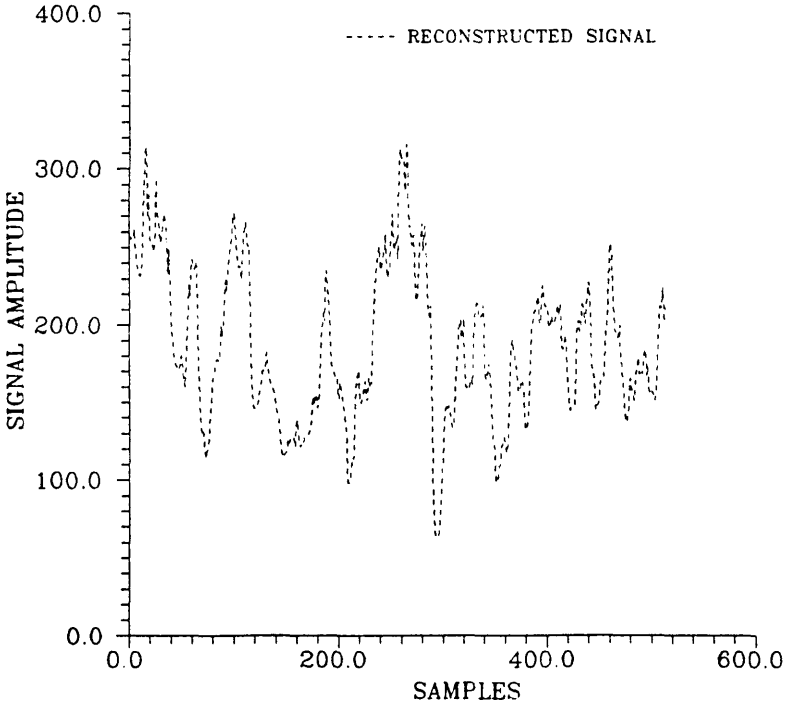


Fig. 5.15d : Reconstruction from the received Hadamard NPT segment corresponding to the format of Fig. 5.3a at α=0.4, with pre- and post-reconstruction filtering; original signal is shown in Fig. 5.13.

interpolating smoothing filter [61,62]. In this filtering approach, a sample is classified as noisy if its magnitude falls outside a specified threshold of the median of samples lying within a moving window centred on the sample in question (in the vicinity of the end points, it is not possible to keep the window centred on the noisy sample - the window length is simply kept constant with the window centred as best as possible around the sample in question). The primary choice for replacing a noisy sample is the value obtained by interpolation based on a number of past samples and the following sample. However, if the following sample is also noisy, the median of samples within a window centred, as best as possible, around it is used for interpolation. In the event that the interpolated sample falls outside the specified threshold of the median, the median is used to replace the noisy sample. The filtering process is initialized by using a median-threshold-decision median filter for filtering the first n_i samples in a segment, where n_i is the number of samples to be used for interpolation. The basic difference in the operation of this filter and that of the median-threshold- decision interpolating smoothing filter is that the median of samples within a window centred as best as possible around a noisy sample, is used to replace the noisy sample.

The reconstructed segment with pre-reconstruction filtering (samples 1 to 256 in Fig. 5.15c) is a great deal better than that obtained without pre-reconstruction filtering (samples 1 to 256 in Fig. 5.15b). The reconstructed segment can be further improved by filtering to remove any spikes, to yield a better reconstructed signal. Fig. 5.15d shows the reconstructed signal with pre- and post-reconstruction filtering. It is a very good approximation of the original Gauss-Markov signal of Fig. 5.13. In the pre-/post-reconstruction filtering algorithm, a window length of six, a threshold of four percent for initialization, a threshold of eight percent for subsequent filtering, and interpolation based on the previous three samples and the following sample, was found to yield very good results.

The median-threshold-decision interpolating filter performs better than the low pass filter and the median filter; it yields a lower mean-square error of reconstruction and preserves details of the signal better. Fig. 5.15e and Fig. 5.15f show the reconstructed signals when a low pass filter and a median filter (window length of six) respectively are used for pre- and post-reconstruction filtering; we can observe that the signal shown in Fig. 5.15d is a better approximation of the original Gauss-Markov signal shown in Fig. 5.13.

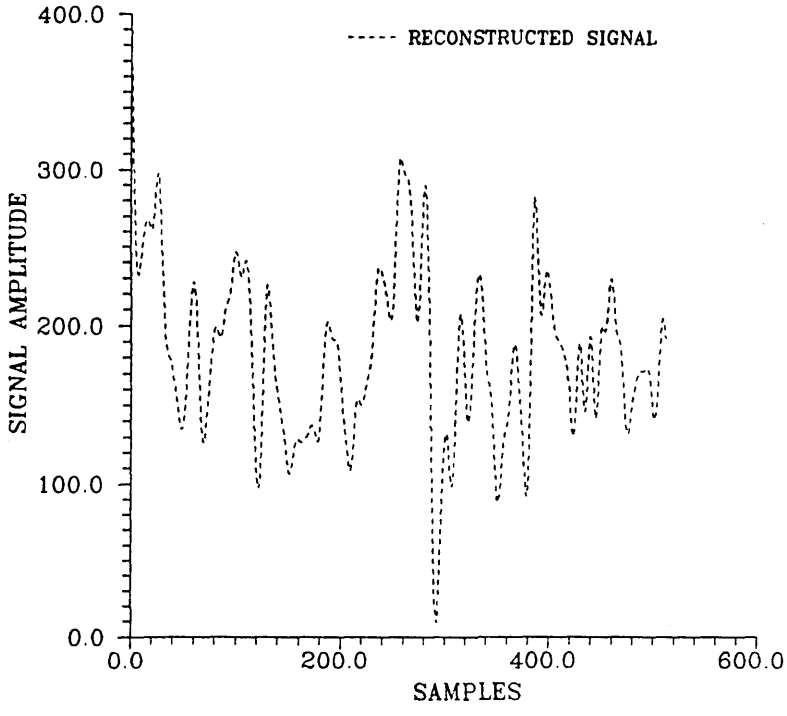


Fig. 5.15e : Reconstruction from the received Hadamard NPT segment corresponding to the format of Fig. 5.3a at α=0.4, with pre- and post-reconstruction low pass filtering; original signal is shown in Fig. 5.13.

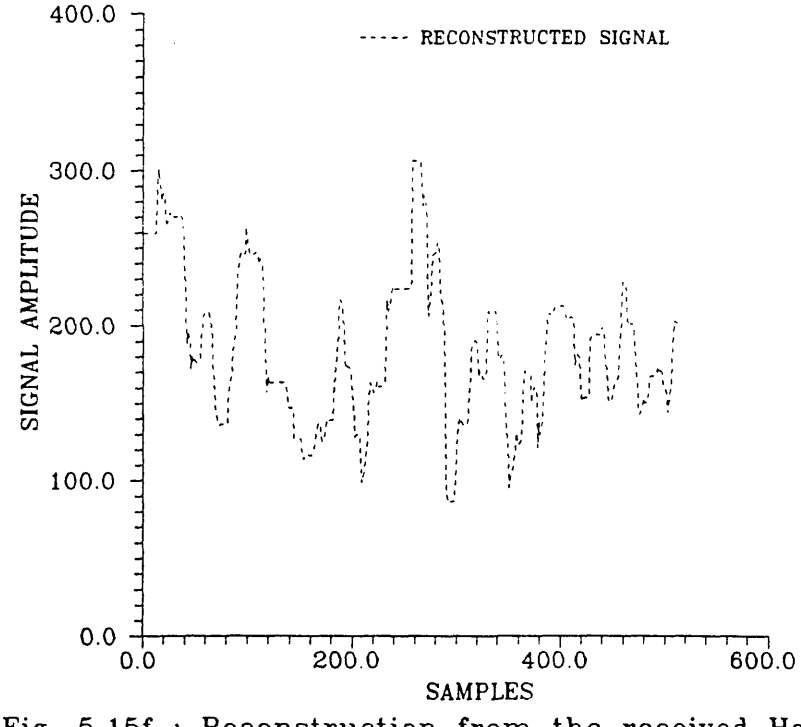


Fig. 5.15f : Reconstruction from the received Hadamard NPT segment corresponding to the format of Fig. 5.3a at α=0.4, with pre- and post-reconstruction median filtering; original signal is shown in Fig. 5.13.

We shall also consider a first order Gauss-Markov signal with low inter-element correlation coefficient. Fig. 5.16 is a plot of 512 samples of a Gauss-Markov signal having a low inter-element correlation coefficient of 0.4. Fig. 5.17a shows the reconstructed signal obtained by applying the fast reconstruction algorithm to the received Hadamard NPT(0.4) samples, corresponding to the format of Fig. 5.3a, with no pre-/post-reconstruction filtering. Fig. 5.17b shows the reconstructed signal with pre- and post-reconstruction filtering. The reconstructed signal in this case is a smoothed version of the original signal.

The above results show that, for first order Gauss-Markov signals having high or low inter-element correlation coefficient, a reasonable version of the signal can be obtained from segments of its Hadamard NPT, using the proposed reconstruction algorithm. A very good approximation of the original signal is obtained for first order Gauss-Markov signals having a high inter-element correlation coefficient, while a smoothed version of the original signal is obtained for first order Gauss-Markov signals having a low inter-element correlation coefficient.

For the formats that can be associated with the fast reconstruction algorithm, an approximate version of a signal can be obtained from segments of its Hadamard NPT, when $\alpha > \frac{1}{2}$. Fig. 5.18a shows the reconstructed signal (original signal is shown in Fig. 5.13) obtained by taking the inverse Hadamard NPT of received samples corresponding to the format of Fig. 5.3a, when $\alpha = 0.75$. Reconstruction is accurate for samples 258 to 512, and poor for the remaining samples. Fig. 5.18b shows the reconstructed signal obtained by applying the fast reconstruction algorithm to the received Hadamard NPT samples, with no pre-/post-reconstruction filtering. It can be observed that the estimate derived from the received samples (samples 257 to 512) is less noisy than that obtained at $\alpha = 0.4$, see Fig. 5.15b. However, the reconstructed "lost " signal segment (samples 1 to 256) at $\alpha = 0.75$ is more noisy than that obtained at $\alpha = 0.4$. The reason for this can be attributed to the factor $\frac{\alpha}{1-\alpha}$ in (5.89) multiplying the sub-Hadamard transforms of the respective estimation errors. Since this factor is greater than unity for $\alpha > \frac{1}{2}$, it has the effect of amplifying the errors in the reconstructed segments.

2) The reconstruction algorithm was simulated for the case of received samples corresponding to the format of Fig. 5.3b; the original signal is the first order Gauss-Markov signal with $\rho = 0.9$, shown in Fig. 5.13. For this format, the received transform samples are no longer contiguous, which implies a discontinuity in the

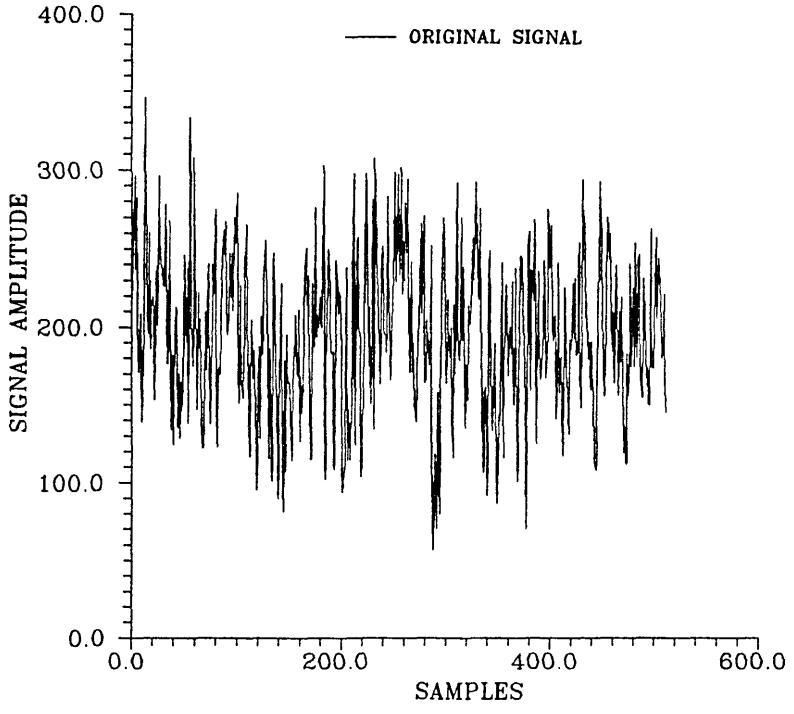


Fig. 5.16 : Original stationary first order Gauss-Markov signal, ρ=0.4.

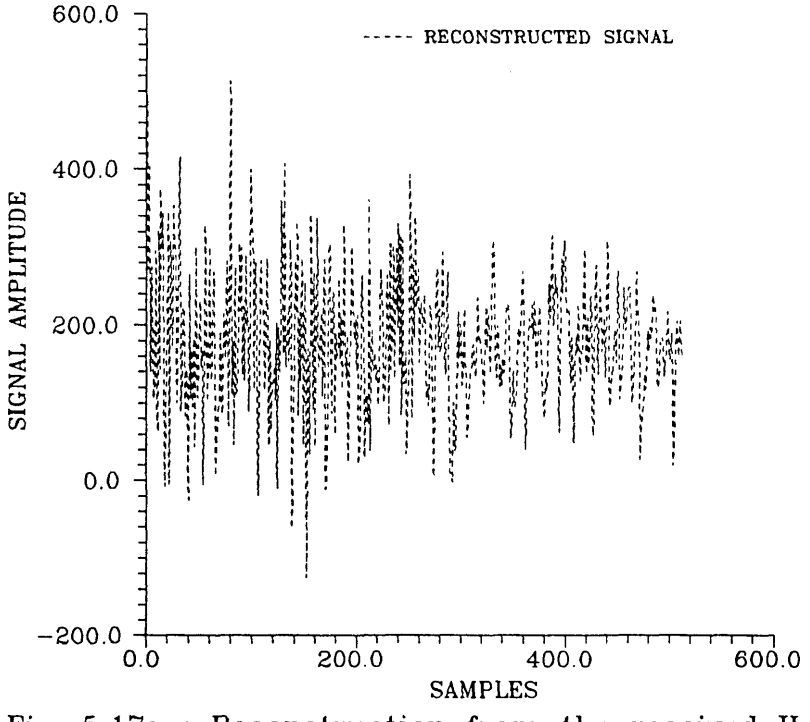


Fig. 5.17a : Reconstruction from the received Hadamard NPT segment corresponding to the format of Fig. 5.3a at α=0.4, with no pre-/ post-reconstruction filtering; original signal is shown in Fig. 5.16.

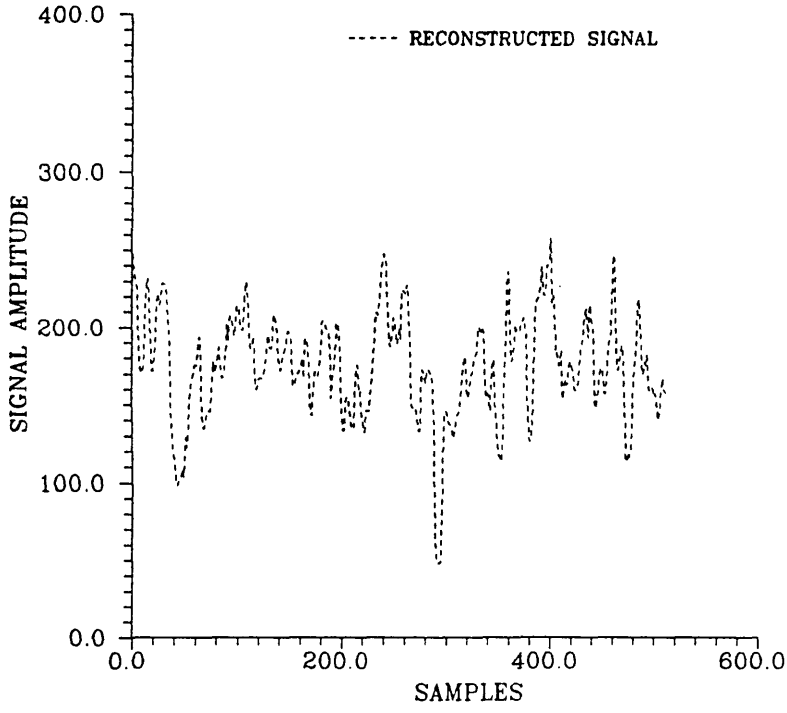


Fig. 5.17b : Reconstruction from the received Hadamard NPT segment corresponding to the format of Fig. 5.3a at α=0.4, with pre- and post-reconstruction filtering; original signal is shown in Fig. 5.16.

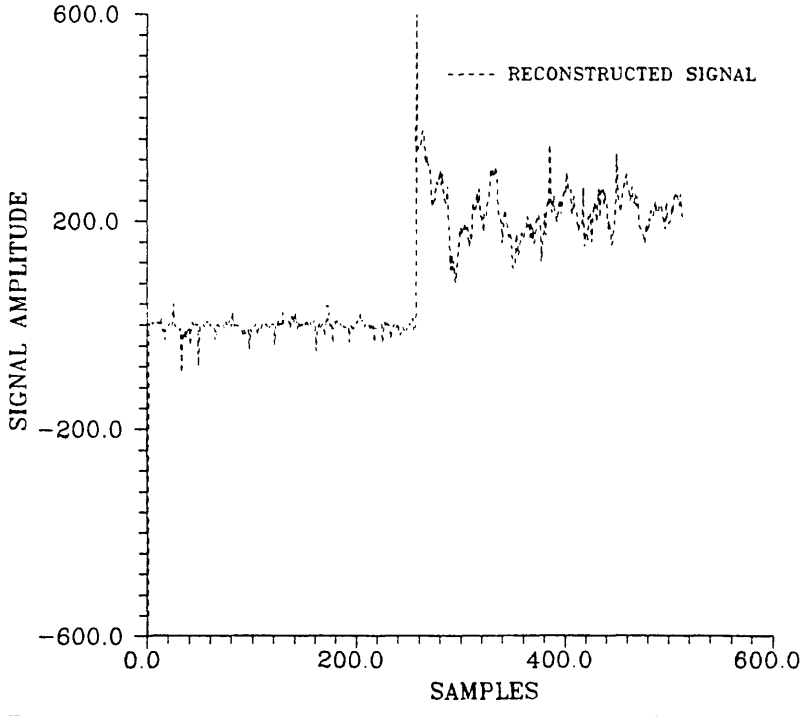


Fig. 5.18a : Result of inverse Hadamard NPT of received samples corresponding to the format of Fig. 5.3a at α=0.75; the original signal is shown in Fig. 5.13.

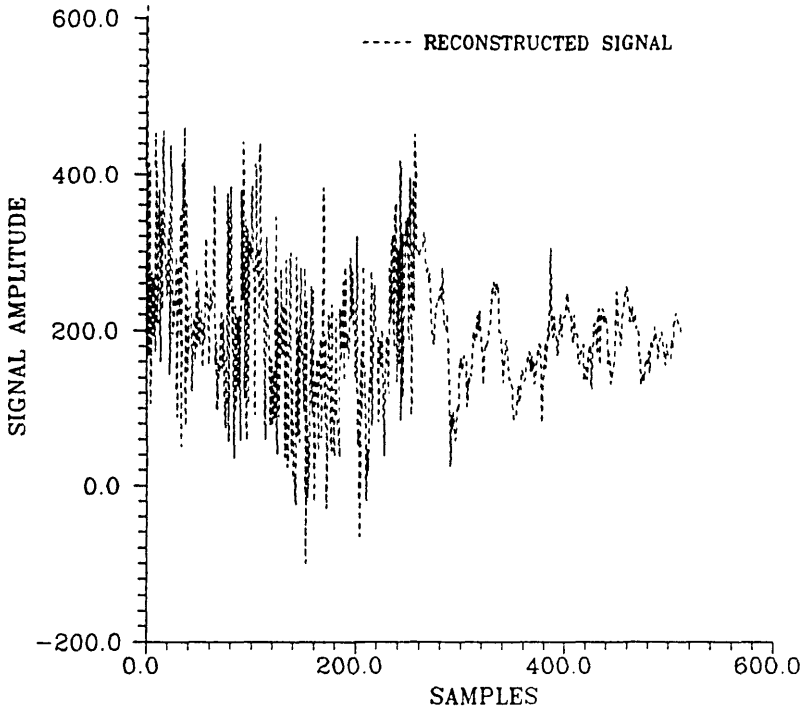


Fig. 5.18b : Reconstruction from the received Hadamard NPT segment corresponding to the format of Fig. 5.3a at α=0.4, with no pre-/ post-reconstruction filtering; original signal is shown in Fig. 5.13.

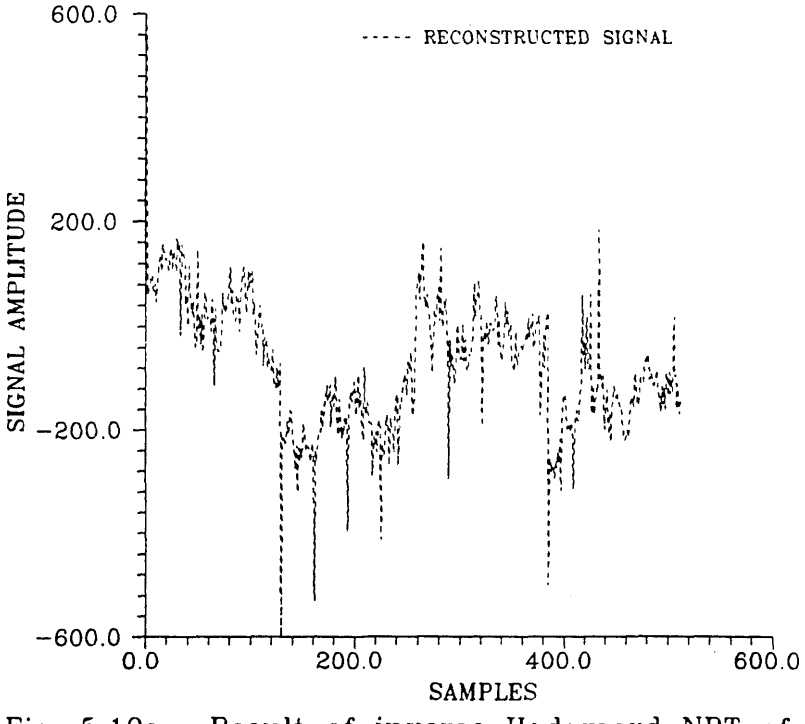


Fig. 5.19a : Result of inverse Hadamard NPT of received samples corresponding to the format of Fig. 5.3b at α=0.4; the original signal is shown in Fig. 5.13.

statistics of the Hadamard NPT components in the respective segments. Fig. 5.19a shows the reconstructed signal obtained by taking the inverse Hadamard NPT(0.4) of the received samples. Fig. 5.19b shows the reconstructed signal obtained by applying the reconstruction algorithm to the received segments, with pre- and post-reconstruction filtering. In the signal segment estimation process, the initial adaptive filter weights used for the successive segments were the converged weights for the previous segment. The reconstructed signal, shown in Fig. 5.19b is a very good approximation of the original signal. However, the mean-square error (MSE) of reconstruction, MSE = 1343.6, is higher than that for the reconstructed signal obtained from the format of Fig. 5.3a, shown in Fig. 5.15b, MSE = 867.5.

3) The reconstruction algorithm was also simulated for a simple format corresponding to the case of loss of even-index vectors. The format considered can be derived from the general case depicted in Fig. 5.8b, with the number of segments $n_s = 2$. For this format, the dominant transform samples, including the "dc " term were received. The original signal used in the simulation is the first order Gauss-Markov signal, $\rho = 0.9$, shown in Fig. 5.13. Fig. 5.20a shows the reconstructed signal obtained by applying the reconstruction algorithm to the received segments, at $\alpha = 0.4$, with no pre-/post-reconstruction filtering. It is observed that the estimates of the signal samples at the beginning of the block (samples 1 to about 90) are very low in magnitude. This is due to the high magnitude of the "dc " sample in relation to the remaining transform samples, which has the effect of slightly "turning off " the filter. An effective remedy against this is to normalize the "dc " sample prior to estimation, by the "coefficient magnitude expansion factor for DC values ", $(CMEF)_{DC}$, given by (2.45) in chapter two. Fig. 5.20b shows the result obtained by making the above modification to the transform samples used for signal segment estimation, with no pre-/post- reconstruction filtering. A greatly improved reconstructed signal is obtained in this case, which can be further improved by pre- and post-reconstruction filtering.

4) The reconstruction algorithm was also simulated for the format shown in Fig. 5.21, where the hatched segments are unknown. The number of samples in each segment is also indicated. The fast reconstruction schemes cannot be directly applied to this format and the required solution is obtained via the iterative reconstruction algorithm given by (5.14).

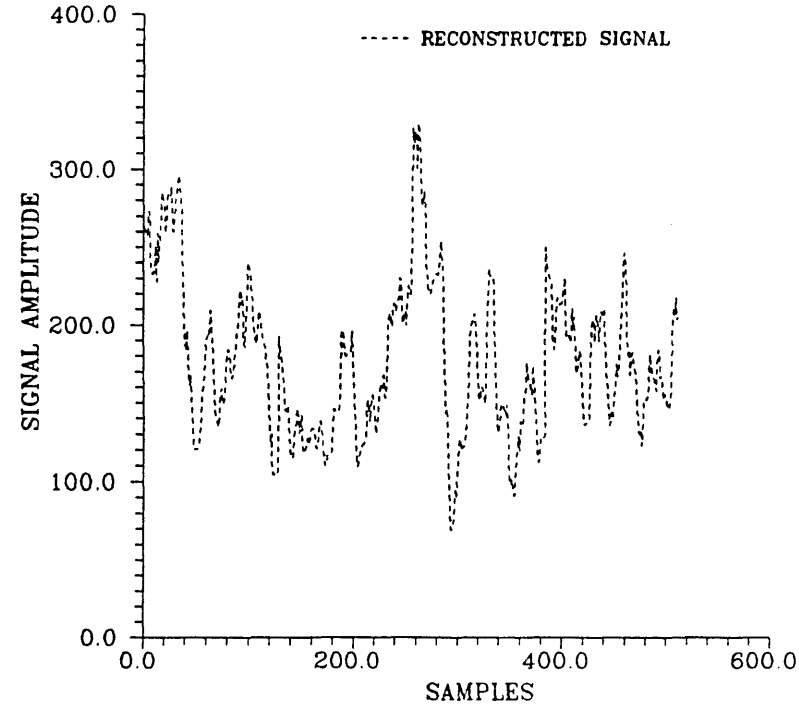


Fig. 5.19b : Reconstruction from the received Hadamard NPT segment corresponding to the format of Fig. 5.3b at α=0.4, with pre- and post-reconstruction filtering; original signal is shown in Fig. 5.13.

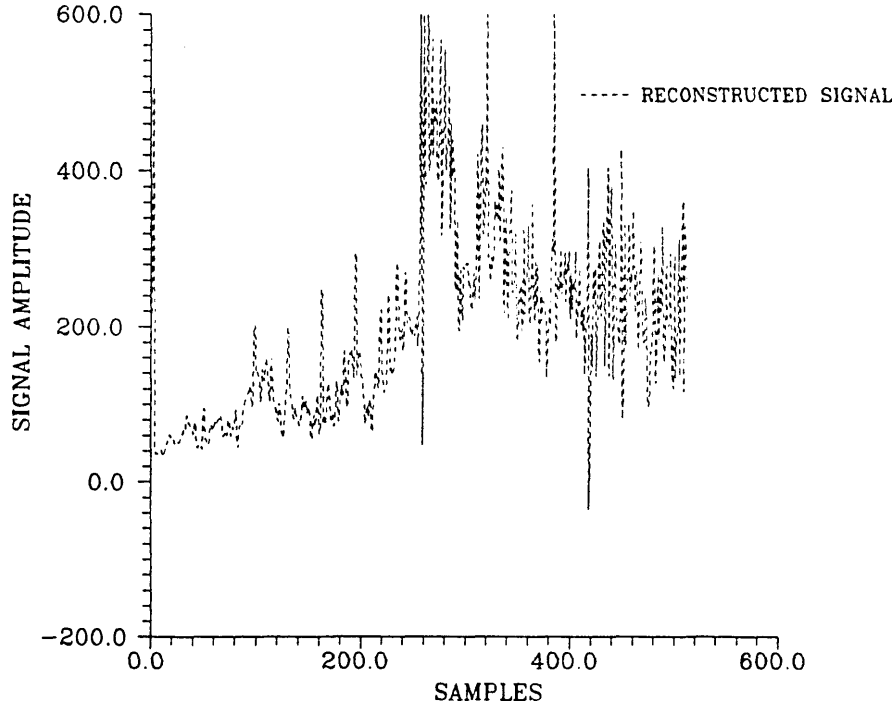


Fig. 5.20a : Reconstruction from the received Hadamard NPT segment corresponding to the format of Fig. 5.8b, with n_s=2, at α=0.4; the original signal is shown in Fig. 5.13.

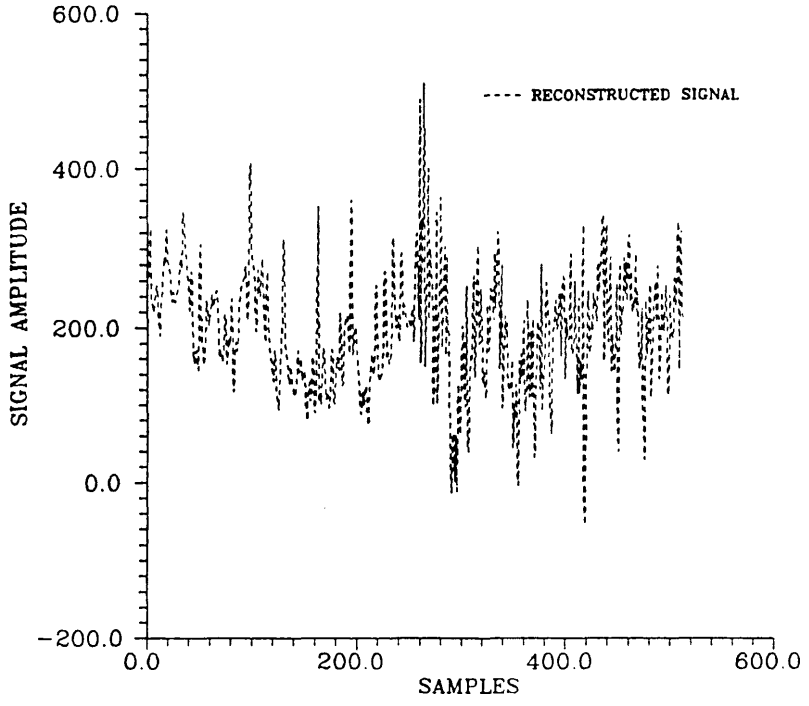
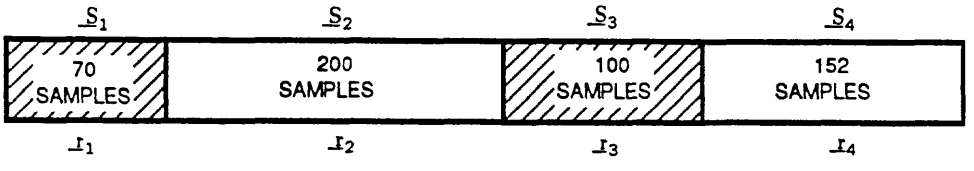


Fig. 5.20b : Reconstruction from the received Hadamard NPT segment corresponding to the format of Fig. 5.8b, with $n_s=2$, at $\alpha=0.4$; using a modified reference signal for estimation.



$\underline{S}_1$, $\underline{S}_3$ = desired (but unknown) signal segments
$\underline{S}_2$, $\underline{S}_4$ = known signal segments
$\underline{I}_1$, $\underline{I}_3$ = desired (but unknown) transform segments
$\underline{I}_2$, $\underline{I}_4$ = known transform segments.

Fig. 5.21 : An iterative Hadamard NPT reconstruction format for which the fast reconstruction schemes cannot be directly applied.

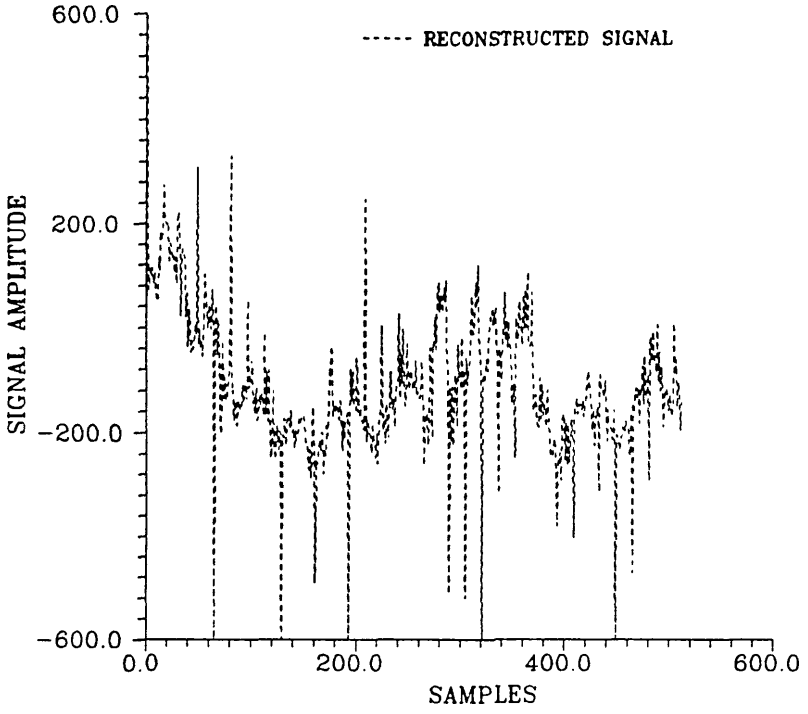


Fig. 5.22a : Result of inverse Hadamard NPT of received samples corresponding to the format of Fig. 5.21 at α=0.4; the original signal is shown in Fig. 5.13.

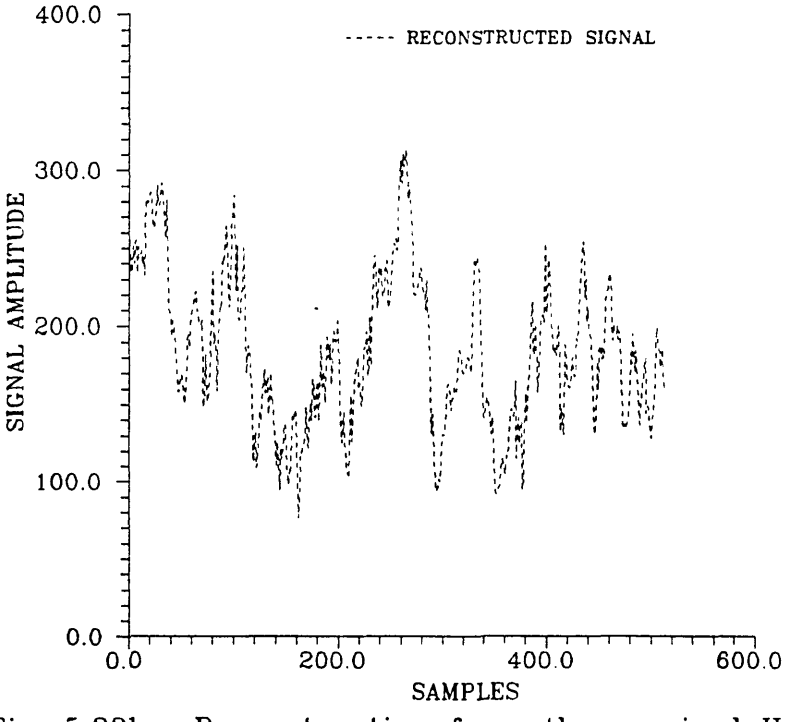


Fig. 5.22b : Reconstruction from the received Hadamard NPT segment corresponding to the format of Fig. 5.21 at α=0.4, with pre- and post-reconstruction filtering; original signal is shown in Fig. 5.13.

Fig. 5.22a shows the result of the inverse Hadamard NPT(0.4) of received Hadamard NPT samples corresponding to the format of Fig. 5.21; the original signal is the stationary first order Gauss-Markov signal shown in Fig. 5.13. Fig. 5.22b shows the reconstructed signal with pre- and post-reconstruction filtering which is a very good approximation of the original signal shown in Fig. 5.13. The result correspond to specifying an ϵ of 1×10^{-2} and 28 iterations were required for convergence. An MSE of 689.03 was obtained which is lower than that obtained in the previously considered cases. This is due to the fact that more transform samples are known for this format than in the previously considered formats. As stated earlier, the number of iterations for convergence is dependent on the choice of ϵ. For example, the choice $\epsilon = 10^{-1}$ requires 23 iterations for convergence.

It is interesting to note that the format of Fig. 5.3b can be obtained from that of Fig. 5.21 by discarding samples 71 to 128 and 371 to 384 in the known segments. Thus, the fast reconstruction schemes can be indirectly applied to the format of Fig. 5.21. In this case, all the available transform samples can be used to obtain the estimate $\hat{S}^W$ but it is only the samples 129 to 256 and 385 to 512 that are used in the fast reconstruction scheme. However, the quality of reconstruction would be poorer than if all the available information was used for reconstruction; there has to be a trade-off between processing speed and reconstructed signal quality.

5.3.2 Reconstruction of Speech Signal

Fig. 5.23 is a plot of 512 samples of a speech signal. The autocorrelation function of the speech signal and that of its Hadamard transform show that there is no significant correlation among the components of the Hadamard transform of the speech signal for a lag of one and above. Hence, only one delay element is needed to generate the reference signal in the ALE algorithm. A six-tap adaptive filter was used in the ALE algorithm described in Fig. 5.12.

1) The reconstruction from received Hadamard NPT segments corresponding to the format of Fig. 5.3a was simulated. Fig. 5.24a shows the reconstructed signal obtained after application of the Hadamard NPT reconstruction algorithm to the received samples at $\alpha = 0.4$, with no pre-/post-reconstruction filtering. Fig. 5.24b shows the reconstructed signal with pre- and post-reconstruction filtering. In this case, although the pre-/post-reconstruction process reduces the spikes in the reconstructed signal, it has the undesired effect of smoothing out some details in

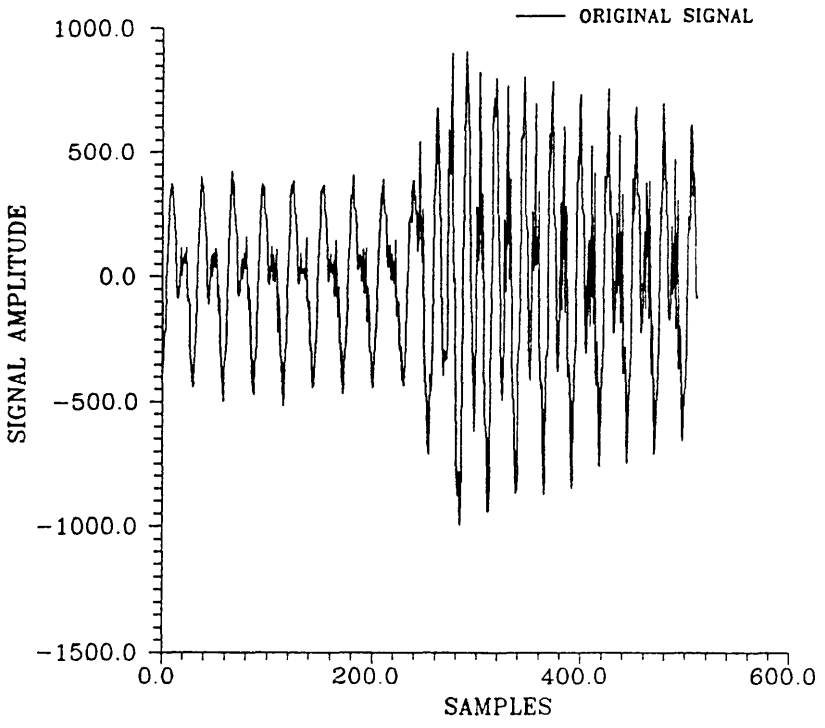


Fig. 5.23 : Original speech signal.

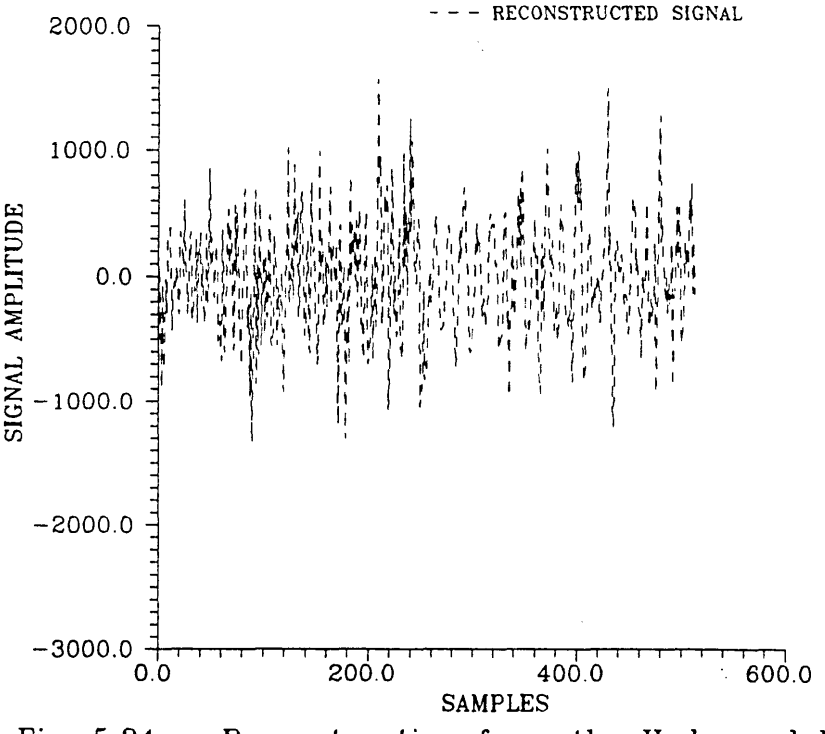


Fig. 5.24a : Reconstruction from the Hadamard NPT segment corresponding to the format of Fig. 5.3a, at α=0.4, with no pre-/post-reconstruction filtering; original signal is shown in Fig. 5.23.

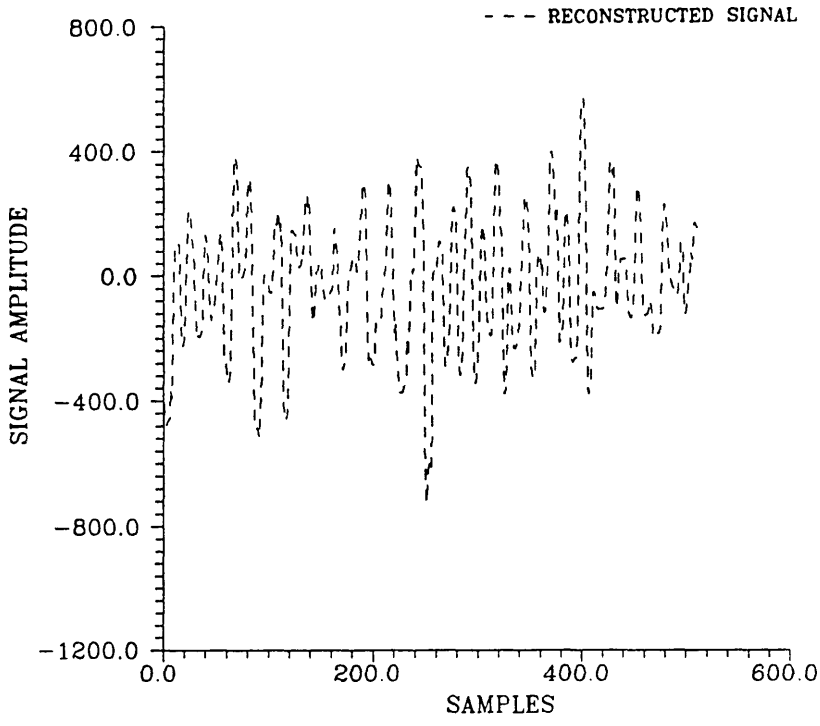


Fig. 5.24b : Reconstruction from the Hadamard NPT segment corresponding to the format of Fig. 5.3a, at α=0.4, with pre- and post-reconstruction filtering; original signal is shown in Fig. 5.23.

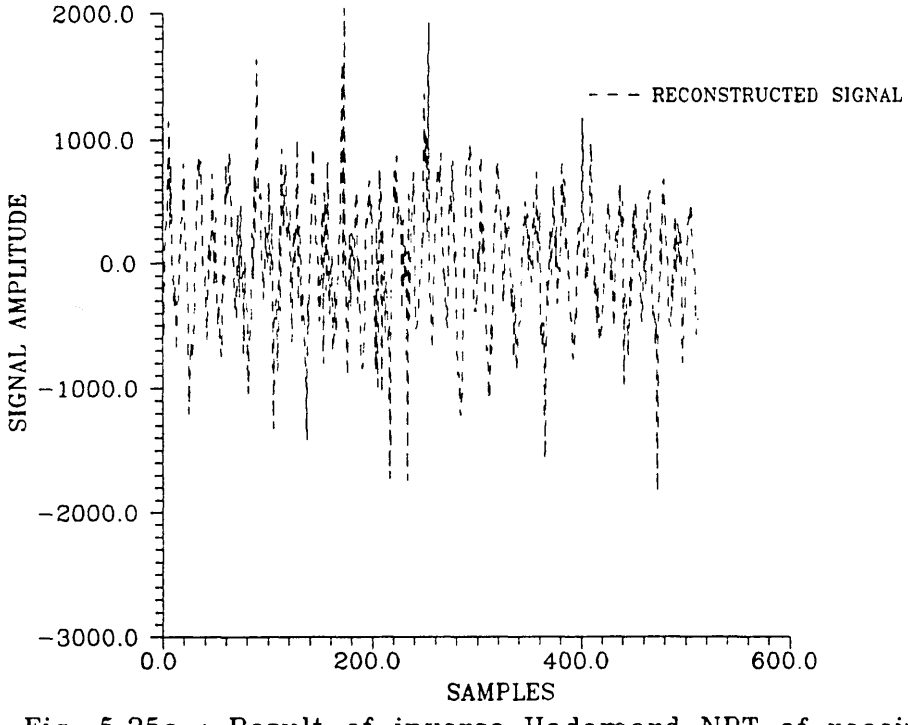


Fig. 5.25a : Result of inverse Hadamard NPT of received samples corresponding to the format of Fig. 5.8b, with n_s=2, at α=0.4; the original signal is shown in Fig. 5.23.

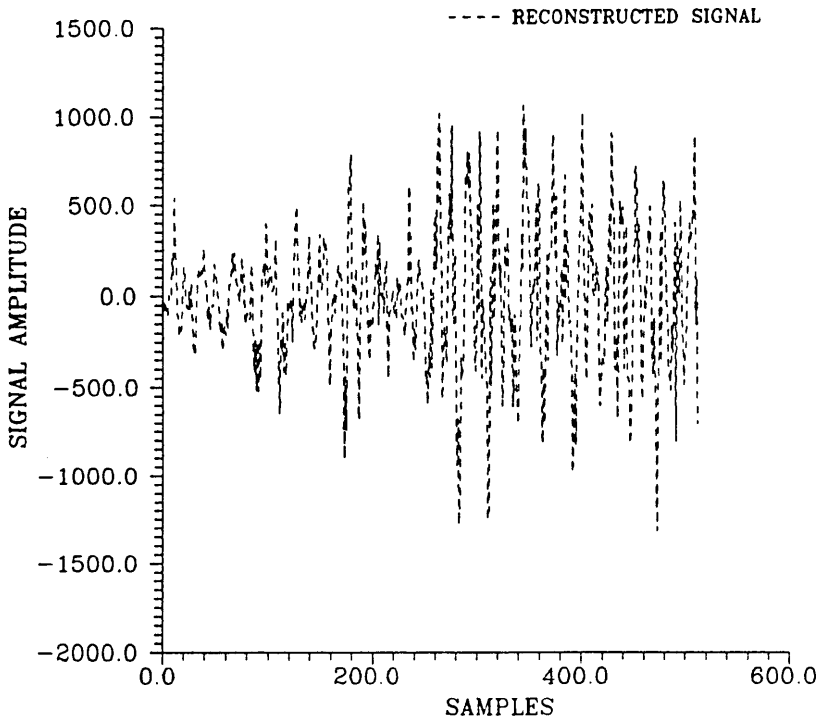


Fig. 5.25b : Reconstruction from the Hadamard NPT segment corresponding to the format of Fig. 5.8b, with n_s=2, at α=0.4; with no pre-/post-reconstruction filtering; original signal is shown in Fig. 5.23.

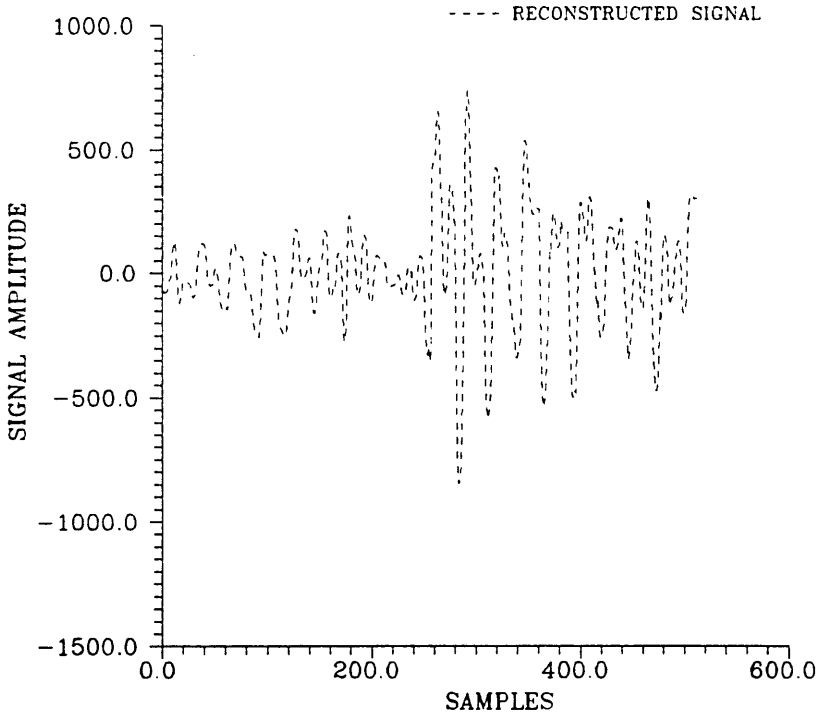


Fig. 5.25c : Reconstruction from the Hadamard NPT segment corresponding to the format of Fig. 5.8b, with n_s=2, at α=0.4; with pre- and post-reconstruction filtering; original signal is shown in Fig. 5.23.

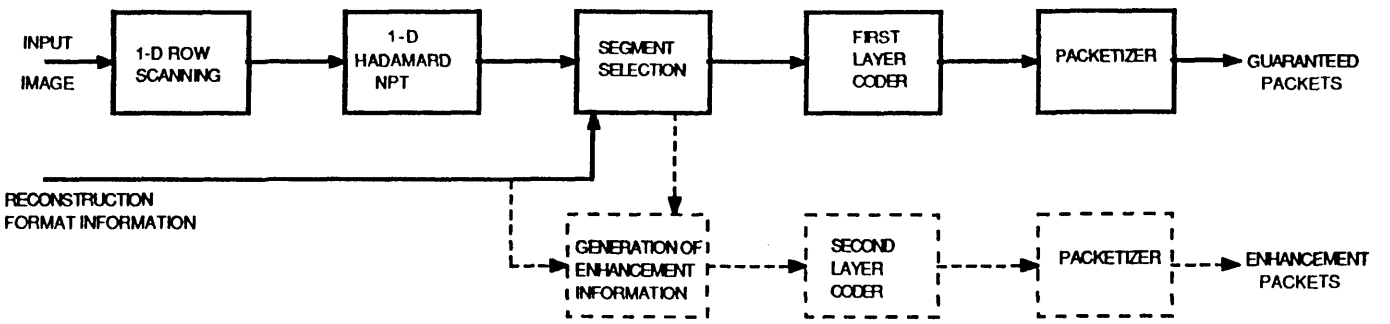
the original signal, more especially in the region of high amplitude samples. See for example samples 260-512 in Fig. 5.24b.

2) The reconstruction from the received samples corresponding to the format of Fig. 5.8b, with $n_s = 2$, was also simulated; this correspond to the loss of an even-index vector. Fig. 5.25a shows the reconstructed signal obtained by taking the inverse Hadamard NPT(0.4) of the received samples. There is a great deal of distortion in the reconstructed signal. The reconstructed signal obtained by application of the reconstruction algorithm to the received samples is shown in Fig. 5.25b. The "dc " sample in this case did not affect the signal estimate; this is due to the fact that the magnitude of the "dc " sample is very small which is linked to the fact that the mean of the original signal shown in Fig. 5.23 is very small. The result obtained by using a modified reference signal in the ALE is similar to that shown in Fig. 5.25b. Fig. 5.25c shows the reconstructed signal with pre- and post-reconstruction filtering. It is also observed that some details of the original signal has been smoothed out as a result of pre- and post-reconstruction filtering.

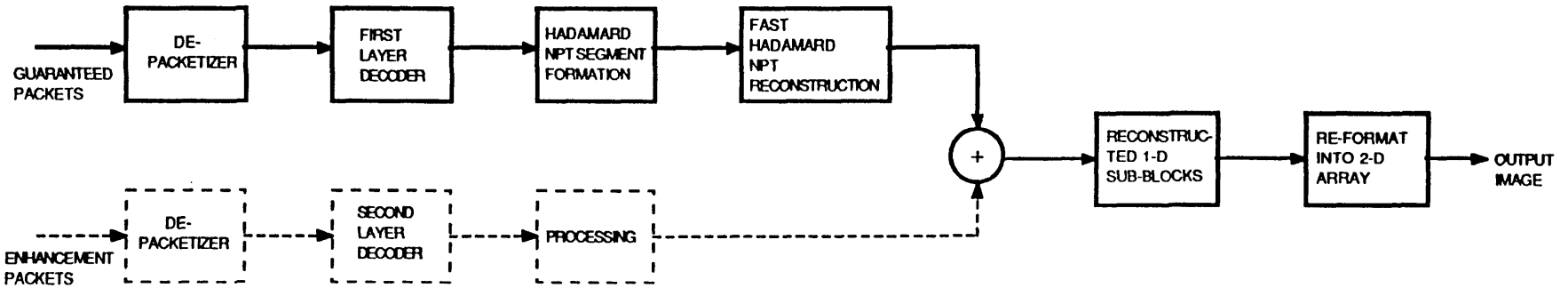
5.4 Application of One-Dimensional Hadamard NPT Reconstruction Formats in Intraframe Packet Transmission of Images

In this section, some of the fast reconstruction formats are investigated for intraframe packet transmission of images. An "Orwell " slotted ring network is assumed, which guarantees the transmission of certain packets. Orwell is a protocol that was primarily developed to carry integrated mixed speech and data services on a slotted ring [63]. The network is able to provide a guaranteed bandwidth for speech sources by controlling access to the slots from the nodes, the data services being given a low priority. However, this network requires the transmitted information to be broken into packets. A common problem is that of packet loss, which could be due to heavy loading of the network or corruption of the address of a packet.

There has been a growing interest in the transmission of packetized image data over an Orwell ring type of network [64,65]. An approach to the problem of packet loss is two-layer coding, where the bit stream of the image data is decomposed into two parts. The first part is transmitted over the guaranteed channel and is referred to as "guaranteed packets ". The second part contains the rest of the image information which does not necessarily have to be received. This consists of "enhancement packets " which, if received, are only used to improve



(a) Transmitter



(b) Receiver

Fig. 5.26 : Two-Layer Intraframe Packet Transmission of Images Using Hadamard NPT Reconstruction.

on the reconstructed picture obtained from the guaranteed packets. In the event of excessive delay of the enhancement packets, they are discarded by the Orwell protocol.

The Hadamard NPT of a signal is very amenable to this type of signal transmission scenario. In the scheme that we propose, certain segments of the Hadamard NPT of one-dimensional sub-blocks of the image (obtained by row-scanning the image) are transmitted as guaranteed packets. These correspond to the formats having a fast reconstruction algorithm. At the receiver, a fast Hadamard NPT reconstruction algorithm is applied to the received packets to yield an approximate version of the original image. The emphasis here is on the reconstruction from guaranteed packets. Other related issues such as the choice of enhancement packets, reconstruction from compressed packets of Hadamard NPT segments, and the effect of transmission errors on the reconstruction from guaranteed packets are considered in chapter seven. Fig. 5.26 is a block diagram of the proposed scheme.

The formats investigated are shown in Fig. 5.27, where the information contained in the guaranteed packets is shown unhatched. It should be noted that it does not imply that all the information in the segment(s) shown unhatched are contained in a single packet. The segments could be broken up to form packets, but the constraint here is that these must be transmitted over the guaranteed channel.

Simulation Results

Experimental results of the reconstruction of images from the various formats of guaranteed packets of Hadamard NPT segments, shown in Fig. 5.27 indicate that the format of Fig. 5.27a yields the best reconstructed pictures in terms of subjective quality and peak signal-to-noise ratio and hence, this format is proposed for packet transmission of images.*

Fig. 5.29a shows the reconstructed picture when 1×256 transforms of sub-blocks of the row-scanned image ALAN (reproduced in Fig. 5.28) are taken, and the inverse Hadamard NPT(0.4) of received segments corresponding to the format of Fig. 5.27a is performed; an offset of 125 was added for the purpose of display, to compensate for the loss of the "dc " sample. It is observed that the information in the right half of the picture has been completely lost. Fig. 5.29b shows the

*The pixel values in the pictures presented in the following have been clipped to between 0 and 255.

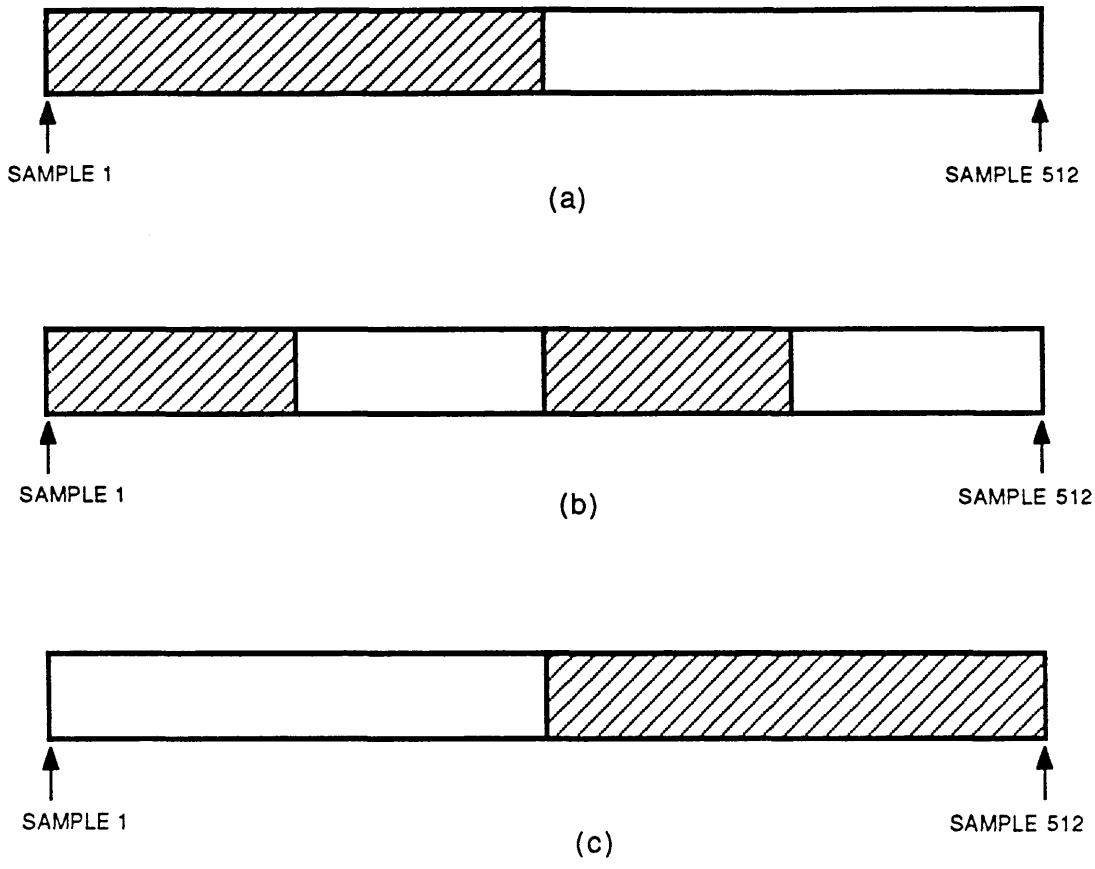


Fig. 5.27 : Formats Investigated For Intraframe Packet Transmission of Images ; the unhatched segments are the ones sent in the guaranteed packets .

reconstructed picture resulting from the application of the fast Hadamard NPT reconstruction algorithm to the received segments. There is a great deal of distortion in the reconstructed picture, but it is better than that obtained by taking the inverse Hadamard NPT of received segments.

Fig. 5.30a shows the reconstructed picture obtained when 1×512 transforms of sub-blocks of the row-scanned image are used, and the inverse Hadamard NPT of received segments corresponding to the format of Fig. 5.27a is performed, with an offset of 125 added. The reconstructed picture obtained by application of the fast Hadamard NPT reconstruction algorithm to the received segments is shown in Fig. 5.30b. Clearly, the reconstructed picture in this case is better than the equivalent one using 1×256 transforms, and there is only a little noticeable distortion.

Some pre-/post-reconstruction filtering techniques were considered for improving the quality of the reconstructed picture. Fig. 5.31a shows the reconstructed picture with pre- and post-reconstruction filtering of the one-dimensional sub-blocks using the median-threshold-decision interpolating filter, which was introduced earlier. A slight blurring is noticeable in the picture and the mean-square error of reconstruction, MSE = 131.52 is higher than that obtained without applying the filtering technique, MSE = 112.25. Fig. 5.31b shows the reconstructed picture with pre- and post-reconstruction one-dimensional median filtering. The blurring of the picture is worse than in the previous case and the mean-square error of reconstruction is also higher, MSE = 204.49. Fig. 5.31c shows the reconstructed picture with pre- and post-reconstruction low pass filtering of the one-dimensional sub-blocks. The low pass filter has effectively cleaned the noise in the reconstructed picture, however, there is a great deal of blurring of the resulting picture; the mean-square error of reconstruction, MSE = 86.26, is lower than in the previously considered cases. Fig. 5.31d shows the result of applying a two-level bi-directional detail-preserving median filter ($2LM^{+}$) (see [66, pp. 78] for the details of this filter) using a 5×5 window, to the reconstructed picture obtained without pre-/post-reconstruction filtering. This corresponds to filtering the image shown in Fig. 5.29b. The best reconstructed picture is obtained and details such as edges are preserved; the mean-square error of reconstruction, MSE = 67.02 is also the lowest.



Fig. 5.28 : Original 8-bit, 256×256 Image ALAN.



Fig. 5.29a : Inverse Hadamard NPT(0.4) of Guaranteed Packets, Format of Fig. 5.27a ; 1×256 Transforms, Image ALAN.



Fig. 5.29b : Hadamard NPT(0.4) Recons. From Guaranteed Packets, Format of Fig. 5.27a ; 1×256 Transforms, Image ALAN. No Pre-/ Post-Recons. Filtering.

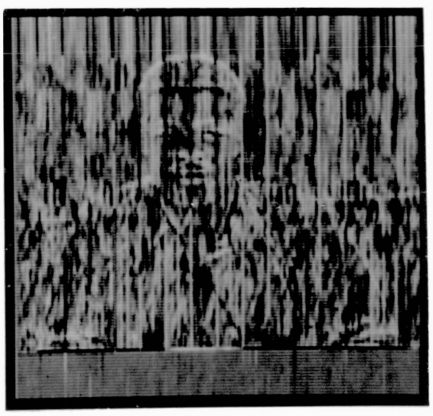


Fig. 5.30a : Inverse Hadamard NPT(0.4) of Guaranteed Packets, Format of Fig. 5.27a ; 1×512 Transforms, Image ALAN.



Fig. 5.30b : Hadamard NPT(0.4) Recons. From Guaranteed Packets, Format of Fig. 5.27a ; 1×512 Transforms, Image ALAN. No Pre-/ Post-Recons. Filtering.



Fig. 5.31a : Hadamard NPT(0.4) Recons. From Guaranteed Packets, Format of Fig. 5.27a ; 1×512 Transforms, Image ALAN. Pre- and Post-Recons. Median-Thresh.-Dec. Interpolating Filtering.



Fig. 5.31b : Hadamard NPT(0.4) Recons. From Guaranteed Packets, Format of Fig. 5.27a ; 1×512 Transforms, Image ALAN. Pre- and Post-Recons. Median Filtering.



Fig. 5.31c : Hadamard NPT(0.4) Recons. From Guaranteed Packets, Format of Fig. 5.27a ; 1×512 Transforms, Image ALAN. Pre- and Post-Recons. Low Pass Filtering.



Fig. 5.31d : Hadamard NPT(0.4) Recons. From Guaranteed Packets, Format of Fig. 5.27a ; 1×512 Transforms, Image ALAN. Post-Recons. Two-Level Bi-directional, Detail-Preserving Median filtering ($2LM^{+}$).

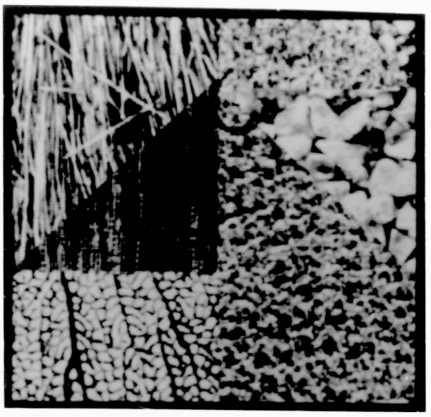


Fig. 5.32 : Original 8-bit, 256×256 Image TEXTURE.

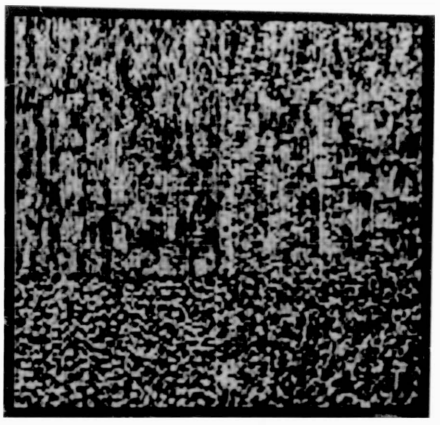


Fig. 5.33a : Inverse Hadamard NPT(0.4) of Guaranteed Packets, Format of Fig. 5.27a ; 1×512 Transforms, Image TEXTURE.

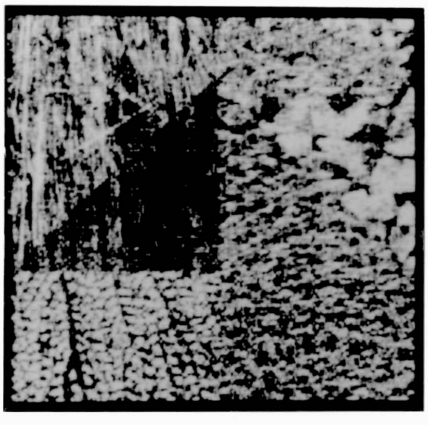


Fig. 5.33b : Hadamard NPT(0.4) Recons. From Guaranteed Packets, Format of Fig. 5.27a ; 1×512 Transforms, Image TEXTURE. No Pre-/Post-Recons. Filtering.

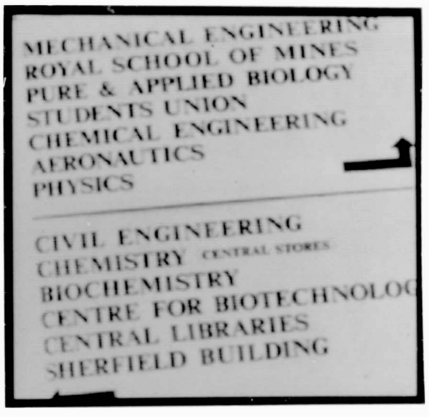


Fig. 5.34 : Original 8-bit, 256×256 Image DOCUMENT.



Fig. 5.35a : Inverse Hadamard NPT(0.4) of Guaranteed Packets, Format of Fig. 5.27a ; 1×512 Transforms, Image DOCUMENT.

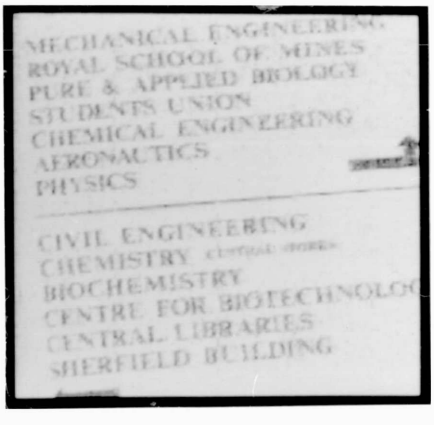


Fig. 5.35b : Hadamard NPT(0.4) Recons. From Guaranteed Packets, Format of Fig. 5.27a ; 1×512 Transforms, Image DOCUMENT. No Pre-/Post-Recons. Filtering.

The effectiveness of the reconstruction scheme when applied to different imagery types was also investigated. Fig. 5.33a shows the reconstructed picture obtained when 1×512 transforms of sub-blocks of the row-scanned image TEXTURE (reproduced in Fig. 5.32) are used, and the inverse Hadamard NPT(0.4) of received segments corresponding to the format of Fig. 5.27a is performed, with an offset of 125 added. The reconstructed picture obtained by application of the fast Hadamard NPT reconstruction algorithm to the received segments is shown in Fig. 5.33b. The subjective quality of the picture is also good, although the peak signal-to-noise ratio (PSNR) is lower than that of the reconstructed image ALAN, shown in Fig. 5.29b.

Fig. 5.35a shows the reconstructed picture obtained when 1×512 transforms of sub-blocks of the row-scanned image DOCUMENT (reproduced in Fig. 5.34) are used, and the inverse Hadamard NPT of received segments corresponding to the format of Fig. 5.27a is performed, with an offset of 125 added. The reconstructed picture obtained by application of the fast Hadamard NPT reconstruction algorithm to the received segments is shown in Fig. 5.35b. The above results show that the reconstruction algorithm is effective in reconstructing lost imagery data. It should be noted that the reconstructed pictures presented correspond to fifty percent packet loss.

In the above simulations, the same 8 bit/sample representation in the original image was retained for the transform samples. However, in applications where there are bandwidth limitations, there is the need for data compression of the information to be transmitted. The reconstruction from compressed packets of Hadamard NPT samples is addressed in chapter seven.

5.5 Summary and Conclusion

The one-dimensional Hadamard NPT domain has been proposed for signal transmission through channels whose quality and characteristics are unpredictable due to non-stationary noise processes or jamming. Signal degradation has been modelled as complete loss of segments of the transmission and the problem of reconstructing a time-varying one-dimensional signal from segments of its Hadamard NPT has been addressed.

Techniques for iteratively reconstructing a time-varying one-dimensional signal from segments of its Hadamard NPT have been developed. An iterative one-

dimensional Hadamard NPT reconstruction algorithm has been introduced. The algorithm requires an estimate of the signal amplitude over the available transform segments. The iterative reconstruction scheme converges for $\alpha \leq 0.464$. Closed-form reconstruction formulae for reconstruction from specific formats of Hadamard NPT segments have been derived. Detailed derivations of these have also been presented. The number of iterations required for convergence is a function of the reconstruction format and the threshold ϵ which measures the similarity between the received transform segments and the corresponding segment of the transform domain iteration vector, at the m^{th} iteration. For $\epsilon = 1 \times 10^{-2}$, between 5 and 28 iterations are required for convergence.

Two fast reconstruction schemes applicable to some signal loss formats, which provide solutions in one iteration, have been introduced.

The effectiveness of the Hadamard NPT reconstruction algorithm in retrieving lost data has been shown for stationary first order Gauss-Markov and speech signals. Pre- and post-reconstruction filtering has been shown to improve the quality of the reconstructed signals. A median-threshold-decision interpolating smoothing filter has been introduced for pre- and post-reconstruction filtering. The filter preserves details of the signal better than the median filter and the low pass filter. It is particularly effective for slowly varying signals but smooths out desirable details in speech signals for example.

Some of the reconstruction formats have been investigated for two-layer intraframe packet transmission of images. The scheme in which the least significant half of 1×512 transformed sub-blocks (i.e. samples 257 to 512) are selected as guaranteed packets yields the best reconstructed pictures and this has been proposed for packet transmission of images. Reconstructed pictures from guaranteed packets, corresponding to fifty percent packet loss have been presented. Two-level bi-directional detail-preserving median filtering has been shown to improve the subjective quality and peak signal-to-noise ratio of reconstructed pictures.

The Hadamard NPT reconstruction scheme has been successfully applied to intraframe packet transmission of different types of imagery.

CHAPTER SIX

ITERATIVE TWO-DIMENSIONAL HADAMARD NATURALNESS-PRESERVING TRANSFORM SIGNAL RECONSTRUCTION WITH APPLICATIONS TO TACTICAL IMAGERY TRANSMISSION

6.1 Introduction and Review of Previous Work

In chapter five, we were mainly concerned with the reconstruction of a time-varying one-dimensional signal from segments of its one-dimensional Hadamard NPT. We developed an iterative one-dimensional Hadamard NPT reconstruction algorithm which we successfully applied to intraframe packet transmission of imagery data.

However, in some applications where two-dimensional data has to be transmitted through channels whose quality and characteristics are unpredictable due to non-stationary noise processes or jamming, there is the constraint that the data be pre-processed in a format that would permit signal recovery in the event of loss of two-dimensional segments of the data. Thus, the focus of this chapter is on two-dimensional signal reconstruction. Specifically, we investigate two-dimensional Hadamard NPT reconstruction of signals that are transmitted through channels which are subject to non-stationary noise processes or jamming.

In military applications, the success of real-time battle planning and other service tactical planning depends on the successful acquisition, transmission and analysis of real-time imagery [54]. "Blocking " by the opposition [3] and other factors such as crowding of the frequency spectrum in times of crisis activity, failure of the error correcting code e.t.c. [54] may result in the loss of two-dimensional segments of the data. Two-dimensional Hadamard NPT reconstruction has important applications in this scenario; we shall be mainly concerned with the application of the two-dimensional Hadamard NPT to the reconstruction of images. A similar problem was considered in [3] but the solution presented assume the knowledge of flat pixel regions within the image. Such an assumption is invalid for highly active images or images with a complicated texture. Here, we introduce an algorithm which makes no such apriori assumption about the original image.

In section 6.2.1, two-dimensional Hadamard NPT pre-processing is discussed. The properties of the two-dimensional Hadamard NPT domain of a signal, which provides the basis for the proposed solution to the signal reconstruction problem are discussed. Section 6.2.2 deals with iterative two-dimensional Hadamard NPT reconstruction. An iterative two-dimensional Hadamard NPT reconstruction algorithm is presented. The algorithm differs from that reported in [3] in the sense that it makes no apriori assumption about the pixel values in the original image and furthermore, it is self-terminating. Examples of iterative two-dimensional Hadamard NPT reconstruction formats are discussed and a clear guideline on the choice of the Hadamard NPT basis parameter α that can be used for signal reconstruction is given.

The results of simulation of the reconstruction of real imagery data from some formats of two-dimensional Hadamard NPT segments are presented in section 6.3.

6.2 Signal Reconstruction From Two-Dimensional Hadamard NPT Segments

6.2.1 Two-Dimensional Hadamard NPT Pre-Processing

We represent the original $N \times N$ two-dimensional data by $\mathbf{F}$. The two-dimensional Hadamard NPT of the data is given by

$$\mathbf{T_F} = \psi\{\alpha\}\,\mathbf{F}\psi\{\alpha\} \tag{6.1}$$

where $\psi\{\alpha\}$ is as defined in (5.1). Thus, $\mathbf{T_F}$ can be expressed as

$$\mathbf{T_F} = \alpha^2\mathbf{F} + \alpha(1-\alpha)[\mathbf{H}_n\mathbf{F} + \mathbf{F}\mathbf{H}_n] + (1-\alpha)^2\mathbf{H}_n\mathbf{F}\mathbf{H}_n \tag{6.2}$$

Equation (6.2) expresses the two-dimensional Hadamard NPT of the data as being made up of three main terms viz a weighting of the original data (i.e. $\alpha^2\mathbf{F}$), a weighting of the sum of cross one-dimensional Hadamard transforms of the data (i.e. $\alpha(1-\alpha)[\mathbf{H}_n\mathbf{F} + \mathbf{F}\mathbf{H}_n]$) and a weighting of the two-dimensional Hadamard transform of the data (i.e. $(1-\alpha)^2\mathbf{H}_n\mathbf{F}\mathbf{H}_n$).

For convenience, we re-write (6.2) as

$$\mathbf{T_F} = \alpha^2\mathbf{F} + \mathbf{Y} \tag{6.3a}$$

where

$$\mathbf{Y} = \alpha(1-\alpha)[\mathbf{H}_n\mathbf{F} + \mathbf{F}\mathbf{H}_n] + (1-\alpha)^2\mathbf{H}_n\mathbf{F}\mathbf{H}_n \tag{6.3b}$$

By virtue of the decorrelation properties of the Hadamard transform, the components of $\alpha^2\mathbf{F}$ and that of $\mathbf{Y}$ are mutually uncorrelated. Furthermore, the correlation range of the weighted signal component, $\alpha^2\mathbf{F}$, is longer than that of the functions of one-dimensional and two-dimensional Hadamard transforms of the data, given by $\mathbf{Y}$.

In a typical scenario, we transmit the Hadamard NPT array $\mathbf{T_F}$ and receive a truncated data array $\tilde{\mathbf{T}}_\mathbf{F}$, which is $\mathbf{T_F}$ with some segments excised. Since the available Hadamard NPT segment(s) contains a weighting of the original data, i.e. $\alpha^2\mathbf{F}$, we can exploit the fact that the correlation range of $\alpha^2\mathbf{F}$ is longer than that of the component $\mathbf{Y}$ to derive an estimate of the signal amplitude, over the correctly received segments. We can then use the estimate derived to solve for an approximation of the lost signal information.

Analogous to one-dimensional Hadamard NPT signal reconstruction, the reconstruction problem comprise two sub-problems, viz

(i) an estimation problem

(ii) developing techniques for reconstructing a signal from segments of its two-dimensional Hadamard NPT.

Solutions to these problems are given in the next section.

6.2.2 Iterative Two-Dimensional Hadamard NPT Signal Reconstruction

Some important notation and operators are first introduced.

Notation :

$\mathbf{F}$ = original two-dimensional data array

$\mathbf{T_F}$ = $\psi\{\alpha\}\,\mathbf{F}\psi\{\alpha\}$; two-dimensional Hadamard NPT of $\mathbf{F}$

$\tilde{\mathbf{T}}_\mathbf{F}$ = truncated $\mathbf{T_F}$; two-dimensional Hadamard NPT of $\mathbf{F}$ with some segments (defined by a $2 \times n_L$ index array $\mathbf{KD}$) excised. n_L is the number of segments excised.

$\tilde{\mathbf{F}}$ = $\psi^{-1}\{\alpha\}\,\tilde{\mathbf{T}}_\mathbf{F}\psi^{-1}\{\alpha\}$; inverse two-dimensional Hadamard NPT of truncated $\mathbf{T_F}$.

$\hat{\mathbf{F}}^W$ = estimate of the original signal, derived from $\tilde{\mathbf{T}}_\mathbf{F}$– the components of $\hat{\mathbf{F}}^W$ are zero at locations corresponding to the truncated samples of $\mathbf{T_F}$ and contain an estimate of the signal amplitude over the known segments of $\mathbf{T_F}$.

$\hat{\mathbf{F}}_m$ = reconstruction of $\mathbf{F}$ at the m^{th} iteration.

$\hat{\mathbf{T}}_{\mathbf{F};m}$ = reconstruction of $\mathbf{T_F}$ at the m^{th} iteration.

Operators :

$\mathbf{S}(\cdot)$ = two-dimensional estimation operator

$\Phi_{\mathbf{KD}}$ = two-dimensional replacement operator, where **KD** is a $2 \times n_L$ array of indices. For example, the operation $\mathbf{A}\Phi_{\mathbf{KD}}\mathbf{B}$ where $\mathbf{KD} = \begin{bmatrix} I_1 & I_2 & I_3 & I_4 \\ J_1 & J_2 & J_3 & J_4 \end{bmatrix}$, replaces the components of matrix **A** whose indices (I, J) satisfy $I_1 \leq I \leq I_2$ and $J_1 \leq J \leq J_2$, with the corresponding components of matrix **B**, as well as replace the components of matrix **A** whose indices satisfy $I_3 \leq I \leq I_4$ and $J_3 \leq J \leq J_4$, with the corresponding components of matrix **B**.

The estimation of signal amplitude over the correctly received segments of $\mathbf{T_F}$ is then modelled by

$$\hat{\mathbf{F}}^W = \mathbf{S}\left(\tilde{\mathbf{T}}_{\mathbf{F}}\right) \tag{6.4}$$

The reconstruction, $\hat{\mathbf{F}}_m$, of $\mathbf{F}$ at the m^{th} iteration is given by

$$\hat{\mathbf{F}}_m = \left[\psi^{-1}\{\alpha\}\left(\hat{\mathbf{T}}_{\mathbf{F};m}\Phi_{\mathbf{KD}}\tilde{\mathbf{T}}_{\mathbf{F}}\right)\psi^{-1}\{\alpha\}\right]\Phi_{\mathbf{KD}}\hat{\mathbf{F}}^W \quad ; \; m = 1, 2, \ldots p \tag{6.5a}$$

where

$$\hat{\mathbf{T}}_{\mathbf{F};m} = \begin{cases} \psi\{\alpha\}\left(\hat{\mathbf{F}}_0\Phi_{\mathbf{KD}}\hat{\mathbf{F}}^W\right)\psi\{\alpha\} & m = 1 \\ \psi\{\alpha\}\hat{\mathbf{F}}_{m-1}\psi\{\alpha\} & m = 2, 3, \ldots p \end{cases} \tag{6.5b}$$

and

$$\hat{\mathbf{F}}_0 = \psi^{-1}\{\alpha\}\tilde{\mathbf{T}}_{\mathbf{F}}\psi^{-1}\{\alpha\} \tag{6.5c}$$

Fig. 6.1 is a detailed block diagram of the iterative two-dimensional reconstruction processor. The processor is made up of three main modules, viz :

(i) an "INITIALIZATION " module which implements equations (6.4) and (6.5*c*),

(ii) a "REPLACEMENT PROCESSOR " module (RPM) which carries out the replacement operations, and

(iii) an "ITERATION " module which implements the iterative reconstruction.

The replacement processor module is a general purpose one. The correct replacement is done by routing the signals through the correct ports. Port A in the RPM is a gated port which allows the signal $\hat{\mathbf{F}}_0$ from the initialization module to be used for replacement at the beginning of the iteration and the signal $\hat{\mathbf{F}}_m$

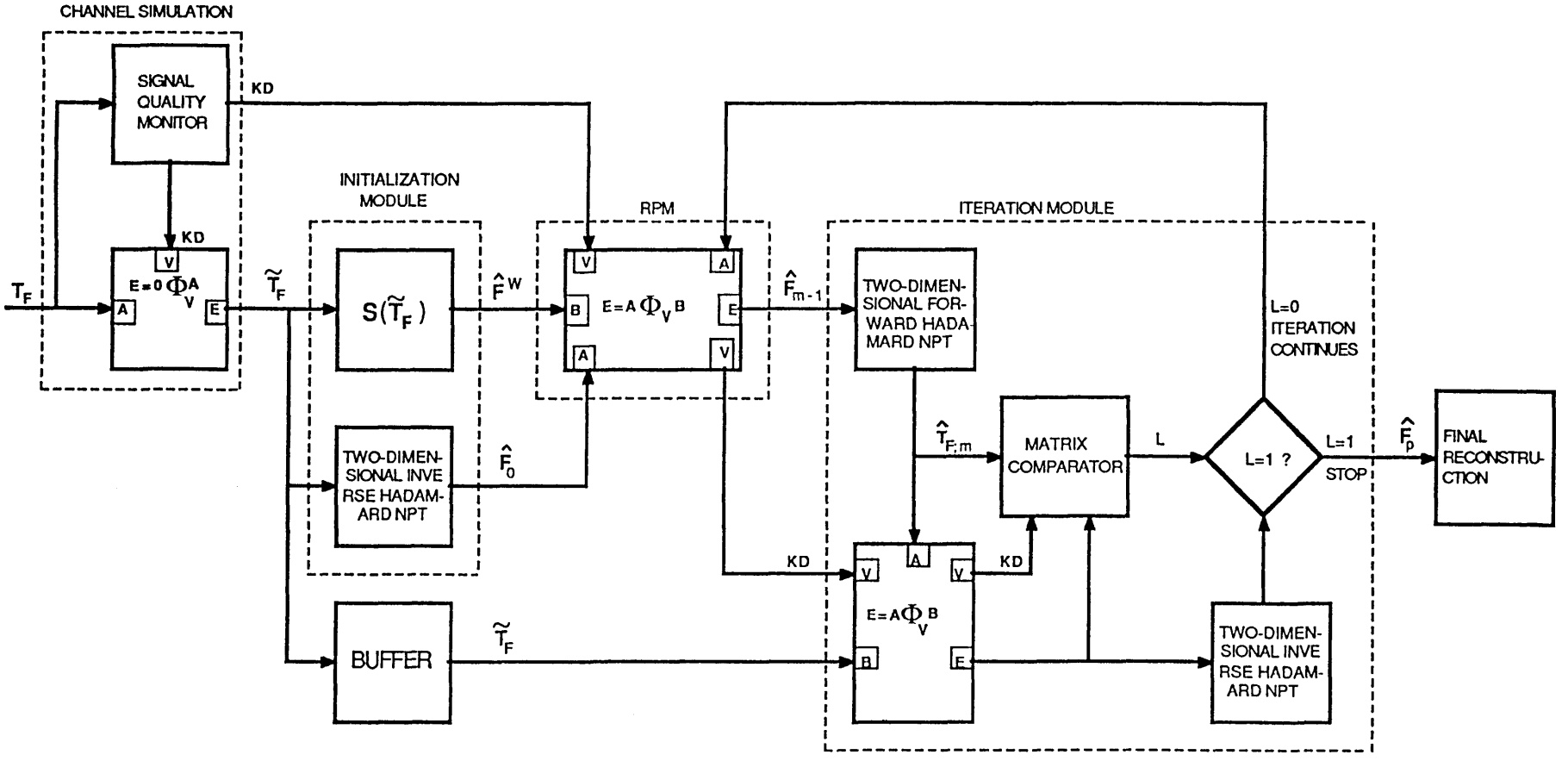


Fig. 6.1 : Detailed Block Diagram of Iterative Two-Dimensional Hadamard NPT Reconstruction Processor.

from the output of the iteration module to be used for replacement at subsequent iterations.

Defining

$$D^{(m)} = d\left(\tilde{\mathbf{T}}_{\mathbf{F}}, \hat{\mathbf{T}}_{\mathbf{F};m}\right)_{\mathbf{KD}} \tag{6.6}$$

as the mean-square error difference between the components of matrix $\tilde{\mathbf{T}}_{\mathbf{F}}$ and $\hat{\mathbf{T}}_{\mathbf{F};m}$ at the locations specified by **KD**, the matrix comparator terminates the iterative reconstruction when

$$\left|D^{(m+1)} - D^{(m)}\right| < \epsilon \tag{6.7}$$

subject to a maximum permissible number of iterations, where ϵ is a user-specified threshold. The choice of ϵ determines the number of iterations required for convergence.

The iterative reconstruction algorithm described by (6.5) converges for $\alpha \leq 0.464$; the proof of convergence is given in appendix III. For m iterations, the scheme requires $2m\,(3N^2 log_2 N + 5N^2)$ operations; conventional least squares solution requires approximately $3N^2 log_2 N + n_k n_u^2 + 5N^2$ operations [3], where n_k and n_u are the number of known and unknown samples of $\mathbf{T}_{\mathbf{F}}$ respectively.

It is worthwhile mentioning that the basic difference between the two-dimensional Hadamard NPT reconstruction processor and the one-dimensional Hadamard NPT reconstruction processor is that the one-dimensional operations in the latter processor are replaced by two-dimensional operations in the former processor.

6.2.2.1 Examples of Iterative Two-Dimensional Hadamard NPT Reconstruction Formats

The iterative reconstruction from specific formats of two-dimensional Hadamard NPT segments is now investigated in detail. In the examples, we consider an $N \times N$ data array and partition this into n_s segments, each of dimension $l_r \times l_c$ with the following constraints :

(i) n_s is an integral power of 2, and $n_s \geq 2$,

(ii) l_r and l_c are integral powers of 2,

(iii) $n_k = n_u$, where n_u is the number of missing samples and n_k is the number of received transform samples.

Thus, we identify two types of formats. The first type, which we shall refer to as "*Type - 1 Formats*", are such that either $l_r = N$ or $l_c = N$ and these are depicted in Fig. 6.2. The second type, which we shall refer to as "*Type - 2 Formats*", are such that $l_r = l_c < N$ and are depicted in Fig. 6.3.

1) Reconstruction From Type - 1 Formats

As an illustration, we shall consider the format of Fig. 6.2a with $n_s = 2$. For convenience, we express the original data array $\mathbf{F}$ as the partitioned matrix

$$\mathbf{F} = \begin{bmatrix} \mathbf{F}_{11} & \mathbf{F}_{12} \\ \mathbf{F}_{21} & \mathbf{F}_{22} \end{bmatrix} \tag{6.8}$$

while the NPT of $\mathbf{F}$ is given by the partitioned matrix

$$\mathbf{T}_{\mathbf{F}} = \begin{bmatrix} \mathbf{T}_{11} & \mathbf{T}_{12} \\ \mathbf{T}_{21} & \mathbf{T}_{22} \end{bmatrix} \tag{6.9}$$

where $\mathbf{T}_{ij}$ and $\mathbf{F}_{ij}$, $1 \leq i,j \leq 2$ are sub-matrices of dimension $\frac{N}{2} \times \frac{N}{2}$.

We define an error matrix $\mathbf{E}$ as

$$\mathbf{E} = \begin{bmatrix} \mathbf{E}_{11} & \mathbf{E}_{12} \\ \mathbf{E}_{21} & \mathbf{E}_{22} \end{bmatrix} \tag{6.10}$$

where $\mathbf{E}_{ij}$ is the sub-matrix of errors incurred in the estimation of the original two-dimensional signal segment $\mathbf{F}_{ij}$. In addition, we express the iteration matrices $\hat{\mathbf{F}}_m$ and $\hat{\mathbf{T}}_{\mathbf{F};m}$ in partitioned form as

$$\hat{\mathbf{F}}_m = \begin{bmatrix} \hat{\mathbf{F}}_{11}^{(m)} & \hat{\mathbf{F}}_{12}^{(m)} \\ \hat{\mathbf{F}}_{21}^{(m)} & \hat{\mathbf{F}}_{22}^{(m)} \end{bmatrix} \tag{6.11}$$

and

$$\hat{\mathbf{T}}_{\mathbf{F};m} = \begin{bmatrix} \hat{\mathbf{T}}_{11}^{(m)} & \hat{\mathbf{T}}_{12}^{(m)} \\ \hat{\mathbf{T}}_{21}^{(m)} & \hat{\mathbf{T}}_{22}^{(m)} \end{bmatrix} \tag{6.12}$$

respectively.

Using (5.1) and the recursive definition of a normalized natural Hadamard matrix of order N, given by (5.24), we express the forward Hadamard NPT kernel as

$$\psi\{\alpha\} = \begin{bmatrix} \left(\alpha \mathbf{I}_{\frac{N}{2}} + c_1 \mathbf{H}_{\frac{N}{2}}\right) & c_1 \mathbf{H}_{\frac{N}{2}} \\ c_1 \mathbf{H}_{\frac{N}{2}} & \left(\alpha \mathbf{I}_{\frac{N}{2}} - c_1 \mathbf{H}_{\frac{N}{2}}\right) \end{bmatrix} \tag{6.13a}$$

$$= \begin{bmatrix} \mathbf{P}_{11} & \mathbf{P}_{12} \\ \mathbf{P}_{21} & \mathbf{P}_{22} \end{bmatrix} \tag{6.13b}$$

where

$$c_1 = \frac{1-\alpha}{\sqrt{2}} \tag{6.13c}$$

Similarly, we express the inverse Hadamard NPT kernel as

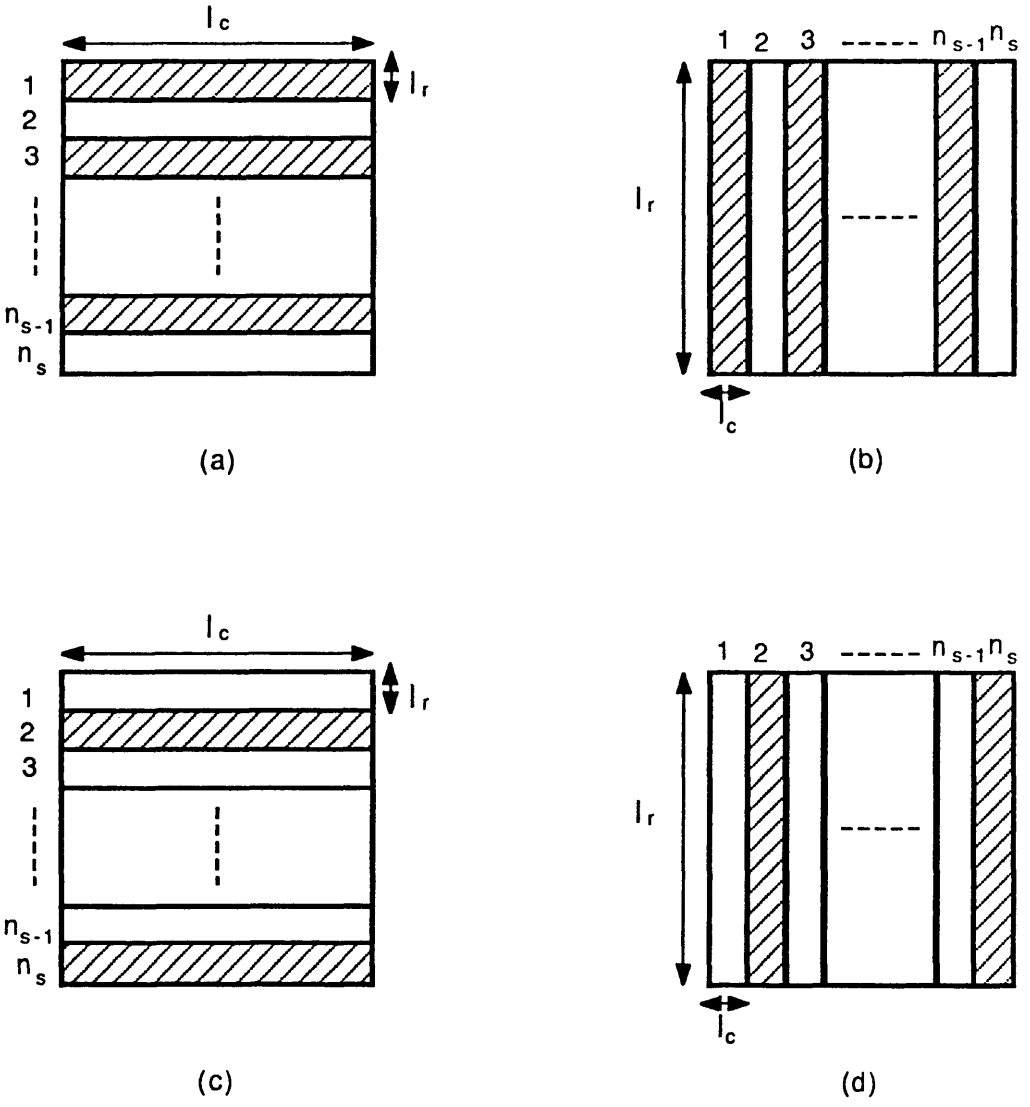
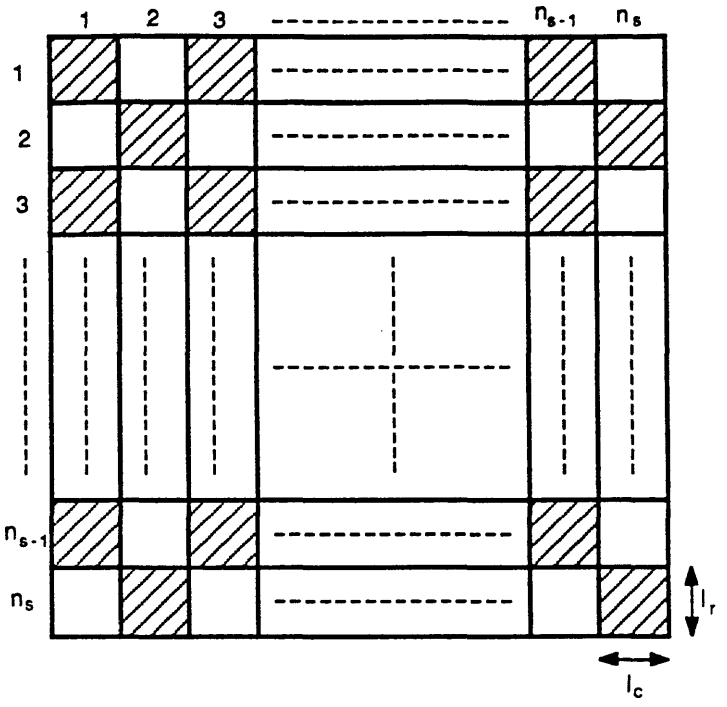
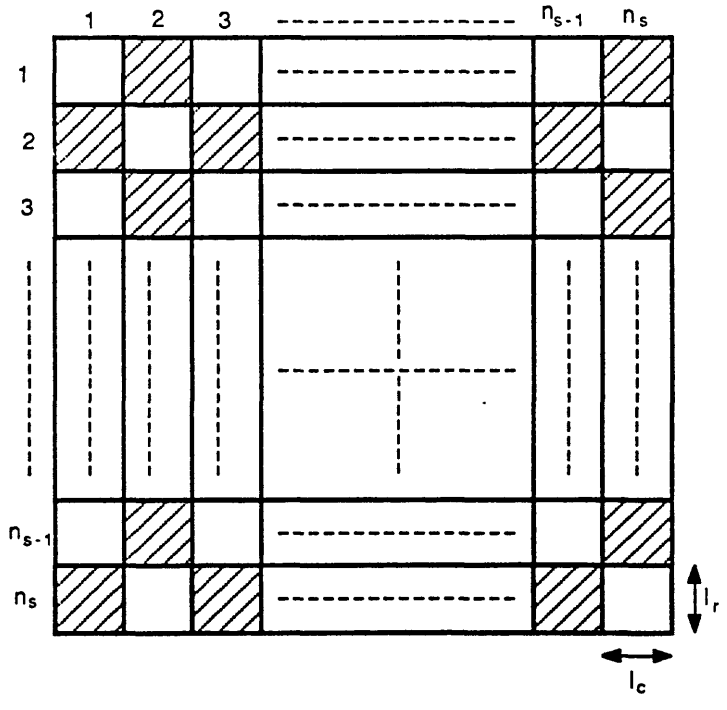


Fig. 6.2 : Type-1 Two-Dimensional Hadamard NPT Reconstruction Formats.



(a)



(b)

Fig. 6.3 : Type-2 Two-Dimensional Hadamard NPT Reconstruction Formats.

$$\psi^{-1}\{\alpha\} = \frac{1}{2\alpha - 1}\begin{bmatrix} \left(\alpha \mathbf{I}_{\frac{N}{2}} - c_1 \mathbf{H}_{\frac{N}{2}}\right) & -c_1 \mathbf{H}_{\frac{N}{2}} \\ -c_1 \mathbf{H}_{\frac{N}{2}} & \left(\alpha \mathbf{I}_{\frac{N}{2}} + c_1 \mathbf{H}_{\frac{N}{2}}\right) \end{bmatrix} \tag{6.14a}$$

$$= \begin{bmatrix} \mathbf{Q}_{11} & \mathbf{Q}_{12} \\ \mathbf{Q}_{21} & \mathbf{Q}_{22} \end{bmatrix} \tag{6.14b}$$

We can relate the two-dimensional transform segments $\mathbf{T}_{ij}$ in (6.9) to the two-dimensional signal segments in (6.8) as follows :

$$\mathbf{T}_{11} = \mathbf{P}_{11}\mathbf{F}_{11}\mathbf{P}_{11} + \mathbf{P}_{12}\mathbf{F}_{21}\mathbf{P}_{11} + \mathbf{P}_{11}\mathbf{F}_{12}\mathbf{P}_{21} + \mathbf{P}_{12}\mathbf{F}_{22}\mathbf{P}_{21} \tag{6.15a}$$

$$\mathbf{T}_{12} = \mathbf{P}_{11}\mathbf{F}_{11}\mathbf{P}_{12} + \mathbf{P}_{12}\mathbf{F}_{21}\mathbf{P}_{12} + \mathbf{P}_{11}\mathbf{F}_{12}\mathbf{P}_{22} + \mathbf{P}_{12}\mathbf{F}_{22}\mathbf{P}_{22} \tag{6.15b}$$

$$\mathbf{T}_{21} = \mathbf{P}_{21}\mathbf{F}_{11}\mathbf{P}_{11} + \mathbf{P}_{22}\mathbf{F}_{21}\mathbf{P}_{11} + \mathbf{P}_{21}\mathbf{F}_{12}\mathbf{P}_{21} + \mathbf{P}_{22}\mathbf{F}_{22}\mathbf{P}_{21} \tag{6.15c}$$

$$\mathbf{T}_{22} = \mathbf{P}_{21}\mathbf{F}_{11}\mathbf{P}_{12} + \mathbf{P}_{22}\mathbf{F}_{21}\mathbf{P}_{12} + \mathbf{P}_{21}\mathbf{F}_{12}\mathbf{P}_{22} + \mathbf{P}_{22}\mathbf{F}_{22}\mathbf{P}_{22} \tag{6.15d}$$

where the $\mathbf{P}_{ij}$, $1 \leq i,j \leq 2$ are defined in (6.13). We can also relate the original two-dimensional signal segments $\mathbf{F}_{ij}$ in (6.8) to the two-dimensional transform segments in (6.9) as follows :

$$\mathbf{F}_{11} = \mathbf{Q}_{11}\mathbf{T}_{11}\mathbf{Q}_{11} + \mathbf{Q}_{12}\mathbf{T}_{21}\mathbf{Q}_{11} + \mathbf{Q}_{11}\mathbf{T}_{12}\mathbf{Q}_{21} + \mathbf{Q}_{12}\mathbf{T}_{22}\mathbf{Q}_{21} \tag{6.16a}$$

$$\mathbf{F}_{12} = \mathbf{Q}_{11}\mathbf{T}_{11}\mathbf{Q}_{12} + \mathbf{Q}_{12}\mathbf{T}_{21}\mathbf{Q}_{12} + \mathbf{Q}_{11}\mathbf{T}_{12}\mathbf{Q}_{22} + \mathbf{Q}_{12}\mathbf{T}_{22}\mathbf{Q}_{22} \tag{6.16b}$$

$$\mathbf{F}_{21} = \mathbf{Q}_{21}\mathbf{T}_{11}\mathbf{Q}_{11} + \mathbf{Q}_{22}\mathbf{T}_{21}\mathbf{Q}_{11} + \mathbf{Q}_{21}\mathbf{T}_{12}\mathbf{Q}_{21} + \mathbf{Q}_{22}\mathbf{T}_{22}\mathbf{Q}_{21} \tag{6.16c}$$

$$\mathbf{F}_{22} = \mathbf{Q}_{21}\mathbf{T}_{11}\mathbf{Q}_{12} + \mathbf{Q}_{22}\mathbf{T}_{21}\mathbf{Q}_{12} + \mathbf{Q}_{21}\mathbf{T}_{12}\mathbf{Q}_{22} + \mathbf{Q}_{22}\mathbf{T}_{22}\mathbf{Q}_{22} \tag{6.16d}$$

The truncated two-dimensional Hadamard NPT transformed matrix, $\tilde{\mathbf{T}}_{\mathbf{F}}$, for the scenario being considered is given by

$$\tilde{\mathbf{T}}_{\mathbf{F}} = \begin{bmatrix} \mathbf{0} & \mathbf{0} \\ \mathbf{T}_{21} & \mathbf{T}_{22} \end{bmatrix} \tag{6.17}$$

The estimate, $\hat{\mathbf{F}}^W$, of the signal amplitude over the known transform segments, derived from $\tilde{\mathbf{T}}_{\mathbf{F}}$, can be expressed as

$$\hat{\mathbf{F}}^W = \begin{bmatrix} \mathbf{0} & \mathbf{0} \\ \hat{\mathbf{F}}_{21} & \hat{\mathbf{F}}_{22} \end{bmatrix} \tag{6.18a}$$

$$= \begin{bmatrix} \mathbf{0} & \mathbf{0} \\ \mathbf{F}_{21} + \mathbf{E}_{21} & \mathbf{F}_{22} + \mathbf{E}_{22} \end{bmatrix} \tag{6.18b}$$

The full derivation of iterates from (6.5), i.e. (6.19) to (6.43), is given in appendix IV (It should be noted that the equation numbers continues in the material in appendix IV).

At the m^{th} $(m \geq 1)$ iteration stage, the segments of the iteration matrix $\hat{\mathbf{T}}_{\mathbf{F};m}$ that is obtained are given by

$$\hat{\mathbf{T}}_{11}^{(m)} = g_m \mathbf{T}_{11} + V_m \left(\mathbf{P}_{12}\mathbf{E}_{21}\mathbf{P}_{11} + \mathbf{P}_{12}\mathbf{E}_{22}\mathbf{P}_{21}\right) \tag{6.40a}$$

$$\hat{\mathbf{T}}_{12}^{(m)} = g_m \mathbf{T}_{12} + V_m \left(\mathbf{P}_{12}\mathbf{E}_{21}\mathbf{P}_{12} + \mathbf{P}_{12}\mathbf{E}_{22}\mathbf{P}_{22}\right) \tag{6.40b}$$

$$\begin{aligned}\hat{\mathbf{T}}_{21}^{(m)} = \mathbf{T}_{21} + \frac{1}{2\alpha - 1}\Big\{&(1 - g_{m-1})\left(c_1^2 \mathbf{I}_{\frac{N}{2}} - \alpha c_1 \mathbf{H}_{\frac{N}{2}}\right)\mathbf{T}_{11} \\ &+ \left(V_{m-1}c_1^2 + 2\alpha - 1\right)\left(\alpha \mathbf{I}_{\frac{N}{2}} - c_1 \mathbf{H}_{\frac{N}{2}}\right)\left(\mathbf{E}_{21}\mathbf{P}_{11} + \mathbf{E}_{22}\mathbf{P}_{21}\right)\Big\}\end{aligned} \tag{6.40c}$$

and

$$\begin{aligned}\hat{\mathbf{T}}_{22}^{(m)} = \mathbf{T}_{22} + \frac{1}{2\alpha - 1}\Big\{&(1 - g_{m-1})\left(c_1^2 \mathbf{I}_{\frac{N}{2}} - \alpha c_1 \mathbf{H}_{\frac{N}{2}}\right)\mathbf{T}_{12} \\ &+ \left(V_{m-1}c_1^2 + 2\alpha - 1\right)\left(\alpha \mathbf{I}_{\frac{N}{2}} - c_1 \mathbf{H}_{\frac{N}{2}}\right)\left(\mathbf{E}_{21}\mathbf{P}_{12} + \mathbf{E}_{22}\mathbf{P}_{22}\right)\Big\}\end{aligned} \tag{6.40d}$$

where g_m is the convergence factor and V_m is the error matrix multiplying factor ; g_m and V_m are recursively given by

$$\begin{aligned} g_m &= \frac{1}{2\alpha - 1}\left(g_{m-1}\left(\alpha^2 - c_1^2\right) - c_1^2\right) \qquad m > 1 \ ; \\ g_0 &= 0 \ , \quad g_1 = \frac{-(1-\alpha)^2}{2(2\alpha - 1)} \end{aligned} \tag{6.41}$$

and

$$\begin{aligned} V_m &= \frac{1}{2\alpha - 1}\left(V_{m-1}\left(\alpha^2 - c_1^2\right) + 2\alpha - 1\right) \qquad m > 1 \ ; \\ V_0 &= 0 \ , \quad V_1 = 1 \end{aligned} \tag{6.42}$$

respectively.

Results of Empirical Investigations of The Behaviour of g_m and V_m

For convergence, the factor g_m in (6.40) must tend to unity with increasing number of iterations. Furthermore, the error multiplying factor V_m should also converge to a finite constant, with a low magnitude. It is observed that the expression for g_m is identical to that for one-dimensional Hadamard NPT reconstruction. Hence, the comments made in section 5.2.3.1 concerning the behaviour of g_m as a function of the number of iterations apply.

The expression for V_m is different from that for one-dimensional reconstruction. Fig. 6.4a shows the error multiplying factor V_m, given by (6.42), as a function of the number of iterations, for four values of α , $\alpha \leq 0.4$. It is observed that V_m converges to a finite constant which we have shown to be given by $\frac{2(1-2\alpha)}{(1-\alpha)^2}$. Fig. 6.4b shows the behaviour of V_m with increasing number of iterations, as the singularity at $\alpha = \frac{1}{2}$ is approached from the left. We can observe oscillations in the values of V_m

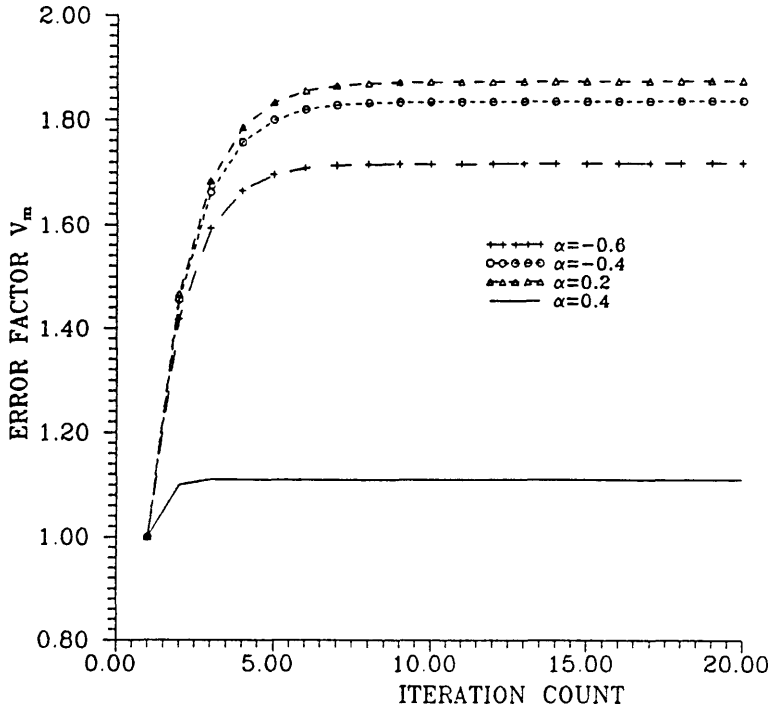


Fig. 6.4a : Error multiplying factor V_m as a function of iteration count; iterative two-dimensional Hadamard NPT reconstruction at $\alpha < 0.45$.

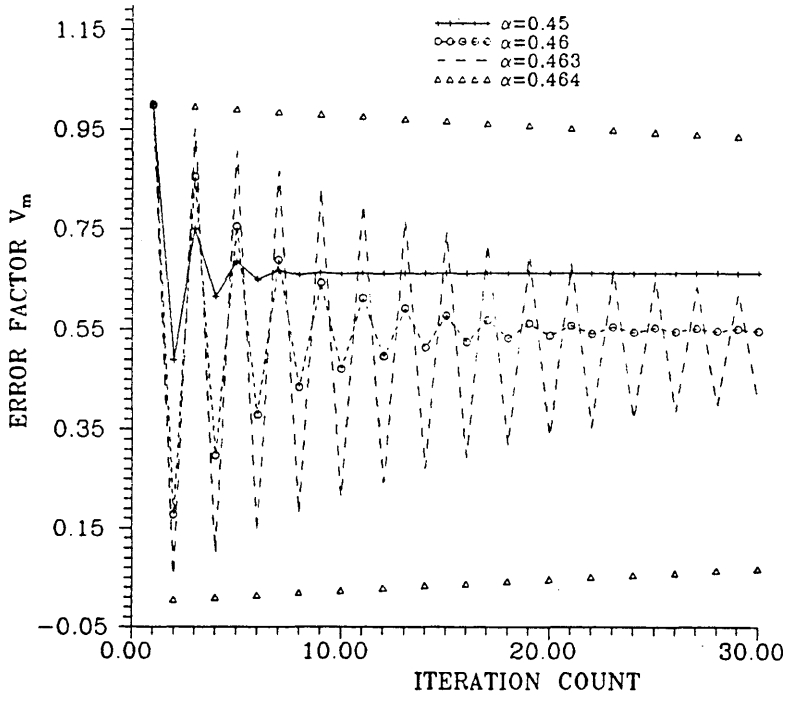


Fig. 6.4b : Error multiplying factor V_m as a function of iteration count; iterative two-dimensional Hadamard NPT reconstruction at $0.45 \leq \alpha < 0.49$.

as iteration progresses, for values of α in the range $0.45 \leq \alpha \leq 0.464$ (it should be noted that the points corresponding to $\alpha = 0.464$ are not joined by a continuous line in the plots). In addition the amplitude of the bounded oscillations increase with increasing values of α in this range but the amplitude of the oscillations decrease with iteration. The oscillations eventually get damped out and convergence is obtained, however, the number of iterations required increases with increasing values of α. For $0.464 < \alpha < 0.5$, the amplitude of the oscillations increase with iteration and eventually become unbounded. Thus, convergence is not obtained for values of α in the range $0.464 < \alpha < 0.5$.

The conclusion that can be drawn from the empirical investigations is that the iterative two-dimensional Hadamard NPT reconstruction algorithm converges for $\alpha \leq 0.464$.

General Result For The Reconstruction From Type - 1 Formats

Based on the results of analyses and simulations, we have shown that for Type - 1 formats, we can express the reconstruction of the missing transform segments at the m^{th} iteration, in terms of the desired (but unknown) transform segments, as

$$\hat{\mathbf{T}}_{ij}^{(m)} = g_m \mathbf{T}_{ij} + \mathcal{F}(E(m,n)) \quad , \; m,n \in \mathbf{KD} \tag{6.44}$$

where i,j index the $l_r \times l_r$ square (in the case of the formats of Fig. 6.2a and Fig. 6.2c) or $l_c \times l_c$ square (in the case of the formats of Fig. 6.2b and Fig. 6.2d) segments of the partitioned matrices $\hat{\mathbf{T}}_{\mathbf{F};m}$ and $\mathbf{T}_{\mathbf{F}}$, $\mathcal{F}(E(m,n))$ is a function of the errors incurred in the estimation of the segments of the original signal from the correctly received two-dimensional Hadamard NPT samples and g_m is the convergence factor which has the same numerical value as that given by (6.41).

In general, the iterative two-dimensional Hadamard NPT reconstruction from these formats yield the required solutions.

2) Reconstruction From Type - 2 Formats

We shall use the format of Fig. 6.3b when $n_s = 2$, as an illustration. Using (6.5), we have shown that we can express the segments of the transform domain iteration matrix at the first iteration, i.e. $\hat{\mathbf{T}}_{\mathbf{F};1}$, as follows

$$\begin{aligned}\hat{\mathbf{T}}_{11}^{(1)} = \mathbf{T}_{11} - \frac{\alpha^2}{(2\alpha-1)^2}\left[\mathbf{T}_{12}\left(c_1^2\mathbf{I}_{\frac{N}{2}} + \alpha c_1 \mathbf{H}_{\frac{N}{2}}\right) + \left(c_1^2\mathbf{I}_{\frac{N}{2}} + \alpha c_1 \mathbf{H}_{\frac{N}{2}}\right)\mathbf{T}_{21}\right] \\ + \mathbf{P}_{11}\mathbf{E}_{11}\mathbf{P}_{11} + \mathbf{P}_{12}\mathbf{E}_{22}\mathbf{P}_{21}\end{aligned} \tag{6.45a}$$

$$\hat{\mathbf{T}}_{12}^{(1)} = -\frac{2c_1^2\left(\alpha^2 - c_1^2\right)}{(2\alpha-1)^2}\mathbf{T}_{12} + \frac{2}{(2\alpha-1)^2}\left(c_1^2\mathbf{I}_{\frac{N}{2}} + \alpha c_1\mathbf{H}_{\frac{N}{2}}\right)\mathbf{T}_{21}\left(c_1^2\mathbf{I}_{\frac{N}{2}} - \alpha c_1\mathbf{H}_{\frac{N}{2}}\right) + \mathbf{P}_{11}\mathbf{E}_{11}\mathbf{P}_{12} + \mathbf{P}_{12}\mathbf{E}_{22}\mathbf{P}_{22} \tag{6.45b}$$

$$\hat{\mathbf{T}}_{21}^{(1)} = -\frac{2c_1^2\left(\alpha^2 - c_1^2\right)}{(2\alpha-1)^2}\mathbf{T}_{21} + \frac{2}{(2\alpha-1)^2}\left(c_1^2\mathbf{I}_{\frac{N}{2}} - \alpha c_1\mathbf{H}_{\frac{N}{2}}\right)\mathbf{T}_{12}\left(c_1^2\mathbf{I}_{\frac{N}{2}} + \alpha c_1\mathbf{H}_{\frac{N}{2}}\right) + \mathbf{P}_{21}\mathbf{E}_{11}\mathbf{P}_{11} + \mathbf{P}_{22}\mathbf{E}_{22}\mathbf{P}_{21} \tag{6.45c}$$

$$\hat{\mathbf{T}}_{22}^{(1)} = \mathbf{T}_{22} + \frac{\alpha^2}{(2\alpha-1)^2}\left[\left(c_1^2\mathbf{I}_{\frac{N}{2}} - \alpha c_1\mathbf{H}_{\frac{N}{2}}\right)\mathbf{T}_{12} + \mathbf{T}_{21}\left(c_1^2\mathbf{I}_{\frac{N}{2}} - \alpha c_1\mathbf{H}_{\frac{N}{2}}\right)\right] + \mathbf{P}_{21}\mathbf{E}_{11}\mathbf{P}_{12} + \mathbf{P}_{22}\mathbf{E}_{22}\mathbf{P}_{22} \tag{6.45d}$$

It is observed that the reconstruction of the missing transform segments $\hat{\mathbf{T}}_{12}^{(1)}$ and $\hat{\mathbf{T}}_{21}^{(1)}$ each contain linear combinations of the desired (but unknown) transform segments $\mathbf{T}_{12}$ and $\mathbf{T}_{21}$. Since the desired transform segments are coupled in the equations, the iterative two-dimensional Hadamard NPT reconstruction from (6.5) would not yield the required solution.

Based on analyses of additional cases and simulations, we have confirmed that the iterative two-dimensional Hadamard NPT reconstruction algorithm would not yield the required solutions for Type - 2 formats.

6.2.2.2 Fast Reconstruction Algorithm

This algorithm provides the required solutions in a single iteration and it is only valid for reconstruction from Type - 1 formats.

The algorithm is based on dividing the reconstruction of the lost transform segments, at the first iteration, by the convergence factor

$$g_1 = -\frac{(1-\alpha)^2}{2(2\alpha-1)} \tag{6.46}$$

Replacement with known segments from $\tilde{\mathbf{T}}_{\mathbf{F}}$ and subsequent inverse two-dimensional Hadamard NPT yields the required solution. For the format of Fig. 6.2a, we have shown that the segments of the final reconstructed signal, $\hat{\mathbf{F}}$, are given by

$$\hat{\mathbf{F}}_{11} = \mathbf{F}_{11} + \mathbf{E}_{21} - \frac{\sqrt{2}\alpha}{1-\alpha}\mathbf{H}_{\frac{N}{2}}\mathbf{E}_{21} \tag{6.47a}$$

$$\hat{\mathbf{F}}_{12} = \mathbf{F}_{12} + \mathbf{E}_{22} - \frac{\sqrt{2}\alpha}{1-\alpha}\mathbf{H}_{\frac{N}{2}}\mathbf{E}_{22} \tag{6.47b}$$

$$\hat{\mathbf{F}}_{21} = \mathbf{F}_{21} + \mathbf{E}_{21} \tag{6.47c}$$

$$\hat{\mathbf{F}}_{22} = \mathbf{F}_{22} + \mathbf{E}_{22} \tag{6.47d}$$

The iterative reconstruction algorithm given by (6.5) also converges to the same solution.

6.2.2.3 Signal Estimation From Two-Dimensional Hadamard NPT Segments

The two-dimensional Hadamard NPT reconstruction algorithm requires an estimate of the signal amplitude over the available transform segments. The quality of the reconstructed signal depends on how well we can estimate the original signal amplitude from the known transform segments.

We stated in section 6.2.1 that the two-dimensional Hadamard NPT domain of a signal $\mathbf{F}$, consists of a weighted original signal component, i.e. $\alpha^2\mathbf{F}$, and another component, $\mathbf{Y}$, which is a function of one-dimensional and two-dimensional Hadamard transforms of the original data (refer to (6.3)). Here, we make use of the fact that the correlation range of the original signal component, i.e. $\alpha^2\mathbf{F}$, is longer than that of the functions of the one-dimensional and two-dimensional Hadamard transforms of the signal, i.e. component $\mathbf{Y}$, to derive an estimate of the original signal component over the available transform segments. Specifically, we employ a two-dimensional adaptive line enhancer (TDALE).

The two-dimensional adaptive line enhancer is a two-dimensional Wiener filter [67,68], which uses a delayed version of the noisy signal as the reference input to the filter. The application of two-dimensional adaptive line enhancing techniques to the estimation of the signal samples $\hat{\mathbf{F}}^W(i,j)$, $i,j \in \mathbf{KD}$, corresponding to the truncated Hadamard NPT matrix $\tilde{\mathbf{T}}_\mathbf{F}$, is described in Fig. 6.5. The arrangement treats the signal component $\alpha^2\mathbf{F}(i,j)$ as "noise " ; thus, the primary input consists of the signal $\mathbf{Y}(i,j)$ and an additive "noise " component $\alpha^2\mathbf{F}(i,j)$, $i,j \in \mathbf{KD}$. The reference input is obtained by passing the signal at the primary input through a two-dimensional delay operator, which delays the signal by Δ_i units along the vertical direction and by Δ_j units along the horizontal direction. The filter used is an $L \times L$ causal adaptive FIR filter.

During the k^{th} iteration, the filter output $\mathbf{F}^O(i,j)$, is obtained by forming the dot product of the filter weight matrix $\mathbf{W}_k$, given by

$$\mathbf{W}_k = \begin{bmatrix} \mathbf{W}_k(0,0) & \mathbf{W}_k(0,1) & \dots & \mathbf{W}_k(0,L-1) \\ \mathbf{W}_k(1,0) & \mathbf{W}_k(1,1) & \dots & \mathbf{W}_k(1,L-1) \\ \vdots & \vdots & \ddots & \vdots \\ \mathbf{W}_k(L-1,0) & \mathbf{W}_k(L-1,1) & \dots & \mathbf{W}_k(L-1,L-1) \end{bmatrix} \tag{6.48}$$

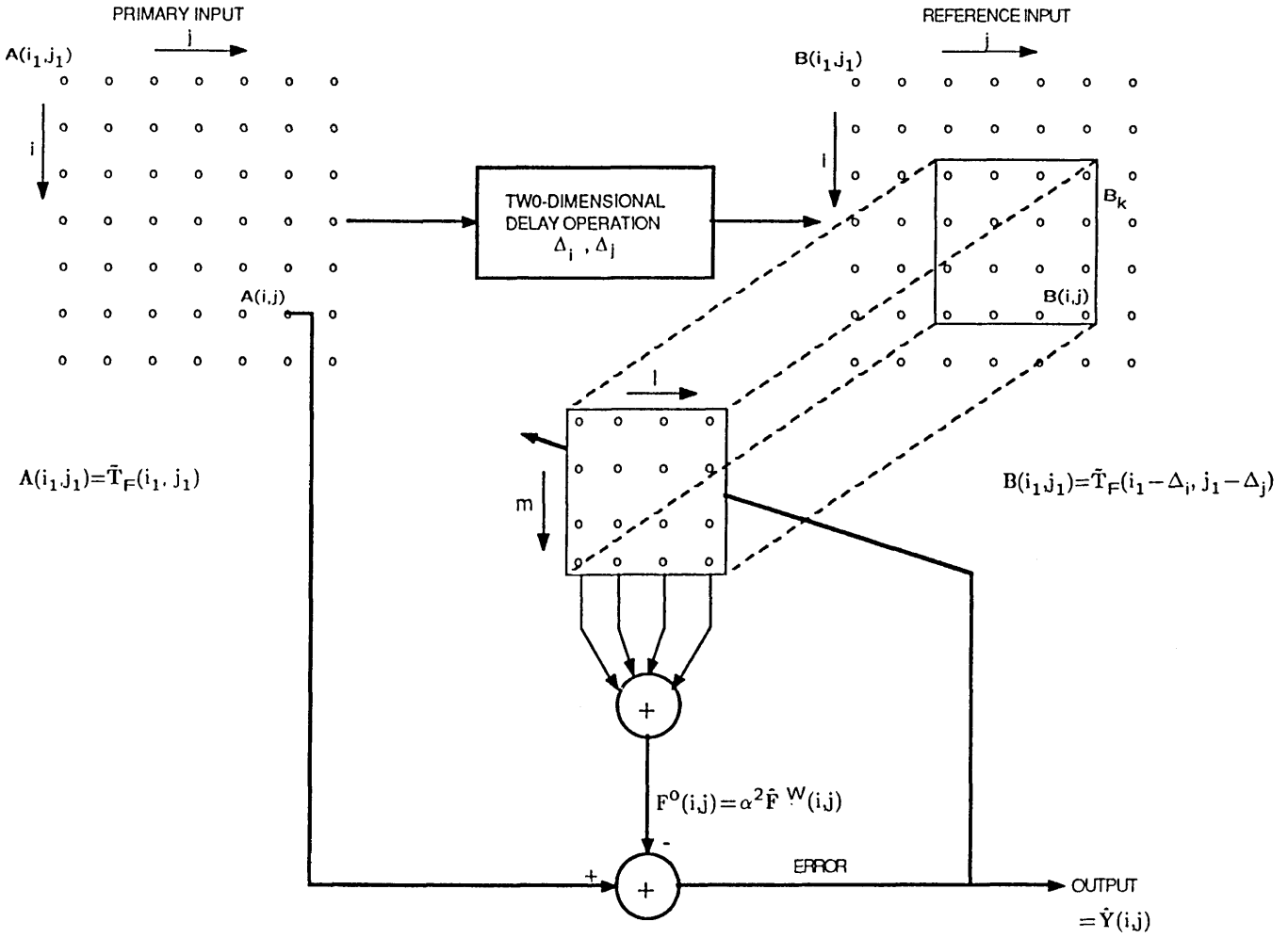


Fig. 6.5 : Two-Dimensional Adaptive Line Enhancer Estimation of Signal Matrix F^{w} From The Truncated Hadamard NPT Matrix, T_F ; i,j $\in$ KD.

with the input data matrix $\mathbf{B}_k$, given by

$$\mathbf{B}_k = \begin{bmatrix} \mathbf{B}(i,j) & \mathbf{B}(i,j-1) & \dots & \mathbf{B}(i,j-L+1) \\ \mathbf{B}(i-1,j) & \mathbf{B}(i-1,j-1) & \dots & \mathbf{B}(i-1,j-L+1) \\ \vdots & \vdots & \ddots & \vdots \\ \mathbf{B}(i-L+1,j) & \mathbf{B}(i-L+1,j-1) & \dots & \mathbf{B}(i-L+1,j-L+1) \end{bmatrix} \tag{6.49}$$

where $\mathbf{B}_k(m,l) = \mathbf{B}(i-m, j-l)$ for $m,l = 0,1,\dots L-1$. The filter output is thus given by

$$\mathbf{F}^O(i,j) = \sum_{m=0}^{L}\sum_{l=0}^{L}\mathbf{W}_k(m,l)\mathbf{B}_k(m,l) \tag{6.50a}$$

$$= \sum_{m=0}^{L}\sum_{l=0}^{L}\mathbf{W}_k(m,l)\mathbf{B}_k(i-m,j-l) \tag{6.50b}$$

By selecting the delays Δ_i and Δ_j to be longer than the effective vertical and horizontal correlation lengths respectively, of the component $\mathbf{Y}(i,j)$ and shorter than the effective vertical and horizontal correlation lengths of the component $\alpha^2\mathbf{F}(i,j)$, the two-dimensional adaptive Wiener filter will respond to cancel an estimate of the $\alpha^2\mathbf{F}(i,j)$ component from the TDALE output as shown in Fig. 6.5. It is these estimates of $\alpha^2\mathbf{F}(i,j)$ that are used to generate the components of the estimation matrix $\hat{\mathbf{F}}^W$.

The adaptive filter weights are iteratively adjusted according to the relation

$$\mathbf{W}_{k+1} = \mathbf{W}_k + \Delta\mathbf{W}_k \tag{6.51}$$

where $\Delta\mathbf{W}_k$ is the correction term at instant k , $k = iN + j$, determined by using an adaptive algorithm, so as to minimize the expected error signal power. We make use of the two-dimensional adaptive LMS algorithm (TDLMS), a detailed description and analysis of which can be found in [68]. It is worthwhile mentioning the fact that the TDLMS algorithm does not require any apriori information about the signal or the noise statistics or correlation properties.

6.3 Simulation, Results and Discussion

The two-dimensional Hadamard NPT reconstruction algorithm was simulated for some reconstruction formats, using 256 x 256, 8-bit monochrome images. The formats investigated are shown in Fig. 6.6, where the hatched segments are unknown.

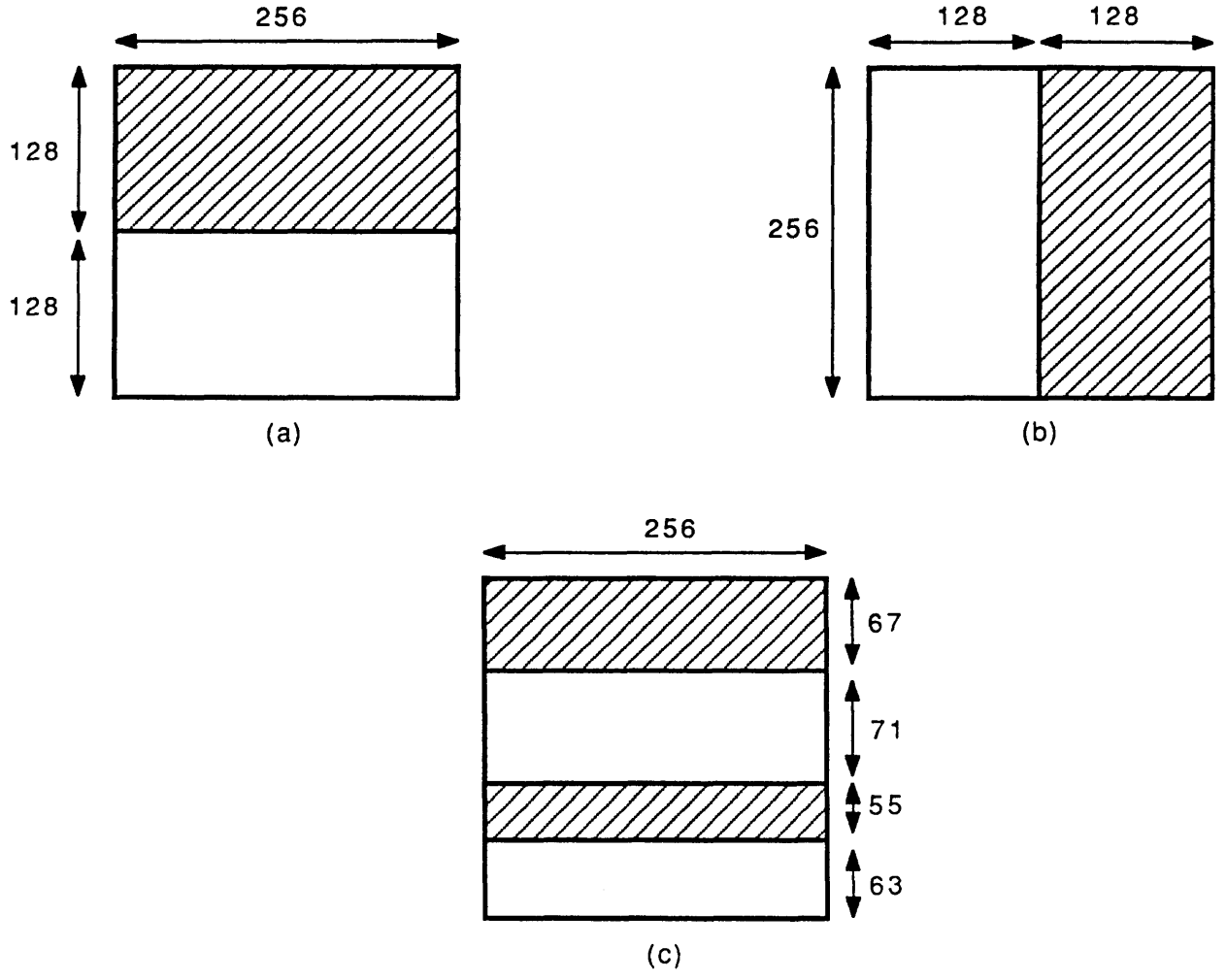


Fig. 6.6 : Some Two-Dimensional Hadamard NPT Reconstruction Formats.

In the simulations, a 2×2 adaptive Wiener filter was used in the TDALE algorithm; the 2×2 filter was found to yield the best results. The first twenty lines of transform samples were used to initialize the algorithm, the LMS adaptation parameter μ was set equal to 7×10^{-7} and delays $\Delta_i = 1$ and $\Delta_j = 1$ were used for generating the reference signal. Prior to the reference signal generation, where applicable, the "dc " coefficient in the received samples was normalized by the two-dimensional "Coefficient Magnitude Expansion Factor for DC Values ", (obtained from (2.45)). Similarly, the "ac " coefficients along the first row and the first column of the array $\tilde{\mathbf{T}}_{\mathbf{F}}$ were normalized by the one-dimensional "Coefficient Magnitude Expansion Factor for DC Values ", (obtained from (2.45)). If the dynamic range of these samples is not reduced, their high magnitude, which is mainly due to the component of the matrix $\mathbf{Y}$, has the effect of creating a low instantaneous signal-to-noise ratio which causes the TDALE to momentarily switch off.

Fig. 6.7a shows the result of inverse two-dimensional Hadamard NPT(0.45) of the received samples corresponding to the format of Fig. 6.6a; the original signal is the image ALAN shown in Fig. 2.7. Most of the information in the original picture has been completely lost. Fig. 6.7b shows the result of applying the fast two-dimensional Hadamard NPT(0.45) reconstruction algorithm to the received samples corresponding to the format of Fig. 6.6a; an MSE of 2441.2 was obtained. It is observed that a greatly improved reconstructed picture is obtained but there is a great deal of distortion in the picture.

Fig. 6.8a shows the result of performing the inverse two-dimensional Hadamard NPT(0.45) of the received samples corresponding to the format of Fig. 6.6b; the original signal is image ALAN shown in Fig. 2.7. There is a great deal of distortion in the reconstructed picture. Fig. 6.8b shows the result of applying the fast two-dimensional Hadamard NPT(0.45) reconstruction algorithm to the received samples corresponding to the format of Fig. 6.6b. This picture contains more information about the original image than that obtained in the picture shown in Fig. 6.8a. An MSE of 2377.2 was obtained and there is a great deal of distortion, noticeable in the reconstructed picture.

Fig. 6.6c is a format to which the fast reconstruction algorithm cannot be applied. However, a solution can be obtained by using the iterative reconstruction algorithm described by (6.5). It was observed empirically that the iterative scheme only yields the required solution for this format, when $\alpha \leq 0.41$. This implies that

the result obtained from the convergence factor g_m in section 6.2.2.1 only apply to fast reconstruction formats. The non-convergence of the algorithm for this format, when $0.41 < \alpha \leq 0.464$, may be attributed to finite computational accuracy. Fig. 6.9a shows the result of inverse two-dimensional Hadamard NPT(0.4) of the received samples corresponding to the format of Fig. 6.6c; the original signal is image ALAN shown in Fig. 2.7. It is observed that the information in the reconstructed picture has been completely lost. Fig. 6.9b shows the result of applying the iterative two-dimensional Hadamard NPT(0.4) reconstruction algorithm to the received transform samples. The converged weights for the first segment were used to initialize the signal amplitude estimation from the second segment of available transform samples. The threshold $\epsilon = 1 \times 10^{-2}$ was used and 23 iterations were required for convergence. An MSE of 4976.3 was obtained and there is a great deal of distortion noticeable in the reconstructed picture, however, some details in the picture are comprehensible.

Some pre-/post-reconstruction filtering techniques were investigated for improving the subjective quality of the reconstructed pictures. In the reconstructed pictures presented above, pixel values lying outside the range 0 to 255 were simply clipped. A pre-/post-reconstruction filtering technique that was devised simply makes a substitution for a pixel value lying outside the range 0 to 255. The pixel value used for substitution is obtained by calculating the median of pixel values lying between 0 and 255 within a window, centred around the pixel whose value is in error. There is the constraint that a minimum number of pixels be used for the median calculation. If this number is not achieved, the window size is increased until the required minimum number of pixels is achieved. Fig. 6.10a shows the result of applying the fast Hadamard NPT(0.45) reconstruction algorithm to the received segments corresponding to the format of Fig. 6.6a, with pre- and post-reconstruction filtering, using the above technique; the original image is ALAN shown in Fig. 2.7. A 3×3 window was used and the minimum number of pixels was set at 4. An MSE of 1693.7 was obtained. The subjective quality of the picture is better than that obtained without applying any pre-/post-reconstruction filtering, shown in Fig. 6.7b. Fig. 6.10b shows the result of applying the fast two-dimensional Hadamard NPT(0.45) reconstruction algorithm to the received samples corresponding to the format of Fig. 6.6a, with pre- and post-reconstruction filtering using a combination of the pixel substitution technique and two-level bi-directional detail-preserving median filtering [66]; the original image is ALAN

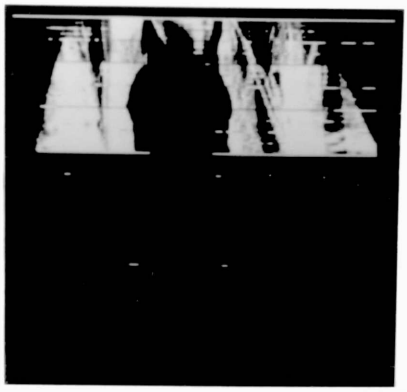


Fig. 6.7a : Inverse 2-D Hadamard NPT(0.45) of Received Samples, Format of Fig. 6.6a, Image ALAN.

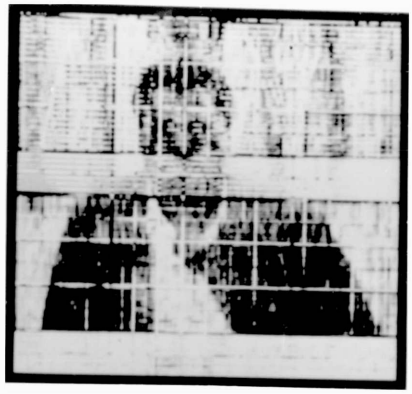


Fig. 6.7b : Fast 2-D Hadamard NPT(0.45) Recons., Format of Fig. 6.6a, Image ALAN. No Pre-/Post-Recons. Filtering.

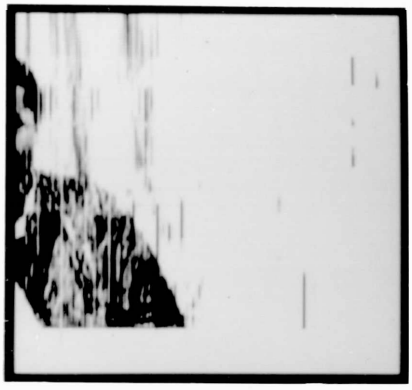


Fig. 6.8a : Inverse 2-D Hadamard NPT(0.45) of Received Samples, Format of Fig. 6.6b, Image ALAN.



Fig. 6.8b : Fast 2-D Hadamard NPT(0.45) Recons., Format of Fig. 6.6b, Image ALAN. No Pre-/Post-Recons. Filtering.

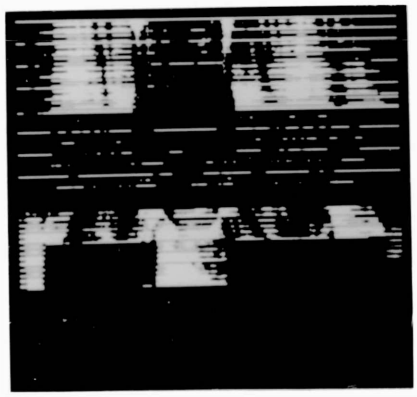


Fig. 6.9a : Inverse 2-D Hadamard NPT(0.4) of Received Samples, Format of Fig. 6.6c, Image ALAN.

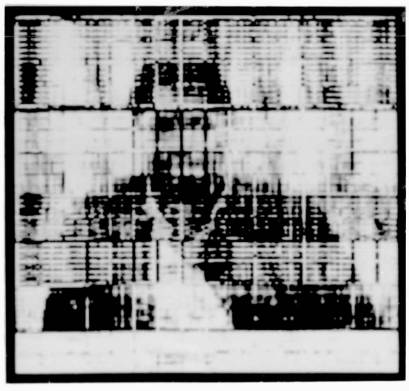


Fig. 6.9b : Iterative 2-D Hadamard NPT(0.4) Recons., Format of Fig. 6.6c, Image ALAN. No Pre-/Post-Recons. Filtering.

shown in Fig. 2.7. A 5×5 window was used for the detail-preserving filtering while the previously mentioned parameters were used for the pixel substitution technique. A lower MSE of 696.3 was obtained and the subjective quality of the reconstructed picture is better than that of Fig. 6.10a.

Using the fast reconstruction algorithm, it is possible to obtain the reconstruction of a signal from segments of its two-dimensional Hadamard NPT, when $\alpha > \frac{1}{2}$. Fig. 6.11a shows the result of inverse two-dimensional Hadamard NPT(0.75) of the received samples corresponding to the format of Fig. 6.6a; the original signal is the image ALAN shown in Fig. 2.7. It is observed that the image information over the segments corresponding to the received transform samples is comprehensible. Fig. 6.11b shows the result of applying the fast two-dimensional Hadamard NPT(0.75) reconstruction algorithm to the received samples corresponding to the format of Fig. 6.6a, with pre- and post-reconstruction pixel substitution; an MSE of 1622.8 was obtained. The subjective quality of the segment corresponding in location to the known transform samples is very good. However, there is a great deal of distortion in the reconstructed segment corresponding in location to the unknown transform samples. This can be attributed to the factor $\frac{\sqrt{2}\alpha}{1-\alpha}$ in (6.47*a*) and (6.47*b*) multiplying the sub-Hadamard transform of the respective estimation errors. Since this factor is greater than unity for $\alpha > \frac{1}{2}$, it has the effect of amplifying the errors.

The two-dimensional Hadamard NPT reconstruction algorithm was also applied to an image having a complicated texture. In this case, we observed that the subjective quality of the reconstructed image depends on the reconstruction format. For example, using the original image TEXTURE shown in Fig. 2.11, the reconstructed segment corresponding in location to the unknown transform samples, from the format of Fig. 6.6a, has no resemblance to that in the original image. Fig. 6.12a shows the result of applying the fast two-dimensional Hadamard NPT(0.45) reconstruction algorithm to the received samples corresponding to the format of Fig. 6.6b, with pre- and post-reconstruction pixel substitution; the original image is TEXTURE. An MSE of 2515.9 was obtained. Some details in the reconstructed picture are comprehensible but there are noticeable distortions in the picture. Fig. 6.12b shows the corresponding result when $\alpha = 0.75$. Again, we observe that the subjective quality of the segment corresponding in location to the known transform segments is very good. However, the segment corresponding in



Fig. 6.10a : Fast 2-D Hadamard NPT (0.45) Recons., Format of Fig. 6.6a, Image ALAN. Pre- and Post-Recon. Pixel Substitution.



Fig. 6.10b : Fast 2-D Hadamard NPT(0.45) Recons., Format of Fig. 6.6a, Image ALAN. Pre- and Post-Recon. Pixel Subs. and Detail-Preserving Median Filtering ($2LM^{+}$).



Fig. 6.11a : Inverse 2-D Hadamard NPT(0.75) of Received Samples, Format of Fig. 6.6a, Image ALAN.



Fig. 6.11b : Fast 2-D Hadamard NPT(0.75) Recons., Format of Fig. 6.6a, Image ALAN. Pre- and Post-Recon. Pixel Substitution.

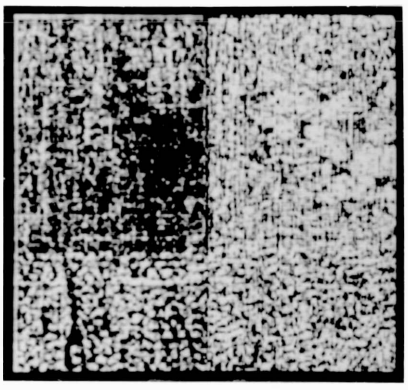


Fig. 6.12a : Fast 2-D Hadamard NPT(0.45) Recon., Format of Fig. 6.6b, Image TEXTURE Pre- and Post-Recon. Pixel Substitution.



Fig. 6.12b : Fast 2-D Hadamard NPT(0.75) Recon., Format of Fig. 6.6b, Image TEXTURE Pre- and Post-Recon. Pixel Substitution.

location to the missing transform samples is greatly distorted, for reasons already given.

6.4 Summary and Conclusion

The problem of transmitting two-dimensional signals through channels whose quality and characteristics are unpredictable due to non-stationary noise processes or jamming has been considered in this chapter. The two-dimensional Hadamard NPT domain has been investigated for such applications. The focus has been on the transmission of tactical imagery data. Signal degradation has been modelled as a complete loss of segments of the transmission and the problem of reconstructing a signal from segments of its two-dimensional Hadamard NPT has been addressed.

Techniques for iteratively reconstructing a two-dimensional signal from segments of its two-dimensional Hadamard NPT have been developed. An iterative two-dimensional Hadamard NPT reconstruction algorithm has been investigated. The reconstruction algorithm requires an estimate of the signal amplitude over the available transform segments. A two-dimensional adaptive line enhancer has been employed for signal amplitude estimation. It has been shown empirically that the iterative reconstruction scheme converges for $\alpha \leq 0.41$. However, for Type - 1 reconstruction formats, the iterative reconstruction is possible for values of α in the range $0.41 < \alpha \leq 0.464$.

The number of iterations required for convergence is a function of the reconstruction format and the threshold ϵ which measures the similarity between the received transform segments and the corresponding segments of the transform domain iteration matrix, at the m^{th} iteration.

A fast reconstruction algorithm applicable to Type - 1 signal loss formats, which provide solutions in one iteration, has been introduced.

The two-dimensional Hadamard NPT reconstruction algorithm has been applied to the reconstruction of imagery data. The subjective quality of the reconstructed imagery data has been shown to be a function of the reconstruction format and the original image content. For original images with little detail, reconstructed pictures are comprehensible. However, some details in highly textured original images are missing from the reconstructed versions.

In general, the quality of the reconstructed signal depends on how well we can estimate the original signal amplitude, over the available transform segments. The subjective quality of the estimated segments of images improves with increasing values of α. However, the subjective quality of the reconstructed segments corresponding in location to the unknown transform samples, become poorer with increasing values of α.

CHAPTER SEVEN

CONSIDERATIONS FOR ONE-DIMENSIONAL AND TWO-DIMENSIONAL HADAMARD NATURALNESS-PRESERVING TRANSFORM RECONSTRUCTION APPLICATIONS

7.1 Introduction

One-dimensional and two-dimensional Hadamard NPT reconstruction techniques have been presented in chapters five and six respectively. This chapter investigates various aspects of one-dimensional and two-dimensional Hadamard NPT reconstruction applications.

A two-layer intraframe packet transmission system using one-dimensional Hadamard NPT reconstruction was proposed in chapter five. We shall be concerned with the performance of this system when used for the transmission of images over low bandwidth channels. In addition, we shall investigate the effect of enhancement packets on the quality of pictures obtained from the system. Furthermore, the effect of errors in the code-word digits used for representing the transmitted information is investigated. These investigations are reported in section 7.2. The results of simulations for the investigations are presented under the respective sub-sections.

The application of two-dimensional Hadamard NPT reconstruction techniques in the transmission of tactical imagery was investigated in chapter six. The performance of the reconstruction technique is further investigated in section 7.3. Specifically, we consider the problem of bandwidth limitations and investigate the effect of data compression on the quality of reconstructed pictures, using the two-dimensional Hadamard NPT reconstruction algorithm. In addition, the effect of errors in the code-word digits used for representing the transmitted information, is investigated. The results of simulations for the investigations are presented under the respective sub-sections.

Hybrid image coding algorithms which are based on one-dimensional Hadamard NPT reconstruction techniques, are presented in section 7.4.

7.2 Considerations For One-Dimensional Hadamard NPT Reconstruction Two-Layer Intraframe Packet Transmission of Images

In one-dimensional Hadamard NPT reconstruction, two-layer intraframe packet transmission of images, (refer to section 5.4, chapter five), the higher order 256 samples from 1×512 Hadamard NPT transformed samples of row-scanned $N \times N$ imagery data, $\mathbf{F}$, are transmitted as guaranteed packets. The rest of the information is sent as enhancement packets and these, if received, are only used to improve on the quality of pictures obtained from guaranteed packets, using the fast one-dimensional Hadamard NPT reconstruction algorithm. A detailed block diagram of this packet transmission system is shown in Fig. 5.26.

7.2.1 Intraframe Packet Transmission of Images Over Low Bandwidth Channels

The results of section 5.4 in chapter five indicate that subjectively good pictures can be obtained from guaranteed packets of Hadamard NPT segments, coded at 8.0 bits per transmitted sample (this is equivalent to 4.0 bits per pixel for each transmitted picture). However, in applications where there are bandwidth limitations, there is the need for data compression of the information to be transmitted. Thus, we investigate the reconstruction of an image from compressed guaranteed packets of its one-dimensional Hadamard NPT samples.

7.2.1.1 Reconstruction of An Image From Guaranteed Packets, Coded Using Hybrid Coding Techniques

Hadamard NPT hybrid coding of images has been discussed in part B, chapter three. Here, we consider the application of transform DPCM techniques to coding the Hadamard NPT samples, corresponding to the guaranteed information in Hadamard NPT reconstruction two-layer intraframe packet transmission of images. In other words, we specify the first layer coder in Fig. 5.26 as a DPCM coder.

The 1×256 higher order Hadamard NPT samples from 1×512 Hadamard NPT transformed samples of the image are stacked to form an $N_s \times 256$ array, where N_s is the total number of 1×512 sub-blocks. Parallel DPCM coding of the respective

columns of the array is then carried out. It is the coded differential signals that are packetized and transmitted.

At the receiver, an approximation of the original transform samples is obtained from the decoded differential signals, using DPCM operators identical to those in the transmitter. The coded 1×256 higher order Hadamard NPT samples are then used to form the truncated Hadamard NPT vectors $\tilde{R}'$, each of which is given by

$$\tilde{R}' = \left[\underline{0} \,|\, \underline{0} \,|\, \underline{r}_3 + \underline{q}_3 \,|\, \underline{r}_4 + \underline{q}_4\right]^T \tag{7.1}$$

where $\underline{r}_j$, $j = 3,4$ are 1×128 vectors of uncoded Hadamard NPT samples, $\underline{q}_j$ is the vector of coding errors of segment $\underline{r}_j$, $j = 3,4$ and $\underline{0}$ is a null vector of dimension 1×128. The fast Hadamard NPT reconstruction scheme 1 (refer to section 5.2.3.2 in chapter five) is then used to obtain an approximate version of the 1×512 samples of the original image. We shall represent the 1×512 reconstructed vector by $\hat{S}$, with

$$\hat{S} = [\underline{\hat{s}}_1 \,|\, \underline{\hat{s}}_2 \,|\, \underline{\hat{s}}_3 \,|\, \underline{\hat{s}}_4]^T \tag{7.2}$$

We have shown that the segments of $\hat{S}$ are given by

$$\underline{\hat{s}}_1 = \underline{s}_1 + \underline{e}'_3 - \frac{\alpha}{1-\alpha}\mathbf{H}_{128}\left(\underline{e}'_3 + \underline{e}'_4\right) + \frac{1}{1-\alpha}\mathbf{H}_{128}\left(\underline{q}_3 + \underline{q}_4\right) \tag{7.3a}$$

$$\underline{\hat{s}}_2 = \underline{s}_2 + \underline{e}'_4 - \frac{\alpha}{1-\alpha}\mathbf{H}_{128}\left(\underline{e}'_3 - \underline{e}'_4\right) + \frac{1}{1-\alpha}\mathbf{H}_{128}\left(\underline{q}_3 - \underline{q}_4\right) \tag{7.3b}$$

$$\underline{\hat{s}}_3 = \underline{s}_3 + \underline{e}'_3 \tag{7.3c}$$

and

$$\underline{\hat{s}}_4 = \underline{s}_4 + \underline{e}'_4 \tag{7.3d}$$

where $\underline{e}'_j$ is a 1×128 vector of errors incurred in the estimation of segment $\underline{s}_j$, $j = 3,4$ from the truncated Hadamard NPT vector $\tilde{R}'$, and $\mathbf{H}_{128}$ is a natural Hadamard matrix of order 128. An approximate version of the original transmitted image, i.e. $\hat{\mathbf{F}}$, is obtained by re-formatting the 1×512 vectors $\hat{S}$, into an $N \times N$ array.

Simulation, Results and Discussion

A first order predictor was used in the DPCM coder. Bits were assigned to the differential signals using the marginal analysis approach [45] and the differential signals were quantized using the optimum Laplacian quantizer.

For bit rates of 1.0 bit per transmitted sample and above, at least one bit was assigned to each sample. This strategy was found to yield reliable results. The

results presented below are for the Hadamard NPT(0.4). Fig. 7.3a shows the reconstructed version of ALAN, when the transform samples used for reconstruction are DPCM coded at 3.0 bits per transmitted sample; this correspond to a rate of 1.5 bits per pixel for the whole picture. An MSE of 138.28 (PSNR = 26.7232 DB) was obtained. The result when the transform samples are not coded (i.e. when 8.0 bits per sample are used for representing the transform samples) is shown in Fig. 7.1 and the MSE in this case is 112.251 (PSNR = 27.629). It is observed that there is little or no noticeable difference in the subjective quality of the two pictures.

Fig. 7.3b shows the reconstructed version of TEXTURE, when the transform samples used for reconstruction are DPCM coded at 3.0 bits per transmitted sample; this correspond to a rate of 1.5 bits per pixel for the entire picture. An MSE of 872.84 (PSNR = 18.7214 DB) was obtained. The result when 8.0 bits per sample are used for representing the transform samples is shown in Fig. 7.2 and the MSE in this case is 828.8065 (PSNR = 18.946 DB). It is observed that there is little noticeable difference in the subjective quality of the two pictures.

Fig. 7.4a shows the reconstructed version of ALAN, when the transform samples used for reconstruction are DPCM coded at 2.0 bits per transmitted sample; this correspond to a rate of 1.0 bit per pixel for the entire picture. A much higher MSE of 222.29 (PSNR = 24.6616 DB) was obtained and there is noticeable degradation in the subjective quality of the picture. Fig. 7.4b shows the reconstructed version of TEXTURE, when the transform samples used for reconstruction are DPCM coded at 2.0 bits per transmitted sample; this correspond to a rate of 1.0 bit per pixel for the entire picture. A higher MSE of 919.879 (PSNR = 18.4935 DB) was obtained but there is little noticeable increase in degradation of the subjective quality of the picture, resulting from reducing the coding rate.

Fig. 7.5a shows the reconstructed version of ALAN, when its Hadamard NPT(0.4) samples, used for reconstruction, are DPCM coded at 1.5 bits per transmitted sample; this correspond to a bit rate of 0.75 bit per pixel for the whole picture. An MSE of 331.61 (PSNR = 22.9245 DB) was obtained and the subjective quality of the picture is very poor. Fig. 7.5b shows the reconstructed version of TEXTURE, when its Hadamard NPT(0.4) samples, used for reconstruction, are DPCM coded at 1.5 bits per transmitted sample; this correspond to a bit rate of 0.75 bit per pixel for the whole picture. An MSE of 952.66 (PSNR = 18.3414 DB) was obtained and the reconstructed picture is subjectively less degraded than the



Fig. 7.1 : Hadamard NPT(0.4) Recons.From Guarant. Packets, Coded at 8.0 Bits/samp., (4.0 Bits/pel.), Image ALAN.

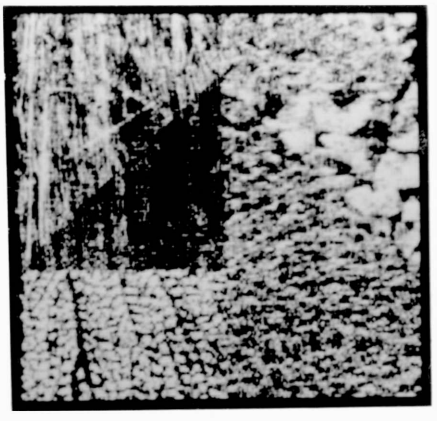


Fig. 7.2 : Hadamard NPT(0.4) Recons. From Guarant. Packets, Coded at 8.0 Bits/samp., (4.0 Bits/pel.), Image TEXTURE.



Fig. 7.3a : Hadamard NPT(0.4) Recons. From Guarant. Packets, DPCM Coded at 3.0 Bits /samp., (1.5 Bits/pel.), Image ALAN.

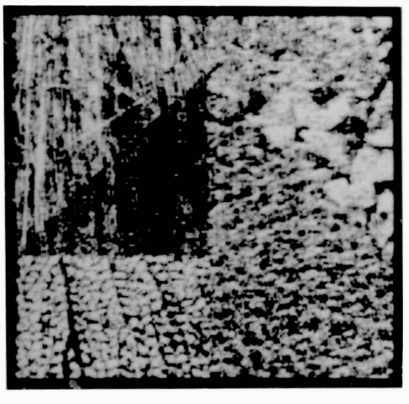


Fig. 7.3b : Hadamard NPT(0.4) Recons. From Guarant. Packets, DPCM Coded at 3.0 Bits /samp., (1.5 Bits/pel.), Image TEXTURE.



Fig. 7.4a : Hadamard NPT(0.4) Recons. From Guarant. Packets, DPCM Coded at 2.0 Bits /samp., (1.0 Bit/pel.), Image ALAN.

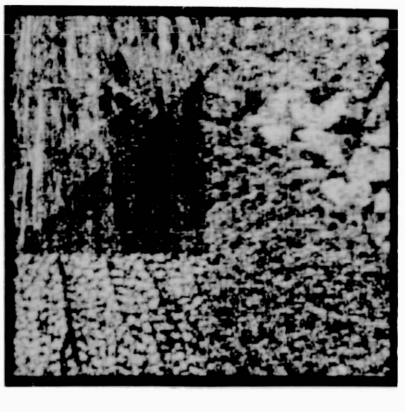


Fig. 7.4b : Hadamard NPT(0.4) Recons. From Guarant. Packets, DPCM Coded at 2.0 Bits /samp., (1.0 Bit/pel.), Image TEXTURE.



Fig. 7.5a : Hadamard NPT(0.4) Recons. From Guarant. Packets, DPCM Coded at 1.5 Bits /samp., (0.75 Bit/pel.), Image ALAN.

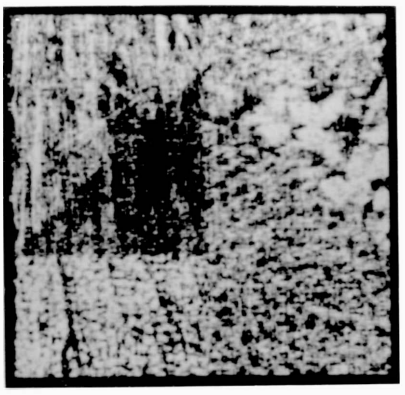


Fig. 7.5b : Hadamard NPT(0.4) Recons. From Guarant. Packets, DPCM Coded at 1.5 Bits /samp., (0.75 Bit/pel.), Image TEXTURE.



Fig. 7.6a : Hadamard NPT(0.4) Recons. From Guarant. Packets, VQ Coded at 1.25 Bits/ samp., (0.625 Bit/pel.), Image ALAN.

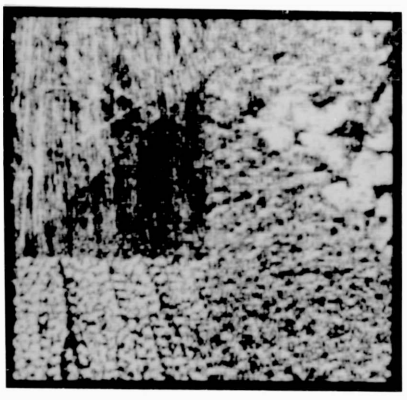


Fig. 7.6b : Hadamard NPT(0.4) Recons. From Guarant. Packets, VQ Coded at 1.25 Bits/ samp., (0.625 Bit/pel.), Image TEXTURE.



Fig. 7.7a : Hadamard NPT(0.4) Recons. From Guarant. Packets, VQ Coded at 0.75 Bit/ samp., (0.375 Bit/pel.), Image ALAN.

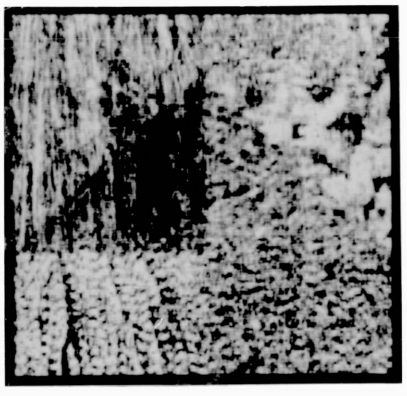


Fig. 7.7b : Hadamard NPT(0.4) Recons. From Guarant. Packets, VQ Coded at 0.75 Bit/ samp., (0.375 Bit/pel.), Image TEXTURE.

corresponding one for the ALAN image, shown in Fig. 7.5a. The above results show that there is little noticeable degradation in the subjective quality of reconstructed pictures, when the Hadamard NPT samples used for reconstruction are DPCM coded at 3.0 bits per transmitted sample and above. Below this rate, there can be severe degradation in the subjective quality of the reconstructed pictures.

In the following sub-sections, we investigate the application of Vector Quantization (VQ) techniques for coding the Hadamard NPT samples, used for reconstruction, at lower bit rates.

7.2.1.2 Reconstruction of An Image From Guaranteed Packets, Coded Using Vector Quantization Techniques

Over the years, VQ has emerged as a robust and powerful data compression technique. The robustness of VQ with respect to compression distortion is linked to a result of Shannon's rate-distortion theory which indicates that a better performance is always achievable in theory by coding vectors instead of scalars, even though the data source is memoryless. The main aim of the work of this section is to employ VQ as a reliable means of coding the guaranteed Hadamard NPT information, necessary for reconstruction, at low bit rates (less than 1.5 bits per transmitted sample). Hence, we shall not attempt to give a comprehensive review of VQ as this has already been given in several places in the literature, for example [69,70]. However, in the next sub-section, we shall give a brief definition of VQ and describe a design algorithm that will be used in the study.

7.2.1.2.1 Definition of Vector Quantization and Vector Quantizer Design

An L-level, z-dimensional vector quantizer is a mapping, Q, of vectors from a z-dimensional real Euclidean vector space $\Re^z$, into a representative subspace $\mathbf{C}$ with L disjoint partitions $\mathbf{C} = [\mathbf{C}_1 \,|\, \mathbf{C}_2 \,|\, \ldots \,|\, \mathbf{C}_L]$, $\mathbf{C} \subset \Re^z$, i.e.

$$Q : \Re^z \rightarrow \mathbf{C} \qquad \mathbf{C} \subset \Re^z \tag{7.4}$$

The mapping $Q(\mathbf{v})$ of vectors $\mathbf{v} \in \Re^z$ is chosen to partition $\Re^z$ into a set of L minimum distortion regions $\mathbf{C}_1, \mathbf{C}_2, \ldots \mathbf{C}_L$. For a given measure of mapping distortion $d(\mathbf{v}, Q(\mathbf{v}))$, an optimal vector quantizer is obtained when the mapping of (7.4) is such that the expected distortion $E\{d(\mathbf{v}, Q(\mathbf{v}))\}$ is a minimum for all possible mapping strategies.

The quantizer Q is completely specified by the reproduction alphabet or codebook $\hat{C} = (\mathbf{u}_i;\ i = 1,2,\ldots L)$ together with the partition, $\mathbf{C} = \{\mathbf{C}_i,\ i = 1,2,\ldots L\}$, of the input vector space into the sets $\mathbf{C}_i = \{\mathbf{v} : Q(\mathbf{v}) = \mathbf{u}_i\}$ of input vectors mapping into the i^{th} codeword. In operation, the quantizer assigns to each input vector $\mathbf{v}$, a reproduction vector $\hat{\mathbf{v}} = Q(\mathbf{v})$, drawn from the finite reproduction alphabet $\hat{C} = (\mathbf{u}_i,\ i = 1,2,\ldots L)$. The associated vector quantizer rate is

$$R_t = log_2 L \qquad bits/vector \tag{7.5a}$$

or

$$r_t = log_2 L^{1/z} \qquad bits/sample \tag{7.5b}$$

The vector quantizer design algorithm that will be used in the investigation is the generalized Lloyd algorithm or the LBG algorithm [71]. The LBG algorithm can be applied to data with a known or unknown probability distribution.

The following steps summarize the LBG algorithm.

1) Given an initial codebook $\hat{C}(0)$, a distortion convergence parameter $\epsilon \geq 0$ and a training sequence $\{\mathbf{v}\}$ of vectors, $\mathbf{v} \in \Re^z$, set the initial average distortion $D_{-1} = \infty$.

At the m^{th} iteration

2) Given $\hat{C}(m) = (\mathbf{u}_i(m),\ i = 1,2,\ldots L)$, effect the minimum distortion mapping $Q : \Re^z \rightarrow \mathbf{C}(m) = \{\mathbf{C}_i(m),\ i = 1,2,\ldots L\}$ of the training sequence, such that $\mathbf{v}_j \in \mathbf{C}_i(m)$ if $d(\mathbf{v}_j, \mathbf{u}_i(m)) \leq d(\mathbf{v}_j, \mathbf{u}_q(m))$, for all q and compute the average distortion

$$D_m = n_{\mathbf{v}}^{-1} \sum_{j=1}^{n_{\mathbf{v}}} \min_{\mathbf{u} \in \hat{C}(m)} d(\mathbf{v}_j, \mathbf{u}) \tag{7.6}$$

where $n_{\mathbf{v}}$ is the total number of vectors in the training sequence .

3) If $(D_{m-1} - D_m) \leq \epsilon D_m$, then stop iterations with $\hat{C}(m)$ as the final codebook. Otherwise go to step 4

4) Find the optimum reproduction codebook $\hat{C}(m+1) = (\mathbf{u}_i(m+1),\ i = 1,2,\ldots L)$ based on $\mathbf{C}(m)$ according to the rule

$$\mathbf{U}_i(m+1) = E\{\mathbf{v} \,|\, Q(\mathbf{v}) : \Re^z \rightarrow \mathbf{C}_i(m)\} \tag{7.7}$$

Set $m = m+1$ and go to step 2.

The algorithm requires an initial representative codebook $\hat{C}(0)$, which may be improved upon in subsequent iterations. Several techniques have been suggested for choosing the initial codebook [69]; we employ the splitting technique [69,70]. Essentially, we start with a one-level quantizer consisting of the centroid of the training sequence. This vector is then split into two vectors by adding a fixed perturbation $\pm\delta$ and the two-level quantizer algorithm is run on this pair to obtain a good two-level quantizer. Each of these two vectors is then split into two close vectors $\mathbf{u}_i + \delta$ and $\mathbf{u}_i - \delta$ and the algorithm is run to produce a good four-level quantizer. The splitting and subsequent optimization is continued until the required codebook is realized.

7.2.1.2.2 Application of VQ To Coding Hadamard NPT Samples For Transmission As Guaranteed Packets

The strategy for VQ coding of the Hadamard NPT samples is similar to the intraframe approach of [72]. The 256 higher order samples from 1×512 Hadamard NPT transformed samples of the image are stacked to form an $N_s \times 256$ array, where N_s is the total number of 1×512 sub-blocks. VQ is then used to exploit the inter-row dependency of the samples of the array, i.e. adopting an intra-column vector formation strategy. It is the reproduction code-words for the vectors that are packetized and transmitted. At the receiver, the decoded code-words are used to address a code-book similar to that in the transmitter, to yield the reproduction vectors. The fast Hadamard NPT reconstruction algorithm is then applied to the reconstructed Hadamard NPT segments, to yield an approximate version of the original transmitted image; (7.3) gives the closed-form expressions for the segments of the reconstructed one-dimensional sub-blocks of the image.

Simulation, Results and Discussion

The training vectors for codebook design were derived from 1×512 Hadamard NPT(0.4) samples of the 256×256 images ALAN (shown in Fig. 2.7), CHOIR (shown in Fig. 2.8), DOCUMENT (shown in Fig. 2.10) and TEXTURE (shown in Fig. 2.11). Each vector was converted to a zero mean and unit standard deviation vector.

The results presented below correspond to the Hadamard NPT basis $\alpha = 0.4$. Fig. 7.6a shows the reconstructed version of ALAN when the guaranteed Hadamard NPT(0.4) samples are VQ coded using a codebook containing 1024,

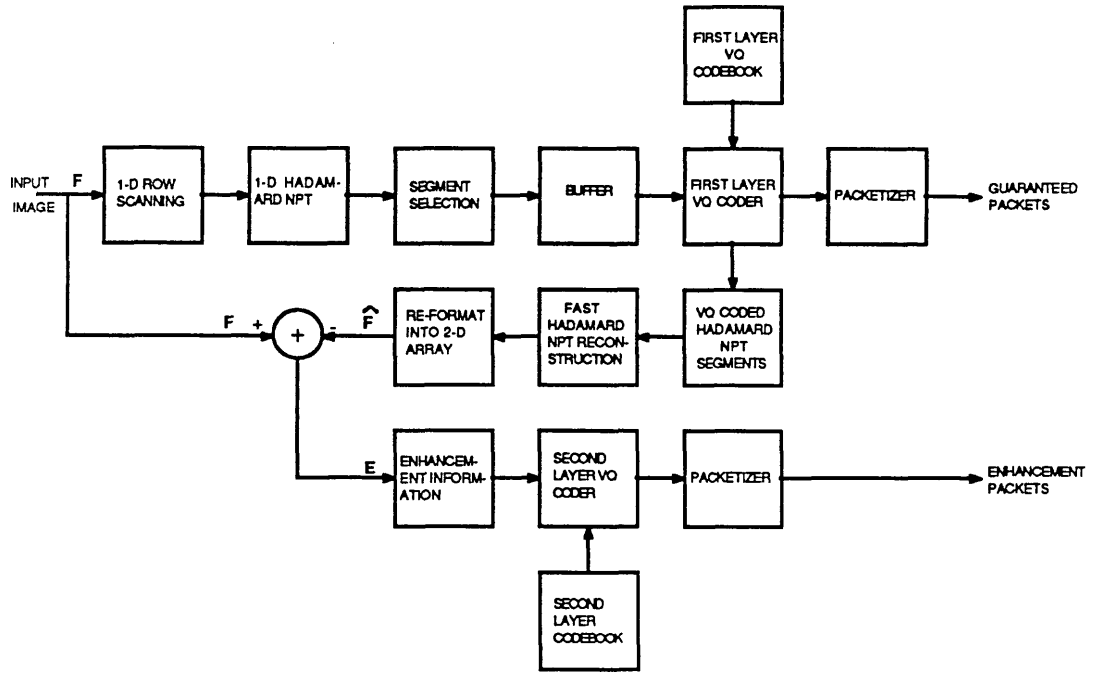
8×1 vectors. This corresponds to coding at 1.25 bits per transmitted sample or 0.625 bit per pixel for the whole picture. An MSE of 134.8682 (PSNR = 26.8317 DB) was obtained. The picture compares very well, subjectively, with the no coding result shown in Fig. 7.1 and the MSE is lower than when the Hadamard NPT(0.4) samples are DPCM coded at 3.0 bits per transmitted sample. Fig. 7.6b shows the reconstructed version of TEXTURE when the guaranteed Hadamard NPT(0.4) samples are VQ coded using the same codebook as that used for Fig. 7.6a. An MSE of 855.4503 (PSNR = 18.8089 DB) was obtained. The subjective quality of the picture compares very well with the no coding result shown in Fig. 7.2 and the PSNR is only 0.137 DB worse than the no coding result.

Fig. 7.7a shows the reconstructed version of ALAN when the guaranteed Hadamard NPT samples are VQ coded using a codebook containing 4096, 16×1 vectors. This corresponds to coding at a rate of 0.75 bit per transmitted sample or 0.375 bit per pixel for the whole picture. An MSE of 153.4789 (PSNR = 26.2703 DB) was obtained. There is an increased degradation in the subjective quality of the reconstructed picture but it is better than that obtained when the transform samples are DPCM coded at 1.5 bits per transmitted sample. Fig. 7.7b shows the reconstructed version of TEXTURE, when its guaranteed Hadamard NPT(0.4) samples are VQ coded using the codebook containing 4096, 16×1 vectors; this corresponds to a rate of 0.75 bit per transmitted sample or 0.375 bit per pixel for the whole picture. An MSE of 855.4595 (PSNR = 18.8088 DB) was obtained. There is only a slight increase in the MSE distortion, compared to when the transform samples are VQ coded at 1.25 bits per transmitted sample. In addition, there is only a slight noticeable increased degradation in the subjective quality of the picture, compared to that of Fig. 7.6b.

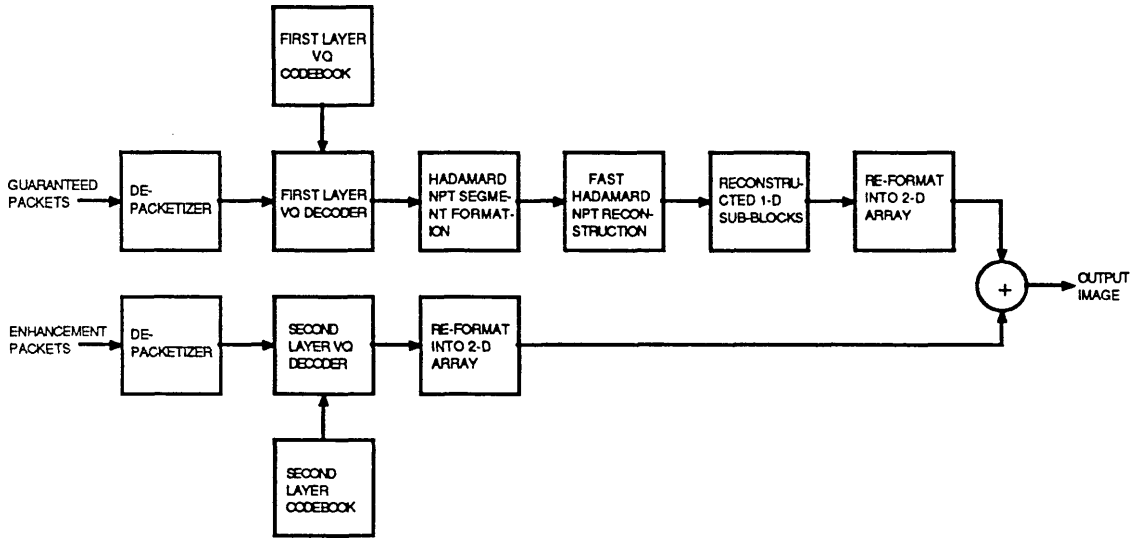
7.2.2 The Transmission of Enhancement Packets

As stated earlier, the second part of the information to be transmitted in two-layer intraframe packet transmission of images consist of enhancement packets. These are only used to improve on the picture obtained from guaranteed packets and they do not necessarily have to be received.

The enhancement packets information generation procedure that we have considered, consists of forming the difference between the original image array $\mathbf{F}$ and a reconstructed version $\hat{\mathbf{F}}$ that is obtained from the coded guaranteed packets of Hadamard NPT samples, at the transmitter. It is the difference array $\mathbf{E} = \mathbf{F} - \hat{\mathbf{F}}$



(a) Transmitter



(b) Receiver

Fig. 7.8 : Detailed Block Diagram of Hadamard NPT Reconstruction Two-Layer Intraframe Packetized Image Transmission System.

that is VQ coded and transmitted as enhancement packets. The reconstruction of $\hat{\mathbf{F}}$ at the coder is made identical to that in the receiver so that picture quality enhancement is realized by adding the received enhancement packets information to the fast Hadamard NPT reconstructed version of the original image, $\hat{\mathbf{F}}$, at the receiver. Fig. 7.8 is a complete block diagram of the transmission protocol.

Simulation, Results and Discussion

A separate codebook was designed for VQ coding of the enhancement packets information. The training sequence vectors were obtained by re-ordering $p \times p$ sub-blocks of the difference array, $\mathbf{E}$, to form $p^2 \times 1$ vectors, which were subsequently used for VQ design; the original images ALAN, CHOIR, DOCUMENT and TEXTURE were used.

In the simulations, the guaranteed packets information was VQ coded using a codebook containing 1024, 8×1 vectors; this corresponds to a transmission rate of 1.25 bits per sample which is equivalent to 0.625 bit per pixel for the whole picture. The corresponding enhancement packets information was VQ coded using a codebook containing 1024, 16×1 vectors, corresponding to a rate of 0.625 bit per pixel. The vectors were obtained by re-ordering 4×4 sub-blocks of the difference array $\mathbf{E}$ into 16×1 vectors. We also assume that each packet contain 50 bits which correspond to 5 vectors per packet.

The results presented below are for the NPT basis $\alpha = 0.4$. Fig. 7.9a shows the final reconstructed version of ALAN when all the enhancement packets are received. The overall transmission rate is 1.25 bits per pixel and an MSE of 29.8957 (PSNR = 33.4747 DB) was obtained. The subjective quality of the picture is very good. Fig. 7.9b shows the reconstructed version of ALAN, when enhancement packets are transmitted, at a loss rate of 10^{-2}. An MSE of 30.9558 (PSNR = 33.2234 DB) was obtained and there is no noticeable degradation in the subjective quality of the reconstructed picture. Fig. 7.9c shows the reconstructed version of ALAN, at enhancement packets loss rate of 10^{-1}. A slightly higher MSE of 40.1176 (PSNR = 32.0975 DB) was obtained. The subjective quality of the picture compares very well with that of Fig. 7.9a and Fig. 7.9b, however, there is a bit of jaggedness noticeable along the right sleeve of ALAN. Empirical results show that the jaggedness of the edges is very slight at an enhancement packet loss rate of 5^{-1} and below. For higher packet loss rates, the jaggedness of the edges become more pronounced. Fig. 7.9d shows the reconstructed version of ALAN at an enhancement packets loss rate



Fig. 7.9a : Hadamard NPT(0.4) Recons. From Guarant. Pack. (VQ Coded at 1.25 Bits/samp.) and all Enh. Pack. (VQ Coded at 0.625 Bit/ samp.), Image ALAN.



Fig. 7.9b : Hadamard NPT(0.4) Recons. From Guarant. Pack. (VQ Coded at 1.25 Bits/samp.) and Enh. Pack. (VQ Coded at 0.625 Bit/samp.) at Enh. Pack. Loss Rate=10^{-2}, Image ALAN.



Fig. 7.9c : Hadamard NPT(0.4) Recons. From Guarant. Pack. (VQ Coded at 1.25 Bits/samp.) and Enh. Pack. (VQ Coded at 0.625 Bit/samp.) at Enh. Pack. Loss Rate=10^{-1}, Image ALAN.



Fig. 7.9d : Hadamard NPT(0.4) Recons. From Guarant. Pack. (VQ Coded at 1.25 Bits/samp.) and Enh. Pack. (VQ Coded at 0.625 Bit/samp.) at Enh. Pack. Loss Rate=2^{-1}, Image ALAN.



Fig. 7.9e : Hadamard NPT(0.4) Recons. From Guarant. Pack. (VQ Coded at 1.25 Bits/samp.) With Two-Level Bi-directional Detail-Preserv. Median Filtering ($2LM^{+}$), Image ALAN.

of 2^{-1}. An MSE of 82.3667 (PSNR = 28.9733 DB) was obtained. The subjective quality of the picture is unacceptable and worse than when enhancement packets are not transmitted, see Fig. 7.6a. The above results show that the reconstructed picture quality is not very sensitive to the loss of enhancement packets. Fig. 7.9e shows the result when no enhancement packets are transmitted but with two-level bi-directional detail-preserving median filtering of the reconstructed picture, i.e. filtering the picture shown in Fig. 7.6a. An MSE of 73.1504 (PSNR = 29.4886 DB) was obtained, which is very much lower than that obtained without filtering, shown in Fig. 7.6a. The reconstructed picture is also less noisy than that shown in Fig. 7.6a, although the picture appears slightly de-focussed.

7.2.3 The Effect of Channel Errors

The effect of errors in the code-word digits used for representing the transmitted information is considered. A binary symmetric channel is assumed and in this context, a bit error is the inversion of a '0' into a '1' and vice versa. The effect of this is separately studied for guaranteed packets and enhancement packets, at various bit-error-rates (BER). The investigation was conducted for the Hadamard NPT basis specified by $\alpha = 0.4$.

Simulation, Results and Discussion

The guaranteed packets information was VQ coded at 1.25 bits per transmitted sample while the enhancement packets information was VQ coded at 0.625 bit per transmitted sample. Empirical investigations show that there is no noticeable effect in the reconstructed pictures, of errors in the code-word digits used for representing the information transmitted as guaranteed packets, at BER = 10^{-4}. Fig. 7.10a shows the reconstructed version of ALAN from VQ coded guaranteed packets, at BER = 10^{-3}. The effect of errors in the code-word digits is slightly noticeable as vertical streaks in the reconstructed picture. An MSE of 144.8461 (PSNR = 26.5217 DB) was obtained. Fig. 7.10b shows the reconstructed version of ALAN from VQ coded guaranteed packets, at BER = 10^{-2}. A higher MSE of 277.8782 (PSNR = 23.6923 DB) was obtained and the vertical streaking is more pronounced.

The effect of errors in the code-word digits used for representing the enhancement information was also investigated; the guaranteed packets were assumed to be transmitted at BER = 0. Fig. 7.11a shows the reconstructed version of ALAN,



Fig. 7.10a : Hadamard NPT(0.4) Recons. From Guarant. Pack. (VQ Coded at 1.25 Bits/samp.) , BER=10^{-3}, Image ALAN



Fig. 7.10b : Hadamard NPT(0.4) Recons. From Guarant. Pack. (VQ Coded at 1.25 Bits/samp.) , BER=10^{-2}, Image ALAN.



Fig. 7.11a : Hadamard NPT(0.4) Recons. From Guarant. Pack. (VQ Coded at 1.25 Bits/samp.) and all Enh. Pack. (VQ Coded at 0.625 Bit/ samp.), BER=20^{-1} For Enh. Inform., Image ALAN.



Fig. 7.11b : Hadamard NPT(0.4) Recons. From Guarant. Pack. (VQ Coded at 1.25 Bits/samp.) and all Enh. Pack. (VQ Coded at 0.625 Bit/ samp.), BER=1 For Enh. Inform., Image ALAN.

when all the enhancement packets are received, at BER = 20^{-1}. An MSE of 61.6822 (PSNR = 30.2292 DB) was obtained and there is very little noticeable degradation in the subjective quality of the picture, compare with Fig. 7.9a. Fig. 7.11b shows the reconstructed version of ALAN, when all the enhancement packets are received at BER = 1 i.e. errors in all the code-word digits used for representing the enhancement packets information. A higher MSE of 99.0351 (PSNR = 28.1729 DB) was obtained and there is little noticeable degradation in the subjective quality of the picture, compare with Fig. 7.9a.

The above results show that errors in the code-word digits used for representing the guaranteed information has more effect on the subjective quality of reconstructed pictures, than errors in the code-word digits used for representing the enhancement information.

7.3 Considerations For Two-Dimensional Hadamard NPT Reconstruction, Tactical Imagery Transmission

Two-dimensional Hadamard NPT reconstruction tactical imagery transmission has been discussed in chapter six. In this section, we consider the problem of channel bandwidth limitations and investigate the reconstruction from segments of compressed two-dimensional Hadamard NPT transformed imagery data. In addition, we also examine the effect of errors in the code-word digits, used for representing the transmitted information. A binary symmetric channel is assumed and a bit error is the inversion of a '0' into a '1' and vice versa. We shall use the Type-1 reconstruction format shown in Fig. 6.6b and the results to be presented correspond to the Hadamard NPT basis $\alpha = 0.45$.

7.3.1 Imagery Reconstruction From Compressed Two-Dimensional Hadamard NPT Segments

VQ technique is considered for data compression of the two-dimensional Hadamard NPT transformed imagery data. This is because the robustness of VQ, with respect to encoding distortion, permits the realization of low data rates. The basic difference between the work of this section and that of chapter six is that the two-dimensional Hadamard NPT transformed imagery data is VQ coded prior to transmission; the reconstructed version of the original image is thus obtained from compressed two-dimensional Hadamard NPT segments.

Simulation, Results and Discussion

The training vectors for codebook design were derived from full-frame two-dimensional Hadamard NPT(0.45) transformed 256 x 256 images ALAN, CHOIR, DOCUMENT and TEXTURE. Prior to vectors formation, the "dc" sample was normalized by the two-dimensional NPT $(CMEF)_{DC}$ while the "ac" samples along the first row and column of the transformed data were normalized by the one-dimensional NPT $(CMEF)_{DC}$. This strategy is aimed at reducing the dynamic range of these samples. An intra-column vector formation approach was adopted although it is also possible to form vectors along the rows or from re-ordered two-dimensional sub-blocks, however, these were not pursued. The vectors were normalized to have zero mean and unit standard deviation.

Fig. 7.12b shows the reconstructed version of ALAN from the Type-1 format of Fig. 6.6b, when the two-dimensional Hadamard NPT transformed data is VQ coded, using a codebook containing 256, 8 x 1 vectors; this corresponds to a rate of 1.0 bit per sample. An MSE of 2642.9 (PSNR = 13.91 DB) was obtained .The result when the transform samples are not coded is shown in Fig. 7.12a. It is observed that there is little difference in the subjective quality of the two pictures. Fig. 7.12c shows the reconstructed version of ALAN from the same Type-1 format of Fig. 6.6b, when the transmitted two-dimensional Hadamard NPT transformed data is VQ coded, using a codebook containing 512, 16 x 1 vectors; this correspond to a rate of 0.5625 bit per transmitted sample. An MSE of 3077.2 (PSNR = 13.25 DB) was obtained. The subjective quality of the picture compares well with the no coding result, but there is a slight noticeable increase in the distortion of the region of the picture corresponding to the unknown transform samples.

7.3.2 The Effect of Channel Errors on Reconstructed Imagery Quality

The effect of errors in the code-word digits used for representing the two-dimensional Hadamard NPT transformed imagery data, on the reconstructed image quality, is also considered. A binary symmetric channel is assumed and a bit error is the conversion of a '0' to a '1' and vice versa.

Simulation, Results and Discussion

The two-dimensional Hadamard NPT(0.45) transformed imagery data was VQ coded prior to transmission, using a codebook containing 256, 8 x 1 vectors; this correspond to a rate of 1.0 bit per sample.



Fig. 7.12a : Fast 2-D Hadamard NPT(0.45) Recons., Format of Fig. 6.6b, No Coding, Image ALAN. No Pre-/Post-Recon. Filt.

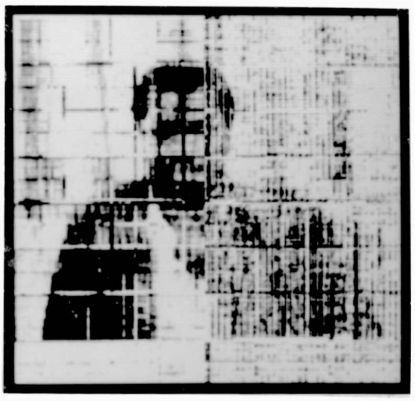


Fig. 7.12b : Fast 2-D Hadamard NPT(0.45) Recons., Format of Fig. 6.6b, VQ Coding at 1.0 Bit/samp., Image ALAN. No Pre-/ Post-Recon. Filt.

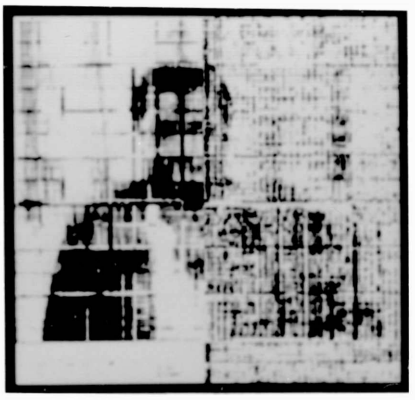


Fig. 7.12c : Fast 2-D Hadamard NPT(0.45) Recons., Format of Fig. 6.6b, VQ Coding at 0.5625 Bit/samp., Image ALAN. No Pre-/ Post-Recon. Filt.

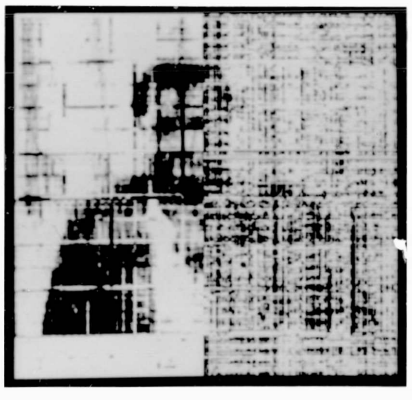


Fig. 7.13a : Fast 2-D Hadamard NPT(0.45) Recons., Format of Fig. 6.6b, VQ Coding at 1.0 Bit/samp., BER=20^{-1}, Image ALAN. No Pre-/Post-Recon. Filt.

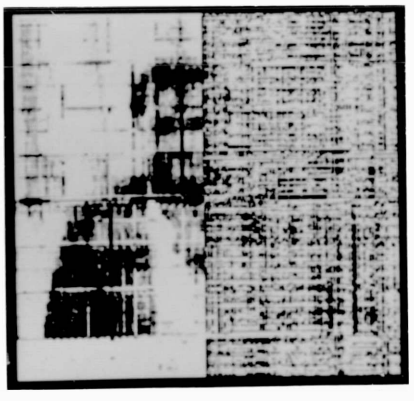


Fig. 7.13b : Fast 2-D Hadamard NPT(0.45) Recons., Format of Fig. 6.6b, VQ Coding at 1.0 Bit/samp., BER=10^{-1}, Image ALAN. No Pre-/Post-Recon. Filt.

Empirical investigations show that there is negligible increase in the distortion of the reconstructed pictures for BER = 10^{-3} and below. However, for BER = 10^{-2}, a slight increase in distortion is noticeable in the region of the picture corresponding to the unknown transform samples. Fig. 7.13a shows the reconstructed version of ALAN from the Type-1 format of Fig. 6.6b, when there are errors at BER = 20^{-1}, in the code-word digits used for representing its VQ coded two-dimensional Hadamard NPT samples; the no error result is shown in Fig. 7.12b. An MSE of 4374.8 (PSNR = 11.72 DB) was obtained. It is observed that the effect of the bit errors manifests mainly as an increase in the distortion, over the region corresponding to the unknown Hadamard NPT samples; the subjective quality of the region corresponding to the known transform segments is more or less unaffected. Fig. 7.13b shows the reconstructed version of ALAN for an identical scheme to that of Fig. 7.13a, but at BER = 10^{-1}. A higher MSE of 6229.9 (PSNR = 10.19 DB) was obtained and the region corresponding to the unknown transform samples is severely distorted, compare with the no error result shown in Fig. 7.12b.

7.4 Hybrid Image Coding Techniques Based on Hadamard Naturalness-Preserving Transform Reconstruction

7.4.1 Introduction

The theme of the work of this section is different from what we have done so far on Hadamard NPT reconstruction applications. In chapter five, we developed an iterative algorithm for reconstructing a signal from segments of its one-dimensional Hadamard NPT. Two fast reconstruction algorithms were introduced. Here, we develop hybrid image coding techniques which are based on Hadamard NPT reconstruction of an approximate version of each image line, at the receiver, using the fast reconstruction scheme 1 (refer to section 5.2.3.2).

A description of the coding algorithm is first presented. Variations of the algorithm are investigated and closed-form expressions for a reconstructed image line, in each of these cases are derived. The theoretical results are confirmed by simulations.

7.4.2 The One-Dimensional Hadamard NPT Reconstruction-Based Hybrid Image Coding Algorithm

We represent the original $N \times N$ image array by $\mathbf{F}$ and define each line of $\mathbf{F}$ as the $1 \times N$ partitioned vector

$$\mathbf{f} = \left[\underline{f}_1 \,|\, \underline{f}_2 \,|\, \underline{f}_3 \,|\, \underline{f}_4\right]^T \tag{7.8}$$

where T denotes the transposition operation.

We perform the one-dimensional natural Hadamard transform of the vector $\mathbf{s} = (1 - \alpha)\mathbf{f}$ to yield the vector

$$\mathbf{h} = [\underline{h}_1 \,|\, \underline{h}_2 \,|\, \underline{h}_3 \,|\, \underline{h}_4]^T \tag{7.9}$$

The vector $\mathbf{h}$ is then truncated by discarding the most significant $\frac{N}{2}$ samples, to yield the vector $\tilde{\mathbf{h}}$ given by

$$\tilde{\mathbf{h}} = [\underline{0} \,|\, \underline{0} \,|\, \underline{h}_3 \,|\, \underline{h}_4]^T \tag{7.10}$$

where $\underline{0}$ is a null vector of dimension $1 \times \frac{N}{4}$. This operation is carried out for each line of $\mathbf{F}$ and the respective vectors $\tilde{\mathbf{h}}$ are stored in the corresponding lines of the array $\tilde{\mathbf{T}}$. The non-zero columns of $\tilde{\mathbf{T}}$ are then coded using a bank of DPCM operators [22,23]. We can express each coded line of $\tilde{\mathbf{T}}$ as the partitioned vector

$$\tilde{\mathbf{h}}' = [\underline{0} \,|\, \underline{0} \,|\, \underline{h}_3 + \underline{e}_3^h \,|\, \underline{h}_4 + \underline{e}_4^h]^T \tag{7.11}$$

where $\underline{e}_j^h$ is the $1 \times \frac{N}{4}$ vector of quantization errors incurred in coding segment $\underline{h}_j$, $j = 3,4$. Due to the fact that the components of $\tilde{\mathbf{h}}$ are low in magnitude, very few bits would be required to code the non-zero columns of $\tilde{\mathbf{T}}$. The coded segments of $\tilde{\mathbf{T}}$, i.e. vectors $\underline{h}_3 + \underline{e}_3^h$ and $\underline{h}_4 + \underline{e}_4^h$, are reconstructed at the receiver, using identical DPCM operators to that in the transmitter.

The following step consists of transmitting the additional information that would permit the reconstruction of each image line at the receiver. This is obtained by discarding (setting to zero) the first $\frac{N}{2}$ samples of each line of the original image $\mathbf{F}$, to yield the array $\tilde{\mathbf{F}}$. Thus, each line of $\tilde{\mathbf{F}}$ can be expressed as

$$\tilde{\mathbf{f}} = \left[\underline{0} \,|\, \underline{0} \,|\, \underline{f}_3 \,|\, \underline{f}_4\right]^T \tag{7.12}$$

A DPCM coder is subsequently used for coding the non-zero portion of $\tilde{\mathbf{F}}$. At the receiver, an identical DPCM operator to that in the transmitter is used to obtain

the coded version of $\tilde{\mathbf{F}}$, i.e. $\tilde{\mathbf{F}}'$, which is then stored in a buffer. Each line of $\tilde{\mathbf{F}}'$ can be expressed as

$$\tilde{\mathbf{f}}' = \left[\underline{0} \,|\, \underline{0} \,|\, \underline{f}_3 + \underline{e}_3^f \,|\, \underline{f}_4 + \underline{e}_4^f\right]^T \tag{7.13}$$

where $\underline{e}_j^f$ is the $1 \times \frac{N}{4}$ vector of errors incurred in coding segment $\underline{f}_j$, $j = 3,4$ of $\mathbf{f}$.

At the receiver, the vectors $\tilde{\mathbf{f}}'$ and $\tilde{\mathbf{h}}'$ are used to form the truncated Hadamard NPT vector $\tilde{\mathbf{r}}'$, thus,

$$\tilde{\mathbf{r}}' = \alpha\tilde{\mathbf{f}}' + \tilde{\mathbf{h}}' \tag{7.14a}$$

$$= \tilde{\mathbf{r}} + \tilde{\mathbf{e}}^t \tag{7.14b}$$

where

$$\tilde{\mathbf{r}} = \alpha\tilde{\mathbf{f}} + \tilde{\mathbf{h}} \tag{7.15}$$

and

$$\tilde{\mathbf{e}}^t = \left[\underline{0} \,|\, \underline{0} \,|\, \underline{e}_3^t \,|\, \underline{e}_4^t\right]^T \tag{7.16a}$$

$$= \left[\underline{0} \,|\, \underline{0} \,|\, \alpha\underline{e}_3^f + \underline{e}_3^h \,|\, \alpha\underline{e}_4^f + \underline{e}_4^h\right]^T \tag{7.16b}$$

The fast Hadamard NPT reconstruction scheme 1, described in section 5.2.3.2 of chapter five is then used to obtain the approximate version of each line, i.e. $\hat{\mathbf{f}}$, using the vectors $\hat{S}^W = \tilde{\mathbf{f}}'$ and $\tilde{R} = \tilde{\mathbf{r}}'$ (note that $\hat{S}^W$ and $\tilde{R}$ have been defined in chapter five).

We have shown that the reconstructed version of each image line is given by

$$\hat{\mathbf{f}} = \left[\hat{\underline{f}}_1 \,|\, \hat{\underline{f}}_2 \,|\, \hat{\underline{f}}_3 \,|\, \hat{\underline{f}}_4\right]^T \tag{7.17}$$

where

$$\hat{\underline{f}}_1 = \underline{f}_1 + \underline{e}_3^f - \frac{\alpha}{1-\alpha}\mathbf{H}_{\frac{N}{4}}\left(\underline{e}_3^f + \underline{e}_4^f\right) + \frac{1}{1-\alpha}\mathbf{H}_{\frac{N}{4}}\left(\underline{e}_3^t + \underline{e}_4^t\right) \tag{7.18a}$$

$$\hat{\underline{f}}_2 = \underline{f}_2 + \underline{e}_4^f - \frac{\alpha}{1-\alpha}\mathbf{H}_{\frac{N}{4}}\left(\underline{e}_3^f - \underline{e}_4^f\right) + \frac{1}{1-\alpha}\mathbf{H}_{\frac{N}{4}}\left(\underline{e}_3^t - \underline{e}_4^t\right) \tag{7.18b}$$

$$\hat{\underline{f}}_3 = \underline{f}_3 + \underline{e}_3^f \tag{7.18c}$$

$$\hat{\underline{f}}_4 = \underline{f}_4 + \underline{e}_4^f \tag{7.18d}$$

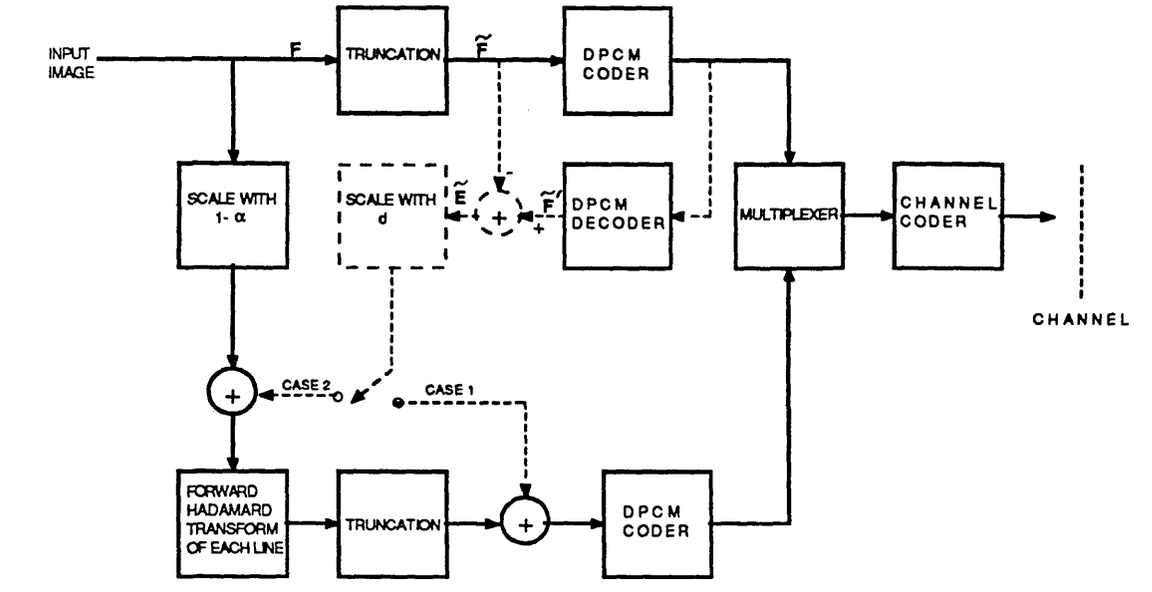
Substituting for $\underline{e}_3^t$ and $\underline{e}_4^t$ from (7.16), we obtain

$$\hat{\underline{f}}_1 = \underline{f}_1 + \underline{e}_3^f + \frac{1}{1-\alpha}\mathbf{H}_{\frac{N}{4}}\left(\underline{e}_3^h + \underline{e}_4^h\right) \tag{7.19a}$$

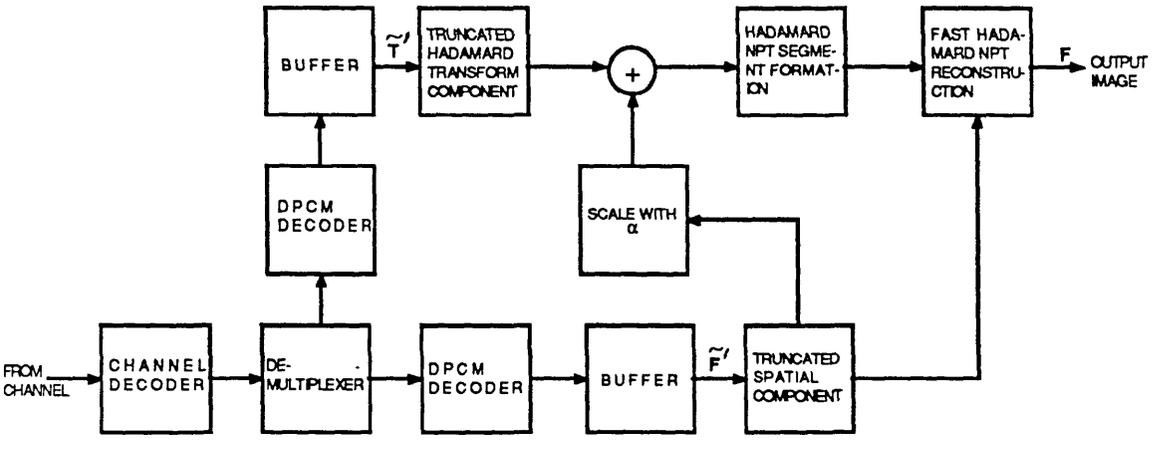
$$\hat{\underline{f}}_2 = \underline{f}_2 + \underline{e}_4^f + \frac{1}{1-\alpha}\mathbf{H}_{\frac{N}{4}}\left(\underline{e}_3^h - \underline{e}_4^h\right) \tag{7.19b}$$

$$\hat{\underline{f}}_3 = \underline{f}_3 + \underline{e}_3^f \tag{7.19c}$$

$$\hat{\underline{f}}_4 = \underline{f}_4 + \underline{e}_4^f \tag{7.19d}$$



(a) Coder



(b) Decoder

Fig. 7.14 : Hybrid Image Coding Using Fast Hadamard NPT Reconstruction.

Fig. 7.14 is a detailed block diagram of the algorithm; the dashed paths describe the variations of the algorithm which are discussed in the following section.

7.4.2.1 Variations of The Hybrid Coding Algorithm

It is observed that the reconstructed segments $\hat{\underline{f}}_1$ and $\hat{\underline{f}}_2$ contain linear combinations of the error terms $\underline{e}_3^f$, $\underline{e}_4^f$, $\underline{e}_3^h$ and $\underline{e}_4^h$. We have investigated the possibility of extracting some of the error terms at the receiver which can then be used to reduce the errors in the reconstructed segments but this has not been possible. In the following, we investigate two techniques which are aimed at reducing the error terms in the segments $\hat{\underline{f}}_1$ and $\hat{\underline{f}}_2$.

Case 1

The first approach considered involves first obtaining the spatial DPCM error vector

$$\tilde{\mathbf{e}}^f = \tilde{\mathbf{f}}' - \tilde{\mathbf{f}} \tag{7.20a}$$

$$= \left[\underline{0}\,|\,\underline{0}\,|\,\underline{e}_3^f\,|\,\underline{e}_4^f\right]^T \tag{7.20b}$$

and then adding a multiple of this vector to the truncated Hadamard transform vector $\tilde{\mathbf{h}}$, to obtain a vector $\tilde{\mathbf{x}}_h$, given by

$$\tilde{\mathbf{x}}_h = \tilde{\mathbf{h}} + d\tilde{\mathbf{e}}^f \tag{7.21}$$

where d is a scale factor. It is the respective vectors $\tilde{\mathbf{x}}_h$ that are used to form the array $\tilde{\mathbf{T}}$, the non-zero columns of which are subsequently DPCM coded. At the receiver, the coded truncated Hadamard NPT vector is obtained from

$$\tilde{\mathbf{r}}' = \alpha\tilde{\mathbf{f}}' + \tilde{\mathbf{x}}_h' \tag{7.22}$$

where $\tilde{\mathbf{x}}_h'$ is the coded version of $\tilde{\mathbf{x}}_h$. The vectors $\tilde{\mathbf{r}}'$ and $\tilde{\mathbf{f}}'$ are then used to reconstruct an approximate version of the image line, i.e. $\hat{\mathbf{f}}$. The segments of $\hat{\mathbf{f}}$ can be obtained by substituting

$$\underline{e}_3^t = (\alpha + d)\underline{e}_3^f + \underline{q}_3 \tag{7.23a}$$

and

$$\underline{e}_4^t = (\alpha + d)\underline{e}_4^f + \underline{q}_4 \tag{7.23b}$$

in (7.18), where $\underline{q}_3$ and $\underline{q}_4$ are respectively the quantization error vectors of the vectors $\underline{h}_3 + d\underline{e}_3^f$ and $\underline{h}_4 + d\underline{e}_4^f$. Thus, we obtain

$$\hat{\underline{f}}_1 = \underline{f}_1 + \underline{e}_3^f + \frac{d}{1-\alpha}\mathbf{H}_{\frac{N}{4}}\left(\underline{e}_3^h + \underline{e}_4^h\right) + \frac{1}{1-\alpha}\mathbf{H}_{\frac{N}{4}}\left(\underline{q}_3 + \underline{q}_4\right) \tag{7.24a}$$

$$\hat{\underline{f}}_2 = \underline{f}_2 + \underline{e}_4^f + \frac{d}{1-\alpha}\mathbf{H}_{\frac{N}{4}}\left(\underline{e}_3^h - \underline{e}_4^h\right) + \frac{1}{1-\alpha}\mathbf{H}_{\frac{N}{4}}\left(\underline{q}_3 - \underline{q}_4\right) \tag{7.24b}$$

$$\hat{\underline{f}}_3 = \underline{f}_3 + \underline{e}_3^f \tag{7.24c}$$

$$\hat{\underline{f}}_4 = \underline{f}_4 + \underline{e}_4^f \tag{7.24d}$$

It is observed that the reconstructed segments $\hat{\underline{f}}_1$ and $\hat{\underline{f}}_2$ each contain linear combinations of the error vectors $\underline{e}_3^f$, $\underline{e}_4^f$, $\underline{e}_3^h$, $\underline{e}_4^h$, $\underline{q}_3$ and $\underline{q}_4$. Furthermore, when $d = 0$, (7.24) reduce to (7.19).

Case 2

The second approach considered entails transmitting the information in such a way that a multiple of sub-Hadamard transforms of the spatial segment coding error vectors $\underline{e}_3^f$ and $\underline{e}_4^f$, i.e. $\mathbf{H}_{\frac{N}{4}}\underline{e}_3^f$ and $\mathbf{H}_{\frac{N}{4}}\underline{e}_4^f$ respectively, are present in the non-zero segments of $\tilde{\mathbf{r}}$. This is achieved by using the Hadamard transform of the vector $\mathbf{y}^f$ given by

$$\mathbf{y}^f = \mathbf{s} + d\tilde{\mathbf{e}}^f \tag{7.25a}$$

$$= (1-\alpha)\mathbf{f} + d\tilde{\mathbf{e}}^f \tag{7.25b}$$

where $\tilde{\mathbf{e}}^f$ is given by (7.20) and d is a scale factor, to form the truncated vector $\tilde{\mathbf{x}}_h$, which is defined by

$$\tilde{\mathbf{x}}_h = [\underline{0}\,|\,\underline{0}\,|\,\underline{x}_3\,|\,\underline{x}_4]^T \tag{7.26}$$

where

$$\underline{x}_3 = \underline{h}_3 - \frac{d(1-\alpha)}{2}\mathbf{H}_{\frac{N}{4}}\left(\underline{e}_3^f + \underline{e}_4^f\right) \tag{7.27}$$

and

$$\underline{x}_4 = \underline{h}_4 - \frac{d(1-\alpha)}{2}\mathbf{H}_{\frac{N}{4}}\left(\underline{e}_3^f - \underline{e}_4^f\right) \tag{7.28}$$

The respective vectors $\tilde{\mathbf{x}}_h$ are then used to form the array $\tilde{\mathbf{T}}$, the columns of which are subsequently DPCM coded. At the receiver, the truncated Hadamard NPT vector $\tilde{\mathbf{r}}'$ is obtained using (7.22). The corresponding vectors $\tilde{\mathbf{r}}'$ and $\tilde{\mathbf{f}}'$ are then used to obtain the reconstructed version of each line, i.e. $\hat{\mathbf{f}}$. The segments of $\hat{\mathbf{f}}$ can be obtained by substituting

$$\underline{e}_3^i = \alpha\underline{e}_3^f - \frac{d(1-\alpha)}{2}\mathbf{H}_{\frac{N}{4}}\left(\underline{e}_3^f + \underline{e}_4^f\right) + \underline{q}_3 \tag{7.29a}$$

and

$$\underline{e}_4^t = \alpha \underline{e}_4^f - \frac{d(1-\alpha)}{2} \mathbf{H}_{\frac{N}{4}} \left(\underline{e}_3^f - \underline{e}_4^f \right) + \underline{q}_4 \tag{7.29b}$$

in (7.18), where $\underline{q}_3$ and $\underline{q}_4$ are respectively the errors incurred in coding vectors $\underline{x}_3$ and $\underline{x}_4$. Thus, we obtain the segments of $\hat{\mathbf{f}}$ as

$$\hat{\underline{f}}_1 = \underline{f}_1 + (1-d)\underline{e}_3^f + \frac{1}{1-\alpha} \mathbf{H}_{\frac{N}{4}} \left(\underline{q}_3 + \underline{q}_4 \right) \tag{7.30a}$$

$$\hat{\underline{f}}_2 = \underline{f}_2 + (1-d)\underline{e}_4^f + \frac{1}{1-\alpha} \mathbf{H}_{\frac{N}{4}} \left(\underline{q}_3 - \underline{q}_4 \right) \tag{7.30b}$$

$$\hat{\underline{f}}_3 = \underline{f}_3 + \underline{e}_3^f \tag{7.30c}$$

$$\hat{\underline{f}}_4 = \underline{f}_4 + \underline{e}_4^f \tag{7.30d}$$

It is observed that if $d = 1$, the error vectors $\underline{e}_3^f$ and $\underline{e}_4^f$ are cancelled from (7.30*a*) and (7.30*b*) respectively.

7.4.3 Simulation, Results and Discussion

The coding algorithms described in the previous section were simulated for a 256 × 256 monochrome image. A DPCM coder was used to code the truncated spatial array $\tilde{\mathbf{F}}$. Similarly, a bank of DPCM coders was used to code the non-zero columns of the truncated array $\tilde{\mathbf{T}}$. The array $\tilde{\mathbf{F}}$ was coded at a higher rate than that used for coding the array $\tilde{\mathbf{T}}$.

Case 1

Fig. 7.15a is a coded version of image ALAN, at an overall rate of 1.75 bits per pixel. This was obtained by coding the non-zero segment of $\tilde{\mathbf{F}}$ at a rate of 2.0 bits per sample and the non-zero segment of $\tilde{\mathbf{T}}$ at a rate of 1.5 bits per sample, with $d = 0$. An MSE of 83.115 was obtained. It is observed that there are noticeable distortions in the left half of the picture; these correspond to (7.24*a*) and (7.24*b*). The subjective quality of the right half of the picture is good and better than that of the left half. Various forms of d were investigated, however, the choice $d = 0$ gave the best result in terms of MSE. Fig. 7.15b shows the result at an overall rate of 1.5 bits per pixel. This was obtained by coding the array $\tilde{\mathbf{F}}$ at 2.0 bits per sample and $\tilde{\mathbf{T}}$ at 1.0 bit per sample. A higher MSE of 91.928 was obtained and the difference in the subjective quality of the left and right halves of the picture becomes more marked. The performance of the coder, with $d = 0$, is independent of the choice of transform basis parameter α.



Fig. 7.15a : Encoded Version of ALAN at 1.75 Bits/pel., Using Hadamard NPT Recons. Hybrid Coding Algorithm; Case 1.



Fig. 7.15b : Encoded Version of ALAN at 1.5 Bits/pel., Using Hadamard NPT Recons. Hybrid Coding Algorithm; Case 1.



Fig. 7.16a : Encoded Version of ALAN at 1.75 Bits/pel., Using Hadamard NPT Recons. Hybrid Coding Algorithm; Case 2.



Fig. 7.16b : Encoded Version of ALAN at 1.5 Bits/pel., Using Hadamard NPT Recons. Hybrid Coding Algorithm; Case 2.

Case 2

In agreement with the result of (7.29), the choice $d = 1$ gave the best result. Fig. 7.16a is a coded version of image ALAN, at an overall rate of 1.75 bits per pixel. This was obtained by coding the non-zero segment of $\tilde{\mathbf{F}}$ at a rate of 2.0 bits per sample and the non-zero segment of $\tilde{\mathbf{T}}$ at a rate of 1.5 bits per sample. The MSE of 50.206 that was obtained is very much lower than the corresponding one for case 1, i.e. MSE = 83.115; an MSE of 82.85 was obtained by using a DPCM coder for coding the whole picture at 2.0 bits per pixel. Furthermore, there is a great deal of improvement in the subjective quality of the picture, compared to that for case 1, shown in Fig. 7.15a. Fig. 7.16b shows the result at an overall rate of 1.5 bits per pixel, obtained by using the same bits distribution as that for case 1. An MSE of 62.718 was obtained, which is very much lower than the corresponding one for case 1, i.e. MSE = 91.928. In addition, the subjective quality of the picture is better than the corresponding one for case 1, shown in Fig. 7.15b.

The results are independent of the choice of the transform basis parameter α.

7.5 Summary and Conclusion

One-dimensional Hadamard NPT reconstruction, two-layer intraframe packet transmission of images, which was proposed in chapter five, has been further investigated. The problem of channel bandwidth limitations has been considered and the reconstruction from guaranteed packets of compressed Hadamard NPT transformed imagery data has been investigated. Using transform DPCM techniques, good subjective quality reconstructed picture has been obtained from coded guaranteed one-dimensional Hadamard NPT samples at 3.0 bits per transmitted sample (this is equivalent to 1.5 bits per pixel for the whole picture) and above. The subjective quality of reconstructed pictures has been shown to deteriorate, when the guaranteed Hadamard NPT transform samples used for reconstruction are DPCM coded at 2.0 bits per transmitted sample. (1.0 bit per pixel for the whole picture) and below. The quality of the reconstructed pictures from DPCM coded guaranteed Hadamard NPT samples has been shown to be dependent on the original image content.

VQ technique has been investigated for coding the guaranteed Hadamard NPT transformed imagery samples at low bit rates. Very good subjective quality reconstructed pictures have been obtained from VQ coded guaranteed Hadamard

NPT transformed imagery samples at a bit rate of 1.25 bits per transmitted sample (0.625 bit per pixel for the whole picture).

The transmission of enhancement information has been shown to improve the quality of reconstructed pictures. It has been shown that very good results can be obtained when VQ is used to code the information transmitted as enhancement packets, at low bit rates. The effect of the loss of enhancement packets on reconstructed picture quality has been shown to be significant only at a high loss rate of 5^{-1} and above.

The effect of errors in the code-word digits used for representing the transmitted information (guaranteed packets and enhancement packets) has been investigated. Errors in the code-word digits used for representing the guaranteed information has been shown to have no noticeable effect on the subjective quality of reconstructed pictures at a BER of 10^{-4} and below. For BER = 10^{-3} and above, errors in the code-word digits used for representing the guaranteed information has been shown to degrade the quality of reconstructed pictures. However, errors in the code-word digits used for representing the enhancement information has been shown to have little or no noticeable effect on the subjective quality of reconstructed pictures.

Two-dimensional Hadamard NPT tactical imagery transmission, which was discussed in chapter six, has been revisited. The problem of signal transmission through limited bandwidth channels has been considered. The effect of coding the two-dimensional Hadamard NPT transformed imagery samples used for reconstruction, on the reconstructed picture quality, has been investigated. VQ coding of the two-dimensional Hadamard NPT samples at 1.0 bit per sample, has been shown to have little noticeable effect on the subjective quality of the reconstructed pictures. The subjective quality of the reconstructed pictures, when the transform samples are VQ coded at a low bit rate of 0.5625 bit per sample, has been shown to compare well with the no coding result, although there is a slight noticeable increase in the distortion of the region of the picture corresponding to the unknown transform samples.

The effect of errors in the code-word digits used for representing the two-dimensional Hadamard NPT transformed samples, used for reconstruction, has been shown to manifest mainly as an increase in the distortion of the region of the

picture corresponding in location to the unknown transform samples. The effect of the errors has been shown to be noticeable at BER of 10^{-2} and above.

Two hybrid image coding techniques, which are based on iterative Hadamard NPT reconstruction of each line of an image, have been proposed. The techniques are variations of a basic technique, which has been described. Results of monochrome image coding, using DPCM coders to code the respective parts of the information needed for reconstruction at the receiver, have been presented. The use of spatial DPCM imposes the restriction of using a block size of at least 128 for a 256×256 image. This has been shown to yield coded pictures having a non-uniform subjective quality, at bit rates of 1.75 bits per pixel and below. The second variation of the coding algorithm has been shown to yield a greatly improved picture in terms of subjective quality and MSE, than the first variation. The performances of the optimum coders in the two cases, are independent of the choice of the transform basis parameter α.

PART III
NATURALNESS-PRESERVING TRANSFORM FILTERING

CHAPTER EIGHT

NATURALNESS-PRESERVING TRANSFORM DOMAIN GENERALIZED WIENER FILTERING

8.1 Introduction

The application of orthogonal transforms in the classical technique of signal estimation known as Wiener filtering has been investigated [5,73]. Specifically, orthogonal transforms have been used to extend Wiener filtering to the processing of discrete signals with emphasis on the reduction of the amount of computation involved in the Wiener filtering process. The generalized Wiener filtering process has also been applied to image enhancement [73].

In this chapter, NPT domain generalized Wiener filtering of discrete signals is developed. NPT generalized Wiener filters are derived. The mathematical model of the NPT generalized Wiener filtering system is presented in section 8.2. A derivation of NPT generalized Wiener filters is given in section 8.3; the formulation is in one dimension. Sub-optimum NPT generalized Wiener filtering systems are examined in section 8.4 and empirical results of their performances, when used for filtering first order stationary Gauss-Markov signals corrupted by additive white noise, are presented. In section 8.5, a new approach to NPT generalized Wiener filtering is examined. Empirical results of the performance of specified filter matrices are presented.

8.2 Mathematical Model of The NPT Generalized Wiener Filter

The block diagram of the one-dimensional NPT generalized Wiener filtering system is shown in Fig. 8.1. $\mathbf{z}$ is the input vector of length N, which is the sum of a data vector $\mathbf{f}$ and a noise vector $\mathbf{w}$. The Wiener filter, $\mathbf{M}$, is in the form of an $N \times N$ matrix. $\psi\{\alpha\}$ and $\psi^{-1}\{\alpha\}$ are $N \times N$ matrices which represent an NPT transform kernel and its inverse respectively, while $\hat{\mathbf{f}}$ is the estimate of the data vector $\mathbf{f}$.

The objective is to design the filter $\mathbf{M}$ in such a way that the expected value of the MSE between $\mathbf{f}$ and $\hat{\mathbf{f}}$ is minimized. For the special case when $\psi\{\alpha\} = \mathbf{I}$, i.e. $\alpha = 1$, the model in Fig. 8.1 reduces to that originally proposed by Wiener. Thus,

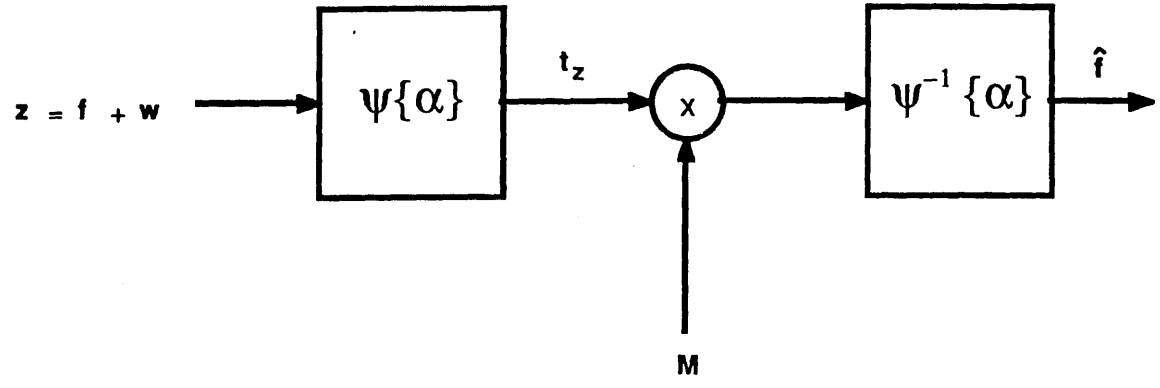


Fig. 8.1 : NPT Generalized Wiener Filtering Model.

the model in Fig. 8.1 is more general and hence the name generalized Wiener filtering.

For many classes of input data, the vector $\mathbf{z}$ can be regarded as a sample of a stationary or non-stationary random process. Denoting the mean vector of the process by $\bar{\mathbf{z}}$, then the data domain covariance matrix is given by

$$\mathbf{C}_{\mathbf{z}} = E\left\{(\mathbf{z}-\bar{\mathbf{z}})(\mathbf{z}-\bar{\mathbf{z}})^T\right\} \tag{8.1}$$

which can be expressed as

$$\mathbf{C}_{\mathbf{z}} = E\left\{\mathbf{z}\mathbf{z}^T\right\} - \bar{\mathbf{z}}\bar{\mathbf{z}}^T \tag{8.2}$$

where $E\{\cdot\}$ represents the mathematical expectation operator and T denotes the transposition operation. The transform domain covariance matrix of the data vector $\mathbf{z}$ is given by

$$\mathbf{C}_{\mathbf{t}_{\mathbf{z}}} = E\left\{(\mathbf{t}_{\mathbf{z}}-\bar{\mathbf{t}}_{\mathbf{z}})(\mathbf{t}_{\mathbf{z}}-\bar{\mathbf{t}}_{\mathbf{z}})^T\right\} \tag{8.3a}$$

$$= E\left\{\mathbf{t}_{\mathbf{z}}\mathbf{t}_{\mathbf{z}}^T\right\} - \bar{\mathbf{t}}_{\mathbf{z}}\bar{\mathbf{t}}_{\mathbf{z}}^T \tag{8.3b}$$

where

$$\mathbf{t}_{\mathbf{z}} = \psi\{\alpha\}\,\mathbf{z} \tag{8.4}$$

Using (8.4) in (8.3b) and making use of (8.2) and the fact that $\psi\{\alpha\}$ is symmetric, (8.3) reduce to

$$\mathbf{C}_{\mathbf{t}_{\mathbf{z}}} = \psi\{\alpha\}\,\mathbf{C}_{\mathbf{z}}\psi\{\alpha\} \tag{8.5}$$

8.3 NPT Generalized Wiener Filter Design

The forward and inverse NPT transform kernels used for the filter design are respectively given by

$$\psi\{\alpha\} = \alpha\mathbf{I} + (1-\alpha)\mathbf{A} \qquad , |\alpha| \leq 1 \tag{8.6}$$

and

$$\psi^{-1}\{\alpha\} = \frac{1}{2\alpha-1}\left[\alpha\mathbf{I} - (1-\alpha)\mathbf{A}\right] \tag{8.7}$$

where $\mathbf{A}$ is a symmetric orthogonal transform kernel. From (8.5 – 8.7), it follows that the data and transform domain covariance matrices are related by a similarity transformation only when $\alpha = 0$ and $\alpha = 1$.

We make the following assumptions in the design of the filter:

1) The data and noise processes have zero means, i.e. $\overline{\mathbf{f}} = \overline{\mathbf{w}} = \mathbf{0}$ which implies that

$$\overline{\mathbf{z}} = \mathbf{0} \tag{8.8a}$$

$$\mathbf{C_f} = E\left\{\mathbf{f}\mathbf{f}^T\right\} \tag{8.8b}$$

$$\mathbf{C_w} = E\left\{\mathbf{w}\mathbf{w}^T\right\} \tag{8.8c}$$

and

$$\mathbf{C_z} = E\left\{\mathbf{z}\mathbf{z}^T\right\} \tag{8.8d}$$

2) The data and noise processes are uncorrelated; i.e.

$$E\left\{\mathbf{f}\mathbf{w}^T\right\} = E\left\{\mathbf{w}\mathbf{f}^T\right\} = \mathbf{0} \tag{8.9}$$

We also make use of the fact that

$$\left[\psi\left\{\alpha\right\}\right]^T = \psi\left\{\alpha\right\} \tag{8.10}$$

and

$$\left[\psi^{-1}\left\{\alpha\right\}\right]^T = \psi^{-1}\left\{\alpha\right\} \tag{8.11}$$

These imply that

$$\mathbf{C}_{\mathbf{t_f}} = \psi\left\{\alpha\right\}\mathbf{C_f}\psi\left\{\alpha\right\} \tag{8.12a}$$

$$\mathbf{C}_{\mathbf{t_w}} = \psi\left\{\alpha\right\}\mathbf{C_w}\psi\left\{\alpha\right\} \tag{8.12b}$$

and

$$\mathbf{C}_{\mathbf{t_z}} = \psi\left\{\alpha\right\}\mathbf{C_z}\psi\left\{\alpha\right\} \tag{8.12c}$$

where $\mathbf{C_f}$, $\mathbf{C_w}$ and $\mathbf{C_z}$ are the data domain covariance matrices of $\mathbf{f}$, $\mathbf{w}$ and $\mathbf{z}$ respectively; $\mathbf{C}_{\mathbf{t_f}}$, $\mathbf{C}_{\mathbf{t_w}}$ and $\mathbf{C}_{\mathbf{t_z}}$ are the transform domain covariance matrices of $\mathbf{f}$, $\mathbf{w}$ and $\mathbf{z}$ respectively.

8.3.1 Derivation of The Optimum NPT Generalized Wiener Filter Matrix

We represent the estimation error vector by $\mathbf{e}$ and is given by

$$\mathbf{e} = \hat{\mathbf{f}} - \mathbf{f} \tag{8.13}$$

The total MSE in estimating $\mathbf{f}$ is thus given by

$$\varepsilon = E\left\{\left\|\hat{\mathbf{f}} - \mathbf{f}\right\|^2\right\} \tag{8.14a}$$

$$= E\left\{\left(\hat{\mathbf{f}} - \mathbf{f}\right)^T\left(\hat{\mathbf{f}} - \mathbf{f}\right)\right\} \tag{8.14b}$$

From the filter model shown in Fig. 8.1, it follows that

$$\hat{\mathbf{f}} = \psi^{-1}\{\alpha\}\,\mathbf{M}\psi\{\alpha\}\,\mathbf{z} \tag{8.15}$$

Expanding (8.14*b*) and substituting (8.15), we obtain

$$\varepsilon = E\left\{\hat{\mathbf{f}}^T\hat{\mathbf{f}}\right\} - E\left\{\hat{\mathbf{f}}^T\mathbf{f}\right\} - E\left\{\mathbf{f}^T\hat{\mathbf{f}}\right\} + E\left\{\mathbf{f}^T\mathbf{f}\right\} \tag{8.16a}$$

$$= E\left\{\mathbf{z}^T\psi\{\alpha\}\,\mathbf{M}^T\psi^{-1}\{\alpha\}\,\psi^{-1}\{\alpha\}\,\mathbf{M}\psi\{\alpha\}\,\mathbf{z}\right\} - E\left\{\mathbf{z}^T\psi\{\alpha\}\,\mathbf{M}^T\psi^{-1}\{\alpha\}\,\mathbf{f}\right\}$$
$$- E\left\{\mathbf{f}^T\psi^{-1}\{\alpha\}\,\mathbf{M}\psi\{\alpha\}\,\mathbf{z}\right\} + E\left\{||\mathbf{f}||^2\right\} \tag{8.16b}$$

or

$$\varepsilon = E\left\{\mathbf{z}^T\psi\{\alpha\}\,\mathbf{M}^T\psi^{-1}\{\alpha\}\,\psi^{-1}\{\alpha\}\,\mathbf{M}\psi\{\alpha\}\,\mathbf{z}\right\} - 2E\left\{\mathbf{z}^T\psi\{\alpha\}\,\mathbf{M}^T\psi^{-1}\{\alpha\}\,\mathbf{f}\right\}$$
$$+ E\left\{||\mathbf{f}||^2\right\} \tag{8.17}$$

where we have made use of the fact that $\psi\{\alpha\}$ and $\psi^{-1}\{\alpha\}$ are symmetric and also that

$$\mathbf{z}^T\mathbf{B}\mathbf{f} = \mathbf{f}^T\mathbf{B}^T\mathbf{z} \tag{8.18}$$

where $\mathbf{z}$ and $\mathbf{f}$ are $N \times 1$ vectors and $\mathbf{B}$ is an $N \times N$ matrix.

Using (8.4), we can express (8.17) as

$$\varepsilon = E\left\{\mathbf{t}_\mathbf{z}^T\mathbf{M}^T\mathbf{Q}\mathbf{M}\mathbf{t}_\mathbf{z}\right\} - 2E\left\{\mathbf{t}_\mathbf{z}^T\mathbf{M}^T\psi^{-1}\{\alpha\}\,\mathbf{f}\right\} + E\left\{||\mathbf{f}||^2\right\} \tag{8.19}$$

where

$$\mathbf{Q} = \psi^{-1}\{\alpha\}\,\psi^{-1}\{\alpha\} \tag{8.20}$$

The optimum filter matrix is obtained by choosing $\mathbf{M}$ in such a way that ε is minimum. Hence, it must satisfy the necessary condition

$$\nabla_\mathbf{M}\varepsilon = \mathbf{0} \tag{8.21}$$

where $\nabla_\mathbf{M}\varepsilon$ is the gradient (generalization of the derivative operation) of ε with respect to the matrix $\mathbf{M}$. Thus, we have

$$E\left\{\nabla_\mathbf{M}\left(\mathbf{t}_\mathbf{z}^T\mathbf{M}^T\mathbf{Q}\mathbf{M}\mathbf{t}_\mathbf{z}\right)\right\} - 2E\left\{\nabla_\mathbf{M}\left(\mathbf{t}_\mathbf{z}^T\mathbf{M}^T\psi^{-1}\{\alpha\}\,\mathbf{f}\right)\right\} + E\left\{\nabla_\mathbf{M}\left(||\mathbf{f}||^2\right)\right\} = \mathbf{0} \tag{8.22}$$

Making use of the relations (these are derived in appendix V)

$$\nabla_\mathbf{B}\left(\mathbf{x}^T\mathbf{B}^T\mathbf{Q}\mathbf{B}\mathbf{x}\right) = \mathbf{Q}^T\mathbf{B}\mathbf{x}\mathbf{x}^T + \mathbf{Q}\mathbf{B}\mathbf{x}\mathbf{x}^T \tag{8.23}$$

$$\nabla_\mathbf{B}\left(\mathbf{x}^T\mathbf{B}^T\mathbf{P}\mathbf{f}\right) = \mathbf{P}\mathbf{f}\mathbf{x}^T \tag{8.24}$$

$$\nabla_\mathbf{B}\left(||\mathbf{x}||^2\right) = \mathbf{0} \tag{8.25}$$

where $\mathbf{B}$, $\mathbf{P}$ and $\mathbf{Q}$ are $N \times N$ matrices, $\mathbf{x}$ and $\mathbf{f}$ are $N \times 1$ vectors, (8.22) becomes

$$E\left\{\mathbf{Q}^T\mathbf{M}\mathbf{t}_z\mathbf{t}_z^T + \mathbf{Q}\mathbf{M}\mathbf{t}_z\mathbf{t}_z^T\right\} = 2E\left\{\psi^{-1}\{\alpha\}\,\mathbf{f}\mathbf{t}_z^T\right\} \tag{8.26}$$

or

$$\left(\mathbf{Q}^T\mathbf{M} + \mathbf{Q}\mathbf{M}\right) E\left\{\mathbf{t}_z\mathbf{t}_z^T\right\} = 2\psi^{-1}\{\alpha\}\, E\left\{\mathbf{f}\mathbf{t}_z^T\right\} \tag{8.27}$$

Using (8.4) in (8.27), we obtain

$$\left(\mathbf{Q}^T + \mathbf{Q}\right)\mathbf{M}\psi\{\alpha\}\, E\left\{\mathbf{z}\mathbf{z}^T\right\}\psi\{\alpha\} = 2\psi^{-1}\{\alpha\}\, E\left\{\mathbf{f}\mathbf{z}^T\right\}\psi\{\alpha\} \tag{8.28}$$

But $\mathbf{z} = \mathbf{f} + \mathbf{w}$, and using $(8.8a - d)$ and (8.9), the following relations hold:

$$E\left\{\mathbf{f}\mathbf{z}^T\right\} = E\left\{\mathbf{f}\,\mathbf{f}^T\right\} = \mathbf{C}_\mathbf{f} \tag{8.29a}$$

and

$$E\left\{\mathbf{z}\mathbf{z}^T\right\} = \mathbf{C}_\mathbf{f} + \mathbf{C}_\mathbf{w} \tag{8.29b}$$

Substituting (8.29a) and (8.29b) in (8.28), we obtain

$$\left(\mathbf{Q}^T + \mathbf{Q}\right)\mathbf{M}\psi\{\alpha\}\left(\mathbf{C}_\mathbf{f} + \mathbf{C}_\mathbf{w}\right)\psi\{\alpha\} = 2\psi^{-1}\{\alpha\}\,\mathbf{C}_\mathbf{f}\psi\{\alpha\} \tag{8.30}$$

Equation (8.30) yields the optimum filter matrix in the following two forms

(i) In terms of the data domain covariance matrices $\mathbf{C}_\mathbf{f}$ and $\mathbf{C}_\mathbf{w}$:

$$\mathbf{M}_0 = 2\left(\mathbf{Q}^T + \mathbf{Q}\right)^{-1}\psi^{-1}\{\alpha\}\,\mathbf{C}_\mathbf{f}\psi\{\alpha\}\left[\psi\{\alpha\}\left(\mathbf{C}_\mathbf{f} + \mathbf{C}_\mathbf{w}\right)\psi\{\alpha\}\right]^{-1} \tag{8.31}$$

$$= 2\left(\mathbf{Q}^T + \mathbf{Q}\right)^{-1}\psi^{-1}\{\alpha\}\,\mathbf{C}_\mathbf{f}\left(\mathbf{C}_\mathbf{f} + \mathbf{C}_\mathbf{w}\right)^{-1}\psi^{-1}\{\alpha\} \tag{8.32}$$

which can be expressed as

$$\mathbf{M}_0 = 2\left(\mathbf{Q}^T + \mathbf{Q}\right)^{-1}\psi^{-1}\{\alpha\}\,\mathbf{M}_r\psi^{-1}\{\alpha\} \tag{8.33}$$

where

$$\mathbf{M}_r = \mathbf{C}_\mathbf{f}\left(\mathbf{C}_\mathbf{f} + \mathbf{C}_\mathbf{w}\right)^{-1} \tag{8.34}$$

Substituting for $\mathbf{Q}$ from (8.20) in (8.33), we obtain

$$\mathbf{M}_0 = 2\left[2\psi^{-1}\{\alpha\}\,\psi^{-1}\{\alpha\}\right]^{-1}\psi^{-1}\{\alpha\}\,\mathbf{M}_r\psi^{-1}\{\alpha\} \tag{8.35}$$

or

$$\mathbf{M}_0 = \psi\{\alpha\}\,\mathbf{M}_r\psi^{-1}\{\alpha\} \tag{8.36}$$

Thus, the optimum filter matrix is dependent on the NPT basis parameter α, $|\alpha| \leq 1$.

(ii) In terms of the transform domain covariance matrices $\mathbf{C}_{t_f}$ and $\mathbf{C}_{t_w}$: from (8.31) and (8.20), we have

$$\mathbf{M}_0 = \psi\{\alpha\}\,\mathbf{C}_\mathbf{f}\psi\{\alpha\}\left[\psi\{\alpha\}\left(\mathbf{C}_\mathbf{f}+\mathbf{C}_\mathbf{w}\right)\psi\{\alpha\}\right]^{-1} \tag{8.37}$$

or

$$\mathbf{M}_0 = \mathbf{C}_{t_f}[\mathbf{C}_{t_f}+\mathbf{C}_{t_w}]^{-1} \tag{8.38}$$

where

$$\mathbf{C}_{t_f} = \psi\{\alpha\}\,\mathbf{C}_\mathbf{f}\psi\{\alpha\} \tag{8.39a}$$

and

$$\mathbf{C}_{t_w} = \psi\{\alpha\}\,\mathbf{C}_\mathbf{w}\psi\{\alpha\} \tag{8.39b}$$

In analogy with the impulse response of a linear system, the matrix $\mathbf{M}_r$ in (8.36) is called the *response matrix* [73].

8.3.2 Minimum Mean-square Error of The Optimum NPT Generalized Wiener Filter

The mean-square error associated with the above optimum filter, given by (8.36) and (8.38), can be obtained as follows. For convenience, we express ε given in (8.14) as

$$\varepsilon = tr\left[E\left\{\left(\hat{\mathbf{f}}-\mathbf{f}\right)\left(\hat{\mathbf{f}}-\mathbf{f}\right)^T\right\}\right] \tag{8.40}$$

where "tr" denotes the trace of a matrix. From (8.40), we have

$$\varepsilon = tr\left[E\left\{\hat{\mathbf{f}}\hat{\mathbf{f}}^T\right\} - E\left\{\hat{\mathbf{f}}\mathbf{f}^T\right\} - E\left\{\mathbf{f}\hat{\mathbf{f}}^T\right\} + E\left\{\mathbf{f}\mathbf{f}^T\right\}\right] \tag{8.41}$$

Using (8.15) and obtaining $\mathbf{M}$ from (8.30), it can be shown that

$$E\left\{\hat{\mathbf{f}}\hat{\mathbf{f}}^T\right\} = E\left\{\mathbf{f}\hat{\mathbf{f}}^T\right\} \tag{8.42a}$$

and

$$E\left\{\hat{\mathbf{f}}\mathbf{f}^T\right\} = \psi^{-1}\{\alpha\}\,\mathbf{M}\psi\{\alpha\}\,\mathbf{C}_\mathbf{f} \tag{8.42b}$$

Substituting (8.42$a-b$) in (8.41) and using (8.8b), we obtain

$$\varepsilon = tr\left[\mathbf{C}_\mathbf{f} - \psi^{-1}\{\alpha\}\,\mathbf{M}\psi\{\alpha\}\,\mathbf{C}_\mathbf{f}\right] \tag{8.43}$$

Substituting $\mathbf{M}_0$ for $\mathbf{M}$ in (8.43), we obtain the expression for the minimum mean-square error as

$$\varepsilon_{min} = tr\left[\mathbf{C}_\mathbf{f} - \mathbf{C}_\mathbf{f}(\mathbf{C}_\mathbf{f}+\mathbf{C}_\mathbf{w})^{-1}\mathbf{C}_\mathbf{f}\right] \tag{8.44}$$

which is exclusively in terms of the data domain covariance matrices and can be computed. It is observed that the minimum mean-square error is independent of the NPT basis employed in the generalized Wiener filter design. This implies that for NPT generalized Wiener filtering systems operating at different values of α, $|\alpha| < 1$, the filtering performance is invariant.

Returning to the filter model in Fig. 8.1 and substituting $\mathbf{M} = \mathbf{M}_0$ from (8.36), we obtain the output of the filter as

$$\hat{\mathbf{f}} = \psi^{-1}\{\alpha\}\left(\psi\{\alpha\}\,\mathbf{M}_r\psi^{-1}\{\alpha\}\right)\psi\{\alpha\}\,\mathbf{z} \tag{8.45a}$$

$$= \mathbf{M}_r\mathbf{z} \tag{8.45b}$$

$$= \mathbf{C_f}(\mathbf{C_f} + \mathbf{C_w})^{-1}\mathbf{z} \tag{8.45c}$$

We obtain the result that the output of the filter, for the choice of filter matrix given by (8.36), is independent of the NPT basis parameter α. However, it must be noted that the fact that (8.36) yields the minimum mean-square error can only be ascertained via the analysis of sections 8.3.1 and 8.3.2. An important fact that is associated with the result of (8.44) is that the performance of an optimum NPT generalized Wiener filtering system for any specified basis parameter α, $|\alpha| < 1$, is identical to that of any optimum orthogonal transform generalized Wiener filtering system.

8.4 Sub-optimal Wiener Filtering

In general, the number of multiplications required to perform the optimal Wiener filtering operation is proportional to N^2 [5, pg. 187] and this constitutes a hindrance to real-time processing. The aim of sub-optimal Wiener filtering is to develop filter matrices that contain a relatively large number of zero entries, while maintaining the mean-square error performance of the resulting filter as close as possible to the optimum filter level. The result of this is that the filter operation $\mathbf{M}\mathbf{t}_\mathbf{z}$ (refer to Fig. 8.1) can be performed with a reduced number of multiplications. We investigate the NPT bases for this purpose.

The sub-optimal Wiener filtering design problem can be regarded as an optimization problem whereby the filter matrix $\mathbf{M}$ is chosen to minimize

$$\begin{aligned}\varepsilon = tr\Big[&\psi^{-1}\{\alpha\}\,\mathbf{M}\psi\{\alpha\}\,(\mathbf{C_f} + \mathbf{C_w})\,\psi\{\alpha\}\,\mathbf{M}^T\psi^{-1}\{\alpha\} \\ &- \psi^{-1}\{\alpha\}\,\mathbf{M}\psi\{\alpha\}\,\mathbf{C_f} - \mathbf{C_f}\psi\{\alpha\}\,\mathbf{M}^T\psi^{-1}\{\alpha\} + \mathbf{C_f}\Big] \\ = tr\left[\psi^{-1}\{\alpha\}\,\mathbf{M}\psi\{\alpha\}\,(\mathbf{C_f} + \mathbf{C_w})\,\psi\{\alpha\}\,\mathbf{M}^T\psi^{-1}\{\alpha\}\right]\end{aligned} \tag{8.46a}$$

$$-tr\left[\psi^{-1}\{\alpha\}\,\mathbf{M}\psi\{\alpha\}\,\mathbf{C}_f\right]-tr\left[\mathbf{C}_f\psi\{\alpha\}\,\mathbf{M}^T\psi^{-1}\{\alpha\}\right]+tr\left[\mathbf{C}_f\right] \qquad (8.46b)$$

subject to the constraint that certain selected elements of $\mathbf{M}$ are zero. The following possibilities are considered.

1) Obtain the sub-optimal filter matrix from the optimum filter matrix by retaining only those elements having a relatively large magnitude. Set the remaining elements to zero.

2) Constrain $\mathbf{M}$ to be a diagonal matrix.

In the following sub-sections, we consider the above two possibilities in more detail and present the results of simulations for sub-optimum NPT generalized Wiener filtering of first order stationary Gauss-Markov signals, corrupted by additive white noise.

8.4.1 Sub-optimal Filtering Using Relatively Large Magnitude Filter Coefficients

In this case, the sub-optimum filter matrix, $\tilde{\mathbf{M}}$, is derived from the optimum filter matrix, $\mathbf{M}_0$, by retaining the highest magnitude n_f filter coefficients and setting the remaining coefficients to zero.

Simulation Results

A simulation was conducted to investigate sub-optimal NPT generalized Wiener filtering using relatively large magnitude filter coefficients. The signal used is a first order stationary Gauss-Markov signal corrupted with additive white noise.

Fig. 8.2 shows the result of using the sub-optimum Hadamard NPT generalized Wiener filter having from 1 to 50 non-zero filter terms, to filter a zero mean, unit variance first order stationary Gauss-Markov signal, $\rho = 0.91$, which has been corrupted by zero mean additive white noise with the signal-to-noise ratio (SNR) equal to unity, using a block size of 16. The plots correspond to the Hadamard NPT bases $\alpha = -0.6$, $\alpha = -0.4$, $\alpha = 0$ and $\alpha = 0.2$. It is observed that for 4 to 10 non-zero filter terms, the Hadamard NPT(0.2) performs better than the Hadamard transform in terms of MSE. In addition, the performances of the Hadamard NPT(0.2) and the Hadamard transform are very similar for 48 to 50 non-zero filter terms. For the remaining cases of non-zero filter terms (≤ 50 in

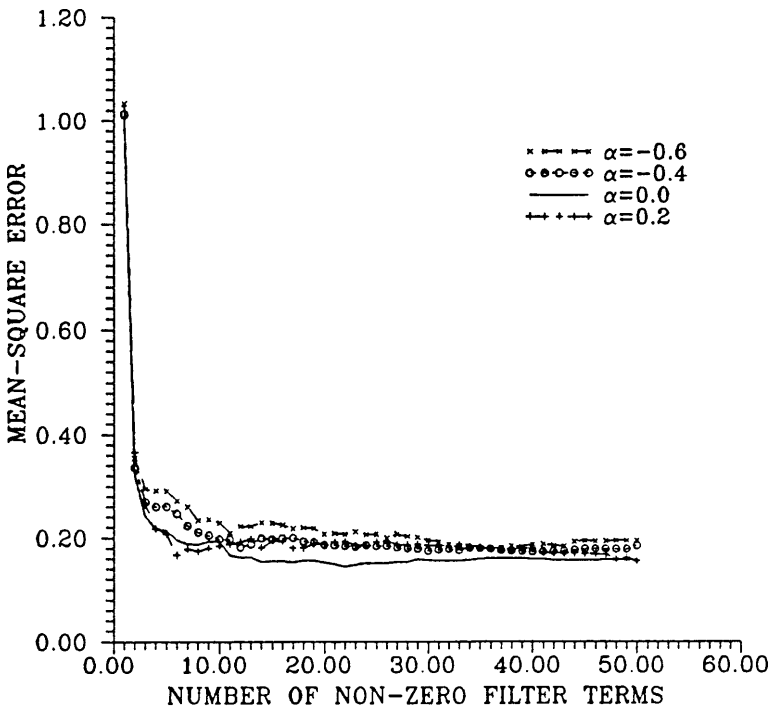


Fig. 8.2 : Sub-optimum Hadamard NPT generalized Wiener filtering of a stationary first order Gauss-Markov signal; ρ=0.91, SNR=1 and block size=16.

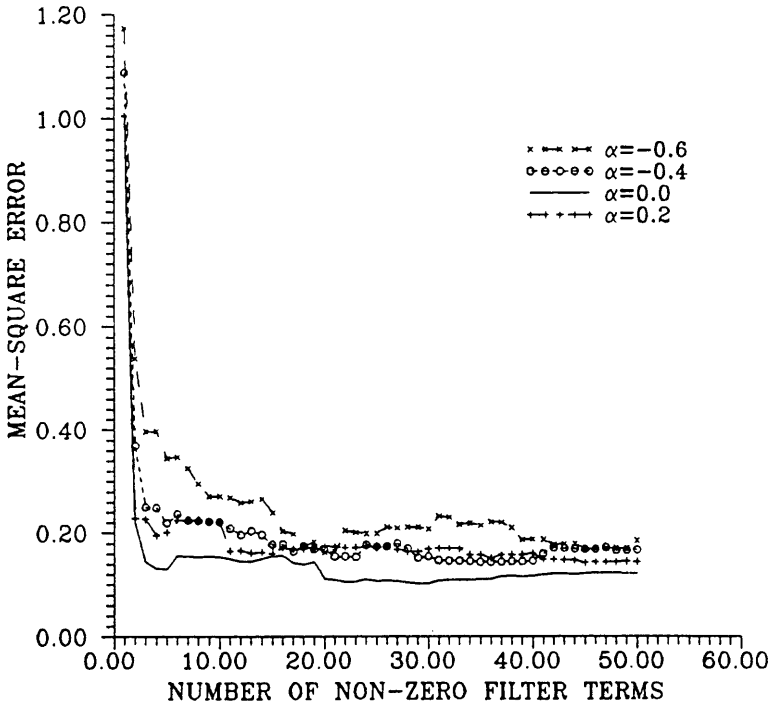


Fig. 8.3 : Sub-optimum sine NPT generalized Wiener filtering of a stationary first order Gauss-Markov signal; ρ=0.91, SNR=1 and block size=16.

number), the Hadamard transform shows superior performance. It is observed that the relative performance of the Hadamard NPT bases varies with the number of non-zero filter terms. Fig. 8.3 shows the result when the sine NPT was used. In this case, the sine transform has the best performance for the different numbers of non-zero filter terms. It is also observed that the relative performance of the sine NPT bases depends on the number of non-zero filter terms used. Fig. 8.4 shows the corresponding result when the SC NPT was used for filtering. It is observed that the SC NPT(-0.6) has the best performance when 29 non-zero filter terms are used for filtering. Furthermore, both the SC NPT(-0.6) and the SC NPT(-0.4) bases perform better than the SC transform when filter terms varying from 31 to 50 in number are used. For the remaining cases of non-zero filter terms (≤ 50), the SC transform shows the best performance. It is also observed that the relative performance of the SC NPT bases is dependent on the number of non-zero filter terms used.

In Fig. 8.5, the three NPT transforms are compared when 10 non-zero filter terms are used to filter the first order stationary Gauss-Markov signal. It should be noted that the points corresponding to the basis parameter α for which the MSE is greater than 2.0 have been excluded from the plots. The relative performance of the NPT transforms can be seen to vary with α. For example, the Hadamard NPT has the best performance when $-1 \leq \alpha < -0.75$ while the SC NPT has the best performance when $-0.75 < \alpha < 0.17$. It is also observed that the basis giving minimum MSE correspond to a value of $\alpha < 0$ for the Hadamard NPT and the SC NPT while it corresponds to a value of $\alpha \approx 0.05$ for the sine NPT.

Fig. 8.6 shows the effect of varying the signal-to-noise ratio for the sub-optimum Hadamard NPT generalized Wiener filtering of the first order Gauss-Markov signal using 10 non-zero filter terms; the points corresponding to α for which the MSE is greater than 2.0 have been excluded from the plots. It is observed that for $-0.8 < \alpha < 0.5$ and $0.8 < \alpha \leq 1.0$, the MSE decreases with increasing signal-to-noise ratio. However, the MSE obtained for SNR = 2 is lower than that obtained for SNR = 10 when $-1 \leq \alpha < -0.8$ and $0.6 < \alpha < 0.82$ (approx.); this is a surprising result and no explanation has been found for this. An additional observation is that the basis giving minimum MSE is dependent on the signal-to-noise ratio. For SNR = 2 and SNR = 10, the basis giving minimum MSE lies within the range $0 < \alpha < 0.25$ while for SNR = 1, it lies within the range $-0.1 < \alpha < 0$.

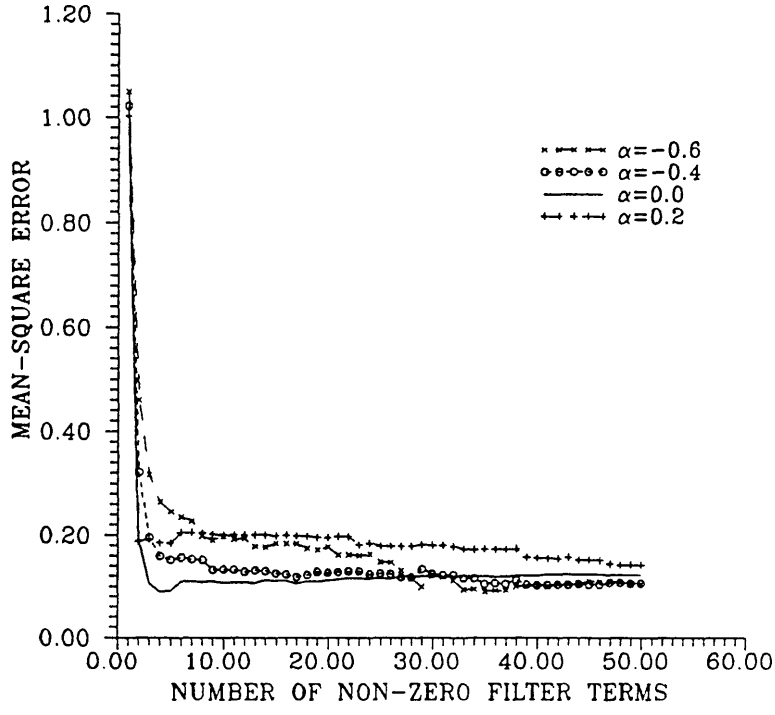


Fig. 8.4 : Sub-optimum SC NPT generalized Wiener filtering of a stationary first order Gauss-Markov signal; ρ=0.91, SNR=1 and block size=16.

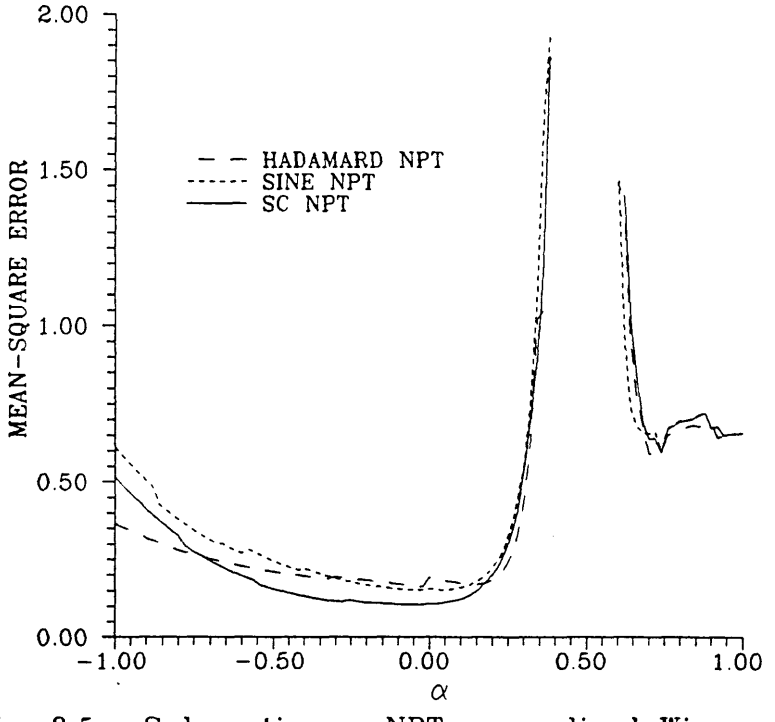


Fig. 8.5 : Sub-optimum NPT generalized Wiener filtering of a stationary first order Gauss-Markov signal, using 10 non-zero filter terms; ρ=0.91, SNR=1 and block size=16.

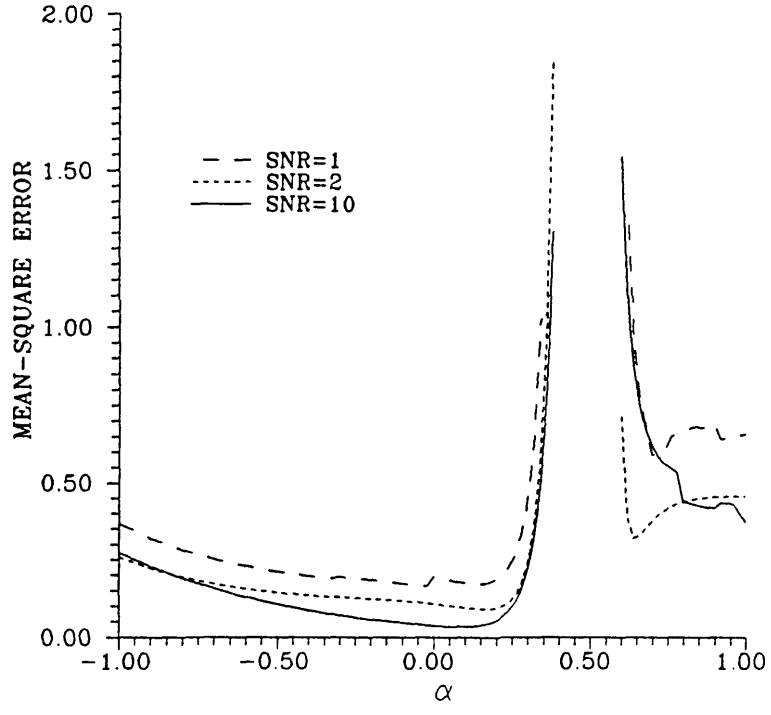


Fig. 8.6 : MSE as a function of α and SNR for sub-optimum Hadamard NPT generalized Wiener filtering of a stationary first order Gauss-Markov signal, using 10 non-zero filter terms; ρ=0.91 and block size=16.

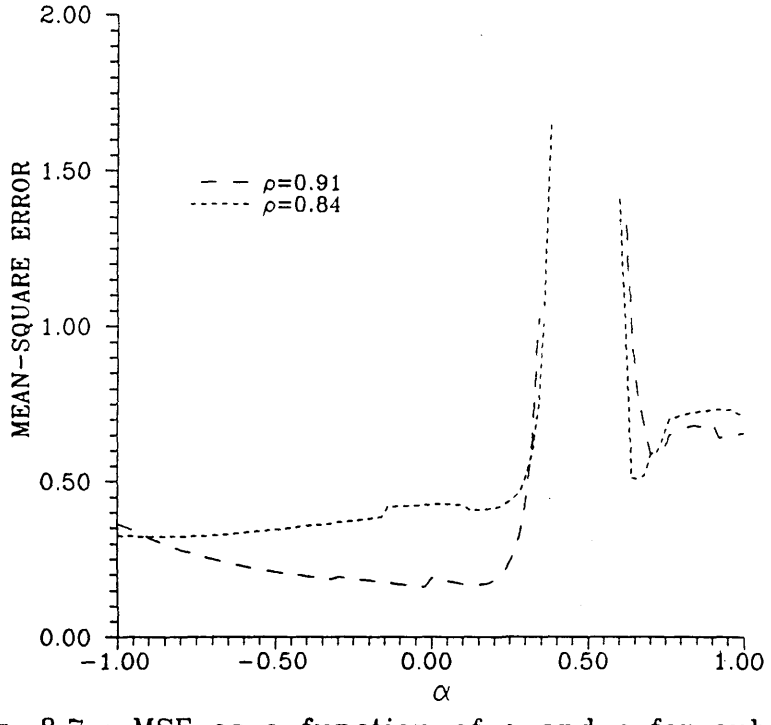


Fig. 8.7 : MSE as a function of α and ρ for sub-optimum Hadamard NPT generalized Wiener filtering of a stationary first order Gauss-Markov signal, using 10 non-zero filter terms; SNR=1 and block size=16.

Fig. 8.7 shows the effect of reducing the inter-element correlation of the original Gauss-Markov signal. The result correspond to using the sub-optimum Hadamard NPT generalized Wiener filter, containing 10 non-zero filter terms and a signal-to-noise ratio of unity. An increase in MSE is observed when the inter-element correlation is reduced from 0.91 to 0.84, for $-0.9 < \alpha < 0.3$ and $0.7 < \alpha \leq 1$. However, for $-1 \leq \alpha < -0.9$, $0.3 < \alpha < 0.5$ and $0.6 < \alpha < 0.8$, a decrease in MSE is observed with reduction of inter-element correlation; this is a surprising result and no explanation has been found for this. For $\rho = 0.84$, the basis giving minimum MSE lies within the range $-1 < \alpha < -0.8$ while for $\rho = 0.91$, the basis giving minimum MSE lies within the range $-0.1 < \alpha < 0$.

8.4.2 Sub-optimal Diagonal Filters

The optimal diagonal filter is the Karhunen-Loève (KL) transform filter. However, due to the complexity of computing the KL transform, the possibility of developing sub-optimal diagonal filter matrices for transforms that posses fast computational algorithms have been considered [5]. Here, we develop sub-optimal diagonal filters based on the NPT transforms.

Filters whose matrices contain only diagonal elements are referred to as *scalar filters*, while those having non-zero off diagonal elements as well, are referred to as *vector filters.*

The desired diagonal filter is obtained by constraining $\mathbf{M}$ in (8.30) to be a diagonal matrix. We define the scalar filter matrix as

$$\mathbf{M}_d = diag\,(m_{11}, m_{22}, \ldots m_{NN}) \tag{8.47}$$

and from (8.20) and (8.30), we obtain

$$m_{ii} = \frac{\mathbf{C}_{t_f}(i,i)}{\mathbf{C}_{t_f}(i,i) + \mathbf{C}_{t_w}(i,i)} \quad , \; i = 1,2 \ldots N \tag{8.48}$$

where $\mathbf{C}_{t_f}$ and $\mathbf{C}_{t_w}$ are given by (8.39*a*) and (8.39*b*) respectively, and $\mathbf{C}_{t_f}(i,i)$, $\mathbf{C}_{t_w}(i,i)$ denote the i^{th} diagonal elements of $\mathbf{C}_{t_f}$ and $\mathbf{C}_{t_w}$ respectively.

The mean-square error associated with $\mathbf{M}_d$ can be obtained from (8.46) as

$$\begin{aligned}\varepsilon_d = {} & tr\left[\psi^{-1}\{\alpha\}\,\mathbf{M}_d\psi\{\alpha\}\,(\mathbf{C}_f + \mathbf{C}_w)\,\psi\{\alpha\}\,\mathbf{M}_d^T\psi^{-1}\{\alpha\}\right] \\ & - tr\left[\psi^{-1}\{\alpha\}\,\mathbf{M}_d\psi\{\alpha\}\,\mathbf{C}_f\right] - tr\left[\mathbf{C}_f\psi\{\alpha\}\,\mathbf{M}_d^T\psi^{-1}\{\alpha\}\right] + tr\left[\mathbf{C}_f\right]\end{aligned} \tag{8.49}$$

Using (8.39*a*) and the fact that $\psi^{-1}\{\alpha\}\,\psi\{\alpha\} = \mathbf{I}$, it follows that

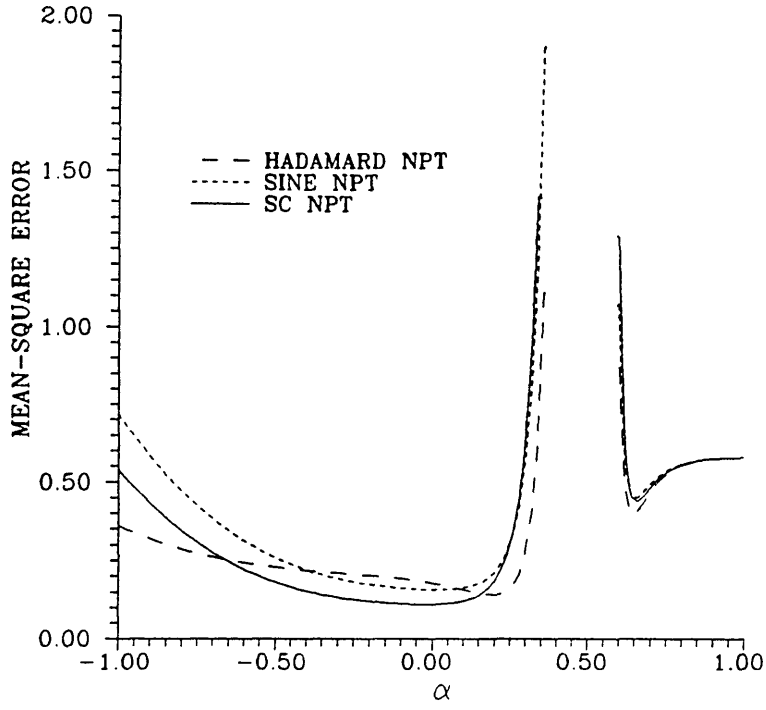


Fig. 8.8 : Mean-square error as a function of α for sub-optimum diagonal NPT generalized Wiener filters; ρ=0.91, SNR=1 and block size = 16.

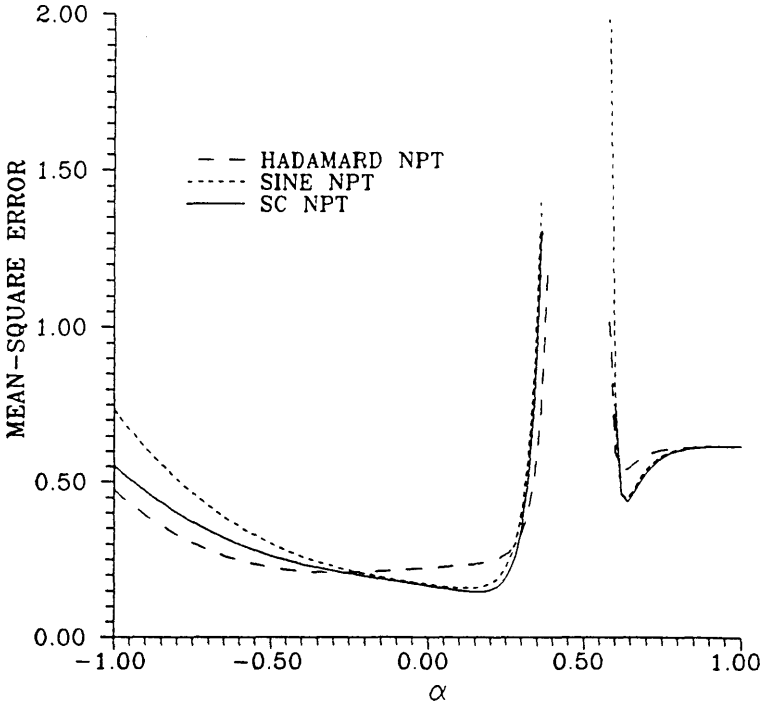


Fig. 8.9 : Mean-square error as a function of α for sub-optimum diagonal NPT generalized Wiener filters; ρ=0.91, SNR=1 and block size = 32.

$$\varepsilon_d = tr\left[\psi^{-1}\{\alpha\}\,\mathbf{M}_d\,(\mathbf{C}_{t_r}+\mathbf{C}_{t_w})\,\mathbf{M}_d\psi^{-1}\{\alpha\}\right]$$
$$-tr\left[\psi^{-1}\{\alpha\}\,\mathbf{M}_d\mathbf{C}_{t_r}\psi^{-1}\{\alpha\}\right]-tr\left[\psi^{-1}\{\alpha\}\,\mathbf{C}_{t_r}\mathbf{M}_d\psi^{-1}\{\alpha\}\right]+tr\left[\mathbf{C}_f\right] \qquad (8.50)$$

Since $\psi^{-1}\{\alpha\}$ is not orthogonal, the first three terms on the right hand side of (8.50) would vary with α and hence the mean-square error will be dependent on α as well.

Simulation Results

Sub-optimal diagonal filtering of stationary first order Gauss-Markov signals, using filter matrices which are based on the NPT transforms, was investigated. Fig. 8.8 shows the result of using sub-optimum diagonal NPT generalized Wiener filters for filtering a zero mean, unit variance stationary first order Gauss-Markov signal, $\rho = 0.91$, corrupted with zero mean white noise, at a signal-to-noise ratio of unity and a block size of 16 was used. It is observed that the relative performance of the filters depends on α. For example, the SC NPT has the best performance for $-0.65 < \alpha < 0.15$ while the Hadamard NPT has the best performance when $-1 \leq \alpha < -0.65$, $0.15 < \alpha < 0.5$ and $0.6 < \alpha < 0.75$. The basis giving minimum MSE is close to $\alpha = 0$ for the SC NPT and the sine NPT while it lies within the range $0.15 < \alpha < 0.25$ for the Hadamard NPT. Fig. 8.9 shows the result when a block size of 32 was used. In this case, it is observed that the SC NPT has the best performance when $-0.3 < \alpha < 0.3$ and $0.6 < \alpha < 1.0$ while the Hadamard NPT has the best performance when $-1 \leq \alpha < -0.3$, $0.3 < \alpha < 0.5$ and over a very small portion of the interval $0.55 < \alpha \leq 0.6$. In addition, the basis giving minimum MSE lies within the range $0.05 < \alpha < 0.25$ for the SC NPT and the sine NPT while it lies within the range $-0.45 < \alpha < -0.2$ for the Hadamard NPT.

The above results show that the performance of the NPT transforms when used for sub-optimum generalized Wiener filtering of first order stationary Gauss-Markov signals corrupted by zero mean additive white noise, depends on the basis parameter α, the number of non-zero filter terms used, the form of the filter matrix (scalar or vector), signal-to-noise ratio and inter-element correlation coefficient. Superior performance to that of the component classical orthogonal transform has been obtained by using an NPT basis $\alpha \neq 0$.

8.4.3 Determination of The Optimum Basis For Sub-optimum Filtering

The results of the previous two sub-sections indicate that the mean-square error of the sub-optimum NPT generalized Wiener filters is dependent on the

basis parameter α. Of importance, however, is the basis giving the minimum MSE of filtering a given noisy signal.

The basis giving minimum MSE is given by

$$\alpha_{opt} = \min_{\alpha}\Big(tr\Big[\psi^{-1}\{\alpha\}\,\tilde{\mathbf{M}}\psi\{\alpha\}\,(\mathbf{C_f}+\mathbf{C_w})\,\psi\{\alpha\}\,\tilde{\mathbf{M}}^T\psi^{-1}\{\alpha\} - \psi^{-1}\{\alpha\}\,\tilde{\mathbf{M}}\psi\{\alpha\}\,\mathbf{C_f} - \mathbf{C_f}\psi\{\alpha\}\,\tilde{\mathbf{M}}^T\psi^{-1}\{\alpha\} + \mathbf{C_f}\Big]\Big) \tag{8.51}$$

For a given sub-optimum filter matrix $\tilde{\mathbf{M}}$ (note that for sub-optimum diagonal filtering, $\tilde{\mathbf{M}} = \mathbf{M}_d$), (8.51) can be solved numerically. We have employed the one-dimensional golden section search algorithm [39].

8.5 A New Approach To NPT Domain Wiener Filtering

In the previous sections, we have been concerned with the classical approach to transform domain generalized Wiener filtering using the NPT transforms. Specifically, given an NPT transform, we determined the best filter to use for filtering a noisy signal based on the model of Fig. 8.1, for specified noise and signal statistics (known signal and noise covariance matrices). However, in this section we pose a slightly different problem: Given a filter matrix that is specified in terms of the NPT matrix, signal and noise covariance matrices, such that for certain choices of the NPT basis parameter α, the performance of the resulting filter matrix (in terms of MSE of filtering) is identical to the performance of the optimum filter matrix of (8.36), we seek the NPT basis parameter α that should be used for transformation such that the mean-square error of filtering a noisy signal is minimum. In other words, given a filter matrix $\mathbf{M}(\psi\{\alpha\}, \mathbf{C_f}, \mathbf{C_w})$ where $\mathbf{C_f}$ and $\mathbf{C_w}$ are the data domain covariance matrices of the signal and noise vectors respectively, and specifying the forward and inverse transforms in Fig. 8.1 as $\psi\{\alpha\}$ and $\psi^{-1}\{\alpha\}$ respectively, we seek the basis parameter α that should be used such that minimum mean-square error of filtering is obtained when the filter matrix $\mathbf{M}(\psi\{\alpha\}, \mathbf{C_f}, \mathbf{C_w})$ is used for filtering the noisy signal.

8.5.1 A Filtering Example

We shall now use an example to illustrate the filtering approach. The forward and inverse transforms are given by $\psi\{\alpha\}$ and $\psi^{-1}\{\alpha\}$ as in Fig. 8.1 but we specify the filter matrix as

$$\mathbf{M}_1 = \psi^{-1}\{\alpha\}\,\mathbf{M}_r\psi\{\alpha\} \tag{8.52}$$

where $\mathbf{M}_r$ is the response matrix given by (8.34); the filter matrix has been obtained by interchanging $\psi\{\alpha\}$ and $\psi^{-1}\{\alpha\}$ in the optimum filter matrix given by (8.36). For this choice, the performance of (8.52) when $\alpha = 0$ or $\alpha = 1$ corresponds to that of the optimum filter matrix of (8.36).

The MSE of filtering, using this arrangement, is obtained by substituting (8.52) in (8.46). Thus, we obtain

$$\begin{aligned}\varepsilon = tr\Big[&\psi^{-1}\{\alpha\}\psi^{-1}\{\alpha\}\mathbf{M}_r\psi^2\{\alpha\}(\mathbf{C_f}+\mathbf{C_w})\psi^2\{\alpha\}\mathbf{M}_r^T\psi^{-1}\{\alpha\}\psi^{-1}\{\alpha\}\\ &-\psi^{-1}\{\alpha\}\psi^{-1}\{\alpha\}\mathbf{M}_r\psi^2\{\alpha\}\mathbf{C_f}-\mathbf{C_f}\psi^2\{\alpha\}\mathbf{M}_r^T\psi^{-1}\{\alpha\}\psi^{-1}\{\alpha\}+\mathbf{C_f}\Big] \qquad (8.53a)\\ = tr\Bigg[&\psi\left\{\frac{2\alpha^2-2\alpha+1}{(2\alpha-1)^2}\right\}\mathbf{M}_r\psi\{2\alpha^2-2\alpha+1\}(\mathbf{C_f}+\mathbf{C_w})\psi\{2\alpha^2-2\alpha+1\}\\ &\cdot\mathbf{M}_r^T\psi\left\{\frac{2\alpha^2-2\alpha+1}{(2\alpha-1)^2}\right\}-\psi\left\{\frac{2\alpha^2-2\alpha+1}{(2\alpha-1)^2}\right\}\mathbf{M}_r\psi\{2\alpha^2-2\alpha+1\}\mathbf{C_f}\\ &-\mathbf{C_f}\psi\{2\alpha^2-2\alpha+1\}\mathbf{M}_r^T\psi\left\{\frac{2\alpha^2-2\alpha+1}{(2\alpha-1)^2}\right\}+\mathbf{C_f}\Bigg] \qquad (8.53b)\end{aligned}$$

which is a function of α and the data domain signal and noise covariance matrices. It should be noted that (8.53*b*) follows from the NPT identities given in chapter two. The basis giving minimum MSE of filtering can be obtained by solving the equation

$$\begin{aligned}\frac{d}{d\alpha}tr\Bigg[&\psi\left\{\frac{2\alpha^2-2\alpha+1}{(2\alpha-1)^2}\right\}\mathbf{M}_r\psi\{2\alpha^2-2\alpha+1\}(\mathbf{C_f}+\mathbf{C_w})\psi\{2\alpha^2-2\alpha+1\}\\ &\cdot\mathbf{M}_r^T\psi\left\{\frac{2\alpha^2-2\alpha+1}{(2\alpha-1)^2}\right\}-\psi\left\{\frac{2\alpha^2-2\alpha+1}{(2\alpha-1)^2}\right\}\mathbf{M}_r\psi\{2\alpha^2-2\alpha+1\}\mathbf{C_f}\\ &-\mathbf{C_f}\psi\{2\alpha^2-2\alpha+1\}\mathbf{M}_r^T\psi\left\{\frac{2\alpha^2-2\alpha+1}{(2\alpha-1)^2}\right\}+\mathbf{C_f}\Bigg]=0 \qquad (8.54a)\end{aligned}$$

subject to

$$\begin{aligned}\frac{d^2}{d\alpha^2}tr\Bigg[&\psi\left\{\frac{2\alpha^2-2\alpha+1}{(2\alpha-1)^2}\right\}\mathbf{M}_r\psi\{2\alpha^2-2\alpha+1\}(\mathbf{C_f}+\mathbf{C_w})\psi\{2\alpha^2-2\alpha+1\}\\ &\cdot\mathbf{M}_r^T\psi\left\{\frac{2\alpha^2-2\alpha+1}{(2\alpha-1)^2}\right\}-\psi\left\{\frac{2\alpha^2-2\alpha+1}{(2\alpha-1)^2}\right\}\mathbf{M}_r\psi\{2\alpha^2-2\alpha+1\}\mathbf{C_f}\\ &-\mathbf{C_f}\psi\{2\alpha^2-2\alpha+1\}\mathbf{M}_r^T\psi\left\{\frac{2\alpha^2-2\alpha+1}{(2\alpha-1)^2}\right\}+\mathbf{C_f}\Bigg]>0 \qquad (8.54b)\end{aligned}$$

This approach is complex and in the alternative, we proceed via the numerical minimization of (8.53) i.e. the bases giving minimum MSE are given by

$$\alpha_i^* = \min_{\alpha} tr\left[\psi\left\{\frac{2\alpha^2-2\alpha+1}{(2\alpha-1)^2}\right\}\mathbf{M}_r\psi\left\{2\alpha^2-2\alpha+1\right\}(\mathbf{C_f}+\mathbf{C_w})\,\psi\left\{2\alpha^2-2\alpha+1\right\}\right.$$
$$\cdot\,\mathbf{M}_r^T\psi\left\{\frac{2\alpha^2-2\alpha+1}{(2\alpha-1)^2}\right\}-\psi\left\{\frac{2\alpha^2-2\alpha+1}{(2\alpha-1)^2}\right\}\mathbf{M}_r\psi\left\{2\alpha^2-2\alpha+1\right\}\mathbf{C_f}$$
$$\left.-\,\mathbf{C_f}\psi\left\{2\alpha^2-2\alpha+1\right\}\mathbf{M}_r^T\psi\left\{\frac{2\alpha^2-2\alpha+1}{(2\alpha-1)^2}\right\}+\mathbf{C_f}\right] \tag{8.55}$$

Suitable algorithms for solving (8.55) can be found in [38,39], for example, the one-dimensional golden section search algorithm has been used.

Simulation, Results and Discussion

Empirical results of filtering a first order stationary Gauss-Markov signal corrupted with additive white noise, using the new filtering approach are presented. It should be noted that the points corresponding to the basis parameter value α for which the MSE is greater than 1.0 have been excluded from the plots. Fig. 8.10 shows the MSE as a function of α for the Hadamard NPT, sine NPT and the SC NPT when all the terms of the filter matrix of (8.52) were used to filter a first order stationary Gauss-Markov signal $\rho = 0.91$, corrupted with additive white noise at unity signal-to-noise ratio, using a block size of 16. For the Hadamard NPT, the bases α_1, α_2 giving minimum MSE of 0.102347 were found to satisfy $|\alpha_1 - 0| = |\alpha_2 - 1|$ with $\alpha_1 = 0.08$ and $\alpha_2 = 0.92$; a higher MSE of 0.120615 is obtained when the filter of (8.36) was used. For the sine NPT, the minimum MSE of 0.120606 was given by the basis $\alpha = 0.01$ while for the SC NPT, the minimum MSE of 0.120507 was given by the basis $\alpha = -0.01$. The improvement over the performance of the filter matrix of (8.36) is higher for the Hadamard NPT than those for the sine NPT and the SC NPT. Fig. 8.11 shows the corresponding result to that of Fig. 8.10, when a block size of 32 was used. The minimum MSE of 0.15003 was obtained for the Hadamard NPT, that for the sine NPT was 0.140102 while for the SC NPT, the minimum MSE was 0.138810. The bases α_1 and α_2 giving minimum MSE were found to satisfy $|\alpha_1 - 0| = |\alpha_2 - 1|$. A higher MSE of 0.152951 was obtained when the filter matrix of (8.36) was used. The improvement over the performance of the matrix of (8.36) is higher for the SC NPT and the sine NPT than it is for the Hadamard NPT.

Fig. 8.12 shows the effect of reducing the inter-element correlation of the original signal, for the Hadamard NPT based filter matrix of (8.52), using a block size of 16 and unity signal-to-noise ratio. It is observed that for $\rho = 0.84$, two minima

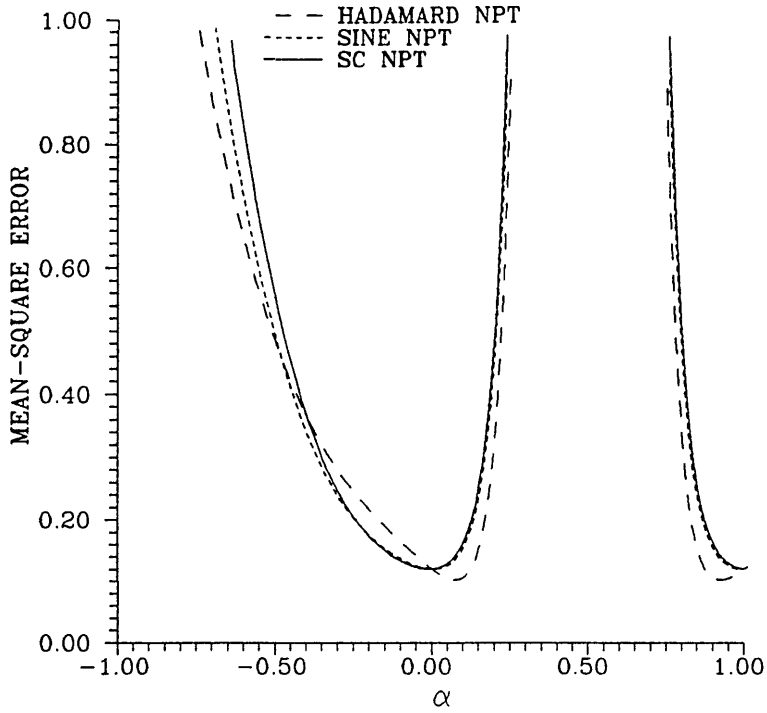


Fig. 8.10 : MSE as a function of α for the NPT generalized Wiener filtering of a stationary first order Gauss-Markov signal, using the matrix of (8.52); ρ=0.91, SNR=1 and block size=16.

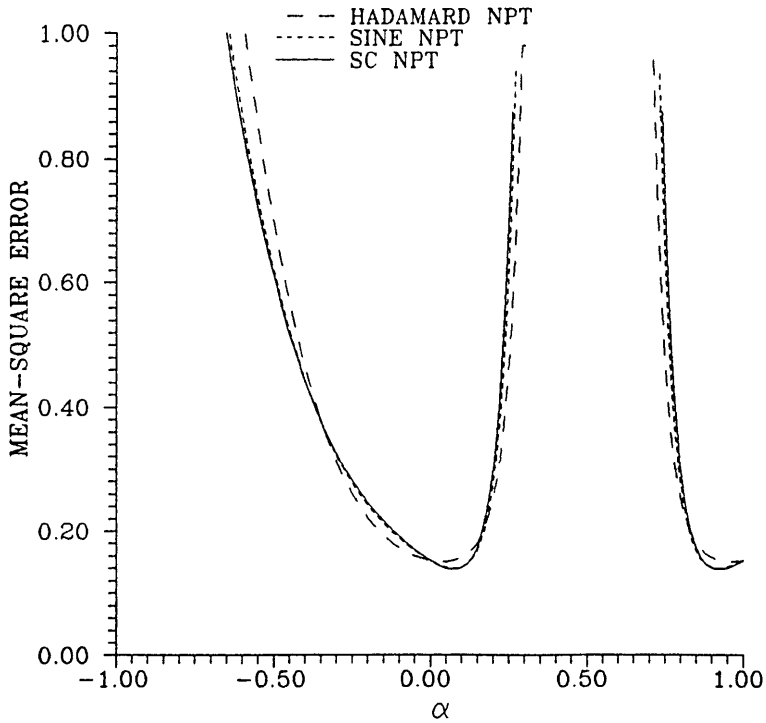


Fig. 8.11 : MSE as a function of α for the NPT generalized Wiener filtering of a stationary first order Gauss-Markov signal, using the matrix of (8.52); ρ=0.91, SNR=1 and block size=32.

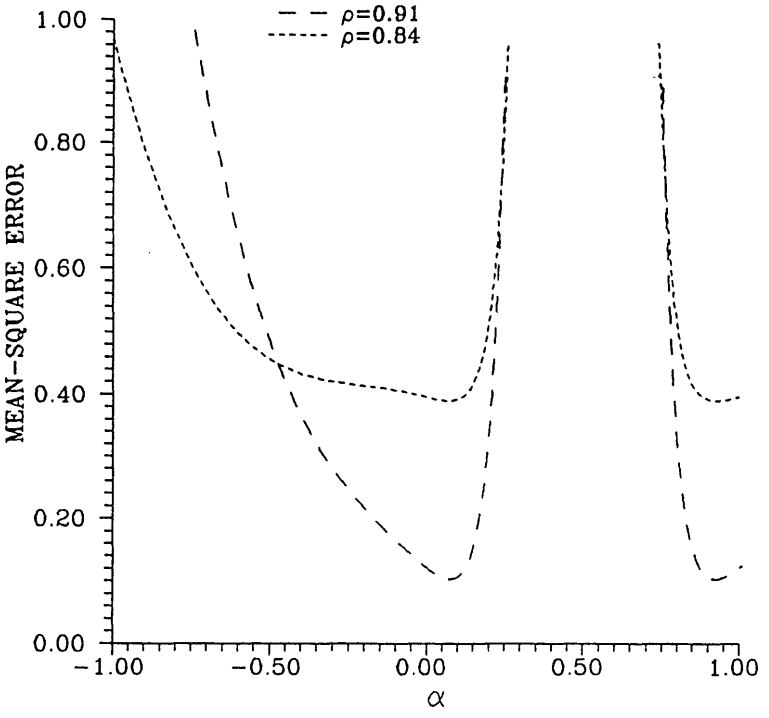


Fig. 8.12 : MSE as a function of α and ρ for the Hadamard NPT generalized Wiener filtering of a stationary first order Gauss-Markov signal, using the matrix of (8.52); SNR=1 and block size=16.

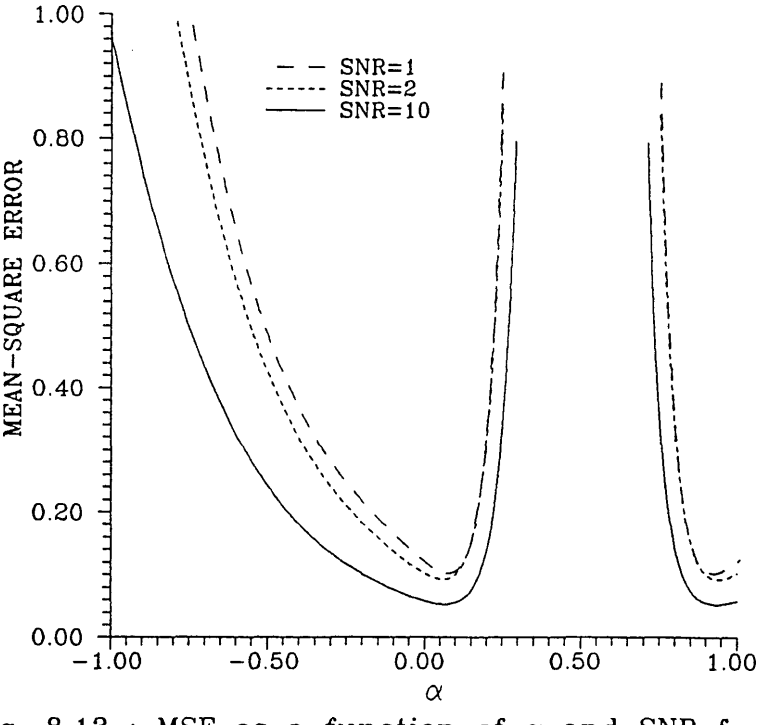


Fig. 8.13 : MSE as a function of α and SNR for the Hadamard NPT generalized Wiener filtering of a stationary first order Gauss-Markov signal, using the matrix of (8.52); ρ=0.91 and block size=16.

α_1 and α_2 are also obtained and these satisfy $|\alpha_1 - 0| = |\alpha_2 - 1|$. The MSE is seen to increase with decrease in inter-element correlation of the signal, except when $-1 \leq \alpha < -0.47$. Fig. 8.13 shows the effect of varying the signal-to-noise ratio, for the Hadamard NPT based filter matrix of (8.52), using a block size of 16 with the inter-element correlation of the original signal being equal to 0.91. It is observed that the MSE decreases with signal-to-noise ratio and there are two minima of MSE in all the cases. Furthermore, the minima α_1, α_2 satisfy the constraint $|\alpha_1 - 0| = |\alpha_2 - 1|$.

Diagonal filters based on the filter matrix of (8.52) were also investigated. Empirical results show that the performance of diagonal filters based on the matrix of (8.52) is identical to that of diagonal filters based on the matrix of (8.36). This result follows from the symmetry of the forward and inverse NPT kernels.

8.5.2 Other Filter Matrices

It is worthwhile mentioning the fact that there are many possible filter matrices that can be specified. The following matrices are some of the possibilities.

$$\mathbf{M}_2 = \psi\{\alpha\}\,\mathbf{M}_r\psi\{\alpha\} \tag{8.56}$$

$$\mathbf{M}_3 = \psi^{-1}\{\alpha\}\,\mathbf{M}_r\psi^{-1}\{\alpha\} \tag{8.57}$$

and

$$\mathbf{M}_4 = \psi\{0\}\,\mathbf{M}_r\psi^{-1}\{\alpha\} \tag{8.58}$$

where $\mathbf{M}_r$ is given by (8.34). The performances of these filters, when used for filtering the first order stationary Gauss-Markov signal, $\rho = 0.91$, corrupted with additive white noise, with the signal-to-noise ratio equal to unity, using a block size of 32, are compared in Fig. 8.14, Fig. 8.15 and Fig. 8.16 for the Hadamard NPT, sine NPT and the SC NPT based filters respectively; it should be noted that all the filter terms have been used. It is observed that for the Hadamard NPT filters, the lowest MSE values obtained when the filter matrices of (8.56), (8.57) and (8.58) are used, are similar in magnitude, while for the sine NPT and SC NPT based filters, the lowest MSE obtained correspond to the filter matrices of (8.52) and (8.58). Furthermore, two minima of MSE are each associated with the matrices of (8.52) and (8.57), for all the three NPT transforms.

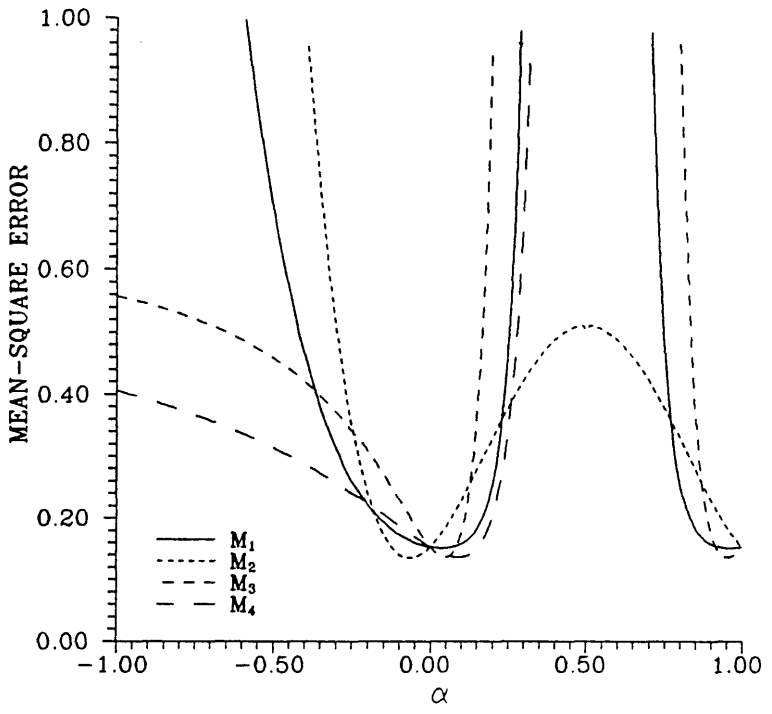


Fig. 8.14 : MSE as a function of α for some Hadamard NPT based filter matrices, when used for filtering a stationary first order Gauss-Markov signal; ρ=0.91, SNR=1 and block size=32.

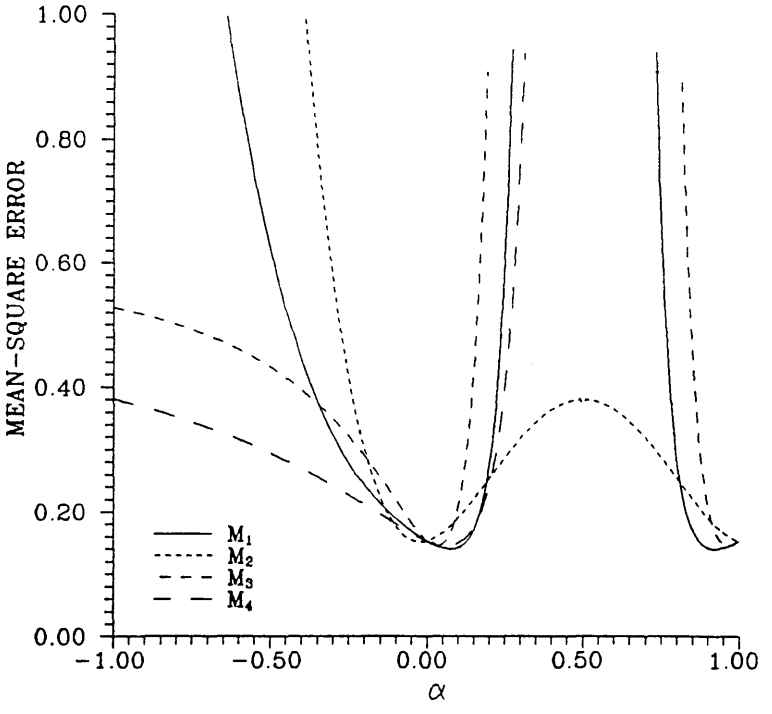


Fig. 8.15 : MSE as a function of α for some sine NPT based filter matrices, when used for filtering a stationary first order Gauss-Markov signal; ρ=0.91, SNR=1 and block size=32.

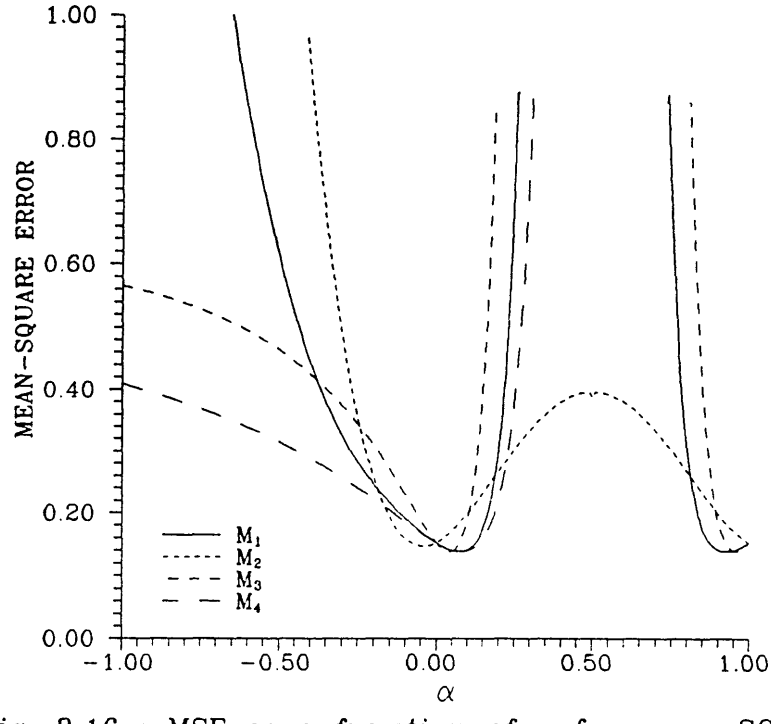


Fig. 8.16 : MSE as a function of α for some SC NPT based filter matrices, when used for filtering a stationary first order Gauss-Markov signal; ρ=0.91, SNR=1 and block size=32.

8.6 Summary and Conclusion

Naturalness-Preserving transform domain generalized Wiener filtering has been developed. We have shown that the performance of an optimum NPT generalized Wiener filtering system for any specified basis parameter value α, $|\alpha| < 1$, is identical to that for any optimum orthogonal transform generalized Wiener filtering system.

Sub-optimum filtering of first order stationary Gauss-Markov signals corrupted with additive white noise, using relatively large magnitude filter terms has been investigated. For certain numbers of non-zero filter terms, superior performance in terms of MSE has been obtained by using a basis different from $\alpha = 0$. The relative performance of the NPT bases has been shown to be dependent on the number of non-zero filter terms used. The relative performance of the NPT transforms has also been shown to vary with the basis parameter value, α.

Sub-optimum diagonal filtering of first order stationary Gauss-Markov signals corrupted with additive white noise has also been investigated. The relative performance of the NPT transforms has been shown to vary with the basis parameter value α, and the block size used. Superior performance in terms of MSE has been obtained by using a basis different from $\alpha = 0$. The problem of choosing the basis giving minimum MSE was briefly considered. Numerical solution of the optimum basis determination problem has been given.

A new approach to NPT generalized Wiener filtering, which essentially consists of specifying filter matrices that are defined in terms of the signal and noise covariance matrices, and the NPT matrix, has been introduced. A variety of filter matrices have been examined and their performances have been investigated empirically. It has been shown that for some NPT basis parameter values, these filters perform better than the optimum NPT generalized Wiener filter obtained using classical design methods, in terms of MSE.

PART IV
SUMMARY, CONCLUSION AND RECOMMENDATIONS FOR FURTHER WORK

CONCLUSIONS

This thesis has focussed on the development, analysis and digital signal processing applications of the Naturalness-Preserving Transforms (NPT). The NPT transforms are a sub-class of hybrid transforms.

Hybrid transforms are linear combinations of orthogonal matrices. The NPT transforms are a special case of hybrid transforms when we require that one of the transforms in the linear combination be the identity matrix.

The hybrid transform kernel is quite general and not every possible linear combination of orthogonal matrices leads to a transform, having an inverse that is definable analytically.

In chapter two, the problem of determining admissible hybrid transforms for digital signal processing applications, based on specified criteria, has been addressed. For computational considerations, admissible hybrid transforms are limited to those comprising a linear combination of two fast orthogonal matrices.

Two theorems which define admissible hybrid transforms comprising a linear combination of commuting (or anti-commuting) involutory orthogonal matrices, have been derived.

An important consequence of the hybrid transform inversion theorem for commuting involutory orthogonal matrices is that it defines a parametric family of admissible NPT transforms for digital signal processing applications. These comprise a linear combination of the identity matrix and a symmetric orthogonal transform.

An associated result of the theorem is the fact that linear combinations of the identity matrix and classical non-symmetric orthogonal transforms such as the discrete cosine transform, Fourier transform, Haar transform e.t.c, are not admissible NPT transforms.

Properties of the parametric family of NPT transforms, some of which are different from those known for classical orthogonal transforms, have been determined. An alternative form of the NPT has also been described.

The NPT domain of typical imagery data has been investigated empirically. An interesting observation made here is that the transform domain of imagery data transformed by certain NPT bases, is visually comprehensible.

An advantage of the NPT transforms is that they are characterized by an infinite number of bases that could be exploited for signal processing applications. In addition, transform basis selection is conveniently and cheaply realized without making any modification to the transform implementation algorithm. Furthermore, the component classical orthogonal transform is selectable by appropriate specification of the NPT parameters.

The NPT transforms have been investigated for a number of digital signal processing applications. A great deal of the reported work represent the pioneering ones in these application areas.

The application of the NPT in image data compression has been the focus of chapter three. In part A, pure two-dimensional NPT coding of monochrome images has been investigated.

The objective of an NPT image coder is to employ the basis or collection of bases giving minimum MSE for coding a given image or image ensemble. Consequently, the algorithm for determining the optimum basis (in the MSE sense) for coding a given image or image ensemble, has been introduced.

The algorithm requires the specification of an empirically determined correction factor and this corrects for the representation of the ratio of the spatial domain MSE to the transform domain MSE by the fourth power of the ratio of the norm of the inverse NPT matrix to the norm of an orthogonal transform matrix.

The correction factor is mainly dependent on the NPT basis parameter α, but has some variations with the transform order, bit rate, NPT transform type, quantization scheme and image content. The number of parameters to be considered in the determination of the correction factor can be reduced by specifying a block size, bit rate, NPT transform type and quantization scheme.

The correction factor has been modelled by a second order polynomial in the basis parameter α, with constant coefficients.

Non-adaptive NPT image coders have been investigated. An interesting feature of these coders is that they employ the optimum NPT basis for coding a given image or image ensemble.

Superior MSE performance to that of the parent classical orthogonal transform has been obtained by using the optimum NPT basis for image coding.

The optimum basis for non-adaptive NPT coding of an image or image ensemble varies with the image content, bit rate, block size, and NPT transform type. Consequently, the non-adaptive NPT image coder is inherently basis adaptive over an image ensemble. However, since the coder employs the same basis and bit allocation for all the sub-blocks of a given image, we have regarded it as a non-adaptive NPT coder.

The important observation that the optimum basis for non-adaptive NPT image coding varies with the image content motivated the introduction of Basis Adaptive NPT Coders (BANPTC).

The basis adaptive NPT coder (BANPTC) is a block classification adaptive transform coding system which features transform basis adaptation according to local image content, in addition to conventional adaptation techniques (bit allocation/quantization).

Superior performance to that of the block classification orthogonal transform based scheme, in terms of MSE, has been obtained by adapting the NPT bases to the local image spatial activity.The MSE improvement has been shown to decrease with increasing block size.

The effect of errors in the code-word digits used for representing the transform coefficients, on the subjective quality of reconstructed pictures, has been investigated. Incorrect basis picture contributions to the reconstructed picture has been shown to have a noticeable effect on the subjective quality of coded pictures at a BER of 10^{-3} and above.

NPT hybrid coding of images has been investigated in part B of chapter three. The coding systems employ one-dimensional NPTs and a bank of DPCM operators.

An algorithm for determining the optimum basis for the hybrid coding of a given image or image sub-array, has been introduced.

The algorithm requires the specification of an empirically determined correction factor which corrects for the modelling of the spatial to transform domain MSE ratio as a function of α, by the second power of the ratio of the norm of the inverse NPT matrix to the norm of an orthogonal transform matrix.

The NPT hybrid image coding correction factor is dependent on the bit rate, image sub-array statistics and NPT transform type. The correction factor has been modelled by a second order polynomial in the basis parameter α, with constant coefficients.

The NPT hybrid image coder is an adaptive hybrid image coder which uses a different transform basis, transform coefficients statistics and bit allocation for coding the respective sub-arrays of the image or image ensemble.

Superior performance, in terms of MSE, over that of the component classical orthogonal transform based scheme, has been obtained by using the optimum NPT basis for hybrid coding of the respective image sub-arrays. The degree of MSE improvement, over that obtained when the orthogonal transform is used, has been shown to vary from one image sub-array to another. In some instances, no MSE improvement has been obtained by using the NPT. It has also been observed that the MSE improvement over that of the orthogonal transform, is higher at low bit rates than at high bit rates.

An additional observation is that the MSE improvement for pure two-dimensional NPT transform coding of images is higher than that for NPT hybrid image coding using one-dimensional transforms, when the respective schemes are compared with the equivalent ones using the parent classical orthogonal transform ($\alpha = 0$) basis.

A rate-distortion theoretic framework for NPT coders has been developed in chapter four. The NPT rate-distortion function ascertains the minimum rate required to transmit or store a given image, in order to achieve a desired fidelity level of reconstructed image, when a specified NPT basis is used for coding the image.

An upper bound of the compression rate subject to a mean-square error (MSE) fidelity constraint has been derived. This bound has been evaluated for a first order stationary Gauss-Markov image and has been used to predict the relative

performance of the respective NPT transforms, for values of the transform basis parameter α satisfying $|\alpha| \leq 0.2$.

The practical relative performance and the prediction of the relative performance that is obtained from the rate-distortion bound are in agreement.

The bound obtained for two-dimensional unconstrained complexity coding of stationary first order Gauss-Markov images has been compared with the performance of practical two-dimensional NPT coders when used for coding stationary first order Gauss-Markov images. An important observation made here is that there is an increase in rate of at least 1 bit/sample as a result of using a finite block size ($N = 8$) for block coding.

The one-dimensional Hadamard NPT domain has been investigated for signal transmission through channels whose quality and characteristics are unpredictable due to non-stationary noise processes or jamming, in chapter five.

Signal degradation has been modelled as a complete loss of segments of the transmitted signal and the problem of reconstructing a signal from segments of its Hadamard NPT has been addressed.

Techniques for iteratively reconstructing a time-varying one-dimensional signal from segments of its Hadamard NPT have been developed. An iterative one-dimensional Hadamard NPT reconstruction algorithm has been introduced.

The algorithm requires an estimate of the signal amplitude over the available transform segments.

Closed-form reconstruction formulae for reconstruction from specific formats of Hadamard NPT segments have been derived.

The convergence of the iterative reconstruction algorithm has been proved in appendix II and the scheme has been shown to converge for $\alpha \leq 0.464$, empirically.

The number of iterations required for convergence is a function of the reconstruction format and the threshold ε which measures the similarity between the correctly received transform segments and the corresponding segments of the transform domain iteration vector, at the m^{th} iteration. For $\varepsilon = 10^{-2}$, it has been shown empirically that between 5 and 28 iterations are required for convergence.

Two fast reconstruction schemes applicable to some signal loss formats, which provide solutions in one iteration, have been introduced .

The one-dimensional Hadamard NPT reconstruction algorithm has been successfully applied to first order stationary Gauss-Markov and speech signals. Adaptive line enhancing technique has been employed for the original signal amplitude estimation from the available segments of the one-dimensional Hadamard NPT transformed signal.

Pre- and post-reconstruction filtering has been shown to improve the quality of the reconstructed signals. A median-threshold-decision interpolating smoothing filter has been introduced for pre- and post-reconstruction filtering. The filter preserves details of the signal better than the median filter and the low pass filter. The filter has been shown to be particularly effective for slowly varying signals but smooths out desirable details in rapidly varying signals.

The application of the fast one-dimensional Hadamard NPT reconstruction algorithm in intraframe two-layer packet transmission of images, has been proposed. The scheme in which the least significant half of 1×512 transformed sub-blocks (i.e. samples 257 to 512) are selected as guaranteed packets has been shown to yield the best reconstructed pictures and this has been proposed for two-layer packet transmission of images.

Good quality reconstructed pictures from guaranteed packets, corresponding to fifty percent packet loss, have been obtained. The Hadamard NPT reconstruction scheme has been successfully applied to intraframe packet transmission of different images.

The problem of transmitting two-dimensional signals through channels whose quality and characteristics are unpredictable due to non-stationary noise processes or jamming has been the focus of chapter six. The two-dimensional Hadamard NPT domain has been investigated for tactical imagery transmission, under this scenario.

Parallel to the one-dimensional Hadamard NPT signal reconstruction problem, signal degradation has been modelled as a complete loss of segments of the transmission and the problem of reconstructing a signal from segments of its two-dimensional Hadamard NPT has been addressed.

An iterative two-dimensional Hadamard NPT reconstruction algorithm has been investigated and the proof of convergence has been given in appendix III. It has been shown empirically that the iterative reconstruction scheme converges for $\alpha \leq 0.41$ and for Type-1 formats, iterative reconstruction is also possible for values of α in the range $0.41 < \alpha \leq 0.464$.

The number of iterations required for convergence is a function of the reconstruction format and the threshold ε which measures the similarity between the received transform segments and the corresponding segments of the transform domain iteration matrix, at the m^{th} iteration.

A fast reconstruction algorithm, applicable to Type-1 signal loss formats, which provide solutions in one iteration, has been introduced. It has been shown that the iterative reconstruction from type-2 formats does not yield the required solutions.

The reconstruction algorithm requires an estimate of the signal amplitude over the available transform segments. A two-dimensional adaptive line enhancer has been employed for this purpose.

The two-dimensional Hadamard NPT reconstruction algorithm has been applied to the reconstruction of imagery data. The subjective quality of the reconstructed imagery data is a function of the reconstruction format and the original image content.

For original images with little detail, reconstructed pictures are comprehensible, however, some details in highly textured images are missing from the reconstructed versions. This is attributed to the poor estimation of the original image segments from the correctly received two-dimensional Hadamard NPT transformed imagery segments.

The subjective quality of the estimated segments of images improves with increasing values of α while the subjective quality of the reconstructed segments corresponding to the unknown transform segments deteriorates with increasing values of α. In general, the quality of the reconstructed signal depends on how well we can estimate the original signal amplitude, from the available transform segments.

With the exception of Type-2 formats, perfect reconstruction is obtained in the event of an errorless estimation of the signal segment corresponding to the correctly received transform segments.

Further developments for one-dimensional and two-dimensional Hadamard NPT applications have been reported in chapter seven.

The one-dimensional Hadamard NPT reconstruction, two-layer intraframe packetized imagery transmission system, which was proposed in chapter five, has been revisited. The problem of channel bandwidth limitations has been addressed and the reconstruction from guaranteed packets of compressed Hadamard NPT transformed imagery samples has been investigated.

Using transform DPCM techniques, good subjective quality reconstructed pictures have been obtained from coded guaranteed one-dimensional Hadamard NPT samples at 3.0 bits per transmitted sample (this is equivalent to 1.5 bits per pixel for the whole picture) and above. However, the subjective quality of reconstructed pictures deteriorates, when the guaranteed Hadamard NPT transformed imagery samples used for reconstruction are DPCM coded at 2.0 bits per transmitted sample (1.0 bit per pixel for the whole picture) and below.

The quality of the reconstructed pictures from DPCM coded guaranteed Hadamard NPT samples is dependent on the original image content and the bit rate.

Vector quantization technique has been used for coding the guaranteed Hadamard NPT transformed imagery samples at low bit rates. Very good subjective quality reconstructed pictures have been obtained from VQ coded guaranteed Hadamard NPT transformed imagery samples at a bit rate of 1.25 bits per transmitted sample (0.625 bit per pixel for the whole picture).

The transmission of additional information as enhancement packets has been shown to improve the quality of reconstructed pictures. Very good reconstructed pictures have been obtained when VQ was used to code the information transmitted as enhancement packets, at low bit rates.

An interesting result that has been obtained is that the loss of enhancement packets has a significant effect on the subjective quality of reconstructed pictures, only at a high loss rate of 5^{-1} and above.

The effect of errors in the code-word digits used for representing the transmitted information has been investigated.

Errors in the code-word digits used for representing the guaranteed information have no noticeable effect on the subjective quality of reconstructed pictures at a BER of 10^{-4} and below. However, for BER = 10^{-3} and above, errors in the code-word digits used for representing the guaranteed information degrades the quality of reconstructed pictures.

For enhancement information, it has been ascertained that errors in the code-word digits used for representing the information have little or no noticeable effect on the subjective quality of reconstructed pictures.

The two-dimensional Hadamard NPT tactical imagery transmission application, which was discussed in chapter six, has been further developed.

The problem of signal transmission through limited bandwidth channels has been addressed. The effect of coding the two-dimensional Hadamard NPT transformed imagery samples used for reconstruction, on the reconstructed picture quality, has been ascertained.

VQ coding of the two-dimensional Hadamard NPT samples at 1.0 bit per sample, has little noticeable effect on the subjective quality of the reconstructed pictures. Furthermore, the subjective quality of the reconstructed pictures, when the transform samples are VQ coded at a low bit rate of 0.5625 bit per sample, compares well with the no coding result, although there is a slight noticeable increase in the distortion of the region of the picture corresponding to the unknown transform samples.

Errors in the code-word digits used for representing the two-dimensional Hadamard NPT transformed samples, used for reconstruction, has been shown to mainly have the effect of increasing the distortion of the region of the picture corresponding to the unknown transform samples. The effect of the errors is noticeable at a BER of 10^{-2} and above.

Image data compression systems which are based on one-dimensional Hadamard NPT reconstruction techniques have been developed. Two hybrid image coding techniques, which are based on fast one-dimensional Hadamard NPT

reconstruction of each line of an image, have been proposed. These are variations of a basic algorithm which has been described.

DPCM coders have been used to code the respective parts of the information needed for reconstruction at the receiver. The use of spatial DPCM imposes the restriction of using a block size of at least 128 for a 256×256 image and this has been shown to yield coded pictures having a non-uniform subjective quality, at bit rates of 1.75 bits per pixel and below.

The second variation of the coding algorithm yields a greatly improved picture in terms of subjective quality and MSE, than the first variation. The performances of the optimum coders in the two cases are independent of the choice of the transform basis parameter, α.

One-dimensional NPT transform domain generalized Wiener filtering has been developed in chapter eight.

An interesting result obtained is that the performance of an optimum NPT generalized Wiener filtering system for any specified basis parameter value α, $|\alpha| < 1$, is identical to that of any optimum orthogonal transform generalized Wiener filtering system.

Sub-optimum filtering of first order stationary Gauss-Markov signals corrupted with additive white noise, using relatively large magnitude filter terms, has been investigated.

For certain numbers of non-zero filter terms, superior performance in terms of MSE has been obtained by using a basis different from $\alpha = 0$. The relative performance of the NPT bases is dependent on the number of non-zero filter terms used. In addition, the relative performance of the different types of NPT transforms varies with the basis parameter value, α.

Sub-optimum diagonal filtering of first order stationary Gauss-Markov signals corrupted with additive white noise has also been investigated.

Superior performance in terms of MSE has been obtained by using a basis different from $\alpha = 0$. In addition, the relative performance of the NPT transforms varies with the basis parameter value α, and the block size used.

The problem of choosing the basis giving minimum MSE was addressed. Numerical solution of the optimum basis determination problem has been given.

A unique approach to NPT generalized Wiener filtering, which essentially consists of specifying filter matrices that are defined in terms of the signal and noise covariance matrices, and the NPT matrix, has been introduced.

A variety of filter matrices have been specified and their performances have been investigated empirically. For some NPT basis parameter values, these filters perform better than the optimum NPT generalized Wiener filter that is obtained using classical design methods, in terms of MSE. Numerical technique has been used to determine the optimum basis (or bases) to be employed for filtering.

Recommendations For Further Work

The areas of further work on NPT transform digital signal processing applications, that have been identified, are as follows.

In NPT image coding, interframe NPT image coding may be pursued.

The feasibility of using the Hadamard NPT for signal transmission through channels whose quality and characteristics are unpredictable due to non-stationary noise processes or jamming has been ascertained. Future efforts may be directed towards the development of techniques for determining the reliable transform segments that can be used for reconstruction.

The one-dimensional Hadamard NPT reconstruction algorithm has been applied to speech signals, however, there is still some scope for further investigations. The development of noise-cleaning algorithms that would improve the subjective quality of reconstructed speech signals can be pursued. It may be instructive also to investigate the performance of the one-dimensional Hadamard NPT reconstruction algorithm for voice applications. For example packetized speech transmission.

Further work on the application of one-dimensional Hadamard NPT reconstruction techniques to the packet transmission of images can be directed towards applying the technique to moving images.

Future efforts on two-dimensional Hadamard NPT tactical imagery transmission applications may be directed towards improving or developing techniques

for the estimation of the pixel values from the correctly received two-dimensional Hadamard NPT segments of the image.

A drawback of using DPCM coders in the Hadamard NPT reconstruction hybrid image coding algorithms is that these lead to coded pictures having a non-uniform subjective quality, at bit rates of 1.75 bits per pixel and below. Further work entails the application of vector quantization techniques to these algorithms.

It is believed that the use of VQ would permit the use of small block sizes which would result in the coding/reconstruction distortion being distributed more uniformly over the reconstructed picture. Furthermore, the use of VQ would permit coding at much lower overall rates.

Future ventures on NPT domain generalized Wiener filtering may be directed towards extending the technique to two dimensions. Applications of the two-dimensional NPT filter to practical problems such as image enhancement may be explored. Research leading to further understanding of the NPT generalized Wiener filtering technique introduced in section 8.5 would also be most invaluable.

APPENDICES

APPENDIX I

DERIVATION OF THE HYBRID TRANSFORM INVERSION THEOREMS

The hybrid transform inversion theorems, which define a family of hybrid transforms comprising a linear combination of two orthogonal matrices were stated in sections 2.3.2.1.1 and 2.3.2.1.2. The derivation of the theorems is outlined below.

We define

$$\psi\{\alpha\} = k_1(\alpha)\mathbf{A}_1 + k_2(\alpha)\mathbf{A}_2 \tag{A1.1}$$

where $k_1(\alpha)$ and $k_2(\alpha)$ are specified functions of a real parameter α; $\mathbf{A}_1$ and $\mathbf{A}_2$ are orthogonal matrices.

We assume the inverse of (A1.1) to be of the form

$$\psi^{-1}\{\alpha\} = \psi\{\underline{\beta}\} = \beta_1\mathbf{B}_1 + \beta_2\mathbf{B}_2 \tag{A1.2}$$

where β_1 and β_2 are unknown parameters; $\mathbf{B}_1$ and $\mathbf{B}_2$ are matrices to be determined.

For (A1.2) to be the inverse of (A1.1), the relation

$$\psi^{-1}\{\alpha\}\,\psi\{\alpha\} = \mathbf{I} \tag{A1.3}$$

must hold.

Using (A1.1) and (A1.2), we can write

$$\begin{aligned}\psi^{-1}\{\alpha\}\,\psi\{\alpha\} &= (\beta_1\mathbf{B}_1 + \beta_2\mathbf{B}_2)(k_1(\alpha)\mathbf{A}_1 + k_2(\alpha)\mathbf{A}_2) \\ &= \beta_1 k_1(\alpha)\mathbf{B}_1\mathbf{A}_1 + \beta_1 k_2(\alpha)\mathbf{B}_1\mathbf{A}_2 + \beta_2 k_1(\alpha)\mathbf{B}_2\mathbf{A}_1 + \beta_2 k_2(\alpha)\mathbf{B}_2\mathbf{A}_2\end{aligned} \tag{A1.4}$$

and substituting (A1.4) in (A1.3), we obtain

$$\beta_1 k_1(\alpha)\mathbf{B}_1\mathbf{A}_1 + \beta_2 k_2(\alpha)\mathbf{B}_2\mathbf{A}_2 + \beta_1 k_2(\alpha)\mathbf{B}_1\mathbf{A}_2 + \beta_2 k_1(\alpha)\mathbf{B}_2\mathbf{A}_1 = \mathbf{I} \tag{A1.5}$$

It should be noted that (A1.5) is just a necessary condition for (A1.2) to be the inverse of (A1.1) and it does not impose any restrictions on the nature of the matrices $\mathbf{B}_1$ and $\mathbf{B}_2$. For example, there may exist various pairs of matrices $\mathbf{B}_1$ and $\mathbf{B}_2$ and weighting parameters β_1,β_2 such that the individual terms

$\beta_i k_j(\alpha)\mathbf{B}_i\mathbf{A}_j$, $i,j = 1,2$, of (*A*1.5) have no resemblance to a diagonal matrix and yet for the four terms to sum equal to an identity matrix. However, there are some special cases of interest and these lead to the hybrid transform inversion theorems. These are considered in the following.

By inspection, we see that (*A*1.5) is satisfied if

$$\beta_1 k_1(\alpha)\mathbf{B}_1\mathbf{A}_1 + \beta_2 k_2(\alpha)\mathbf{B}_2\mathbf{A}_2 = \mathbf{I} \tag{A1.6a}$$

and

$$\beta_1 k_2(\alpha)\mathbf{B}_1\mathbf{A}_2 + \beta_2 k_1(\alpha)\mathbf{B}_2\mathbf{A}_1 = \mathbf{O} \tag{A1.6b}$$

It should be noted that we could equally have chosen the terms on the left hand side of (*A*1.6*a*) to sum equal to the null matrix and the terms on the left hand side of (*A*1.6*b*) to sum equal to the identity matrix; however, the final result would still be the same as what the present choice would give.

From (*A*1.6*b*), we obtain

$$\beta_1\mathbf{B}_1 = -\beta_2\frac{k_1(\alpha)}{k_2(\alpha)}\mathbf{B}_2\mathbf{A}_1\mathbf{A}_2^{-1} \tag{A1.7}$$

and substituting (*A*1.7) in (*A*1.6*a*), we obtain

$$-\beta_2\frac{k_1^2(\alpha)}{k_2(\alpha)}\mathbf{B}_2\mathbf{A}_1\mathbf{A}_2^{-1}\mathbf{A}_1 + \beta_2 k_2(\alpha)\mathbf{B}_2\mathbf{A}_2 = \mathbf{I} \tag{A1.8}$$

There are two special cases of interest for which (*A*1.8) is satisfied. In these cases, we impose restrictions on the matrices $\mathbf{A}_1$ and $\mathbf{A}_2$, which enable us to determine the matrices $\mathbf{B}_1$ and $\mathbf{B}_2$.

Case 1

If $\mathbf{A}_1$ and $\mathbf{A}_2$ are commuting involutory matrices, then

$$\mathbf{A}_1\mathbf{A}_2^{-1} = \mathbf{A}_2\mathbf{A}_1^{-1} \tag{A1.9}$$

Using (*A*1.9) in (*A*1.8), we obtain

$$-\beta_2\frac{k_1^2(\alpha)}{k_2(\alpha)}\mathbf{B}_2\mathbf{A}_2 + \beta_2 k_2(\alpha)\mathbf{B}_2\mathbf{A}_2 = \mathbf{I} \tag{A1.10}$$

and further manipulation yields

$$\mathbf{B}_2\mathbf{A}_2 = \frac{k_2(\alpha)}{\beta_2[k_2^2(\alpha) - k_1^2(\alpha)]}\mathbf{I} \tag{A1.11}$$

Substituting (*A*1.11) in (*A*1.6*a*), we obtain

$$\beta_1 k_1(\alpha)\mathbf{B}_1\mathbf{A}_1 + \frac{k_2^2(\alpha)}{[k_2^2(\alpha) - k_1^2(\alpha)]}\mathbf{I} = \mathbf{I} \tag{A1.12}$$

and further simplification yields

$$\mathbf{B}_1\mathbf{A}_1 = \frac{k_1(\alpha)}{\beta_1[k_1^2(\alpha) - k_2^2(\alpha)]}\mathbf{I} \tag{A1.13}$$

From (*A*1.11) and (*A*1.13), we obtain

$$\mathbf{B}_1 = \frac{k_1(\alpha)}{\beta_1[k_1^2(\alpha) - k_2^2(\alpha)]}\mathbf{A}_1^{-1} \tag{A1.14a}$$

and

$$\mathbf{B}_2 = \frac{k_2(\alpha)}{\beta_2[k_2^2(\alpha) - k_1^2(\alpha)]}\mathbf{A}_2^{-1} \tag{A1.14b}$$

Substituting (*A*1.14*a*) and (*A*1.14*b*) in (*A*1.2), and using the fact that $\mathbf{A}_1$ and $\mathbf{A}_2$ are involutory matrices, we obtain the desired inverse transform of (*A*1.1) as

$$\psi^{-1}\{\alpha\} = \frac{1}{k_1^2(\alpha) - k_2^2(\alpha)}[k_1(\alpha)\mathbf{A}_1 - k_2(\alpha)\mathbf{A}_2] \tag{A1.15}$$

Case 2

If $\mathbf{A}_1$ and $\mathbf{A}_2$ are anti-commuting involutory matrices, then

$$\mathbf{A}_1\mathbf{A}_2^{-1} = -\mathbf{A}_2\mathbf{A}_1^{-1} \tag{A1.16}$$

Using (*A*1.16) in (*A*1.8), we obtain

$$\beta_2\frac{k_1^2(\alpha)}{k_2(\alpha)}\mathbf{B}_2\mathbf{A}_2 + \beta_2 k_2(\alpha)\mathbf{B}_2\mathbf{A}_2 = \mathbf{I} \tag{A1.17}$$

which with further manipulation yields

$$\mathbf{B}_2\mathbf{A}_2 = \frac{k_2(\alpha)}{\beta_2[k_1^2(\alpha) + k_2^2(\alpha)]}\mathbf{I} \tag{A1.18}$$

Substituting (*A*1.18) in (*A*1.6*a*), we obtain

$$\beta_1 k_1(\alpha)\mathbf{B}_1\mathbf{A}_1 + \frac{k_2^2(\alpha)}{[k_1^2(\alpha) + k_2^2(\alpha)]}\mathbf{I} = \mathbf{I} \tag{A1.19}$$

and further simplification yields

$$\mathbf{B}_1\mathbf{A}_1 = \frac{k_1(\alpha)}{\beta_1[k_1^2(\alpha) + k_2^2(\alpha)]}\mathbf{I} \tag{A1.20}$$

From (*A*1.18) and (*A*1.20), we obtain

$$\mathbf{B}_1 = \frac{k_1(\alpha)}{\beta_1[k_1^2(\alpha) + k_2^2(\alpha)]}\mathbf{A}_1^{-1} \tag{A1.21a}$$

and

$$\mathbf{B}_2 = \frac{k_2(\alpha)}{\beta_2[k_1^2(\alpha) + k_2^2(\alpha)]}\mathbf{A}_2^{-1} \qquad (A1.21b)$$

Using ($A1.21a$) and ($A1.21b$) in ($A1.2$), and the fact that $\mathbf{A}_1$ and $\mathbf{A}_2$ are involutory matrices, we obtain the desired inverse transform of ($A1.1$) as

$$\psi^{-1}\{\alpha\} = \frac{1}{k_1^2(\alpha) + k_2^2(\alpha)}[k_1(\alpha)\mathbf{A}_1 + k_2(\alpha)\mathbf{A}_2] \qquad (A1.22)$$

which completes the derivation of the hybrid transform inversion theorems.

A necessary condition for the inverse of a linear combination of two matrices to be given by the hybrid transform inversion theorems is that the matrices must be involutory. Furthermore, the two matrices in the linear combination must either commute or anti-commute. For orthogonal matrices $\mathbf{A}_1$ and $\mathbf{A}_2$, the condition that each $\mathbf{A}_i$ must be an involutory matrix imply that the above theorems apply only to a linear combination of two commuting or anti-commuting symmetric orthogonal matrices.

APPENDIX II

PROOF OF CONVERGENCE OF THE ITERATIVE ONE-DIMENSIONAL HADAMARD NPT RECONSTRUCTION ALGORITHM

The iterative one-dimensional Hadamard NPT reconstruction algorithm has been described in section 5.2.3. The proof of convergence of the algorithm is now given.

The forward Hadamard NPT matrix can be expressed as

$$\psi\{\alpha\} = \alpha\mathbf{I} + (1-\alpha)\mathbf{H}_n = \mathbf{M}^T\mathbf{D}\mathbf{M} \tag{A2.1}$$

where $\mathbf{M}$ is an orthogonal matrix of order 2^n and $\mathbf{D}$ is the diagonal matrix

$$\mathbf{D} = \begin{bmatrix} \mathbf{I}_{\frac{N}{2}} & 0 \\ 0 & (2\alpha-1)\mathbf{I}_{\frac{N}{2}} \end{bmatrix} \tag{A2.2}$$

and $\mathbf{I}_{\frac{N}{2}}$ is an identity matrix of order 2^{n-1}.

The vector of samples of the Hadamard NPT of the signal vector S, is given by

$$R = \mathbf{M}^T\mathbf{D}\mathbf{M}S \tag{A2.3}$$

It follows that the vector S can be expressed as

$$S = \mathbf{M}^T\mathbf{D}^{-1}\mathbf{M}R \tag{A2.4}$$

We can write

$$S = [S_k \quad S_u]^T \tag{A2.5a}$$

and

$$R = [R_k \quad R_u]^T \tag{A2.5b}$$

where S_k and R_k are vectors of n_k samples each, known from S and R respectively. Similarly, S_u and R_u are vectors of n_u samples each, unknown from S and R respectively; we consider that $n_k \geq n_u$.

Using (A2.3)-(A2.5), we can express the unknown vectors as

$$S_u = \mathbf{M}_u^T\mathbf{D}^{-1}\mathbf{M}_u R_u + \mathbf{M}_u^T\mathbf{D}^{-1}\mathbf{M}_k R_k \tag{A2.6}$$

and

$$R_u = \mathbf{M}_u^T \mathbf{D} \mathbf{M}_u S_u + \mathbf{M}_u^T \mathbf{D} \mathbf{M}_u S_k \qquad (A2.7)$$

where $\mathbf{M}_u$ and $\mathbf{M}_k$ are sub-matrices derived from $\mathbf{M}$ in order to determine S_u in terms of R_u and R_k, and also to determine R_u in terms of S_u and S_k; $\mathbf{M}_u$ is of dimension $N \times n_u$ while $\mathbf{M}_k$ is of dimension $N \times n_k$. (A2.6) and (A2.7) can be expressed as

$$\begin{bmatrix} S_u \\ R_u \end{bmatrix} = \begin{bmatrix} \mathbf{0} & \mathbf{M}_u^T \mathbf{D}^{-1} \mathbf{M}_u \\ \mathbf{M}_u^T \mathbf{D} \mathbf{M}_u & \mathbf{0} \end{bmatrix} \begin{bmatrix} S_u \\ R_u \end{bmatrix} + \begin{bmatrix} \mathbf{M}_u^T \mathbf{D}^{-1} \mathbf{M}_k R_k \\ \mathbf{M}_u^T \mathbf{D} \mathbf{M}_k S_k \end{bmatrix} \qquad (A2.8)$$

which is seen to be of the form

$$\omega = \mathbf{G}\omega + \kappa \qquad (A2.9)$$

where ω is the unique solution vector and κ is a known vector; the matrix $\mathbf{G}$ is of dimension $2n_u \times 2n_u$.

If $\omega^{(0)}$ is an approximation of ω, then a sequence of iterates can be defined as

$$\omega^{(m+1)} = \mathbf{G}\omega^{(m)} + \kappa \qquad ; \; m \geq 0 \qquad (A2.10)$$

The error vector $\varepsilon^{(m)}$ at the m^{th} iteration is given by

$$\varepsilon^{(m)} = \omega^{(m)} - \omega \qquad (A2.11)$$

The iterative scheme would converge to the true solution if

$$\lim_{m \to \infty} \varepsilon^{(m)} = \underline{0} \qquad (A2.12)$$

This condition is equivalent to requiring that [55]

$$\lim_{m \to \infty} \mathbf{G}^m = \mathbf{0} \qquad (A2.13)$$

which obtains if the spectral radius of $\mathbf{G}$, i.e. $\rho(\mathbf{G})$, is less than unity. In other words, the eigenvalues of $\mathbf{G}$, λ_i, must satisfy

$$|\lambda_i| < 1 \qquad (A2.14)$$

The characteristic polynomial of $\mathbf{G}$ is given by

$$|\lambda \mathbf{I}_{2u} - \mathbf{G}| = \begin{vmatrix} \lambda \mathbf{I}_u & -\mathbf{M}_u^T \mathbf{D}^{-1} \mathbf{M}_u \\ -\mathbf{M}_u^T \mathbf{D} \mathbf{M}_u & \lambda \mathbf{I}_u \end{vmatrix} \qquad (A2.15)$$

where $\mathbf{I}_{2u}$ is an identity matrix of order $2n_u$ and $\mathbf{I}_u$ is an identity matrix of order n_u. Making use of the fact that

$$\begin{vmatrix} \mathbf{A} & \mathbf{B} \\ \mathbf{C} & \mathbf{D} \end{vmatrix} = |\mathbf{A}| \, |\mathbf{D} - \mathbf{C}\mathbf{A}^{-1}\mathbf{B}| \qquad (A2.16)$$

we can write

$$|\lambda \mathbf{I}_{2u} - \mathbf{G}| = \lambda^{n_u} \left| \lambda \mathbf{I}_u - \mathbf{M}_u^T \mathbf{D} \mathbf{M}_u \left(\frac{1}{\lambda} \mathbf{I}_u \right) \mathbf{M}_u^T \mathbf{D}^{-1} \mathbf{M}_u \right| \tag{A2.17a}$$

$$= |\lambda^2 \mathbf{I}_u - \mathbf{M}_u^T \mathbf{D} \mathbf{M}_u \mathbf{M}_u^T \mathbf{D}^{-1} \mathbf{M}_u| \tag{A2.17b}$$

We define

$$\mathbf{Q} = \mathbf{M}_u^T \mathbf{D} \mathbf{M}_u \mathbf{M}_u^T \mathbf{D}^{-1} \mathbf{M}_u \tag{A2.18}$$

and represent the eigenvalues of $\mathbf{Q}$ by μ_i. The characteristic polynomial of $\mathbf{Q}$ is given by

$$f(\mu_i) = |\mu \mathbf{I}_u - \mathbf{Q}| \tag{A2.19}$$

From (A2.17b) and (A2.19), it follows that the n_u eigenvalues of G are related to the n_u eigenvalues of $\mathbf{Q}$ by

$$\lambda_i^2 = \mu_i \tag{A2.20}$$

Thus, we can prove the convergence of the iterative reconstruction process by proving that the eigenvalues of $\mathbf{Q}$, i.e. μ_i , $i = 1, 2, \ldots n_u$, all satisfy the constraint $|\mu_i| < 1$. Writing

$$\mathbf{D} \mathbf{M}_u \mathbf{M}_u^T \mathbf{D}^{-1} = (\mathbf{D} \mathbf{M}_u) (\mathbf{M}_u^T \mathbf{D}^{-1}) \equiv \mathbf{A}\mathbf{B} \tag{A2.21}$$

it follows that

$$\mathbf{M}_u^T \mathbf{D}^{-1} \mathbf{D} \mathbf{M}_u \equiv \mathbf{B}\mathbf{A} = \mathbf{I}_u \tag{A2.22}$$

Hence [56], $\mathbf{D} \mathbf{M}_u \mathbf{M}_u^T \mathbf{D}^{-1}$ and $\mathbf{M}_u^T \mathbf{D}^{-1} \mathbf{D} \mathbf{M}_u$ have the same eigenvalues except that $\mathbf{D} \mathbf{M}_u \mathbf{M}_u^T \mathbf{D}^{-1}$ has extra $(N - n_u)$ zero eigenvalues. Since any $N \times N$ matrix, $\mathbf{X}$ is unitarily similar to an upper triangular matrix whose diagonal entries are the eigenvalues of $\mathbf{X}$ arranged in any prescribed order [57], we can write

$$\mathbf{D} \mathbf{M}_u \mathbf{M}_u^T \mathbf{D}^{-1} = \mathbf{C}^T \begin{bmatrix} \mathbf{L}_u & \mathbf{Z} \\ \mathbf{0} & \mathbf{0}_{N-n_u} \end{bmatrix} \mathbf{C} \tag{A2.23a}$$

$$= \mathbf{C}^T \mathbf{L} \mathbf{C} \tag{A2.23b}$$

where $\mathbf{C}$ is an orthogonal matrix, $\mathbf{L}_u$ and $\mathbf{L}$ are upper triangular matrices, with the diagonal entries of $\mathbf{L}$ all equal to unity; $\mathbf{Z}$ is a matrix which is not relevant to the analysis and $\mathbf{0}_{N-n_u}$ is a null matrix of order $N - n_u$.

Using (A2.23), we can write

$$\mathbf{M}_u^T \mathbf{D} \mathbf{M}_u \mathbf{M}_u^T \mathbf{D}^{-1} \mathbf{M}_u = \mathbf{M}_u^T \mathbf{C}^T \mathbf{L} \mathbf{C} \mathbf{M}_u \tag{A2.24}$$

and expressing

$$\mathbf{M}_u^T \mathbf{C}^T = \mathbf{Y}_u^T \tag{A2.25}$$

it follows that $\mathbf{Y}_u$ can be regarded as a sub-matrix of the orthogonal matrix

$$\mathbf{Y}^T = \mathbf{C}^T\mathbf{L}^T \tag{A2.26}$$

Thus, the spectral norm of $\mathbf{Y}_u$, i.e. $\|\mathbf{Y}_u\|$, satisfy $\|\mathbf{Y}_u\| < 1$.

Using (*A*2.25), we can express (*A*2.24) as

$$\mathbf{M}_u^T\mathbf{D}\mathbf{M}_u\mathbf{M}_u^T\mathbf{D}^{-1}\mathbf{M}_u = \mathbf{Y}_u^T\mathbf{L}\mathbf{Y}_u \tag{A2.27}$$

The spectral norm of (*A*2.27) is given by

$$\left\|\mathbf{Y}_u^T\mathbf{L}\mathbf{Y}_u\right\| \leq \left\|\mathbf{Y}_u^T\right\| \|\mathbf{L}\| \|\mathbf{Y}_u\| \tag{A2.28}$$

and since the spectral radius of $\mathbf{L}$ is unity, it follows that

$$\left\|\mathbf{Y}_u^T\mathbf{L}\mathbf{Y}_u\right\| < 1 \tag{A2.29}$$

which implies that the magnitudes of all the eigenvalues of $\mathbf{M}_u^T\mathbf{D}\mathbf{M}_u\mathbf{M}_u^T\mathbf{D}^{-1}\mathbf{M}_u$ are all less than unity. This follows from the fact that the spectral norm of a matrix is greater than or equal to its spectral radius [55]. From (*A*2.20), it is clear that the magnitudes of the eigenvalues of $\mathbf{G}$ are all less than unity. This proves the convergence of the iterative Hadamard NPT reconstruction algorithm.

We wish to point out that in establishing the proof of convergence, we have made use of the fact that the non-zero eigenvalues of the matrix $\mathbf{D}\mathbf{M}_u\mathbf{M}_u^T\mathbf{D}^{-1}$ are equal to the eigenvalues of the matrix $\mathbf{M}_u^T\mathbf{D}^{-1}\mathbf{D}\mathbf{M}_u$. However, the matrix $\mathbf{D}^{-1}$ does not exist for $\alpha = \frac{1}{2}$, meaning that the eigenvalues of $\mathbf{M}_u^T\mathbf{D}^{-1}\mathbf{D}\mathbf{M}_u$ and the non-zero eigenvalues of $\mathbf{D}\mathbf{M}_u\mathbf{M}_u^T\mathbf{D}^{-1}$ are unbounded at $\alpha = \frac{1}{2}$. It is conjectured that this may lead to an instability of the algorithm in the vicinity of the singularity at $\alpha = \frac{1}{2}$. Further analysis and empirical results, which are presented in section 5.2.3.1 show that convergence of the iterative Hadamard NPT reconstruction algorithm is only obtained for $\alpha \leq 0.464$.

APPENDIX III

PROOF OF CONVERGENCE OF THE ITERATIVE TWO-DIMENSIONAL HADAMARD NPT RECONSTRUCTION ALGORITHM

The iterative two-dimensional Hadamard NPT reconstruction algorithm is described in section 6.2.2. The proof of convergence of the algorithm is as follows.

The two-dimensional Hadamard NPT of the $N \times N$ original signal, $\mathbf{F}$, can be expressed as

$$\mathbf{T_F} = \mathbf{M}^T\mathbf{DMFM}^T\mathbf{DM} \tag{A3.1}$$

where $\mathbf{M}$ is an orthogonal matrix.

From (A3.1), we can write

$$\mathbf{D}\left(\mathbf{MFM}^T\right) = \left(\mathbf{MT_FM}^T\right)\mathbf{D}^{-1} \tag{A3.2}$$

We define

$$\mathbf{D} = diag\left(d_1, d_2, \ldots, d_N\right) \tag{A3.3}$$

$$\mathbf{Q} = (q_{ij}) = \mathbf{MFM}^T \tag{A3.4}$$

and

$$\mathbf{R} = (r_{ij}) = \mathbf{MT_FM}^T \tag{A3.5}$$

where the entries q_{ij} and r_{ij} are linear functions of all the entries of $\mathbf{F}$ and $\mathbf{T_F}$ respectively. In addition, we define the vectors

$$\mathbf{q}^T = [q_{11}, q_{12}, \ldots, q_{1N}, q_{21}, q_{22}, \ldots, q_{2N}, \ldots, q_{N1}, \ldots, q_{NN}] \tag{A3.6}$$

which is obtained by row-stacking the entries of $\mathbf{Q}$ and

$$\mathbf{r}^T = [r_{11}, r_{12}, \ldots, r_{1N}, r_{21}, r_{22}, \ldots, r_{2N}, \ldots, r_{N1}, \ldots, r_{NN}] \tag{A3.7}$$

which is obtained by row-stacking the entries of $\mathbf{R}$; the vectors $\mathbf{q}$ and $\mathbf{r}$ are each of dimension $N^2 \times 1$.

Using (A3.2), it follows that

$$\mathbf{D}_1\mathbf{q} = \mathbf{D}_2\mathbf{r} \tag{A3.8}$$

where

$$\mathbf{D}_1 = diag\,(d_1, \ldots d_1, d_2, \ldots d_2, \ \ldots, d_N, \ldots, d_N) \tag{A3.9}$$

and

$$\mathbf{D}_2 = diag\left(\frac{1}{d_1}, \frac{1}{d_2}, \ldots, \frac{1}{d_N}, \frac{1}{d_1}, \frac{1}{d_2}, \ldots, \frac{1}{d_N}, \frac{1}{d_1}, \ldots, \frac{1}{d_N}\right) \tag{A3.10}$$

; $\mathbf{D}_1$ and $\mathbf{D}_2$ are each of dimension $N^2 \times N^2$.

Making use of the fact that the entries of vectors $\mathbf{q}$ and $\mathbf{r}$ are linear functions of the entries of $\mathbf{F}$ and $\mathbf{T_F}$ respectively, we can write

$$\mathbf{D}_1\mathbf{X}\mathbf{f}_\mathbf{F} = \mathbf{D}_2\mathbf{X}\mathbf{t}_\mathbf{F} \tag{A3.11}$$

where

$$\mathbf{f}_\mathbf{F}^T = [f_{11}, f_{12}, \ldots, f_{1N}, f_{21}, \ldots f_{2N}, \ldots f_{N1}, \ldots f_{NN}] \tag{A3.12}$$

$$\mathbf{t}_\mathbf{F}^T = [t_{11}, t_{12}, \ldots, t_{1N}, t_{21}, \ldots t_{2N}, \ldots t_{N1}, \ldots t_{NN}] \tag{A3.13}$$

and $\mathbf{X}$ is an orthogonal matrix given by

$$\mathbf{X} = \mathbf{C} \otimes \mathbf{C} \tag{A3.14}$$

Thus, we can express (A3.12) as

$$\mathbf{f}_\mathbf{F} = \mathbf{X}^T \left(\mathbf{D}_3^{-1}\right) \mathbf{X}\mathbf{t}_\mathbf{F} \tag{A3.15}$$

from which it follows that

$$\mathbf{t}_\mathbf{F} = \mathbf{X}^T\mathbf{D}_3\mathbf{X}\mathbf{f}_\mathbf{F} \tag{A3.16}$$

where

$$\mathbf{D}_3 = \mathbf{D}_2^{-1}\mathbf{D}_1 \tag{A3.17}$$

We can write

$$\mathbf{f}_\mathbf{F} = [\mathbf{f}_{\mathbf{F};k} \,|\, \mathbf{f}_{\mathbf{F};u}]^T \tag{A3.18a}$$

and

$$\mathbf{t}_\mathbf{F} = [\mathbf{t}_{\mathbf{F};k} \,|\, \mathbf{t}_{\mathbf{F};u}]^T \tag{A3.18b}$$

where $\mathbf{f}_{\mathbf{F};k}$ and $\mathbf{t}_{\mathbf{F};k}$ are vectors of n_k samples each, known from $\mathbf{f}_\mathbf{F}$ and $\mathbf{t}_\mathbf{F}$ respectively. Similarly, $\mathbf{f}_{\mathbf{F};u}$ and $\mathbf{t}_{\mathbf{F};u}$ are vectors of n_u samples each, unknown from $\mathbf{f}_\mathbf{F}$ and $\mathbf{t}_\mathbf{F}$ respectively; we consider that $n_k \geq n_u$.

Using (A3.15)-(A3.18), we can express the unknown vectors as

$$\mathbf{f}_{\mathbf{F};u} = \mathbf{X}_u^T\mathbf{D}_3^{-1}\mathbf{X}_u\mathbf{t}_{\mathbf{F};u} + \mathbf{X}_u^T\mathbf{D}_3^{-1}\mathbf{X}_k\mathbf{t}_{\mathbf{F};k} \tag{A3.19a}$$

and

$$\mathbf{t}_{\mathbf{F};u} = \mathbf{X}_u^T\mathbf{D}_3\mathbf{X}_u\mathbf{f}_{\mathbf{F};u} + \mathbf{X}_u^T\mathbf{D}_3\mathbf{X}_k\mathbf{f}_{\mathbf{F};k} \tag{A3.19b}$$

where $\mathbf{X}_u$ and $\mathbf{X}_k$ are sub-matrices derived from $\mathbf{X}$ in order to determine $\mathbf{f}_{\mathbf{F};u}$ in terms of $\mathbf{t}_{\mathbf{F};u}$ and $\mathbf{t}_{\mathbf{F};k}$, and also to determine $\mathbf{t}_{\mathbf{F};u}$ in terms of $\mathbf{f}_{\mathbf{F};u}$ and $\mathbf{f}_{\mathbf{F};k}$; $\mathbf{X}_u$ is of dimension $N^2 \times n_u$ while $\mathbf{X}_k$ is of dimension $N^2 \times n_k$.

We can express (*A*3.19) in matrix form as

$$\begin{bmatrix} \mathbf{f}_{\mathbf{F};u} \\ \mathbf{t}_{\mathbf{F};u} \end{bmatrix} = \begin{bmatrix} \mathbf{0} & \mathbf{X}_u^T \mathbf{D}_3^{-1} \mathbf{X}_u \\ \mathbf{X}_u^T \mathbf{D}_3 \mathbf{X}_u & \mathbf{0} \end{bmatrix} \begin{bmatrix} \mathbf{f}_{\mathbf{F};u} \\ \mathbf{t}_{\mathbf{F};u} \end{bmatrix} + \begin{bmatrix} \mathbf{X}_u^T \mathbf{D}_3^{-1} \mathbf{X}_k \mathbf{t}_{\mathbf{F};k} \\ \mathbf{X}_u^T \mathbf{D}_3 \mathbf{X}_k \mathbf{f}_{\mathbf{F};k} \end{bmatrix} \qquad (A3.20)$$

which is of the form

$$\omega = \mathbf{G}\omega + \kappa \qquad (A3.21)$$

If $\omega^{(0)}$ is an approximation of ω, then a sequence of iterates can be defined as

$$\omega^{(m+1)} = \mathbf{G}\omega^{(m)} + \kappa \qquad ; \; m \geq 0 \qquad (A3.22)$$

The iterative scheme would converge to the true solution if [55]

$$\lim_{m \to \infty} \mathbf{G}^m = \mathbf{0} \qquad (A3.23)$$

which obtains if the eigenvalues of $\mathbf{G}$, λ_i, satisfy the constraint

$$|\lambda_i| < 1 \qquad (A3.24)$$

The analysis from this point onwards is similar to that carried out for one-dimensional reconstruction in appendix II and shall not be repeated here. Essentially, we set $\mathbf{M}_u^T = \mathbf{X}_u^T$ and $\mathbf{D} = \mathbf{D}_3$ in (*A*2.8) and the proof follows in a straightforward fashion.

APPENDIX IV

DERIVATION OF THE RESULT OF EQUATION (6.40), CHAPTER SIX

The material contained in this appendix was removed from chapter six to permit its easier reading; it immediately follows (6.18*b*).

Initialization

We perform the inverse two-dimensional Hadamard NPT of $\tilde{\mathbf{T}}_{\mathbf{F}}$ (given by (6.17)) to obtain the matrix $\hat{\mathbf{F}}_0$, which is given by

$$\hat{\mathbf{F}}_0 = \begin{bmatrix} \hat{\mathbf{F}}_{11}^{(0)} & \hat{\mathbf{F}}_{12}^{(0)} \\ \hat{\mathbf{F}}_{21}^{(0)} & \hat{\mathbf{F}}_{22}^{(0)} \end{bmatrix} \tag{6.19}$$

where

$$\hat{\mathbf{F}}_{11}^{(0)} = \mathbf{Q}_{12}\mathbf{T}_{21}\mathbf{Q}_{11} + \mathbf{Q}_{12}\mathbf{T}_{22}\mathbf{Q}_{21} \tag{6.20a}$$

$$\hat{\mathbf{F}}_{12}^{(0)} = \mathbf{Q}_{12}\mathbf{T}_{21}\mathbf{Q}_{12} + \mathbf{Q}_{12}\mathbf{T}_{22}\mathbf{Q}_{22} \tag{6.20b}$$

$$\hat{\mathbf{F}}_{21}^{(0)} = \mathbf{Q}_{22}\mathbf{T}_{21}\mathbf{Q}_{11} + \mathbf{Q}_{22}\mathbf{T}_{22}\mathbf{Q}_{21} \tag{6.20c}$$

$$\hat{\mathbf{F}}_{22}^{(0)} = \mathbf{Q}_{22}\mathbf{T}_{21}\mathbf{Q}_{12} + \mathbf{Q}_{22}\mathbf{T}_{22}\mathbf{Q}_{22} \tag{6.20d}$$

Replace the sub-matrices $\hat{\mathbf{F}}_{21}^{(0)}$ and $\hat{\mathbf{F}}_{22}^{(0)}$ in $\hat{\mathbf{F}}_0$ with the estimates $\hat{\mathbf{F}}_{21}$ and $\hat{\mathbf{F}}_{22}$ respectively, to obtain the matrix $\hat{\mathbf{F}}_0'$, whose two-dimensional segments are

$$\check{\mathbf{F}}_{11}^{(0)} = \hat{\mathbf{F}}_{11}^{(0)} = \mathbf{Q}_{12}\mathbf{T}_{21}\mathbf{Q}_{11} + \mathbf{Q}_{12}\mathbf{T}_{22}\mathbf{Q}_{21} \tag{6.21a}$$

$$\check{\mathbf{F}}_{12}^{(0)} = \hat{\mathbf{F}}_{12}^{(0)} = \mathbf{Q}_{12}\mathbf{T}_{21}\mathbf{Q}_{12} + \mathbf{Q}_{12}\mathbf{T}_{22}\mathbf{Q}_{22} \tag{6.21b}$$

$$\check{\mathbf{F}}_{21}^{(0)} = \hat{\mathbf{F}}_{21} = \mathbf{Q}_{21}\mathbf{T}_{11}\mathbf{Q}_{11} + \mathbf{Q}_{22}\mathbf{T}_{21}\mathbf{Q}_{11} + \mathbf{Q}_{21}\mathbf{T}_{12}\mathbf{Q}_{21} + \mathbf{Q}_{22}\mathbf{T}_{22}\mathbf{Q}_{21} + \mathbf{E}_{21} \tag{6.21c}$$

and

$$\check{\mathbf{F}}_{22}^{(0)} = \hat{\mathbf{F}}_{22} = \mathbf{Q}_{21}\mathbf{T}_{11}\mathbf{Q}_{12} + \mathbf{Q}_{22}\mathbf{T}_{21}\mathbf{Q}_{12} + \mathbf{Q}_{21}\mathbf{T}_{12}\mathbf{Q}_{22} + \mathbf{Q}_{22}\mathbf{T}_{22}\mathbf{Q}_{22} + \mathbf{E}_{22} \tag{6.21d}$$

Iteration 1

Forward Two-Dimensional Hadamard NPT

Perform the forward two-dimensional Hadamard NPT of the matrix $\hat{\mathbf{F}}_0'$, whose segments are given by (6.21), to obtain the respective segments of the matrix $\hat{\mathbf{T}}_{\mathbf{F};1}$.

Thus, we have

$$\hat{\mathbf{T}}_{11}^{(1)} = \mathbf{P}_{11}\check{\mathbf{F}}_{11}^{(0)}\mathbf{P}_{11} + \mathbf{P}_{11}\check{\mathbf{F}}_{12}^{(0)}\mathbf{P}_{21} + \mathbf{P}_{12}\check{\mathbf{F}}_{21}^{(0)}\mathbf{P}_{11} + \mathbf{P}_{12}\check{\mathbf{F}}_{22}^{(0)}\mathbf{P}_{21} \tag{6.22a}$$

$$\begin{aligned}
&= \left\{\mathbf{P}_{11}\mathbf{Q}_{12}\mathbf{T}_{21}\mathbf{Q}_{11}\mathbf{P}_{11} + \mathbf{P}_{11}\mathbf{Q}_{12}\mathbf{T}_{22}\mathbf{Q}_{21}\mathbf{P}_{11}\right\} + \left\{\mathbf{P}_{11}\mathbf{Q}_{12}\mathbf{T}_{21}\mathbf{Q}_{12}\mathbf{P}_{21}\right. \\
&\quad \left. + \mathbf{P}_{11}\mathbf{Q}_{12}\mathbf{T}_{22}\mathbf{Q}_{22}\mathbf{P}_{21}\right\} + \left\{\mathbf{P}_{12}\mathbf{Q}_{21}\mathbf{T}_{11}\mathbf{Q}_{11}\mathbf{P}_{11} + \mathbf{P}_{12}\mathbf{Q}_{21}\mathbf{T}_{12}\mathbf{Q}_{21}\mathbf{P}_{11}\right. \\
&\quad + \mathbf{P}_{12}\mathbf{Q}_{22}\mathbf{T}_{21}\mathbf{Q}_{11}\mathbf{P}_{11} + \mathbf{P}_{12}\mathbf{Q}_{22}\mathbf{T}_{22}\mathbf{Q}_{21}\mathbf{P}_{11} + \mathbf{P}_{12}\mathbf{E}_{21}\mathbf{P}_{11}\Big\} + \Big\{\mathbf{P}_{12}\mathbf{Q}_{21}\mathbf{T}_{11}\mathbf{Q}_{12}\mathbf{P}_{21} \\
&\quad + \mathbf{P}_{12}\mathbf{Q}_{21}\mathbf{T}_{12}\mathbf{Q}_{22}\mathbf{P}_{21} + \mathbf{P}_{12}\mathbf{Q}_{22}\mathbf{T}_{21}\mathbf{Q}_{12}\mathbf{P}_{21} + \mathbf{P}_{12}\mathbf{Q}_{22}\mathbf{T}_{22}\mathbf{Q}_{22}\mathbf{P}_{21} \\
&\quad \left. + \mathbf{P}_{12}\mathbf{E}_{22}\mathbf{P}_{21}\right\}
\end{aligned} \tag{6.22b}$$

$$\begin{aligned}
&= \left\{\frac{1}{(2\alpha-1)^2}\Big[-\left(\alpha^2-c_1^2\right)\left(c_1^2\mathbf{I}_{\frac{N}{2}} + \alpha c_1\mathbf{H}_{\frac{N}{2}}\right)\mathbf{T}_{21}\right. \\
&\quad \left. + \left(c_1^2\mathbf{I}_{\frac{N}{2}} + \alpha c_1\mathbf{H}_{\frac{N}{2}}\right)\mathbf{T}_{22}\left(c_1^2\mathbf{I}_{\frac{N}{2}} + \alpha c_1\mathbf{H}_{\frac{N}{2}}\right)\Big]\right\} \\
&\quad + \left\{\frac{1}{(2\alpha-1)^2}\Big[c_1^2\left(c_1^2\mathbf{I}_{\frac{N}{2}} + \alpha c_1\mathbf{H}_{\frac{N}{2}}\right)\mathbf{T}_{21}\right. \\
&\quad \left. - \left(c_1^2\mathbf{I}_{\frac{N}{2}} + \alpha c_1\mathbf{H}_{\frac{N}{2}}\right)\mathbf{T}_{22}\left(c_1^2\mathbf{I}_{\frac{N}{2}} + \alpha c_1\mathbf{H}_{\frac{N}{2}}\right)\Big]\right\} + \left\{\frac{1}{(2\alpha-1)^2}\Big[-c_1^2\left(\alpha^2-c_1^2\right)\mathbf{T}_{11}\right. \\
&\quad + c_1^2\mathbf{T}_{12}\left(c_1^2\mathbf{I}_{\frac{N}{2}} + \alpha c_1\mathbf{H}_{\frac{N}{2}}\right) + \left(\alpha^2-c_1^2\right)\left(c_1^2\mathbf{I}_{\frac{N}{2}} + \alpha c_1\mathbf{H}_{\frac{N}{2}}\right)\mathbf{T}_{21} \\
&\quad \left. - \left(c_1^2\mathbf{I}_{\frac{N}{2}} + \alpha c_1\mathbf{H}_{\frac{N}{2}}\right)\mathbf{T}_{22}\left(c_1^2\mathbf{I}_{\frac{N}{2}} + \alpha c_1\mathbf{H}_{\frac{N}{2}}\right)\Big] + \mathbf{P}_{12}\mathbf{E}_{21}\mathbf{P}_{11}\right\} \\
&\quad + \left\{\frac{1}{(2\alpha-1)^2}\Big[c_1^4\mathbf{T}_{11} - c_1^2\mathbf{T}_{12}\left(c_1^2\mathbf{I}_{\frac{N}{2}} + \alpha c_1\mathbf{H}_{\frac{N}{2}}\right) - c_1^2\left(c_1^2\mathbf{I}_{\frac{N}{2}} + \alpha c_1\mathbf{H}_{\frac{N}{2}}\right)\mathbf{T}_{21}\right. \\
&\quad \left. + \left(c_1^2\mathbf{I}_{\frac{N}{2}} + \alpha c_1\mathbf{H}_{\frac{N}{2}}\right)\mathbf{T}_{22}\left(c_1^2\mathbf{I}_{\frac{N}{2}} + \alpha c_1\mathbf{H}_{\frac{N}{2}}\right)\Big] + \mathbf{P}_{12}\mathbf{E}_{22}\mathbf{P}_{21}\right\}
\end{aligned} \tag{6.22c}$$

$$= \left[\frac{-(1-\alpha)^2}{2(2\alpha-1)}\right]\mathbf{T}_{11} + \mathbf{P}_{12}\mathbf{E}_{21}\mathbf{P}_{11} + \mathbf{P}_{12}\mathbf{E}_{22}\mathbf{P}_{21} \tag{6.22d}$$

$$\hat{\mathbf{T}}_{12}^{(1)} = \mathbf{P}_{11}\check{\mathbf{F}}_{11}^{(0)}\mathbf{P}_{12} + \mathbf{P}_{11}\check{\mathbf{F}}_{12}^{(0)}\mathbf{P}_{22} + \mathbf{P}_{12}\check{\mathbf{F}}_{21}^{(0)}\mathbf{P}_{12} + \mathbf{P}_{12}\check{\mathbf{F}}_{22}^{(0)}\mathbf{P}_{22} \tag{6.23a}$$

$$\begin{aligned}
&= \left\{\mathbf{P}_{11}\mathbf{Q}_{12}\mathbf{T}_{21}\mathbf{Q}_{11}\mathbf{P}_{12} + \mathbf{P}_{11}\mathbf{Q}_{12}\mathbf{T}_{22}\mathbf{Q}_{21}\mathbf{P}_{12}\right\} + \left\{\mathbf{P}_{11}\mathbf{Q}_{12}\mathbf{T}_{21}\mathbf{Q}_{12}\mathbf{P}_{22}\right. \\
&\quad \left. + \mathbf{P}_{11}\mathbf{Q}_{12}\mathbf{T}_{22}\mathbf{Q}_{22}\mathbf{P}_{22}\right\} + \left\{\mathbf{P}_{12}\mathbf{Q}_{21}\mathbf{T}_{11}\mathbf{Q}_{11}\mathbf{P}_{12} + \mathbf{P}_{12}\mathbf{Q}_{21}\mathbf{T}_{12}\mathbf{Q}_{21}\mathbf{P}_{12}\right. \\
&\quad + \mathbf{P}_{12}\mathbf{Q}_{22}\mathbf{T}_{21}\mathbf{Q}_{11}\mathbf{P}_{12} + \mathbf{P}_{12}\mathbf{Q}_{22}\mathbf{T}_{22}\mathbf{Q}_{21}\mathbf{P}_{12} + \mathbf{P}_{12}\mathbf{E}_{21}\mathbf{P}_{12}\Big\} \\
&\quad + \Big\{\mathbf{P}_{12}\mathbf{Q}_{21}\mathbf{T}_{11}\mathbf{Q}_{12}\mathbf{P}_{22} + \mathbf{P}_{12}\mathbf{Q}_{21}\mathbf{T}_{12}\mathbf{Q}_{22}\mathbf{P}_{22} + \mathbf{P}_{12}\mathbf{Q}_{22}\mathbf{T}_{21}\mathbf{Q}_{12}\mathbf{P}_{22} \\
&\quad \left. + \mathbf{P}_{12}\mathbf{Q}_{22}\mathbf{T}_{22}\mathbf{Q}_{22}\mathbf{P}_{22} + \mathbf{P}_{12}\mathbf{E}_{22}\mathbf{P}_{22}\right\}
\end{aligned} \tag{6.23b}$$

$$= \left\{ \frac{1}{(2\alpha-1)^2} \left[\left(c_1^2 \mathbf{I}_{\frac{N}{2}} + \alpha c_1 \mathbf{H}_{\frac{N}{2}} \right) \mathbf{T}_{21} \left(c_1^2 \mathbf{I}_{\frac{N}{2}} - \alpha c_1 \mathbf{H}_{\frac{N}{2}} \right) \right. \right.$$
$$\left. \left. + c_1^2 \left(c_1^2 \mathbf{I}_{\frac{N}{2}} + \alpha c_1 \mathbf{H}_{\frac{N}{2}} \right) \mathbf{T}_{22} \right] \right\} + \left\{ \frac{1}{(2\alpha-1)^2} \left[- \left(c_1^2 \mathbf{I}_{\frac{N}{2}} + \alpha c_1 \mathbf{H}_{\frac{N}{2}} \right) \mathbf{T}_{21} \left(c_1^2 \mathbf{I}_{\frac{N}{2}} - \alpha c_1 \mathbf{H}_{\frac{N}{2}} \right) \right. \right.$$
$$\left. \left. - (\alpha^2 - c_1^2) \left(c_1^2 \mathbf{I}_{\frac{N}{2}} + \alpha c_1 \mathbf{H}_{\frac{N}{2}} \right) \mathbf{T}_{22} \right] \right\} + \left\{ \frac{1}{(2\alpha-1)^2} \left[c_1^2 \mathbf{T}_{11} \left(c_1^2 \mathbf{I}_{\frac{N}{2}} - \alpha c_1 \mathbf{H}_{\frac{N}{2}} \right) \right. \right.$$
$$+ c_1^4 \mathbf{T}_{12} - \left(c_1^2 \mathbf{I}_{\frac{N}{2}} + \alpha c_1 \mathbf{H}_{\frac{N}{2}} \right) \mathbf{T}_{21} \left(c_1^2 \mathbf{I}_{\frac{N}{2}} - \alpha c_1 \mathbf{H}_{\frac{N}{2}} \right) - c_1^2 \left(c_1^2 \mathbf{I}_{\frac{N}{2}} + \alpha c_1 \mathbf{H}_{\frac{N}{2}} \right) \mathbf{T}_{22} \Big]$$
$$\left. + \mathbf{P}_{12} \mathbf{E}_{21} \mathbf{P}_{12} \right\} + \left\{ \frac{1}{(2\alpha-1)^2} \left[- c_1^2 \mathbf{T}_{11} \left(c_1^2 \mathbf{I}_{\frac{N}{2}} - \alpha c_1 \mathbf{H}_{\frac{N}{2}} \right) - c_1^2 (\alpha^2 - c_1^2) \mathbf{T}_{12} \right. \right.$$
$$\left. \left. + \left(c_1^2 \mathbf{I}_{\frac{N}{2}} + \alpha c_1 \mathbf{H}_{\frac{N}{2}} \right) \mathbf{T}_{21} \left(c_1^2 \mathbf{I}_{\frac{N}{2}} - \alpha c_1 \mathbf{H}_{\frac{N}{2}} \right) + (\alpha^2 - c_1^2) \left(c_1^2 \mathbf{I}_{\frac{N}{2}} + \alpha c_1 \mathbf{H}_{\frac{N}{2}} \right) \mathbf{T}_{22} \right] \right.$$
$$\left. + \mathbf{P}_{12} \mathbf{E}_{22} \mathbf{P}_{22} \right\} \tag{6.23c}$$

$$= \left[\frac{-(1-\alpha)^2}{2(2\alpha-1)} \right] \mathbf{T}_{12} + \mathbf{P}_{12} \mathbf{E}_{21} \mathbf{P}_{12} + \mathbf{P}_{12} \mathbf{E}_{22} \mathbf{P}_{22} \tag{6.23d}$$

$$\hat{\mathbf{T}}_{21}^{(1)} = \mathbf{P}_{21} \check{\mathbf{F}}_{11}^{(0)} \mathbf{P}_{11} + \mathbf{P}_{21} \check{\mathbf{F}}_{12}^{(0)} \mathbf{P}_{21} + \mathbf{P}_{22} \check{\mathbf{F}}_{21}^{(0)} \mathbf{P}_{11} + \mathbf{P}_{22} \check{\mathbf{F}}_{22}^{(0)} \mathbf{P}_{21} \tag{6.24a}$$

$$= \left\{ \mathbf{P}_{21} \mathbf{Q}_{12} \mathbf{T}_{21} \mathbf{Q}_{11} \mathbf{P}_{11} + \mathbf{P}_{21} \mathbf{Q}_{12} \mathbf{T}_{22} \mathbf{Q}_{21} \mathbf{P}_{11} \right\} + \left\{ \mathbf{P}_{21} \mathbf{Q}_{12} \mathbf{T}_{21} \mathbf{Q}_{12} \mathbf{P}_{21} + \mathbf{P}_{21} \mathbf{Q}_{12} \mathbf{T}_{22} \mathbf{Q}_{22} \mathbf{P}_{21} \right\}$$
$$+ \left\{ \mathbf{P}_{22} \mathbf{Q}_{21} \mathbf{T}_{11} \mathbf{Q}_{11} \mathbf{P}_{11} + \mathbf{P}_{22} \mathbf{Q}_{21} \mathbf{T}_{12} \mathbf{Q}_{21} \mathbf{P}_{11} + \mathbf{P}_{22} \mathbf{Q}_{22} \mathbf{T}_{21} \mathbf{Q}_{11} \mathbf{P}_{11} \right.$$
$$\left. + \mathbf{P}_{22} \mathbf{Q}_{22} \mathbf{T}_{22} \mathbf{Q}_{21} \mathbf{P}_{11} + \mathbf{P}_{22} \mathbf{E}_{21} \mathbf{P}_{11} \right\} + \left\{ \mathbf{P}_{22} \mathbf{Q}_{21} \mathbf{T}_{11} \mathbf{Q}_{12} \mathbf{P}_{21} + \mathbf{P}_{22} \mathbf{Q}_{21} \mathbf{T}_{12} \mathbf{Q}_{22} \mathbf{P}_{21} \right.$$
$$\left. + \mathbf{P}_{22} \mathbf{Q}_{22} \mathbf{T}_{21} \mathbf{Q}_{12} \mathbf{P}_{21} + \mathbf{P}_{22} \mathbf{Q}_{22} \mathbf{T}_{22} \mathbf{Q}_{22} \mathbf{P}_{21} + \mathbf{P}_{22} \mathbf{E}_{22} \mathbf{P}_{21} \right\} \tag{6.24b}$$

$$= \left\{ \frac{1}{(2\alpha-1)^2} \left[- c_1^2 (\alpha^2 - c_1^2) \mathbf{T}_{21} + c_1^2 \mathbf{T}_{22} \left(c_1^2 \mathbf{I}_{\frac{N}{2}} + \alpha c_1 \mathbf{H}_{\frac{N}{2}} \right) \right] \right\}$$
$$+ \left\{ \frac{1}{(2\alpha-1)^2} \left[c_1^4 \mathbf{T}_{21} - c_1^2 \mathbf{T}_{22} \left(c_1^2 \mathbf{I}_{\frac{N}{2}} + \alpha c_1 \mathbf{H}_{\frac{N}{2}} \right) \right] \right\}$$
$$+ \left\{ \frac{1}{(2\alpha-1)^2} \left[(\alpha^2 - c_1^2) \left(c_1^2 \mathbf{I}_{\frac{N}{2}} - \alpha c_1 \mathbf{H}_{\frac{N}{2}} \right) \mathbf{T}_{11} \right. \right.$$
$$- \left(c_1^2 \mathbf{I}_{\frac{N}{2}} - \alpha c_1 \mathbf{H}_{\frac{N}{2}} \right) \mathbf{T}_{12} \left(c_1^2 \mathbf{I}_{\frac{N}{2}} + \alpha c_1 \mathbf{H}_{\frac{N}{2}} \right) + (\alpha^2 - c_1^2)^2 \mathbf{T}_{21}$$
$$\left. \left. - (\alpha^2 - c_1^2) \mathbf{T}_{22} \left(c_1^2 \mathbf{I}_{\frac{N}{2}} + \alpha c_1 \mathbf{H}_{\frac{N}{2}} \right) \right] \right.$$
$$\left. + \mathbf{P}_{22} \mathbf{E}_{21} \mathbf{P}_{11} \right\} + \left\{ \frac{1}{(2\alpha-1)^2} \left[- c_1^2 \left(c_1^2 \mathbf{I}_{\frac{N}{2}} - \alpha c_1 \mathbf{H}_{\frac{N}{2}} \right) \mathbf{T}_{11} \right. \right.$$
$$+ \left(c_1^2 \mathbf{I}_{\frac{N}{2}} - \alpha c_1 \mathbf{H}_{\frac{N}{2}} \right) \mathbf{T}_{12} \left(c_1^2 \mathbf{I}_{\frac{N}{2}} + \alpha c_1 \mathbf{H}_{\frac{N}{2}} \right) - c_1^2 (\alpha^2 - c_1^2) \mathbf{T}_{21}$$
$$\left. \left. + (\alpha^2 - c_1^2) \mathbf{T}_{22} \left(c_1^2 \mathbf{I}_{\frac{N}{2}} + \alpha c_1 \mathbf{H}_{\frac{N}{2}} \right) \right] + \mathbf{P}_{22} \mathbf{E}_{22} \mathbf{P}_{21} \right\} \tag{6.24c}$$

$$= \mathbf{T}_{21} + \frac{1}{2\alpha - 1}\left(c_1^2 \mathbf{I}_{\frac{N}{2}} - \alpha c_1 \mathbf{H}_{\frac{N}{2}}\right)\mathbf{T}_{11} + \mathbf{P}_{22}\mathbf{E}_{21}\mathbf{P}_{11} + \mathbf{P}_{22}\mathbf{E}_{22}\mathbf{P}_{21} \tag{6.24d}$$

$$\hat{\mathbf{T}}_{22}^{(1)} = \mathbf{P}_{21}\check{\mathbf{F}}_{11}^{(0)}\mathbf{P}_{12} + \mathbf{P}_{21}\check{\mathbf{F}}_{12}^{(0)}\mathbf{P}_{22} + \mathbf{P}_{22}\check{\mathbf{F}}_{21}^{(0)}\mathbf{P}_{12} + \mathbf{P}_{22}\check{\mathbf{F}}_{22}^{(0)}\mathbf{P}_{22} \tag{6.25a}$$

$$\begin{aligned} &= \left\{\mathbf{P}_{21}\mathbf{Q}_{12}\mathbf{T}_{21}\mathbf{Q}_{11}\mathbf{P}_{12} + \mathbf{P}_{21}\mathbf{Q}_{12}\mathbf{T}_{22}\mathbf{Q}_{21}\mathbf{P}_{12}\right\} + \left\{\mathbf{P}_{21}\mathbf{Q}_{12}\mathbf{T}_{21}\mathbf{Q}_{12}\mathbf{P}_{22}\right. \\ &\quad \left. + \mathbf{P}_{21}\mathbf{Q}_{12}\mathbf{T}_{22}\mathbf{Q}_{22}\mathbf{P}_{22}\right\} + \left\{\mathbf{P}_{22}\mathbf{Q}_{21}\mathbf{T}_{11}\mathbf{Q}_{11}\mathbf{P}_{12} + \mathbf{P}_{22}\mathbf{Q}_{21}\mathbf{T}_{12}\mathbf{Q}_{21}\mathbf{P}_{12}\right. \\ &\quad \left. + \mathbf{P}_{22}\mathbf{Q}_{22}\mathbf{T}_{21}\mathbf{Q}_{11}\mathbf{P}_{12} + \mathbf{P}_{22}\mathbf{Q}_{22}\mathbf{T}_{22}\mathbf{Q}_{21}\mathbf{P}_{12} + \mathbf{P}_{22}\mathbf{E}_{21}\mathbf{P}_{12}\right\} + \left\{\mathbf{P}_{22}\mathbf{Q}_{21}\mathbf{T}_{11}\mathbf{Q}_{12}\mathbf{P}_{22}\right. \\ &\quad \left. + \mathbf{P}_{22}\mathbf{Q}_{21}\mathbf{T}_{12}\mathbf{Q}_{22}\mathbf{P}_{22} + \mathbf{P}_{22}\mathbf{Q}_{22}\mathbf{T}_{21}\mathbf{Q}_{12}\mathbf{P}_{22} + \mathbf{P}_{22}\mathbf{Q}_{22}\mathbf{T}_{22}\mathbf{Q}_{22}\mathbf{P}_{22}\right. \\ &\quad \left. + \mathbf{P}_{22}\mathbf{E}_{22}\mathbf{P}_{22}\right\} \end{aligned} \tag{6.25b}$$

$$\begin{aligned} &= \left\{\frac{1}{(2\alpha-1)^2}\left[c_1^2\mathbf{T}_{21}\left(c_1^2\mathbf{I}_{\frac{N}{2}} - \alpha c_1\mathbf{H}_{\frac{N}{2}}\right) + c_1^4\mathbf{T}_{22}\right]\right\} + \left\{\frac{1}{(2\alpha-1)^2}\left[-c_1^2\mathbf{T}_{21}\left(c_1^2\mathbf{I}_{\frac{N}{2}} - \alpha c_1\mathbf{H}_{\frac{N}{2}}\right)\right.\right. \\ &\quad \left.\left. - c_1^2\left(\alpha^2 - c_1^2\right)\mathbf{T}_{22}\right]\right\} + \left\{\frac{1}{(2\alpha-1)^2}\left[-\left(c_1^2\mathbf{I}_{\frac{N}{2}} - \alpha c_1\mathbf{H}_{\frac{N}{2}}\right)\mathbf{T}_{11}\left(c_1^2\mathbf{I}_{\frac{N}{2}} - \alpha c_1\mathbf{H}_{\frac{N}{2}}\right)\right.\right. \\ &\quad \left. - c_1^2\left(c_1^2\mathbf{I}_{\frac{N}{2}} - \alpha c_1\mathbf{H}_{\frac{N}{2}}\right)\mathbf{T}_{12} - \left(\alpha^2 - c_1^2\right)\mathbf{T}_{21}\left(c_1^2\mathbf{I}_{\frac{N}{2}} - \alpha c_1\mathbf{H}_{\frac{N}{2}}\right)\right. \\ &\quad \left.\left. - c_1^2\left(\alpha^2 - c_1^2\right)\mathbf{T}_{22}\right] + \mathbf{P}_{22}\mathbf{E}_{21}\mathbf{P}_{12}\right\} \\ &\quad + \left\{\frac{1}{(2\alpha-1)^2}\left[\left(c_1^2\mathbf{I}_{\frac{N}{2}} - \alpha c_1\mathbf{H}_{\frac{N}{2}}\right)\mathbf{T}_{11}\left(c_1^2\mathbf{I}_{\frac{N}{2}} - \alpha c_1\mathbf{H}_{\frac{N}{2}}\right)\right.\right. \\ &\quad + \left(\alpha^2 - c_1^2\right)\left(c_1^2\mathbf{I}_{\frac{N}{2}} - \alpha c_1\mathbf{H}_{\frac{N}{2}}\right)\mathbf{T}_{12} + \left(\alpha^2 - c_1^2\right)\mathbf{T}_{21}\left(c_1^2\mathbf{I}_{\frac{N}{2}} - \alpha c_1\mathbf{H}_{\frac{N}{2}}\right) \\ &\quad \left.\left. + \left(\alpha^2 - c_1^2\right)^2\mathbf{T}_{22}\right] + \mathbf{P}_{22}\mathbf{E}_{22}\mathbf{P}_{22}\right\} \end{aligned} \tag{6.25c}$$

$$= \mathbf{T}_{22} + \frac{1}{2\alpha - 1}\left(c_1^2 \mathbf{I}_{\frac{N}{2}} - \alpha c_1 \mathbf{H}_{\frac{N}{2}}\right)\mathbf{T}_{12} + \mathbf{P}_{22}\mathbf{E}_{21}\mathbf{P}_{12} + \mathbf{P}_{22}\mathbf{E}_{22}\mathbf{P}_{22} \tag{6.25d}$$

Replace the sub-matrices $\hat{\mathbf{T}}_{21}^{(1)}$ and $\hat{\mathbf{T}}_{22}^{(1)}$ with $\mathbf{T}_{21}$ and $\mathbf{T}_{22}$ respectively (these are obtained from $\tilde{\mathbf{T}}_{\mathbf{F}}$) to yield the matrix $\hat{\mathbf{T}}'_{\mathbf{F};1}$, whose segments are

$$\check{\mathbf{T}}_{11}^{(1)} = \hat{\mathbf{T}}_{11}^{(1)} = g_1\mathbf{T}_{11} + V_1\left(\mathbf{P}_{12}\mathbf{E}_{21}\mathbf{P}_{11} + \mathbf{P}_{12}\mathbf{E}_{22}\mathbf{P}_{21}\right) \tag{6.26a}$$

$$\check{\mathbf{T}}_{12}^{(1)} = \hat{\mathbf{T}}_{12}^{(1)} = g_1\mathbf{T}_{12} + V_1\left(\mathbf{P}_{12}\mathbf{E}_{21}\mathbf{P}_{12} + \mathbf{P}_{12}\mathbf{E}_{22}\mathbf{P}_{22}\right) \tag{6.26b}$$

$$\check{\mathbf{T}}_{21}^{(1)} = \mathbf{T}_{21} \tag{6.26c}$$

$$\check{\mathbf{T}}_{22}^{(1)} = \mathbf{T}_{22} \tag{6.26d}$$

where

$$g_1 = \frac{-(1-\alpha)^2}{2(2\alpha - 1)} \tag{6.27a}$$

and

$$V_1 = 1 \tag{6.27b}$$

We observe that (6.26*a*) and (6.26*b*) respectively express the sub-matrices $\hat{\mathbf{T}}_{11}^{(1)}$ and $\hat{\mathbf{T}}_{12}^{(1)}$ in terms of the desired (but unknown) two-dimensional transform segments $\mathbf{T}_{11}$ and $\mathbf{T}_{12}$. If the estimation error sub-matrices $\mathbf{E}_{21}$ and $\mathbf{E}_{22}$ are null matrices (errorless estimation of the original signal segments $\mathbf{F}_{21}$ and $\mathbf{F}_{22}$), multiplying the segments $\check{\mathbf{T}}_{11}^{(1)}$ and $\check{\mathbf{T}}_{12}^{(1)}$ of $\hat{\mathbf{T}}'_{\mathbf{F};1}$ by $\frac{-2(2\alpha-1)}{(1-\alpha)^2}$ and performing the inverse two-dimensional Hadamard NPT of the resulting matrix would yield a perfectly reconstructed original transmitted signal, $\mathbf{F}$.

In the following, we further investigate the iterative reconstruction process, and derive expressions for the reconstructed segments at the m^{th} iteration.

Inverse Two-Dimensional Hadamard NPT

The inverse two-dimensional Hadamard NPT of the matrix $\hat{\mathbf{T}}'_{\mathbf{F};1}$, whose segments are given by (6.26), yields the matrix $\hat{\mathbf{F}}'_1$ whose two-dimensional segments are given by

$$\check{\mathbf{F}}_{11}^{(1)} = \mathbf{Q}_{11}\check{\mathbf{T}}_{11}^{(1)}\mathbf{Q}_{11} + \mathbf{Q}_{11}\check{\mathbf{T}}_{12}^{(1)}\mathbf{Q}_{21} + \mathbf{Q}_{12}\check{\mathbf{T}}_{21}^{(1)}\mathbf{Q}_{11} + \mathbf{Q}_{12}\check{\mathbf{T}}_{22}^{(1)}\mathbf{Q}_{21} \tag{6.28a}$$

$$= g_1\left(\mathbf{Q}_{11}\mathbf{T}_{11}\mathbf{Q}_{11} + \mathbf{Q}_{11}\mathbf{T}_{12}\mathbf{Q}_{21}\right) + \mathbf{Q}_{12}\mathbf{T}_{21}\mathbf{Q}_{11} + \mathbf{Q}_{12}\mathbf{T}_{22}\mathbf{Q}_{21}$$
$$+ V_1\left(\mathbf{Q}_{11}\mathbf{P}_{12}\mathbf{E}_{21}\mathbf{P}_{11}\mathbf{Q}_{11} + \mathbf{Q}_{11}\mathbf{P}_{12}\mathbf{E}_{22}\mathbf{P}_{21}\mathbf{Q}_{11} + \mathbf{Q}_{11}\mathbf{P}_{12}\mathbf{E}_{21}\mathbf{P}_{12}\mathbf{Q}_{21}\right.$$
$$\left. + \mathbf{Q}_{11}\mathbf{P}_{12}\mathbf{E}_{22}\mathbf{P}_{22}\mathbf{Q}_{21}\right) \tag{6.28b}$$

$$= g_1\left(\mathbf{Q}_{11}\mathbf{T}_{11}\mathbf{Q}_{11} + \mathbf{Q}_{11}\mathbf{T}_{12}\mathbf{Q}_{21}\right) + \mathbf{Q}_{12}\mathbf{T}_{21}\mathbf{Q}_{11} + \mathbf{Q}_{12}\mathbf{T}_{22}\mathbf{Q}_{21}$$
$$+ V_1\mathbf{Q}_{11}\mathbf{P}_{12}\mathbf{E}_{21} \tag{6.28c}$$

$$\check{\mathbf{F}}_{12}^{(1)} = \mathbf{Q}_{11}\check{\mathbf{T}}_{11}^{(1)}\mathbf{Q}_{12} + \mathbf{Q}_{11}\check{\mathbf{T}}_{12}^{(1)}\mathbf{Q}_{22} + \mathbf{Q}_{12}\check{\mathbf{T}}_{21}^{(1)}\mathbf{Q}_{12} + \mathbf{Q}_{12}\check{\mathbf{T}}_{22}^{(1)}\mathbf{Q}_{22} \tag{6.29a}$$

$$= g_1\left(\mathbf{Q}_{11}\mathbf{T}_{11}\mathbf{Q}_{12} + \mathbf{Q}_{11}\mathbf{T}_{12}\mathbf{Q}_{22}\right) + \mathbf{Q}_{12}\mathbf{T}_{21}\mathbf{Q}_{12} + \mathbf{Q}_{12}\mathbf{T}_{22}\mathbf{Q}_{22}$$
$$+ V_1\left(\mathbf{Q}_{11}\mathbf{P}_{12}\mathbf{E}_{21}\mathbf{P}_{11}\mathbf{Q}_{12} + \mathbf{Q}_{11}\mathbf{P}_{12}\mathbf{E}_{22}\mathbf{P}_{21}\mathbf{Q}_{12} + \mathbf{Q}_{11}\mathbf{P}_{12}\mathbf{E}_{21}\mathbf{P}_{12}\mathbf{Q}_{22}\right.$$
$$\left. + \mathbf{Q}_{11}\mathbf{P}_{12}\mathbf{E}_{22}\mathbf{P}_{22}\mathbf{Q}_{22}\right) \tag{6.29b}$$

$$= g_1\left(\mathbf{Q}_{11}\mathbf{T}_{11}\mathbf{Q}_{12} + \mathbf{Q}_{11}\mathbf{T}_{12}\mathbf{Q}_{22}\right) + \mathbf{Q}_{12}\mathbf{T}_{21}\mathbf{Q}_{12} + \mathbf{Q}_{12}\mathbf{T}_{22}\mathbf{Q}_{22}$$
$$+ V_1\mathbf{Q}_{11}\mathbf{P}_{12}\mathbf{E}_{22} \tag{6.29c}$$

$$\check{\mathbf{F}}_{21}^{(1)} = \mathbf{Q}_{21}\check{\mathbf{T}}_{11}^{(1)}\mathbf{Q}_{11} + \mathbf{Q}_{21}\check{\mathbf{T}}_{12}^{(1)}\mathbf{Q}_{21} + \mathbf{Q}_{22}\check{\mathbf{T}}_{21}^{(1)}\mathbf{Q}_{11} + \mathbf{Q}_{22}\check{\mathbf{T}}_{22}^{(1)}\mathbf{Q}_{21} \tag{6.30a}$$

$$= g_1\left(\mathbf{Q}_{21}\mathbf{T}_{11}\mathbf{Q}_{11} + \mathbf{Q}_{21}\mathbf{T}_{12}\mathbf{Q}_{21}\right) + \mathbf{Q}_{22}\mathbf{T}_{21}\mathbf{Q}_{11} + \mathbf{Q}_{22}\mathbf{T}_{22}\mathbf{Q}_{21}$$
$$+ V_1\left(\mathbf{Q}_{21}\mathbf{P}_{12}\mathbf{E}_{21}\mathbf{P}_{11}\mathbf{Q}_{11} + \mathbf{Q}_{21}\mathbf{P}_{12}\mathbf{E}_{22}\mathbf{P}_{21}\mathbf{Q}_{11} + \mathbf{Q}_{21}\mathbf{P}_{12}\mathbf{E}_{21}\mathbf{P}_{12}\mathbf{Q}_{21}\right.$$
$$\left. + \mathbf{Q}_{21}\mathbf{P}_{12}\mathbf{E}_{22}\mathbf{P}_{22}\mathbf{Q}_{21}\right) \tag{6.30b}$$

$$= g_1\left(\mathbf{Q}_{21}\mathbf{T}_{11}\mathbf{Q}_{11} + \mathbf{Q}_{21}\mathbf{T}_{12}\mathbf{Q}_{21}\right) + \mathbf{Q}_{22}\mathbf{T}_{21}\mathbf{Q}_{11} + \mathbf{Q}_{22}\mathbf{T}_{22}\mathbf{Q}_{21}$$
$$+ V_1\mathbf{Q}_{21}\mathbf{P}_{12}\mathbf{E}_{21} \tag{6.30c}$$

$$\check{\mathbf{F}}_{22}^{(1)} = \mathbf{Q}_{21}\check{\mathbf{T}}_{11}^{(1)}\mathbf{Q}_{12} + \mathbf{Q}_{21}\check{\mathbf{T}}_{12}^{(1)}\mathbf{Q}_{22} + \mathbf{Q}_{22}\check{\mathbf{T}}_{21}^{(1)}\mathbf{Q}_{12} + \mathbf{Q}_{22}\check{\mathbf{T}}_{22}^{(1)}\mathbf{Q}_{22} \tag{6.31a}$$

$$= g_1\left(\mathbf{Q}_{21}\mathbf{T}_{11}\mathbf{Q}_{12} + \mathbf{Q}_{21}\mathbf{T}_{12}\mathbf{Q}_{22}\right) + \mathbf{Q}_{22}\mathbf{T}_{21}\mathbf{Q}_{12} + \mathbf{Q}_{22}\mathbf{T}_{22}\mathbf{Q}_{22}$$
$$+ V_1\left(\mathbf{Q}_{21}\mathbf{P}_{12}\mathbf{E}_{21}\mathbf{P}_{11}\mathbf{Q}_{12} + \mathbf{Q}_{21}\mathbf{P}_{12}\mathbf{E}_{22}\mathbf{P}_{21}\mathbf{Q}_{12} + \mathbf{Q}_{21}\mathbf{P}_{12}\mathbf{E}_{21}\mathbf{P}_{12}\mathbf{Q}_{22}\right.$$
$$\left. + \mathbf{Q}_{21}\mathbf{P}_{12}\mathbf{E}_{22}\mathbf{P}_{22}\mathbf{Q}_{22}\right) \tag{6.31b}$$

$$= g_1\left(\mathbf{Q}_{21}\mathbf{T}_{11}\mathbf{Q}_{12} + \mathbf{Q}_{21}\mathbf{T}_{12}\mathbf{Q}_{22}\right) + \mathbf{Q}_{22}\mathbf{T}_{21}\mathbf{Q}_{12} + \mathbf{Q}_{22}\mathbf{T}_{22}\mathbf{Q}_{22}$$
$$+ V_1\mathbf{Q}_{21}\mathbf{P}_{12}\mathbf{E}_{22} \tag{6.31c}$$

The spatial domain iteration matrix $\hat{\mathbf{F}}_1$ is obtained by replacing the submatrices $\check{\mathbf{F}}_{21}^{(1)}$ and $\check{\mathbf{F}}_{22}^{(1)}$ in $\hat{\mathbf{F}}_1'$ with $\hat{\mathbf{F}}_{21}$ and $\hat{\mathbf{F}}_{22}$ respectively. The segments of $\hat{\mathbf{F}}_1$ are given by

$$\hat{\mathbf{F}}_{11}^{(1)} = \check{\mathbf{F}}_{11}^{(1)} = g_1\left(\mathbf{Q}_{11}\mathbf{T}_{11}\mathbf{Q}_{11} + \mathbf{Q}_{11}\mathbf{T}_{12}\mathbf{Q}_{21}\right) + \mathbf{Q}_{12}\mathbf{T}_{21}\mathbf{Q}_{11} + \mathbf{Q}_{12}\mathbf{T}_{22}\mathbf{Q}_{21}$$
$$+ V_1\mathbf{Q}_{11}\mathbf{P}_{12}\mathbf{E}_{21} \tag{6.32a}$$

$$\hat{\mathbf{F}}_{12}^{(1)} = \check{\mathbf{F}}_{12}^{(1)} = g_1\left(\mathbf{Q}_{11}\mathbf{T}_{11}\mathbf{Q}_{12} + \mathbf{Q}_{11}\mathbf{T}_{12}\mathbf{Q}_{22}\right) + \mathbf{Q}_{12}\mathbf{T}_{21}\mathbf{Q}_{12} + \mathbf{Q}_{12}\mathbf{T}_{22}\mathbf{Q}_{22}$$
$$+ V_1\mathbf{Q}_{11}\mathbf{P}_{12}\mathbf{E}_{22} \tag{6.32b}$$

$$\hat{\mathbf{F}}_{21}^{(1)} = \hat{\mathbf{F}}_{21} = \mathbf{Q}_{21}\mathbf{T}_{11}\mathbf{Q}_{11} + \mathbf{Q}_{21}\mathbf{T}_{12}\mathbf{Q}_{21} + \mathbf{Q}_{22}\mathbf{T}_{21}\mathbf{Q}_{11} + \mathbf{Q}_{22}\mathbf{T}_{22}\mathbf{Q}_{21}$$
$$+ \mathbf{E}_{21} \tag{6.32c}$$

and

$$\hat{\mathbf{F}}_{22}^{(1)} = \hat{\mathbf{F}}_{22} = \mathbf{Q}_{21}\mathbf{T}_{11}\mathbf{Q}_{12} + \mathbf{Q}_{21}\mathbf{T}_{12}\mathbf{Q}_{22} + \mathbf{Q}_{22}\mathbf{T}_{21}\mathbf{Q}_{12} + \mathbf{Q}_{22}\mathbf{T}_{22}\mathbf{Q}_{22}$$
$$+ \mathbf{E}_{22} \tag{6.32d}$$

Iteration 2

Forward Two-Dimensional Hadamard NPT

Perform the forward two-dimensional Hadamard NPT of the matrix $\hat{\mathbf{F}}_1$ whose segments are given by (6.32), to obtain the matrix $\hat{\mathbf{T}}_{\mathbf{F};2}$ whose segments are

$$\hat{\mathbf{T}}_{11}^{(2)} = \mathbf{P}_{11}\check{\mathbf{F}}_{11}^{(1)}\mathbf{P}_{11} + \mathbf{P}_{11}\check{\mathbf{F}}_{12}^{(1)}\mathbf{P}_{21} + \mathbf{P}_{12}\check{\mathbf{F}}_{21}^{(1)}\mathbf{P}_{11} + \mathbf{P}_{12}\check{\mathbf{F}}_{22}^{(1)}\mathbf{P}_{21} \tag{6.33a}$$

$$\begin{aligned}
&= \left\{g_1\mathbf{P}_{11}\mathbf{Q}_{11}\mathbf{T}_{11}\mathbf{Q}_{11}\mathbf{P}_{11} + g_1\mathbf{P}_{11}\mathbf{Q}_{11}\mathbf{T}_{12}\mathbf{Q}_{21}\mathbf{P}_{11} + \mathbf{P}_{11}\mathbf{Q}_{12}\mathbf{T}_{21}\mathbf{Q}_{11}\mathbf{P}_{11}\right. \\
&\quad \left. + \mathbf{P}_{11}\mathbf{Q}_{12}\mathbf{T}_{22}\mathbf{Q}_{21}\mathbf{P}_{11} + V_1\mathbf{P}_{11}\mathbf{Q}_{11}\mathbf{P}_{12}\mathbf{E}_{21}\mathbf{P}_{11}\right\} + \left\{g_1\mathbf{P}_{11}\mathbf{Q}_{11}\mathbf{T}_{11}\mathbf{Q}_{12}\mathbf{P}_{21}\right. \\
&\quad + g_1\mathbf{P}_{11}\mathbf{Q}_{11}\mathbf{T}_{12}\mathbf{Q}_{22}\mathbf{P}_{21} + \mathbf{P}_{11}\mathbf{Q}_{12}\mathbf{T}_{21}\mathbf{Q}_{12}\mathbf{P}_{21} + \mathbf{P}_{11}\mathbf{Q}_{12}\mathbf{T}_{22}\mathbf{Q}_{22}\mathbf{P}_{21} \\
&\quad \left. + V_1\mathbf{P}_{11}\mathbf{Q}_{11}\mathbf{P}_{12}\mathbf{E}_{22}\mathbf{P}_{21}\right\} + \left\{\mathbf{P}_{12}\mathbf{Q}_{21}\mathbf{T}_{11}\mathbf{Q}_{11}\mathbf{P}_{11} + \mathbf{P}_{12}\mathbf{Q}_{21}\mathbf{T}_{12}\mathbf{Q}_{21}\mathbf{P}_{11}\right. \\
&\quad + \mathbf{P}_{12}\mathbf{Q}_{22}\mathbf{T}_{21}\mathbf{Q}_{11}\mathbf{P}_{11} + \mathbf{P}_{12}\mathbf{Q}_{22}\mathbf{T}_{22}\mathbf{Q}_{21}\mathbf{P}_{11} + \mathbf{P}_{12}\mathbf{E}_{21}\mathbf{P}_{11}\left.\right\} \\
&\quad + \left\{\mathbf{P}_{12}\mathbf{Q}_{21}\mathbf{T}_{11}\mathbf{Q}_{12}\mathbf{P}_{21} + \mathbf{P}_{12}\mathbf{Q}_{21}\mathbf{T}_{12}\mathbf{Q}_{22}\mathbf{P}_{21} + \mathbf{P}_{12}\mathbf{Q}_{22}\mathbf{T}_{21}\mathbf{Q}_{12}\mathbf{P}_{21}\right. \\
&\quad \left. + \mathbf{P}_{12}\mathbf{Q}_{22}\mathbf{T}_{22}\mathbf{Q}_{22}\mathbf{P}_{21} + \mathbf{P}_{12}\mathbf{E}_{22}\mathbf{P}_{21}\right\}
\end{aligned} \tag{6.33b}$$

$$\begin{aligned}
&= \left\{\frac{1}{(2\alpha-1)^2}\left[g_1(\alpha^2-c_1^2)^2\mathbf{T}_{11} - g_1(\alpha^2-c_1^2)\mathbf{T}_{12}\left(c_1^2\mathbf{I}_{\frac{N}{2}} + \alpha c_1\mathbf{H}_{\frac{N}{2}}\right)\right.\right. \\
&\quad - (\alpha^2-c_1^2)\left(c_1^2\mathbf{I}_{\frac{N}{2}} + \alpha c_1\mathbf{H}_{\frac{N}{2}}\right)\mathbf{T}_{21} + \left(c_1^2\mathbf{I}_{\frac{N}{2}} + \alpha c_1\mathbf{H}_{\frac{N}{2}}\right)\mathbf{T}_{22}\left(c_1^2\mathbf{I}_{\frac{N}{2}} + \alpha c_1\mathbf{H}_{\frac{N}{2}}\right)\left.\right] \\
&\quad \left. + \frac{V_1(\alpha^2-c_1^2)}{2\alpha-1}\mathbf{P}_{12}\mathbf{E}_{21}\mathbf{P}_{11}\right\} + \left\{\frac{1}{(2\alpha-1)^2}\left[-g_1c_1^2(\alpha^2-c_1^2)\mathbf{T}_{11}\right.\right. \\
&\quad + g_1(\alpha^2-c_1^2)\mathbf{T}_{12}\left(c_1^2\mathbf{I}_{\frac{N}{2}} + \alpha c_1\mathbf{H}_{\frac{N}{2}}\right) + c_1^2\left(c_1^2\mathbf{I}_{\frac{N}{2}} + \alpha c_1\mathbf{H}_{\frac{N}{2}}\right)\mathbf{T}_{21} \\
&\quad \left.\left. - \left(c_1^2\mathbf{I}_{\frac{N}{2}} + \alpha c_1\mathbf{H}_{\frac{N}{2}}\right)\mathbf{T}_{22}\left(c_1^2\mathbf{I}_{\frac{N}{2}} + \alpha c_1\mathbf{H}_{\frac{N}{2}}\right)\right] + \frac{V_1(\alpha^2-c_1^2)}{2\alpha-1}\mathbf{P}_{12}\mathbf{E}_{22}\mathbf{P}_{21}\right\} \\
&\quad + \left\{\frac{1}{(2\alpha-1)^2}\left[-c_1^2(\alpha^2-c_1^2)\mathbf{T}_{11} + c_1^2\mathbf{T}_{12}\left(c_1^2\mathbf{I}_{\frac{N}{2}} + \alpha c_1\mathbf{H}_{\frac{N}{2}}\right)\right.\right. \\
&\quad + (\alpha^2-c_1^2)\left(c_1^2\mathbf{I}_{\frac{N}{2}} + \alpha c_1\mathbf{H}_{\frac{N}{2}}\right)\mathbf{T}_{21} - \left(c_1^2\mathbf{I}_{\frac{N}{2}} + \alpha c_1\mathbf{H}_{\frac{N}{2}}\right)\mathbf{T}_{22}\left(c_1^2\mathbf{I}_{\frac{N}{2}} + \alpha c_1\mathbf{H}_{\frac{N}{2}}\right)\left.\right] \\
&\quad \left. + \mathbf{P}_{12}\mathbf{E}_{21}\mathbf{P}_{11}\right\} + \left\{\frac{1}{(2\alpha-1)^2}\left[c_1^4\mathbf{T}_{11} - c_1^2\mathbf{T}_{12}\left(c_1^2\mathbf{I}_{\frac{N}{2}} + \alpha c_1\mathbf{H}_{\frac{N}{2}}\right)\right.\right. \\
&\quad - c_1^2\left(c_1^2\mathbf{I}_{\frac{N}{2}} + \alpha c_1\mathbf{H}_{\frac{N}{2}}\right)\mathbf{T}_{21} + \left(c_1^2\mathbf{I}_{\frac{N}{2}} + \alpha c_1\mathbf{H}_{\frac{N}{2}}\right)\mathbf{T}_{22}\left(c_1^2\mathbf{I}_{\frac{N}{2}} + \alpha c_1\mathbf{H}_{\frac{N}{2}}\right)\left.\right] \\
&\quad \left. + \mathbf{P}_{12}\mathbf{E}_{22}\mathbf{P}_{21}\right\}
\end{aligned} \tag{6.33c}$$

$$\begin{aligned}
&= \frac{1}{2\alpha-1}\left(g_1(\alpha^2-c_1^2) - c_1^2\right)\mathbf{T}_{11} + \frac{1}{2\alpha-1}\left(V_1(\alpha^2-c_1^2) + 2\alpha - 1\right)\left\{\mathbf{P}_{12}\mathbf{E}_{21}\mathbf{P}_{11}\right. \\
&\quad \left. + \mathbf{P}_{12}\mathbf{E}_{22}\mathbf{P}_{21}\right\}
\end{aligned} \tag{6.33d}$$

$$\hat{\mathbf{T}}_{12}^{(2)} = \mathbf{P}_{11}\check{\mathbf{F}}_{11}^{(1)}\mathbf{P}_{12} + \mathbf{P}_{11}\check{\mathbf{F}}_{12}^{(1)}\mathbf{P}_{22} + \mathbf{P}_{12}\check{\mathbf{F}}_{21}^{(1)}\mathbf{P}_{12} + \mathbf{P}_{12}\check{\mathbf{F}}_{22}^{(1)}\mathbf{P}_{22} \tag{6.34a}$$

$$\begin{aligned}
&= \left\{g_1\mathbf{P}_{11}\mathbf{Q}_{11}\mathbf{T}_{11}\mathbf{Q}_{11}\mathbf{P}_{12} + g_1\mathbf{P}_{11}\mathbf{Q}_{11}\mathbf{T}_{12}\mathbf{Q}_{21}\mathbf{P}_{12} + \mathbf{P}_{11}\mathbf{Q}_{12}\mathbf{T}_{21}\mathbf{Q}_{11}\mathbf{P}_{12}\right. \\
&\quad \left. + \mathbf{P}_{11}\mathbf{Q}_{12}\mathbf{T}_{22}\mathbf{Q}_{21}\mathbf{P}_{12} + V_1\mathbf{P}_{11}\mathbf{Q}_{11}\mathbf{P}_{12}\mathbf{E}_{21}\mathbf{P}_{12}\right\} + \left\{g_1\mathbf{P}_{11}\mathbf{Q}_{11}\mathbf{T}_{11}\mathbf{Q}_{12}\mathbf{P}_{22}\right. \\
&\quad + g_1\mathbf{P}_{11}\mathbf{Q}_{11}\mathbf{T}_{12}\mathbf{Q}_{22}\mathbf{P}_{22} + \mathbf{P}_{11}\mathbf{Q}_{12}\mathbf{T}_{21}\mathbf{Q}_{12}\mathbf{P}_{22} + \mathbf{P}_{11}\mathbf{Q}_{12}\mathbf{T}_{22}\mathbf{Q}_{22}\mathbf{P}_{22} \\
&\quad \left. + V_1\mathbf{P}_{11}\mathbf{Q}_{11}\mathbf{P}_{12}\mathbf{E}_{22}\mathbf{P}_{22}\right\} + \left\{\mathbf{P}_{12}\mathbf{Q}_{21}\mathbf{T}_{11}\mathbf{Q}_{11}\mathbf{P}_{12} + \mathbf{P}_{12}\mathbf{Q}_{21}\mathbf{T}_{12}\mathbf{Q}_{21}\mathbf{P}_{12}\right. \\
&\quad \left. + \mathbf{P}_{12}\mathbf{Q}_{22}\mathbf{T}_{21}\mathbf{Q}_{11}\mathbf{P}_{12} + \mathbf{P}_{12}\mathbf{Q}_{22}\mathbf{T}_{22}\mathbf{Q}_{21}\mathbf{P}_{12} + \mathbf{P}_{12}\mathbf{E}_{21}\mathbf{P}_{12}\right\} \\
&\quad + \left\{\mathbf{P}_{12}\mathbf{Q}_{21}\mathbf{T}_{11}\mathbf{Q}_{12}\mathbf{P}_{22} + \mathbf{P}_{12}\mathbf{Q}_{21}\mathbf{T}_{12}\mathbf{Q}_{22}\mathbf{P}_{22} + \mathbf{P}_{12}\mathbf{Q}_{22}\mathbf{T}_{21}\mathbf{Q}_{12}\mathbf{P}_{22}\right. \\
&\quad \left. + \mathbf{P}_{12}\mathbf{Q}_{22}\mathbf{T}_{22}\mathbf{Q}_{22}\mathbf{P}_{22} + \mathbf{P}_{12}\mathbf{E}_{22}\mathbf{P}_{22}\right\}
\end{aligned} \tag{6.34b}$$

$$\begin{aligned}
&= \left\{\frac{1}{(2\alpha-1)^2}\left[-g_1\left(\alpha^2-c_1^2\right)\mathbf{T}_{11}\left(c_1^2\mathbf{I}_{\frac{N}{2}} - \alpha c_1\mathbf{H}_{\frac{N}{2}}\right) - g_1c_1^2\left(\alpha^2-c_1^2\right)\mathbf{T}_{12}\right.\right. \\
&\quad \left.\left. + \left(c_1^2\mathbf{I}_{\frac{N}{2}} + \alpha c_1\mathbf{H}_{\frac{N}{2}}\right)\mathbf{T}_{21}\left(c_1^2\mathbf{I}_{\frac{N}{2}} - \alpha c_1\mathbf{H}_{\frac{N}{2}}\right) + c_1^2\left(c_1^2\mathbf{I}_{\frac{N}{2}} + \alpha c_1\mathbf{H}_{\frac{N}{2}}\right)\mathbf{T}_{22}\right]\right. \\
&\quad \left. + \frac{V_1\left(\alpha^2-c_1^2\right)}{2\alpha-1}\mathbf{P}_{12}\mathbf{E}_{21}\mathbf{P}_{12}\right\} + \left\{\frac{1}{(2\alpha-1)^2}\left[g_1\left(\alpha^2-c_1^2\right)\mathbf{T}_{11}\left(c_1^2\mathbf{I}_{\frac{N}{2}} - \alpha c_1\mathbf{H}_{\frac{N}{2}}\right)\right.\right. \\
&\quad + g_1\left(\alpha^2-c_1^2\right)^2\mathbf{T}_{12} - \left(c_1^2\mathbf{I}_{\frac{N}{2}} + \alpha c_1\mathbf{H}_{\frac{N}{2}}\right)\mathbf{T}_{21}\left(c_1^2\mathbf{I}_{\frac{N}{2}} - \alpha c_1\mathbf{H}_{\frac{N}{2}}\right) \\
&\quad \left.\left. - \left(\alpha^2-c_1^2\right)\left(c_1^2\mathbf{I}_{\frac{N}{2}} + \alpha c_1\mathbf{H}_{\frac{N}{2}}\right)\mathbf{T}_{22}\right] + \frac{V_1\left(\alpha^2-c_1^2\right)}{2\alpha-1}\mathbf{P}_{12}\mathbf{E}_{22}\mathbf{P}_{22}\right\} \\
&\quad + \left\{\frac{1}{(2\alpha-1)^2}\left[c_1^2\mathbf{T}_{11}\left(c_1^2\mathbf{I}_{\frac{N}{2}} - \alpha c_1\mathbf{H}_{\frac{N}{2}}\right) + c_1^4\mathbf{T}_{12} - \left(c_1^2\mathbf{I}_{\frac{N}{2}} + \alpha c_1\mathbf{H}_{\frac{N}{2}}\right)\mathbf{T}_{21}\left(c_1^2\mathbf{I}_{\frac{N}{2}} - \alpha c_1\mathbf{H}_{\frac{N}{2}}\right)\right.\right. \\
&\quad \left.\left. - c_1^2\left(c_1^2\mathbf{I}_{\frac{N}{2}} + \alpha c_1\mathbf{H}_{\frac{N}{2}}\right)\mathbf{T}_{22}\right] + \mathbf{P}_{12}\mathbf{E}_{21}\mathbf{P}_{12}\right\} + \left\{\frac{1}{(2\alpha-1)^2}\left[-c_1^2\mathbf{T}_{11}\left(c_1^2\mathbf{I}_{\frac{N}{2}} - \alpha c_1\mathbf{H}_{\frac{N}{2}}\right)\right.\right. \\
&\quad - c_1^2\left(\alpha^2-c_1^2\right)\mathbf{T}_{12} + \left(c_1^2\mathbf{I}_{\frac{N}{2}} + \alpha c_1\mathbf{H}_{\frac{N}{2}}\right)\mathbf{T}_{21}\left(c_1^2\mathbf{I}_{\frac{N}{2}} - \alpha c_1\mathbf{H}_{\frac{N}{2}}\right) \\
&\quad \left.\left. + \left(\alpha^2-c_1^2\right)\left(c_1^2\mathbf{I}_{\frac{N}{2}} + \alpha c_1\mathbf{H}_{\frac{N}{2}}\right)\mathbf{T}_{22}\right] + \mathbf{P}_{12}\mathbf{E}_{22}\mathbf{P}_{22}\right\}
\end{aligned} \tag{6.34c}$$

$$\begin{aligned}
&= \frac{1}{2\alpha-1}\left(g_1\left(\alpha^2-c_1^2\right)-c_1^2\right)\mathbf{T}_{12} + \frac{1}{2\alpha-1}\left(V_1\left(\alpha^2-c_1^2\right)+2\alpha-1\right)\left\{\mathbf{P}_{12}\mathbf{E}_{21}\mathbf{P}_{12}\right. \\
&\quad \left. + \mathbf{P}_{12}\mathbf{E}_{22}\mathbf{P}_{22}\right\}
\end{aligned} \tag{6.34d}$$

$$\hat{\mathbf{T}}_{21}^{(2)} = \mathbf{P}_{21}\check{\mathbf{F}}_{11}^{(1)}\mathbf{P}_{11} + \mathbf{P}_{21}\check{\mathbf{F}}_{12}^{(1)}\mathbf{P}_{21} + \mathbf{P}_{22}\check{\mathbf{F}}_{21}^{(1)}\mathbf{P}_{11} + \mathbf{P}_{22}\check{\mathbf{F}}_{22}^{(1)}\mathbf{P}_{21} \tag{6.35a}$$

$$\begin{aligned}
&= \left\{g_1\mathbf{P}_{21}\mathbf{Q}_{11}\mathbf{T}_{11}\mathbf{Q}_{11}\mathbf{P}_{11} + g_1\mathbf{P}_{21}\mathbf{Q}_{11}\mathbf{T}_{12}\mathbf{Q}_{21}\mathbf{P}_{11} + \mathbf{P}_{21}\mathbf{Q}_{12}\mathbf{T}_{21}\mathbf{Q}_{11}\mathbf{P}_{11}\right. \\
&\quad \left. + \mathbf{P}_{21}\mathbf{Q}_{12}\mathbf{T}_{22}\mathbf{Q}_{21}\mathbf{P}_{11} + V_1\mathbf{P}_{21}\mathbf{Q}_{11}\mathbf{P}_{12}\mathbf{E}_{21}\mathbf{P}_{11}\right\} + \left\{g_1\mathbf{P}_{21}\mathbf{Q}_{11}\mathbf{T}_{11}\mathbf{Q}_{12}\mathbf{P}_{21}\right. \\
&\quad \left. + g_1\mathbf{P}_{21}\mathbf{Q}_{11}\mathbf{T}_{12}\mathbf{Q}_{22}\mathbf{P}_{21} + \mathbf{P}_{21}\mathbf{Q}_{12}\mathbf{T}_{21}\mathbf{Q}_{12}\mathbf{P}_{21} + \mathbf{P}_{21}\mathbf{Q}_{12}\mathbf{T}_{22}\mathbf{Q}_{22}\mathbf{P}_{21}\right.
\end{aligned}$$

$$+ V_1\mathbf{P}_{21}\mathbf{Q}_{11}\mathbf{P}_{12}\mathbf{E}_{22}\mathbf{P}_{21}\Big\} + \Big\{\mathbf{P}_{22}\mathbf{Q}_{21}\mathbf{T}_{11}\mathbf{Q}_{11}\mathbf{P}_{11} + \mathbf{P}_{22}\mathbf{Q}_{21}\mathbf{T}_{12}\mathbf{Q}_{21}\mathbf{P}_{11}$$
$$+ \mathbf{P}_{22}\mathbf{Q}_{22}\mathbf{T}_{21}\mathbf{Q}_{11}\mathbf{P}_{11} + \mathbf{P}_{22}\mathbf{Q}_{22}\mathbf{T}_{22}\mathbf{Q}_{21}\mathbf{P}_{11} + \mathbf{P}_{22}\mathbf{E}_{21}\mathbf{P}_{11}\Big\}$$
$$+ \Big\{\mathbf{P}_{22}\mathbf{Q}_{21}\mathbf{T}_{11}\mathbf{Q}_{12}\mathbf{P}_{21} + \mathbf{P}_{22}\mathbf{Q}_{21}\mathbf{T}_{12}\mathbf{Q}_{22}\mathbf{P}_{21} + \mathbf{P}_{22}\mathbf{Q}_{22}\mathbf{T}_{21}\mathbf{Q}_{12}\mathbf{P}_{21}$$
$$+ \mathbf{P}_{22}\mathbf{Q}_{22}\mathbf{T}_{22}\mathbf{Q}_{22}\mathbf{P}_{21} + \mathbf{P}_{22}\mathbf{E}_{22}\mathbf{P}_{21}\Big\} \tag{6.35b}$$

$$= \Bigg\{\frac{1}{(2\alpha-1)^2}\Big[-g_1\left(\alpha^2-c_1^2\right)\left(c_1^2\mathbf{I}_{\frac{N}{2}} - \alpha c_1\mathbf{H}_{\frac{N}{2}}\right)\mathbf{T}_{11}$$
$$+ g_1\left(c_1^2\mathbf{I}_{\frac{N}{2}} - \alpha c_1\mathbf{H}_{\frac{N}{2}}\right)\mathbf{T}_{12}\left(c_1^2\mathbf{I}_{\frac{N}{2}} + \alpha c_1\mathbf{H}_{\frac{N}{2}}\right)$$
$$- c_1^2\left(\alpha^2-c_1^2\right)\mathbf{T}_{21} + c_1^2\mathbf{T}_{22}\left(c_1^2\mathbf{I}_{\frac{N}{2}} + \alpha c_1\mathbf{H}_{\frac{N}{2}}\right)\Big] - \frac{V_1}{2\alpha-1}c_1\mathbf{H}_{\frac{N}{2}}\left(c_1^2\mathbf{I}_{\frac{N}{2}} - \alpha c_1\mathbf{H}_{\frac{N}{2}}\right)\mathbf{E}_{21}\mathbf{P}_{11}\Bigg\}$$
$$+ \Bigg\{\frac{1}{(2\alpha-1)^2}\Big[g_1c_1^2\left(c_1^2\mathbf{I}_{\frac{N}{2}} - \alpha c_1\mathbf{H}_{\frac{N}{2}}\right)\mathbf{T}_{11} - g_1\left(c_1^2\mathbf{I}_{\frac{N}{2}} - \alpha c_1\mathbf{H}_{\frac{N}{2}}\right)\mathbf{T}_{12}\left(c_1^2\mathbf{I}_{\frac{N}{2}} + \alpha c_1\mathbf{H}_{\frac{N}{2}}\right)$$
$$+ c_1^4\mathbf{T}_{21} - c_1^2\mathbf{T}_{22}\left(c_1^2\mathbf{I}_{\frac{N}{2}} + \alpha c_1\mathbf{H}_{\frac{N}{2}}\right)\Big] - \frac{V_1}{2\alpha-1}c_1\mathbf{H}_{\frac{N}{2}}\left(c_1^2\mathbf{I}_{\frac{N}{2}} - \alpha c_1\mathbf{H}_{\frac{N}{2}}\right)\mathbf{E}_{22}\mathbf{P}_{21}\Bigg\}$$
$$+ \Bigg\{\frac{1}{(2\alpha-1)^2}\Big[\left(\alpha^2-c_1^2\right)\left(c_1^2\mathbf{I}_{\frac{N}{2}} - \alpha c_1\mathbf{H}_{\frac{N}{2}}\right)\mathbf{T}_{11} - \left(c_1^2\mathbf{I}_{\frac{N}{2}} - \alpha c_1\mathbf{H}_{\frac{N}{2}}\right)\mathbf{T}_{12}\left(c_1^2\mathbf{I}_{\frac{N}{2}} + \alpha c_1\mathbf{H}_{\frac{N}{2}}\right)$$
$$+ \left(\alpha^2-c_1^2\right)^2\mathbf{T}_{21} - \left(\alpha^2-c_1^2\right)\mathbf{T}_{22}\left(c_1^2\mathbf{I}_{\frac{N}{2}} + \alpha c_1\mathbf{H}_{\frac{N}{2}}\right)\Big] + \mathbf{P}_{22}\mathbf{E}_{21}\mathbf{P}_{11}\Bigg\}$$
$$+ \Bigg\{\frac{1}{(2\alpha-1)^2}\Big[-c_1^2\left(c_1^2\mathbf{I}_{\frac{N}{2}} - \alpha c_1\mathbf{H}_{\frac{N}{2}}\right)\mathbf{T}_{11} + \left(c_1^2\mathbf{I}_{\frac{N}{2}} - \alpha c_1\mathbf{H}_{\frac{N}{2}}\right)\mathbf{T}_{12}\left(c_1^2\mathbf{I}_{\frac{N}{2}} + \alpha c_1\mathbf{H}_{\frac{N}{2}}\right)$$
$$- c_1^2\left(\alpha^2-c_1^2\right)\mathbf{T}_{21} + \left(\alpha^2-c_1^2\right)\mathbf{T}_{22}\left(c_1^2\mathbf{I}_{\frac{N}{2}} + \alpha c_1\mathbf{H}_{\frac{N}{2}}\right)\Big]$$
$$+ \mathbf{P}_{22}\mathbf{E}_{22}\mathbf{P}_{21}\Bigg\} \tag{6.35c}$$

$$= \mathbf{T}_{21} + \frac{1}{2\alpha-1}\Big\{(1-g_1)\left(c_1^2\mathbf{I}_{\frac{N}{2}} - \alpha c_1\mathbf{H}_{\frac{N}{2}}\right)\mathbf{T}_{11}$$
$$+ \left(V_1c_1^2 + 2\alpha - 1\right)\left(\alpha\mathbf{I}_{\frac{N}{2}} - c_1\mathbf{H}_{\frac{N}{2}}\right)\left(\mathbf{E}_{21}\mathbf{P}_{11} + \mathbf{E}_{22}\mathbf{P}_{21}\right)\Big\} \tag{6.35d}$$

and

$$\hat{\mathbf{T}}_{22}^{(2)} = \mathbf{P}_{21}\check{\mathbf{F}}_{11}^{(1)}\mathbf{P}_{12} + \mathbf{P}_{21}\check{\mathbf{F}}_{12}^{(1)}\mathbf{P}_{22} + \mathbf{P}_{22}\check{\mathbf{F}}_{21}^{(1)}\mathbf{P}_{12} + \mathbf{P}_{22}\check{\mathbf{F}}_{22}^{(1)}\mathbf{P}_{22} \tag{6.36a}$$
$$= \Big\{g_1\mathbf{P}_{21}\mathbf{Q}_{11}\mathbf{T}_{11}\mathbf{Q}_{11}\mathbf{P}_{12} + g_1\mathbf{P}_{21}\mathbf{Q}_{11}\mathbf{T}_{12}\mathbf{Q}_{21}\mathbf{P}_{12} + \mathbf{P}_{21}\mathbf{Q}_{12}\mathbf{T}_{21}\mathbf{Q}_{11}\mathbf{P}_{12}$$
$$+ \mathbf{P}_{21}\mathbf{Q}_{12}\mathbf{T}_{22}\mathbf{Q}_{21}\mathbf{P}_{12} + V_1\mathbf{P}_{21}\mathbf{Q}_{11}\mathbf{P}_{12}\mathbf{E}_{21}\mathbf{P}_{12}\Big\} + \Big\{g_1\mathbf{P}_{21}\mathbf{Q}_{11}\mathbf{T}_{11}\mathbf{Q}_{12}\mathbf{P}_{22}$$
$$+ g_1\mathbf{P}_{21}\mathbf{Q}_{11}\mathbf{T}_{12}\mathbf{Q}_{22}\mathbf{P}_{22} + \mathbf{P}_{21}\mathbf{Q}_{12}\mathbf{T}_{21}\mathbf{Q}_{12}\mathbf{P}_{22} + \mathbf{P}_{21}\mathbf{Q}_{12}\mathbf{T}_{22}\mathbf{Q}_{22}\mathbf{P}_{22}$$
$$+ V_1\mathbf{P}_{21}\mathbf{Q}_{11}\mathbf{P}_{12}\mathbf{E}_{22}\mathbf{P}_{22}\Big\} + \Big\{\mathbf{P}_{22}\mathbf{Q}_{21}\mathbf{T}_{11}\mathbf{Q}_{11}\mathbf{P}_{12} + \mathbf{P}_{22}\mathbf{Q}_{21}\mathbf{T}_{12}\mathbf{Q}_{21}\mathbf{P}_{12}$$
$$+ \mathbf{P}_{22}\mathbf{Q}_{22}\mathbf{T}_{21}\mathbf{Q}_{11}\mathbf{P}_{12} + \mathbf{P}_{22}\mathbf{Q}_{22}\mathbf{T}_{22}\mathbf{Q}_{21}\mathbf{P}_{12} + \mathbf{P}_{22}\mathbf{E}_{21}\mathbf{P}_{12}\Big\}$$
$$+ \Big\{\mathbf{P}_{22}\mathbf{Q}_{21}\mathbf{T}_{11}\mathbf{Q}_{12}\mathbf{P}_{22} + \mathbf{P}_{22}\mathbf{Q}_{21}\mathbf{T}_{12}\mathbf{Q}_{22}\mathbf{P}_{22} + \mathbf{P}_{22}\mathbf{Q}_{22}\mathbf{T}_{21}\mathbf{Q}_{12}\mathbf{P}_{22}$$

$$+ \mathbf{P}_{22}\mathbf{Q}_{22}\mathbf{T}_{22}\mathbf{Q}_{22}\mathbf{P}_{22} + \mathbf{P}_{22}\mathbf{E}_{22}\mathbf{P}_{22}\Big\} \tag{6.36b}$$

$$\begin{aligned}
&= \Bigg\{\frac{1}{(2\alpha-1)^2}\Big[g_1\left(c_1^2\mathbf{I}_{\frac{N}{2}} - \alpha c_1\mathbf{H}_{\frac{N}{2}}\right)\mathbf{T}_{11}\left(c_1^2\mathbf{I}_{\frac{N}{2}} - \alpha c_1\mathbf{H}_{\frac{N}{2}}\right) + g_1c_1^2\left(c_1^2\mathbf{I}_{\frac{N}{2}} - \alpha c_1\mathbf{H}_{\frac{N}{2}}\right)\mathbf{T}_{12} \\
&+ c_1^2\mathbf{T}_{21}\left(c_1^2\mathbf{I}_{\frac{N}{2}} - \alpha c_1\mathbf{H}_{\frac{N}{2}}\right) + c_1^4\mathbf{T}_{22}\Big] - \frac{V_1}{2\alpha-1}c_1\mathbf{H}_{\frac{N}{2}}\left(c_1^2\mathbf{I}_{\frac{N}{2}} - \alpha c_1\mathbf{H}_{\frac{N}{2}}\right)\mathbf{E}_{21}\mathbf{P}_{12}\Bigg\} \\
&+ \Bigg\{\frac{1}{(2\alpha-1)^2}\Big[-g_1\left(c_1^2\mathbf{I}_{\frac{N}{2}} - \alpha c_1\mathbf{H}_{\frac{N}{2}}\right)\mathbf{T}_{11}\left(c_1^2\mathbf{I}_{\frac{N}{2}} - \alpha c_1\mathbf{H}_{\frac{N}{2}}\right) \\
&- g_1\left(\alpha^2 - c_1^2\right)\left(c_1^2\mathbf{I}_{\frac{N}{2}} - \alpha c_1\mathbf{H}_{\frac{N}{2}}\right)\mathbf{T}_{12} \\
&- c_1^2\mathbf{T}_{21}\left(c_1^2\mathbf{I}_{\frac{N}{2}} - \alpha c_1\mathbf{H}_{\frac{N}{2}}\right) - c_1^2\left(\alpha^2 - c_1^2\right)\mathbf{T}_{22}\Big] - \frac{V_1}{2\alpha-1}c_1\mathbf{H}_{\frac{N}{2}}\left(c_1^2\mathbf{I}_{\frac{N}{2}} - \alpha c_1\mathbf{H}_{\frac{N}{2}}\right)\mathbf{E}_{22}\mathbf{P}_{22}\Bigg\} \\
&+ \Bigg\{\frac{1}{(2\alpha-1)^2}\Big[-\left(c_1^2\mathbf{I}_{\frac{N}{2}} - \alpha c_1\mathbf{H}_{\frac{N}{2}}\right)\mathbf{T}_{11}\left(c_1^2\mathbf{I}_{\frac{N}{2}} - \alpha c_1\mathbf{H}_{\frac{N}{2}}\right) - c_1^2\left(c_1^2\mathbf{I}_{\frac{N}{2}} - \alpha c_1\mathbf{H}_{\frac{N}{2}}\right)\mathbf{T}_{12} \\
&- \left(\alpha^2 - c_1^2\right)\mathbf{T}_{21}\left(c_1^2\mathbf{I}_{\frac{N}{2}} - \alpha c_1\mathbf{H}_{\frac{N}{2}}\right) - c_1^2\left(\alpha^2 - c_1^2\right)\mathbf{T}_{22}\Big] + \mathbf{P}_{22}\mathbf{E}_{21}\mathbf{P}_{12}\Bigg\} \\
&+ \Bigg\{\frac{1}{(2\alpha-1)^2}\Big[\left(c_1^2\mathbf{I}_{\frac{N}{2}} - \alpha c_1\mathbf{H}_{\frac{N}{2}}\right)\mathbf{T}_{11}\left(c_1^2\mathbf{I}_{\frac{N}{2}} - \alpha c_1\mathbf{H}_{\frac{N}{2}}\right) + \left(\alpha^2 - c_1^2\right)\left(c_1^2\mathbf{I}_{\frac{N}{2}} - \alpha c_1\mathbf{H}_{\frac{N}{2}}\right)\mathbf{T}_{12} \\
&+ \left(\alpha^2 - c_1^2\right)\mathbf{T}_{21}\left(c_1^2\mathbf{I}_{\frac{N}{2}} - \alpha c_1\mathbf{H}_{\frac{N}{2}}\right) + \left(\alpha^2 - c_1^2\right)^2\mathbf{T}_{22}\Big] + \mathbf{P}_{22}\mathbf{E}_{22}\mathbf{P}_{22}\Bigg\}
\end{aligned} \tag{6.36c}$$

$$\begin{aligned}
&= \mathbf{T}_{22} + \frac{1}{2\alpha-1}\Big\{(1-g_1)\left(c_1^2\mathbf{I}_{\frac{N}{2}} - \alpha c_1\mathbf{H}_{\frac{N}{2}}\right)\mathbf{T}_{12} \\
&+ \left(V_1c_1^2 + 2\alpha - 1\right)\left(\alpha\mathbf{I}_{\frac{N}{2}} - c_1\mathbf{H}_{\frac{N}{2}}\right)\left(\mathbf{E}_{21}\mathbf{P}_{12} + \mathbf{E}_{22}\mathbf{P}_{22}\right)\Big\}
\end{aligned} \tag{6.36d}$$

We replace the sub-matrices $\hat{\mathbf{T}}_{21}^{(2)}$ and $\hat{\mathbf{T}}_{22}^{(2)}$ in $\hat{\mathbf{T}}_{\mathbf{F};2}$ with $\mathbf{T}_{21}$ and $\mathbf{T}_{22}$ respectively (obtained from $\tilde{\mathbf{T}}_{\mathbf{F}}$) to yield the matrix $\hat{\mathbf{T}}'_{\mathbf{F};2}$ whose segments are

$$\check{\mathbf{T}}_{11}^{(2)} = \hat{\mathbf{T}}_{11}^{(12)} = g_2\mathbf{T}_{11} + V_2\left(\mathbf{P}_{12}\mathbf{E}_{21}\mathbf{P}_{11} + \mathbf{P}_{12}\mathbf{E}_{22}\mathbf{P}_{21}\right) \tag{6.37a}$$

$$\check{\mathbf{T}}_{12}^{(2)} = \hat{\mathbf{T}}_{12}^{(2)} = g_2\mathbf{T}_{12} + V_2\left(\mathbf{P}_{12}\mathbf{E}_{21}\mathbf{P}_{12} + \mathbf{P}_{12}\mathbf{E}_{22}\mathbf{P}_{22}\right) \tag{6.37b}$$

$$\check{\mathbf{T}}_{21}^{(2)} = \mathbf{T}_{21} \tag{6.37c}$$

$$\check{\mathbf{T}}_{22}^{(2)} = \mathbf{T}_{22} \tag{6.37d}$$

where

$$g_2 = \frac{1}{2\alpha-1}\left(g_1\left(\alpha^2 - c_1^2\right) - c_1^2\right) \tag{6.38a}$$

and

$$V_2 = \frac{1}{2\alpha-1}\left(V_1\left(\alpha^2 - c_1^2\right) + 2\alpha - 1\right) \tag{6.38b}$$

; g_1 and V_1 are already defined in (6.27a) and (6.27b) respectively.

Inverse Two-Dimensional Hadamard NPT

By comparing (6.37) with (6.26), it is clear that performing the inverse two-dimensional Hadamard NPT of the matrix $\hat{\mathbf{T}}'_{\mathbf{F};2}$ whose segments are given by (6.37) would yield a matrix $\hat{\mathbf{F}}'_2$, whose segments can be obtained by replacing g_1 and V_1 in (6.28*c*), (6.29*c*), (6.30*c*) and (6.31*c*), with g_2 and V_2 respectively. Replacement of $\check{\mathbf{F}}^{(2)}_{21}$ and $\check{\mathbf{F}}^{(2)}_{22}$ in $\hat{\mathbf{F}}'_2$ with $\hat{\mathbf{F}}_{21}$ and $\hat{\mathbf{F}}_{22}$ respectively (obtained from $\hat{\mathbf{F}}^W$) yields the iteration matrix $\hat{\mathbf{F}}_2$, whose segments are given by

$$\hat{\mathbf{F}}^{(2)}_{11} = \check{\mathbf{F}}^{(2)}_{11} = g_2\left(\mathbf{Q}_{11}\mathbf{T}_{11}\mathbf{Q}_{11} + \mathbf{Q}_{11}\mathbf{T}_{12}\mathbf{Q}_{21}\right) + \mathbf{Q}_{12}\mathbf{T}_{21}\mathbf{Q}_{11} + \mathbf{Q}_{12}\mathbf{T}_{22}\mathbf{Q}_{21} + V_2\mathbf{Q}_{11}\mathbf{P}_{12}\mathbf{E}_{21} \tag{6.39a}$$

$$\hat{\mathbf{F}}^{(2)}_{12} = \check{\mathbf{F}}^{(2)}_{12} = g_2\left(\mathbf{Q}_{11}\mathbf{T}_{11}\mathbf{Q}_{12} + \mathbf{Q}_{11}\mathbf{T}_{12}\mathbf{Q}_{22}\right) + \mathbf{Q}_{12}\mathbf{T}_{21}\mathbf{Q}_{12} + \mathbf{Q}_{12}\mathbf{T}_{22}\mathbf{Q}_{22} + V_2\mathbf{Q}_{11}\mathbf{P}_{12}\mathbf{E}_{22} \tag{6.39b}$$

$$\hat{\mathbf{F}}^{(2)}_{21} = \hat{\mathbf{F}}_{21} = \mathbf{Q}_{21}\mathbf{T}_{11}\mathbf{Q}_{11} + \mathbf{Q}_{21}\mathbf{T}_{12}\mathbf{Q}_{21} + \mathbf{Q}_{22}\mathbf{T}_{21}\mathbf{Q}_{11} + \mathbf{Q}_{22}\mathbf{T}_{22}\mathbf{Q}_{21} + \mathbf{E}_{21} \tag{6.39c}$$

and

$$\hat{\mathbf{F}}^{(2)}_{22} = \hat{\mathbf{F}}_{22} = \mathbf{Q}_{21}\mathbf{T}_{11}\mathbf{Q}_{12} + \mathbf{Q}_{21}\mathbf{T}_{12}\mathbf{Q}_{22} + \mathbf{Q}_{22}\mathbf{T}_{21}\mathbf{Q}_{12} + \mathbf{Q}_{22}\mathbf{T}_{22}\mathbf{Q}_{22} + \mathbf{E}_{22} \tag{6.39d}$$

Iteration m

We can infer, based on the results of the previous two iterations, that by continuing the iterative two-dimensional Hadamard NPT reconstruction process to the m^{th} $(m \geq 1)$ iteration stage, the segments of the iteration matrix $\hat{\mathbf{T}}_{\mathbf{F};m}$ that is obtained are given by

$$\hat{\mathbf{T}}^{(m)}_{11} = g_m\mathbf{T}_{11} + V_m\left(\mathbf{P}_{12}\mathbf{E}_{21}\mathbf{P}_{11} + \mathbf{P}_{12}\mathbf{E}_{22}\mathbf{P}_{21}\right) \tag{6.40a}$$

$$\hat{\mathbf{T}}^{(m)}_{12} = g_m\mathbf{T}_{12} + V_m\left(\mathbf{P}_{12}\mathbf{E}_{21}\mathbf{P}_{12} + \mathbf{P}_{12}\mathbf{E}_{22}\mathbf{P}_{22}\right) \tag{6.40b}$$

$$\hat{\mathbf{T}}^{(m)}_{21} = \mathbf{T}_{21} + \frac{1}{2\alpha - 1}\Big\{\left(1 - g_{m-1}\right)\left(c_1^2\mathbf{I}_{\frac{N}{2}} - \alpha c_1\mathbf{H}_{\frac{N}{2}}\right)\mathbf{T}_{11} + \left(V_{m-1}c_1^2 + 2\alpha - 1\right)\left(\alpha\mathbf{I}_{\frac{N}{2}} - c_1\mathbf{H}_{\frac{N}{2}}\right)\left(\mathbf{E}_{21}\mathbf{P}_{11} + \mathbf{E}_{22}\mathbf{P}_{21}\right)\Big\} \tag{6.40c}$$

and

$$\hat{\mathbf{T}}^{(m)}_{22} = \mathbf{T}_{22} + \frac{1}{2\alpha - 1}\Big\{\left(1 - g_{m-1}\right)\left(c_1^2\mathbf{I}_{\frac{N}{2}} - \alpha c_1\mathbf{H}_{\frac{N}{2}}\right)\mathbf{T}_{12} + \left(V_{m-1}c_1^2 + 2\alpha - 1\right)\left(\alpha\mathbf{I}_{\frac{N}{2}} - c_1\mathbf{H}_{\frac{N}{2}}\right)\left(\mathbf{E}_{21}\mathbf{P}_{12} + \mathbf{E}_{22}\mathbf{P}_{22}\right)\Big\} \tag{6.40d}$$

where g_m is the convergence factor and V_m is the error multiplying factor ; g_m and V_m are recursively given by

$$g_m = \frac{1}{2\alpha - 1}\left(g_{m-1}\left(\alpha^2 - c_1^2\right) - c_1^2\right) \qquad m > 1 \ ;$$
$$g_0 = 0 \ , \quad g_1 = \frac{-(1-\alpha)^2}{2(2\alpha - 1)} \tag{6.41}$$

and

$$V_m = \frac{1}{2\alpha - 1}\left(V_{m-1}\left(\alpha^2 - c_1^2\right) + 2\alpha - 1\right) \qquad m > 1 \ ;$$
$$V_0 = 0 \ , \quad V_1 = 1 \tag{6.42}$$

respectively.

Replacing the sub-matrices $\hat{\mathbf{T}}_{21}^{(m)}$ and $\hat{\mathbf{T}}_{22}^{(m)}$ in $\hat{\mathbf{T}}_{\mathbf{F};m}$ with $\mathbf{T}_{21}$ and $\mathbf{T}_{22}$ (obtained from $\tilde{\mathbf{T}}_{\mathbf{F}}$) to yield the matrix $\hat{\mathbf{T}}'_{\mathbf{F};m}$ and performing the inverse two-dimensional Hadamard NPT of $\hat{\mathbf{T}}'_{\mathbf{F};m}$, we obtain the matrix $\hat{\mathbf{F}}'_m$ whose segments are given by

$$\check{\mathbf{F}}_{11}^{(m)} = g_m\left(\mathbf{Q}_{11}\mathbf{T}_{11}\mathbf{Q}_{11} + \mathbf{Q}_{11}\mathbf{T}_{12}\mathbf{Q}_{21}\right) + \mathbf{Q}_{12}\mathbf{T}_{21}\mathbf{Q}_{11} + \mathbf{Q}_{12}\mathbf{T}_{22}\mathbf{Q}_{21}$$
$$+ V_m\mathbf{Q}_{11}\mathbf{P}_{12}\mathbf{E}_{21} \tag{6.43a}$$
$$\check{\mathbf{F}}_{12}^{(m)} = g_m\left(\mathbf{Q}_{11}\mathbf{T}_{11}\mathbf{Q}_{12} + \mathbf{Q}_{11}\mathbf{T}_{12}\mathbf{Q}_{22}\right) + \mathbf{Q}_{12}\mathbf{T}_{21}\mathbf{Q}_{12} + \mathbf{Q}_{12}\mathbf{T}_{22}\mathbf{Q}_{22}$$
$$+ V_m\mathbf{Q}_{11}\mathbf{P}_{12}\mathbf{E}_{22} \tag{6.43b}$$
$$\check{\mathbf{F}}_{21}^{(m)} = g_m\left(\mathbf{Q}_{21}\mathbf{T}_{11}\mathbf{Q}_{11} + \mathbf{Q}_{21}\mathbf{T}_{12}\mathbf{Q}_{21}\right) + \mathbf{Q}_{22}\mathbf{T}_{21}\mathbf{Q}_{11} + \mathbf{Q}_{22}\mathbf{T}_{22}\mathbf{Q}_{21}$$
$$+ V_m\mathbf{Q}_{21}\mathbf{P}_{12}\mathbf{E}_{21} \tag{6.43c}$$
$$\check{\mathbf{F}}_{22}^{(m)} = g_m\left(\mathbf{Q}_{21}\mathbf{T}_{11}\mathbf{Q}_{12} + \mathbf{Q}_{21}\mathbf{T}_{12}\mathbf{Q}_{22}\right) + \mathbf{Q}_{22}\mathbf{T}_{21}\mathbf{Q}_{12} + \mathbf{Q}_{22}\mathbf{T}_{22}\mathbf{Q}_{22}$$
$$+ V_m\mathbf{Q}_{21}\mathbf{P}_{12}\mathbf{E}_{22} \tag{6.43d}$$

APPENDIX V

DERIVATION OF SOME RESULTS USED IN THE NPT GENERALIZED WIENER FILTER DESIGN

Result 1

$$\nabla_{\mathbf{B}} \left(\mathbf{x}^T \mathbf{B}^T \mathbf{Q} \mathbf{B} \mathbf{x}\right) = \mathbf{Q}^T \mathbf{B} \mathbf{x} \mathbf{x}^T + \mathbf{Q} \mathbf{B} \mathbf{x} \mathbf{x}^T \tag{A5.1}$$

$\mathbf{x}$ is the $N \times 1$ vector

$$\mathbf{x}^T = [\mathbf{x}_1 \, \mathbf{x}_2 \, \ldots \, \mathbf{x}_N] \tag{A5.2}$$

where the superscript T denotes transposition operation; $\mathbf{B}$ is the $N \times N$ matrix

$$\mathbf{B} = \begin{bmatrix} b_{11} & b_{12} & \cdots & b_{1N} \\ b_{21} & b_{22} & \cdots & b_{2N} \\ \vdots & \vdots & \ddots & \vdots \\ b_{N1} & b_{N2} & \cdots & b_{NN} \end{bmatrix} \tag{A5.3}$$

and $\mathbf{Q}$ is the $N \times N$ matrix

$$\mathbf{Q} = \begin{bmatrix} q_{11} & q_{12} & \cdots & q_{1N} \\ q_{21} & q_{22} & \cdots & q_{2N} \\ \vdots & \vdots & \ddots & \vdots \\ q_{N1} & q_{N2} & \cdots & q_{NN} \end{bmatrix} \tag{A5.4}$$

For convenience, we consider the case $N = 3$ and define

$$U = \mathbf{x}^T \mathbf{B}^T \mathbf{Q} \mathbf{B} \mathbf{x} \tag{A5.5}$$

Substituting for $\mathbf{x}$, $\mathbf{B}$ and $\mathbf{Q}$ from $(A5.2 - A5.3)$ in $(A5.5)$, we have

$$U = [x_1 \quad x_2 \quad x_3] \begin{bmatrix} b_{11} & b_{21} & b_{31} \\ b_{12} & b_{22} & b_{32} \\ b_{13} & b_{23} & b_{33} \end{bmatrix} \begin{bmatrix} q_{11} & q_{12} & q_{13} \\ q_{21} & q_{22} & q_{23} \\ q_{31} & q_{32} & q_{33} \end{bmatrix} \begin{bmatrix} b_{11} & b_{12} & b_{13} \\ b_{21} & b_{22} & b_{23} \\ b_{31} & b_{32} & b_{33} \end{bmatrix} \begin{bmatrix} x_1 \\ x_2 \\ x_3 \end{bmatrix} \tag{A5.6}$$

or

$$U = [r_1 \quad r_2 \quad r_3] \begin{bmatrix} q_{11} & q_{12} & q_{13} \\ q_{21} & q_{22} & q_{23} \\ q_{31} & q_{32} & q_{33} \end{bmatrix} \begin{bmatrix} r_1 \\ r_2 \\ r_3 \end{bmatrix} \tag{A5.7}$$

where

$$r_1 = b_{11}x_1 + b_{12}x_2 + b_{13}x_3 \tag{A5.8a}$$

$$r_2 = b_{21}x_1 + b_{22}x_2 + b_{23}x_3 \tag{A5.8b}$$

$$r_3 = b_{31}x_1 + b_{32}x_2 + b_{33}x_3 \tag{A5.8c}$$

It follows that

$$U = \begin{bmatrix} y_1 & y_2 & y_3 \end{bmatrix} \begin{bmatrix} r_1 \\ r_2 \\ r_3 \end{bmatrix} \tag{A5.9}$$

where

$$y_1 = r_1 q_{11} + r_2 q_{21} + r_3 q_{31} \tag{A5.10a}$$

$$y_2 = r_1 q_{12} + r_2 q_{22} + r_3 q_{23} \tag{A5.10b}$$

$$y_3 = r_1 q_{13} + r_2 q_{23} + r_3 q_{33} \tag{A5.10c}$$

therefore

$$U = y_1 r_1 + y_2 r_2 + y_3 r_3 \tag{A5.11}$$

By definition [5],

$$\nabla_{\mathbf{B}} U = \begin{bmatrix} \frac{\partial U}{\partial b_{11}} & \frac{\partial U}{\partial b_{12}} & \frac{\partial U}{\partial b_{13}} \\ \frac{\partial U}{\partial b_{21}} & \frac{\partial U}{\partial b_{22}} & \frac{\partial U}{\partial b_{23}} \\ \frac{\partial U}{\partial b_{31}} & \frac{\partial U}{\partial b_{32}} & \frac{\partial U}{\partial b_{33}} \end{bmatrix} \tag{A5.12}$$

Substituting (A5.10) into (A5.11), we have

$$\begin{aligned} U = {} & r_1^2 q_{11} + r_1 r_2 q_{21} + r_1 r_3 q_{31} + r_1 r_2 q_{12} + r_2^2 q_{22} \\ & + r_2 r_3 q_{32} + r_1 r_3 q_{13} + r_2 r_3 q_{23} + r_3^2 q_{33} \end{aligned} \tag{A5.13}$$

The individual entries of (A5.12) are as follows

$$\frac{\partial U}{\partial b_{11}} = (r_1 q_{11} + r_2 q_{21} + r_3 q_{31} + r_1 q_{11} + r_2 q_{12} + r_3 q_{13})\, x_1 \tag{A5.14a}$$

$$\frac{\partial U}{\partial b_{12}} = (r_1 q_{11} + r_2 q_{21} + r_3 q_{31} + r_1 q_{11} + r_2 q_{12} + r_3 q_{13})\, x_2 \tag{A5.14b}$$

$$\frac{\partial U}{\partial b_{13}} = (r_1 q_{11} + r_2 q_{21} + r_3 q_{31} + r_1 q_{11} + r_2 q_{12} + r_3 q_{13})\, x_3 \tag{A5.14c}$$

$$\frac{\partial U}{\partial b_{21}} = (r_1 q_{12} + r_2 q_{22} + r_3 q_{32} + r_1 q_{21} + r_2 q_{22} + r_3 q_{23})\, x_1 \tag{A5.14d}$$

$$\frac{\partial U}{\partial b_{22}} = (r_1 q_{12} + r_2 q_{22} + r_3 q_{32} + r_1 q_{21} + r_2 q_{22} + r_3 q_{23})\, x_2 \tag{A5.14e}$$

$$\frac{\partial U}{\partial b_{23}} = (r_1 q_{12} + r_2 q_{22} + r_3 q_{32} + r_1 q_{21} + r_2 q_{22} + r_3 q_{23})\, x_3 \tag{A5.14f}$$

$$\frac{\partial U}{\partial b_{31}} = (r_1 q_{13} + r_2 q_{23} + r_3 q_{33} + r_1 q_{31} + r_2 q_{32} + r_3 q_{33})\, x_1 \tag{A5.14g}$$

$$\frac{\partial U}{\partial b_{32}} = (r_1 q_{13} + r_2 q_{23} + r_3 q_{33} + r_1 q_{31} + r_2 q_{32} + r_3 q_{33})\, x_2 \tag{A5.14h}$$

$$\frac{\partial U}{\partial b_{33}} = (r_1 q_{13} + r_2 q_{23} + r_3 q_{33} + r_1 q_{31} + r_2 q_{32} + r_3 q_{33})\, x_3 \tag{A5.14i}$$

Substituting (A5.14) into (A5.12), we obtain

$$\begin{aligned} \nabla_{\mathbf{B}} U = {} & \begin{bmatrix} q_{11} & q_{21} & q_{31} \\ q_{12} & q_{22} & q_{32} \\ q_{13} & q_{23} & q_{33} \end{bmatrix} \begin{bmatrix} x_1 r_1 & x_2 r_1 & x_3 r_1 \\ x_1 r_2 & x_2 r_2 & x_3 r_2 \\ x_1 r_3 & x_2 r_3 & x_3 r_3 \end{bmatrix} \\ & + \begin{bmatrix} q_{11} & q_{12} & q_{13} \\ q_{21} & q_{22} & q_{23} \\ q_{31} & q_{32} & q_{33} \end{bmatrix} \begin{bmatrix} x_1 r_1 & x_2 r_1 & x_3 r_1 \\ x_1 r_2 & x_2 r_2 & x_3 r_2 \\ x_1 r_3 & x_2 r_3 & x_3 r_3 \end{bmatrix} \end{aligned} \tag{A5.15}$$

But

$$\begin{bmatrix} x_1r_1 & x_2r_1 & x_3r_1 \\ x_1r_2 & x_2r_2 & x_3r_2 \\ x_1r_3 & x_2r_3 & x_3r_3 \end{bmatrix} = \begin{bmatrix} b_{11} & b_{12} & b_{13} \\ b_{21} & b_{22} & b_{23} \\ b_{31} & b_{32} & b_{33} \end{bmatrix} \begin{bmatrix} x_1^2 & x_2x_1 & x_3x_1 \\ x_1x_2 & x_2^2 & x_3x_2 \\ x_1x_3 & x_2x_3 & x_3^2 \end{bmatrix} \tag{A5.16a}$$

$$= \begin{bmatrix} b_{11} & b_{12} & b_{13} \\ b_{21} & b_{22} & b_{23} \\ b_{31} & b_{32} & b_{33} \end{bmatrix} \begin{bmatrix} x_1 \\ x_2 \\ x_3 \end{bmatrix} \begin{bmatrix} x_1 & x_2 & x_3 \end{bmatrix} \tag{A5.16b}$$

and using (A5.16) in (A5.15), we obtain

$$\nabla_{\mathbf{B}} \left(\mathbf{x}^T \mathbf{B}^T \mathbf{Q} \mathbf{B} \mathbf{x} \right) = \mathbf{Q}^T \mathbf{B} \mathbf{x} \mathbf{x}^T + \mathbf{Q} \mathbf{B} \mathbf{x} \mathbf{x}^T \tag{A5.17}$$

Result 2

$$\nabla_{\mathbf{B}} \left(\mathbf{x}^T \mathbf{B}^T \mathbf{P} \mathbf{f} \right) = \mathbf{P}^T \mathbf{f} \mathbf{x}^T \tag{A5.18}$$

The vector $\mathbf{x}$ and the matrix $\mathbf{B}$ are defined in (A5.2) and (A5.3) respectively. $\mathbf{f}$ is the $N \times 1$ vector

$$\mathbf{f}^T = [f_1 \quad f_2 \quad \dots \quad f_N] \tag{A5.19}$$

and $\mathbf{P}$ is the $N \times N$ matrix

$$\mathbf{P} = \begin{bmatrix} p_{11} & p_{12} & \cdots & p_{1N} \\ p_{21} & p_{22} & \cdots & p_{2N} \\ \vdots & \vdots & \ddots & \vdots \\ p_{N1} & p_{N2} & \cdots & p_{NN} \end{bmatrix} \tag{A5.20}$$

Again, for convenience, we consider the case $N = 3$ and define

$$U = \mathbf{x}^T \mathbf{B}^T \mathbf{P} \mathbf{f} \tag{A5.21}$$

Substituting (A5.2), (A5.3), (A5.19) and (A5.20) into (A5.21), we obtain

$$U = r_1c_1 + r_2c_2 + r_3c_3 \tag{A5.22}$$

where

$$r_1 = b_{11}x_1 + b_{12}x_2 + b_{13}x_3 \tag{A5.23a}$$

$$r_2 = b_{21}x_1 + b_{22}x_2 + b_{23}x_3 \tag{A5.23b}$$

$$r_3 = b_{31}x_1 + b_{32}x_2 + b_{33}x_3 \tag{A5.23c}$$

and

$$c_1 = p_{11}f_1 + p_{12}f_2 + p_{13}f_3 \tag{A5.24a}$$

$$c_2 = p_{21}f_1 + p_{22}f_2 + p_{23}f_3 \tag{A5.24b}$$

$$c_3 = p_{31}f_1 + p_{32}f_2 + p_{33}f_3 \tag{A5.24c}$$

Substituting (A5.23) into (A5.22), we obtain

$$U = c_1 (b_{11}x_1 + b_{12}x_2 + b_{13}x_3) + c_2 (b_{21}x_1 + b_{22}x_2 + b_{23}x_3) + c_3 (b_{31}x_1 + b_{32}x_2 + b_{33}x_3) \tag{A5.25}$$

Using the definition of $\nabla_{\mathbf{B}}U$ given by (*A*5.12) and the expression for U from (*A*5.25), we obtain

$$\nabla_{\mathbf{B}}U = \begin{bmatrix} x_1c_1 & x_2c_1 & x_3c_1 \\ x_1c_2 & x_2c_2 & x_3c_2 \\ x_1c_3 & x_2c_3 & x_3c_3 \end{bmatrix} \tag{A5.26}$$

or

$$\nabla_{\mathbf{B}}U = \begin{bmatrix} c_1 \\ c_2 \\ c_3 \end{bmatrix} [x_1 \quad x_2 \quad x_3] \tag{A5.27}$$

Substituting for c_1, c_2 and c_3 from (*A*5.24) and after some matrix manipulations, we obtain

$$\nabla_{\mathbf{B}}U = \begin{bmatrix} p_{11} & p_{12} & p_{13} \\ p_{21} & p_{22} & p_{23} \\ p_{31} & p_{32} & p_{33} \end{bmatrix} \begin{bmatrix} f_1 \\ f_2 \\ f_3 \end{bmatrix} [x_1 \quad x_2 \quad x_3] \tag{A5.28}$$

or

$$\nabla_{\mathbf{B}}U = \mathbf{P}\mathbf{f}\mathbf{x}^T \tag{A5.29}$$

REFERENCES

1. W. K. Pratt, *Digital Image Processing*, John Wiley and Sons, 1978.

2. R. J. Clarke, *Transform Coding of Images*, Academic Press, 1985.

3. R. Yarlagadda and J. Hershey, "A Naturalness-Preserving Transform for Image Coding and Reconstruction ", IEEE Transactions on Acoustics, Speech and Signal Processing, vol. ASSP-33, No. 4, Aug. 1985, pp. 1005-1012.

4. A. K. Jain, "A Sinusoidal Family of Unitary Transforms ", IEEE Transactions on Pattern Analysis and Machine Intelligence, vol. PAMI-1, No. 4, Oct. 1979, pp. 356-365.

5. N. Ahmed and K. R. Rao, *Orthogonal Transforms for Digital Signal Processing*, Springer Verlag, Berlin and New York, 1970.

6. F. Ayres Jr., *Theory and Problems of Matrices*, McGraw-Hill International Book Company, New York, 1974.

7. R. Yarlagadda and J. Hershey, "A Note on The Eigenvectors of Hadamard Matrices of Order 2^n ", Linear Algebra and Its Application, vol. 45, 1982, pp. 43-53.

8. W. k. Pratt, J. Kane and H. C. Andrews, "Hadamard Transform Image Coding ", Proc. IEEE, vol. 57, No. 1, January 1969, pp. 58-68.

9. R. C. Gonzalez and P. Wintz, *Digital Image Processing*, Addison-Wesley, Reading, MA, 1977.

10. A. K. Jain, "A Fast Karhunen-Loève Transform for a Class of Random Processes ", IEEE Transactions on Communications, vol. COM-24, Sept. 1976, pp. 1023-1029.

11. H. Kitajima, "A Symmetric Cosine Transform ", IEEE Transactions on Computers, vol. C-29, No. 4, April 1980, pp. 317-323.

12. P. Lancaster, *Theory of Matrices*, Academic Press, New York, 1969

13. R. J. Clarke, "On The Dynamic Range of Coefficients Generated in The Transform Processing of Digitised Data ", Proc. IEE, vol. 132, Pt. F, No. 2 : Comm. Radar Signal Processing, April 1985, pp. 107-110.

14. A. K. Jain, "Advances in Mathematical Models for Image Processing ", Proc. IEEE, vol. 69, No. 5, May 1981, pp. 502-528.

15. N. Ahmed, T. Natarajan, K. R. Rao, "Discrete Cosine Transform ", IEEE Transactions on Computers, vol. C-23, 1974, pp. 90-93.

16. W. K. Pratt, W. Chen and L. R. Welch, "Slant Transform Image Coding ", IEEE Transactions on Communications, vol. COM-22, No. 8, August 1974, pp. 1075-1093.

17. W. K. Cham and R. J. Clarke, "Application of The Principle of Dyadic Symmetry to The Generation of Orthogonal Transforms ", Proc. IEE, vol. 133, Pt. F, No. 3, June 1986, pp. 264-270.

18. R. J. Clarke, "Application of Sine Transform in Image Processing ", Electronics letters, vol. 19, No. 13, June 1983, pp. 490-491.

19. C. E. Shannon, *The Mathematical Theory of Communication*, University of Illinois Press, Urbana, Illinois, 1949.

20. A. K. Jain, "Image Data Compression : A Review ", Proc. IEEE, vol. 69, No. 3, March 1981, pp. 349-384.

21. H. G. Musmann, P. Pirsch and H. Grallert, "Advances in Picture Coding ", Proc. IEEE, vol. 73, No. 4, April 1985, pp. 523-548.

22. A. Habibi, "Hybrid Coding of Pictorial Data ", IEEE Transactions on Communications, vol. COM-22, No. 5, May 1974, pp. 614-624.

23. J. B. O'Neal, "Predictive Quantizing Systems (Differential Pulse Code Modulation) For The Transmission of Television Signals ", Bell System Technical Journal 45, May-June 1966, pp. 689-721.

24. A. Habibi, "Survey of Adaptive Image Coding Techniques ", IEEE Transactions on Communications, vol. COM-25, No. 11, Nov. 1977, pp. 1275-1284.

25. M. Kanefsky and C. Fong, "Predictive Source Coding Techniques Using Maximum Likelihood Prediction For Compression of Digitized Images ", IEEE Transactions on Information Theory, vol. IT-30, No. 5, September 1984, pp. 722-727.

26. S. T. Alexander and S. A. Rajala, "Image Compression Results Using the LMS Adaptive Algorithm ", IEEE Transactions on Acoustics, Speech and Signal Processing, vol. ASSP-33, No. 3, June 1985, pp. 712-714.

27. A. K. Jain, "Image Coding Via a Nearest Neighbours Image Model ", IEEE Transactions on Communications, vol. COM-23, No. 3 March 1975, pp. 318-331.

28. P. A. Wintz, "Transform Picture Coding ", Proc. IEEE, vol. 60, No. 7, July 1972, pp. 809-820.

29. H. J. Landau and D. Slepian, "Some Computer Experiments in Picture Processing For Bandwidth Reduction ", Bell System Technical Journal, vol. 50, No. 5, May-June 1971, pp. 1525-1540.

30. A. Habibi and P. A. Wintz, "Image Coding by Linear Transformation and Block Quantization ", IEEE Transactions on Communication Technology, vol. COM-19, No. 1, February 1971, pp. 50-62.

31. T. C. Chen and T. P. de Figueiredo, " An Image Transform Coding Scheme Based on Spatial Domain Considerations ", IEEE Transactions on Pattern Analysis and Machine Intelligence, vol. PAMI-5, No. 3, May 1983, pp. 332-337.

32. P. M. Farrelle and A. K. Jain, "Recursive Block Coding - A New Approach to Transform Coding ", IEEE Transactions on Communications, vol. COM-34, No. 2, February 1986, pp. 161-179.

33. J. A. Roese, W. K. Pratt and G. S. Robinson, "Interframe Cosine Transform Image Coding ", IEEE Transactions on Communications, vol. COM-25, No. 11, November 1977, pp. 1329-1338.

34. J. Roese, "Hybrid Transform-Predictive Image Coding ", in Image Transmission Techniques (W. K. Pratt, editor), Academic Press, New York, 1979, pp. 157-187.

35. A. O. Osinubi and R. A. King, "Naturalness-Preserving Transform Coding of Monochrome Images ", Proc. Fifth International Conference on Digital Processing of Signals in Communications, Loughborough, U. K., September 1988, pp. 267-275.

36. A. O. Osinubi and R. A. King, "Predictive Naturalness-Preserving Transform Coding of Monochrome Images ", Proc. MELECON '89, Lisbon, Portugal, April 1989.

37. S. H. Wang and A. K. Jain, *Applications of Stochastic Models For Image Data Compression*, Research Report, Department of Electrical Engineering, University of California, Davis, 1979.

38. R. P. Brent, *Algorithms For Minimization Without Derivatives*, Prentice Hall, 1973.

39. W. H. Press, B. P. Flannery, S. A. Teukolsky and W. T. Vetterling, *Numerical Recipes*, Cambridge University Press, New York, 1986.

40. A. Segall, "Bit Allocation and Encoding For Vector Sources ", IEEE Transactions on Information Theory, vol. IT-22, No. 2, March 1976, pp. 162-169.

41. B. Fox, "Discrete Optimization Via Marginal Analysis ", Management Science, vol. 13, No. 3, November 1966, pp. 210-216.

42. P. A. Wintz and A. J. Kurtenbach, "Waveform Error Control in PCM Telemetry ", IEEE Transactions on Information Theory, vol. IT-14, 1968, pp. 650-661.

43. J. J. Y. Huang and P. M. Schultheiss, "Block Quantization of Correlated Gaussian Random Variables ", IEEE Transactions on Communication Systems, vol. CS-11, September 1963, pp. 289-296.

44. L. D. Davisson, "Rate-Distortion Theory and Applications ", Proc. IEEE, vol. 60, July 1972, pp. 800-808.

45. K. Tzou, "A Fast Computational Approach to The Design of Block Quantization " IEEE Transactions on Acoustics, Speech and Signal Processing, vol. ASSP-35, No. 2, February 1987, pp. 235-237.

46. A. Papoulis, *Probability, Random Variables, and Stochastic Processes*, McGraw-Hill Book Company, 1985.

47. J. Max, "Quantizing For Minimum Distortion ", IEEE Transactions on Information Theory, vol. IT 16, 1960, pp. 7-12.

48. W. Mauersberger, "An Adaptive Transform Coding System Based on Two-Dimensional Classification ", Proc. Picture Coding Symposium, Ipswich, U. K., Paper 12.1, 1979.

49. W. Chen and C. H. Smith, "Adaptive Coding of Monochrome and Colour Images ", IEEE Transactions on Communications, vol. COM-25, No. 11, November 1977, pp. 1285-1292.

50. W. K. Pratt, editor, *Image Transmission Techniques*, Academic Press, 1979.

51. T. Berger, *Rate-Distortion Theory : A mathematical Basis for Data Compression*, Englewood Cliffs, N.J., Prentice Hall, 1971.

52. D. J. Sakrison and V. R. Algazi, " Comparison of Line-by-Line and Two-Dimensional Encoding of Random Images ", IEEE Transactions on Information Theory, vol. IT-17, No. 4, July 1971, pp. 386-398.

53. L. D. Davisson, " The Theoretical Analysis of Data Compression Systems ", Proc. IEEE, vol. 56, No. 2, February 1968, pp. 176-186.

54. J. Hershey, H. Gates, B. Fields, J. Cosgrove and R. Yarlagadda, "Military Tactical Imagery ", J. Electronic Defense, vol. 6, October 1983, pp. 127-132.

55. R. S. Varga, *Matrix Iterative Analysis*, Englewood Cliffs, N. J., Prentice-Hall, 1962.

56. J. H. Wilkinson, *The Algebraic Eigenvalue Problem*, Oxford, England : Clarendon, 1965.

57. J. S. Frame, "Matrix Functions and Applications ", IEEE Spectrum, vol. 1, April 1964, pp. 102-108.

58. J. S. Orfanidis, *Optimum Signal Processing*, Macmillan, New York, 1985.

59. B. Widrow et al, "Adaptive Noise Cancelling : Principles and Applications ", Proc. IEEE, vol. 63, December 1975, pp. 1692-1716.

60. B. Widrow et al, "Stationary and Non-Stationary Learning Characteristics of The LMS Adaptive Filter ", Proc. IEEE, vol. 64, August 1976, pp. 1151-1162.

61. A. O. Osinubi and R. A. King, " Naturalness-Preserving Transform (NPT) Reconstruction of Signals Degraded by Non-Stationary Noise Processes ", Proc. IEEE International Conference on Acoustics, Speech and Signal Processing, Glasgow, U. K., May 1989, pp. 1199-1202.

62. A. O. Osinubi and R. A. King, " One-Dimensional Hadamard Naturalness-Preserving Transform Reconstruction of Signals Degraded by Non-Stationary Noise Processes ", submitted for publication in IEEE Transactions on Acoustics, Speech and Signal Processing.

63. R. M. Falconer and J. L. Adams, " 'Orwell' : A Protocol For an Integrated Services Local Network ", British Telecom Technol. J., vol. 3, No. 4, October 1985, pp. 27-35.

64. Proc. IEE Colloquium on "Packet Video ", London, May 1989.

65. IEEE Journal on Selected Areas in Communications, vol. 7, No. 5, Special Issue on Packet Speech and Video, June 1989.

66. A. Nieminen, P. Heinonen and Y. Neuvo, "A New Class of Detail-Preserving Filters For Image Processing ", IEEE Transactions on Pattern Analysis and Machine Intelligence, vol. PAMI-9, No. 1, January 1987, pp. 74-90.

67. M. P. Ekstrom, "Realizable Wiener Filtering in Two-Dimensions ", IEEE Transactions on Acoustics, Speech and Signal Processing, vol. ASSP-30, No. 1, February 1982, pp. 31-40.

68. M. M. Hadhoud and D. W. Thomas, "Two-Dimensional Adaptive LMS (TDLMS) Algorithm ", IEEE Transactions on Circuits and Systems, vol. 35, No. 5, May 1988, pp. 485-494.

69. R. M. Gray, "Vector Quantization ", IEEE ASSP Magazine, April 1984, pp. 4-28.

70. N. M. Nasrabadi and R. A. King, "Image Coding Using Vector Quantization : A Review ", IEEE Transactions on Communications, vol. 36, No. 8, August 1988, pp. 957-971.

71. Y. Linde, A. Buzo and R. M. Gray, "An algorithm for Vector Quantizer Design ", IEEE Transactions on Communications, vol. COM-28, No. 1, January 1980, pp. 84-95.

72. N. M. Nasrabadi and R. A. King, "A New Image Coding Technique Using Transform Vector Quantization ", IEEE ICASSP, California, 1984, pp. 19-21.

73. W. K. Pratt, "Generalized Wiener Filtering Computation Techniques ", IEEE Transactions on Computers, vol. C-21, No. 7, pp. 636-641, July 1972.

74. A. Graham, *Kronecker Products and Matrix Calculus With Applications*, Ellis Horwood Limited, Chichester, England, 1981.

75. G. S. Rogers, *Matrix Derivatives*, Marcel Dekker Inc., 1981.

76. H. Kitajima and T. Shimono, "Residual Correlation of The Hadamard Transforms of Stationary Markov-1 Signals", IEEE Transactions on Communications, vol. COM-31, No. 1, January 1983, pp. 119-121.